Newcastle University

Northern Institute for Cancer Research

Biological mechanisms of disease relapse in childhood medulloblastoma

Rebecca Maree Hill

Thesis submitted in partial fulfilment of the requirements

for the degree of Doctor of Philosophy

Newcastle University

Faculty of Medical Sciences

Northern Institute for Cancer Research

October 2014

Declaration

I certify that no part of the material documented in this thesis has previously been submitted for a degree or other qualification in this or any other university. I declare that this thesis represents my own unaided work, carried out by myself, except where it is acknowledged otherwise in the thesis text.

Rebecca Maree Hill

October 2014

Acknowledgements

I would like to thank my supervisors Prof Steven Clifford and Prof Simon Bailey for their unstinting support, enthusiasm and encouragement throughout this project. Next I would like to thank all the members of the Paediatric Brain Tumour Group at the Northern Institute for Cancer Research who have helped make these last 4 years some of the most enjoyable in my career. In particular I would like to thank Dr Janet Lindsey for introducing me to, and teaching me, the laboratory techniques utilised in the paired relapse study (Chapter 3), and her assistance during this aspect of the project. In addition, I would like to thank Dr Ed Schwalbe for his patience and support in the bioinformatic analysis of the Infinium methylation 450K array, reported in Chapter 5. I would also like to thank Dr Louis Chesler and his group, the Pediatric Solid Tumour Biology and Therapeutics Team at The Institute of Cancer Research. The work by the Pediatric Solid Tumour Biology and Therapeutics Team is reported as part of this thesis in Chapter 4, as their own discoveries are pertinent to the findings in this study, which are described in Chapter 3.

Within the Northern Institute for Cancer Research, Prof Deborah Tweddle and Prof Christine Harrison, my thesis progression overseers, have helped to ensure that my project has run smoothly and their insightful contributions have enriched and improved this thesis. In addition, I would like to thank Prof Josef Vormoor for his invaluable support and advice throughout both my clinical and academic career. Finally, I would like to thank my funders, Action Medical Research, and their fundraisers, whose tireless efforts to raise money have made this project possible.

Dedication

I would like to dedicate this thesis to the patients and families who have contributed to this work. Without their commitment to improving the lives of all children with medulloblastoma, none of this would have been possible. In particular I would like to dedicate this study to the first young person I met in my career to be diagnosed with a relapsed medulloblastoma. He was the bravest young man I have ever come across and I will continue this work in memory of you.

Abstract

Over 30% of patients diagnosed with a medulloblastoma experience disease recurrence. Relapse is almost universally fatal, only infants who receive delayed radiotherapy at disease recurrence typically survive long term. Consequently relapse is the single leading cause of mortality disease-wide. Improved understanding of medulloblastoma at diagnosis has led to the identification of four distinct molecular subgroups with differing biology and outcome. These comprise of medulloblastomas associated with WNT and SHH pathway disruption (MB_{WNT} and MB_{SHH} respectively), and Group 3 and Group 4 tumours (MB_{Group3} and MB_{Group4}). In contrast, very little is understood about the disease at recurrence, and at present there are only two published studies interrogating the biology of relapsed medulloblastoma. However, improved understanding of the biology at relapse is critical to improving treatment. Events at disease relapse could be explored as therapeutic targets or, if predictive of disease recurrence, provide an opportunity to escalate upfront therapy with the aim of preventing relapse.

This study compiled a cohort of medulloblastoma tumours sampled at relapse (n=29), paired with their diagnostic counterparts. All clinicopathological and molecular features, with an established relationship to disease prognosis at diagnosis, were interrogated in this paired relapse cohort. With the exception of molecular subgroup, all features investigated displayed evidence of alteration and predominantly acquisition at recurrence. Most strikingly, the emergence of combined p53-MYC defects was commonly observed at relapse and these features were associated with locally aggressive, rapidly progressive disease following relapse. Through collaborative work, this discovery was explored further, with the development of a novel GTML/*Trp53* $^{KI/KI}$ mouse model which faithfully recapitulated the clinicopathological and molecular features of the p53-MYC human tumours, and demonstrated the dependency of tumourigenesis and maintenance on this genetic interaction. Moreover, therapeutic inhibition of Aurora A kinase using MLN8237 in these mouse tumours led to degradation of MYCN, tumour reduction and prolonged survival.

A novel genome-wide DNA methylation analysis was next undertaken in the paired relapse cohort, focusing on MB_{Group4} tumours, to interrogate maintained and acquired DNA methylation events between diagnosis and relapse, which may play a role in tumour development. Individual CpG sites on the Infinium DNA methylation 450K array were assessed for changes in their DNA methylation status between diagnosis and relapse. Fifteen candidate genes demonstrated tumour-specific methylation states that emerged at relapse and correlated with gene expression. The T-box and Homeobox gene families accounted for 8/15 (53%) candidates identified. Both these families are reportedly important for tumour development in other cancers. In addition, several studies suggest that epigenetic mechanisms, such as DNA methylation, play a regulatory role in their gene expression.

Finally, a large cohort of medulloblastoma tumours (n=206), sampled at diagnosis, from patients who are known to go on and recur, was assembled to investigate any subgroup-specific patterns and timings of relapse. MB_{WNT} rarely relapsed, whereas MB_{SHH} frequently relapsed at both local and distant sites, but were the tumour subgroup most readily salvaged by radiotherapy in patients who were not treated with craniospinal irradiation (CSI) at diagnosis (8/12, 67%). Both MB_{Group3} and MB_{Group4} were widely metastatic at recurrence (34/41 (83%) and 52/61 (85%)) but contrastingly MB_{Group3} relapsed quickly (p=0.0022), whereas MB_{Group4} relapsed more slowly (p=0.0008). In patients who did not receive upfront CSI, *MYC* amplification at diagnosis was associated with rapid disease progression after relapse (p=0.0003). No diagnostic feature was significantly associated with time to death following relapse in the cohort of patients who received upfront CSI. This finding was supported by data from the paired relapse cohort where, in patients who received upfront CSI, it was the biological features of the tumour at relapse and not diagnosis, which were associated with disease course.

In summary, this study has discovered emergent combined p53-MYC defects at medulloblastoma relapse which are associated with disease behaviour, identified potentially epigenetically regulated candidate genes in relapsed MB_{Group4} tumours, and shown that the patterns of disease relapse are associated with radiotherapy and molecular subgroup. Together these findings demonstrate that medulloblastoma tumour biology is significantly different at relapse and that the timings and location of

disease recurrence should be considered in the context of molecular subgroup and treatment. Biopsy at disease recurrence is now essential to validate and expand on these novel findings, interrogate all molecular subgroups at disease recurrence, and translate these discoveries into improved outcomes for the patients suffering from this devastating diagnosis.

List of Abbreviations

4-OHT	4-hydroxytamoxifen
A	Adenine
ALK	Anaplastic lymphoma receptor tyrosine kinase
AML	Acute myeloid leukaemia
APC	Adenomatous polyposis coli
Atoh1	Atonal homologue 1
ATP	Adenine triphosphate
ATRT	Atypical teratoid/rhabdoid tumours
BAC	Bacterial artificial chromosome
BET	Bromodomain and extraterminal domain
Blbp	Brain lipid binding protein
BMIQ	Beta-mixture quantile
bp	Base pair
BSA	Bovine serum albumin
BTIC	Brain tumour-initiating cell
C	Cytosine
CA	California
CCLG	Children's Cancer and Leukaemia Group
CDK6	Cyclin-dependent kinase 6
cDNA	Complementary DNA
CGNPs	Cerebellar granule neuron precursors
ChIP	Chromatin immunoprecipitation
CIMP	CpG island methylator phenotype
CLA	Classic
CML	Chronic myeloid leukaemia
CNS	Central nervous system
CNS-PNET	CNS primitive neuroectodermal tumour
CRUK	Cancer Research UK

CSC	Cancer stem cell
CSF	Cerebrospinal fluid
CSI	Craniospinal irradiation
CT	Connecticut
CTP	Cytosine triphosphate
ddNTP	Dideoxynucleotide
DDX3X	Dead box helicase3, X linked gene
DIPG	Diffuse intrinsic pontine glioma
DM	Double minutes
DMSO	Dimethyl sulfoxide
DN	Desmoplastic/nodular
DNA	Deoxyribonucleic acid
DNMT	DNA methyltransferases
dNTP	Deoxynucleotide
Dox	Doxycycline
dsDNA	Double stranded deoxyribonucleic acid
EFS	Event free survival
EGFR	Epidermal growth factor receptor
E-SIOP	European International Society of Paediatric Oncology
ETANTR	Embryonal tumour with abundant neuropil and true rosettes
Ex3	Exon 3
FCS	Foetal calf serum
FDR	False discovery rate
FFPE	Formalin fixed, paraffin embedded
FGF1	Fibroblast growth factor 1
FGF2	Fibroblast growth factor 2
FISH	Fluorescence in situ hybridisation
Flx	Flox
FVB/NJ	Friend Virus B-type/NIH Jackson

G	Guanine
GBM	Glioblastoma
GFAP	Glial fibrillary acidic protein
GFP	Green fluorescent protein
Glt1	Glutamate transporter 1
GTP	Guanine triphosphate
H&E	Haematoxylin and eosin
H3F3A	H3 histone, family 3A
HCl	Hydrochloric acid
HDAC	Histone deacetylase
HFRT	Hyperfractionated radiotherapy
HGG	High grade glioma
HSR	Homogenously staining regions
i(17q)	Isochromosome 17q
IA	Iowa
IL	Illinois
IN	Indiana
IPA	Ingenuity Pathway Analysis
IQ	Intelligence quotient
IS	Internal standard
KDM6A	Lysine (K)-specific demethylase 6A
LCA	Large cell/anaplastic
LFS	Li-Fraumeni syndrome
LGG	Low grade glioma
Lin	Lineage
LNA	Locked nucleic acid
LOH	Loss of heterozygosity
Luc	Luciferase
MA	Massachusetts

MBEN	Medulloblastoma with extensive nodularity
MB_{NOS}	Medulloblastoma not otherwise specified
MB_{Group3}	Medulloblastoma group 3 subgroup
MB_{Group4}	Medulloblastoma group 4 subgroup
MB_{SHH}	Medulloblastoma SHH subgroup
MB_{WNT}	Medulloblastoma WNT subgroup
$MgCl_2$	Magnesium Chloride
miRNAs	MicroRNAs
ml	Millilitre
MLL	Mixed-lineage leukaemia
MLPA	Multiplex ligation-dependent probe amplification
MO	Missouri
MRI	Magnetic resonance imaging
MRM	Multiple reaction monitoring
mRNA	Messenger RNA
MRS	Magnetic resonance spectroscopy
ND2	Neurogenic differentiation 2
NDUFAF3	NADH dehydrogenase assembly factor 3
Neurod2	Neurogenic differentiation 2
NF-1	Neurofibromatosis type 1
NJ	New Jersey
NK	Natural killer
nm	Nanometre
NMB	Newcastle Medulloblastoma
NMF	Non-negative matrix factorization
NSCs	Neural stem cells
NY	New York
OS	Overall survival
OTX2	Orthodenticle Homeobox 2 gene

PA	Pennsylvania
PBC	Peak-based correction
PBS	Phosphate buffered saline
PBTG	Paediatric Brain Tumour Group
PCR	Polymerase chain reaction
PDGFB	Platelet derived growth factor B
PDGFC	Platelet derived growth factor C
PFS	Progression free survival
Pik3ca	PI3K catalytic-α polypeptide
PLA	Proximity ligation assay
Prom1	Prominin 1
QC	Quality control
QT-PCR	Quantitative PCR
Rcf	Relative centrifugal force
RefSeq	Reference Sequence
RFP	Red fluorescent protein
RIN	RNA integrity number
RNA	Ribonucleic acid
RT-PCR	Real time PCR
SB	Sleeping beauty
SHH	Sonic hedgehog
Smoa1	Activated mutant of smoothened
SNP	Single nucleotide polymorphisms
SSC	Saline sodium citrate
SSCTM	Saline sodium citrate, tween, milk
ssDNA	Single stranded DNA
STR	Subtotal resection
SVM	Support vector machine
SWAN	Subset-quantile within array normalization

SWI/SNF	Switch/sucrose non fermentable
T	Thymine
Tam	Tamoxifen
TBE	Tris-Borate-EDTA
TE	Tris-EDTA
TERT	Telomerase reverse transcriptase
TET	Ten-eleven translocation
THBS1	Thrombospondin 1
T_m	Melting temperature
TN	Tennessee
TSP-1	Thrombospondin-1
TSS	Transcriptional start site
tTA	Tetracycline transactivator
TTP	Thymine triphosphate
TX	Texas
VEGF	Vascular endothelial growth factor
VEGFA	Vascular endothelial growth factor A
VEGFC	Vascular endothelial growth factor C
VHL	Von Hippel-Lindau
w/v	Weight/volume
WA	Washington
WES	Whole exome sequencing
WGA	Whole genome amplification
WGS	Whole genome sequencing
WI	Wisconsin
WNT	Wnt/Wingless
WT	Wild type
µl	Microlitre

Table of Contents

List of Figures

Chapter 1

Chapter 2

Chapter 3

Chapter 4

Chapter 5

Chapter 6

Chapter 9

List of Tables

Chapter 1

Chapter 2

Chapter 3

Chapter 6

Chapter 9

Chapter 1. Introduction

1.1 Definition of cancer

Cancer, in its simplest terms is used to describe a disease process where there is uncontrolled and unregulated replication of cells. To circumvent the normal cell regulatory mechanisms, cancer cells must overcome numerous barriers, both intrinsic and extrinsic, to gain a survival advantage and continue to multiply, populate a tumour and disseminate throughout the body (metastasise). Cancer is a heterogeneous disease which develops over time and different cell populations within a tumour acquire different properties, such as the ability to invade or metastasise. Despite advances in the treatment of cancer, worldwide it still remains one of the biggest challenges faced by science and modern medicine today (Pelengaris and Khan, 2006).

1.2 Health burden of cancer

1.2.1 Worldwide incidence of cancer

More than one in three people will be diagnosed with a form of cancer during their lifetime. The occurrence and distribution of cancers varies across the world with a higher incidence experienced in developed countries such as the USA, UK, Australia and New Zealand. However, whilst the incidence of cancer is highest in developed countries (Figure 1.1), due to of the distribution of people around the globe, over half of all the world's cancer diagnoses occur in the developing world (CRUK, 2011).

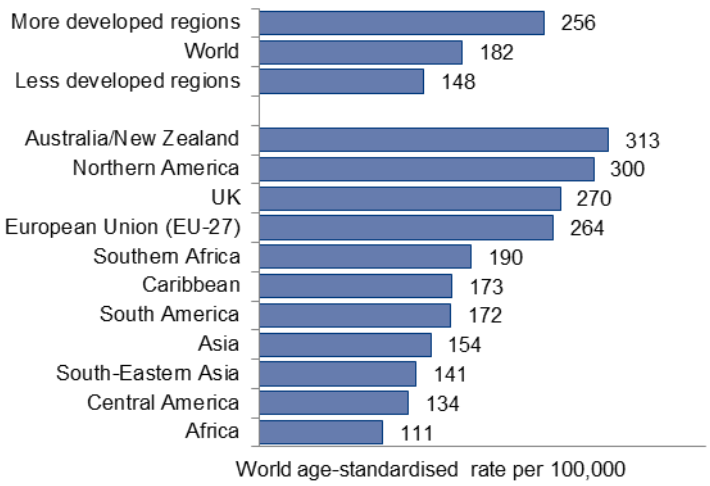

Figure 1.1 Worldwide incidence of cancer per 100,000 people in 2008. Figure adapted from Cancer Worldwide and in the UK (CRUK, 2011).

1.2.2 UK incidence of cancer

In the UK alone, 300 000 people were diagnosed with cancer in 2011 with lung, prostate, breast and bowel (Figure 1.2) being the commonest primary locations observed (CRUK, 2014b). Women and men suffer from different types of cancer with breast cancer being the commonest in women, and cancer of the prostate the commonest diagnosis in men. There is both a gender and age bias in the incidence of cancer as men are more likely to develop cancer, and the rate of cancer increases with advancing age with over half of all cancers diagnosed in people older than 50 years (CRUK, 2014b).

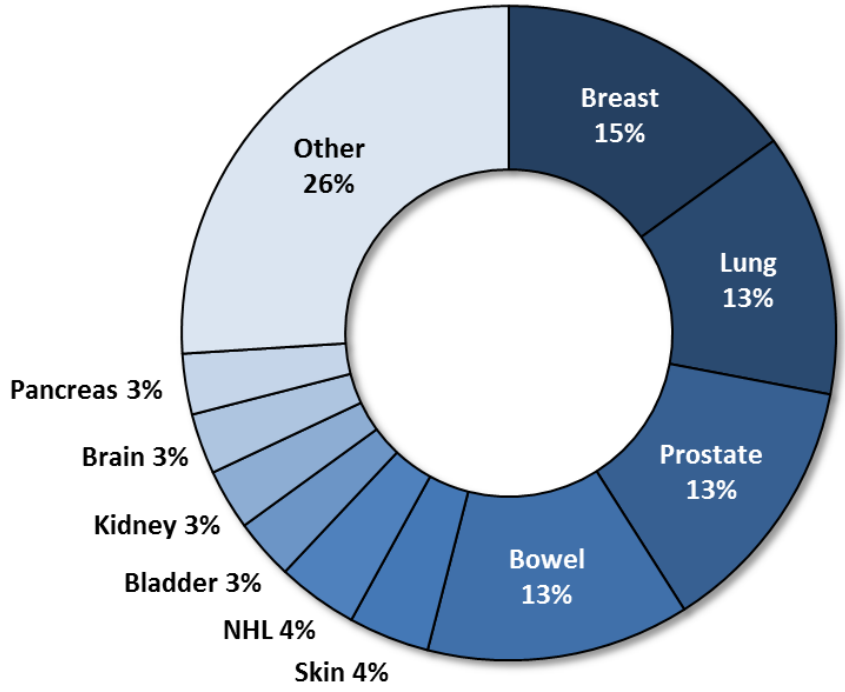

Figure 1.2 Percentage incidence of the ten commonest cancers observed in the UK. NHL, Non-Hodgkin's lymphoma. Figure adapted from Cancer incidence and mortality in the UK (CRUK, 2014b).

1.2.3 Incidence of childhood cancer

Cancer diagnosed between the ages of 0-14 years is rare (1% of all cancers), with approximately 1600 new diagnoses made annually in the UK (CRUK, 2014c). Of these, the most common diagnoses are the haematological malignancies (leukaemia and lymphoma) with tumours arising in the central nervous system (CNS) being the most common 'solid' tumour (Figure 1.3).

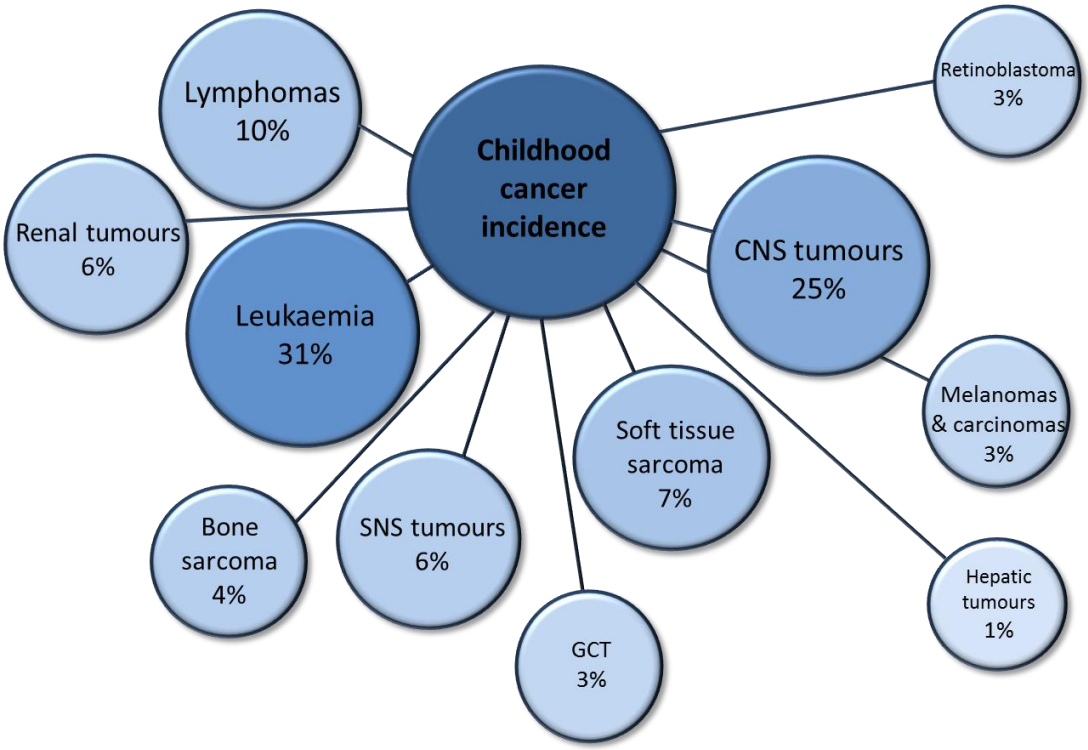

Figure 1.3 Illustrative diagram highlighting the percentage incidence of childhood cancer within the UK. CNS, central nervous system; SNS, sympathetic nervous system; GCT, germ cell tumour. Figure adapted from Childhood Cancer Great Britain & UK (CRUK, 2010).

The incidence of childhood cancer has risen in the UK over the last 50 years by approximately 40%. This is believed to be due to a combination of improved diagnoses and better reporting systems. In contrast, however, survival from childhood cancer has greatly improved as a result of better treatment strategies and therapeutic advances. Five year survival rates for childhood cancer are currently 82% and whilst there are still advances to be made to cure all children of their disease, treatment strategies are now also focusing on long term quality of survival and minimising late effects (CRUK, 2014c). Consequently the challenges and aims of treating childhood cancer today can be divided into two broad strategies; firstly identifying, treating and curing those tumours that currently have a poor prognosis and overall survival (OS) rate and secondly, safely reducing therapies responsible for morbid late effects whilst maintaining survival for those cancers that are currently successfully cured long term.

1.3 The hallmarks of cancer

It is well recognised that cancer occurs following multiple processes which enable the cancer cells to escape normal growth control, develop, grow and metastasise. During this multistep process it is estimated that up to seven events, either genetic or epigenetic, are required by cancer cells for tumour development. The mechanisms by which cancer cells acquire these aberrations and overcome the normal regulatory processes imposed are not fully understood. Conceptually they consist of six established characteristics which are summarised below (Figure 1.4). More recently, additional mechanisms which contribute to the maintenance and progression of the disease have also been described and are similarly displayed in Figure 1.4 (Knudson, 1971; Hanahan and Weinberg, 2000; Pelengaris and Khan, 2006; Hanahan and Weinberg, 2011).

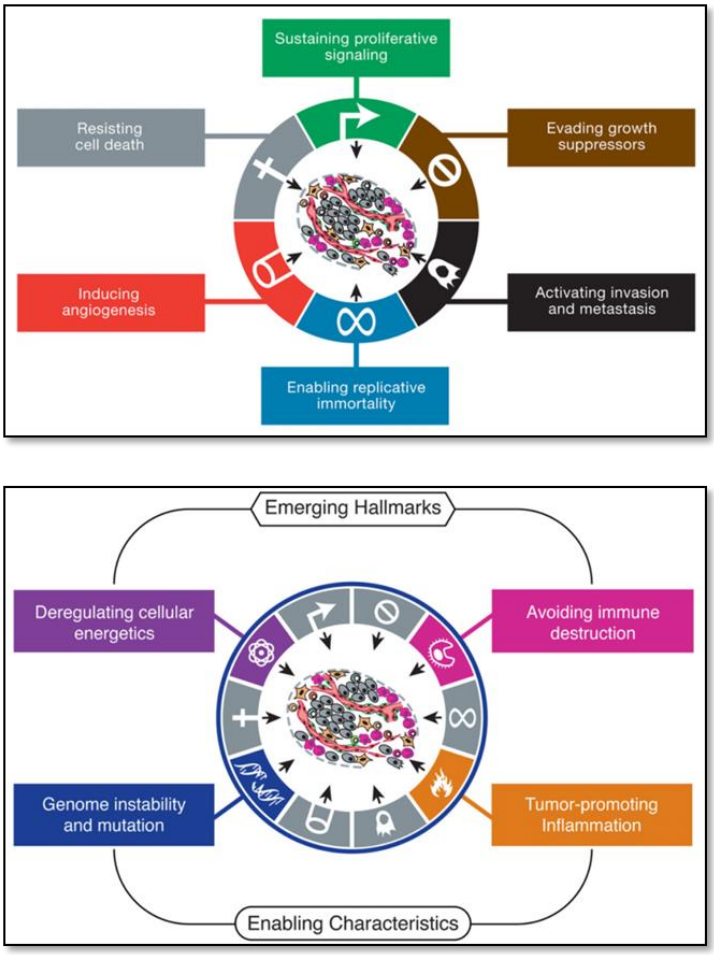

Figure 1.4 Established and emerging hallmarks of cancer. Illustration summarising the six hallmarks of cancer (top panel) followed by more recent emerging and enabling characteristics (bottom panel) that have been recently proposed by Hanahan and Weinberg (2011).

1.3.1 Sustained proliferative signalling

In order to enable cancers cells to continuously proliferate, the normal balance of cell growth and division is disrupted. Cell growth is controlled by a balance of positive and negative signals which are either local in origin (paracrine) or distant (endocrine). Complex pathways are integral to this process; growth factors bind to intracellular or cell surface receptors and engage downstream intracellular enzymes or transcription factors which activate the cell cycle and growth machinery. Typically, for cell growth to occur in the correct environment, growth factors also require integrin cell-adhesion. These processes, however, are difficult to investigate experimentally, as they are typically paracrine in nature, transient and localised making accessing these events challenging. What is understood is that cancer cells can acquire alternative proliferative signalling mechanisms to maintain survival and growth. These mechanisms include; hyper-sensitivity to growth factors due to increased growth factor receptors, modified receptor structures which enable independent unregulated signalling, excess self-production of growth factors, recruitment of growth factors from nearby normal cells, and downstream control of growth factor signalling pathways (Pelengaris and Khan, 2006; Hanahan and Weinberg, 2011).

1.3.2 Evading growth suppressors

In addition to sustaining proliferation and growth, cancer cells must also evade the normal growth suppressive mechanisms. Two key cellular processes are in place to suppress growth; contact inhibition and tumour suppressor genes. Contact inhibition is the process where densely populated, neighbouring cells, form cell-to-cell contacts which in turn inhibits further growth and division. An example of contact inhibition is the coupling of the cell-surface adhesion molecular E-cadherin, to a transmembrane receptor tyrosine kinase such as the epidermal growth factor receptor (EGF). This process is mediated by Merlin, the cytoplasmic product of the *NF2* gene. Merlin strengthens the cell-to-cell adhesions formed and can also sequester growth factors leading to the overall suppression of growth. Loss of Merlin, through mutations in the *NF2* gene, occurs in the cancer predisposition syndrome neurofibromatosis type II and is an example of how cancer can evade one of the growth suppressive mechanisms (Hanahan and Weinberg, 2011).

Tumour suppressor genes encode for proteins which either inhibit or slow cell proliferation. Their role is to prevent abnormal cells with damaged DNA from entering or progressing through the cell cycle and they either induce growth arrest, to allow the repair of the damaged cell, or cell death known as apoptosis. Examples of tumour suppressor genes are *RB1* and *TP53* (discussed in section 1.4.1, Table 1.1) which both encode for proteins involved in cell cycle control (Rb and p53 respectively). In brief, Rb is responsible for determining whether a cell should continue to grow and divide whereas p53 halts the cycle of a cell with DNA damage and elects to either repair that cell or trigger apoptosis if the cell is beyond rescue. Both these mechanisms can be circumvented by cancer cells, and aberrations in the Rb and p53 pathways are frequently discovered with mutations in *TP53* being the most frequently found mutations (~50%) in adult cancers (Hanahan and Weinberg, 2011).

1.3.3 Resisting cell death

There are a variety of mechanisms adopted by cancer cells to resist apoptosis. Abnormalities within the p53 pathway, such as mutation of the *TP53* gene, enable cancer cells to avoid death. A similar affect is achieved by the down-regulation of other pro-apoptotic factors, such as *BAX* or *BBC3* (Figure 1.6), or the up-regulation of survival and anti-apoptotic factors (*BCL2* or *BCL2L1*). Other forms of cell death such as autophagy are less well understood, and enhancement of this process can be both deleterious as well as beneficial to cancer cells. Finally, cell death via necrosis can be advantageous to tumours as the release of the cell contents attracts inflammatory cells which in turn stimulates growth via processes such as angiogenesis (Pelengaris and Khan, 2006; Hanahan and Weinberg, 2011).

1.3.4 Enabling replicative immortality

Normal cells have a finite ability to replicate, with the endpoint being either senescence, where cells cease to divide but remain viable, or cell death (apoptosis). Telomeres, located at the end of chromosomes, progressively shorten after each cell division and it is this process which determines the number of divisions a cell can undergo. Once telomeres are eroded, the chromosome ends are no longer protected and cells enter a crisis phase where the majority of cells die. Cells surviving this crisis phase typically express telomerase, a ribonucleoprotein with DNA polymerase activity which stabilises and maintains the shortened telomere ends by adding repeat

segments of DNA. These cells are consequently immortalised; a characteristic feature displayed by both cell lines and cancer cells (up to 90% of all tumours) and the reactivation of telomerase correlates directly with the sustained growth of many advanced cancers (Hanahan and Weinberg, 2011; Shay and Wright, 2011). Other mechanisms by which cells can achieve immortalisation are through increased expression of telomerase reverse transcriptase (*TERT*), the protein subunit of telomerase. This can be achieved via hypermethylation or mutations in the promoter region of the gene (section 1.4.7). Other alternative mechanism also recently discovered for telomere lengthening include loss-of-function mutations in the telomere binding proteins encoded by *DAXX* and *ATRX* (Shay and Wright, 2011; Castelo-Branco *et al.*, 2013; Killela *et al.*, 2013; Lindsey *et al.*, 2014).

1.3.5 Inducing angiogenesis

The normal process of blood vessel growth, angiogenesis, is rarely activated in developed tissue except when stimulated to do so by injury for example, to enable healing. In tumourigenesis and cancer progression, angiogenesis is central to the survival of cancer cells and is inevitably activated relatively early in cancer development (Pelengaris and Khan, 2006; Hanahan and Weinberg, 2011). Pathological activation of vascularisation in tumourigenesis is attributed to the imbalance of pro and anti-angiogenic factors and this 'angiogenic switch' is believed to be triggered by the relative hypoxia and increased metabolic load found within a tumour (Baeriswyl and Christofori, 2009).

Vascular endothelial growth factor A (*VEGFA*) is a member of the gene family responsible for inducing placental growth. It plays a central role in regulating both normal and pathological angiogenesis. In pathological angiogenesis, VEGFA binds to its tyrosine kinase receptor VEGFR-2, which is located on the endothelial cells within blood vessels, and promotes abnormal vascularisation within the tumour. Additional members of same gene family such as VEGFC are also involved in inducing angiogenesis by binding to their tyrosine kinase receptors. Other well recognised stimulators in this process are fibroblast growth factor 1 and 2 (*FGF1* and *FGF2*) and platelet derived growth factor B and C (*PDGFB* and *PDGFC*) all of which induce endothelial cell migration and proliferation (Pelengaris and Khan, 2006; Baeriswyl and Christofori, 2009; Hanahan and Weinberg, 2011).

Anti-angiogenic factors disrupted during the vascularisation of tumours include thrombospondin-1 (*THBS1*), an extracellular matrix glycoprotein which inhibits growth factor mobilisation and endothelial migration and promotes endothelial cell apoptosis. In addition the proteolytic cleavage products of collagen (endostatin, tumstatin and canstatin), interferon-α, interferon-β and angiostatin are all potent inhibitors of angiogenesis. Both inhibitors and stimulators of vascularisation can be produced by cancer cells themselves or by neighbouring inflammatory cells which have invaded the tumour. Once angiogenesis has begun patterns of vascularisation vary from tumour to tumour due to the spectrum of ongoing stimulation resulting in some tumours being highly vascularised and others relatively under-vascularised (Pelengaris and Khan, 2006; Baeriswyl and Christofori, 2009; Hanahan and Weinberg, 2011).

1.3.6 Activating invasion and metastasis

Understanding the biology of invasion and metastasis of cancer cells is an evolving field but recent advances propose a sequential mechanisms which is summarised in Figure 1.5 below (Talmadge and Fidler, 2010) .

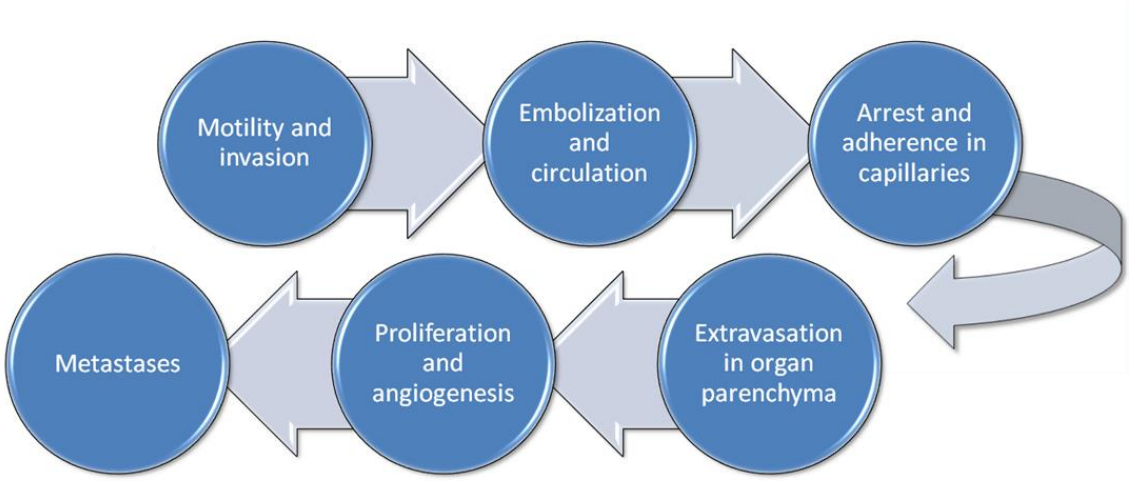

Figure 1.5 The sequential process of metastasis. Figure adapted from Talmadge and Fidler, 2010.

Not all cells within a tumour have the properties which enable them to invade and metastasise. In addition, as illustrated in Figure 1.5, invasion and metastasis is a multistep process with rate limiting steps along the way and failure to progress from one step to the next will delay or halt the process. Cancer cells attain invasive

properties through inappropriate activation of matrix-degrading enzymes alongside altered epithelial intercellular adhesion. Cells either enter the blood or lymphatic circulation directly, or break away from the primary malignancy and proliferate in the stromal tissue until they discover an appropriate lymph node or blood vessel to enter the circulation through (motility and invasion, embolization and circulation, Figure 1.5). Typically cancer cells become trapped within a capillary because of their relatively large size compared to the vessel diameter (arrest and adherence in capillaries, Figure 1.5).

However, certain tumour types have a predilection for particular organs and it is hypothesised that specific tumour cells require specific microenvironments to successfully invade and proliferate. Moreover, if a cancer cell is circulating via the lymphatic system the most likely metastatic sites are the lymph nodes located in the drainage region of the primary tumour. Here, cancer cells face additional challenges to overcome due to the differing microenvironment and large population of cytotoxic T cells found in lymph nodes. Once a cancer cell has established itself at a secondary site with an appropriate microenvironment, the processes of proliferation and angiogenesis (Figure 1.5 and section 1.3.5) begins again. When invasion and metastasis occurs varies, and there is an emerging body of evidence which suggests that the metastatic process can be initiated both early and late on in cancer development (Pelengaris and Khan, 2006; Hanahan and Weinberg, 2011).

1.3.7 Advances in understanding the biology of cancer

In addition to the six established hallmarks already discussed (section 1.3.1-1.3.6), two new hallmarks and further enabling features concerned with cancer development have now been described (Figure 1.4). The new hallmarks are i) mechanisms to avoid destruction by the immune system and ii) the modification of cellular metabolisms to create the most ideal circumstances for neoplastic proliferation. The enabling characteristics are i) genomic instability and ii) promoting an inflammatory response (Hanahan and Weinberg, 2011).

Genomic instability is an enabling feature for the majority of cancers and plays a key role in tumourigenesis and progression. It is best defined as an increased tendency to spontaneously acquire DNA damage, from the nucleotide level (*e.g.* DNA mutations) to

gross changes at the chromosomal level (*e.g.* chromothripsis). Disruptions of many cellular processes are associated with genomic instability such as DNA damage and repair mechanisms, telomere function (section 1.3.4) and cell cycle regulation. As such, the process results in a highly mutable genome allowing the more rapid acquisition of beneficial aberrations for tumour progression (Pelengaris and Khan, 2006; Hanahan and Weinberg, 2011; Rausch *et al.*, 2012).

Finally, the innate inflammatory response, elicited by cancer cells, which historically was thought to be the immune system attempting to eliminate the cancer cells, is now believed to also be an enabling event in cancer development. Tumour promoting effects of inflammation include the ability of immune cells to supply growth factors, pro-angiogenic factors and survival factors. All of these features contribute to many of the already established hallmarks of cancer and enabling features in tumour development described above (section 1.3.1-1.3.6) and illustrated in Figure 1.4 (Hanahan and Weinberg, 2011).

1.4 Models of tumourigenesis in cancer development

As described in section 1.3, cancer development is a multistep process. In order for these steps to occur, many genetic and epigenetic aberrations must develop, typically in tumour suppressor genes and oncogenes, to enable a cancer cell to grow, multiply, invade and metastasise (Figure 1.5). These two classes of genes are described below in section 1.4.1 and 1.4.2, along with the key models proposed for tumour development (sections 1.4.3-1.4.7).

1.4.1 Tumour suppressor genes

A tumour suppressor gene encodes for a protein which guards the cell against DNA damage. Tumour suppressor genes have a variety of functions such as monitoring critical checkpoints at the G1 or G2 phase in the cell cycle, initiating repair, inducing growth arrest or preventing inappropriate signalling for cell growth (Pelengaris and Khan, 2006). It was initially proposed that all tumour suppressor genes were recessive, *i.e.* both alleles required an aberration to lead to loss-of-function of the encoded protein. Knudson's 'two hit' theory, which explored the inheritance of retinoblastoma, supported this and proposed that a child who develops this particular tumour of the retina, inherits one defective *RB1* allele from a parent (germline), followed by a second (somatic), deletion, insertion, nonsense mutation or missense mutation of the remaining functioning *RB1* allele sometime later (Knudson, 1971; Pelengaris and Khan, 2006; Ali *et al.*, 2010).

This hypothesis is based on the understanding that one normal copy and one abnormal copy (heterozygosity of the *RB1* gene) is not adequate for a malignant retinoblastoma tumour to develop. In the absence of a germline mutation in the *RB1* gene, unilateral retinoblastoma can still arise but typically later on in childhood which allows time for the acquisition of separate aberrations of both *RB1* alleles (Cavenee *et al.*, 1983). However, whilst loss of heterozygosity of the *RB1* gene leads to tumourigenesis, this is not true for all tumour suppressor genes.

The *TP53* gene, for example, is the most frequently mutated gene in adult cancers (Hanahan and Weinberg, 2011). It has been shown that missense heterozygous mutations can act in a dominant negative way and still lead to loss of p53 function. Other mechanisms which lead to loss of p53 function include deletion of one or both

of the *TP53* alleles, which are located on the short arm of chromosome 17 (17p13.1) or amplification of *MDM2*, the negative regulator of p53 (Figure 1.6), which leads to excess degradation of the p53 protein (de Vries *et al.*, 2002; Wijnhoven *et al.*, 2007; Carr-Wilkinson *et al.*, 2010).

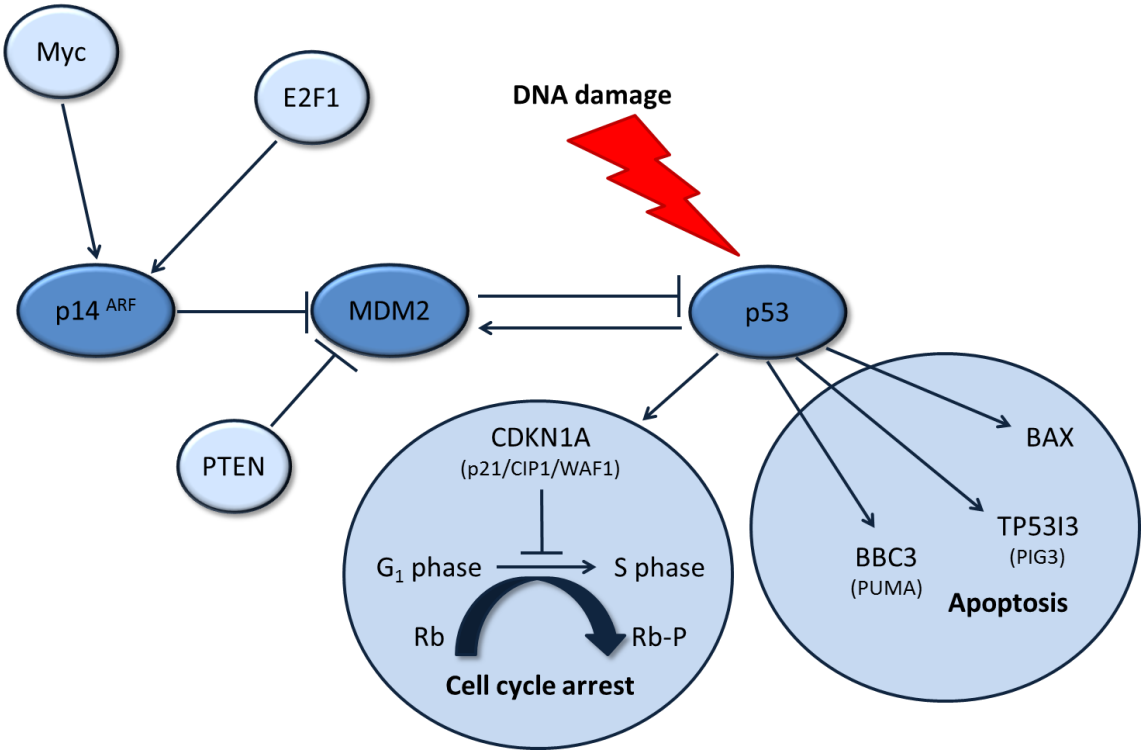

Figure 1.6 Illustrative diagram representing the p53 pathway. p53 responds to DNA damage by activating cell cycle arrest via transcription of *CDKN1A* or apoptosis through transcription of *BAX, TP53I3* and *BBC3*. A feedback loop with *MDM2* regulates p53 with *MDM2* degrading p53. *MDM2* in turn is inhibited by $p14^{ARF}$ along with *PTEN* indirectly and $p14^{ARF}$ responds to *MYC* and *E2F*. Figure adapted from Carr *et al*., 2006.

Since the discovery of the *RB1* gene and the *TP53* gene as tumour suppressor, several other genes important in cancer development have subsequently been characterised as tumour suppressors and examples of these are summarised in Table 1.1.

Gene	Nomenclature	Function	Chromosome location	Associated tumour types
RB1	Retinoblastoma 1	Cell cycle regulator	13q14.2	retinoblastoma, bladder cancer, osteogenic sarcoma
TP53	Tumour protein p53	Induces cell cycle arrest, apoptosis, senescence, DNA repair or changes in metabolism	17p13.1	Variety of human cancers and Li-Fraumeni syndrome
CDKN2A	Cyclin-dependent kinase inhibitor 2A	Cell cycle regulator	9p21	Variety of human cancers
APC	Adenomatous polyposis coli	Antagonist of the Wnt signalling pathway	5q21-q22	Colon cancer
BRCA1	Breast cancer 1	DNA repair	17q21	Breast and ovarian cancer
BRCA2	Breast cancer 2	DNA repair	13q12.3	Breast and ovarian cancer
MSH2	mutS homolog 2	DNA mismatch repair	2p21	Hereditary nonpolyposis colon cancer
MLH1	mutL homolog 1	DNA mismatch repair	3p21.3	Hereditary nonpolyposis colon cancer
VHL	von Hippel-Lindau	Transcription elongation	3p25.3	Renal cancer, haemangioblastoma, pheochromoctoma
PTCH1	Patched 1	Development and differentiation	9q22.3	Medulloblastoma, basal cell carcinoma and Gorlin sydrome
PTEN	Phosphatase and tensin homolog	Signalling	10q23.3	Variety of human cancers
WT1	Wilms' tumour 1	Transcription regulator	11p13	Wilms' tumour
NF1	Neurofibromin 1	Ras inactivation	17q11.2	Neurofibromas, sarcomas, gliomas and Neurofibromatosis type 1
NF2	Neurofibromin 2	Cytoskeleton	22q12.2	Schwannomas, astrocytomas, meningiomas and Neurofibromatosis type II

Table 1.1 Examples of commonly occurring tumour suppressor genes genetically down-regulated in many types of cancer. Genes are shown alongside their current nomenclature with a summary of their function, chromosomal location and associated tumour types. Table adapted from Pelengaris and Khan (2006).

1.4.2 Oncogenes

Oncogenes are cancer causing genes which, when functioning normally are a class of genes known as proto-oncogenes. Proto-oncogenes are typically growth factors, transcription factors, signal transducers or receptors and are responsible for cellular mechanisms such as growth, division or survival. Their abnormal activation via aberrations such as mutations, amplifications and chromosomal rearrangements, alongside the accumulation of other defects such as loss of a tumour suppressor can lead to tumour maintenance or tumourigenesis. Several examples of oncogenes alongside their associated tumour types are highlighted in Table 1.2. Two key instances of aberrant proto-oncogene activation are discussed below; the chromosomal rearrangement creating the fusion gene *BCR-ABL*, and point mutations, amplifications and overexpression of the *MYC* gene family; *MYC*, *MYCN* and *MYCL* (Vita and Henriksson, 2006).

The BCR-ABL fusion protein, encoded for by the fusion gene *BCR-ABL* is cancer causing in certain types of leukaemia. It was first discovered in 1960 (Nowell and Hungerford, 1960) in the karyotypes of patients with chronic myeloid leukaemia (CML) and is created from the reciprocal translocation of chromosomal material between chromosome 9 and 22; t(9;22)(q34;911). Whilst the normal function of *BCR* is not known, *ABL1* is a classic proto-oncogene encoding a tyrosine kinase implicated in cellular processes such as division and differentiation. The fusion gene *BCR-ABL* leads to constitutive activation of the *ABL1* proto-oncogene and a cancer causing phenotype (Druker *et al.*, 2001).

MYC protein is a transcription factor involved in a variety of regulatory processes in the cell such as cell cycle progression, differentiation, growth, cell motility and proliferation (Figure 1.7). Normally the expression of *MYC* is tightly regulated with high levels of expression when a cell enters the cell cycle and low levels of expression when a cell is quiescent. The *MYC* gene family are widely activated in a variety of adult and childhood cancers via several mechanisms. For example, in haematological malignancies such as Burkitt's lymphoma or diffuse large cell lymphoma *MYC* translocations and overexpression are the activating mechanisms, whereas in solid tumours such as neuroblastoma and medulloblastoma amplifications of *MYC* and *MYCN,* are observed (Vita and Henriksson, 2006; Bretones *et al.*, 2014).

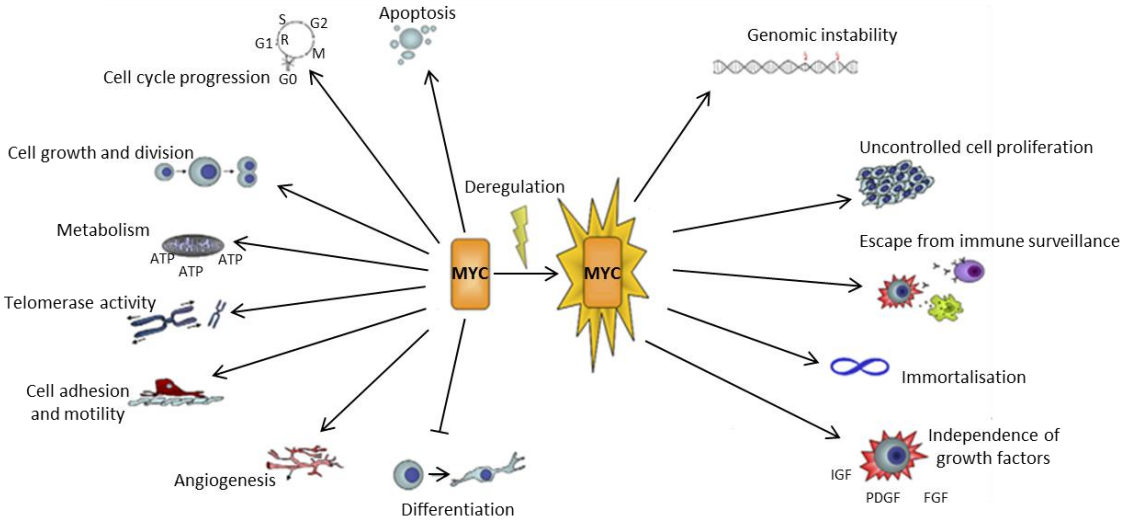

Figure 1.7 The cellular processes controlled by MYC during normal conditions and tumourigenesis. Left; normal cell processes that MYC regulates, right; deregulation of MYC leads to multiple tumorigenic processes such as genomic instability, uncontrolled cell proliferation, escape from immune surveillance, immortalisation and independence from growth factors. Figure taken from Vita and Henriksson, 2006.

Gene	Nomenclature	Function	Chromosome location	Associated tumour types
ABL1	ABL proto-oncogene 1, non-receptor tyrosine kinase	Cell division, adhesion, differentiation, and response to stress	9q34.1	Chronic myeloid leukaemia
VAV1	Vav 1 guanine nucleotide exchange factor	T-cell and B-cell development and activation	19p13.2	Haematological malignancies
NRAS	Neuroblastoma RAS viral oncogene homolog	GTPase activity	1p13.2	Rectal cancer, follicular thyroid cancer and autoimmune lymphoproliferative syndrome
BRAF	B-Raf proto-oncogene, serine/threonine kinase	Cell division, differentiation, and secretion	7q34	Non-Hodgkin lymphoma, colorectal cancer, malignant melanoma and thyroid carcinoma
EGFR	Epidermal growth factor receptor	Transmembrane glycoprotein, member of the protein kinase superfamily	7p12	Lung cancer
ERBB2	V-erb-b2 avian erythroblastic leukaemia	Epidermal growth factor receptor family of receptor tyrosine kinases	17q12	Breast and ovarian tumours
RUNX1	Runt-related transcription factor 1	Transcription factor involved normal haematopoiesis	21q22.3	Leukaemia
MYCN	V-myc avian myelocytomatosis viral	Transcription factor involved in brain development	2p24.3	Neuroblastoma and medulloblastoma
MDM2	MDM2 proto-oncogene, E3 ubiquitin protein ligase	p53-binding protein	12q14.3-q15	Sarcomas
MYC	V-myc avian myelocytomatosis viral	Cell cycle progression, apoptosis and cellular transformation	8q24.21	Haematopoietic tumours, leukaemias and lymphomas
MET	MET proto-oncogene, receptor tyrosine kinase	Hepatocyte growth factor receptor	7q31	Papillary renal carcinoma
CCND1	Cyclin D1	Cell cycle progression	11q13	Breast cancer, squamous cell carcinoma of the head and neck and bladder cancer
CDK4	Cyclin-dependent kinase 4	Cell cycle G1 phase progression	12q14	Multiple cancers including sarcomas

Table 1.2 Examples of commonly occurring oncogenes up-regulated in many types of cancer. Genes are shown alongside their current nomenclature with a summary of their function, chromosomal location and associated tumour types. Table adapted from Pelengaris and Khan (2006).

1.4.3 The genetic model for tumourigenesis

In 1990 Fearon and Vogelstein proposed a genetic model for the tumourigenesis of colorectal cancer (Fearon and Vogelstein, 1990). Here they hypothesised that the sequential accumulation of aberrations such as activation of oncogenes (section 1.4.2) and loss of tumour suppressor genes (section 1.4.1) led to benign tumours, in this instance adenomas, developing into carcinomas. These events in turn led to a survival advantage with the aberration(s) enabling the cancer cell to multiply; a process known as clonal expansion (Figure 1.8). They also proposed that it was not the order but the accumulation of events that was important, with up to seven events required by a cancer cell for tumourigenesis to occur (Knudson, 1971; Fearon and Vogelstein, 1990; Pelengaris and Khan, 2006).

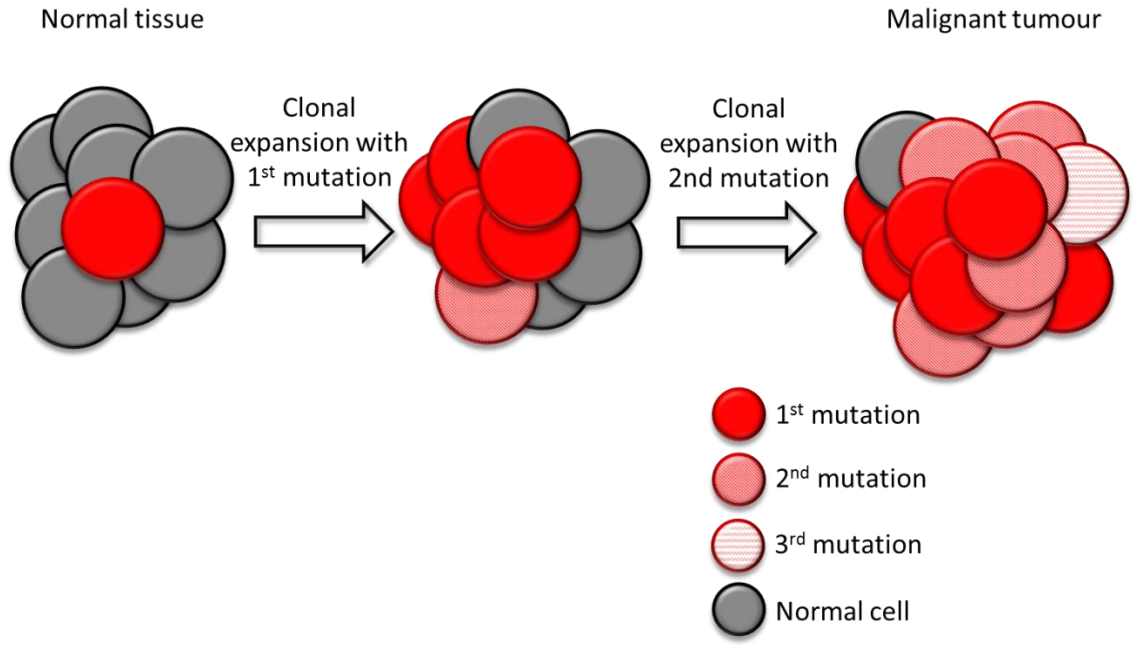

Figure 1.8 Illustrative example of mutation accumulation in tumourigenesis. The 1st mutation acquired expands clonally before a 2nd and 3rd mutation are acquired. Each clone, in turn, expands the population of cells with that specific aberration and provides heterogeneity within the arising malignant tumour.

This model of genetic accumulation is also observed in many other tumours such as breast cancer, ependymoma and leukaemia. In addition it is now recognised that aberrations within DNA repair mechanisms can accelerate this process of accumulation

with distinct repair pathways disrupted in specific tumour types. For example, homologous recombination genes are disrupted in breast and ovarian cancer, colon cancer exhibits aberrations in DNA mismatch repair and homologous recombination pathways, whereas prostate cancer displays aberrations in both homologous recombination and nucleotide-excision repair mechanism (Shackney *et al.*, 1996; Milde *et al.*, 2009; Dietlein *et al.*, 2014; Esposito and So, 2014).

1.4.4 The cancer stem cell model of tumour development and maintenance

The cancer stem cell (CSC) model is a hierarchical model proposed for tumour development whereby a small population of CSCs possesses the ability to populate and propagate the tumour (Figure 1.10). This is in contrast to the non-hierarchical clonal evolution model where genetic features are accumulated within clones of cancer cells (Figure 1.8). These two models are not mutually exclusive, and both models can account for tumour development, maintenance and importantly the molecular heterogeneity frequently observed in multiple cancer types as illustrated below in Figure 1.9 and Figure 1.10 (Hanahan and Weinberg, 2011; Visvader and Lindeman, 2012).

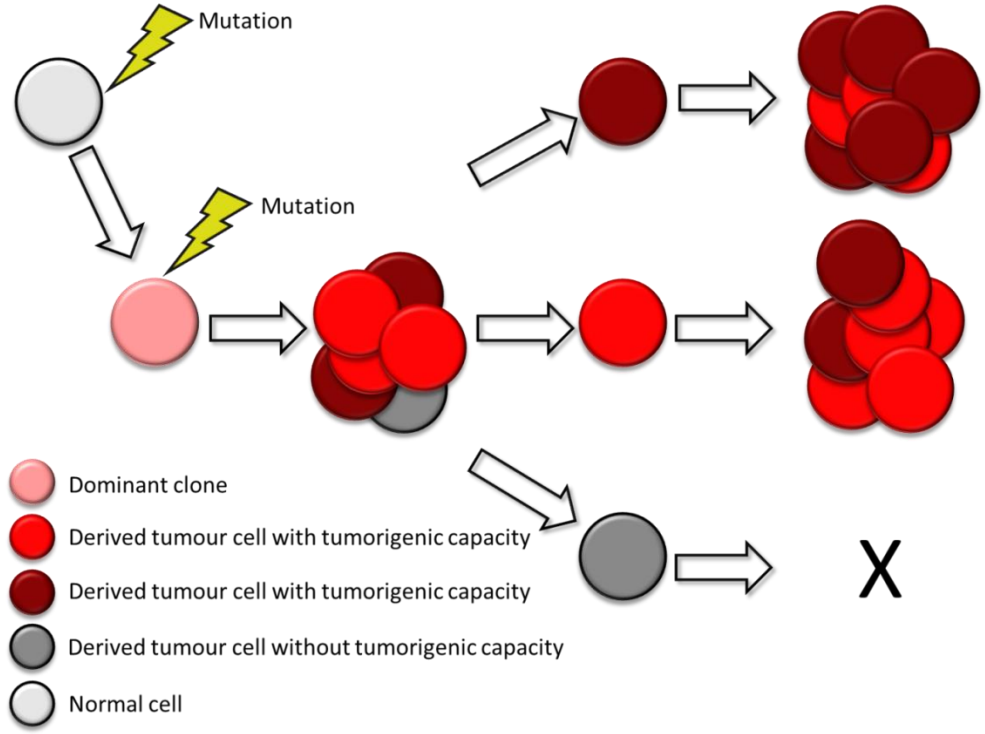

Figure 1.9 Illustrative example of the clonal evolution model. Tumour cells arise from the dominant clone, generate other tumour cells, some with and some without tumorigenic capacity. Figure adapted from Visvader and Lindeman, 2012.

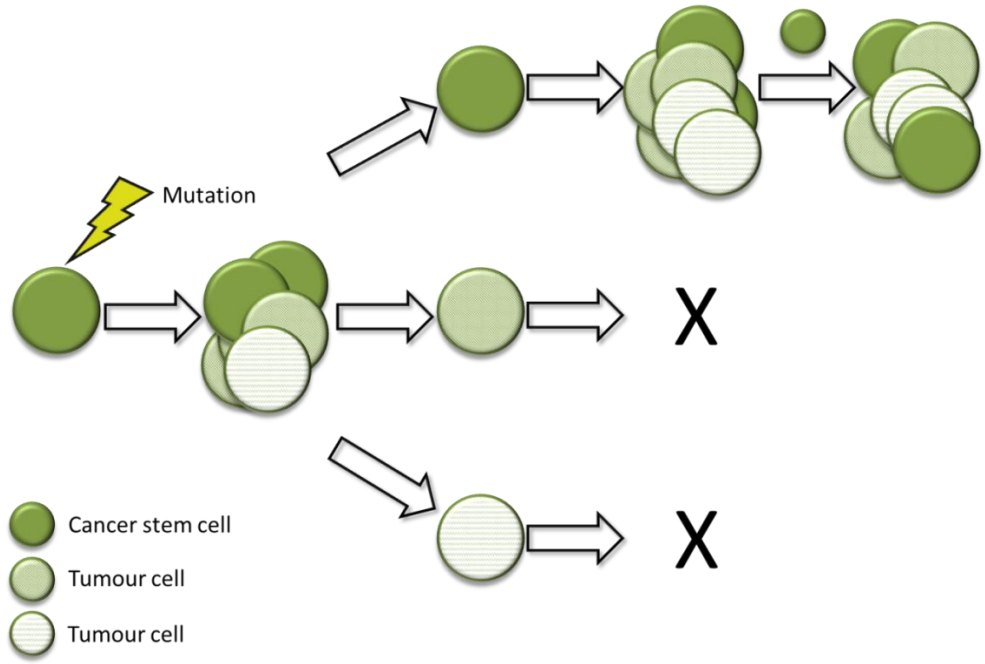

Figure 1.10 Illustrative example of the cancer stem cell model. Small subsets of cancer stem cells sustain tumourigenesis whereas all other tumour cells do not have this ability. The CSC continues to maintain the malignant tumour as it grows and develop. Figure adapted from Visvader and Lindeman, 2012.

CSCs do not necessarily originate from normal stem cells but do have properties such as self-renewal and multi-potency. They have been attributed to treatment resistance and populating recurrences and theoretically must be eradicated to achieve cure. Not all cells within the tumour have these abilities, or the need to be destroyed but the theory implies that all cells within the malignancy have been derived from a CSC as illustrated in Figure 1.10 (Nguyen *et al.*, 2012; Visvader and Lindeman, 2012).

The concept of CSCs has been postulated for several decades with the first notable publications in the 1960s where, for example, genetic evidence of the clonal progression of CML was reported (Levan *et al.*, 1963) and the clonal origin of tumours was first demonstrated *in vivo* (Kleinsmith and Pierce, 1964). As momentum has grown in this field there are now multiple theories emerging as to how CSCs propagate tumours and convey heterogeneity, such as a single subset of CSCs populating a tumour (Figure 1.10), multiple subsets of populating CSCs, dormant CSCs which lead to recurrence over a period of time, evolution of a novel CSC leading to a dominant CSC clone and tumour progression and finally CSCs which have an unstable phenotype resulting in phenotypic reversion (Visvader and Lindeman, 2012).

Clinically, CSCs offer an attractive therapeutic option. Various approaches have been attempted, such as targeting the critical pathways for CSC maintenance or the use of monoclonal antibodies towards CSC surface markers. The CSC niche, the tumour microenvironment which interacts bi-directionally with the CSCs, has also provided a target in certain tumours, for example in glioblastoma (GBM), a highly malignant brain tumour for which there is currently no curative therapy (Gilbertson and Rich, 2007). However the clinical utility of the CSC concept has yet to be proven with most pre-clinical models that demonstrate a response requiring both CSC focused therapy and adjuvant chemotherapy (Visvader and Lindeman, 2012). Further work is required to evaluate the importance of CSCs in particular in tumour resistance, progression and disease recurrence.

1.4.5 Epigenetics and cancer

Epigenetics is the study of heritable changes in gene expression or cellular phenotype which do not correspond with a change in the DNA nucleotide sequences. The interaction of epigenetic mechanisms, such as DNA methylation, chromatin remodelling and histone modification, can regulate gene expression. As demonstrated in Figure 1.11, an epigenetically silenced gene will display DNA methylation upstream of the promoter region and the promoter CpG island will be occupied by the Polycomb complex which mediates chromatin modulation. Transcriptionally inactive genes have compressed DNA with extensive methylation downstream, compacted nucleosomes and repressive histone modifiers such as the trimethylation of lysine 27 residue on histone 3 (Baylin and Jones, 2011).

Transcriptionally active genes (Figure 1.11) display the active histone modification of trimethylation on lysine residue 4, histone 3 (H3K4me3), alongside acetylation of key lysine residues in histone 3 and histone 4. Transcriptional elongation is facilitated by the variant histone H2A.Z, and trimethylation of histone 3, lysine residue 36 (H3K36me3). The transcriptional start site (TSS) has an open configuration with distal enhancers such as H3K4me1 (Baylin and Jones, 2011).

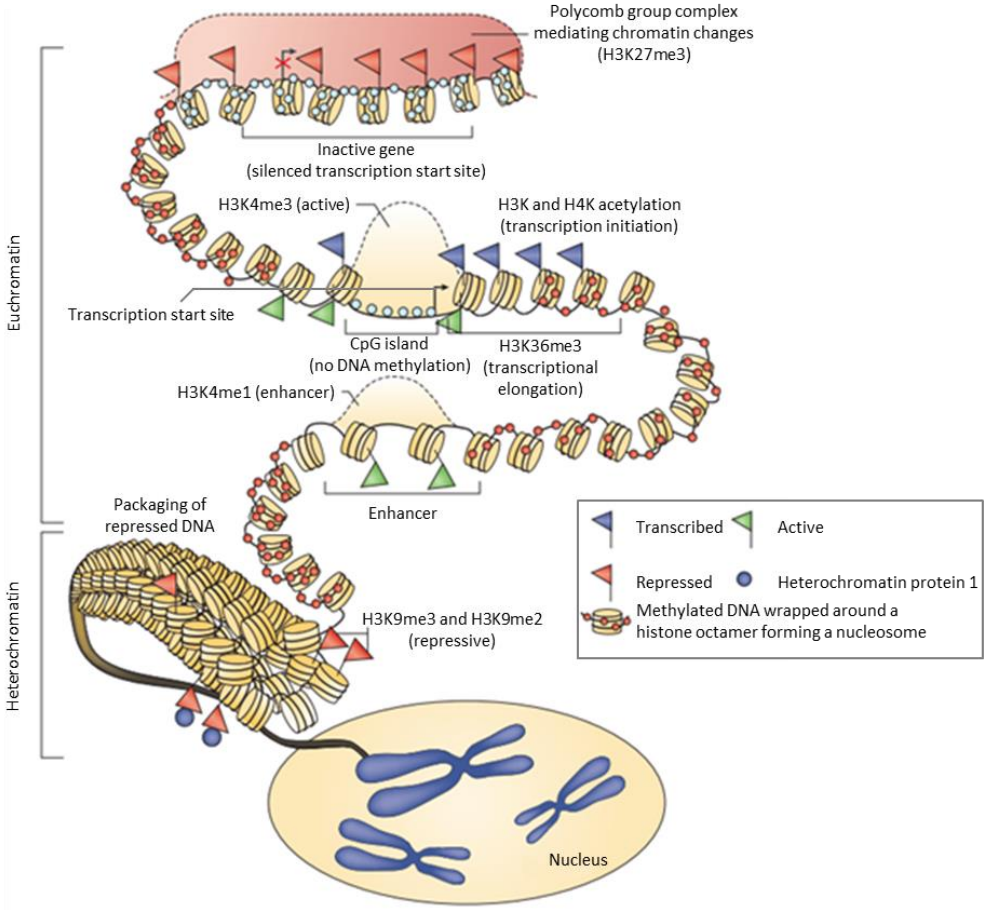

Figure 1.11 The normal human epigenome. Both a silenced gene with repressive histone marks (H3K27me3) at the transcription start site and a transcribed gene are demonstrated. DNA hypomethylation at the promoter CpG island followed by downstream acetylation of H3K/H4K to aide in transcription initiation, H3K36me3 for transcriptional elongation and the signature histone modification for enhancers H3K4me1, are present for transcription. The packaging and folding of repressed methylated DNA, (H3K9me3 and H3K9me2), into chromosomes located to the nucleus is also shown. Figure adapted from Baylin and Jones, 2011.

1.4.6 The cancer epigenome

Since the early 1980s there has been a growing body of evidence demonstrating that epigenetic and genetic mechanisms co-occur in the development of cancer (Feinberg and Tycko, 2004; Jones and Baylin, 2007). There are currently four epigenetic mechanisms which can lead to alterations in gene expression (Figure 1.12) and may therefore play a role in cancer development. These are summarised in sections 1.4.6.1-1.4.6.3 and comprise of DNA methylation, microRNAs (miRNAs) and their connection to the up-regulation of DNA methyltransferase (DNMT) and hypermethylation of gene

promoters, histone modifications (methylation and acetylation) and chromatin remodelling (Hadnagy *et al.*, 2008; Baylin and Jones, 2011).

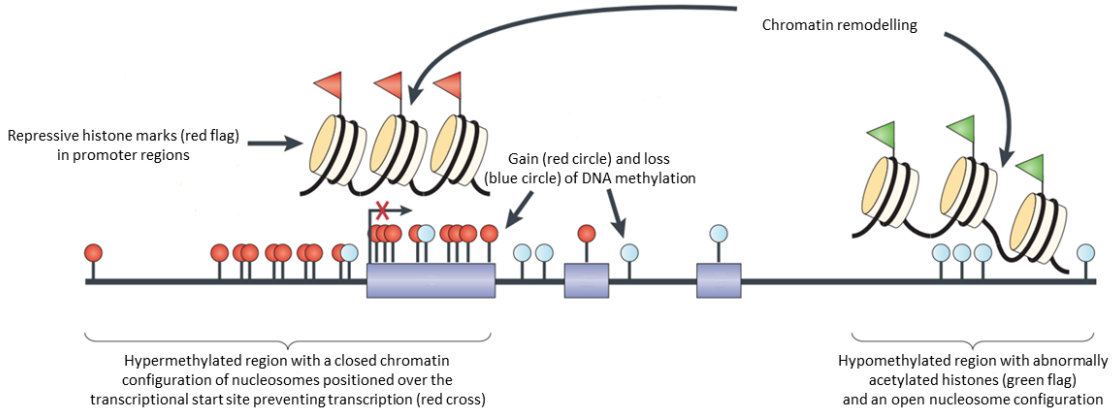

Figure 1.12 The cancer epigenome. Diagram demonstrating the epigenetic mechanisms associated with tumour development and maintenance. Figure adapted from Baylin and Jones, 2011.

1.4.6.1 DNA methylation

1.4.6.1.1 DNA methylation in normal development

CpG sites are symmetrical linear dinucleotides, which, through evolution, have been progressively lost due to the ability of the methylated cytosine (C) to deaminate and become thymine (T). CpG residues which have escaped depletion are thought to play an important role in normal development and gene expression (Issa, 2004). CpG islands are GC rich regions of DNA which contain a relatively high proportion of CpG sites. Approximately 60% of all genes have CpG islands associated with their promoter region which are typically unmethylated. Importantly however, a small number of CpG islands do become normally methylated, for example in X-linked or imprinted genes. When this occurs the methylated DNA is wrapped around histones and compacted into nucleosomes, which also harbour repressive histone marks and deacetylated histones. This focally establishes the chromatin as inactive and subsequently silences the gene as shown in Figure 1.11 (Bird, 2002).

It is not fully understood how DNA methylation patterns are established. The enzyme family of DNMTs can transfer methyl groups onto DNA. Cooperation between different

members of this family of enzymes (*e.g. DNMT1, DNMT3A* and *DNMT3B*) facilitates and maintains the tissue-specific normal DNA methylation patterns. *DNMT1* is the main member of the family responsible for the maintenance of DNA methylation and is assisted by *DNMT3A* and *DNMT3B*. Conversely there are also enzyme systems important in development which remove methyl groups from DNA such as the ten-eleven translocation (TET) family of proteins (Baylin and Jones, 2011; Gros *et al.*, 2012).

1.4.6.1.2 Aberrant promoter region DNA methylation

DNA methylation is critical to explaining the epigenome of cancer and is thus far the most widely studied epigenetic mechanism in this field. Methylation imbalances are frequently observed in cancer cells, such as aberrant hypermethylation at promoter associated CpG islands (Figure 1.12) leading to gene silencing, as well as more widespread hypomethylation outside of these regions (Costello and Plass, 2001; Sidransky, 2002; Dedeurwaerder *et al.*, 2011). Recent advances have enabled the characterisation of hundreds of genes within a variety of cancers which display promoter region hypermethylation. Examples include *CDKN2A* which displays promoter hypermethylation in several cancers and encodes the tumour suppressor $p14^{ARF}$, as well as the tumour suppressor gene Von Hippel-Lindau (*VHL*), which is silenced in renal cancer, and *RASSF1A* which is epigenetically silenced in medulloblastoma (Table 1.3). These high frequency events however, are rare and some of the most commonly reported examples are shown in Table 1.3. The relevance of other, low frequency, hypermethylation events observed in cancer is not fully understood. It is possible that these rarer epigenetic events cluster in the same signaling pathways, or complement genetic events such as mutations to create the cancer phenotype (Lindsey *et al.*, 2005; Baylin and Jones, 2011; Levesley *et al.*, 2011).

Gene	Nomenclature	Function	Chromosome location	Associated tumour types
CDKN2A	Cyclin-dependent kinase inhibitor 2A	DNA mismatch repair	9p21	Wide variety of tumours including colon, gastric and endometrial tumours
THBS1	Thrombospondin 1	Mediates cello-to-cell and cell-to-matrix interactions	15q15	Gliomas
VHL	von Hippel-Lindau tumour suppressor, E3 ubiquitin	Ubiquitin ligase component	3p25.3	Renal tumours and haemangioblastomas
RASSF1A	Ras association domain family member 1	DNA repair	3p21.3	Variety of cancer types
BRCA1	Breast cancer 1	DNA repair	17q21	Breast and ovarian cancer
RB1	Retinoblastoma 1	Cell cycle regulator	13q14.2	retinoblastoma, bladder cancer, osteogenic sarcoma
APC	Adenomatous polyposis coli	Antagonist of the Wnt signalling pathway	5q21-q22	Colon cancer
SFRP1	Secreted frizzled-related protein 1	Activation of Wnt signalling	8p11.21	Colon cancer
HOXA9	Homeobox A9	Regulates gene expression, morphogenesis and differentiation	7p15.2	Leukaemia and neuroblastoma
CDH1	Cadherin 1, type 1, E-cadherin	Cell adhesion	16q22.1	Gastric, breast colorectal, thyroid and ovarian cancer
CDH13	Cadherin 13	Cell adhesion	16q.23.3	Many tumour types including breast and lung cancer
SOCS1	Suppressor of cytokine signalling 1	Inhibitor of JAK-STAT pathway	16p.13.13	Liver cancer and myeloma
SOCS3	suppressor of cytokine signalling 3	Inhibitor of JAK-STAT pathway	17q25.3	Lung cancer

Table 1.3 Examples of genes silenced by CpG island hypermethylation in many types of cancer. Genes are shown alongside their current nomenclature with a summary of their function, chromosomal location and associated tumour types. Table adapted from Pelengaris and Khan (2006).

1.4.6.1.3 Global methylation patterns and sub-classification of tumours

Increasingly, global DNA methylation patterns in cancer are being used to sub-stratify tumours which historically have been thought of as one disease. Examples include medulloblastoma (Hovestadt *et al.*, 2013; Schwalbe *et al.*, 2013b), GBM (Sturm *et al.*, 2012) and chronic lymphocytic leukemia (Kulis *et al.*, 2012). Importantly these derived subgroups correlate with clinicopathological variables, molecular features and prognosis. It is postulated that these global methylation patterns witnessed are biologically relevant and relate to the epigenetic imprint of the cancer cell of origin (Kulis *et al.*, 2012).

1.4.6.1.4 DNA hypermethylation and disruption of microRNAs

miRNAs are defined as short, non-coding RNAs which function by targeting the coding messenger RNA (mRNA) to fine-tune or regulate gene expression. There is increasing evidence to suggest that miRNAs are both effectors and targets in aberrant DNA hypermethylation observed in cancer. For example, promoter hypermethylation which leads to pathway disruption can repress the transcription of miRNAs and subsequently up-regulate the oncogenic targets of these microRNAs which, in turn, promotes tumour progression (Baylin and Jones, 2011). Studies have also shown that enforced expression of the miRNA-29 family demonstrates indirect and direct interactions with the DNA methyltransferases *DNMT1, DNMT3A* and *DNMT3B* (section 1.4.6.1.1), which lowers their expression and leads to a reduction in global DNA methylation. This subsequently fosters the re-expression of important tumour suppressor genes in both lung cancer and AML models supporting the role of miRNA-29 suppression in tumourigenesis and its therapeutic utility (Fabbri *et al.*, 2007; Garzon *et al.*, 2009).

1.4.6.2 Histones

1.4.6.2.1 Normal function and modification of histones

Histones are the major protein component of chromatin and are responsible for packaging and organising DNA. There are two classes of histones; core histones (H2A, H2B, H3 and H4), which share a similar structure of terminal tails and a central fold domain, and linker histones (H1 and H5). DNA is wrapped around the octameric histone unit which consists of eight core histones (two of H2A, H2B, H3 and H4) to form a nucleosome. The linker histone H1 binds the DNA in place and the nucleosomes are further wound into efficiently packed chromosomes. Post translational modifications of histones leads to alterations in the chromatin conformation, and thus form another epigenetic mechanism to regulate gene expression (Hadnagy *et al.*, 2008; Baylin and Jones, 2011).

Normal enhancing modifications of histones, such as trimethylation of lysine 4 of the core histone H3, (H3K4me3), flank nucleosome depleted regions of the DNA making these regions more amenable to transcription. Trimethylation of lysine 36, (H3K36me3), facilitates transcriptional elongation whereas destabilisation of the nucleosome structure due to acetylation of H3 and H4 enhances transcription initiation. Repressive modifications also occur, for example, methylation at the lysine 9 residue of H3, (H3K9me2 and H3K9me3, Figure 1.11). Histone methyltransferases and demethylases can remove lysine methylation marks on histones. Similarly histone acetyltransferases and deacetylases, acetylate and deacetylate histones, respectively. A summary of the key histone modifications witnessed in the normal epigenetic regulation of gene transcription and expression are displayed in Table 1.4 (Hadnagy *et al.*, 2008; Baylin and Jones, 2011).

Histone	Class	Lysine	Modification	Role in transcription	Nomenclature
3	Core	4	methylation	Enhancement	H3K4me1
		4	Trimethylation	Enhancement	H3K4me3
		36	Trimethylation	Elongation	H3K36me3
3	Core		Acetylation	Enhancement	
4	Core		Acetylation	Enhancement	
3	Core	9	Dimethyltion	Repression	H3K9me2
		9	Trimethylation	Repression	H3K9me3
		27	Trimethylation	Repression	H3K27me3

Table 1.4 Summary of the major histone modifications observed in the epigenetic regulation of gene expression. K, lysine; me, methylation.

1.4.6.2.2 Abnormal histone modifications in cancer

The role of aberrant histone modifications in cancer is less well understood. Recent advances support the importance of these aberrations as an epigenetic mechanism in tumourigenesis (Figure 1.12). Abnormal gains of repressive histone marks or loss of enhancing ones can occur through a variety of ways including rearrangement or mutations of genes which undertake these histone modifications (section 1.4.7). For example, H3K27me3, which is critical in the normal balance of gene activity, is frequently deregulated in several types of cancer including B-cell lymphoma, ovarian cancer, breast cancer and paediatric high grade gliomas (Martinez-Garcia and Licht, 2010; Greer and Shi, 2012; Bender *et al.*, 2013). Similarly, abnormal acetylation of histones 3 and 4 are observed in many tumour types such as oesophageal cancer, breast cancer and lymphoma (Piekarz *et al.*, 2004; Chen *et al.*, 2011; Huang *et al.*, 2011).

1.4.6.3 Chromatin

1.4.6.3.1 Normal chromatin architecture

Chromatin consists of DNA and proteins (histones) which combine to strengthen and package DNA. As already eluded to, the conformation of chromatin, either closed or open, is another epigenetic mechanism which can regulate the expression of genes. The structure of chromatin will vary normally depending on the phase of the cell cycle and DNA access required, with a tightly packed, condensed conformation (heterochromatin) during metaphase and an open structure (euchromatin) during interphase to allow transcriptional machinery access (Figure 1.11).

1.4.6.3.2 Chromatin remodeling and cancer

Abnormal chromatin architecture can play a vital role in cancer (Figure 1.12). One highly studied example is the switch/sucrose non fermentable (SWI/SNF) chromatin remodeling complex, a tumour suppressor which disrupts histone-DNA interactions in an adenosine triphosphate (ATP)-dependent fashion. The SWI/SNF complex regulates transcription and comprises of 11-15 proteins. Mutations and deletions of the genes encoding these proteins, for example *SMARCB1* and *SMARCA4,* are observed in many types of cancer such as the rare childhood brain tumour, atypical teratoid/rhabdoid tumour (ATRT). In ATRTs, greater than 90% of tumours demonstrate inactivation of *SMARCB1*, and more recent reports also identify *SMARCA4* mutations in a small subset of cases (Banine *et al.*, 2005; Hasselblatt *et al.*, 2011; Tolstorukov *et al.*, 2013).

1.4.7 Genetics meets epigenetics

There is no one unified model for the development of cancer. There is evidence to support the genetic model for tumourigenesis with mutation accumulation (section 1.4.3) and the non-hierarchical clonal evolution model as well as reports supporting the hierarchical system of cancer stem cells (section 1.4.4). Similarly cancer is not uniquely a genetic disease, and epigenetic mechanisms are increasingly implicated in tumour development and maintenance. For example, many tumour suppressor genes are both genetically and epigenetically silenced (*e.g. APC*, *RB1* and *CDKN2A,* Table 1.1 and Table 1.3). Moreover, as described in section 1.4.6.3.2, the genetic inactivation of SMARCB1 due to mutation or deletion of the *SMARCB1* gene is an example of a genetic aberration disrupting an epigenetic mechanism. It is now well recognised that there are a high number of aberrations in many cancers of genes which encode proteins associated with epigenetic mechanisms (Plass *et al.*, 2013).

Examples of this cross-over of mechanisms are found in mixed-lineage leukemia (MLL) rearranged leukemia, where histone methyltransferase no longer functions normally due to chromosomal translocations. The resultant fusion proteins lead to both abnormal histone acetylation and methylation (Slany, 2009). Another example is the highly malignant paediatric brain tumour, GBM, whose epigenome is rapidly being elucidated. This tumour has epigenetic subgroups (section 1.4.6.1.3) which are biologically distinct. Two of these subgroups are defined by mutations in the H3 histone, family 3A (*H3F3A*) which affect critical amino acids, lysine 27 (K27) and glycine

34 (G34), of the core histone. Further work has demonstrated that in the K27 mutant subgroup, reduced methylation in the repressive histone mark H3K27me3 alone, or in combination with global DNA hypomethylation, are major epigenetic processes allowing the aberrant upregulation of genes witnessed in this subgroup (Sturm *et al.*, 2012; Bender *et al.*, 2013).

Finally, combined epigenetic and genetic aberrations are observed in the disruption of *TERT*, a catalytic subunit of telomerase which lengthens telomeres, allowing cancer cells to evade apoptosis and become immortal (section 1.3.4). Recent studies in several tumour types have demonstrated that hypermethylation upstream of the TSS of *TERT* can lead to increased expression of the gene, as oppose to the epigenetic gene silencing following promoter hypermethylation described in section 1.4.6.1.2. This finding is particularly true in high grade tumours, as in comparison low grade tumours and normal tissue display unmethylated CpG sites upstream of the TSS. Importantly, expression of *TERT* in normal tissue is not associated with hypermethylation, and tumours that evolve from low grade to high grade (*e.g.* low to high grade gliomas (HGG)), show increasing levels of methylation upstream of the TSS with a corresponding rise in *TERT* expression (Castelo-Branco *et al.*, 2013; Lindsey *et al.*, 2014).

Somatic mutations of the *TERT* promoter, also leading to elevated expression are frequently found in cancer (Killela *et al.*, 2013; Koelsche *et al.*, 2013; Remke *et al.*, 2013). Moreover, a recent study in medulloblastoma shows that these hotspot mutations are mutually exclusive to *TERT* promoter hypermethylation, and together are prognostically significant, providing insight into how epigenomic and genomic events complement each other to derive the cancer phenotype (Lindsey *et al.*, 2014). All these examples underpin the importance of understanding both the genome and epigenome within the context of the cancer phenotype. Moreover, there are exciting therapeutic agents being developed in this field, such as histone deacetylase inhibitors (HDAC, section 1.5.1.3), which offer potential novel treatment opportunities (Baylin and Jones, 2011; Plass *et al.*, 2013).

1.5 Therapeutic targeting in cancer

Understanding the hallmarks of cancer (section 1.3) along with the genetic and epigenetic aberrations (section 1.4) that contribute to these processes has created the opportunity to therapeutically target these mechanisms and aberrations. Examples of these targeted therapies are shown in Figure 1.13 and some key agents are discussed in section 1.5.1 and 1.5.2.

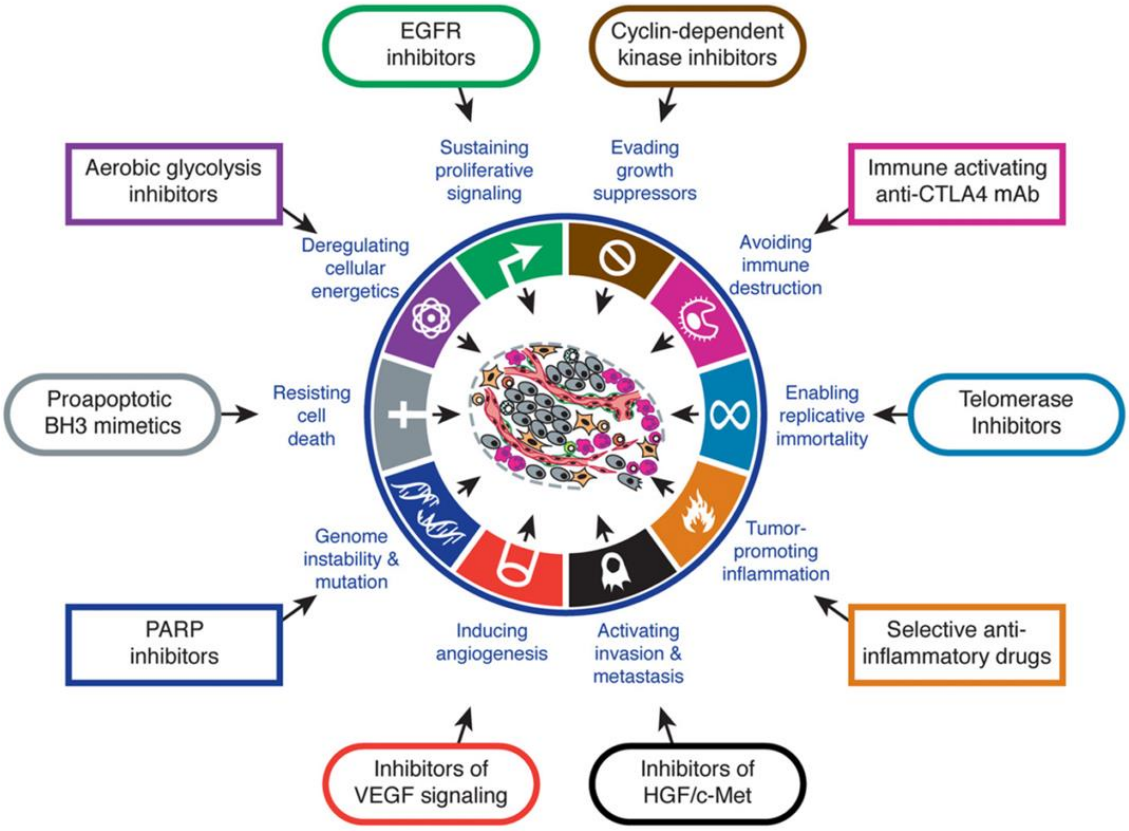

Figure 1.13 Schematic illustrating the therapeutic targeting of the hallmarks of cancer. Figure taken from Hanahan and Weinberg, 2011.

1.5.1 Reactivation of tumour suppressor genes

As already described in section 1.4.1, loss-of-function in tumour suppressor genes plays a key role in cancer development. Therapeutic agents now exist which reactivate these genes. Examples include nutlins which reactivate *TP53*, or DNMT inhibitors and HDAC inhibitors, both of which can lead to the reactivation of epigenetically silenced tumour suppressor genes.

1.5.1.1 Nutlins

Targeting the interaction between *MDM2* and p53 to stimulate the tumour suppressor activity of p53 is an attractive therapeutic option (Chene, 2003). Nutlins 1, 2 and 3 are analogs of cis-imidazole and competitively block the p53-*MDM2* interaction (Figure 1.6) by selectively binding to the p53-binding domain of *MDM2*. This group of agents have been show to display anti-tumorigenic activity *in vitro* and *in vivo* for a variety of paediatric tumours including medulloblastoma (Kunkele *et al.*, 2012; Carol *et al.*, 2013; Van Maerken *et al.*, 2013) and first in man studies of the nutlin compound RG7112, in adult cancers such as AML and liposarcoma, have also shown promise (Ray-Coquard *et al.*, 2012).

1.5.1.2 DNA methyltransferase inhibitors

As already described, hypermethylation in the promoter region of tumour suppressor genes can lead to gene silencing (Table 1.3). The enzyme family of DNMTs are responsible for transferring methyl groups onto DNA (section 1.4.6). Inhibition of DNMT utilising either nucleoside on non-nucleoside analogues, can target aberrant DNA hypermethylation in cancer. Nucleoside inhibitors are incorporated into the DNA before they can inhibit DNMT whereas non-nucleoside inhibitors do not require DNA incorporation and can block the action DNMT directly. This, in turn, interrupts the process of DNA methylation leading to the reactivation of epigenetically silenced genes (Hadnagy *et al.*, 2008).

It has been demonstrated that the strategy of inhibiting DNA methylation via pan-inhibition of DNMT is effective in cancers such as AML, chronic myelomonocytic leukaemia and myelodysplastic syndrome. Approved agents for the treatment of these conditions are the first generation nucleoside inhibitors azacitibine and decitabine. Both these drugs are also in phase II trials for solid tumours such as melanoma, prostate and ovarian cancer. Non-nucleoside analogues such as flavonoids have demonstrated demethylating activity in pre-clinical studies although their utility as an anti-cancer therapy is unclear. More developed agents include the anti-hypertensive hydralazine and the anti-arrhythmic procainamide, both of which have the secondary effect of DNMT inhibition. Several other non-nucleoside inhibitors are under investigation but as yet none of them have enter clinical trials for the treatment of cancer (Gros *et al.*, 2012; Kirschbaum *et al.*, 2014).

1.5.1.3 Histone deacetylase inhibitors

Alterations of histone acetylation are observed in many cancers such as AML, breast and ovarian malignancies (Figure 1.12). Inhibition of histone deacetylase (HDAC) is believed to have several effects; re-expression of epigenetically silence tumour suppressor genes, generation of oxidative stress leading to early chromatid separation, and an ineffective mitotic spindle assembly checkpoint. There are many examples of HDAC inhibitors such as vorinostat, panobinostat and romidepsin. Many of these agents are in phase I-III trials such as vorinostat which is being investigated for the treatment for mesothelioma, AML, myelodysplastic syndrome and T-cell lymphoma (Hadnagy *et al.*, 2008; Witt *et al.*, 2012; Di Costanzo *et al.*, 2014; Kirschbaum *et al.*, 2014).

1.5.2 Targeting oncogenes

The upregulation of oncogenes are critical to the development of cancer. Multiple oncogenes have been identified (Table 1.2) and are now therapeutic targets for the treatment of cancer (section 1.5.2.1-1.5.2.3).

1.5.2.1 Imatinib

Imatinib was first discovered in the late 1990s following a screening program for compounds with the ability to inhibit protein kinases through binding at their ATP site. Pre-clinically, compound CGP 57148 was found to be a potent inhibitor of the ABL proto-oncogene (section 1.4.2 and Table 1.2), whilst not significantly inhibiting the majority of other tyrosine kinases (Druker *et al.*, 1996). This compound was developed into imatinib for use initially in CML, a first of its kind in this class of molecularly targeted drugs to be used in cancer therapy. It was well tolerated in phase I trials and showed significant anti-leukemic effects (Druker *et al.*, 2001).

Imatinib has revolutionised the current treatment of CML and its use has been broadened to include other types of leukemia with the *BCR-ABL* translocation. However, primary and acquired resistance to imatinib does exist, through mechanism such as point mutations within the target fusion gene *BCR-ABL*, or through alternative pathways of disease progression (*e.g.* activation of the *SRC*-kinase family). This has led to the development of other *BCR-ABL* targeted agents, such as dasatinib and nilotinib, which have greater potencies for both non-mutant and mutant *BCR-ABL* when

compared to imatinib. Other inhibitors which target the alternate pathways to resistance, such as *SRC*-kinase family, have also been developed. These include the dual *SRC* and *ABL* kinase inhibitor bosutinib, which has shown efficacy following failure to treat CML with imatinib, dasatinib and nilotinib (Kujawski and Talpaz, 2007; Saglio *et al.*, 2010; Khoury *et al.*, 2012).

1.5.2.2 Aurora A kinase inhibitors

Aurora kinases are mitotic kinases critical for the cellular processes of mitosis and division and were identified in the mid-1990s. There are three homologs, A, B and C, with Aurora A kinase being involved in mechanisms such as mitotic entry, spindle assembly and chromosome alignment during metaphase. Currently there are multiple Aurora kinase inhibitors in various stages of development, some that are pan-inhibitors whereas others specifically inhibit Aurora A, examples of which are listed in Table 1.5 (Kollareddy *et al.*, 2012).

Compound	Selectivity	*In vitro* IC_{50}	Pre-clinical activity	Stage of development
MLN8237	Aurora A	1nM	Solid tumours and leukemias	Phase II
ENMD-2076	Aurora A	14nM	Solid tumours and multiple myeloma	Phase II
MK-5108	Aurora A	0.064nM	Solid tumours	Phase I

IC_{50}, half maximal inhibitory concentration; nM, nanomolar; AML, acute myeloid leukaemia

Table 1.5 Aurora kinase A inhibitors in clinical trials. Table adapted from Kollareddy *et al.,* 2012.

1.5.2.2.1 MLN8237

MLN8237 is a second generation Aurora A inhibitor which has been shown to have *in vitro* efficacy in a variety of paediatric cancers including rhabdomyosaroma, Ewing's sarcoma, GBM, ALL and neuroblastoma. *In vitro* in neuroblastoma (section 1.7.3), Aurora A protein, independent of its kinase activity, binds to MYCN, the protein encoded by *MYCN* (Figure 1.14), stabilises it and prevents proteasomal degradation of the MYCN onco-protein (Otto *et al.*, 2009). The Aurora A kinase inhibitor MLN8237, disrupts the complex formed between Aurora A and MYCN, promoting MYCN degradation leading to prolonged survival and tumour regression *in vivo* (Brockmann *et al.,* 2013).

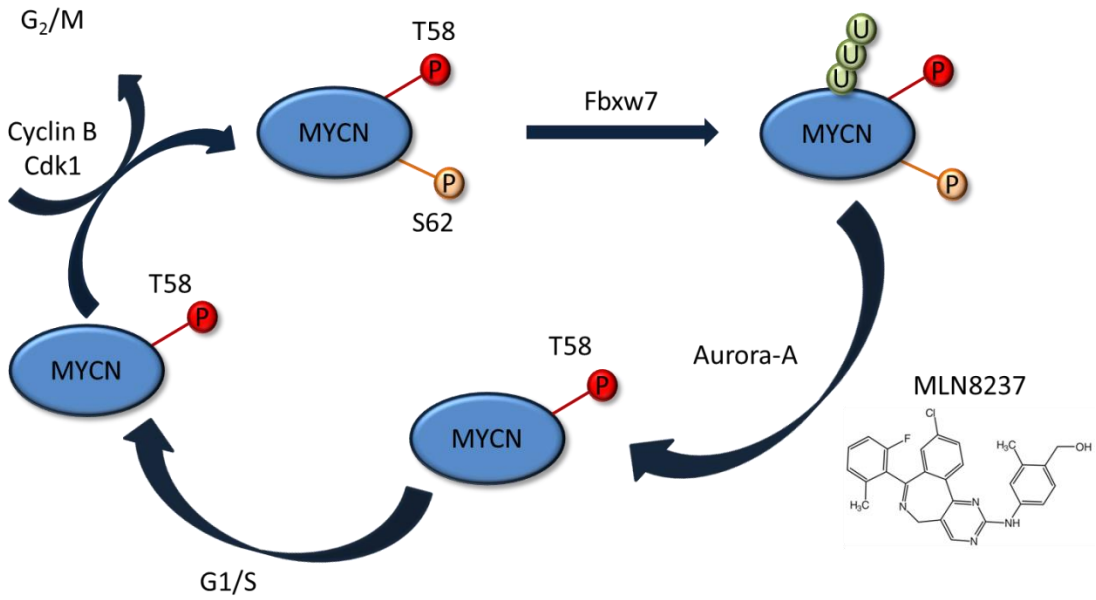

Figure 1.14 Disruption of MYCN degradation by MLN8237 inhibition of Aurora A. The MYCN/Aurora A complex prevents degradation of the MYCN protein by Fbxw7 which normally recognises MYCN in G_2/M when it is doubly phosphorylated (S62 and T58) and mediates the ubiquitination of phosphorylated MYCN. MLN8237 disrupts the MYCN/Aurora A complex, returning the degradation process to normal. U, Ubiquitin; P, phosphate. Figure adapted from Kollareddy *et al.,* 2012 and Brockmann *et al.,* 2013.

1.5.2.3 Bromodomain and extraterminal domain inhibition

The bromodomain and extraterminal domain (BET) family are important in cellular processes such as transcription, cell growth and epigenetic memory. The BET family comprise of four genes; *BRD2*, *BRD3*, *BRD4* and *BRDT*. Inhibition of the BET family has utility in the treatment of many types of haematological malignancies as well as the highly aggressive epithelial cancer NUT midline carcinoma (Puissant *et al.*, 2013; Di Costanzo *et al.*, 2014).

1.5.2.3.1 JQ1

JQ1, a novel thienotriazolo-1,4-diazepine, was the first selective inhibitor of the BET family and works by competitively binding to the lysine pocket of the bromodomain. JQ1 has multiple mechanisms of action, such as disruption of the binding between *MYC* and *BRD4* leading to suppression of the *MYC* oncogene. Recent *in vitro* and *in vivo* work has also identified that JQ1 has efficacy in the treatment of *MYCN* amplified neuroblastoma and leads to downregulation of the expression of the *MYCN* oncogene as well as the *MYC* oncogene. *BRD4* also binds to the promoter region of *MYCN,* and,

similar to *MYC*, inhibition by JQ1 leads to a disruption of this interaction and downregulation of *MYCN*. JQ1 is therefore a novel agent which targets two of the *MYC* gene family of oncogenes and may have utility in the treatment of a variety of *MYC* and *MYCN* driven malignancies (Puissant *et al.*, 2013; Di Costanzo *et al.*, 2014).

1.5.3 The future of targeted therapies

Many of the above mentioned targeted therapies show promise in pre-clinical and early phase trials, and more developed agents such as imatinib, are the standard treatment for *BCR-ABL* positive leukaemia. However, tumour resistance and evolution still occur following targeted treatment, as highlighted by the discussion in section 1.5.2.1, and calls for second line agents, for example in primary and secondary resistance to imatinib. Strategies can, and have, been put in place to overcome mechanisms of tumour resistance, for example the development of dasatinib, nilotinib or bosutinib (section 1.5.2.1). However, it is highly likely that the therapeutic strategies of the future will encompass both targeted treatments alongside more traditional cytotoxic therapies, in a variety of combinations to successfully evade tumour resistance, improve outcomes and also reduce long term toxicity.

1.6 Paediatric tumours

Paediatric malignancies are rare (section 1.2.3) with approximately 1600 new cancer diagnoses made per annum in the UK in children aged between 0-14 years (CRUK, 2014c). As oppose to adult malignancies, paediatric cancers are less due to environmental factors and are more frequently observed in children with hereditary syndromes, although the overall incidence of familial and genetic syndromes associated with childhood malignancies is still low (Stiller, 2004). Hereditary syndromes, for example Li-Fraumeni syndrome, which are linked to childhood cancers also have important wider medical considerations, and have historically provided crucial insights into the development of sporadic childhood malignancies (discussed in section 1.8.7). In addition, many of the tumour types witnessed in childhood, such as neuroblastoma, rhabdomyosarcoma and hepatoblastoma, are rarely seen in adulthood (Pinkerton *et al.*, 2007) and therefore the research and treatment of paediatric tumours has often evolved separately to that of adult malignancies.

1.6.1 Central nervous system tumours in childhood

Paediatric malignancies are typically thought of as either liquid; leukaemia and lymphoma, or solid; bone, brain and soft tissue tumours (Pelengaris and Khan, 2006). Tumours that occur within the CNS are the most common solid tumour observed in childhood (section 1.2.3 and Figure 1.3), with over 400 new diagnoses per year in the UK, and approximately 600 when including young adults (Figure 1.15). Typically CNS tumours originate within the brain tissue itself, and certain malignancies have the ability to metastasis via the cerebrospinal fluid (CSF). Less frequently, CNS tumours can arise from the spinal cord such as ependymomas. Tumours originating from glial cells (gliomas, section 1.6.1.1) are the most commonly diagnosed CNS tumours, account for approximately 43% of all cases, and are a spectrum from low grade to high grade (Louis *et al.*, 2007). The second most frequently observed group are embryonal tumours in the CNS (19%, section 1.6.1.2), followed by ependymomas (section 1.6.1.3) the third most common childhood brain tumour (CRUK, 2010).

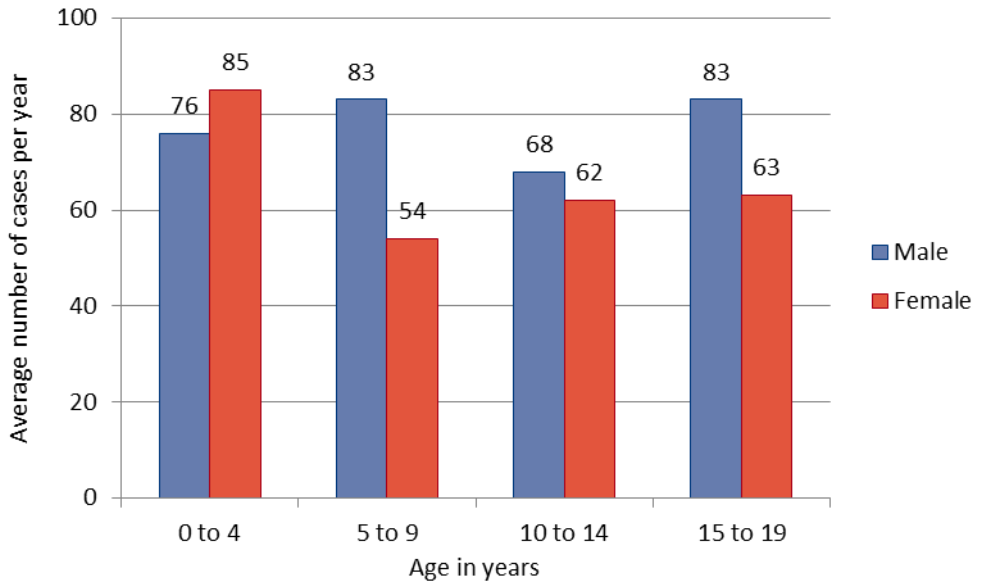

Figure 1.15 Average number of new CNS tumours diagnosed per year in the UK between 2009-2011. Figure adapted from CRUK (CRUK, 2014a).

1.6.1.1 Gliomas

Gliomas are a diverse spectrum of tumours classified as either low grade (grade I and II), or high grade (grade III and IV). These classifications reflect the behaviour of the tumour with low grade tumours being more 'benign' in nature and indolent and high grade being more 'malignant' and aggressive in their disease course (Hargrave, 2009).

1.6.1.1.1 Low grade gliomas

Low grade gliomas (LGGs) commonly arise from the optic pathway or cerebellum but can occur anywhere within the CNS. Astrocytic tumours originate from astrocytes and include the subtypes; pilomyxoid, pilocytic, subependymal giant cell, diffuse astrocytomas and pleomorphic xanthoastrocytoma (Louis *et al.*, 2007). The most commonly witnessed LGGs in childhood are pilocytic astrocytomas. Unlike in adult LGGs, malignant transformation of these tumours rarely occurs in childhood, although more aggressive disease behaviour and metastases within the CSF has been observed in the paediatric age group (Hargrave, 2009).

LGGs are particularly associated with the neurocutaneous condition neurofibromatosis type 1 (NF-1). *NF1* is a tumour suppressor gene (Table 1.1) and is an inhibitor of the RAS signalling pathway and involved in control of the *mTOR* pathway. Sporadic LGGs

have, in recent years, been associated with aberrations of the *BRAF* oncogene (Table 1.2), a cytosolic serine-threonine kinase and member of the RAF kinase family (Dasgupta and Haas-Kogan, 2013). Two established *BRAF* aberrations in paediatric LGGs are the activating point mutation, *BRAF* V600E, which is linked to a poorer prognosis and found in grade II LGGs, and the *KIAA1549-BRAF* fusion gene which is associated with the majority of pilocytic astrocytomas. The identification of *BRAF* aberrations such as the point mutation V600E has provided the opportunity to use the *BRAF* V600E targeted agent dabrafenib, which is currently in a UK's Children's Cancer and Leukaemia Group (CCLG) phase I trial for mutation positive paediatric solid tumours such as LGGs. However, it is the fusion gene, *KIAA1549-BRAF*, that is more commonly observed in this group of tumours, and use of dabrafenib in this context is not established and conversely may encourage tumour growth (Hargrave, 2009; Schiffman *et al.*, 2010; Dasgupta and Haas-Kogan, 2013).

1.6.1.1.2 High grade gliomas

High grade gliomas (HGGs) encompass anaplastic astrocytomas (grade III) and GBM (grade IV) which are both believed to either originate from, or histopathologically resemble, glial cells (Phillips *et al.*, 2006). Grading is used to assess the malignancy of the tumour, prognosticate and direct treatment decisions. For example, grade III tumours are malignant tumours with nuclear atypia and elevated mitotic activity. Similarly grade IV tumours are malignant with a higher frequency of mitotic bodies and evidence of tumour necrosis (Louis *et al.*, 2007).

Much work has recently been undertaken in these devastating tumours which have a 5 year survival below 10% (Phillips *et al.*, 2006; Sturm *et al.*, 2012). Critical mutations and epigenetically defined subgroups have been identified for GBM in both paediatric and adult GBM (section 1.4.6.1.3 and 1.4.7). Overall, six subgroups have recently been described, with 30-40% of GBMs in children and young people associated with disrupted epigenetic mechanisms such as *IDH1* mutations (also linked to *TP53* mutations) or mutations of the *H3F3A* gene which affect the lysine residues K27 or G34 (section 1.4.7). The other three subgroups are associated with copy number variations such as *PDGFRA* amplification, *EGFR* amplification, deletion of *CDKN2A*, chromosome 7 gain and chromosome 10 loss. These subgroups cluster separately, according to their DNA methylation patterns, and importantly are associated with differing tumour

locations and prognosis. For example, GBMs with a *H3F3A* mutation affecting the K27 residue are located in the midline (thalamus or pons), and have a poorer overall survival. *IDH1* mutated tumours are located in the cerebral hemispheres (frontal and temporal lobe) and have a better overall survival (Sturm *et al.*, 2012).

Alongside the epigenetic features recently described for GBM, paediatric HGGs are also associated with the point mutation *BRAF* V600E in up to 20% of cases (section 1.6.1.1.1). These mutations are often linked to the concomitant deletion of *CDKN2A*. (Schiffman *et al.*, 2010; Dasgupta and Haas-Kogan, 2013). Similar to LGGs (section 1.6.1.1.1) dabrafenib is currently in a CCLG phase I trial for mutation positive tumours. In addition to this trial, use of the targeted agent bevacizumab, a VEGF inhibitor (section 1.3.5), is currently open in a CCLG phase II study for paediatric HGG.

1.6.1.2 Embryonal brain tumours

Under the current WHO guidelines embryonal brain tumours consist of ATRTs, CNS primitive neuroectodermal tumours (CNS-PNETs) and medulloblastoma (Louis *et al.*, 2007).

1.6.1.2.1 ATRTs

ATRTs are an extremely rare (<5% of paediatric brain tumours), and aggressive form of intracranial tumour which occur both in the infratentorial and supratentorial regions of the brain (Figure 1.16).

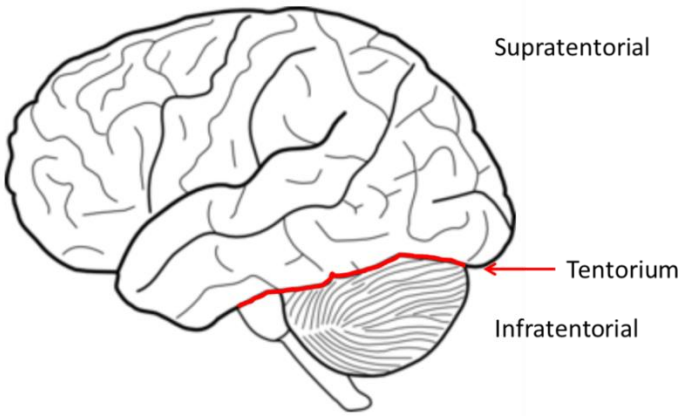

Figure 1.16 Illustration demonstrating the supratentorial and infratentorial regions of the brain.

They occur predominantly in children under the age of 3 years, and it is this group of patients who typically present with disseminated disease and do extremely poorly, with an OS of less than 15%. Tumours display pathological heterogeneity which historically gave rise to difficulty in their confident identification. Consequently ATRTs were commonly misdiagnoses as medulloblastomas, choroid plexus carcinomas and CNS-PNETs. However, more recently, the identification of *SMARCB1* loss in greater than 90% of tumours (section 1.4.6.3.2), with a corresponding lack of expression of the protein it encodes (commonly referred to as INI-1, section 2.2), has rapidly improved the histopathological diagnostic certainty of this tumour. Despite these advances, treating these tumours remains challenging. It is also becoming clear that they are not genetically homogenous, and the importance of epigenetic and other molecular events in tumour development are emerging (Tekautz *et al.*, 2005; Hasselblatt *et al.*, 2011; Dufour *et al.*, 2012a).

1.6.1.2.2 CNS-PNETs

CNS-PNETs, historically considered alongside medulloblastoma and previously referred to as supratentorial PNETs (Figure 1.16), are now separately defined (Louis *et al.*, 2007). They are rare, accounting for approximately 3-5% of all brain tumours in childhood, and have an OS of approximately 50%, despite receiving similar multimodal treatment to patients diagnosed with medulloblastoma. They are again pathologically heterogeneous, currently divided into four subtypes; CNS neuroblastoma, CNS ganglioneuroma, medulloepithelioma and ependymoblastoma. However, the histological classification of these aggressive supratentorial tumours is challenging and they are often reclassified as other paediatric tumours such as ATRTs. Moreover, an additional histological entity, 'embryonal tumour with abundant neuropil and true rosettes' (ETANR) has recently been proposed as a further variant of CNS-PNET. These histological difficulties are increasingly corroborated by the expanding amount of data available on the genome and epigenome of these complex tumours. Recent findings suggest that the DNA methylation patterns of these tumours more closely relate to other paediatric brain tumours, rather than other CNS-PNETs , raising important questions regarding the biology of this tumour entity, appropriateness of current clinical classification, and future treatment approaches (Picard *et al.*, 2012; Schwalbe *et al.*, 2013a; Kleinman *et al.*, 2014; Korshunov *et al.*, 2014).

1.6.1.3 Ependymomas

Ependymomas account for 3-6% of all CNS tumours and can occur anywhere in the CNS, although they most frequently arise intracranially in children. There are currently three histological subtypes of ependymomas; myxopapillary ependymoma (grade I), ependymoma (grade II) and anaplastic ependymoma (grade III). At present anaplastic subtype, younger age group and incomplete surgical resection are all associated with a poor outcome. However, despite this understanding, and histological similarities between ependymoma subtypes, tumours can exhibit a wide range of outcomes with 5 year PFS ranging from 30-60%. (Louis *et al.*, 2007; Wani *et al.*, 2012).

Recent breakthrough discoveries have identified two biologically defined subgroups of infratentorial ependymomas (Figure 1.16). The first subgroup (group A), occurs more frequently in young children, have a male preponderance and extremely poor prognosis. Group A tumours demonstrate a balanced genome with only gain of chromosome 1 and loss of chromosome 22 repeatedly observed. Over-expression of genes associated with angiogenesis, wound healing, cell migration and cell adhesion have also been reported in this group. In addition, group A tumours also display promoter hypermethylation (section 1.4.6.1.2) known as the 'CpG island methylator phenotype' (CIMP). Group B tumours are witnessed in older patients, and have a better prognosis (>95% 5 year OS). These tumours are genomically unstable with frequent copy number aberrations such as loss of chromosome 1, 2, 3, 6, 8, 10, 14q, 17q ,22q and gain of 4, 5q, 7, 9, 11, 12, 15q, 18, 20, 21q. Overexpression of genes involved in microtubule assembly, mitochondria metabolism and ciliogenesis have also been described in this subgroup (Archer and Pomeroy, 2011; Witt *et al.*, 2011; Wani *et al.*, 2012; Mack *et al.*, 2014).

Recent pre-clinical work in supratentorial ependymomas (Figure 1.16), has identified the common occurrence of the oncogenic fusion gene *C11orf95-RELA* as a driver of tumourigenesis through aberrant stimulation of the NF-κB signalling pathway (Parker *et al.*, 2014). These discoveries, along with pre-clinical high-throughput drug screening, are altering and advancing the understanding and treatment of ependymoma. Agents such as 5-fluorouracil have been identified to have efficacy in this normally chemo-resistant tumour (Atkinson *et al.*, 2011). However, further advances are required if survival for paediatric ependymoma, is to be improved.

1.7 Relapsed paediatric tumours

Relapsed disease is frequently observed in many of the malignancies already discussed such as HGG and the embryonal brain tumours; ependymomas, CNS-PNETS and ATRTs. Limited investigations into the patterns, treatment and biology of these tumours have been reported (Phillips *et al.*, 2006; Merchant *et al.*, 2008; Messahel *et al.*, 2009; Pizer *et al.*, 2011a; Bouffet *et al.*, 2012; Fangusaro, 2012; Sottoriva *et al.*, 2013; Bode *et al.*, 2014; Hoffman *et al.*, 2014). Further insights into relapsed paediatric malignancies have been attained from studies in non-CNS paediatric tumours such as relapsed neuroblastoma (Carr *et al.*, 2006; Carr-Wilkinson *et al.*, 2010). While recurrent CNS-PNETS have historically been considered together with relapsed medulloblastoma in trials (Pizer *et al.*, 2011a; Bode *et al.*, 2014), other relapsed CNS and embryonal tumours and their relevance to relapsed medulloblastoma are summarised below.

1.7.1 Recurrent high grade glioma

Paediatric HGGs are highly malignant and aggressive brain tumours which, as detailed in section 1.6.1.1.2, have a 5 year overall survival rate below 10% (Phillips *et al.*, 2006; Sturm *et al.*, 2012). Typically following treatment; maximal surgical resection, focal radiotherapy and chemotherapy, (although the benefit of chemotherapy in paediatric HGG is unclear), the tumour will progress or recur and most children will succumb to their disease (Fangusaro, 2012). Treatment resistance has been attributed to intratumoural heterogeneity with different molecular subgroup signatures observed within the same tumour. This molecular heterogeneity compounds the challenge of treatment resistance in HGG. Clonal evolution, and a heterogeneous surviving subpopulation of treatment resistant cells, which may be stem-cell-like, adds to the complexity of recurrent disease (Phillips *et al.*, 2006; Gilbertson and Rich, 2007; Sottoriva *et al.*, 2013). These findings raise important questions with regards to the molecular subgroup evolution in medulloblastoma, and whether subgroup remains the same or changes at disease relapse.

1.7.2 Relapsed ependymoma

Ependymoma is the second most common malignant CNS tumour observed in childhood (section 1.6.1.3). It is typically treated with maximal surgical resection and focal radiotherapy, although recent pre-clinical work has identified a limited number of chemotherapeutic agents which may have efficacy in the treatment of this tumour

(Atkinson *et al.*, 2011). Recurrent disease is common in ependymoma, occurring in 20-70% of all patients diagnosed with the tumour. At present, relapsed disease is rarely curable with reports of only up to 25% of patients being rescued with re-treatment at disease recurrence. Similar to medulloblastoma, recent advances in the understanding of the biology of disease at diagnosis have been reported and are summarised in section 1.6.1.3 (Archer and Pomeroy, 2011; Witt *et al.*, 2011; Wani *et al.*, 2012; Mack *et al.*, 2014). However, very little is known about the biology at relapse.

What has been reported in ependymoma is the successful re-treatment of patients at disease recurrence with radiotherapy. Bouffet *et al*., (2012) for example, reported a series of 18 patients who received full dose focal radiotherapy (54Gy) to the tumour bed, coupled with CSI (36Gy) in metastatic recurrences. Encouragingly 3 year OS was 81%, compared to 10% in relapsed patients who did not receive radiotherapy at this time-point. Moreover, the interval to next recurrence, (third presentation), was significantly increased following re-irradiation. However follow-up of these patients was short, (2 years), and therefore it is difficult to comment on the long term side effects of re-irradiation. Similar findings following stereotactic radiosurgery for recurrent ependymoma (n=12) have recently been reported by Hoffman *et al*., (2014). Here they report a significantly prolonged interval to second recurrence following radiation therapy (p=0.008) and a 3 years OS of 89%. However, radiation necrosis was observed and was symptomatic in 25% of patients.

Other attempts at re-irradiation for disease recurrence have not been as successful, but still convey either a survival benefit or good local disease control (Merchant *et al.*, 2008; Messahel *et al.*, 2009). Re-irradiation at relapse is a growing practice in recurrent ependymoma and is providing important information on its safety and efficacy in the craniospinal axis. While this treatment comes with significant long term morbidity, as discussed in section 1.8.6 and 1.9.1, it may also provide, at present, the best chance of cure in patients who relapse with other CNS tumours (Merchant *et al.*, 2008; Zacharoulis *et al.*, 2010; Atkinson *et al.*, 2011; Bouffet *et al.*, 2012; Hoffman *et al.*, 2014; Muller *et al.*, 2014).

1.7.3 Neuroblastoma

Neuroblastoma is the most common extra-cranial solid tumour in paediatrics. It is embryonal in origin, and predominantly occurs during childhood. It arises from the sympathoadrenal lineage of the developing neural crest, most commonly the adrenal medulla. Neuroblastoma is a complicated, heterogeneous disease with a clinical outcome that varies from complete tumour regression, to high-risk refractory or recurrent disease. Characteristic molecular features include, activating mutations of the gene encoding the anaplastic lymphoma receptor tyrosine kinase (*ALK*), amplification of *MYCN* (section 1.4.2) and intra-chromosomal rearrangements, all of which convey a poor prognosis. Disruption of the p53 pathway is also important in the disease, in particular at relapse where acquisition or maintenance of p53 pathway defects (*TP53* mutations, $p14^{ARF}$ methylation/deletion and *MDM2* amplification, Figure 1.6) are enriched, suggesting a role in chemoresistance and subsequent demise of the patient (Carr *et al.*, 2006; Carr-Wilkinson *et al.*, 2010; Petroni *et al.*, 2012; Cheung and Dyer, 2013). These findings, of acquisition of p53 pathway defects at disease recurrence, suggest that the biology of disease at relapse differs from diagnosis in neuroblastoma. This raises important questions to address in studying other relapsed disease, including medulloblastoma, and highlights the necessity of studying paired tumour samples at both time-points to understand the molecular evolution of tumour biology.

1.8 Medulloblastoma

1.8.1 Incidence, epidemiology and outcomes

Medulloblastoma is the most common malignant CNS tumour of childhood, and accounts for approximately 90 new paediatric cancer diagnoses per year in the UK (Pizer and Clifford, 2008). In comparison to other childhood cancers (section 1.2.3), medulloblastoma is disproportionately responsible for a high frequency (~10%) of childhood cancer deaths (Pizer and Clifford, 2009). There is a male preponderance in the disease (1.7: 1, male: female), and tumours typically occur in the first decade of life. The peak incidence is between 4-7 years but medulloblastoma can occur in neonates and infants as well as teenagers and young adults (Pizer and Clifford, 2008).

Outcome after multimodal therapy (section 1.8.5) is variable, with 5 year OS rates in standard-risk disease around 80% (Lannering *et al.*, 2012). However, for those patients with high-risk disease, which is distinguished from standard-risk disease by the presence of metastatic disease, large cell/anaplastic (LCA) histology, <3 years of age or a residual tumour of >1.5cm^2 post-surgery, the outcome is much poorer with a 5 year OS rate of 25-65% (Crawford *et al.*, 2007; Pizer and Clifford, 2009; Ellison, 2010; Gajjar *et al.*, 2012). Despite advances in our understanding of the disease at diagnosis, >30% of all children with a medulloblastoma will experience disease recurrence, which is almost universally fatal especially in patients who received craniospinal irradiation (CSI) at initial diagnosis (Pizer *et al.*, 2011a; Jones *et al.*, 2012; Ramaswamy *et al.*, 2013).

1.8.2 Diagnosing medulloblastoma

The presentation of patients with medulloblastoma varies and is often dependent on the age of the child. Medulloblastomas are infratentorial (posterior fossa) tumours occurring below the tentorium, within the cerebellum (Figure 1.16). Typically they give rise to the triad of symptoms attributed to disruption of the CSF flow and raised intracranial pressure (ICP); early morning headaches, vomiting, and papilloedema leading to visual disturbances. Children may also exhibit localised 'cerebellar signs' such as ataxia, nystagmus and speech disturbances. However, the symptoms and signs in a younger child are more subtle due to the ability of the unfused skull to expand and compensate for raised ICP. This is compounded by their inability to report symptoms

and leads to a different spectrum of symptoms and signs in the infant age group, with increasing head circumference, developmental delay or loss of developmental milestones often worrying features present at diagnosis (Pizer and Clifford, 2008).

Following a history and examination suggestive of a space occupying lesion within the cranium the next investigation of choice in a medically stable patient would be imaging. A gadolinium contrast enhanced magnetic resonance imaging (MRI) of the entire CNS (brain and spinal cord) to look for primary tumour and metastases, is superior in quality to computed tomography (CT), and the preferred investigation.

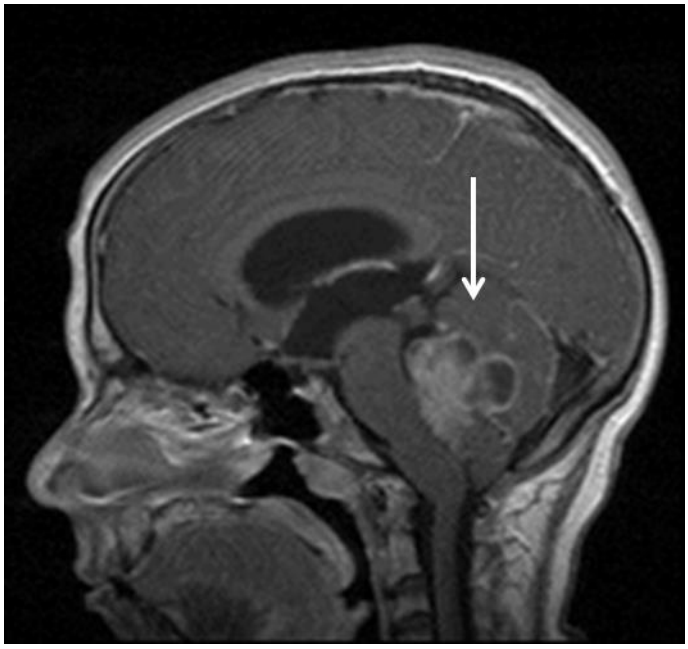

Figure 1.17 Sagittal MRI of a medulloblastoma. Image demonstrates a posterior fossa tumour consistent with the appearances of a medulloblastoma (arrow). Image kindly provided by Prof Simon Bailey (PBTG, Paediatric Brain Tumour Group).

Advances in MRI technology such as diffusion weighted images and magnetic resonance spectroscopy (MRS), have improved the diagnostic capabilities and interpretation of this imaging modality (Panigrahy *et al.*, 2006; Rumboldt *et al.*, 2006). However, it is not always possible to confidently differentiate from other posterior fossa tumours such as ependymomas (section 1.6.1.3) or pilocytic astrocytomas (section 1.6.1.1.1). MRI is critical however, in confirming the presence of a tumour, aiding in surgical planning and staging of the disease.

1.8.3 Staging of medulloblastoma

Current practice uses the Chang's operative staging system (Chang *et al.*, 1969) to assess and stage the extent of metastatic disease (Table 1.6). Alongside an MRI, a lumbar puncture must be performed to sample and assess for the presence of tumour cells in the CSF (M1 disease). Metastatic disease is present in up to 35% of patients at diagnosis (Gandola *et al.*, 2009). If there is clinical suspicion of widely disseminated disease outside the CNS (M4 stage), for instance in extensive M3 disease, other clinically appropriate imaging techniques such as a bone scan, can be performed as disease can rarely spread to bone or other extra-CNS sites such as the liver (Cakir *et al.*, 2004; Gajjar *et al.*, 2006).

Metastatic (M) stage	Definition
M0	No metastases
M1	Presence of tumour cells in the CSF
M2	Intracranial metastases
M3	Spinal metastases
M4	Metastases outside of the CNS

Table 1.6 Metastatic staging of medulloblastoma. Classification based on Chang's criteria (Chang *et al.*, 1969; Dufour *et al.*, 2012b).

1.8.4 Histological diagnosis and classification

The diagnosis of medulloblastoma is currently confirmed histopathologically and while this can be performed on a biopsy sample, typically upfront treatment of all posterior fossa tumours require complete or near complete surgical excision. Therefore, confirmatory histological diagnosis of medulloblastoma follows neurosurgical resection of the tumour. Medulloblastoma, like all other embryonal brain tumours (section 1.6.1.2), is histologically heterogeneous and currently comprises of five main pathological subtypes. These are classic (CLA, 73%), desmoplastic/nodular (DN, 10%), medulloblastoma with extensive nodularity (MBEN), anaplastic and large cell (Louis *et al.*, 2007), with the latter two subtypes being routinely combined to form the subtype LCA, which combined account for approximately 17% of all tumours (Ellison, 2010).

Historically it was crucial to firstly correctly identify medulloblastomas over and above other tumours that can occur in the posterior fossa such as ATRTs (section 1.6.1.2). However, it is now becoming increasingly important to not only confirm the diagnosis of medulloblastoma, but define the pathological subtype as well. These histological variants have prognostic significance and, alongside the growing body of molecular information as well as other clinical factors in medulloblastoma, are utilised to direct current and future therapeutic strategies (McManamy *et al.*, 2007; Pizer and Clifford, 2009; Ellison, 2010; Leary *et al.*, 2011; Taylor *et al.*, 2012).

1.8.4.1 Classic histology

Medulloblastomas exhibiting sheets of small, round, blue cells with a high nuclear: cytoplasmic ratio, are subtyped as CLA histopathology. This subtype is observed in over 70% of tumours (Figure 1.18). Nuclear pleomorphism, mitotic figures and apoptotic bodies are seen in this pathological variant as are occasional rosettes of cells (Ellison, 2010).

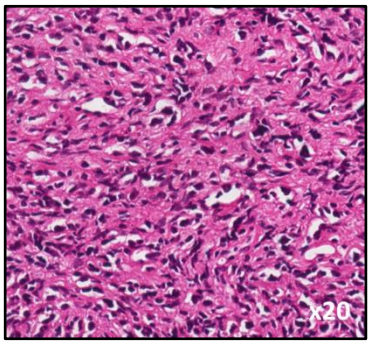

Figure 1.18 Medulloblastoma with classic histology. Haemotoxylin and eosin (H&E) stain demonstrating CLA histology with nuclear pleomorphism, mitotic and apoptotic bodies. Image obtained from the tumour arising in patient 6 (Chapter 3) at diagnosis.

1.8.4.2 Desmoplastic nodular medulloblastoma and medulloblastoma with extensive nodularity

Both DN medulloblastoma and MBEN demonstrate nodules which consist of differentiated neurocytic cells with intranodular regions of desmoplasia. This is easiest visualised on a reticulin stain (Figure 1.19), which is used to detect reticulin fibres made of type III collagen. This silver stain is part of the standard panel of immunohistochemistry performed on a suspected medulloblastoma tumour sample

(section 2.2). In MBEN, the nodules are extensive and dominant with sparse intranodular desmoplasia, whereas in DN medulloblastoma the nodules are less frequent (Figure 1.19). Intranodular neurocytic cells express synaptophysin, another stain performed as part of the histopathological assessment of a tumour sample (section 2.2). Both DN medulloblastomas and MBEN convey a good prognosis in the infant subgroup, which is typically defined as patients under the age of 3 years (McManamy *et al.*, 2007; Ellison, 2010; Leary *et al.*, 2011).

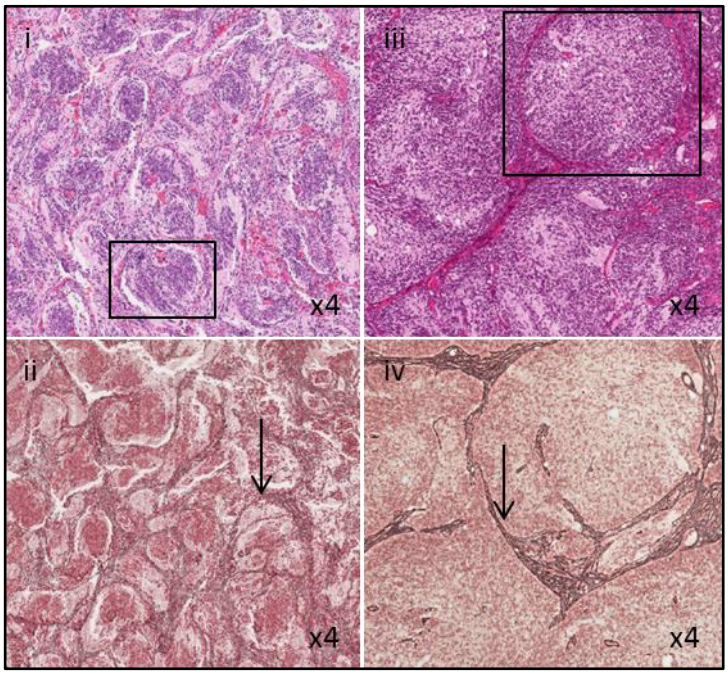

Figure 1.19 Low power images of medulloblastoma with extensive nodularity and desmoplastic nodular histology. Images obtained from the tumours arising in patient 3 (Chapter 3) demonstrating MBEN subtype with dominant nodules (square) and sparse intranodular desmoplasia at diagnosis on H&E (i) and reticulin staining (arrow) (ii) and DN subtype with large, less frequent nodules (square) at relapse on H&E (iii) and reticulin stain (arrow) (iv).

1.8.4.3 Large cell/anaplastic histology

Large cell and anaplastic medulloblastomas have similar features and typically co-occur. As a result they are routinely considered together as one histological subtype, LCA. Large cells are observed with a single nucleolus and round nuclei. Anaplastic cells demonstrate significant cytological pleomorphism and accompanying features of cell wrapping and irregular patterns of nuclei known as cell moulding (Figure 1.20). Both cell types show apoptosis and a high mitotic index. Importantly, LCA is associated with

a poorer outcome and is currently used to define high-risk disease and direct treatment strategies (Pizer and Clifford, 2009; Ellison, 2010; Pizer *et al.*, 2011b).

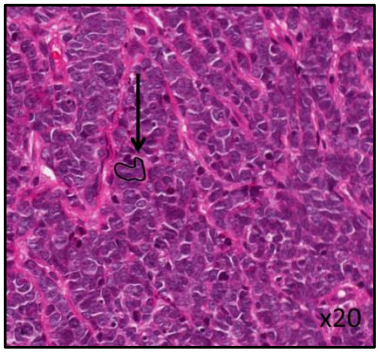

Figure 1.20 Medulloblastoma with large/cell anaplastic histology. H&E stain demonstrating LCA histology with large pleomorphic cells (arrow and outlined) when compared to CLA histology (Figure 1.18). Image obtained from the tumour arising at relapse in patient 6 (Chapter 3).

1.8.5 Treatment of medulloblastoma

Currently multimodal treatment strategies and risk-adapted stratification of medulloblastoma therapy in the UK and Europe-wide rely on clinicopathological variables alone. Standard-risk patients are defined as those at diagnosis who are; i) greater than 3 years old, ii) have M0 disease (Table 1.6), iii) have less than 1.5cm^2 of residual tumour after surgical resection, and iv) have CLA, DN or MBEN histological subtype (Pizer *et al.*, 2011b). All other patients who do not meet these criteria, such as those with metastatic disease or LCA histology, are classified as having high-risk disease and, with the exception of infants, receive escalated therapy (Gajjar *et al.*, 2006; Gandola *et al.*, 2009).

However, the advent of molecular treatment stratification is upon us, with new trials already in advanced stages of development or underway. For example, in Europe the PNET5 trial, coordinated by the European International Society of Paediatric Oncology (E-SIOP) is due to open imminently, and in certain centres in the USA the SJMB12 trial, coordinated by St Jude Children's Research Hospital (Memphis, TN), is currently recruiting. These protocols will radically alter treatment approaches for medulloblastoma. They aim to appropriately escalate or de-escalate therapy according to each patients predicted outcome which is determined by both clinicopathological

and molecular variables and will be discussed in more detail in section 1.8.8 (Pizer and Clifford, 2009; Morfouace *et al.*, 2014).

In brief therefore, the current principles of multimodal treatment in medulloblastoma comprise of a complete or near complete upfront surgical resection, followed by craniospinal irradiation (CSI) with a directed boost towards the primary tumour in the posterior fossa. Patients with standard-risk disease receive adjuvant chemotherapy, with the E-SIOP PNET4 regimen, the most recent standard-risk trial to be completed in Europe, comprising of vincristine, cisplatin and lomustine. This trial had two treatment arms of either standard fractionated radiotherapy or hyperfractionated radiotherapy (HFRT, discussed further in section 1.8.6) and reported a 5 year OS of 77% and 78% for the two treatment arms respectively (Lannering *et al.*, 2012).

High-risk disease protocols are less well defined. Patients typically receive escalated therapy, for example in the form of risk-adapted CSI or HFRT alongside high dose chemotherapy with autologous stem cell transplant. The SJMB-96 utilised risk-adapted CSI and a cyclophosphamide based high-dose chemotherapy regimen and reported a 5 year OS of up to 70% (Gajjar *et al.*, 2006). In other reports, the use of HFRT for high-risk disease alongside a chemotherapy regimen consisting of methotrexate, etoposide, cyclophosphamide and carboplatin achieved a 5 year OS of 73% (Gandola *et al.*, 2009). Whilst both these trials were promising, the treatment of high-risk disease remains a considerable challenge and these improvements in OS have not always been reproducible in other centres around the world. The 5 year OS of high-risk medulloblastoma is therefore difficult to capture but is more likely to be between 25-65% (Crawford *et al.*, 2007; Pizer and Clifford, 2009; Ellison, 2010; Gajjar *et al.*, 2012).

1.8.6 Long term sequelae of medulloblastoma treatment

Since the addition of chemotherapy to treatment protocols of medulloblastoma the dose of radiotherapy has successfully been reduced but is still a necessary modality for the majority of patients (Packer *et al.*, 2006). Predominantly CSI, but also neurosurgery, can affect many aspects of neurocognitive function in long term survivors, and the quality of survival is increasingly influencing treatment strategies and interventions (Pizer and Clifford, 2009). Typically, survivors have been thought to suffer from a lower than average intelligence quotient (IQ). This is due to the inability

of survivors to acquire new skills and understanding. Consequently they do not display the traditional increase in IQ with age that is seen in their healthy peers.

While a reduced IQ alone will have long term consequences in schooling and higher education, the neurological damage following CSI is more complex. Survivors of brain tumours also display lower adaptive functioning; the age appropriate ability to independently complete tasks of daily living, as well as difficulties with areas of executive function, such as working memory; integral for obtaining new information. Survivors also display emotional, physical, social and behavioral problems and over time will develop endocrinopathies, such as growth and sex hormone deficiencies, which require life-long treatment (Ashford *et al.*, 2014; Bull *et al.*, 2014; Knight *et al.*, 2014).

Understanding the interplay of all these neurocognitive deficits, alongside treatment factors is difficult. Radiotherapy avoidance strategies are in place for infants with medulloblastoma as the long term side effects are too devastating for such a young and developing brain. As a result of this strategy it has become apparent that a subpopulation of infants with localised, DN disease (section 1.8.4.2) can potentially achieve long term survival without requiring radiotherapy at all. Infants with DN medulloblastoma are reported to experience an OS of 85%, an equivalently good survival to that of older, standard-risk patients. This subpopulation of infants will benefit in the future from elimination of radiotherapy as an upfront strategy and instead it will only be employed as salvage treatment if disease recurs (Leary *et al.*, 2011).

Other attempts to improve long term survival while preserving or improving quality of survival include the use of HFRT in the standard-risk E-SIOP, PNET4 trial (section 1.8.5). This was a randomised study comparing standard CSI with HFRT with the aim of improving tumour control, due to the dose escalation permitted in HFRT, without an increase in late effects. To date there is no evidence of benefit using HFRT in standard-risk disease either for tumour control or quality of survival (5 year OS of 77% and 78% for the 2 arms). However, the full range of late-effects is yet to be evaluated in this study, as the median follow-up at review of this trial was only 4.8 years (Lannering *et al.*, 2012).

1.8.7 Initial insights into the molecular biology of medulloblastoma

Medulloblastoma is associated with several cancer predisposition syndromes; most notably Li- Fraumeni syndrome (LFS), Turcot syndrome (Type A) and Gorlin syndrome. As a result of these associations, initial research into the molecular biology of medulloblastoma focused on understanding whether the pathways disrupted in these syndromes played a wider role in the development of sporadic medulloblastoma (Northcott *et al.*, 2012a).

1.8.7.1 Li-Fraumeni syndrome

LFS was described in 1969 following observations of frequent childhood cancers within the same family. It is a cancer predisposition disorder whereby there is classically a germline mutation of the tumour suppressor gene *TP53* (section 1.4.1, Table 1.1). It is non-syndromic without physical phenotypical features, and therefore often only suspected by obtaining a strong family history of cancer. The diagnosis is also suspected in isolated specific tumour types in childhood which are strongly associated with LFS such as adrenocortical carcinoma and choroid plexus carcinoma, or in young women who have early onset breast cancer without identifiable *BRCA1* or *BRCA2* (Table 1.1) mutations (Chompret *et al.*, 2000; Gonzalez *et al.*, 2009).

The classic definition for LFS is a proband diagnosed with a sarcoma under the age of 45 years, with a first-degree relative with cancer below the age of 45 years, and another first-degree/second-degree relative with cancer under the age of 45 years or a sarcoma at any time in their life. The classic component tumour spectrum is shown in Figure 1.21 and includes sarcomas, brain tumours, breast cancer and adrenocortical carcinoma. Over time the tumour spectrum has increased to include for example gastric cancer, melanoma and germ cell tumours. The diversity of tumour types is possibly explained by an increasingly complex *TP53* genotype such as polymorphisms and copy number variations (Gonzalez *et al.*, 2009; Malkin, 2011).

Medulloblastoma is one of the component tumours of LFS and recent discoveries of an unexpectedly high frequency of germline *TP53* mutations in one of the subgroups of medulloblastoma (section 1.8.8.2) has led to the proposal that LFS is underestimated in the disease (Rausch *et al.*, 2012). Moreover, this insight into the relationship between LFS and medulloblastoma led to the interrogation of *TP53* status in sporadic

disease, and somatic mutations of the *TP53* gene are known to be one of the most frequently observed mutations disease-wide (~10%) and will be discussed further in section 1.8.8.1 and 1.8.8.2 (Northcott *et al.*, 2012a; Rausch *et al.*, 2012; Zhukova *et al.*, 2013).

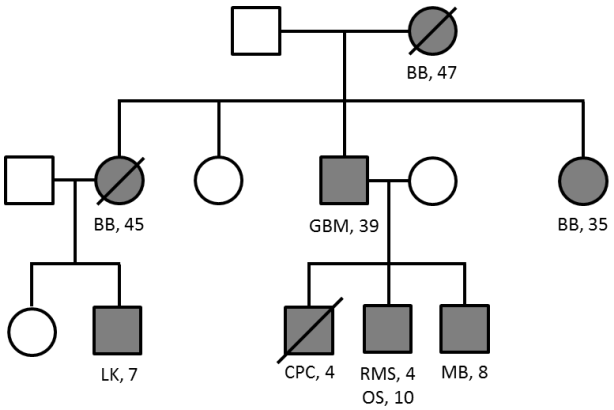

Figure 1.21 Li-Fraumeni family pedigree. Illustrative example of a family with inherited LFS also demonstrating the genetic anticipation observed in the syndrome. Circle, female; square, male; grey, affected; diagonal line, deceased; BB, bilateral breast cancer; LK, leukaemia; OS, osteosarcoma; RMS, rhabdomyosarcoma; CPC, choroid plexus carcinoma; GBM, glioblastoma; MB, medulloblastoma; number, age at diagnosis in years. Figure adapted from Malkin, 2011.

1.8.7.2 Turcot syndrome

Turcot syndrome is another cancer syndrome which includes a predisposition to medulloblastoma as well as GBM (section 1.6.1.1.2), ependymoma (section 1.6.1.3), colon cancer, thyroid papillary carcinoma, basal cell carcinoma, leukemia and lymphoma. Unlike LFS, patients have phenotypic features of café au lait spots, sebaceous cysts and pigmented ocular fundi lesions. There are two types of Turcot syndrome, type A and type B. Type A is associated with medulloblastoma and is a result of a mutation in the adenomatous polyposis coli gene (*APC*, Table 1.1), a member of the canonical Wnt/wingless (WNT) signaling pathway (Figure 1.22). Type B, which is associated GBM (section 1.6.1.1.2) and ependymoma (section 1.6.1.3), has mutations in the DNA mismatch repair genes; *MLH1, MLH2, MLH3, PMS1 and PMS2* (de Bont *et al.*, 2008; Gorovoy and de Alba Campomanes, 2014).

Similar to LFS, the discovery of *APC* mutations in medulloblastomas associated with Turcot syndrome led to the investigation of other WNT pathway components in sporadic medulloblastoma. It is now well established that somatic mutations of the *CTNNB1* of the WNT pathway, which encodes the protein β-catenin, occur in approximately 10% of all medulloblastomas, and this subgroup of tumours is discussed further in section 1.8.8.1 (de Bont *et al.*, 2008; Northcott *et al.*, 2012a; Taylor *et al.*, 2012; Gorovoy and de Alba Campomanes, 2014).

1.8.7.3 Gorlin syndrome

Gorlin syndrome is also known as nevoid basal cell carcinoma syndrome. It is predominantly associated with the formation of basal cell carcinomas but also predisposes to medulloblastoma. Phenotypic features include vertebral abnormalities, polydactyly and a coarse facial appearance. Mutations of genes within the sonic hedgehog (SHH) pathway (*PTCH1*, *PTCH2* and *SUFU*) are frequently observed (Torrelo *et al.*, 2014). Subsequent investigation of the SHH pathway (Figure 1.22) in non-syndromic medulloblastomas revealed somatic mutations of *PTCH* and *SUFU* alongside mutations of *SMO* and amplifications of *GLI1 and GL2*, all components of the SHH pathway (Figure 1.22). Combined these SHH pathway aberrations are found in up to a third of sporadically arsing medulloblastomas, and form their own molecular subgroup which is discussed in section 1.8.8.2 (Northcott *et al.*, 2012a; Taylor *et al.*, 2012).

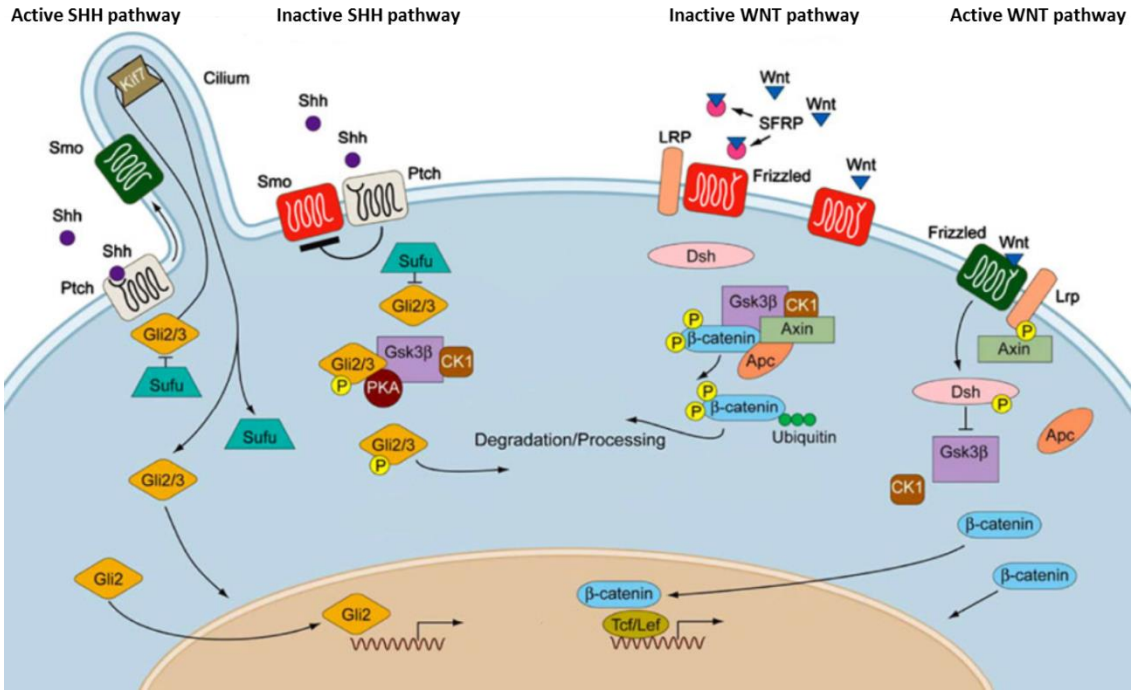

Figure 1.22 The sonic hedgehog and Wnt/Wingless signaling pathways. Inactive SHH pathway; Ptch receptors inhibit Smo (red) preventing Smo from accessing the primary cilium, Sufu binds Gli2 and Gli3, Gli2 is also degraded. Active SHH pathway; Ptch no longer represses Smo (green) which locates into the cilium, Sufu does not bind to Gli2 and Gli3, Gli2 translocates to the nucleus where it activates transcription. Inactive WNT pathway; phosphorylated β-catenin is degraded. Active WNT pathway; β-catenin translocates to the nucleus where it activates transcription. Figure adapted from Ellison, 2010.

1.8.8 Molecular subgrouping

It is now well established that medulloblastoma comprises of four genetically and epigenetically (section 1.4.6.1.3) defined subgroups, with their own distinct clinicopathological demographics, recurrent molecular aberrations and outcomes (Figure 1.23). These four subgroups were largely identified through the convergence of transcriptomic data which subgrouped medulloblastoma into anything from four to six separate molecular subgroups. Leaders in the field of medulloblastoma research reached a consensus agreement in 2012 that there are four principal, molecularly defined, subgroups in medulloblastoma. However, within these four subgroups there is likely to be further sub-classifications which would account for the variable number of subgroups originally reported (Thompson *et al.*, 2006; Kool *et al.*, 2008; Cho *et al.*, 2011; Northcott *et al.*, 2011b; Taylor *et al.*, 2012).

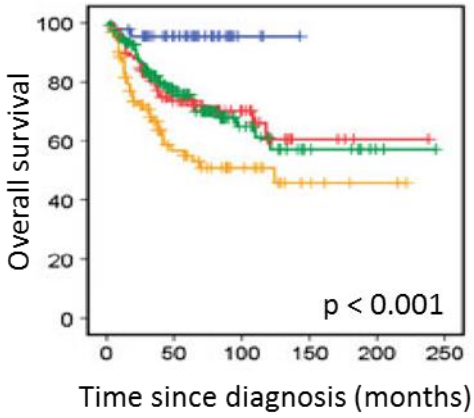

Figure 1.23 Overall survival difference between the four molecular subgroups of medulloblastoma. MB_{WNT}, blue; MB_{SHH}, red; MB_{Group3}, yellow; MB_{Group4}, green. Figure adapted from Kool *et al*., 2012.

The most well defined and understood subgroups are medulloblastomas associated with WNT pathway disruption (MB_{WNT}, section 1.8.7.2 and Figure 1.22) and medulloblastomas associated with aberrations of the SHH pathway (MB_{SHH}, section 1.8.7.3 and Figure 1.22). The two remaining subgroups, Group 3 and Group 4, (MB_{Group3} and MB_{Group4} respectively) are less well characterised but recent years have seen an expansion of genomic and epigenomic data across all subgroups (Kool *et al.*, 2012; Northcott *et al.*, 2012a; Taylor *et al.*, 2012).

1.8.8.1 WNT subgroup

1.8.8.1.1 Clinical, pathological and molecular features of MB_{WNT}

MB_{WNT} is the least common subgroup and accounts for approximately 10% of all medulloblastomas. They occur equally in boys and girls, typically around the median age of 9 years and readily display CLA histology, although rarely there have been reports of LCA in this subgroup (section 1.8.4). Initial insights into WNT pathway involvement in tumourigenesis were revealed due to the association of Turcot syndrome (type A) and medulloblastoma (section 1.8.7.2). Mutations in exon 3 of the *CTNNB1* gene, which is pathognomonic for MB_{WNT} membership, leads to nuclear accumulation of the encoded protein, β-catenin. This protein accumulation in the nucleus of tumour cells can be examined by immunohistochemistry and serves as a surrogate test to confirm molecular subgroup (Clifford *et al.*, 2006; Northcott *et al.*, 2012a; Taylor *et al.*, 2012).

Another surrogate marker for MB_{WNT} membership is monosomy 6 which can be examined by Fluorescence *in situ* Hybridisation (FISH). This is a frequently (~85%) observed copy number variation in this otherwise balanced genomic subgroup. Importantly, patients with MB_{WNT} have a favorable prognosis (Figure 1.23 and Figure 1.24) with long term OS in excess of 90%. This is despite the relatively frequent occurrence of *TP53* mutations in this subgroup (~12% of MB_{WNT}) which has traditionally been thought of as a poor prognostic marker. Recent work however has revealed that it is the subgroup context of *TP53* mutations which is important in medulloblastoma, and MB_{SHH} with *TP53* mutations drive the poor prognosis of this additional molecular feature. MB_{WNT} tumours with a *TP53* mutation still have a good OS, comparable to those MB_{WNT} with wild type *TP53* (Clifford *et al.*, 2006; Pfaff *et al.*, 2010; Tabori *et al.*, 2010; Lindsey *et al.*, 2011; Kool *et al.*, 2012; Northcott *et al.*, 2012a; Taylor *et al.*, 2012; Zhukova *et al.*, 2013; Shih *et al.*, 2014).

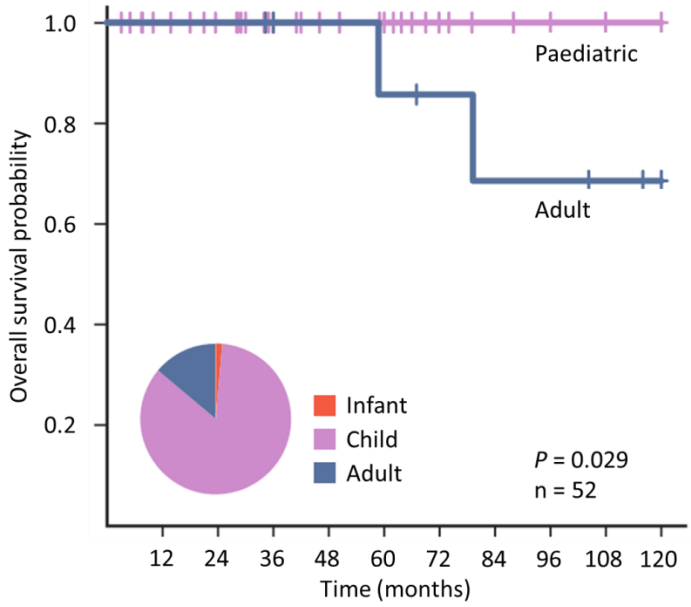

Figure 1.24 Kaplan-Meier overall survival curves for MB_{WNT}. Ten year overall survival; demonstrating a good prognosis for MB_{WNT} molecular subgroup in children. Figure adapted from Shih *et al.,* 2014.

Other recurrent aberrations more recently identified through a variety of sequencing techniques, (Sanger sequencing (section 2.4), whole-genome sequencing (WGS) and whole-exome sequencing (WES)), include mutations of the dead box helicase3, X linked gene (*DDX3X*) which are reported in up to 50% of MB_{WNT}. *DDX3X* is part of a gene family encoding for dead box proteins which are associated with multiple cellular mechanisms such as regulation of the cell cycle. Mutations within this gene alter the RNA binding conformation, and consequently modify protein function. Mutations of the histone and chromatin modifiers, *MLL2* (12%, sections 1.4.6.2.2 and 1.4.7) and *SMARCA4* (26%, section 1.4.6.3.2) respectively, are also enriched in this subgroup (Parsons *et al.*, 2011; Jones *et al.*, 2012; Northcott *et al.*, 2012a; Pugh *et al.*, 2012; Robinson *et al.*, 2012).

1.8.8.1.2 Therapeutic stratification of MB_{WNT}

Despite the increasing number of molecular aberrations associated with MB_{WNT}, evidence suggests that it is subgroup membership that is the overriding biomarker related to prognosis, and other features such as *TP53* mutation, monosomy 6 and metastatic disease, play less of a role in determining outcome (Pfaff *et al.*, 2010; Lindsey *et al.*, 2011; Kool *et al.*, 2012; Zhukova *et al.*, 2013; Shih *et al.*, 2014). As such,

trials are either in development, or underway, to reduce the therapy given to this group. In particular, radiotherapy reductions are planned for this good prognosis subgroup with the aim of reducing long term side effects specific to this treatment modality (section 1.8.6) while maintaining the high OS rates (Pizer and Clifford, 2009).

While deciding on the appropriate treatment reduction is one challenge, determining an appropriate clinical test to identify patients with MB_{WNT} in the first instance is also difficult and, at present, international consensus is yet to be reached. Immunohistochemical staining for nuclear accumulation of the β-catenin protein has proven robust when assessed uniformly (Ellison, 2010), and is currently utilised in the SJMB12 protocol coordinated by St Jude Children's Research Hospital (Memphis, TN). Examination for monosomy 6 by FISH or polymerase chain reaction (PCR) DNA sequencing analysis for the hotspot mutations observed in exon 3 of the *CTNNB1* gene have been proposed as potential tests to identify this subgroup (Taylor *et al.*, 2012). Currently, mutation screening alongside immunohistochemistry are the favoured analyses by E-SIOP for the upcoming PNET5 trial (section 1.8.5). Additionally, MB_{WNT} along with MB_{SHH}, MB_{Group3} and MB_{Group4} cluster distinctly according to both their gene expression and DNA methylation signatures (section 1.4.6.1.3, 1.8.8 and 2.11). Minimal gene expression (Northcott *et al.*, 2011c; Schwalbe *et al.*, 2011), and DNA methylation signature assays (PBTG unpublished work, section 6.3.6.2), are at various stages of development to assign not only MB_{WNT} membership but MB_{SHH}, MB_{Group3} and MB_{Group4} membership as well.

1.8.8.1.3 Mouse models of MB_{WNT}

Evidence now suggests that MB_{WNT} have a distinct developmental origin to that of other medulloblastomas (Gibson *et al.*, 2010). It has been demonstrated in *Ctnnb1*-mutant mice that aberrant cell collections in the dorsal brainstem most commonly resemble progenitor cells derived from the lower rhombic lip. Further work in *Ctnnb1*-mutant mice on a background of *Trp53* deletion ($Trp53^{flx/flx}$) demonstrated that upon aging, 15% of *Ctnnb1*-mutant; $Trp53^{flx/flx}$ mice developed CLA medulloblastomas, connected to the dorsal brainstem, with immunoprofiles most closely resembling MB_{WNT}. Cross-species genomic comparison of the transcriptomes of these tumours, demonstrated that the *Ctnnb1*-mutant mice tumour profiles clustered only with their human MB_{WNT} counterparts. This evidence supports the hypothesis that MB_{WNT}

tumours differ in their developmental origin when compared to MB_{SHH} (section 1.8.8.2), and uniquely originate from progenitor cells within the dorsal brainstem (Gibson *et al.*, 2010). Further work to model this disease subgroup has shown that mice harbouring *Pik3ca*^{E545K} mutations, also reported in human MB_{WNT}, develop tumours with 100% penetrance which recapitulate human MB_{WNT} in *Blbp*-Cre;*Ctnnb1*$^{+/lox(Ex3)}$;*Tp53*$^{+/flx}$ transgenic mice (Robinson *et al.*, 2012; Poschl *et al.*, 2014). A summary of all the key features in MB_{WNT} is provided below (Figure 1.25).

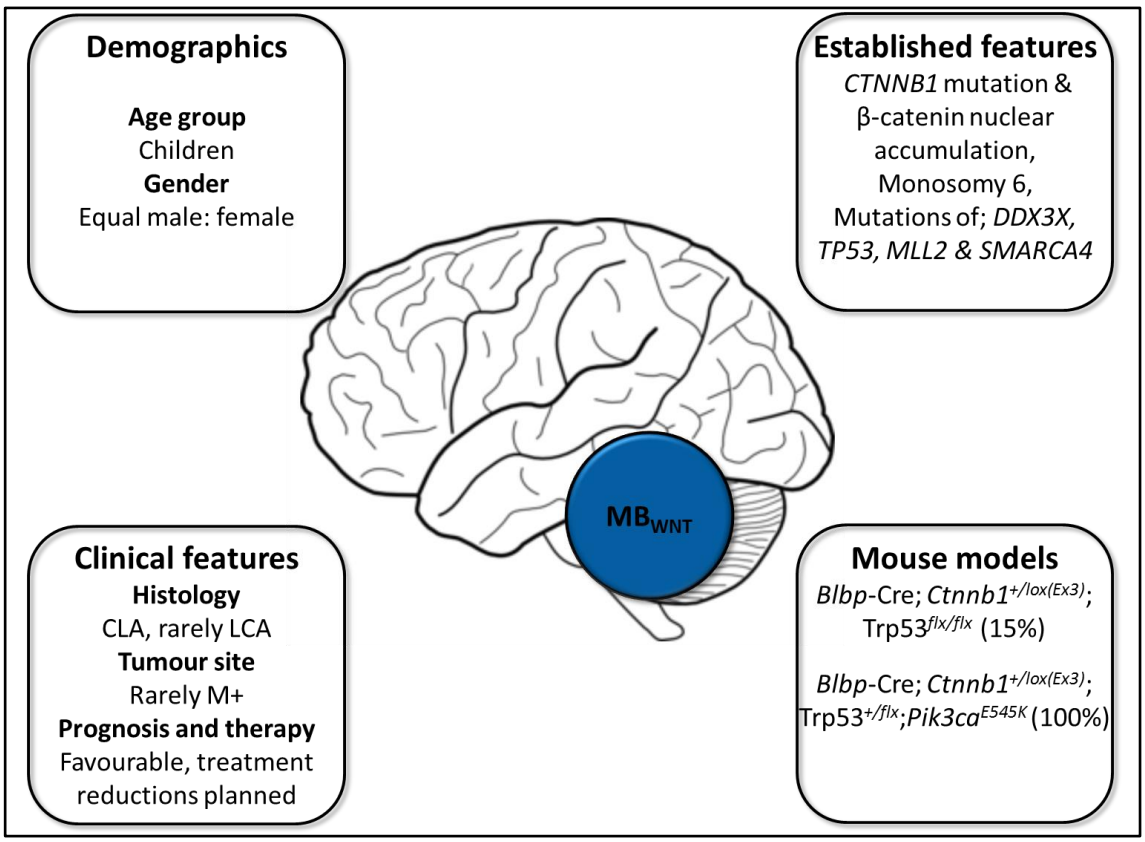

Figure 1.25 Summary of the main clinical, pathological, molecular features and mouse models associated with MB_{WNT}. CLA, classic histology; LCA, large cell/anaplastic; M+, metastatic disease; *Blbp*, brain lipid binding protein; Ex3, exon 3; Pik3ca, PI3K catalytic-α polypeptide; *Flx*, flox. Mouse models; percentage tumour penetrance in parenthesis.

1.8.8.2 SHH subgroup

1.8.8.2.1 Clinical, pathological and molecular features of MB_{SHH}

MB_{SHH} is named after the SHH pathway (Figure 1.22) which is disrupted in this subgroup and drives tumour initiation. MB_{SHH} is associated with amplifications (*GLI1* and *GLI2*), somatic and germline mutations of the SHH pathway (*SUFU*, *PTCH* and *SMO*, section 1.8.7.3). Together mutations within the SHH pathway are found in approximately 87% of sporadic MB_{SHH} tumours (Kool *et al.*, 2014). MB_{SHH} display a bimodal age distribution, and commonly occur in teenagers and young adults or infants (<3 years old), with a paucity of MB_{SHH} during the childhood years. There is an equal gender distribution but otherwise these tumours are clinically and biologically heterogeneous, with variable outcomes, pathology and molecular aberrations. For example, infants with DN histology (section 1.8.4.2) have a good prognosis and many of these young patients are able to avoid CSI (section 1.8.6), whereas older patients tend to have an intermediate prognosis (Figure 1.26). However, unlike $MB_{WNT,}$ the interplay of clinicopathological and molecular events within this subgroup does significantly affect OS in both univariate and multivariate analyses (McManamy *et al.*, 2007; Ellison, 2010; Leary *et al.*, 2011; Taylor *et al.*, 2012; Shih *et al.*, 2014).

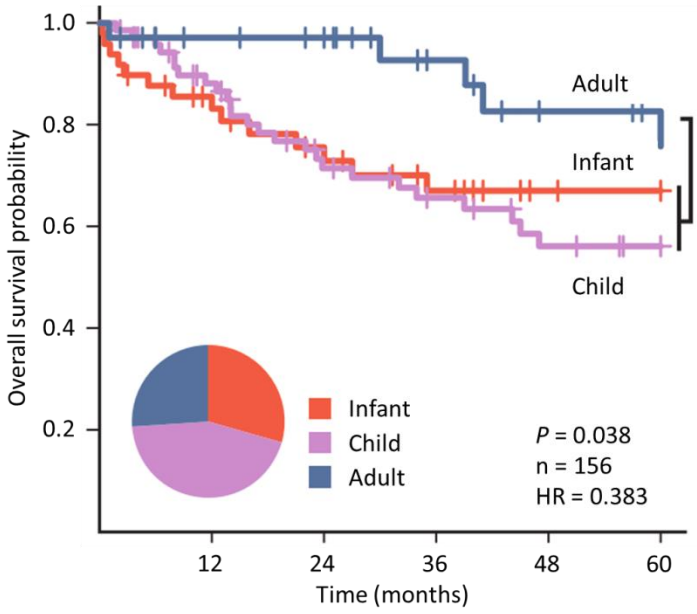

Figure 1.26 Kaplan-Meier overall survival curves for MB_{SHH}. Overall survival demonstrating a variable outcome by age for MB_{SHH} molecular subgroup. Figure adapted from Shih *et al.,* 2014.

Germline and somatic *TP53* mutations are enriched within this subgroup (up to 20%). Studies report that *TP53* mutations convey an extremely poor prognosis in all MB_{SHH} (5 year OS of 41%). *TP53* mutations are frequently found in tumours sampled from children diagnosed with a MB_{SHH} between the ages of 5-18 years and, in this age group, predict an extremely poor OS with over 70% of patients with *TP53* mutant-MB_{SHH} succumbing to their disease. This is irrespective of whether mutations are somatic or germline (LFS, section 1.8.7.1). In addition to the association with age and LFS, *TP53* mutant-MB_{SHH} frequently exhibit LCA histology, 17p loss or *MYCN* amplifications, and combined *TP53*-*MYCN* defects occur in approximately 6% of MB_{SHH} (Pfaff *et al.*, 2010; Jones *et al.*, 2012; Zhukova *et al.*, 2013; Kool *et al.*, 2014). Recent findings have also linked *GLI2* amplifications with *TP53* mutations (Kool *et al.*, 2014). Moreover, copy number aberrations of components in the p53 pathway such as *PPM1D* and *MDM4* amplification have been described, although their impact on prognosis is not clear (Northcott *et al.*, 2012b).

Chromothripsis (section 1.3.7), whereby there are alternating copy number states and chromosomal rearrangements attributed to one single event shattering the chromosome, has similarly been linked to germline *TP53* mutations in this subgroup. This suggests that preceding *TP53* mutations lead to the chromothripsis phenomenon, and also highlights the importance of considering undiagnosed LFS in patients with MB_{SHH} (Rausch *et al.*, 2012). Patients displaying chromothripsis with MB_{SHH} also have a significantly worse outcome (Shih *et al.*, 2014).

MYCN amplification in isolation is found in approximately 8% of MB_{SHH} and conveys a poor prognosis. Similarly amplification of the SHH pathway member *GLI2* is predictive of a poor outcome as is 17p loss, 14q loss and 10q gain (Korshunov *et al.*, 2011; Northcott *et al.*, 2011a; Pezzolo *et al.*, 2011; Taylor *et al.*, 2012; Shih *et al.*, 2014). *DDX3X* mutations (section 1.8.8.1) are present in around 12% of MB_{SHH}, as well as amplifications of IGF signalling genes (for example *IGF1R*) and PI3K genes. Mutations and aberrations of the *TERT* promoter region have also been recently described. As already discussed in section 1.4.7, increased expression of *TERT* via mutually exclusive genetic and epigenetic mechanisms, leads to telomere lengthening and evasion of apoptosis by cancer cells. *TERT* promoter aberrations occur in >75% of non-infant MB_{SHH}, convey an improved prognosis, and represent the most common additionally

disrupted pathway within the MB_{SHH} subgroup (Jones *et al.*, 2012; Northcott *et al.*, 2012a; Northcott *et al.*, 2012b; Pugh *et al.*, 2012; Robinson *et al.*, 2012; Koelsche *et al.*, 2013; Remke *et al.*, 2013; Kool *et al.*, 2014; Lindsey *et al.*, 2014).

1.8.8.2.2 Therapeutic stratification, targeted therapies and quality of survival in MB_{SHH}

It is important to consider all these multiple, recurrent genetic and epigenetic events described in the MB_{SHH} subgroup when deriving improved therapeutic stratification and prognostication. A recent multivariate analyses (Shih *et al.*, 2014), integrating the majority, but not all, of the proposed clinical, pathological and molecular biomarkers in medulloblastoma reported that for MB_{SHH} the consideration of *GLI2* amplification, 14q loss and metastatic disease provides the most robust model for discerning high, standard and low risk patients in this subgroup. Importantly, absence of all three poor prognostic features conveys an OS comparable to the favourable prognosis of MB_{WNT} tumours (Figure 1.24). While this report is promising (Shih *et al.*, 2014), further work is required to assess some of the features of MB_{SHH} not included in these multivariate analyses, such as *TP53* mutations and *TERT* promoter mutations/methylation status.

Treatment strategies targeted towards inhibiting the SHH pathway are currently underway in phase I/II studies for medulloblastoma, having shown efficacy in other SHH pathway driven cancers such as basal cell carcinoma (Low and de Sauvage, 2010). Use of the agent GDC-0449, a selective inhibitor of *SMO* (Figure 1.22), has shown early promise. However, tumours with aberrations of the SHH pathway downstream of *SMO* (amplification of *GLI2* for example) are likely to exhibit primary resistance to this agent and, following administration of GDC-0449 to sensitive tumours, secondary resistance has been acquired. Furthermore, the long term effects of using these agents in young patients are unknown, and concerns focus on growth abnormalities and abnormal development. It therefore follows, given the evidence of tumour resistance and concerns around late effects, that targeted therapies may need to be part of a multi-agent rather than single-agent strategy (Rudin *et al.*, 2009; Ng and Curran, 2011; Northcott *et al.*, 2012a; Kool *et al.*, 2014).

Similarly as we move towards subgroup-specific stratified treatments, so should long term follow-up analysis. Firstly, to account for the variable effects of molecularly defined and potentially targeted treatment strategies and secondly, to understand how the differing biology of the four subgroups influences the long term health outcomes of survivors. Recent evidence, for example, suggests that despite their intermediate prognosis, patients with MB_{SHH} have a better quality of survival, even when compared to MB_{WNT} survivors who had equivalent treatment and better OS (Bull *et al.*, 2014).

1.8.8.2.3 Mouse models of MB_{SHH}

It has also been demonstrated that MB_{SHH} tumours arise from differing cells of origin when compared to MB_{WNT}. This is firstly borne out by observations in both human and mouse, where MB_{SHH} tumours are located in the cerebral hemispheres rather than on the surface of the dorsal brainstem like MB_{WNT} tumours (section 1.8.8.1). This observation is further supported by findings in mouse models of MB_{SHH}. There are currently multiple mouse models of MB_{SHH} which are either constitutive knockout or transgenic models (Poschl *et al.*, 2014). The knockout models occur on a background of a single inactivated *Ptch1* allele, and develop sporadic MB_{SHH} with a penetrance of approximately 15%, which improves to 100% in *Trp53*$^{-/-}$ mice (Goodrich *et al.*, 1997; Wetmore *et al.*, 2000; Northcott *et al.*, 2012a). In *Ptch1*$^{+/-}$ MB_{SHH} mouse models, tumours have been shown to originate in granule neuron precursor cells arising from the upper rhombic lip (Gibson *et al.*, 2010).

Transgenic models however, either mimic SHH pathway disruption, by overexpressing neurogenic differentiation 2 (Neurod2 or "ND2")-SmoA1, or by targeting the inactivation of *Ptch1* in granule precursor cells by crossing a knockout *Ptch1* mouse with a *Math1-cre* transgenic mouse (Helms *et al.*, 2000; Schuller *et al.*, 2007). These transgenic models develop tumours with increased penetrance that anatomically, and histologically resemble MB_{SHH} (Hallahan *et al.*, 2004; Hatton *et al.*, 2008; Yang *et al.*, 2008). Further work has demonstrated that in the transgenic mice *hGFAP-cre::SmoM2-YFP*$^{Fl/+}$ and *Math1-cre::SmoM2-YFP*$^{Fl/+}$, which disrupts the SHH pathway via a mutated *SMO* allele (*SmoM2-YFP*), tumours arise from granule neuron precursor cells derived from of the cochlear nuclei of the lower rhombic lip. This cell of origin still remains distinct from the pre-cerebellar lower rhombic lip cell of origin of MB_{WNT}, described in

section 1.8.8.1. These multiple cells of origin from both the upper rhombic lip and cochlear nuclei of the lower rhombic lip for MB_{SHH} could go part way to explaining the heterogeneity frequently observed in this molecular subgroup (Grammel *et al.*, 2012).

Most recently Wu *et al*., (2012), describes a model where the expression of the sleeping beauty transposon system in a *Math1* transgenic mouse, bred with transgenic T2/Onc mice on a background of hemizygous *Ptch1* inactivation, develop highly aggressive, metastatic medulloblastomas similar in their dissemination to human MB_{SHH} (Wu *et al.*, 2012). A summary of these models alongside the key clinical, pathological and molecular features in MB_{SHH} are shown in Figure 1.27.

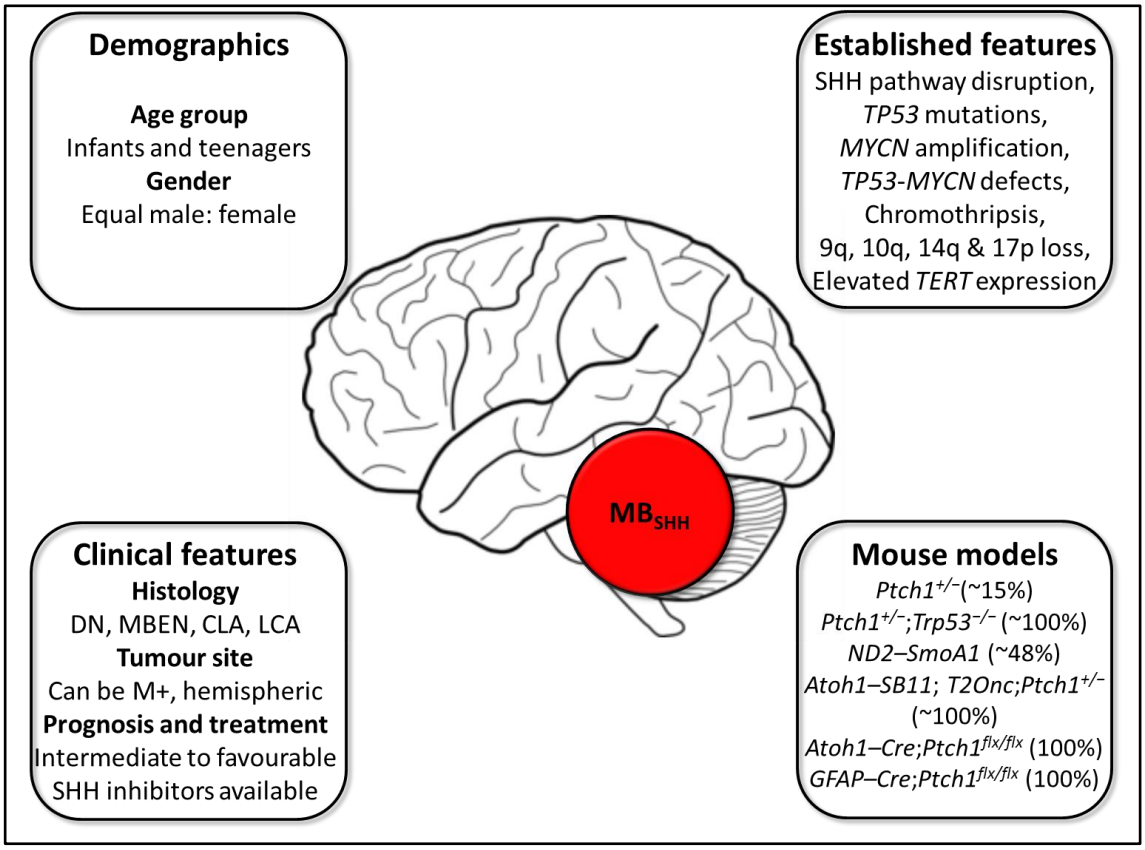

Figure 1.27 Summary of the main clinical, pathological, molecular features and mouse models associated with MB_{SHH}. DN, desmoplastic/nodular histology; MBEN, medulloblastoma with extensive nodularity; CLA, classic histology; LCA, large cell/anaplastic; M+, metastatic disease; ND2, neurogenic differentiation 2; Smoa1; activated mutant of smoothened; Atoh1, atonal homologue 1; SB, sleeping beauty; Flx, flox; GFAP, glial fibrillary acidic protein. Mouse models; percentage tumour penetrance in parenthesis.

1.8.8.3 Group 3 subgroup

1.8.8.3.1 Clinical, pathological and molecular features of MB_{Group3}

MB_{Group3} occur in infancy and childhood, display a male predominance (2:1) and account for approximately 27% of all medulloblastomas. Both LCA and CLA histological appearances are observed in MB_{Group3}, with enrichment of LCA in infants. They are frequently metastatic with approximately 30-50% of patients presenting with distant disease. As such, MB_{Group3}, across all age groups, conveys the worst prognosis of all four molecular subgroups (Figure 1.23 and Figure 1.28). Despite this poor prognosis, little is known about the molecular biology of MB_{Group3} tumours. Certain genes associated with retinal development are over-expressed in this subgroup, but their role in tumourigenesis is unclear, and unlike MB_{WNT} and MB_{SHH} there is no defined molecular event or pathway implicated yet in the initiation of this tumour subgroup (Kool *et al.*, 2012; Northcott *et al.*, 2012a; Taylor *et al.*, 2012).

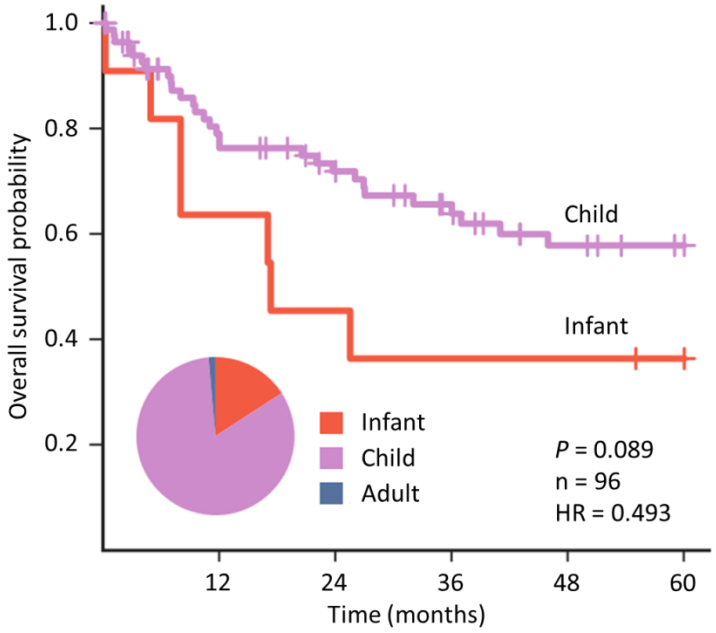

Figure 1.28 Kaplan-Meier overall survival curves for MB_{Group3}. Overall survival demonstrating a universally poor, but significantly worse outcome in infants, with MB_{Group3}. Figure adapted from Shih *et al.,* 2014.

Overall the MB_{Group3} genome is highly variable with copy number aberrations and tetraploidy being common events. High levels of *MYC* expression and frequent amplification is observed in up to 17% of MB_{Group3} tumours. Similarly, amplification and

overexpression of the orthodenticle Homeobox 2 gene (*OTX2*), which normally encodes a transcription factor involved in craniofacial and brain development but is believed to play an oncogenic role in medulloblastoma, is observed in approximately 8% of MB_{Group3}. Other cytogenetic abnormities include deletions of chromosome 10q (~50%), 16q (50%), and 17p (~40%), gains of 1q (35%), 7 (55%), and 17q (~60%) along with the combined loss of 17p and gain of 17q known as isochromsome 17 (i(17q)). *SMARCA4* (~10%) and *MLL2* mutations (4%), are also noted in this subgroup as they are in MB_{WNT} (Parsons *et al.*, 2011; Jones *et al.*, 2012; Kool *et al.*, 2012; Northcott *et al.*, 2012a; Northcott *et al.*, 2012b; Pugh *et al.*, 2012; Robinson *et al.*, 2012; Taylor *et al.*, 2012; Shih *et al.*, 2014).

1.8.8.3.2 Therapeutic stratification in MB_{Group3}

In the recent multivariate analysis by Shih *et al*., (2014) a selection of FISH biomarkers, including some of the cytogenetic aberrations associated with MB_{Group3} (*MYC*, Ch11, Ch17p and Ch17q) were assessed for their role in improving subgroup-specific prognostication. In this study patients with metastatic disease, i(17q) or *MYC* amplification identify a high-risk group of MB_{Group3}, but crucially the absence of all three of these poor prognostic markers reveals a standard-risk group of patients. This is in contrast to previous analyses by Kool *et al*., (2012), who observe a non-significant difference in OS between metastatic and non-metastatic MB_{Group3} . This may be due to cohort size or differing types of analyses between the two studies.

In addition to these attempts to improve prognostication in MB_{Group3}, patients with MB_{Group3} or MB_{Group4} tumours in the currently recruiting SJMB12 trial, (St Jude Children's Research Hospital, Memphis, TN), will receive chemotherapy that has demonstrated efficacy in pre-clinical MB_{Group3} models. This comprises of gemcitabine and pemetrexed, which are established cytotoxic drugs in the paediatric setting, cross the blood brain barrier and target purine, pyrimidine and folate metabolism. Both agents showed promise in pre-clinical medulloblastoma studies, where survival was significantly increased in MB_{Group3} neurospheres and mice harbouring both murine MB_{Group3} and patient derived xenografts of MB_{Group3} tumours (Morfouace *et al.*, 2014).

1.8.8.3.3 Mouse models of MB_{Group3}

Models of MB_{Group3} have been described following orthotopic transplantation of *Trp53*-inactivated cerebellar stem or progenitor cells which have been transformed by Myc expression (Kawauchi *et al.*, 2012; Pei *et al.*, 2012). The only spontaneous model of MB_{Group3} is the GTML (*Glt1–tTA/TRE–MYCN–Luc*) MYCN-driven transgenic mouse model which is described in detail in Chapter 4 (Swartling *et al.*, 2010; Poschl *et al.*, 2014). A summary of the key MB_{Group3} features are summarised in Figure 1.29.

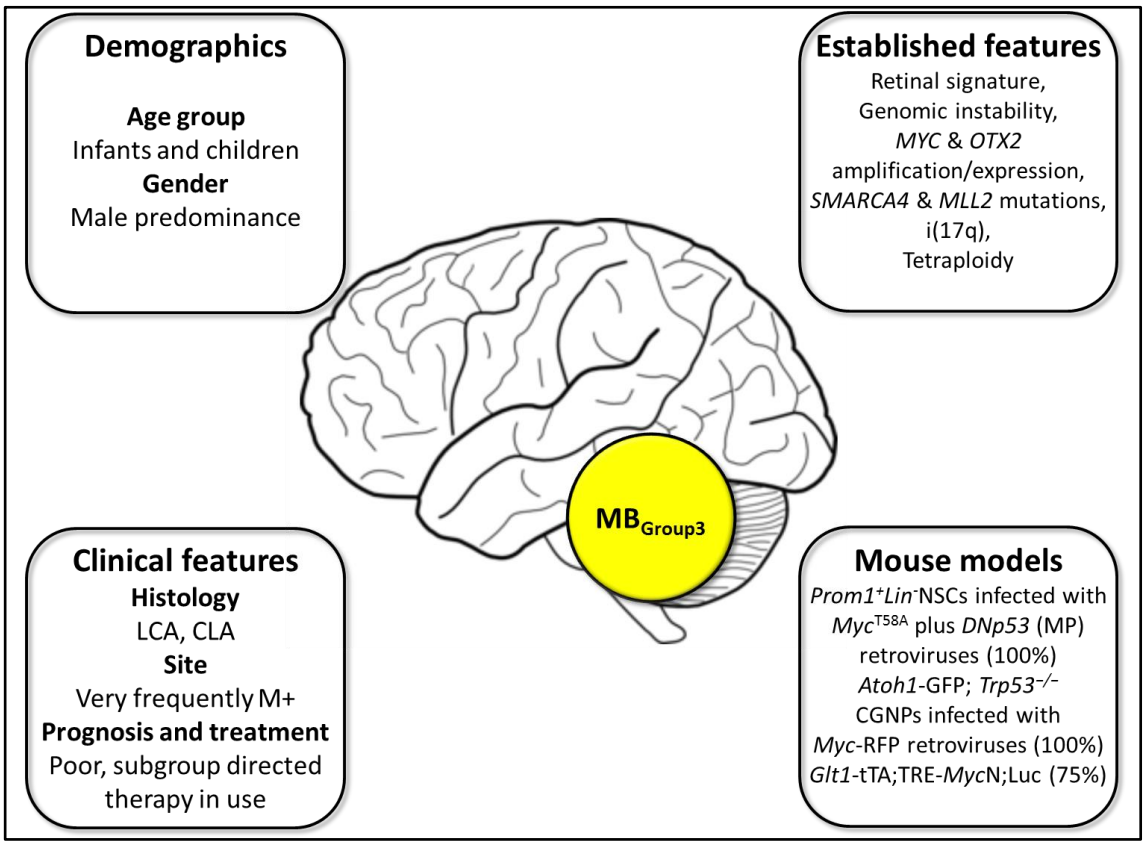

Figure 1.29 Summary of the main clinical, pathological, molecular features and mouse models associated with MB_{Group3}. LCA, large cell/anaplastic; CLA, classic histology; M+, metastatic disease; *Prom1*, prominin 1; Lin, lineage; NSCs, neural stem cells; Atoh1, atonal homologue 1; GFP, green fluorescent protein; CGNPs, cerebellar granule neuron precursors; RFP, red fluorescent protein; Glt1, glutamate transporter 1; tTA, tetracycline transactivator; Luc, luciferase. Mouse models; percentage tumour penetrance in parenthesis.

1.8.8.4 Group 4 subgroup

1.8.8.4.1 Clinical, pathological and molecular features of MB_{Group4}

This is the largest subgroup of medulloblastoma accounting for a third of all tumours diagnosed. MB_{Group4} have a male bias across all ages and occur predominantly in children but also occasionally in adults and infancy. They are often metastatic, display CLA histology and convey an intermediate prognosis. Similar to MB_{Group3}, the molecular pathogenesis of MB_{Group4} is not understood and while multiple expression analyses have noted the association, and over-representation of genes involved in neuronal development and differentiation, the underlying role these pathways play in MB_{Group4} development is unclear (Kool *et al.*, 2012; Northcott *et al.*, 2012a; Taylor *et al.*, 2012).

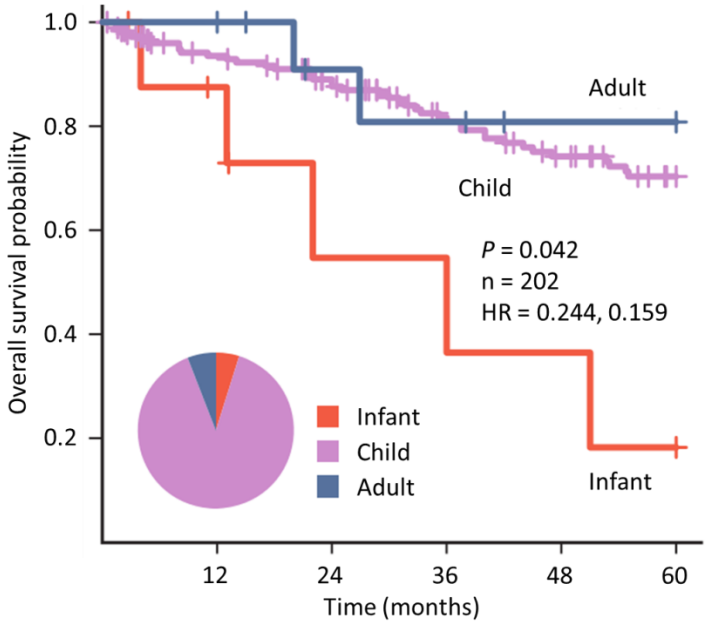

Figure 1.30 Kaplan-Meier overall survival curves for MB_{Group4}. Overall survival demonstrating an intermediate prognosis for MB_{Group4}, with a significantly worse outcome in the few infant-MB_{Group4}. Figure adapted from Shih *et al.,* 2014.

Tetraploidy, as well as recurrent cytogenetic abnormalities, such as amplification of *MYCN* and cyclin-dependent kinase 6 (*CDK6*), another proto-oncogene which normally assists in the regulation of cell cycle progression, are associated with approximately 6% and 5% of MB_{Group4} respectively. Loss of 17p as well as i(17q) is most frequently found in this subgroup and is the most common cytogenetic aberration (>60%). Deletions of *NFKBIA* and *USP4*, both components of the NF-κB pathway, are observed, and female

patients typically show loss of one copy of the X chromosome. In addition, there are reports of mutations in lysine (K)-specific demethylase 6A (*KDM6A,* 13%), *MLL3* (~5%), occasional *TP53* and *TERT* mutations as well as chromothripsis in MB_{Group4}. However, while *TERT* promoter mutations are a rare occurrence, in contrast to their presence in MB_{SHH}, initial findings suggest that these aberrations convey a poor prognosis (Parsons *et al.*, 2011; Jones *et al.*, 2012; Kool *et al.*, 2012; Northcott *et al.*, 2012a; Northcott *et al.*, 2012b; Pugh *et al.*, 2012; Rausch *et al.*, 2012; Robinson *et al.*, 2012; Taylor *et al.*, 2012; Remke *et al.*, 2013; Zhukova *et al.*, 2013; Shih *et al.*, 2014).

1.8.8.4.2 Therapeutic stratification in MB_{Group4}

Shih *et al*., (2014) proposed that stratifying patients with; metastatic MB_{Group4} as high-risk, loss of Ch11 or gain of Ch17 as low risk, and standard-risk as those patients who demonstrated none of these features, improves prognostication in this subgroup. Surprisingly no poor prognosis molecular markers were identified in these analyses, including *MYCN* amplification which is in contrast to its role in MB_{SHH}. These few and unclear observations, combined with the absence of known drivers of tumourigenesis, and critically no mouse models of MB_{Group4} (Poschl *et al.*, 2014), emphasise the urgent need for further study in MB_{Group4}, the most common molecular subgroup, and yet the most poorly understood (Figure 1.31).

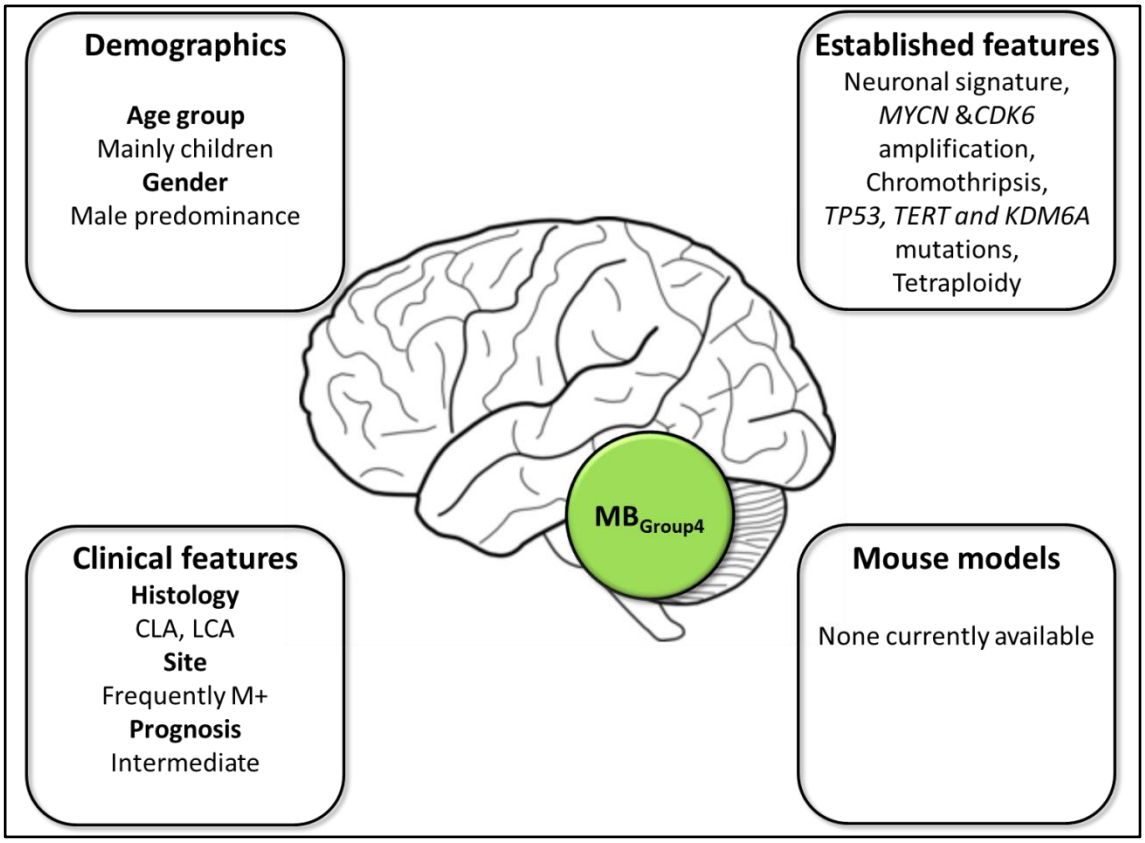

Figure 1.31 Summary of the main clinical, pathological and molecular features associated with MB_{Group4}. CLA, classic histology; LCA, large cell/anaplastic; M+, metastatic disease.

1.8.8.5 Summary of molecular subgrouping in medulloblastoma

The four molecular subgroups of medulloblastoma display unique clinical, pathological genetic and epigenetic features. Recent studies suggest that these subgroups represent distinct tumour entities with differing cells of origin. This is reflected in their varying gene expression and DNA methylation profiles, cytogenetic aberrations and mutation spectrum. However, there is also crossover between the molecular aberrations found across subgroups, such as *TP53* mutations, *MYC* and *MYCN* amplifications, as well as a variety of recently described mutations in histone and chromatin modifiers (*e.g. SMARCA4, MLL*2, *MLL3* and *KDM6A*). The interplay of many of these aberrations, as well as clinicopathological features varies according to molecular subgroup. In view of this data, it is now clear that pre-clinical research, clinical treatment stratification and future therapies, alongside extended survival analyses in medulloblastoma, must now be interpreted in the context of molecular subgroup.

1.9 Relapsed medulloblastoma

1.9.1 Impact, survival and treatment of relapsed disease

Overall survival rates for children diagnosed with medulloblastoma are approximately 80% for patients with standard-risk disease and 25-65% for high-risk disease. Despite improved survival rates, recurrence will occur in over 30% of patients with an enrichment of relapses in the infant age group, attributable to the avoidance of CSI in this patient population. Relapsed disease is almost universally fatal, and is therefore the single leading cause of death for children with medulloblastoma. (Crawford *et al.*, 2007; Pizer and Clifford, 2008; Pizer and Clifford, 2009; Dunkel *et al.*, 2010; Ellison, 2010; Gajjar *et al.*, 2012; Jones *et al.*, 2012; Northcott *et al.*, 2012a; Ramaswamy *et al.*, 2013).

In view of these dismal outcomes for relapsed disease, various treatment strategies have been administered including protocols consisting of re-resection, high-dose chemotherapy with stem cell rescue, and salvage radiotherapy for unirradiated patients (Gajjar *et al.*, 1994; Grodman *et al.*, 2009; Massimino *et al.*, 2009; Dunkel *et al.*, 2010; Gajjar and Pizer, 2010; Pizer *et al.*, 2011a). Together, the administration of high-dose chemotherapy across multiple studies for medulloblastoma and CNS-PNET recurrences, achieves an overall survival of less than 5% (Gajjar and Pizer, 2010).

Other more novel combinations have been attempted, such as metronomic therapy, oral etoposide, temozolamide, irinotecan and the *VEGFA* inhibitor bevacizumab, as well as phase I trials of the SHH pathway inhibitor, Vismodegib (GDC-0449). However, many of these studies are case reports or phase I/II trials, aimed at establishing the maximum tolerated dose of an agent, assessing adverse effects and investigating disease response. The intention of these studies is not to achieve cure, and therefore often does not have long term survival data. However, Aguilera *et al*., (2013) does report a PFS of 15-55 months in three patients who received bevacizumab, temozolamide and irinotecan at relapse. Padovani *et al*., (2011) reported an isolated long term survivor, (median follow-up 28 months), following the administration of metronomic temozolamide alongside re-irradiation. Similarly, Kim *et al*., (2013) reported an isolated long term survivor following high-dose chemotherapy and radiotherapy, and one long term survivor following combination chemotherapy alone

(Ruggiero *et al.*, 2010; Sterba *et al.*, 2010; Aguilera *et al.*, 2011; Padovani *et al.*, 2011; Sondhi *et al.*, 2012; Aguilera *et al.*, 2013; Gajjar *et al.*, 2013; Grill *et al.*, 2013; Kim *et al.*, 2013).

Despite this variety of treatments, there is no standard of care for children suffering from relapsed medulloblastoma. None of the therapies discussed have shown any consistent benefit, or improvement in long term survival, with the exception of a minority of radiotherapy naive infants who receive this modality of treatment at relapse, albeit with significant neurological long term effects (Muller *et al.*, 2014). In the study by Muller *et* al., (2014), seventeen patients, the majority of whom were infants at diagnosis (median age 2.9 years, range 1.7-5 years), underwent CSI as part of a salvage strategy at relapse. Eleven of these patients progressed and died. However the 5 year OS was reported as 39%, suggesting that a small number of infants who did not receive CSI at initial diagnosis, could benefit and survive long term following CSI delivery at relapse (Muller *et al.*, 2014).

1.9.2 The biology of relapsed disease

As already discussed in section 1.8, there has been an impressive expansion of genomic and epigenomic human data, alongside *in vitro* and *in vivo* studies, leading to a better understanding of medulloblastoma biology at diagnosis. However, this has not occurred in the disease at relapse with only two published studies to date, summarised below, which have interrogated the biology of recurrent medulloblastoma (Korshunov *et al.*, 2008; Ramaswamy *et al.*, 2013).

1.9.2.1 Accumulation of molecular aberrations in medulloblastoma at relapse

The hypothesis of the study by Korshunov *et al.*, (2008), based on observations in other tumour types, was that medulloblastoma exhibited molecular progression at relapse. Korshunov *et al*., (2008), collated a cohort of 28 medulloblastoma tumours sampled at relapse, which were paired with their counterpart tumours sampled at diagnosis. This study was carried out prior to the current understanding of molecular subgrouping in medulloblastoma, and aimed to compare recurrence patterns and pathological subtype, alongside a panel of five cytogenetic markers. The markers

selected (*MYC*, *MYCN*, 17p, 17q and 6q), were assessed by FISH and utilised to determine whether molecular progression over time occurred in medulloblastoma.

At diagnosis 26/28 (93%) patients had M0 disease, and all patients received multimodal therapy consisting of neurosurgical resection, CSI and adjuvant chemotherapy (vincristine, lomustine and cisplatin). There was a male preponderance (3:1, male: female), with a median age at recurrence of 14 years (range 3-37). Early relapses occurred in 16/28 (57%) cases, which was defined as disease recurrence less than 4 years after initial diagnosis. Thirteen cases had isolated local recurrences, six demonstrated local disease with leptomeningeal spread (one of these patients had spread outside the CNS as well) and nine had isolated leptomeningeal disease. All patients underwent surgical re-resection at recurrence with eighteen samples obtained from the local recurrence, and ten samples from metastatic disease sites.

Patients with LCA disease at diagnosis (n=4) had a significantly shorter time to relapse ($p< 0.001$). Interestingly ten patients exhibited histopathological changes, with CLA histology in their tumours sampled at diagnosis evolving to demonstrate features of anaplasia in their respective tumours at relapse. Thirteen tumours showed cytogenetic aberrations at diagnosis, and this group of patients had a non-significant reduction in both time to relapse and OS. At relapse, seven tumours demonstrated cytogenetic aberrations not previously observed in their paired tumour at diagnosis, with abnormalities of 17q most commonly acquired (n=5). Gain of 6q (n=2) and *MYCN* (n=2) amplification, were also observed in samples taken at relapse where the diagnostic profiles were balanced. Both examples of acquired 6q gain occurred in tumours which also acquired 17q abnormalities. Conversely, two metastatic lesions sampled at relapse showed maintenance of i(17)q but loss of *MYCN* amplification.

This study was the first published dataset to report the temporal progression and accumulation of both histopathological and cytogenetic events in medulloblastoma. While only a limited set of biological features were assessed, Korshunov *et al*., (2008), provided the first insights into the biology of recurrent disease highlighting that firstly, it is not always the same as the disease at diagnosis, and secondly, further studies are required to improve understanding and outcomes for this fatal disease.

1.9.2.2 Subgroup-specific patterns of relapse in medulloblastoma

Ramaswamy *et al*,. (2013) combined three independent cohorts (cohort 1, n=5; cohort 2, n=29; cohort 3, n=17) of relapsed medulloblastoma samples, paired with tumours taken at diagnosis. Molecular subgroup was assigned at both diagnosis and relapse in cohort 1 and 2 by nanoString (Northcott *et al.*, 2011c), a targeted gene expression profiling technique, which revealed that molecular subgroup did not change between diagnosis and relapse. This finding was confirmed in cohort 3 where a panel of four immunohistochemistry antibodies, which had previously been reported (MB_{WNT}, β-catenin; MB_{SHH}, SFRP1; MB_{Group3}, NPR3 and MB_{Group4}, KCNA1), was adopted to assign molecular subgroup in this latter validation cohort (Clifford *et al.*, 2006; Northcott *et al.*, 2011b).

Patterns and timings of recurrence were analysed in a subgroup-specific manner, in extended cohorts, where tumour tissue was not available at relapse and subgroup had been assigned on samples obtained at diagnosis (cohort 1, n=30; cohort 2, n=77; cohort 3, n=96). This report suggests that there are subgroup-specific patterns of relapse, with local recurrences dominating in MB_{SHH} and distant relapses occurring more frequently in MB_{Group3} and MB_{Group4}. Relapse disease in MB_{WNT} was unsurprisingly rare, given their overall good prognosis (section 1.8.8.1), and MB_{Group4} tumours had a prolonged time to death (TTD). This study provides further evidence to support the notion that the four molecular subgroups within medulloblastoma are distinct, with subgroup stability over time strengthening the evidence that they arise from different cells of origin (section 1.8.8.1 and 1.8.8.2). Ramaswamy *et al*,. (2013) also reinforces the importance of analysing medulloblastoma in the context of the four molecular subgroups at all time-points in the disease course, and provides initial insights into the subgroup-specific patterns of disease relapse.

1.10 Summary and aims

Medulloblastoma is the most common malignant CNS tumour of childhood. Current survival rates following multi-modal therapy have plateaued at approximately 80% for children with standard-risk disease, and 25-65% for those displaying high-risk features. Moreover, the long term neurological sequelae following multimodal treatment highlights that advances in our therapeutic strategies are essential if we are to not only improve survival, but the quality of that survival as well. Consequently in recent years there has been a rapid expansion of data on the disease at diagnosis. This has led to the identification of four distinct molecular subgroups with unique demographic, clinical, pathological, epigenetic and genetic features, and it is now believed that these four subgroups represent distinct disease entities with different cells of origin.

Two of the medulloblastoma molecular subgroups are well characterised (MB_{WNT} and MB_{SHH}) and treatment reductions are either in place, or planned for MB_{WNT}, and phase I trials are underway for SHH pathway inhibitors in the disease. Despite these developments, there is still a greater understanding of these two subgroups required, such as the interplay of other features and novel events on prognosis. Little is known about the driving events in MB_{Group3} and MB_{Group4} which represent the poorest prognosis or largest subgroup observed, respectively. Efforts therefore continue to focus predominantly on the characterisation, modelling and discovery of novel events in the disease at diagnosis.

Relapsed medulloblastoma is almost universally fatal. Typically only infants who are treated at recurrence with salvage radiotherapy have a chance of surviving their disease. Despite this dismal outcome, and the appreciation of the natural course of the disease, *i.e.* patients rarely die from other causes except disease recurrence, very little is understood about relapsed disease. At present there is no unifying treatment approach or trial for relapsed medulloblastoma. This has made studying the disease at recurrence difficult, and is compounded by the fact that routine sampling of a suspected recurrent lesion is rarely performed, as the diagnosis is commonly made by radiological assessment alone. Therefore there have only been two published studies which have attempted to interrogate the biology of medulloblastoma at relapse.

The characterisation of medulloblastoma at relapse is crucial to providing future new therapeutic targets and critical insights into the biology of the disease. This in turn, may identify patients at greater risk of disease recurrence, enabling their upfront treatment to be escalated and tailored accordingly, and their risk of recurrence reduced. Moreover, the identification of molecular events at disease relapse, could be explored in the future as therapeutic targets, proving new approaches to control or cure disease at this time-point. This project therefore aims to comprehensively investigate the clinical, pathological and molecular features of relapsed medulloblastoma, and provide essential new understanding into the mechanisms of disease recurrence to identifying events predictive of or specific to relapse.

The aims and approaches undertaken are;

1. Assemble a large cohort of relapsed tumours, paired with their diagnostic counterparts. Within this cohort, comprehensively characterise all the established molecular features with validated relationships to prognosis currently understood in the disease at diagnosis, with the aim of identifying associations between relapsed medulloblastoma features and disease behaviour. These events could next be explored as either prognostic biomarkers or therapeutic targets in the medulloblastoma at recurrence (Chapter 3 and Chapter 4).

2. Interrogate the epigenome of relapsed medulloblastoma utilising the paired relapsed cohort assembled in Chapter 3, to identify events specific to or predictive of relapse. Validate these discoveries with relation to expression, in an independent cohort, and provide the foundation for future functional work to identify novel epigenetic events in relapsed medulloblastoma. These epigenetic events could further be exploited as either prognostic biomarkers or therapeutic targets (Chapter 5).

3. Assemble a large cohort of medulloblastoma tumour samples taken at diagnosis from patients who have subsequently relapsed with their disease. Utilise this extensively characterised relapsing cohort to investigate the subgroup-specific clinical, pathological and molecular features of relapsed disease at diagnosis, which may further inform disease course and behaviour at relapse. Moreover, this relapsing cohort provides an additional future resource to either identify prognostic biomarkers, or investigate the utility of events discovered in aims 1 and 2, that may be predictive of relapse (Chapter 6).

Chapter 2. Materials and Methods

2.1 Extraction of nucleic acids

Extractions of tumour DNA from FFPE (formalin fixed, paraffin embedded) and tumour DNA and RNA from frozen material were performed by myself, Dr Janet Lindsey and Ms Amanda Smith (PBTG). Extracted tumour DNA was also kindly provided by Dr Michael Taylor (Arthur and Sonia Labatt Brain Tumour Research Centre, Hospital for Sick Children, University of Toronto, Toronto, Canada) and Prof Stefan Pfister (Department of Paediatric Haematology and Oncology, Heidelberg University Hospital, Heidelberg, Germany).

2.1.1 DNA extraction

DNA extractions from FFPE tumour material were performed using the Qiagen QIAamp ® DNA FFPE tissue kit (Qiagen, Venlo, Netherlands) according to the manufacturer's instructions. High molecular weight DNA was obtained from frozen tissue using the Qiagen DNeasy ® blood and tissue kit (Qiagen, Venlo, Netherlands). Extracted DNA was stored at -80°C.

2.1.2 Quality control of DNA

2.1.2.1 NanoDrop spectrophotometry

DNA was assessed using the NanoDrop 1000 Spectrophotometer (Thermo Fisher Scientific, Waltham, MA, USA). NanoDrop spectrophotometry is able to measure nucleic acid concentrations as low as 1ng/µl and purity in liquid samples as small as 1µl by utilising the differences in optical density between nucleic acids and protein. Nucleotides, DNA and RNA all absorb UV light at a wavelength of 260nm. The greater the amount of DNA or RNA in a sample, the more UV light is absorbed, providing a measure of sample DNA or RNA concentration. The absorbance ratio at wavelengths 260nm/280nm (maximum protein absorbency) is utilised to assess the purity of a sample, as impurities have absorbance at different wavelengths *e.g.* EDTA, phenol and carbohydrates, wavelength of 230nm (Sedlackova *et al.*, 2013).

2.1.2.2 Qubit ® fluorometer

Double stranded DNA (dsDNA) was evaluated using the Qubit ® PicoGreen dsDNA broad-range assay kit according to the manufacturer's instructions (Invitrogen, Carlsbad, CA, USA). This assay is highly selective for dsDNA and uses intercalating fluorescent dyes to determine DNA concentrations as low as 25pg/ml. Whilst the

PicoGreen reagent is not specific to dsDNA, once bound to dsDNA, fluorescent enhancement is 1000-fold greater than bound PicoGreen reagent to single stranded DNA (ssDNA, Figure 2.1). It is also able to detect RNA-DNA hybrids, and as a result of these features is able to reliably quantify dsDNA, the main advantage over NanoDrop spectrophotometry (Sedlackova *et al.*, 2013).

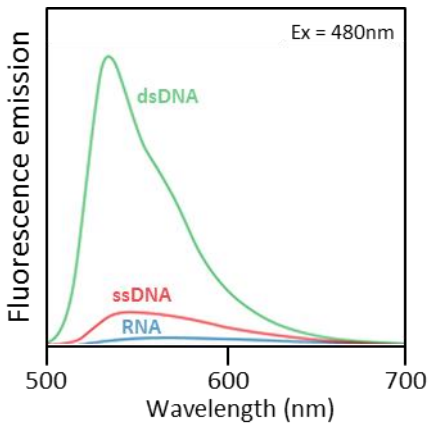

Figure 2.1 Illustrative example demonstrating the difference in fluorescence emission between dsDNA, ssDNA and RNA upon binding to the PicoGreen dsDNA reagent. Figure taken from Life Technologies, Nucleic acid quantitation in solution, www. lifetechnologies.com.

2.1.3 RNA extraction

RNA was extracted using Trizol reagent (Invitrogen, Carlsbad, CA, USA) according to manufacturer's guidelines. Extracted RNA was stored at -80 °C.

2.1.4 Quality control of RNA

Assessment of the quantity and integrity of total RNA was performed using the Agilent RNA 6000 Nano Kit on the Agilent Bioanalyzer (Agilent Technologies, Santa Clara, CA, USA) according to the manufacturer's instructions. This system allows visualisation of RNA integrity and impurities, has a quantitative range of 25-500ng/µl, and reports the RNA Integrity Number (RIN), which is a software tool designed to provide a measure of RNA degradation.

2.1.5 Combined DNA/RNA extraction

Combined extractions of tumour DNA and RNA were carried out using the Qiagen AllPrep extraction kit using standard methods (Qiagen, Venlo, Netherlands). Quality

control of extracted nucleic acids was performed as descried in section 2.1.2 and 2.1.4. Extracted products were stored at -80 °C.

2.2 Histopathology

Immunohistochemistry slides were prepared by Ms Sarah Leigh Nicholson (former member of the PBTG), Miss Anna Long (former member of the PBTG) and Dr Stephen Crosier (PBTG). FFPE tumour blocks were sectioned at a thickness of 5µm on a microtome, floated in a water bath at 40°C, and transferred onto Superfrost Plus slides (VWR International, East Grinstead, UK). A panel of stains were performed using standard techniques, to assess the medulloblastoma pathological variant according to the current 2007 World Health Organization (WHO) classification of central nervous system tumours (Louis *et al.*, 2007).

The immunohistochemical stains undertaken were; H&E, for morphological assessment; reticulin, for morphological assessment and expression in DN variant of medulloblastoma; GFAP, normally expressed in astrocytes within the CNS; synaptophysin, expressed in the intranodular regions of DN medulloblastoma; neurofilament protein expression, differentiates neurons from glial cells; Ki-67, marker of cellular proliferation; Vimentin, mesenchymal expression; INI-1, differentiates between medulloblastoma (immunopositive) and ATRT (immunonegative); β-catenin, nuclear localisation in MB_{WNT} (section 1.8.8.1); and p53, nuclear expression in p53 pathway disruption.

Central pathology review was performed according to the current 2007 WHO classification of tumours (Louis *et al.*, 2007) by three neuropathologists, Dr Thomas Jacques, Prof Stephen Wharton and Dr Keith Robson, from the CCLG. Pathological variant was assigned as CLA, DN, MBEN or LCA, as described in section 1.8.4. If the pathological variant was unable to be assigned it was recorded as a medulloblastoma not otherwise specified (MB_{NOS}).

2.3 Polymerase Chain Reaction

PCR was first described in the 1980s by Kary Mullis (Mullis *et al.*, 1986) and is a technique used to specifically amplify a segment of DNA. To target the desired DNA, primers of 18-25 nucleotides in length are designed to complement the DNA sequences which flank the target DNA segment. In designing primers, the nucleotide sequence selected should not be repeated elsewhere in the genome and ideally have an even distribution of the four bases Cytosine (C), Guanine (G), Thymine (T) and Adenine (A). The melting temperature (T_m, mid-point in the transition between dsDNA and ssDNA) of the forward and reverse primers should also be within 5°C of each other (Dieffenbach *et al.*, 1993).

The process of PCR consists of three stages; denaturation, primer annealing and DNA synthesis. Denaturation of human DNA, where hydrogen bonds between dsDNA break forming ssDNA, typically occurs at approximately 94°C. The conditions for primer annealing depends on the T_m of the primer pairs but is usually 5°C below the T_m (50-70°C) and allows the primers to align to their complementary DNA sequence. Finally, DNA synthesis, which occurs at 70-75 °C in the presence of DNA polymerase and the four deoxyribonucleotide triphosphates (dNTP), is the process whereby primers initiate the creation of the desired complementary DNA. This process is repeated in cycles to allow for the exponential amplification of the desired DNA product.

2.3.1 TP53 mutation analysis

PCR based direct sequence analysis of exons 2-11 (Table 2.1), within the DNA binding domain of *TP53*, was performed on all samples within the paired relapse cohort (Chapter 3). Following the identification of mutations within exons 5-8, alongside the latest understanding of *TP53* mutation distribution in medulloblastoma (Zhukova *et al.*, 2013), all samples within the relapsing cohort (Chapter 6) were screened for *TP53* mutations in exons 5-8 only. Fast PCR was optimised for all exons (2-11) in this mutation screen, which used a hot start polymerase system, a technique which increased the specificity and reduced the time taken to perform the PCR reactions.

One 20µl reaction required 2µl of both forward and reverse primers (Table 2.1), at a final concentration of 10µM, 5µl of RNAase free water, 25ng of total tumour DNA (in 1µl of RNAse free water) and 10µl of GeneAmp® Fast PCR Master Mix (Life

Technologies, Paisley, UK). A negative control of the same reaction mix without DNA was performed for each experiment to confirm that there was no DNA contamination of the reagents. PCR reactions were run on the Applied Biosystems® 9800 Fast Thermal Cycler (Life Technologies, Paisley, UK, Table 2.2).

Location	Forward sequence 5'-3'	Reverse sequence 5'-3'
Exon 2	CCAGGGTTGGAAGCGTCTC	GACAAGAGCAGAAAGTCAGTCC
Exon 3/4	CATGGGACTGACTTTCTGCTC	CTTCATCTGGACCTGGGTCT
Exon 4 (part)	GGACGATATTGAACAATGGTT	ATGGAAGCCAGCCCCTCAG
Exon 4	GGCTGAGGACCTGGTCCTCTGA	GCCAGGCATTGAAGTCTCATGG
Exon 5	ATCTGTTCACTTGTGCCCTG	CAACCAGCCCTGTCGTCTCTC
Exon 6	GCCTCTGATTCCTCACTGAT	GGAGGGCCACTGACAACCA
Exon 7	AAGGCGCACTGGCCTCATCTT	CAGGGGTCAGAGGCAAGCAGA
Exon 8	GAGCCTGGTTTTTTAAATGG	TTTGGCTGGGGAGAGGAGCT
Exon 9	AGCGAGGTAAGCAAGCAGG	GCCCCAATTGCAGGTAAAACAG
Exon 10	CTTCTCCCCCTCCTCTGTTGC	GAAGGCAGGATGAGAATGGA
Exon 11	GGCACAGACCCTCTCACTCAT	TGCTTCTGACGCACACCTATT

Table 2.1 Primer sequences for *TP53* mutation screen. Forward and reverse nucleotide sequences for primer pairs utilised in the PCR reactions for exons 2-11 of the *TP53* gene.

Temperature	Time	Cycles
95°C	45 seconds	
94°C	0 seconds	35
64°C	15 seconds	
72°C	45 seconds	
4°C	Hold	

Table 2.2 Thermocycler settings for fast PCR reaction. Temperature settings, duration and number of cycles required for fast PCR reaction; exons 2-11 of the *TP53* gene.

2.3.2 CTNNB1 mutation analysis

PCR of the GSK-3β phosphorylation domain of *CTNNB1* (nucleotides 791-1070), the mutational hotspot within the *CTNNB1* gene associated with MB_{WNT} subgroup membership, was analysed using a standard PCR technique (Ellison *et al.*, 2005; Taylor *et al.*, 2012). One 20µl reaction contained 2µl of both forward and reverse primers (10µM final concentration, Table 2.3), 2µl of PCR buffer, 1.5µl $MgCl_2$ (10mM), 0.8µl dNTP (5mM), 0.2µl of *Taq* polymerase (5U/ µl), 9.5µl of RNAse free water and a total of

50ng of DNA (25ng/µl). A negative control of the same reaction mix without DNA was performed for each experiment to confirm that there was no DNA contamination of the reagents. The PCR reaction was run on the GeneAmp ® PCR System 9700 thermocycler (Applied Biosystems, Life Technologies, Paisley, UK) with the following settings (Table 2.4).

Forward sequence 5'-3'	Reverse sequence 5'-3'
TCCAATCTACTAATGCTAATACTG	TAAGGCAATGAAAAATAATACTC

Table 2.3 Primer sequences for *CTNNB1* mutation screen. Forward and reverse nucleotide sequences for the primer pairs utilised in the PCR reaction for *CTNNB1*.

Temperature	Time	Cycles
95°C	45 seconds	
95°C	30 seconds	
53°C	30 seconds	40
72°C	30 seconds	
72°C	5 minutes	
4°C	Hold	

Table 2.4 Thermocycler settings for standard PCR reaction. Temperature settings, duration and number of cycles required for *CTNNB1* PCR reaction.

2.3.3 Agarose gel electrophoresis

Agarose gel electrophoresis was used to separate different length strands of amplified DNA. It works on the principle that DNA, being negatively charged, will travel through an agarose gel when an electrical current is passed through the gel. Different percentage (w/v) gels can be made, with lower percentage (w/v) gels allowing the travel of larger DNA strands and *vice versa* for smaller DNA segments. A DNA ladder is run alongside the amplified product to allow estimation of the DNA strand length and confirmation of the desired PCR product.

For both *TP53* and *CTNNB1* mutational analysis, gel electrophoresis on a 2% (w/v) agarose gel confirmed the presence and length of the desired amplified product (Figure 2.2). The 2% (w/v) agarose gel was made by microwave heating 40mls of 1xTris-Borate-EDTA (TBE, Table 2.5) with 0.8g of molecular grade agarose powder

(Bioline, London, UK). Once dissolved, 4µl of GelRed™ Nucleic Acid Gel Stain (Biotium, Hayward, CA, USA) was added to the solution. Gels were cast in appropriately sized moulds with combs to create individual wells (Scientific Laboratory Supplies, East Riding, UK), set at room temperature and immersed in 1xTBE gel bath (Scientific Laboratory Supplies, East Riding, UK). The first well was loaded with 4µl of PCR markers (Promega, Madison, WI, USA) as a reference DNA ladder. Subsequent wells were loaded with 5µl of PCR product, which had all been individually premixed with 1µl of PCR loading dye (Promega, Madison, WI, USA). Gels were run at 150volts for 10 minutes and visualised under UV light using a G:Box (Syngene, Cambridge, UK).

Component	Amount
H_2O	700ml
Tris	108g
Boric acid	55g
EDTA (0.5M)	40ml
Additional H_2O is added to male a final volume of 1l Made to pH 8.3 using additional Hydrochloric acid	

Table 2.5 Recipe for 10xTBE. 1xTBE; 100ml of 10xTBE added to 900mls of H_2O.

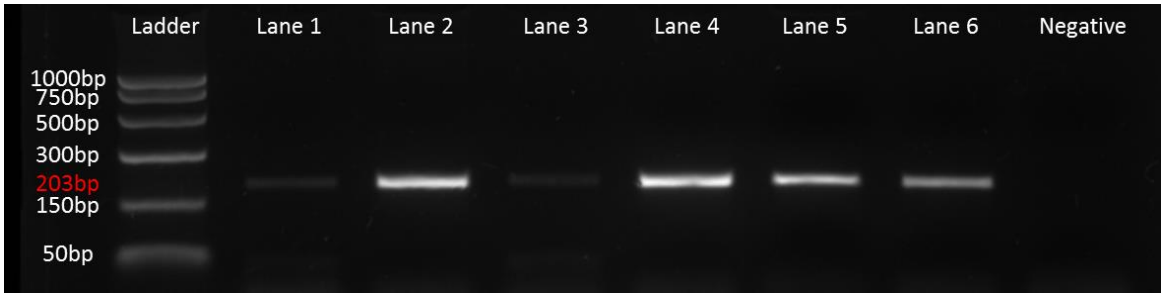

Figure 2.2 Gel electrophoresis demonstrating amplified PCR products. Lane 1-6 all show DNA bands for exon 6, *TP53*. Lane 1 and 3 show low intensity bands, reflecting the differing quality of DNA extracted from tumour samples. Negative control is blank confirming that there is no DNA contamination of the reagents. Ladder band sizes are shown (left) and PCR product size is highlighted in red; bp, base pairs.

2.3.4 PCR purification

PCR purification was undertaken using the Purelink® PCR Purification Kit (Life Technologies, Paisley, UK) according to the manufacturer's instructions. Samples were stored at 4°C until sequenced.

2.4 DNA Sequencing

Sanger sequencing was first described in 1977 by Frederick Sanger and colleagues (Sanger *et al.*, 1977). It is an enzymatic method where ssDNA is the template for making complementary DNA using DNA polymerase. There are four reactions using the four dNTPs (ATP, TTP, CTP and GTP), along with a dideoxynucleotide (ddNTP), which lacks a hydroxyl group at both the 2' and 3' carbon positions and acts as a chain terminator. Automated DNA sequencing utilises fluorophores, a non-isotopic chemical group, to label the primers and dNTPs enabling the four reactions to occur simultaneously. As the reactions occur the DNA strand, now labelled with distinct fluorophores, elongates until the ddNTP is randomly inserted ending the reactions and terminating the chain. During automated sequencing the intensity of the fluorescent signals from the labelled DNA strand is recorded and outputted as an intensity profile for each of the four fluorophores, allowing the sequence to be read and interpreted (Figure 2.3). Sanger sequencing was outsourced in this study to DBS GENOMICS (Durham University, UK) and Eurofins Genomics (Ebersberg, Germany) and performed on an ABI sequencer (Applied Biosystems, Life Technologies, Paisley, UK). Sequence analysis was undertaken on SeqMan 5.05, MegAlign 5.05 (©1993-2002 DNASTAR) and Mutation Surveyor (Dna Variant Analaysis, SoftGenetics, PA, USA).

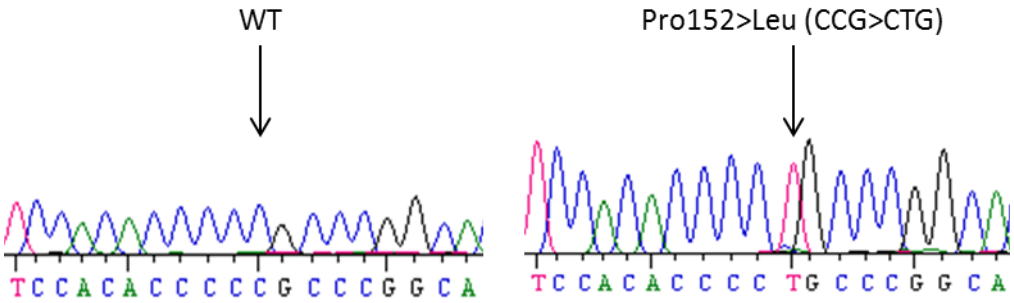

Figure 2.3 Sequence analysis of *TP53* exon 5. Wild type (WT) sequence is shown on the left panel, homozygous missense mutation demonstrated on the right panel. Pro, proline, Leu, leucine.

2.5 Next Generation Sequencing

Next generation sequencing is a high throughput sequencing technology which parallelises the sequencing process and enables thousands to millions of sequencing reads to be produced. The Fluidigm Access Array System (Fluidigm Corporation, San Francisco, CA, USA) combines tagged, target specific primers with sample specific primer pairs, (four primer amplicon tagging scheme), which reduces the time required for enrichment of the target sequence. Target specific primers for exon 5 of *TP53* were used as previously described (Grossmann *et al.*, 2011), and combined a sequence specific primer and a universal Fluidigm tag (Table 2.6).

Location	Forward sequence 5'-3'	Reverse sequence 5'-3'
Fludigm tag	ACACTGACGACATGGTTCTACA	TACGGTAGCAGAGACTTGGTCT
Exon 5	CACTTGTGCCCTGACTTTCA	CACTCGGATAAGATGCTGAGG

Table 2.6 Next generation sequencing target specific primers for *TP53*, exon 5. Forward and reverse nucleotide sequences for the primers required for the Fluidigm tag and exon 5 of the *TP53* gene.

PCR reaction preparation (Table 2.7), and thermocycler settings (Table 2.8), were performed as per the Fluidigm Access Array System directions (Fluidigm Corporation, San Francisco, CA, USA). PCR fragment size and quantitation size were confirmed using the Agilent DNA 1000 Kit for the Agilent 2100 BioAnalyzer (Agilent Technologies, Santa Clara, CA, USA). PCR products were purified using the Agencourt AMPure beads according to the manufacturer's instructions (Beckman Coulter UK Ltd, High Wycombe, UK). In brief, PCR products were bound to AMPure magnetic beads, allowing the separation of contaminants, which were aspirated, from bound products. PCR fragments were washed in 70% ethanol, air dried and then eluted in PCR certified water. The AMPure magnetic beads were separated from the eluted PCR fragments using the DynaMag™-96 Side Skirted Magnetic Particle Concentrator (Invitrogen, Carlsbad, CA, USA). Purified PCR products were then combined with barcoded primers from the Access Array Barcode Library, pooled and run in a single sequencing experiment on the 454 FLX titanium sequencer (454 Life Sciences, a Roche company, CT, USA).

Component	Volume per reaction (µl)	Final concentration
10x FastStart High Fidelity Reaction Buffer without $MgCl_2$ *	0.5	1x
25 mM $MgCl_2$ *	0.9	4.5mM
Dimethyl sulfoxide (DMSO) *	0.25	5%
10mM PCR Grade Nucleotide Mix *	0.1	200µM each
5 U/µl FastStart High Fidelity Enzyme Blend *	0.05	0.05 U/µl
20x Access Array Loading Reagent #	0.25	1x
2 µM Access Array Barcoded Primers # for the 454 FLX Titanium Sequencer *	1	400nM
DNA	0.83	10ng/µl
RNAase free water	0.12	10mM
Target Specific Primers #	1	
Total	5	

* Roche, Indianapolis, IN, USA

Fluidigm, San Francisco, CA, USA

Table 2.7 Reaction preparation for next generation sequencing. Each component of the reaction alongside the final volume and concentration per reaction are shown. Current suppliers of every component are also highlighted.

Temperature	Time	Cycles
50°C	2 minutes	1
70°C	20 minutes	1
95°C	10 minutes	1
95°C	15 seconds	10
60°C	30 seconds	
72°C	1 minute	
95°C	15 seconds	2
80°C	30 seconds	
60°C	30 seconds	
72°C	1 minute	
95°C	15 seconds	8
60°C	30 seconds	
72°C	1 minute	
95°C	15 seconds	2
80°C	30 seconds	
60°C	30 seconds	
72°C	1 minute	
95°C	15 seconds	8
60°C	30 seconds	
72°C	1 minute	
95°C	15 seconds	5
80°C	30 seconds	
60°C	30 seconds	
72°C	1 minute	

Table 2.8 Thermocycler settings for next generation sequencing PCR reaction.
Temperature settings, duration and number of cycles required for the PCR reaction prior to next generation sequencing of exon 5 of the *TP53* gene are shown.

2.6 Fluorescence *in situ* hybridisation (FISH)

FISH is a cytogenetic technique used to detect chromosomal abnormalities such as amplifications, deletions and translocations. DNA probes which hybridise to the chromosome are either labelled directly or indirectly with fluorophores, which can be visualised using certain wavelengths of light. The digoxigenin and the biotin-streptavidin system are two common examples of indirect labelling. DNA probes are labelled indirectly, with a nucleotide containing a modified reporter molecule such as digoxigenin (*Digitalis* steroid) or biotin (vitamin B_7). In the digoxigenin system, a digoxigenin-specific antibody acts as a fluorescently labelled affinity molecule, binding to the reporter molecule (digoxigenin) after it has been incorporated into the DNA, and thus allows for detection of the reporter molecule. For the biotin-streptavidin technique, streptavidin is the fluorescently labelled affinity molecule which binds to biotin, the reporter molecule.

2.6.1 Probe preparation

Bacterial artificial chromosome (BAC) cloned DNA sequences (Wellcome Trust Sanger Institute, Cambridge, UK) were used as probes for the four chromosomal regions of interest; *MYC*, *MYCN*, chromosome 17p and 17q (Lamont *et al.*, 2004). These probes were subsequently labelled using the nick-translation technique. Using this method, single strand breaks known as 'nicks' are introduced by an endonuclease into the DNA. As a result, the exposed 3' terminus of the nick acts as a start point for the introduction of fluorescently labelled nucleotides. Using DNA polymerase the labelled nucleotides replace the existing nucleotides, which are removed 5' to 3', and the DNA sequence is translated.

DNA probes were labelled using the Nick-Translation Kit (Vysis, Abbott Molecular, IL, USA). The reaction was combined according to the manufacturer's instructions (Table 2.9), briefly centrifuged and vortexed, and then incubated at 15°C for 16 hours on the GeneAmp ® PCR System 9700 thermocycler (Applied Biosystems, Life Technologies, Paisley, UK), to allow for the translation of unlabelled nucleotides to labelled nucleotides.

Component	Volume per reaction (µl)
RNAase free water [#] with 1µg DNA	19
Biotin-16-dTUP (50nmol) * or Digoxigenin-11-dUTP (25nmol) *	1
0.1mM dTTP [#]	5
0.1mM dNTP [#]	10
Nick translation enzyme [#]	5
10x Nick translation buffer [#]	5
Total	45

* Roche, Indianapolis, IN, USA

[#] Vysis, Abbott Molecular, IL, USA

Table 2.9 Reaction preparation for probe labelling by nick translation. Each component and their concentration alongside the final volume per reaction are shown. Current suppliers of every component are also highlighted.

The reaction was terminated on ice, and probe size was determined by running 6µl of the reaction on a 0.8% (w/v) agarose gel (section 2.3.3) in parallel with an appropriate DNA ladder (PCR markers, Promega, Madison, WI, USA). For probe precipitation, the reagents were added in order (Table 2.10), vortexed and transferred onto dry ice for 15 minutes. The reaction was centrifuged at 16 000xg relative centrifugal force (rcf) in a pre-cooled Eppendorf centrifuge 5415R (Eppendorf, Hauppauge, NY, USA) at 4° for 20 minutes. The liquid supernatant was aspirated, and pellet vacuum dried for 5 minutes at 16 000xg (rcf) in an Eppendorf concentrator 5301 (Eppendorf, Hauppauge, NY, USA). The pellet was re-suspended in hybridisation mix (Table 2.11) at a ratio of 4:1, hybridisation mix to nick translation mixture (128µl: 32µl), vortexed, incubated for 60 minutes at 37°C and stored at -20°C.

Component	Volume per reaction (µl)
Nick translation reaction locus specific probe	24
Nick translation reaction centromeric probe	8
Human Cot-1 DNA (1mg/ml) *	6
Salmon Sperm DNA #	16
3M sodium acetate #	5.4
100% Ethanol at -20°C	148.5
Total	217.9

* Invitrogen, Carlsbad, CA, USA

Life Technologies, Paisley, UK

Table 2.10 Mixture for precipitation of probes labeled by nick translation. Each component and their final volume per reaction are shown. Current suppliers of every component are also highlighted. Salmon sperm DNA is added to block non-specific binding of hybridisation probe. Human Cot-1 DNA contains repetitive DNA sequences and is also utilised to block non-specific hybridisation by binding to repetitive DNA sequences.

Component	Volume per reaction (ml)
Deionised formamide containing 20% dextran sulphate *	5ml
10x saline sodium citrate (SSC) #	2ml
Distilled water	3ml
Total	10ml

* Sigma-Aldrich, St. Louis, MO, USA

20x SSC (Invitrogen, Carlsbad, CA, USA) containing 3.0 M NaCl and 0.3M sodium citrate at pH 7.0 was diluted according to requirements with deionised water.

Table 2.11 Hybridisation mix for re-suspension of probes labelled by nick translation. Each component and their final volume per reaction are shown. Current suppliers of every component are also highlighted

2.6.2 Isolation of nuclei

FFPE tumour tissue curls, cut to 15µm, were dewaxed in 1ml of xylene for 5 minutes at 12 100xg (rcf, Eppendorf miniSpin, Eppendorf, Hauppauge, NY, USA). The dewaxing was repeated after removal of the supernatant, and the pellet re-suspended in 1ml of 100% ethanol. The sample was centrifuged for 5 minutes at 12 100xg (rcf) and supernatant aspirated. Re-suspension was repeated with 50% (v/v) ethanol and

phosphate buffered saline (PBS, Life Technologies, Paisley, UK) respectively. Tissue pellets were digested for 2 hours with 500µl of 0.5% (w/v) pepsin (Sigma-Aldrich, MO, USA) in 0.01M hydrochloric acid (HCl). If digestion was not complete on visual inspection, a further 250µl of 0.5% (w/v) pepsin was added and digestion continued for a total of 3 hours. Foetal calf serum (FCS) was added (500µl) to terminate digestion and samples were next centrifuged at 12 100xg (rcf).

The supernatant was removed, tissue re-suspended in 1ml of PBS, passed through a 70µM nylon mesh filter (Thermo Fisher Scientific, Waltham, MA, USA) at 8000xg (rcf) for 10 minutes and collected in a 50ml falcon tube. This process was repeated with a further 1ml of PBS added to the original tube to remove any residual tissue. The filtrate in the falcon tube was aspirated and the remaining tissue, containing the isolated nuclei, was re-suspended in 1ml of PBS. Using cuvettes and pre-cut filter cards (Thermo Fisher Scientific, Waltham, MA, USA) to create a central density of nuclei, 80-100µl of this solution was centrifuged onto superfrost plus slides (VWR International, East Grinstead, UK) in a Cytospin 2 Centrifuge (Thermo Shandon, Runcorn, UK). Cytospins for each sample were assessed by light microscopy (Optika, Ponteranica, Italy) to determine the volume of solution required to create the desired nuclei density.

2.6.3 Fluorescence in situ hybridisation protocol

Cytospin slides were warmed at 37°C for 10 minutes in a water bath (Thermo Fisher Scientific, Waltham, MA, USA). Slides were dried, nuclei covered with 100µl of pepsin solution (Sigma-Aldrich, MO, USA, 4mg per 1ml 0.2M HCl), and incubated in a humidified slide chamber at 37°C for 16 minutes. Cytospin slides were next washed in distilled water followed by PBS and graded alcohols (v/v, 75%, 85% and 95%) and air dried. The probe solution (Section 2.6.1) was warmed to 37°C for 15 minutes in a digital dry bath (Labnet, Edison, NJ, USA), vortexed and briefly centrifuged at 12 100xg (rcf). Probe solution (2.5µl) was added to the centre of each slide which was covered with a circular coverslip (VWR International, East Grinstead, UK) and sealed with rubber glue. Slides were placed on a hot plate (VELP Scientifica, Usmate, Italy) at 75°C for 5 minutes to denature and then incubated overnight in a dark humidified chamber at 37°C.

Following overnight hybridisation, cover slips were removed from each slide by agitating them at 37°C in 2x saline sodium citrate (SSC, Invitrogen, Carlsbad, CA, USA). Slides were washed twice, 5 minutes each, at 43°C, in variably stringent solutions which was determined by the degree of background staining. *MYCN s*lides were washed in 40ml of 1xSSC/30% formamide (56ml 1xSSC and 24ml formamide, Sigma-Aldrich, MO, USA) and *MYC*, 17p and 17q slides were washed in 40ml of 0.5xSSC/30% formamide (56ml 0.5xSSC and 24ml formamide). All slides were subsequently washed at 37°C in 2xSSC for a further 5 minutes.

Cytospins were incubated at 37°C in 100µl of 4xSSCTM (saline sodium citrate, Tween and milk, Table 2.12) for 15 minutes in a humidified chamber before each antibody was sequentially applied as described in Table 2.13. Each antibody application was separated by two washes in 4xSSCTM (Table 2.12) for 4 minutes at 43°C to minimise unspecific antibody binding followed by two final 4 minute washes in 2xSSC at 37°C.

Component	Volume
Tween/Igepal CA-630 *	250µl
4xSSC #	500ml
Powdered milk	1.5ml

* Sigma-Aldrich, St. Louis, MO, USA

Invitrogen, Carlsbad, CA, USA

Table 2.12 Saline sodium citrate, tween and milk recipe. Each component and their volume are shown. Current suppliers of every component are also highlighted.

Order	Antibody	Dilution in 4xSSCTM	Duration (minutes)
1	Anti-digoxigenin fluorescein, Fab fragments *	1:20	30
2	Polyclonal rabbit anti-sheep immunoglobulins #	1:50	20
3	Polyclonal swine anti-rabbit immunoglobulins #	1:40	20
4	Texas red avidin DCS ~	1:500	20

* Roche, Indianapolis, IN, USA

Dako, Glostrup, Denmark

~ Vector, Peterborough, UK

Table 2.13 Order of antibody application, dilution and duration for FISH. Antibodies are displayed in order of application (1-4) alongside their final dilution in 4xSSCTM and duration of incubation at 37°C. Current suppliers of each antibody are also highlighted.

Slides were agitated in PBS for 1 minute, dehydrated in sequential alcohols (v/v, 75%, 85% and 95% respectively) and air dried in the dark. Each slide had 20µl of Vectashield® mounting medium with DAPI added (Vector, Peterborough, UK), followed by a 25mmx25mm coverslip (VWR International, East Grinstead, UK) before being examined by two independent scorers (Dr Janet Lindsey and myself) using fluorescence microscopy (Olympus BX16, Olympus, Tokyo, Japan). The scoring methods for chromosome 17 status are detailed in section 3.3.2.2. *MYC* and *MYCN* FISH slides were scored as previously described (Ellison *et al.*, 2011). Amplification was defined as a gene locus: centromeric ratio greater than 4: 1 respectively in 5% or more nuclei scored, with evidence of double minutes (DM) or homogenously staining regions (HSR).

2.7 Multiplex ligation-dependent probe amplification

Multiplex ligation-dependent probe amplification (MLPA) is a multiplex PCR method that can be used to detect copy number aberrations at multiple (typically up to 40) different loci of interest (Schouten *et al.*, 2002). It is a semi-quantitative technique and identifies changes in probe signals of interest relative to probe signals at reference/control loci. The method requires small amounts of DNA (20ng-100ng) and consists of four steps; denaturation and hybridisation, ligation, PCR reaction and fragment analysis. Each MLPA probe consists of two oligonucleotide sequences which bind to adjacent sites on the sample DNA prior to the ligation reaction. Within the oligonucleotide sequences are; complementary nucleotides (hybridising sequence) for the loci of interest, a stuffer sequence so that each ligated probe is unique in length to allow fragment analysis to differentiate between multiple loci, and universal primers for the PCR reaction to occur (Figure 2.4). Only the ligated oligonucleotides are amplified during the PCR reaction and give a signal, enabling the products of interest to be separated and measured by electrophoresis.

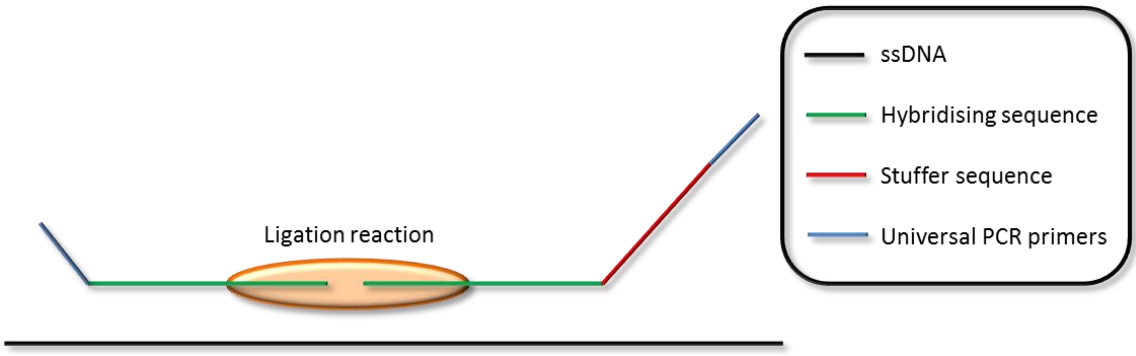

Figure 2.4 Schematic showing a standard MLPA probe bound to a ssDNA target sequence prior to ligation reaction.

MLPA was carried out as per the manufactures two-tube protocol using the SALSA ® reagents for MLPA, P200-1 reference probe mix and Cy5.0 PCR primers (MRC-Holland, Amsterdam, Netherlands). In brief, a custom made probe mix was prepared consisting of oligonucleotide sequences for the three genes of interest (*MYC, MYC* and *MDM2*) along with two control genes (*TBP* and *B2M*, Table 2.14). Each oligonucleotide, supplied at 20nmol (Metabion International, Martinsried, Germany) was re-suspended with 200µl of Tris-EDTA buffer (TE buffer solution, Sigma-Aldrich, MO, USA) to make a

stock solution of 100µM which was stored at -20°C. Working dilutions of the oligonucleotides (*MYC, MYC, MDM2, TBP* and *B2M*) were made with 10µl of stock solution and 990µl of TE buffer (1µM) and stored at -20°C. The custom probe mix was made by combining 0.8µl of each 1µM oligonucleotide (working dilution), with TE buffer to a final volume of 200 µl (stored at -20°C).

Gene of interest	Oligonucleotide I 5'-3'	Oligonucleotide II 5'-3'
MYC	CTACGCAGCGCCTCCCTCCACTTGCAGTTCCGCACT ACTACGCTGACTCTAGATTGGATCTTGCTGGCAC	GGGTTCCCTAAGGGTTGGAGTGC CACGTCTCCACACATCAGCACAA
MYCN	GCTTGAGAACGAGCTGTGGGGCATGCAGTTCCGC ACTACTACGCTGATCTAGATTGGATCTTGCTGGCAC	GGGTTCCCTAAGGGTTGGAG AGCTGGGTCACGGAGATGCT
MDM2	CAGAAGATTATAGCCTTAGTGAAGAAGGACAA GAACTCTCTTCTAGATTGGATCTTGCTGGCAC	GGGTTCCCTAAGGGTTGGAGATCAGTTTA GTGTAGAATTTGAAGTTGAATCTCTCGACT
TBP	CTTACGCTCAGGGCTTGGCCTCCTG CATCTAGATTGGATCTTGCTGGCAC	GGGTTCCCTAAGGGTTGGATCAT GGATCAGAACAACAGCCTGCCAC
B2M	GATGTCTCGCTCCGTGGCCTTATGCA GTTTCTAGATTGGATCTTGCTGGCAC	GGGTTCCCTAAGGGTTGGA CTGACAGCATTCGGGCCGA

Table 2.14 Oligonucleotide sequences for MLPA. Oligonucleotide sequences (I, forward; II reverse) for the three loci of interest (*MYC, MYCN* and *MDM2*) and two additional reference loci (*TBP* and *B2M*) are shown.

2.7.1 Denaturation and hybridisation

DNA (2.5µl, total amount 20-100ng) was denatured at 98°C for 5 minutes and cooled to 25°C. For one hybridisation reaction 0.5µl of P200-1 reference probe mix, 0.25µl of custom made probe mix (section 2.7) and 0.75µl of MLPA buffer were mixed and added to each DNA sample (total reaction volume 4µl). Samples were incubated at 95°C for 1 minute, and heated at 60°C for 16 hours overnight on a GeneAmp ® PCR System 9700 thermocycler (Applied Biosystems, Life Technologies, Paisley, UK).

2.7.2 Ligation reaction

The ligase reaction mix was prepared within 1 hour before use and stored on ice. Each reaction contained 1.5µl of ligase 65 buffer A, 1.5µl of ligase 65 buffer B and 12.5µl of RNAse free water which was vortexed before 0.5µl of Ligase 65 was added to make a total volume of 16µl. Samples were cooled from 60°C (section 2.7.1) to 54°C before the ligase mix was added (total reaction volume 20µl). The reaction was incubated at 54°C for 15 minutes before being heated to 98°C for 5 minutes.

2.7.3 PCR reaction

In separate PCR tubes, 2µl of SALSA ® PCR buffer, 13µl of RNAse free water and 5µl of the MLPA reaction (section 2.7.2) were combined. Next, 5µl of the polymerase reaction (1µl of SALSA ® PCR primers, 1µl of SALSA ® enzyme dilution buffer, 2.75µl of RNAse free water and 0.25µl of SALSA ®polymerase) was added to each tube and the PCR reaction started on a GeneAmp ® PCR System 9700 thermocycler (Table 2.15, Applied Biosystems, Life Technologies, Paisley, UK).

Temperature	Time	Cycles
95°C	30 seconds	
60°C	30 seconds	35
72°C	1 minute	
72°C	20 minutes	
4°C	Hold	

Table 2.15 Thermocycler settings for MLPA PCR reaction. Temperature settings, duration and number of cycles required for MLPA PCR reaction are shown.

2.7.4 Fragment analysis

Separation of amplified products using electrophoresis was performed on the Beckman Coulter CEQ™ 880 Genetic Analysis System (Beckman Coulter UK Ltd, High Wycombe, UK), and results were analysed using GeneMarker ® Version 1.75 (SoftGenetics, PA, USA). *MYC, MYCN* and *MDM2* copy numbers were measured relative to the two reference genes (*TBP* and *B2M)* in the custom made probemix along with two additional reference loci in the P200-1 probemix (7q31 and 14q22). Normal DNA diploid controls were run on the MLPA assay (n=7) and used to define cut-offs for the detection of copy number elevation (> 2 standard deviations of the mean). Any tumour sample showing elevated copy number versus three or more reference loci (*TBP*, *B2M*, 7q31 and 14q22) on two separate replicate assays was deemed to have copy number elevation of that gene.

2.7.5 Validation of MLPA assay

MLPA results for individual samples were compared to FISH (section 2.6), the standard technique for measuring *MYC* and *MYCN* amplification (section 2.6.3). In an initial pilot study, 55 tumour samples for *MYC* and 52 tumour samples for *MYCN* had FISH and

MLPA data correlated (Figure 2.5 and Figure 2.6). Overall, MLPA reliably detected tumours with no *MYC/MYCN* amplification and when amplification of *MYC* was present in >30% of nuclei, and amplification of *MYCN* in >10% of nuclei. In tumour samples with lower-level copy number changes, MLPA delivered an intermediate copy number score requiring FISH validation to confirm the degree of amplification or gain (gene locus: centromeric ratio >1:1 but ≤ 4:1).

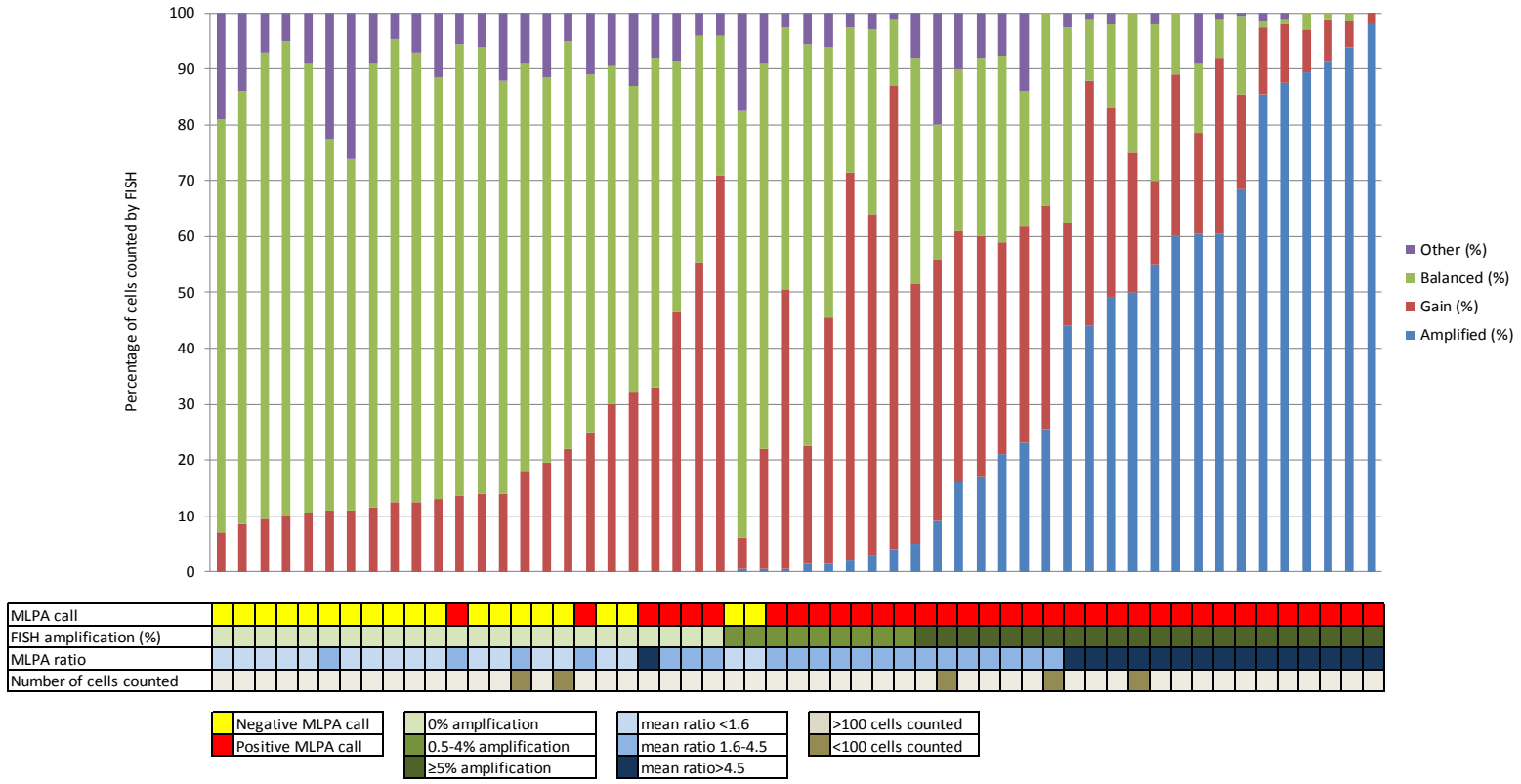

Figure 2.5 Comparison of *MYC* copy number status as detected by MLPA and FISH. Figure shows the percentage of amplified nuclei, gained nuclei and balanced nuclei counted for each sample alongside their positive or negative MLPA score (as defined in section 2.7.4). Overall, 22 MLPA positive samples showed amplification by FISH (section 2.6.3), and no amplified cases produced a negative MLPA result. MLPA was therefore 100% sensitive for detecting *MYC* amplified cases and 61% specific, as it identified 13 cases that were not amplified although several of these cases had high levels of gain as displayed in the figure.

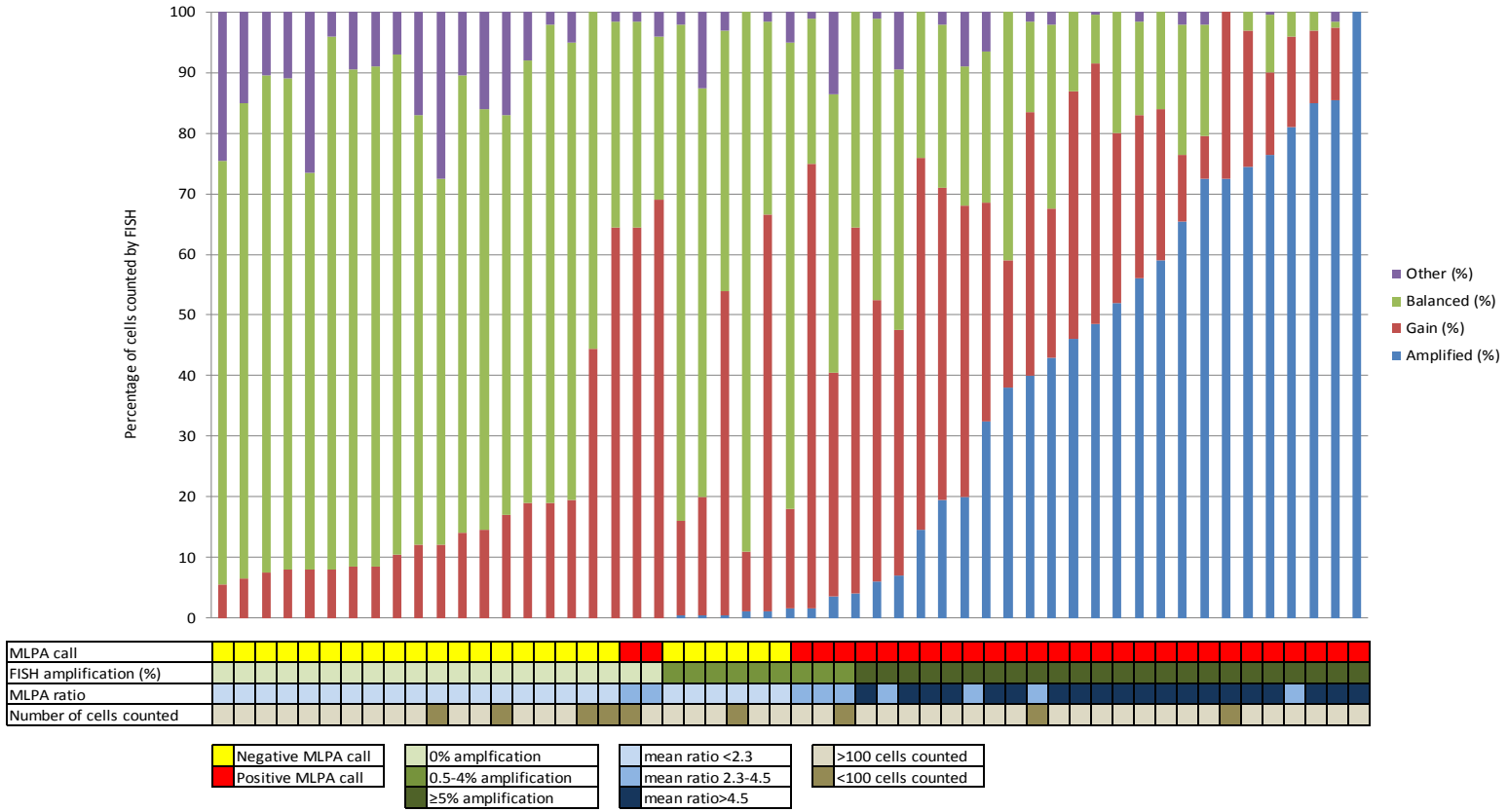

Figure 2.6 Comparison of *MYCN* copy number status as detected by MLPA and FISH. Figure shows the percentage of amplified nuclei, gained nuclei and balanced nuclei counted for each sample alongside their positive or negative MLPA score (as defined in section 2.7.4). Overall, 24 MLPA positive cases showed amplification by FISH (section 2.6.3). No amplified cases produced a negative MLPA result. MLPA was therefore 100% sensitive for detecting *MYCN* amplified cases and 83% specific, as it identified 5 cases that were not amplified although all of these cases had either high levels of gain or a low level amplification in <5% of cells as displayed in the figure.

2.8 Survival analysis

Cancer survival analyses typically measure event free survival (EFS) and OS. EFS is a measure of the time from initial diagnosis to an event such as relapse, disease progression or another pre-defined event unique to that cancer or treatment. OS measures the time from initial diagnosis to death of any cause and therefore includes toxic deaths due to treatment complications as well as deaths unrelated to the cancer or its associated therapy.

For the purpose of survival analysis within medulloblastoma studies, EFS is defined as the time from diagnosis to disease progression if remission is not achieved, or disease recurrence, if there is documented evidence of no visible disease in the interim period between initial therapy and recurrence. Consequently, all events used to calculate EFS in this study were disease recurrence. OS remained as the time from initial diagnosis to the time of death, or if the patient was still alive the data was censored at the date of last follow-up. Those patients who died of causes unrelated to their disease were excluded from OS analyses but remained in the EFS analyses. TTD was calculated as the difference between EFS (date of relapse) and OS (date of death or last follow-up). All survival analyses were performed in R (R Development Core Team, 2014).

2.8.1 Univariate testing

The Log-rank test is a test of significance and is applied to compare survival between two or more groups of interest with the null hypothesis that there is no difference between these groups. A p value of <0.05 indicates that there is a significant difference in survival between the two comparison groups, although if multiple comparisons are performed this must be corrected for using an appropriate technique such as the Bonferroni procedure which is discussed in section 2.10. The advantage of this method is it accounts for the total survival experience and was used across all observation periods (EFS, OS and TTD, section 2.8). Censored data is handled in the same way as the Kaplan-Meier method, *i.e.* the data is not included in the analysis beyond the point of censorship (Bland and Altman, 2004).

Kaplan-Meier plots are survival curves which estimate the proportion of patients surviving at a given time-point. An event, such as death of disease or disease relapse, is

represented as a step down in the graph, as the proportion of patients not suffering the event reduces. Censored data are indicated by vertical lines on the plot but do not affect the overall shape of the survival curve, making the assumption that had the patient's data not been censored, their prospects of surviving the disease were equal to those remaining (Bland and Altman, 1998).

2.8.2 Multivariate testing

Multivariate testing using a statistical model allows survival to be assessed in relation to many variables at the same time; for example, metastatic stage, gender and pathology. The Cox proportional hazard model (Bradburn *et al.*, 2003) is the statistical model of choice in medical research and was used to assess the contribution of multiple clinicopathological and molecular variables to EFS, OS and TTD. It is a nonparametric, multi linear, regression model, which reports the size of effect (hazard ratio and their 95% confidence intervals) and how each variable jointly impacts on survival. The hazard ratio is an estimate of the ratio of the hazard rates in relation to two variables or two groups of patients. A ratio of 1 indicates no difference between the variables compared. Hazard ratios with 95% confidence intervals greater than 1 indicate a variable is significantly and positively associated with the probability of an event, ratios with 95% confidence intervals less than 1 are significantly and negatively associated (Bradburn *et al.*, 2003; Clark *et al.*, 2003).

2.9 Comparative and correlative analyses

Contingency tables and subsequent comparative analyses of the frequency and distribution of clinicopathological variables were generated and undertaken using Fisher's exact test in GraphPad Prism version 6.05 (GraphPad Software, Inc., San Diego, CA, USA). Clinicopathological and molecular variables were tested for association using Fisher's exact test and performed in R (R Development Core Team, 2014). Data was categorised for each variable including continuous data, such as age which was categorised as ≥ 4 years or < 4 years old, and results with a p value of <0.05 were considered significant, once appropriately corrected for multiple testing (section 2.10).

2.10 Correction for multiple testing

Upon testing multiple variables and consequently multiple null hypotheses, the possibility of witnessing a significant result by chance, and incorrectly rejecting the null

hypothesis increases. To account for this, the Bonferroni procedure was applied to both univariate survival analyses and correlative analyses (section 2.8.1 and 2.9 respectively). It is a conservative method, which corrects the p value by multiplying it by the number of tests performed (Bland and Altman, 1995).

2.11 Molecular subgrouping on the Infinium Methylation 450K array

The quality control of tumour DNA samples and experimental procedures undertaken on the Infinium methylation 450K array are described in section 3.3.2.1, 5.3.6 and 6.3.6.1. Molecular subgrouping assignment using non-negative matrix factorisation (NMF) was performed by Dr Ed Schwalbe (PBTG) as previously described (Schwalbe *et al.*, 2013b). NMF is a technique which reduces the variation of a high dimensional dataset to a more manageable set of metagenes, which represent patterns of variation in the original dataset. In brief, a filtered 450K array dataset containing the most variably methylated probes (A) was reduced to two matrices (H and W). The H matrix typically represents the expression of the metagenes, although in this instance it refers to DNA methylation, and is the number of samples (M) from the original dataset A, by the number of metagenes identified (k). The W matrix represents the correlation of each input probe (N) with each metagene identified and its dimensions are defined by these two variables (N by k, Figure 2.7).

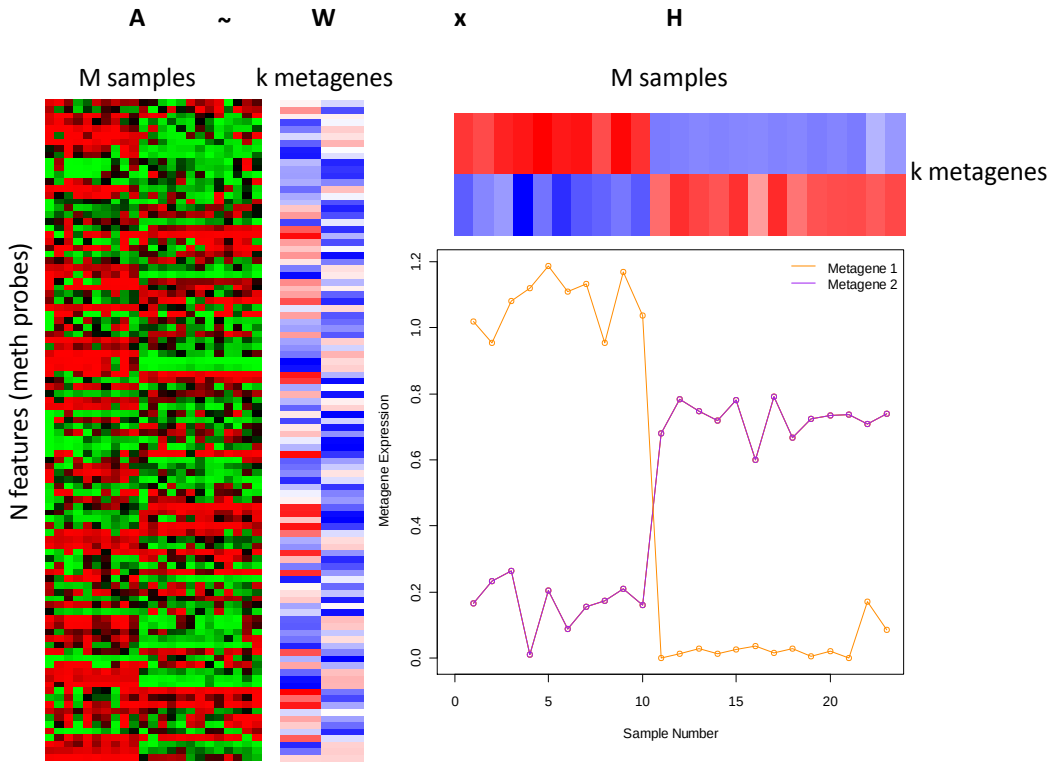

Figure 2.7 Illustrative example of non-negative matrix factorisation demonstrating 2 metagenes corresponding to 2 groups. Heatmap A shows 100 methylation probes for 23 medulloblastoma samples. (Green, unmethylated probes; red, methylated probes; black, hemi-methylated probes.) NMF factorises matrix A into the W and H matrices. The W matrix has size N rows by k columns, (k = number of metagenes). Each data point for W represents the coefficient of a methylation probe with that particular metagene. (Blue, probes with low correlation to the metagene; red, probes with high correlation.) Matrix H has k rows and M columns where M is the number of samples and each column represents the metagene expression profile for each sample. (Blue, low metagene expression; red, high metagene expression.) Line graph illustrates the clear difference in metagene expression between the two classes. Image kindly provided by Dr Ed Schwalbe (PBTG).

After identifying the metagenes, dataset A was then clustered using resampling techniques which varied the number of clusters and metagenes from three to ten to identify the most robust clustering solution. In this instance, five metagenes and four clusters were the most stable solution and used to assign molecular subgroup membership (Figure 2.8). NMF is considered to be a superior clustering technique for biological datasets as it identifies the major components of variation in the dataset, and is robust to noise that is typically of high-dimensional biological datasets. In addition, identified metagenes can also be used across multiple datasets to project subgroup membership using the original predetermined W matrices (Hovestadt *et al.*, 2013; Schwalbe *et al.*, 2013b).

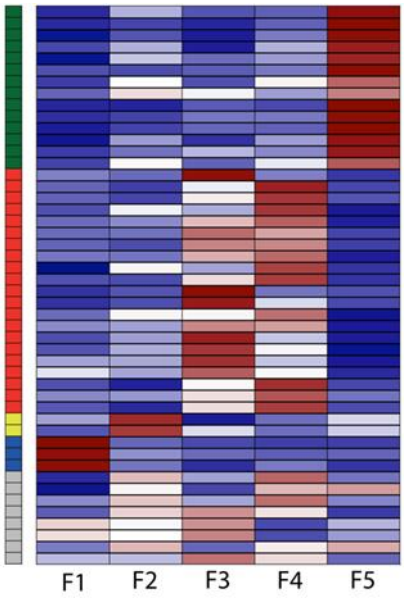

Figure 2.8 Metagene patterns of tumours sampled at diagnosis and relapse in the paired relapse cohort. Five metagenes are shown (F1-F5) with F3 and F4 identifying MB_{SHH} reflecting the heterogeneity within this subgroup (section 1.8.8.2). Each sample is represented by a row with confidently assign samples labelled; MB_{Grp4}, green; MB_{SHH}, red; MB_{Grp3}, yellow; MB_{WNT}, blue and unconfidently assigned samples in grey (MB_{NOS}).

Chapter 3. Combined *MYC* gene family amplification and p53 pathway defects emerge at medulloblastoma relapse and identify locally aggressive, rapidly progressive disease

3.1 Introduction

Recent years have witness a rapid expansion in the knowledge and understanding of the molecular biology of medulloblastoma at diagnosis (Northcott *et al.*, 2012a; Taylor *et al.*, 2012). This, in turn, has influenced global clinical practice to treat the disease, with new therapeutic stratification and treatment options increasingly based on the interplay of molecular markers alongside clinical features (Pizer and Clifford, 2009; Morfouace *et al.*, 2014). The biology of the disease at relapse however, remains poorly understood with a limited number of molecular studies and clinical trials available to inform future research and treatment strategies (Korshunov *et al.*, 2008; Pizer *et al.*, 2011a; Ramaswamy *et al.*, 2013).

In other paediatric tumour types such as neuroblastoma, a neural crest cell tumour arising from the sympathetic nervous system (section 1.7.3), studies have shown that acquisition of defects in the p53 pathway frequently occur at relapse (Carr-Wilkinson *et al.*, 2010). Moreover, in HGGs (section 1.6.1.1.2), tumour heterogeneity gives rise to intratumoural molecular subgroup variation and evolution of subgroup is seen at disease relapse (Phillips *et al.*, 2006; Sottoriva *et al.*, 2013). Two initial studies in relapsed medulloblastoma, summarised in section 1.9.2, have shown that some molecular features are altered at relapse (Korshunov *et al.*, 2008), with more recent findings suggesting that molecular subgroup does not change over time (Ramaswamy *et al.*, 2013). However, the established medulloblastoma clinicopathological and molecular features, have yet to be comprehensively interrogated at relapse.

This chapter focuses on the investigation of molecular features with validated relationships to disease prognosis at diagnosis, within a cohort of medulloblastoma samples taken at relapse (n=29), paired with their tumour sampled at diagnosis, and correlates these findings with disease behaviour and clinicopathological features at both time-points. Tumour samples taken at diagnosis and relapse are interrogated for molecular subgroup status (MB_{WNT}, MB_{SHH}, MB_{Group3} and MB_{Group4}), which is associated with particular clinical demographics, molecular features and disease behaviour (Taylor *et al.*, 2012). Additionally, chromosome 17 defects, the most common cytogenetic abnormality observed in medulloblastoma (predominantly MB_{Group3} and MB_{Group4}), and polyploidy, a feature noted in MB_{Group3} and MB_{Group4}, are investigated in view of their association with a poorer outcome (Pfister *et al.*, 2009; Ellison *et al.*,

2011; Jones *et al.*, 2012; Northcott *et al.*, 2012a; Taylor *et al.*, 2012; Shih *et al.*, 2014). Specific genetic aberrations also associated with a poor prognosis, such as *MYC* and *MYCN* amplification, *TP53* mutation (predictive of a poor prognosis in MB_{SHH}) and other p53 pathway defects (*MDM2* amplification and $p14^{ARF}$ deletion/methylation) are assessed (Frank *et al.*, 2004; Pfister *et al.*, 2009; Pizer and Clifford, 2009; Ellison *et al.*, 2011; Northcott *et al.*, 2012a; Ryan *et al.*, 2012; Zhukova *et al.*, 2013; Shih *et al.*, 2014). Combined, these investigations provide a comprehensive investigation of the established features in medulloblastoma at disease relapse, and an initial insight into the biology and behaviour of recurrent medulloblastoma.

3.2 Aims

The aims of this chapter are to;

- Collect a cohort of tumour samples obtained at medulloblastoma relapse alongside their counterpart sample taken at diagnosis.

- Collate and centrally review all clinical and pathological data within this cohort, including a detailed assessment of the disease patterns at relapse.

- Investigate tumour samples taken at both time-points for molecular disease features with established importance and relationships to prognosis in the disease at diagnosis.

- Undertake correlative, univariate and multivariate analyses of all clinical, pathological and molecular variables to identify associations between relapsed medulloblastoma features and disease behaviour.

3.3 Materials and methods

3.3.1 Cohort assembly and preparation

Tumour tissue was obtained from UK CCLG institutions and collaborating centres (Pizer *et al.*, 2011a) for 29 patients at the time of relapse, 26 of these samples had material available from their tumour resected at diagnosis. Tumour material was predominantly FFPE (diagnosis n=24, relapse n=27) with frozen material available for two additional diagnostic and two relapse samples, alongside duplicate frozen material for 15/51 FFPE samples. All investigations carried out on human tissue in this study were part of a CCLG-approved biological study (BS-2007-04) with ethics approval from the Newcastle/North Tyneside Research Ethics Committee (reference 07/Q0905/71).

3.3.1.1 Collation of clinical data and patterns of relapse

Detailed clinical data was collated by Prof Simon Bailey (PBTG) from all treatment centres and centrally reviewed. Information was gathered at both diagnosis and relapse on; gender, age, treatment (degree of surgical resection, chemotherapy and radiotherapy regimen), site(s) of disease, date of last follow-up and cause of death where appropriate. Metastatic stage at diagnosis was assigned according to Chang's criteria (Chang *et al.*, 1969), whereas patterns of disease relapse were recorded as local and/or distant site, nodular and/or diffuse. These criteria were designed to capture the diverse patterns of relapse witnessed in the disease (Perreault *et al.*, 2013). Treatment intent at relapse was also recorded as either palliative or curative.

3.3.1.2 Central pathology review

All tumours were centrally reviewed by a panel of three CCLG neuropathologists as previously described (section 2.2). Where possible pathological variant was assigned according to the current WHO criteria (Louis *et al.*, 2007), otherwise a tumour was confirmed as a MB_{NOS}.

3.3.1.3 Extraction of nucleic acids

Extractions of nucleic acids from FFPE and frozen samples were performed as detailed in section 2.1. Quality of extracted material was assessed by Nanodrop spectrophotometry for investigations of the established molecular pathways (section 2.1.2.1) and Quibit fluorometer for samples proceeding onto the Infinium methylation 450K array (section 2.1.2.2 and 5.3.6).

3.3.1.4 Confirming the identity of the paired tumour samples

Microsatellites are highly variable lengths of typically di, tri or tetra nucleotide repeats and can be used, for example, in linkage analysis, assessment of segmental chromosomal copy number abnormalities or in this instance, confirmation that DNA obtained from two independent tumour samples originated from the same patient. To assess the lengths of a series of up to fourteen microsatellite markers for each patient, PCR and subsequent analysis was performed by Dr Janet Lindsey (PBTG), using previously reported primer sequences that flanked the microsatellite regions of interest (Randerson-Moor *et al.*, 2001; Jung *et al.*, 2004; Langdon *et al.*, 2006).

Location	Forward sequence 5'-3'	Reverse sequence 5'-3'
d9s942	GCAAGATTCCAAACAGTA	CTCATCCTGCGGAAACCATT
d9s1748	CACCTCAGAAGTCAGTGAGT	GTGCTTGAAATACACCTTTCC
d5s346	ACTCACTCTAGTGATAAATCGGG	AGCAGATAAGACAGTATTACTAGTT
d2s123	AAACAGGATGCCTGCCTTTA	GGACTTTCCACCTATGGGAC
MYCL	TGGGGTCTGCTTAGCTCACT	GTCCTCAGATCATCCCCAGA
d18s69	GCAGTCTGGAAATCCTCTTT	ATGTTCCCCGCTATTGTACT
d10s197	ACCACTGCACTTCAGGTGAC	GTGATACTGTCCTCAGGTCTCC
TP53	AGGGATACTATTCAGCCCGAGGTG	ACTGCCACTCCTTGCCCCATTC
d17s2196	CCAACATCTAGAATTAATCAGAATC	ATATTTCAATATTGTAACCAGTCCC
d17s936	ATTTGAAACCACAACAGCA	AGGTATATGCCCACCCC
d17s969	ATCTAATCTGTCATTCATCTATCCA	AACTGCAGTGCTGCATCATA
d17s974	AGACCCTGTCTCAGATAGATGG	TAAAATAGAAAGTGCCCCTCC
d17s786	TACAGGGATAGGTAGCCGAG	GGATTTGGGCTCTTTTGTAA
d17s1866	TGGATTCTGTAGTCCCAGG	GGTTCAAAGACAACTCCCC

Table 3.1 Primer sequences for microsatellite markers.

Each 15µl PCR reaction contained 1.5µl of forward and reverse primers (10µM, Table 3.1), 1.5µl of PCR buffer, 0.9µl $MgCl_2$ (10mM), 0.6µl dNTP (5mM), 0.15µl Taq polymerase (5U/µl), 7.35µl of RNAse free water and 1.5µl of DNA (25ng/µl). The PCR reaction was run on the GeneAmp ® PCR System 9700 thermocycler (Applied Biosystems, Life Technologies, Paisley, UK), with 1 cycle at 94°C for 10 minutes followed by 40 cycles of 95°C for 1 minute, 55°C for 1 minute and 72°C for 1 minute followed by 1 cycle of 72°C for 5 minutes. Fragment analysis (Figure 3.1) of amplified products using electrophoresis was performed on the Beckman Coulter CEQTM 880 Genetic Analysis System (UK Ltd, High Wycombe, UK). All 26 cases, where tumour DNA

was available at diagnosis and relapse, demonstrated corresponding microsatellite profiles, confirming the matched nature of the paired samples.

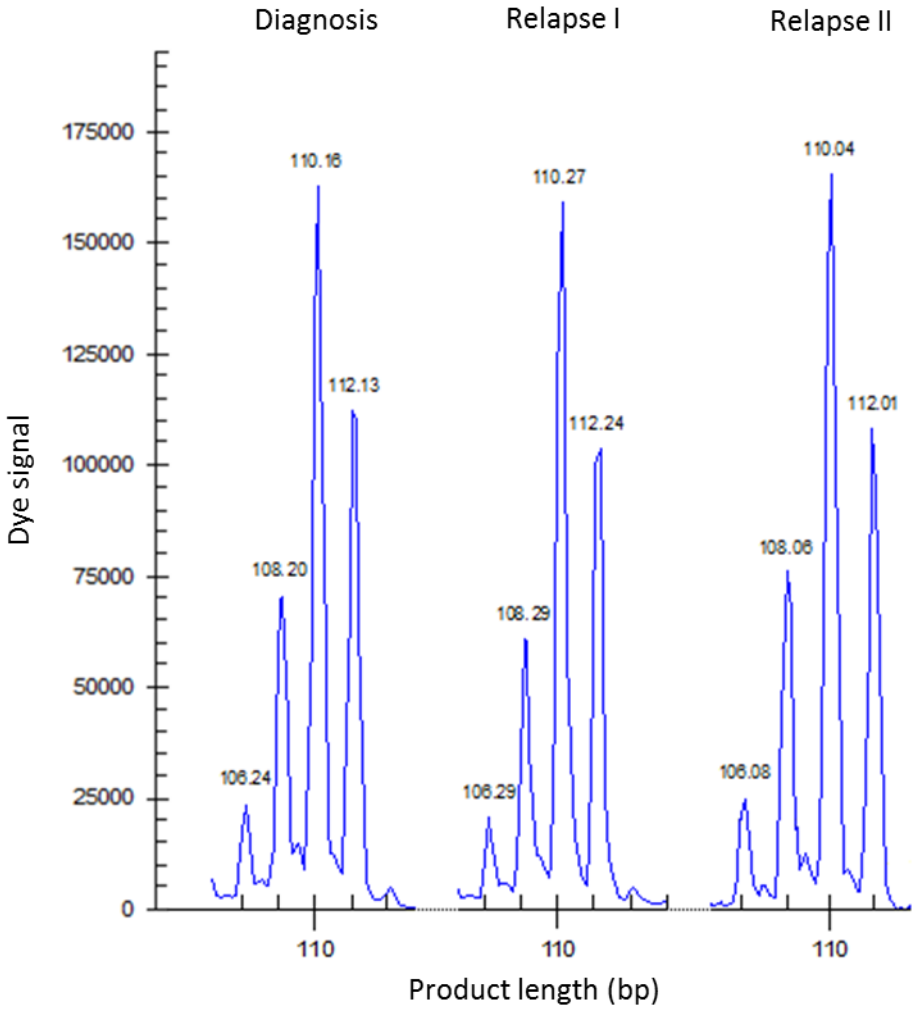

Figure 3.1 Fragment analysis for microsatellite marker d9s1748. Traces show identical fragment lengths in tumours sampled at three different time-points confirming that they have been sampled from the same patient.

3.3.2 Selection of pathways and techniques for investigation

Investigations carried out on the paired relapse cohort focused on interrogating those pathways which play a role in the tumourigenesis of medulloblastoma at diagnosis as well as molecular features known to be important in other embryonal tumours at relapse. Molecular features examined included molecular subgroup, chromosome 17, the p53 pathway, *MYC* gene family (*MYC/MYCN*) status and polyploidy as detailed in section 3.1.

3.3.2.1 Molecular subgroup

All tumour samples were examined for *CTNNB1* mutation, associated with MB_{WNT} subgroup status as detailed in section 2.3.2. Where DNA was of sufficient quantity and quality, as determined by the Qubit fluorometer (section 2.1.2.2), samples were analysed on the Infinium methylation 450K array at the Wellcome Trust Clinical Research Facility, University of Edinburgh, UK, according to the manufacturer's protocols (section 5.3.6, Illumina Inc. San Diego, CA, USA). Sample requirements for this array were a DNA concentration of ≥50ng/µl and total amount of 2µg extracted from FFPE material or 750ng extracted from frozen tissue. A total of 49/55 samples in the paired relapse cohort met these criteria and were processed to assess their molecular subgroup as described in section 2.11.

3.3.2.2 Chromosome 17

Assessment of chromosome 17 by FISH was undertaken for 17p and 17q (section 2.6). Each sample slide was scored by two independent assessors with a total of 200 non-overlapping nuclei recorded with reference to the number of centromeric probes versus locus specific probe (17p13.3 and 17q12). Counts were divided into the total number of nuclei demonstrating a loss (locus specific probe count < centromeric probe count), gain (locus specific probe count > centromeric probe count) or balanced status (locus specific probe count = centromeric probe count). Both 17p and 17q status were combined for each tumour sample and the overall chromosome 17 status designated as balanced, 17p loss or i(17q) as previously described (Nicholson *et al.*, 2000). In brief, each slide was assigned an average signal score, for example if there were 70% of nuclei demonstrating two locus specific signals with two centromeric (2/2), and 30% of nuclei demonstrating one locus specific signal with two centromeric (1/2) the score

would be 0.85 ((2/2 x 0.7) + (1/2 x 0.3)). With thresholds set at < 0.8 for loss and >1.2 for gain, this example would be a balanced profile.

3.3.2.3 The p53 pathway

Assessment of the p53 pathway focused on analysing the *TP53* gene mutation status by PCR based direct sequencing (section 2.3.1), *MDM2* amplification by MLPA (section 2.7) and hypermethylation or deletion of the $p14^{ARF}$ gene. Methylation status of the $p14^{ARF}$ was obtained from Infinium methylation 450K array (section 3.3.2.1 and 5.3.6, Illumina Inc. San Diego, CA, USA). Deletion of $p14^{ARF}$ was initially assessed using microsatellite markers d9s942 and d9s1748 (section 3.3.1.4), as loss of heterozygosity (LOH) at these loci is suggestive of a heterozygous deletion (Randerson-Moor *et al.*, 2001). Conformation of copy number status was performed for three samples demonstrating LOH using the Infinium methylation 450K array (n=2) or the Illumina human omniexpress array (n=1, Illumina Inc. San Diego, CA, USA). Sample requirements for the Illumina human omniexpress array were identical to the requirements for the Infinium methylation 450K array (section 3.3.2.1). Copy number analysis was performed by Dr E Schwalbe (PBTG) using R (R Development Core Team, 2014) as previously reported (Northcott *et al.*, 2012b; Sturm *et al.*, 2012). Copy number estimates were normalised by quantile normalisation and segmented using the Circular Binary Segmentation (CBS) algorithm. The copy number segments were subsequently interrogated and classified as balanced, gained or lost.

3.3.2.4 MYC gene family

MYC gene family status (*MYC* and *MYCN*) were assessed by FISH (section 2.6). One hundred nuclei were assessed by two independent scorers, with reference to the number of centromeric probes, locus specific probes and the relationship between the two counts (section 2.6.3). Tumour samples were deemed to show *MYC* or *MYCN* amplification if the gene locus: centromeric ratio was greater than 4: 1 respectively in 5% or more nuclei scored with evidence of DM or HSR (Ellison *et al.*, 2011). Alongside FISH analysis, an MLPA assay was developed to interrogate and screen multiple loci of interest including *MYC* and *MYCN* (section 2.7).

3.3.2.5 Polyploidy

Polyploidy was assessed for each tumour sample with FISH slides undertaken to interrogate multiple regions of interest (*MYC*, *MYCN*, 17p and 17q). Centromeric counts were categorised as balanced (2n), elevated (>2n) or other (<2n). Polyploidy was assigned where the modal centromeric category was >2n across 2 or more loci.

3.3.3 Independent control cohort

To compare, in a subgroup-specific manner, the incidence of molecular events discovered at relapse with their expected rate at diagnosis, a large independent control cohort of tumours sampled at diagnosis was assembled (n=344). All cases were assigned their molecular subgroup utilising the Infinium methylation 450K array as previously described (section 2.11 and 5.3.6, Illumina Inc. San Diego, CA, USA), and assessed for *TP53* mutations, *MYC* and *MYCN* amplification as discussed in section 2.3.1, 2.6 and 2.7 respectively. An overview of this cohort is shown in Table 3.2. The reduced number of MB_{SHH} and MB_{Group3} observed can be explained by the exclusion of patients not receiving upfront CSI. These patients are typically in the infant age group which is enriched for MB_{SHH} and MB_{Group3} (Kool *et al.*, 2012; Northcott *et al.*, 2012a; Taylor *et al.*, 2012) and therefore underrepresented in this cohort.

Clinicopathological features and molecular subgroup		Control cohort
Gender	Male	219/344 (64%)
	Female	125/344 (36%)
	Male:female ratio	1.75:1
Age	Age range in years	1.4-39.6
	Infants (<4 years)	35/344 (10%)
	Children (4-16 years)	294/344 (86%)
	Adults (>16 years)	15/344 (4%)
Pathology	CLA	258/325 (79%)
	DN	26/325 (8%)
	LCA	41/325 (13%)
Metastatic stage	M-	259/341 (76%)
	M+	82/341 (24%)
Resection	GTR	244/337 (72%)
	STR	93/337 (28%)
Molecular subgroup	MB_{SHH}	65/344 (19%)
	MB_{WNT}	48/344 (14%)
	MB_{Group3}	72/344 (21%)
	MB_{Group4}	159/344 (46%)

Table 3.2 Clinicopathological and molecular subgroup demographics of the independent control cohort sampled at diagnosis. CLA, classic histology; DN, desmoplastic/nodular histology; LCA, large cell/anaplastic histology; M-, M0/M1 disease; M+, M2+ disease; GTR, gross total resection; STR, subtotal resection.

3.4 Results

3.4.1 Comparing the paired relapsed cohort with historic studies

To assess the distribution and frequency of clinicopathological and molecular features in the paired relapsed cohort, independent, well annotated, historic studies of medulloblastoma tumours, sampled at diagnosis, were used to perform comparison analyses (McManamy *et al.*, 2007; Pfister *et al.*, 2009; Pfaff *et al.*, 2010; Kool *et al.*, 2012; Lannering *et al.*, 2012; Ryan *et al.*, 2012).

3.4.1.1 Metastatic disease is enriched in the paired relapse cohort

The paired relapse cohort consisted of 29 patients with a male to female ratio of 1.6: 1 and a median age at diagnosis of 8.6 years (range 0.1-33.7 years). High-risk features, namely metastatic disease (M1+) as defined by Chang's criteria (Chang *et al.*, 1969), subtotal resection (STR, <1.5cm^2 residuum after surgical resection), LCA pathology and infant age group were assessable in 27/29 (93%) patients. For the purposes of comparisons with reported high-risk features in the selected historic studies, infant age group was defined as <4 years old. Overall 24/27 (89%) patients in the paired relapse cohort demonstrated at least one high-risk feature at diagnosis (Figure 3.2).

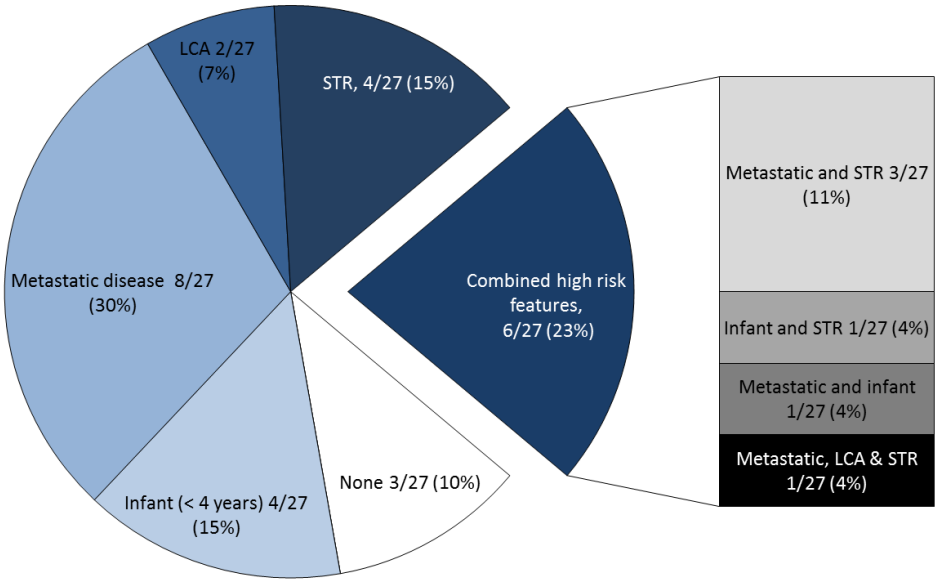

Figure 3.2 Proportion of assessable high-risk features present in the paired relapse study cohort at diagnosis. Metastatic disease, M1+ disease; LCA, large cell/anaplastic histology; STR, subtotal resection.

Clinicopathological features in the paired relapse cohort at diagnosis were compared to historic studies of tumours sampled at diagnosis, and demonstrated that for gender, age and pathological subtype incidence was comparable, but subtotal resection was enriched (p=0.0657, Fisher's exact test) and metastatic disease was significantly more common in the paired relapse cohort at diagnosis (p=0.0026, Fisher's exact test, Table 3.3). Similarly, at relapse, metastatic disease was the only clinicopathological feature significantly enriched in comparison to historic studies of medulloblastomas sampled at diagnosis (p<0.0001, Fisher's exact test, Table 3.3). The majority of patients who were fully staged at relapse (n=24) demonstrated distant sites of disease (18/24, 75%).

Clinicopathological features		Historic studies [#]	Paired relapse study			
			Diagnosis	p value	Relapse	p value
Gender	Male	585/952 (61%)	18/29 (62%)	1	18/29 (62%)	1
	Female	367/952 (39%)	11/29 (38%)		11/29 (38%)	
	Male:female ratio	1.6:1	1.6:1		1.6:1	
Age	Age range in years	0.3-52	0.1-33.7	0.6261 *	2.3-36.3	1 *
	Infants (<4 years)	167/943 (17%)	6/29 (21%)		5/29 (17%)	
	Children (4-16 years)	599/943 (64%)	22/29 (76%)		19/29 (66%)	
	Adults (>16 years)	177/943 (19%)	1/29 (3%)		5/29 (17%)	
Pathology	CLA	938/1277 (74%)	16/26 (61%)	1 *	14/24 (58%)	0.1073 *
	DN	183/1277 (14%)	7/26 (27%)		4/24 (17%)	
	LCA	156/1277 (12%)	3/26 (12%)		6/24 (25%)	
Metastatic stage	M -	608/834 (73%)	9/22 (41%)	**0.0026**	6/24 (25%)	**<0.0001**
	M +	226/834 (27%)	13/22 (59%)		18/24 (75%)	
Resection	GTR	267/317 (84%)	20/29 (69%)	0.0657	na	
	STR	50/317 (16%)	9/29 (31%)		na	

Table 3.3 Comparison of clinicopathological features in the paired relapse study with historic studies of tumours sampled at diagnosis. [#] Historic studies (McManamy *et al.*, 2007; Kool *et al.*, 2012; Lannering *et al.*, 2012). * Patients with the specific feature were compared against all others without that feature. CLA, classic histology; DN, desmoplastic/nodular histology; LCA, large cell/anaplastic histology; M-, M0 disease; M+, M1+ disease; GTR, gross total resection; STR, subtotal resection; na, not applicable. p, Fisher's exact test.

3.4.1.2 High-risk molecular features are enriched at relapse

Whilst the incidence of all molecular aberrations interrogated have not been reported in historic studies of tumours sampled at diagnosis (*e.g.* polyploidy, $p14^{ARF}$ aberrations and *MDM2* status), comparisons between the frequency and distribution of molecular subgroup, *MYC* and *MYCN* amplification, *TP53* mutation and chromosome 17 defects were possible.

MB_{SHH} was enriched at diagnosis within the paired relapse cohort, whereas MB_{Group3} was under-represented when compared to the typical subgroup distribution at diagnosis (p=0.0402 and 0.0355 respectively, Fisher's exact test). This is most likely reflective of current clinical practice coupled with the increased incidence of relapse in infants, which is discussed further in Chapter 6 (section 6.4.3). The remainder of molecular features examined at diagnosis (section 3.3.2) revealed that while high-risk molecular events were present at diagnosis in the paired relapse cohort (*e.g. TP53* mutation, *MYC* and *MYCN* amplification), unlike the high-risk clinicopathological factors, (section 3.4.1.1) these molecular aberrations were not significantly enriched at diagnosis (Table 3.4).

In contrast, the majority of molecular events interrogated at relapse in the paired relapse cohort were significantly more frequent, when compared to historic studies of tumours sampled at diagnosis, most notably the occurrences of *TP53* mutation, *MYC* and *MYCN* amplification (Table 3.4). This observation suggests that there is progression of the molecular biology over time between diagnosis and relapse in medulloblastoma as previously reported by Korshunov *et al,.*(2008). This hypothesis is explored further in the following comparisons made within the relapse cohort between the paired tumour samples taken at both diagnosis and relapse (section 3.4.2).

Molecular features		Historic studies #	Paired relapse study			
			Diagnosis	p value	Relapse	p value
Molecular subgroup	MB_{SHH}	153/550 (28%)	12/25 (48%)	**0.0402 ***	12/25 (48%)	**0.0402 ***
	MB_{WNT}	60/550 (11%)	2/25 (8%)	1 *	2/25 (8%)	1 *
	MB_{Group3}	149/550 (27%)	2/25 (8%)	**0.0355 ***	2/25 (8%)	**0.0355 ***
	MB_{Group4}	188/550 (34%)	9/25 (36%)	0.8324 *	9/25 (36%)	0.8324 *
Molecular defects	*MYC/MYCN* amplification	50/552 (9%)	2/25 (8%)	1	9/29 (31%)	**0.0012**
	MYC amplification	17/552 (3%)	1/25 (4%)	0.5549	4/29 (14%)	**0.0166**
	MYCN amplification	33/552 (6%)	1/25 (4%)	1	5/29 (17%)	**0.034**
	TP53 mutations	21/310 (7%)	4/26 (15%)	0.1157	8/29 (28%)	**0.0013**
	Chromosome 17 defects	138/260 (53%)	8/21 (38%)	0.2562	10/21 (48%)	0.6562

Table 3.4 Comparison of molecular features in the paired relapse study with historic studies of tumours sampled at diagnosis. # Historic studies (Pfister *et al.*, 2009; Pfaff *et al.*, 2010; Ryan *et al.*, 2012). * Patients with the specific feature were compared against all others without that feature.

3.4.2 Clinicopathological and molecular features evolve between diagnosis and relapse

To address the theory that there is progression of clinicopathological and molecular features in medulloblastoma over time, analyses to interrogate the differences between tumour samples taken at relapse and their diagnostic counterparts was undertaken. This comprised of examining the frequencies and distributions of all the clinical, pathological and molecular features investigated at diagnosis and relapse (section 3.1). An overview of the clinicopathological and molecular features for all 29 patients in the paired relapse cohort are summarised in Table 3.5 followed by a detailed analyses and commentary of the pertinent findings.

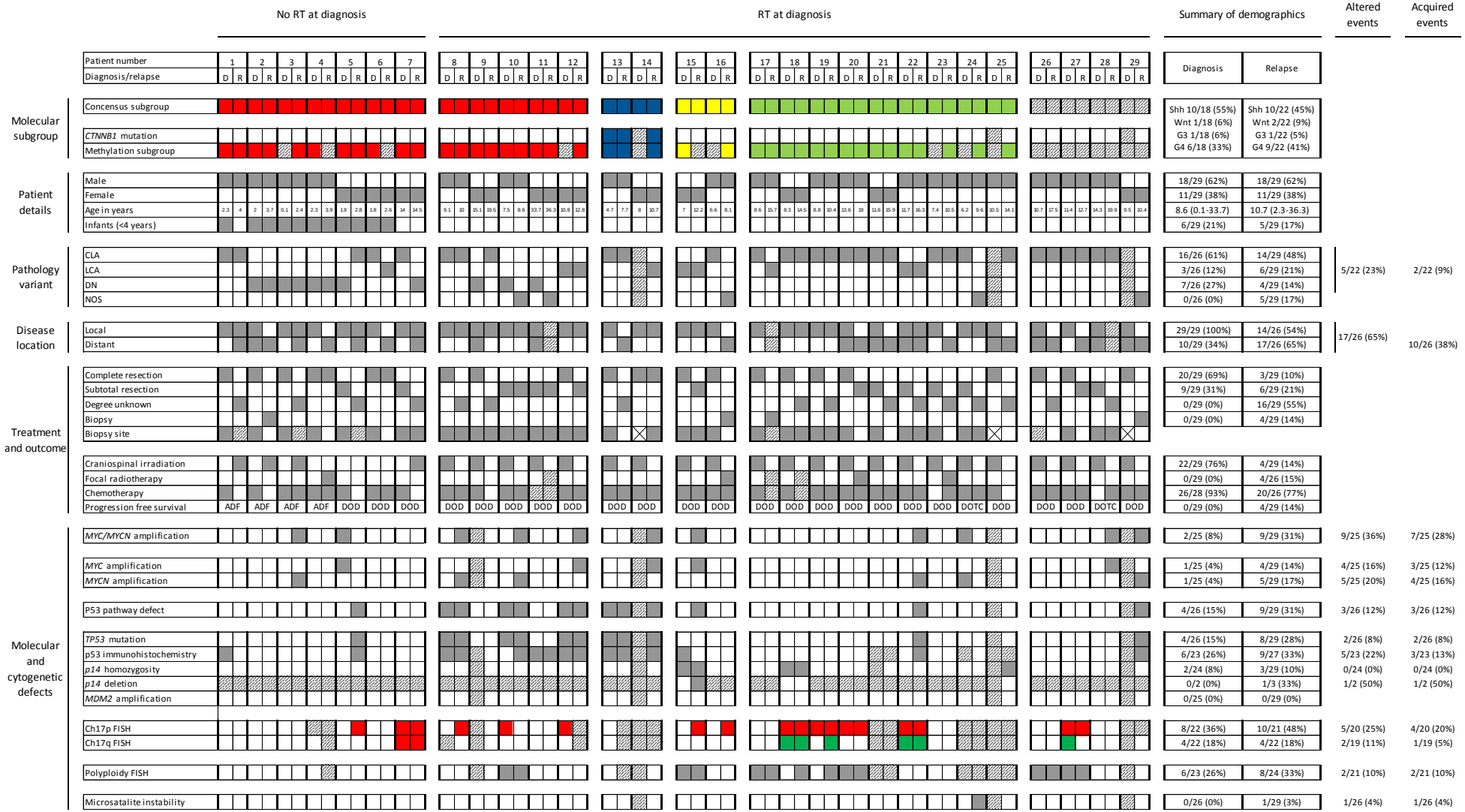
No RT at diagnosis
RT at diagnosis
Summary of demographics
Altered events
Acquired events
Patient number
Diagnosis/relapse
Diagnosis
Relapse
Molecular subgroup
Concensus subgroup
Shh 10/18 (55%) Wnt 1/18 (6%) G3 1/18 (6%) G4 6/18 (33%)
Shh 10/22 (45%) Wnt 2/22 (9%) G3 1/22 (5%) G4 9/22 (41%)
CTNNB1 mutation
Methylation subgroup
Patient details
Male
18/29 (62%)
18/29 (62%)
Female
11/29 (38%)
11/29 (38%)
Age in years
8.6 (0.1-33.7)
10.7 (2.3-36.3)
Infants (<4 years)
6/29 (21%)
5/29 (17%)
Pathology variant
CLA
16/26 (61%)
14/29 (48%)
LCA
3/26 (12%)
6/29 (21%)
5/22 (23%)
2/22 (9%)
DN
7/26 (27%)
4/29 (14%)
NOS
0/26 (0%)
5/29 (17%)
Disease location
Local
29/29 (100%)
14/26 (54%)
Distant
10/29 (34%)
17/26 (65%)
17/26 (65%)
10/26 (38%)
Treatment and outcome
Complete resection
20/29 (69%)
3/29 (10%)
Subtotal resection
9/29 (31%)
6/29 (21%)
Degree unknown
0/29 (0%)
16/29 (55%)
Biopsy
0/29 (0%)
4/29 (14%)
Biopsy site
Craniospinal irradiation
22/29 (76%)
4/29 (14%)
Focal radiotherapy
0/29 (0%)
4/26 (15%)
Chemotherapy
26/28 (93%)
20/26 (77%)
Progression free survival
0/29 (0%)
4/29 (14%)
Molecular and cytogenetic defects
MYC/MYCN amplification
2/25 (8%)
9/29 (31%)
9/25 (36%)
7/25 (28%)
MYC amplification
1/25 (4%)
4/29 (14%)
4/25 (16%)
3/25 (12%)
MYCN amplification
1/25 (4%)
5/29 (17%)
5/25 (20%)
4/25 (16%)
P53 pathway defect
4/26 (15%)
9/29 (31%)
3/26 (12%)
3/26 (12%)
TP53 mutation
4/26 (15%)
8/29 (28%)
2/26 (8%)
2/26 (8%)
p53 immunohistochemistry
6/23 (26%)
9/27 (33%)
5/23 (22%)
3/23 (13%)
p14 homozygosity
2/24 (8%)
3/29 (10%)
0/24 (0%)
0/24 (0%)
p14 deletion
0/2 (0%)
1/3 (33%)
1/2 (50%)
1/2 (50%)
MDM2 amplification
0/25 (0%)
0/29 (0%)
Ch17p FISH
8/22 (36%)
10/21 (48%)
5/20 (25%)
4/20 (20%)
Ch17q FISH
4/22 (18%)
4/22 (18%)
2/19 (11%)
1/19 (5%)
Polyploidy FISH
6/23 (26%)
8/24 (33%)
2/21 (10%)
2/21 (10%)
Microsatalite instability
0/26 (0%)
1/29 (3%)
1/26 (4%)
1/26 (4%)

Table 3.5 Detailed clinical, pathological and molecular characteristics of the paired relapse cohort at diagnosis (D) and relapse (R), showing altered and acquired features at relapse. Demographic frequencies, altered and acquired events are shown as a proportion and percentage of the data available for each variable. Consensus molecular subgroup (red, MB_{SHH}; blue, MB_{WNT}; yellow, MB_{Group3}; green, MB_{Group4}). Pathology variant (CLA, classic; LCA, large-cell/anaplastic; DN, desmoplastic/nodular; NOS, medulloblastoma not otherwise specified). Disease location (local, M0/M1; distant, M2+). Current status (ADF, alive disease-free; DOD, died of disease; DOTC, died of treatment complications). Chromosome 17 status (red, loss; green, gain). Feature present, grey square; feature absent, white square; data not available, diagonal hatching; biopsy sample not available, crossed square.

3.4.2.1 Molecular subgroups are stable between diagnosis and relapse

Molecular subgrouping, achieved by PCR based DNA sequencing analysis of *CTNNB1* (Table 3.6 and section 2.3.2) and the Infinium methylation 450K array (section 3.3.2.1), was confidently assigned in 40/49 (82%) tumour samples within the paired relapse cohort (Figure 3.3, section 2.11). Two cases had *CTNNB1* mutations, both of which were located in exon 3, part of the GSK-3β phosphorylation domain of the gene and the known mutational hotspot in MB_{WNT} (Ellison *et al.*, 2005; Taylor *et al.*, 2012). Both these cases alone also clustered with MB_{WNT} on the Infinium methylation 450K array (Table 3.5 and Figure 3.3). In total, 15/15 (100%) assessable pairs maintained molecular subgroup, as determined by their DNA methylation patterns at both time-points (Table 3.5). This discovery corroborated recent findings from an independent study, which similarly reported that molecular subgroup did not alter at relapse in medulloblastoma (Ramaswamy *et al.*, 2013).

Patient number	Mutated gene	Protein	Acquired mutation	Molecular Subgroup
13	*CTNNB1*	Ser34Phe	No	MB_{WNT}
14	*CTNNB1*	Ser37deletion	Unknown	MB_{WNT}

Phe, Phenylalanine, Ser, Serine.

Table 3.6 Details of *CTNNB1* mutations identified in the paired relapse cohort.

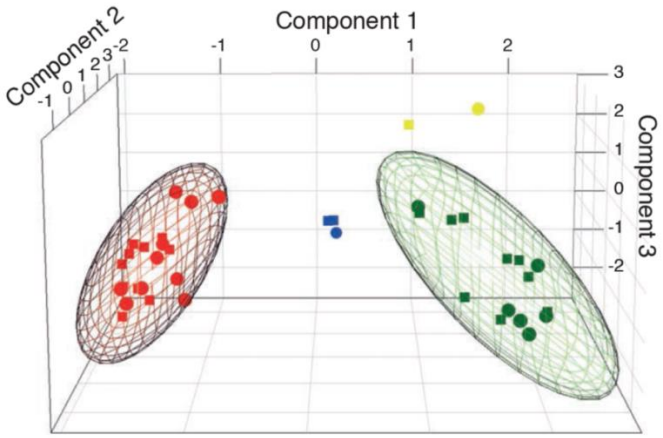

Figure 3.3 Principal component analysis of medulloblastoma subgroups at diagnosis and relapse. Consensus molecular subgroups: red, MB_{SHH}; blue, MB_{WNT}; yellow, MB_{Group3}; green, MB_{Group4}. Subgroups assigned at diagnosis are represented by circles and those assigned at relapse by squares.

3.4.2.2 Acquisition at relapse of high-risk clinicopathological features

The incidence of clinicopathological features between diagnosis and relapse within the paired relapse cohort were altered (Table 3.5). Acquisition of LCA histology and distant disease (M2+) was demonstrated between paired samples (2/22, 9% and 10/26, 38% respectively, Figure 3.4). While the frequency of LCA at diagnosis and relapse was not significantly different (p=0.2814, Fisher's exact test), the occurrence of distant disease (M2+) was significantly enriched at relapse when compared to diagnosis (p=0.0315, Fisher's exact test).

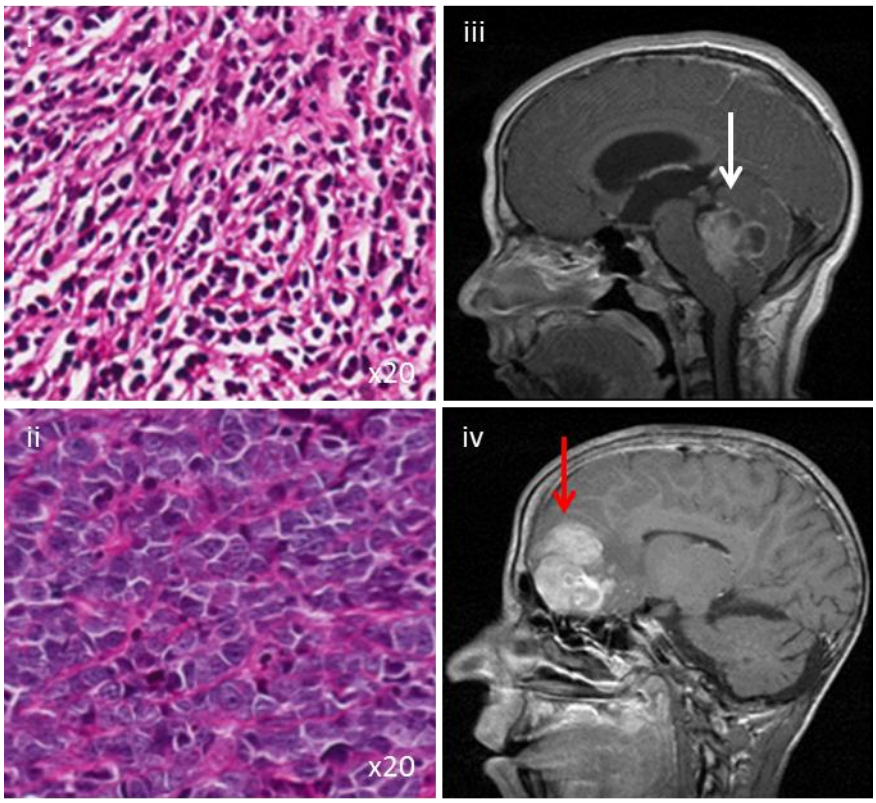

Figure 3.4 Acquisition of high-risk clinicopathological features at medulloblastoma relapse. H&E stain demonstrating (i) CLA histology at diagnosis and development of LCA at relapse (ii). Sagittal view of an MRI kindly provided by Prof Simon Bailey (PBTG) showing (iii) local disease at diagnosis (white arrow) with a large, distant, frontal lesion (red arrow) at disease recurrence (iv).

3.4.2.3 Acquisition at relapse of high-risk molecular features

All of the molecular features examined, with the exception of *MDM2*, demonstrated evidence of acquired defects at relapse. Microsatellite instability, polyploidy, chromosome 17 defects, *TP53* mutations, $p14^{ARF}$ defects, *MYC* and *MYCN* amplifications were observed in tumours sampled at relapse where the paired sample showed no evidence of that defect (Table 3.5). Acquisition of microsatellite instability and polyploidy (Figure 3.5) were witnessed in only one paired tumour sample respectively, whereas all other aberrations demonstrated acquisition in multiple cases and are discussed in detail below.

3.4.2.3.1 Chromosome 17 defects are acquired in relapsed disease

Chromosome 17 defects were acquired at relapse in five tumours (5/20 assessable pairs, 25%) but the overall frequency of chromosome 17 defects was not significantly enriched when compared to diagnosis in the paired relapse cohort (p=0.7557, Fisher's exact test).

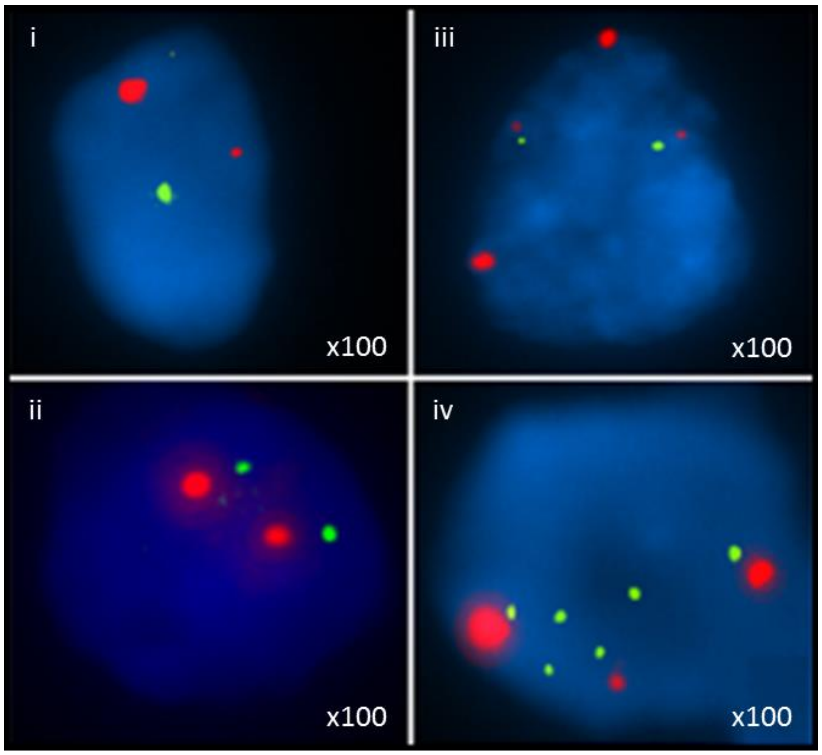

Figure 3.5 Acquisition of Chromosome 17 defects between diagnosis and relapse. FISH images demonstrating 17p loss (i), with a balanced 17q profile (ii) at diagnosis, evolving into i(17)q and evidence of polyploidy with 17p loss (iii), and 17q gain(iv) at relapse. Green, locus specific probe; red, centromeric probe.

3.4.2.3.2 p53 pathway defects are maintained or emerge at relapse

No evidence of *MDM2* amplification or *p14*^{ARF} hypermethylation was discovered at either diagnosis or relapse. Acquisition of other p53 pathway defects were observed in three patients (*TP53* mutation and *p14*^{ARF} deletion, Table 3.5 and Figure 3.6). These defects were consistent with the typically reported pathway defects in the disease at diagnosis (Frank *et al.*, 2004; Zhukova *et al.*, 2013), and compliments the theory of tumour molecular evolution over time, first proposed by Korshunov *et al.*, (2008).

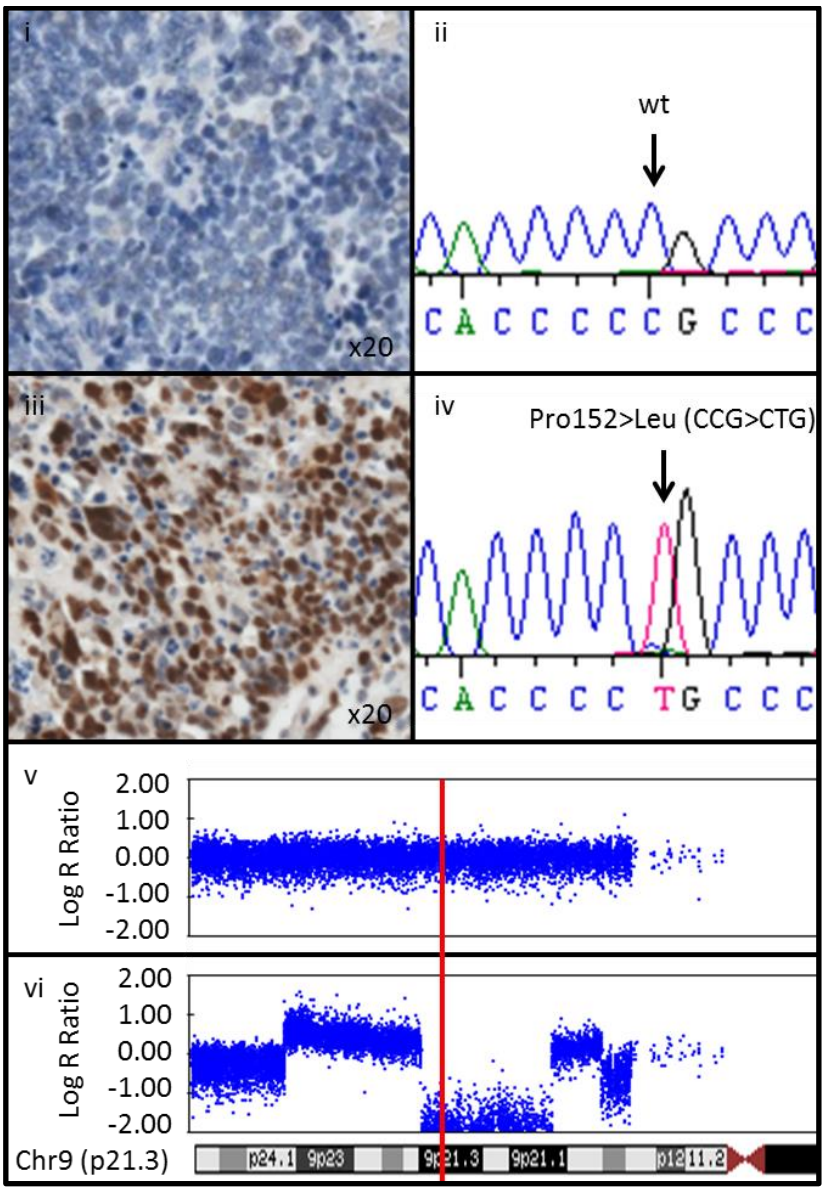

Figure 3.6 Acquisition of p53 pathway defects at relapse. (i) Normal negative immunohistochemical staining of the p53 protein with wild type copy (wt, arrow) of the *TP53* gene (ii) at diagnosis. Acquisition at relapse of a homozygous *TP53* mutation (arrow) as demonstrated by Sanger sequencing (iv) and corresponding nuclear accumulation of the p53 protein (iii). (v) Normal copy number profile of chromosome 9p with loss of one copy of the *p14*^{ARF} locus (red line) at relapse (vi).

Importantly, no case showed loss of a p53 pathway defect and in total 8/29 (28%) patients demonstrated *TP53* mutations at relapse, two of which were acquired and 1/29 (3%) demonstrated deletion of the $p14^{ARF}$ gene (Figure 3.6 and Table 3.5). Whilst the frequency of *TP53* mutations at relapse was significantly enriched when compared to independent historic studies (Table 3.4), the increased incidence of p53 pathway defects between diagnosis and relapse within the paired relapse cohort was not significant (p=0.3387, Fisher's exact test). All *TP53* mutations observed had been reported on the *TP53* database (Soussi *et al.*, 2006) and located within exons 4-9 which encodes for the DNA binding domain of p53, the region most frequently mutated in medulloblastoma (Pfaff *et al.*, 2010; Zhukova *et al.*, 2013).

Patient number	Mutated gene	Protein	Homozygous	Acquired mutation	Molecular Subgroup
5	*TP53*	Gly245Val	No	Yes	MB_{SHH}
8	*TP53*	Arg282Trp	Yes	No	MB_{SHH}
10	*TP53*	Arg282Trp	Yes	No	MB_{SHH}
12	*TP53*	Arg273His	Yes	No	MB_{SHH}
13	*TP53*	Arg158Cys & Arg282Trp	No	No	MB_{WNT}
14	*TP53*	Arg273His	No	Unknown	MB_{WNT}
22	*TP53*	Pro152Leu	Yes	Yes	MB_{Group4}
29	*TP53*	Arg175His	No	Unknown	Unknown

Arg, Arginine; Cys, Cysteine; His, Histidine; Leu, Leucine; Pro, Proline; Trp, Tryptophan; Val, Valine; na, not applicable.

Table 3.7 Nature of *TP53* mutations that are maintained or acquired at medulloblastoma relapse.

3.4.2.3.3 MYC gene family amplifications frequently emerge at relapse

Amplification of *MYC* and *MYCN* was the most frequently acquired defect observed at relapse (7/25 assessable paired samples, 28%). This was a significantly increased rate of amplification when compared to tumours sampled at diagnosis within the paired relapse cohort (p=0.0467, Fisher's exact test and Figure 3.7). This finding corroborates the earlier observations by Korshunov *et el*., (2008, section 1.9.2.1) of molecular progression over time in medulloblastoma, as they also observed acquisition of *MYCN* amplification at relapse in a minority of cases (2/28, 7%).

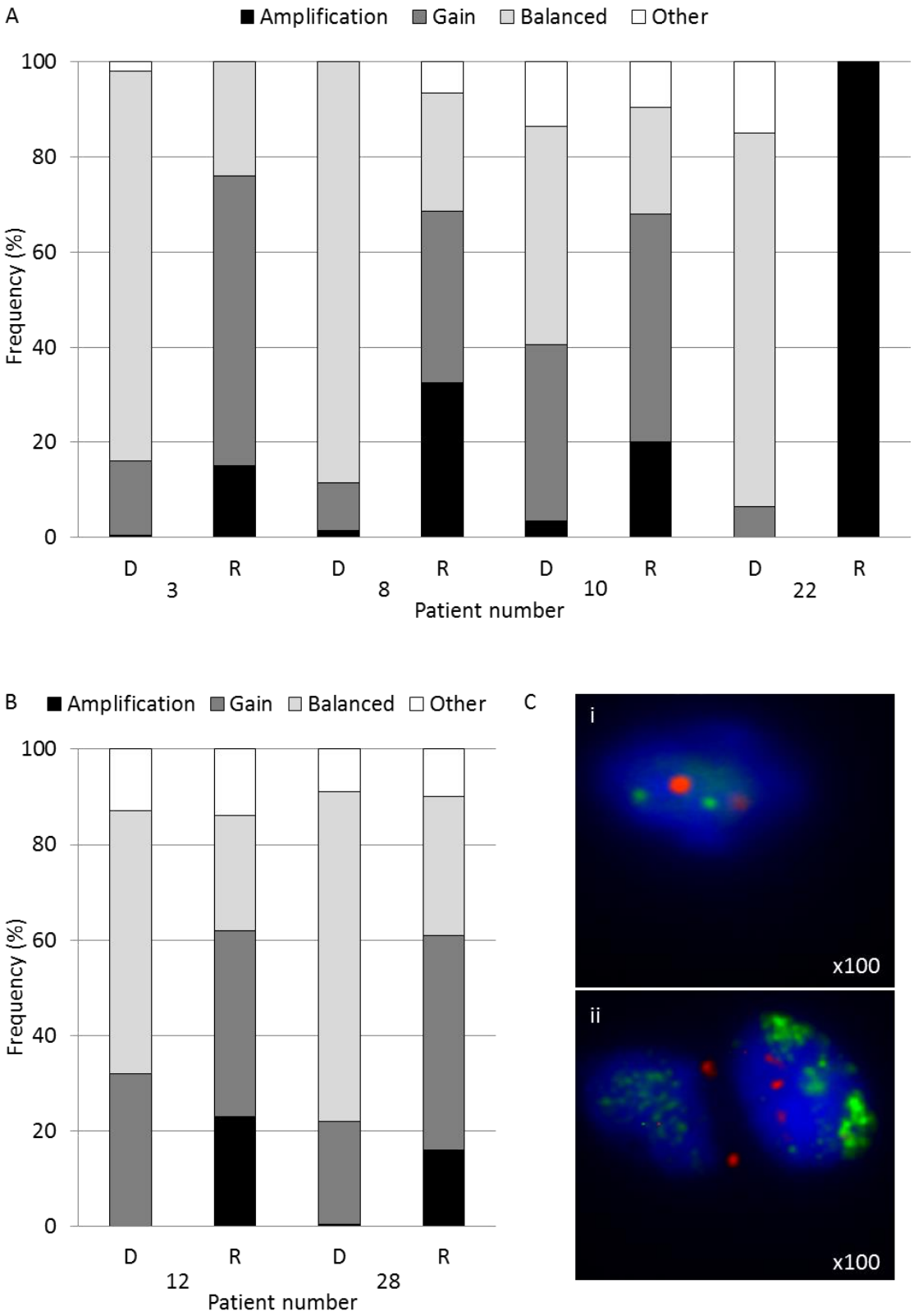

Figure 3.7 *MYC* and *MYCN* defects at diagnosis and relapse. (A) *MYCN* amplification at relapse (R) with varying statuses at diagnosis (low levels of amplification; patient 3, 8 and 10, gain in patient 22). (B) *MYC* amplification at relapse following high levels of gain (patient 12) or low levels of amplification (patient 28) at diagnosis. (C) FISH images demonstrating a balanced profile at diagnosis (i) and amplification at relapse (ii). Green, locus specific probe; red, centromeric probe.

3.4.3 Overall survival in the paired relapse cohort

The median time to relapse in the paired relapse cohort was 2.6 years (range 0.7-7.1 years) with a median age at recurrence of 10.7 years (range 2.4-36.3 years). Twenty-five patients (85%) died following relapse; 23/29 (79%) died of their disease, 2/29 (7%) died of other causes (Table 3.5). Of note, none of the patients who received standard initial therapy, consisting of upfront CSI (22/29, 76%) survived their disease recurrence. Only 4/29 (14%) survived their relapse, all of whom were infants (<4 years) at diagnosis who received salvage radiotherapy at disease recurrence (median OS 17 years, range 8.9-19.2 years). In both univariate and multivariate analyses infant age group was the most significant established clinical feature associated with OS (Figure 3.8 and Table 3.8).

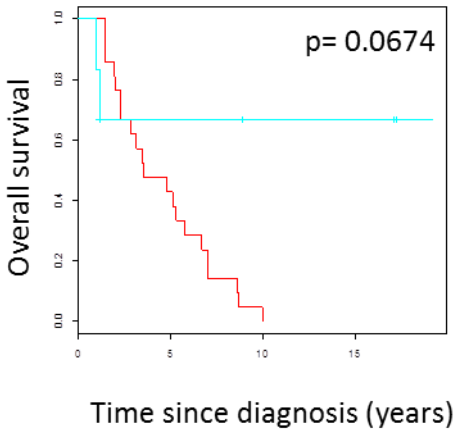

Figure 3.8 Kaplan-Meier plot demonstrating the difference in overall survival between infants and non-infants in the paired relapse cohort. Blue line, infant age group; red line, non-infant age group. p, Log rank test, Bonferroni corrected.

Clinicopathological feature		Number of patients	Univariate			Multivariate
			HR	95% CI	p value	p value
Age	Infant	6/29 (21%)	0.171	0.04-0.77	**0.021**	**0.021***
	Non infant	23/29 (79%)				
Gender	Male	18/29 (62%)	0.385	0.16-0.92	**0.032**	ns
	Female	11/29 (38%)				
RT at diagnosis	Yes	22/29 (76%)	3.715	1.05-13.21	**0.043**	ns
	No	7/29 (24%)				
Resection	STR	9/29 (31%)	2.281	0.9-5.79	0.083	ns
	GTR	20/29 (69%)				
Pathology	LCA	3/26 (12%)	1.758	0.49-6.33	0.388	ns
	Non LCA	23/26 (88%)				
Metastatic stage	M+	10/29 (34%)	0.886	0.37-2.10	0.784	ns
	M-	19/29 (66%)				

Table 3.8 Cox proportional hazard models assessing the significance of clinicopathological features on OS. Unadjusted p values are reported. RT, radiotherapy; STR, subtotal resection; GTR, gross total resection; LCA, large cell/anaplastic histology; M+, M2+ disease; M-, M0/M1 disease; ns, not significant; HR, hazard ratio; CI, confidence interval.

3.4.4 Analyses of relapsing patients who received upfront craniospinal irradiation

In view of the OS differences within the paired relapse cohort between infants and non-infants, and the survival advantage conveyed by salvage radiotherapy at relapse the following analyses were carried out on those patients >4 years old who received comparable upfront standard treatment (n=22, surgical resection, CSI and chemotherapy).

3.4.4.1 MYC gene family amplification and p53 pathway defects are significantly associated at relapse

All interrogated clinical, pathological and molecular features with validated relationships to poor prognoses in the disease at diagnosis (section 3.1) were tested for association at diagnosis and relapse in the paired relapse cohort. These results, summarised in Figure 3.9, demonstrated that at diagnosis no features were significantly associated with each other but importantly, at relapse, several events showed evidence of association. These were; p53 pathway defects and LCA histology (4/20 assessable cases, 20%, p=0.03, Fisher's exact test), p53 pathway defects and

MYCN amplification (4/22, 18%, p=0.01, Fisher's exact test), LCA histology and *MYC* gene family amplification (4/20 assessable cases, 20%, p=0.03, Fisher's exact test) and p53 pathway defects and *MYC* gene family amplification (7/22, 32%, p=0.0004, Fisher's exact test).

With the exception of p53 pathway defects and LCA histology, which was observed in 1/19 (5%) assessable cases at diagnosis, none of the other correlations at relapse were witnessed in the paired relapse cohort at diagnosis (p53 pathway defects and *MYCN* amplification, LCA histology and *MYC* gene family amplification and p53 pathway defects and *MYC* gene family amplification). Furthermore, following correction using the Bonferroni procedure for type I errors (familywise error rate, section 2.10) the association of *MYC* gene family amplification and p53 pathway defects remained the only significant finding at medulloblastoma relapse (p=0.02, Fisher's exact test).

A

p53 defect	Ch17 defects	LCA	Gender	Resection	Metastatic disease	Ploidy	MB_{Group4}	MB_{SHH}	*MYC* amplification	*MYCN* amplification
0.57(1)										
0.53(1)	0.57(1)									
1(1)	1(1)	0.22(1)								
1(1)	1(1)	1(1)	1(1)							
0.25(1)	1(1)	1(1)	0.66(1)	0.38(1)						
1(1)	1(1)	1(1)	1(1)	0.59(1)	1(1)					
0.08(1)	0.57(1)	1(1)	0.33(1)	0.62(1)	0.62(1)	1(1)				
0.06(1)	1(1)	1(1)	0.33(1)	1(1)	1(1)	1(1)				
MYC amplification not detected at diagnosis										
1(1)		1(1)	1(1)	0.39(1)	1(1)		1(1)	1(1)		

B

p53 defect	Ch17 defects	LCA	Gender	Resection	Metastatic disease	Ploidy	MB_{Group4}	MB_{SHH}	*MYC* amplification	*MYCN* amplification	*MYC/MYCN* amplification
0.57(1)											
0.03(1)	1(1)										
0.39(1)	1(1)	0.28(1)									
0.37(1)	1(1)	0.28(1)	0.17(1)								
0.37(1)	0.62(1)	1(1)	0.37(1)		1(1)						
0.05(1)	1(1)	0.58(1)	0.33(1)		0.31(1)	0.28(1)					
0.33(1)	0.22(1)	1(1)	0.33(1)		0.09(1)	0.3(1)					
0.12(1)	1(1)	0.05(1)	0.12(1)		0.09(1)	0.59(1)	0.21(1)	1(1)			
0.01(0.49)	1(1)	0.51(1)	1(1)		1(1)	0.59(1)	1(1)	0.17(1)			
0.0004(0.02)	1(1)	**0.03**(1)	0.39(1)		0.17(1)	0.19(1)	0.13(1)	0.27(1)			

Figure 3.9 Correlative analysis of the association between clinicopathological and molecular features at diagnosis (A) and relapse (B). Raw p values (Fisher's exact test) reported in individual boxes, Bonferroni corrected p values in parentheses; Ch17, chromosome 17; LCA, large cell/anaplastic histology; diagonally hatched boxes, comparison not appropriate/available; bold, significant raw p value; yellow box, significant finding following Bonferroni correction.

3.4.4.2 MYC and p53 defects are either detected at low levels at diagnosis or acquired de novo at relapse

Following the identification of combined p53 pathway defects and *MYC* gene family amplification which emerged at relapse (p53-MYC), it was evident that tumours sampled at relapse acquired *MYC* gene family amplification following either low levels of amplified cells (<5%) at diagnosis (patient 8 and 10, Figure 3.10), or no detectable amplified cells at diagnosis (patient 12 and 22, Figure 3.10). *TP53* mutations were either maintained at relapse (patient 8, 10 and 12, Figure 3.10) or acquired *de novo* at relapse in one patient (patient 22, Figure 3.10), who on next generation sequencing demonstrated no evidence of a mutation at diagnosis in approximately 2000 reads (Figure 3.10).

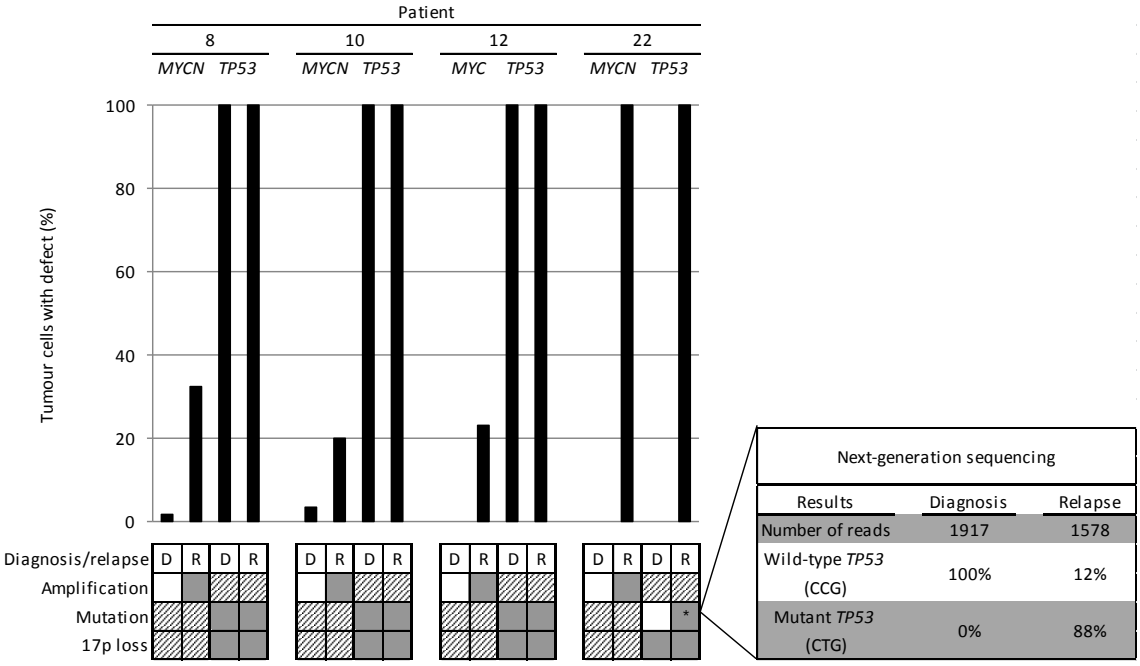

Figure 3.10 Mechanisms for acquisition of molecular defects at relapse. Estimated percentages of *TP53* mutated tumour cells (Sanger sequencing peak heights, mutant versus wild type) and *MYC/MYCN* amplified cells (by FISH). D, diagnosis; R, relapse; diagonally hatched box, data not relevant; white box, negative results; grey box; positive result. * Expanded box; next generation sequencing reads for *TP53* exon 5, patient 22.

3.4.4.3 TP53 mutations predict a shortened time to relapse

All clinicopathological and molecular features at diagnosis and relapse were analysed to determine their association with time to relapse (EFS). These univariate and multivariate analyses included the variable of combined p53-MYC defects which emerged at relapse (section 3.4.4.1). The results of these Cox proportional hazard models are summarised in Table 3.9 and demonstrate that in univariate analyses p53 pathway defects at diagnosis (4/19, 21%, p=0.007), MB_{SHH} membership (5/14, 36%, p=0.035) and *MYCN* amplification at relapse (4/22, 18%, p=0.044) all conveyed a significantly shortened time to relapse.

Importantly these first two features, p53 pathway defects and MB_{SHH}, are closely related. While p53 pathway defects and MB_{SHH} were not significantly associated at diagnosis in this study (p=0.06, Fisher's exact test, Figure 3.9), 3/4 (75%) of the cases with a p53 pathway defect at diagnosis belonged to the MB_{SHH} subgroup. The p53 pathway defects were *TP53* mutations in the DNA binding domain in all three cases. Moreover, only 2/5 (40%) of MB_{SHH} did not demonstrate a *TP53* mutation. These observations are consistent with other recent reports that *TP53* mutations convey a poor prognosis in MB_{SHH} (Zhukova *et al.*, 2013; Kool *et al.*, 2014). This is particularly true between the ages of 5-18 years, which was corroborated by these three cases of MB_{SHH} with *TP53* mutations who were all diagnosed with a medulloblastoma in this age range (patient 8, 10 and 12, age range 7.5-10.8 years, Table 3.5). It is also reported that patients with a MB_{SHH} tumour and a *TP53* mutation are more likely to harbour a germline *TP53* mutation consistent with LFS (section 1.8.7.1), however, no germline DNA was available to test this hypotheses in these three individuals (Rausch *et al.*, 2012; Zhukova *et al.*, 2013; Kool *et al.*, 2014).

The third significant feature associated with a shortened time to relapse was *MYCN* amplification at relapse. *MYCN* amplification at diagnosis conveys a poor prognosis in MB_{SHH} and 2/4 (50%) cases identified to have a *MYCN* amplification at relapse were assigned to the MB_{SHH} subgroup. The presence of the defect at relapse, but not at diagnosis, and its association with a rapid time to relapse can be explained in several ways. Firstly 2/4 (50%) of those cases with *MYCN* amplification at relapse exhibited MB_{SHH} membership and *TP53* mutations at diagnosis and therefore it could be these molecular events that drove the tumour to recur quickly. Importantly, 3/4 (75%), of

tumours with *MYCN* amplification at relapse, when sampled at diagnosis exhibited low levels (<5%) of *MYCN* amplification. These findings may support the theory that this aggressive sub-population of *MYCN* amplified cells which, following the selective pressure of treatment, expanded rapidly to populate an early, recurrent tumour (Figure 3.7). In the single case that does not show any amplified nuclei at diagnosis (patient 22) there are two possibilities as to why *MYCN* amplification could predict a rapid time to relapse. Firstly, that there was a sub-population of *MYCN* amplified cells that, due to tumour heterogeneity, were not sampled at diagnosis. Secondly, that *MYCN* amplification was acquired *de novo*, but early in the treatment course leading to a reduced time to relapse.

To further address these hypotheses a multivariate Cox proportional hazard model, inclusive of all univariate variables analysed, was performed (Table 3.9). This demonstrated that the only factor significantly associated with EFS was the presence of a *TP53* mutation at diagnosis (p=0.007) and no other event added to this model. *TP53* mutations are known to convey a poor prognosis in a subgroup-specific manner. Interestingly, 2/4 (50%) patients with a *TP53* mutation at diagnosis were classified as having standard-risk disease in this cohort (patient 8 (MB_{SHH}) and 13 (MB_{WNT})). Together, these findings re-emphasise the importance of overlaying molecular biomarkers to stratify new therapeutic approaches in a subgroup-specific manner in medulloblastoma at diagnosis.

Variable		Number of cases	Univariate			Multivariate
			HR	95% CI	p value	p value
p53 pathway defect at diagnosis	Yes	4/19 (21%)	6.887	1.69-28.14	**0.007**	**0.007***
	No	15/19 (79%)				
Subgroup	MB_{SHH}	5/14 (36%)	3.929	1.1-14.03	**0.035**	ns
	MB_{Group4}	9/14 (64%)				
MYCN amplification at relapse	Yes	4/22 (18%)	3.257	1.03-10.28	**0.044**	ns
	No	18/22 (82%)				
p53 pathway defect at relapse	Yes	8/22 (36%)	2.593	0.99-6.79	0.053	ns
	No	14/22 (64%)				
p53 pathway defect & *MYC/MYCN* amplification at relapse	Yes	7/22 (32%)	2.451	0.92-6.49	0.071	ns
	No	15/22 (68%)				
Ploidy at relapse	Yes	8/18 (44%)	0.357	0.12-1.1	0.073	ns
	No	10/18 (56%)				
Ploidy at diagnosis	Yes	6/16 (38%)	0.444	0.14-1.46	0.180	ns
	No	10/16 (62%)				
Ch17 defects at diagnosis	Yes	7/15 (47%)	2.005	0.67-6.01	0.215	ns
	No	8/15 (53%)				
MYC/MYCN amplification at relapse	Yes	8/22 (36%)	1.723	0.69-4.31	0.245	ns
	No	14/22 (64%)				
Ch17 defects at relapse	Yes	8/15 (53%)	1.952	0.62-6.08	0.249	ns
	No	7/15 (47%)				
Metastatic stage at diagnosis	M +	9/22 (41%)	0.697	0.29-1.68	0.422	ns
	M -	13/22 (59%)				
Pathology at relapse	LCA	5/16 (31%)	0.712	0.22-2.26	0.565	ns
	Non LCA	11/16 (69%)				
Metastatic stage at relapse	M +	10/19 (53%)	0.793	0.31-2.01	0.625	ns
	M -	9/19 (47%)				
Gender	Male	14/22 (64%)	0.812	0.32-2	0.650	ns
	Female	8/22 (36%)				
Resection at diagnosis	STR	7/22 (32%)	1.243	0.49-3.19	0.651	ns
	GTR	15/22 (68%)				
Pathology at diagnosis	LCA	3/19 (16%)	1.127	0.31-4.06	0.855	ns
	Non LCA	16/19 (84%)				
MYC amplification at relapse	Yes	4/22 (18%)	0.954	0.32-2.89	0.934	ns
	No	18/22 (82%)				

Table 3.9 Univariate and multivariate Cox proportional hazard models interrogating the relationship between all clinicopathological and molecular variables and time to relapse. HR, hazard ratio; CI, confidence interval; Ch17, chromosome 17; M+, M2+; M0, M0/M1; LCA, large cell/anaplastic histology; STR, subtotal resection; GTR, gross total resection; bold, significant; ns, not significant. Features witnessed as a single event were not included.

3.4.4.4 Combined p53 pathway defects and MYC gene family amplification predict a rapid time to death following relapse

All clinicopathological and molecular features were analysed to determine their association with TTD (Table 3.10). For the purposes of these analyses the data for the patients who died of treatment complications (n=2) were censored (section 2.8).

Variable		Number of cases	Univariate			Multivariate
			HR	95% CI	p value	p value
p53 pathway defect & *MYC/MYCN* amplification at relapse	Yes	7/20 (35%)	8.185	1.93-34.19	**0.004**	**0.004 ***
	No	13/20 (65%)				
MYC/MYCN amplification at relapse	Yes	7/20 (35%)	8.185	1.93-34.19	**0.004**	ns
	No	13/20 (65%)				
p53 pathway defect at relapse	Yes	8/20 (40%)	3.692	1.26-10.78	**0.017**	ns
	No	12/20 (60%)				
MYCN amplification at relapse	Yes	4/20 (20%)	5.633	1.35-23.44	**0.017**	ns
	No	16/20 (80%)				
Pathology at diagnosis	LCA	3/17 (18%)	6.304	1.22-32.45	**0.028**	ns
	Non LCA	14/17 (82%)				
p53 pathway defect at diagnosis	Yes	4/17 (24%)	2.919	0.86-9.91	0.086	ns
	No	13/17 (76%)				
Ch17 defects at relapse	Yes	8/14 (57%)	3.149	0.78-12.71	0.107	ns
	No	6/14 (43%)				
MYC amplification at relapse	Yes	3/20 (15%)	2.905	0.74-11.39	0.126	ns
	No	17/20 (85%)				
Subgroup	MB_{SHH}	5/13 (38%)	2.272	0.67-7.67	0.186	ns
	MB_{Group4}	8/13 (62%)				
Ch17 defects at diagnosis	Yes	7/14 (50%)	2.207	0.68-7.15	0.187	ns
	No	7/14 (50%)				
Pathology at relapse	LCA	5/17 (29%)	1.613	0.53-4.88	0.397	ns
	Non LCA	12/17 (71%)				
Metastatic stage at diagnosis	M+	8/20 (40%)	1.45	0.57-3.68	0.439	ns
	M-	12/20 (60%)				
Gender	Male	12/20 (60%)	0.728	0.29-1.86	0.506	ns
	Female	8/20 (40%)				
Ploidy at relapse	Yes	8/17 (47%)	0.835	0.31-2.25	0.722	ns
	No	9/17 (53%)				
Metastatic stage at relapse	M+	10/18 (56%)	0.857	0.33-2.26	0.754	ns
	M-	8/18 (44%)				
Ploidy at diagnosis	Yes	6/15 (40%)	1.03	0.36-2.99	0.956	ns
	No	9/15 (60%)				
Resection at diagnosis	STR	5/20 (25%)	0.994	0.32-3.07	0.992	ns
	GTR	15/20 (75%)				

Table 3.10 Univariate and multivariate Cox proportional hazard models interrogating the relationship between all clinicopathological and molecular variables and time to death. HR, hazard ratio; CI, confidence interval; LCA, large cell/anaplastic histology; Ch17, chromosome 17; M+, M2+; M0, M0/M1; STR, subtotal resection; GTR, gross total resection; bold, significant; ns, not significant. Features witnessed as a single event were not included.

In univariate analyses the most significant variable associated with a shortened TTD was combined p53 pathway defects and *MYC* gene family amplification (p53-MYC) at relapse, present in 7/20 (35%, p=0.004) patients. In addition to this finding p53 pathway defects at relapse and *MYCN* amplification at relapse both independently predicted a shorted TTD post relapse (8/20, 40%, p=0.017 and 4/20, 20%, p=0.017 respectively). Both these variables however were identifying a similar population of patients to the variable of combined p53-MYC defects (Table 3.5). This was also true for *MYC* gene family amplification at relapse which identified the same cohort of 7/20 patients (35%, p=0.004). One patient demonstrated *MYC* amplification at relapse in isolation (patient 28, Table 3.5) but died of treatment complication and was therefore excluded from these analyses (Table 3.5).

Finally LCA histology at diagnosis, an established poor prognostic marker in medulloblastoma (Pizer and Clifford, 2009; Ellison, 2010; Pizer *et al.*, 2011b), was also significantly associated with a reduced TTD (3/17 assessable cases, 18%, p=0.028). The three patients exhibiting LCA at diagnosis, however, all went on to develop p53-MYC defects. To understand the interplay of these events a multivariate analysis was performed and revealed that combined p53-MYC defects remained the only significant variable associated with rapidly progressive disease at relapse and no other variable added to the Cox proportional hazard model (p=0.004, Table 3.10). This significant finding is illustrated in the following Kaplan-Meier survival curves (Figure 3.11) which reports the Log rank, Bonferroni corrected p values for patients with p53-MYC defects for time to relapse (p=1) and TTD (p=0.0165). These analyses further support the association of p53-MYC defects and TTD which remained the only significant variable following Log rank analyses and correction for multiple testing (section 2.10).

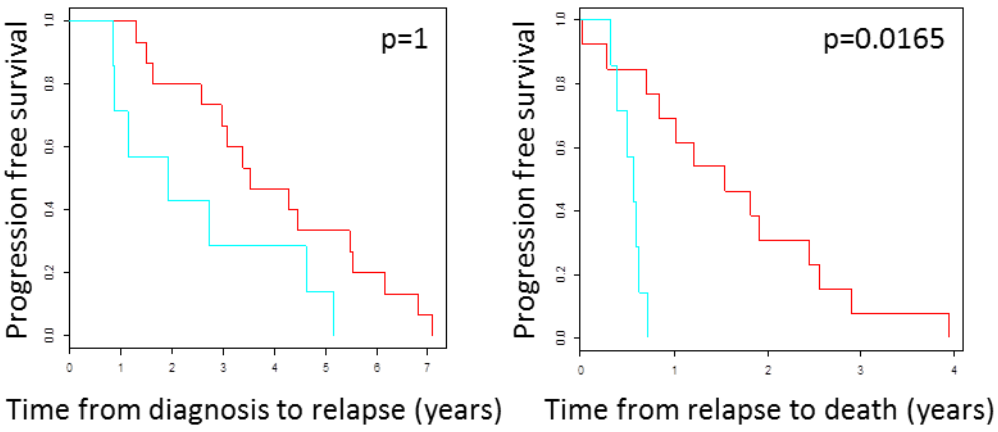

Figure 3.11 Survival of patients harbouring combined p53 pathway defects and *MYC* gene family amplification at relapse. Left, Kaplan-Meier curve demonstrating no significant difference in time from diagnosis to relapse between patients with p53-MYC defects (blue line) and patients without p53-MYC defects (red line). Right, Kaplan-Meier curve demonstrating a significant difference in time from relapse to death between patients with p53-MYC defects (blue line) and patients without p53-MYC defects (red line). p, Log rank test, Bonferroni corrected.

3.4.4.5 Relapsed tumours with combined p53-MYC defects are locally aggressive

At relapse, p53 pathway defects and *MYC* gene family amplification were the only features examined that were significantly associated with each other. No other features demonstrated a significant association after correction for multiple testing at either diagnosis or relapse (Figure 3.9). Furthermore, combined p53-MYC defects were the only feature in multivariate analyses significantly associated with a rapidly progressive disease course following relapse. This is the first report of emergent molecular events at medulloblastoma relapse to show an association with disease prognosis. The clinical, pathological and molecular features of the seven cases demonstrating combined p53-MYC defects at relapse are summarised in Table 3.11. This summary highlights important clinicopathological and molecular observations in this subgroup of patients.

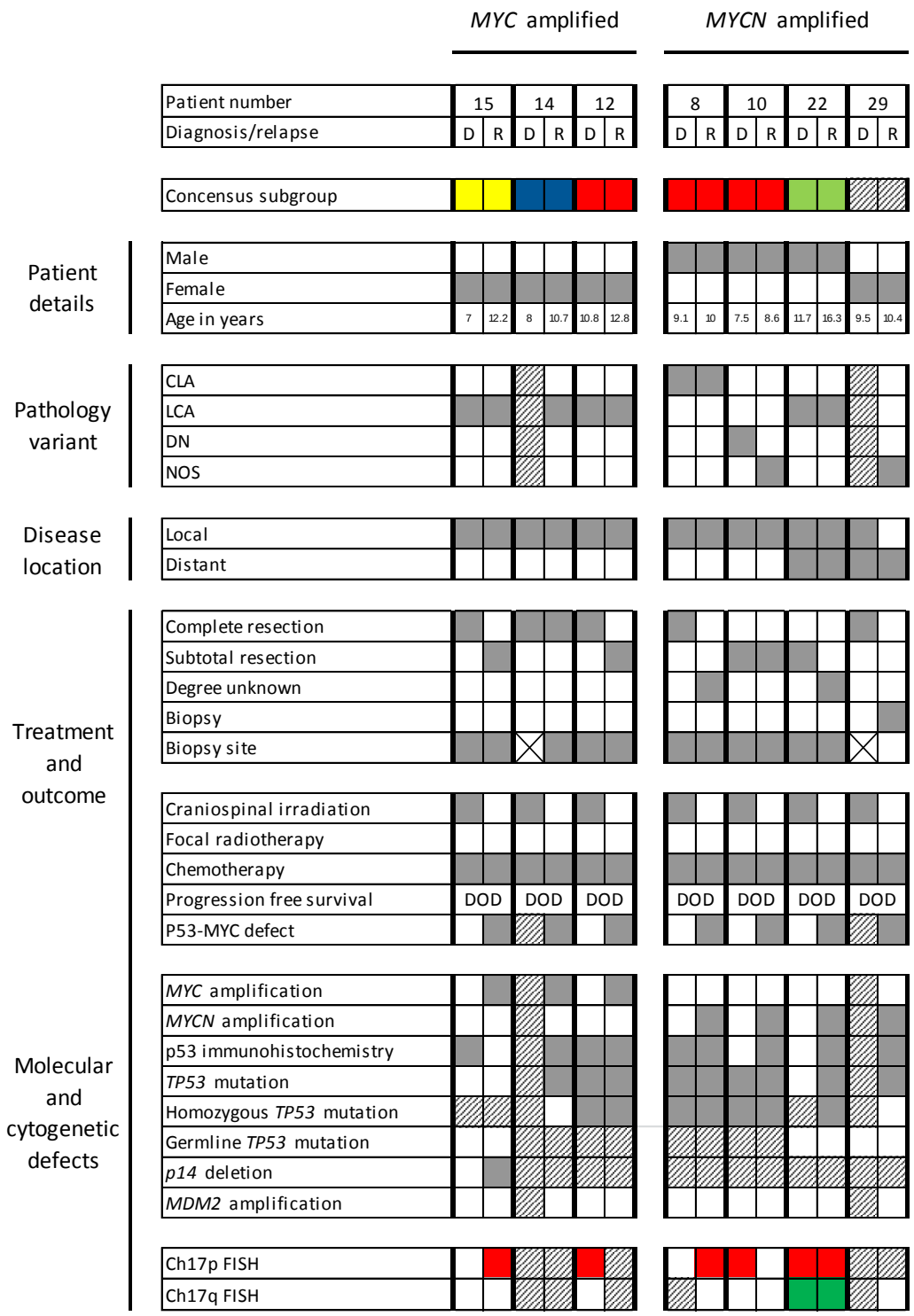

Table 3.11 Detailed clinical, pathological and molecular demographics of patients with combined p53 pathway defects and *MYC* gene family defects at relapse. Consensus molecular subgroup (red, MB_{SHH}; blue, MB_{WNT}; yellow, MB_{Group3}; green, MB_{Group4}). Pathology variant (CLA, classic; LCA, large-cell/anaplasia; DN, nodular/desmoplastic; NOS, medulloblastoma not otherwise specified). Disease location (local, M0/M1; distant, M2+) current status (DOD, died of disease). Chromosome 17 status (red, loss; green, gain). D, diagnosis; R, relapse. Feature present, grey square; feature absent, white square; data not available, diagonal hatching; biopsy sample not received, crossed square.

Disease at relapse was local in 5/7 cases (70%) and significantly associated with LCA at relapse in 4/5 assessable cases (80%, p=0.0099, Fisher's exact test). Tumours with combined p53-MYC defects were therefore locally extremely aggressive, and in the main, non-metastatic (2/7, 30%, demonstrated distant disease sites at relapse). *TP53* mutations were homozygous in 4/6 (67%) cases and heterozygous in 2/6 (33%). No evidence of germline mutations were found in 2/6 (33%) assessable cases which demonstrated a *TP53* mutation at relapse, and loss of 17p was observed in 2/6 (33%) cases with a *TP53* mutation at relapse, both of which were homozygous.

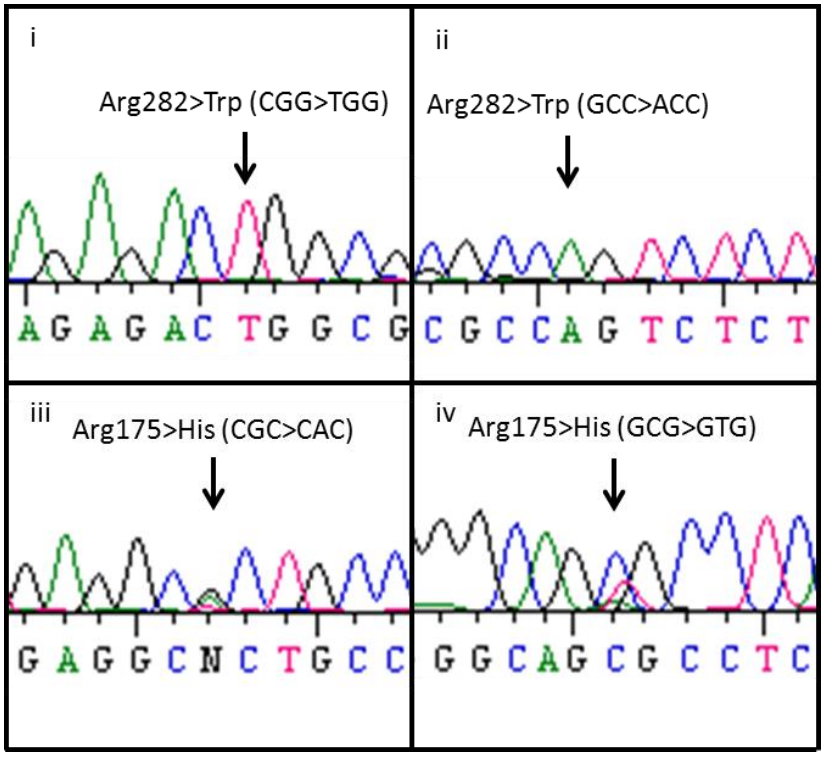

Figure 3.12 Homozygous and heterozygous *TP53* mutations in tumours with combined p53 pathway defects and *MYC* gene family amplification. Forward (i) and reverse (ii) Sanger sequence demonstrating a homozygous *TP53* mutation in codon 282 from the tumour sampled at relapse in patient 8. Forward (iii) and reverse (iv) Sanger sequencing demonstrating a heterozygous *Tp53* mutation in codon 175 from the tumour sampled at relapse in patient 29 (see also Table 3.7).

Typically, combined *TP53* mutation and *MYCN* amplification is a phenomenon normally only observed in ~6% of MB_{SHH} at diagnosis (Jones *et al.*, 2012; Zhukova *et al.*, 2013; Kool *et al.*, 2014). In this study at relapse, combined p53-MYC defects were witnessed across all 4 molecular subgroups in combinations that are not reported in the disease at diagnosis such as; *TP53-MYC* defects in MB_{WNT} and MB_{SHH}, *$p14^{ARF}$-MYC* defects in MB_{Group3} and *TP53-MYCN* defects in MB_{Group4} (Table 3.11).

3.4.4.6 Combined p53-MYC defects are not observed in MB_{WNT}, MB_{Group3} and MB_{Group4} in independent cohorts of tumours sampled at diagnosis

To analyse the incidence of combined p53-MYC defects in a subgroups specific manner at relapse, and compare this to the incidence at diagnosis, a large independent control cohort of tumours sampled at diagnosis (section 3.3.3), was assessed for combined defects (*TP53* mutation and *MYC/MYCN* amplification) alongside molecular subgroup. A further published dataset (Northcott *et al.*, 2012b) was utilised to analyse the combination of *$p14^{ARF}$-MYC* defects in MB_{Group3}, the specific combination identified in MB_{Group3} at relapse in this study. The results of these analyses are reported in Figure 3.13 and demonstrate that no combined p53-MYC defects were found in MB_{WNT}, MB_{Group3} and MB_{Group4} at diagnosis. In MB_{SHH} at diagnosis, *TP53-MYCN* defects were identified at diagnosis in 8/65 (12%) cases, however the incidence at relapse was significantly greater (p=0.0250, 3/5, 60%). The discovery at relapse of combined p53-MYC defects enriched in MB_{SHH}, and the isolated examples observed in MB_{WNT} (1/2, 50%) and MB_{Group3} (1/2, 50%) is a significant finding when compared to the frequency of all these events at diagnosis (p=0.0250, 0.0400 and 0.0156 respectively, Fisher's exact test, Figure 3.13). The isolated example of *TP53-MYCN* defects at relapse in MB_{Group4} (1/9, 11%) was also unique at relapse, but not significant when compared to diagnosis (p=0.0536, Fisher's exact test, Figure 3.13).

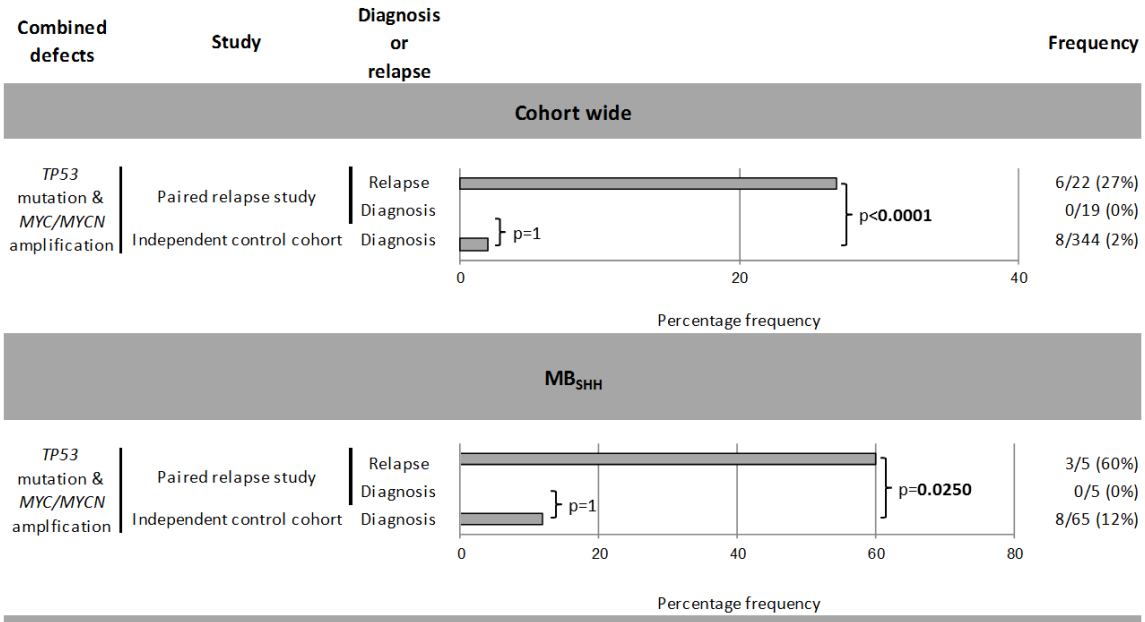

MB_{WNT}, MB_{Group3} and MB_{Group4}

Molecular subgroup	Combined defects	Independent control cohort	Paired relapse study			
		Diagnosis	Diagnosis	p value	Relapse	p value
MB_{WNT}	*TP53* mutation & *MYC* amplification *	0/48 (0%)	0/1 (0%)	1	1/2 (50%)	**0.0400**
MB_{Group3}	$p14^{ARF}$ homozygous deletion & *MYC* amplification #	0/124 (0%)	0/2 (0%)	1	1/2 (50%)	**0.0159**
MB_{Group4}	*TP53* mutation & *MYCN* amplification *	0/159 (0%)	0/8 (0%)	1	1/9 (11%)	0.0536

Figure 3.13 Subgroup distribution of combined p53-MYC defects in the paired relapse cohort compared to a large independent cohort of tumours sampled at diagnosis. No examples of combined *TP53* mutation and *MYC/MYCN* amplification found in MB_{WNT} (n=48), MB_{Group3} (n=72) or MB_{Group4} (n=159) sampled at diagnosis. *Compared against patients receiving upfront radiotherapy. # Compared against patients aged 3-16 years from Northcott *et al.,* (2012b). p, Fisher's exact test versus independent control cohorts, significant values are in bold.

3.5 Discussion

3.5.1 Molecular subgroup does not change at relapse

Recent work in this study and by others (Ramaswamy *et al.*, 2013) has demonstrated, by differing techniques, (methylation profiling, expression signatures and immunohistochemistry) that molecular subgroup does not change between diagnosis and relapse. This supports the theory that the four different medulloblastoma subgroups originate from different embryonal cells (Gibson *et al.*, 2010; Grammel *et al.*, 2012) with the molecular event(s) determining subgroup being common to all tumour cells and present in whichever cells repopulate the relapse tumour. So whilst intratumoural heterogeneity is observed for other events such as *MYC* gene family amplification (Figure 3.7), these findings suggest that molecular subgroup heterogeneity does not occur in medulloblastoma, unlike other brain tumours such as GBM, (Phillips *et al.*, 2006; Sottoriva *et al.*, 2013). Subgroup stability also has important implications for subgroup targeted therapies, *e.g.* SHH inhibitors (section 1.8.8.2), which could be appropriately selected for use at relapse, even if subgroup was determined at diagnosis.

3.5.2 High-risk medulloblastoma features at diagnosis

Clinical and pathological variables currently used for treatment stratification (STR, LCA, M1+ disease and infant age group) to determine high-risk from standard-risk disease (Pizer *et al.*, 2011b) are enriched within this relapsed cohort and do aid in the identification of a population of patients at diagnosis who are likely to have a poor outcome (section 3.4.1.1). Metastatic disease (M1+) was significantly enriched at diagnosis within this cohort and only three out of the twenty-seven fully assessable patients at diagnosis had standard-risk disease (Figure 3.2). Infant age group was reported as the only current high-risk variable to significantly impact OS (section 3.4.3) as while the paired relapsed cohort was enriched for infant patients, as would be expected given their reduced upfront therapy (section 1.8.5), four infants were salvaged with RT and adjuvant therapy at relapse (Figure 3.8).

Acknowledged high-risk molecular features, such as *MYC/MYCN* amplification (Pizer and Clifford, 2009; Northcott *et al.*, 2012a; Ryan *et al.*, 2012), were not enriched at diagnosis. However, the presence of *TP53* at diagnosis predicted a shorter time to

relapse in the non-infant group who received upfront RT (section 3.4.4.3). The presence of *TP53* mutations in three MB_{SHH} at diagnosis also emphasised the interplay of these two molecular features as a poor prognostic marker (Zhukova *et al.*, 2013) highlighting the potential role of directed molecular investigation to improve upfront treatment stratification of this heterogeneous subgroup (section 1.8.8.2).

3.5.3 High-risk medulloblastoma features are enriched and emerge medulloblastoma at relapse

When compared to historic independent cohorts sampled at diagnosis, the incidence of metastatic disease (M1+), *TP53* mutation, *MYC* and *MYCN* amplification were significantly enriched at relapse in the paired relapse cohort (Table 3.3 and Table 3.4). Moreover, on comparing the clinical, pathological and molecular profiles of relapsed patients with their diagnostic counterparts, molecular aberrations were frequently acquired and rarely lost (Table 3.5). This was observed on multiple occasions for chromosome 17 defects (section 3.4.2.3.1), p53 pathway defects (section 3.4.2.3.2) and *MYC* gene family amplification (section 3.4.2.3.3). The emergence of molecular features at relapse occurred following no evidence of the aberration at diagnosis or, low levels of that aberration, for example *MYCN* amplification in <5% of nuclei examined at diagnosis (Figure 3.7 and Figure 3.10). These findings suggest that the molecular progression observed in medulloblastoma at relapse can be attributed to two differing mechanisms, either clonal evolution or *de novo* acquisition.

3.5.4 Clonal evolution versus de novo acquisition of molecular defects at relapse

As highlighted in Figure 3.7 and Figure 3.10, the progression or acquisition of molecular aberrations at relapse either occurred following low levels of the same defect detectable at diagnosis or, in the absence of that defect at diagnosis. These mechanisms can therefore be considered as two different models, similar in design to the previously described models of tumourigenesis in section 1.4, but now taking into account the continuing process of tumour development after a malignant tumour has initially developed, received treatment and then recurred.

The clonal evolution model, first proposed in the 1970s (Nowell, 1976), describes the stepwise selection, expansion and progression of sub-populations of tumours cells. In this model, a treatment resistant, sub-population or clone of cells, present at low levels when the tumour was sampled at diagnosis, survives due to selective pressure following the administration of treatment, and expands to populate the tumour at relapse. This model explains some of the observations in the paired relapse cohort, for example in patient 8 (Figure 3.7 and Figure 3.10), where there was a low level (<5%) of *MYCN* amplified cells in the tumour sampled at diagnosis, but a much higher proportion (>30%) of amplified cells in the counterpart tumour sampled at relapse. Whether this surviving sub-population of cells has stem-like properties (section 1.4.4), is an area of ongoing research in brain tumours, in particular GBM (section 1.6.1.1.2), another highly malignant brain tumour which exhibits genetic heterogeneity and treatment resistance at relapse (Gilbertson and Rich, 2007; Aktipis *et al.*, 2011; Andor *et al.*, 2014).

The second mechanism of emergent defects at relapse is *de novo* acquisition, observed for example in patient 22 (Figure 3.7 and Figure 3.10). This patient demonstrated no evidence of *MYCN* amplification in 200 nuclei scored in their tumour sampled at diagnosis. Conversely, all 200 nuclei counted in the tumour sampled at relapse demonstrated *MYCN* amplification. A similar finding is noted for *TP53* mutation in this case where, on deep sequencing analysis in approximately 2000 reads, no *TP53* mutation was noted in the tumour at diagnosis, whereas almost all tumour cells sequenced at relapse (>1500 reads) showed evidence of mutation (Figure 3.10).

De novo acquisition of p53 pathway defects have been reported *in vivo* (*TP53* mutations) following treatment with both RT and chemotherapy (Lowe *et al.*, 1994), as well as in other paediatric embryonal tumours such as neuroblastoma (*TP53* mutations, $p14^{ARF}$ methylation and deletion, section 1.7.3) at various time-points; post chemotherapy, disease progression and disease recurrence (Carr *et al.*, 2006; Carr-Wilkinson *et al.*, 2010). These findings of emergent defects at medulloblastoma relapse therefore support both mechanisms; clonal expansion and *de novo* acquisition and both models are summarised in Figure 3.14.

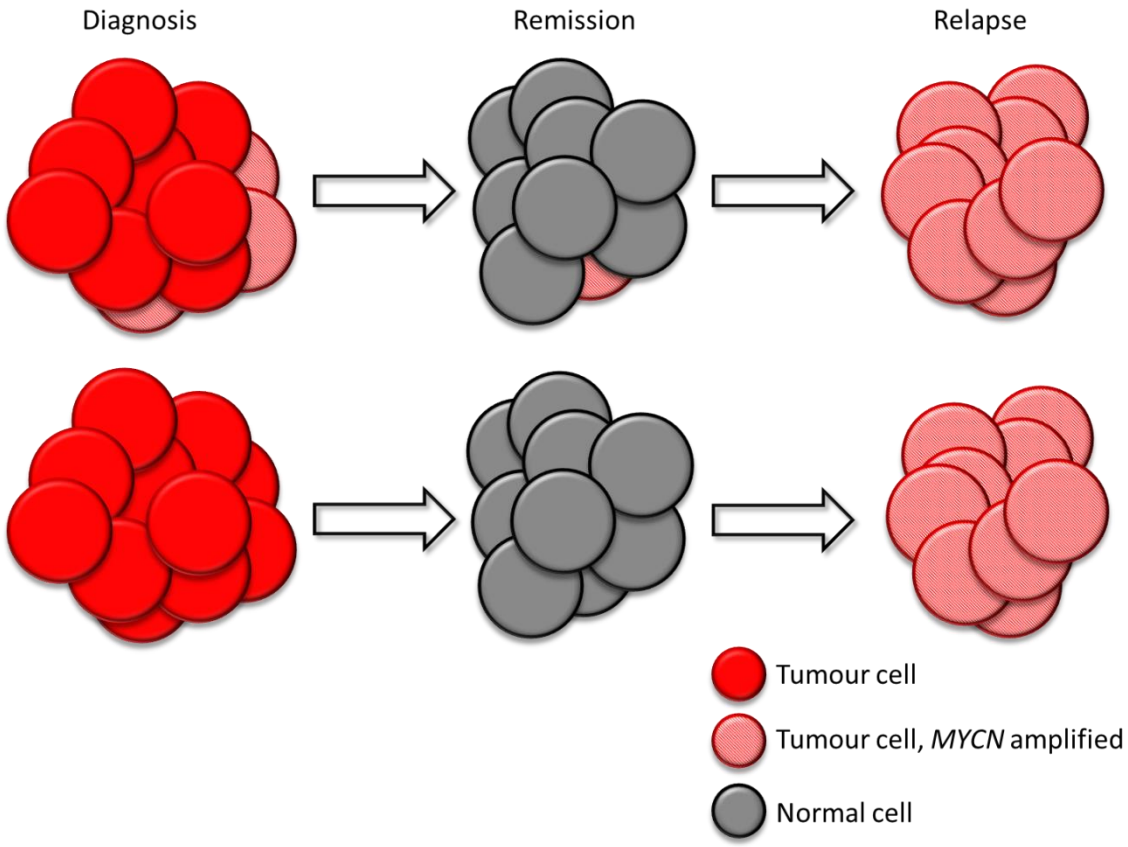

Figure 3.14 Illustrative example of the two mechanisms for acquisition of defects at relapse; clonal expansion and *de novo* acquisition. Top panel, clonal expansion; low level evidence of the molecular aberration (*MYCN* amplification) at diagnosis which remains undetected at remission but populates the tumour at relapse. Bottom panel, *de novo* acquisition; *MYCN* amplification is not present at diagnosis but is acquired during the time between remission and relapse.

3.5.5 Combined p53 and MYC gene family amplifications are a biomarker of aggressive disease at relapse

Individually *MYC* gene family amplification and p53 pathway defects are known to convey a poor prognosis at diagnosis in a subgroup-specific way (Pizer and Clifford, 2009; Northcott *et al.*, 2012a; Ryan *et al.*, 2012; Zhukova *et al.*, 2013; Shih *et al.*, 2014). Combined p53-MYC defects were not observed in our paired relapse cohort at diagnosis, and were only evident in MB_{SHH} in our large independent control cohort of samples taken at diagnosis (section 3.4.4.6). This was consistent with independently reported findings by Zhukova *et al*., (2013).

The relationship between combined p53-MYC defects and survival has never been formally analysed in medulloblastoma at diagnosis or relapse. This study has shown, for the first time, that *MYC* gene family amplification and p53 pathway defects frequently co-occur at relapse and define locally aggressive, rapidly progressive disease (Figure 3.11). This association with aggressive disease behaviour was independent of molecular subgroup in multivariate analysis (Table 3.10), and combined p53-MYC defects were found in all four subgroups, in combinations that were not observed in the disease at diagnosis, for example *TP53-MYC* defects in MB_{WNT} and MB_{SHH}, $p14^{ARF}$-*MYC* defects in MB_{Group3} and *TP53-MYCN* defects in MB_{Group4} (section 3.4.4.5).

3.5.6 p53 pathway defects and MYC gene family amplification interact

The frequent observation of emergent and combined p53-MYC defects at relapse (7/22, 32%) suggested that these two events interact to define rapidly progressive and locally aggressive disease. While we were unable to directly assess this for all human tumours demonstrating combined defects, one tumour, sampled at relapse from patient 22 (Figure 3.10), demonstrated 100% *de novo* acquisition of both *MYCN* amplification by FISH and *TP53* mutation on next generation sequencing. This further supported the hypothesis that combined p53-MYC defects co-occurred at a cellular level. To explore the p53-MYC interaction functionally, collaborations with Dr Louis Chesler and his group, the Pediatric Solid Tumour Biology and Therapeutics Team at The Institute of Cancer Research were undertaken and are discussed in Chapter 4.

3.6 Summary

Recurrent disease is the poorest prognostic factor in childhood medulloblastoma with only infants who receive radiotherapy at relapse surviving despite, in the present study, many older children having treatment with curative intent as part of the Recurrent PNET (CNS 2000 01) trial (Pizer *et al.*, 2011a). Current treatment risk stratification still has merit in the diagnostic setting, as demonstrated by the enrichment of high-risk clinicopathological features in the paired relapse cohort at diagnosis (section 3.4.1.1). However, subgroup-specific treatment stratification is now in development at diagnosis with the aim of reducing long term side effects in low risk groups (MB_{WNT}, section 1.8.8.1.2) and escalating treatment in those patients with high-risk disease (Pizer and Clifford, 2009; Morfouace *et al.*, 2014) . These advancements have not translated into the disease at relapse where little is understood about the biology of disease at this time-point.

The present paired relapse study reports, at diagnosis and relapse, all the clinicopathological and molecular variables with established relationships to disease behaviour at diagnosis. At relapse, almost all clinicopathological and molecular features examined show examples of alteration, and predominately acquisition of poor prognosis features with the only unchanged feature being molecular subgroup (section 3.4.2.1-3.4.2.3). However, it is the emergence of high-risk molecular events at relapse that is significantly enriched when compared to both the paired diagnostic tumour samples, and independent historic cohorts of tumours sampled at diagnosis (section 3.4.1.2 and 3.4.2.3).

The most striking and significant example of altered molecular biology at relapse is the emergence of frequent p53 pathway defects together with *MYC* gene family amplification. These combined defects demonstrated the most significant association with disease behaviour at relapse, identifying a group of patients (7/22, 32%) with rapidly progressive disease at the point of relapse. Moreover, p53-MYC defects occurred in patients who typically only had local disease (5/7, 71%), a feature not commonly found in this cohort (section 3.4.1.1). In addition, these combined defects were observed in all four molecular subgroups in unique combinations, not previously described in the disease (section 3.4.4.6).

This paired relapse study highlights the difficulty in successful treating medulloblastoma at relapse, and provides compelling evidence for further investigations into the disease at this time-point. No patients who received standard upfront multi-modal treatment survived their disease recurrence. This was despite the fact that many had aggressive re-treatment at relapse (Pizer *et al.*, 2011a). Importantly, the biology of relapsed disease evolves and is different to the disease at diagnosis. Events such as combined p53-MYC defects that are not detectable at diagnosis emerge, and interact at relapse. These combined defects are the first described molecular events to be significantly associated with aggressive disease behaviour at recurrence and emphasise the necessity of understanding the molecular biology of relapsed disease by sampling tumours at this time-point. Moreover combined p53-MYC defects have, at present, potential utility in directing current treatment decisions at medulloblastoma relapse. In the future this molecular biomarker could be targeted therapeutically to improve the outcome of this rapidly progressive disease course (Chapter 4).

Further studies in relapsed medulloblastoma are now essential. Interrogating the epigenome and genome of disease at both diagnosis and relapse for events predictive of or specific to relapse could, in turn, identify therapeutic targets. Validation of the findings reported in this chapter is also required in a separate cohort to confirm the frequent presence of p53-MYC defects at relapse, and their association with an aggressive and devastating disease course.

Chapter 4. MYC and p53 interactions can be modelled and therapeutically targeted in GTML mice

4.1 Introduction

To further explore the relationship between *MYC* gene family amplification and p53 pathway defects, the following work was performed by Dr Louis Chesler and his group, the Pediatric Solid Tumour Biology and Therapeutics Team at The Institute of Cancer Research (Sutton, UK). This chapter has therefore been undertaken separate to this study but included in this thesis due to its pertinent discoveries and relevance to relapsed medulloblastoma. The methods, written by Dr Louis Chesler and his group, and results, which they have provided, are reported in this additional chapter along with a discussion of the key findings.

4.2 Materials and methods

These experiments were designed and carried out by Dr Louis Chesler and his group (Pediatric Solid Tumour Biology and Therapeutics Team, The Institute of Cancer Research, Sutton, UK).

4.2.1 Immunohistochemistry

Mouse tumour samples were fixed in 4% paraformaldehyde in PBS for at least 24 hours, decalcified with 0.3M EDTA and processed using the Leica ASP300S tissue processor (Leica Microsystems, Milton Keynes, UK). Sections were cut at 4µM for H&E staining and immunohistochemistry as previously described (Chesler *et al.*, 2006). Antibodies used for immunohistochemistry were: MYCN (OP-13, Merck-Millipore, Darmstadt, Germany), Ki-67 (556003, BD Biosciences, NJ, USA), GFAP (Z0334, DAKO, Glostrup, Denmark), Cleaved Caspase 3 (9664, Cell Signalling Technology, MA, USA), Synaptophysin (180130, Life Technologies, CA, USA), Gli1 (2534, Cell Signalling Technology, MA, USA), Phospho-Ser10-Histone H3 (9706, Cell Signalling Technology, MA, USA).

4.2.2 In situ RNA analysis

Dual colour RNA *in situ* hybridization was performed using the RNAscope 2-plex Chromogenic Reagent Kit (Advanced Cell Diagnostics, CA, USA) according to the manufacturer's instructions. Paired double-Z oligonucleotide probes were designed against *Cdkn1a* using custom software as previously described (Wang *et al.*, 2012). Custom mouse *Cdkn1a*-specific RNA target Z probe pairs (20), provided by Advanced Cell Diagnostics (CA, USA) targeted bps 19 through 1240 of the *Cdkn1a* cDNA sequence (NM_007669.4). Probe sets specific for mouse *Ubc* (ubiquitin C), *Polr2a* (DNA-directed RNA polymerase II subunit RPB1) and *Ppib* (Peptidylprolyl Isomerase B, Cyclophilin B) as well as the probe set against the *dapB* (dihydrodipicolinate reductase) gene from *B. subtilis* were obtained from Advanced Cell Diagnostics (CA, USA).

FFPE tissue blocks were sectioned at 4µm. Slides were baked for 1 hour at 60°C prior to use. After de-paraffinisation and dehydration, the tissues were air dried and treated with peroxidase blocker before boiling at 100-104°C in a pre-treatment solution for 15 minutes. Protease was then applied for 30 minutes at 40°C. Target probes for each two-gene combination were premixed and hybridized together for 2 hours at 40°C,

followed by a series of signal amplification and washing steps. All hybridizations at 40°C were performed in a HybEZ Hybridisation System (Advanced Cell Diagnostics, CA, USA). Following the RNAscope assay, samples were counterstained for 2 minutes with 50% Gill's Haematoxylin diluted in dH_20. Hybridisation signals were detected by sequential chromogenic reactions using red and green chromogens and RNA staining signal was identified as red and green punctate dots. Each sample was quality controlled for RNA integrity with a probe specific to the *Ppib* housekeeping gene; only samples with an average of >4 dots per cell were included for analysis. Negative control background staining was evaluated using a probe specific to the bacterial *dapB* gene; only samples with an average of <1 dot per 10 cells were included for analysis. To verify that the RNAscope method was performed with technical accuracy, references slides consisting of FFPE HeLa cell pellets were tested for *Ppib* and *dapB* expression in parallel with tissue sample quality control (QC).

4.2.3 In situ proximity ligation assay

Duolink *in situ* proximity ligation assay (PLA; Olink Bioscience, Uppsala, Sweden) was performed according to the manufacturer's instructions. Briefly, GTML/*Trp53*$^{KI/KI}$ neurospheres were fixed in 4% paraformaldehyde for 20 minutes, permeabilised with 0.5% Triton X-100 (Sigma-Aldrich, MO, USA), and blocked with 1% bovine serum albumin (BSA) for 30 minutes at room temperature, followed by incubation with paired primary antibodies, MYCN (OP-13, Merck-Millipore, Darmstadt, Germany) with Aurora A (GeneTex, CA, USA), overnight at 4°C. PLA detection was performed as recommended by the manufacturer. Images were taken and analysed using the Zeiss LSM700 confocal microscope (Jena, Germany) and analysed using DuoLink image analysis software (Olink Bioscience, Uppsala, Sweden).

4.2.4 In vivo experiments

All experiments were performed in accordance with guidelines specified in the local ethical review panel, the UK Home Office Animals Scientific Procedures Act 1986 and the UK National Cancer Research Institute guidelines for the welfare of animals in cancer research (Workman *et al.*, 2010). The GTML mouse model has been described previously (Swartling *et al.*, 2010). The *Trp53*$^{KI/KI}$ mice were kindly provided by G.I. Evan (Christophorou *et al.*, 2005) and crossed with GTML animals into a background of the Friend Virus B-type/NIH Jackson (FVB/NJ) inbred strain (Taketo *et al.*, 1991). To image

for bioluminescence expression, animals were injected with 75mg kg^{-1} D-luciferin in saline (Perkin Elmer, MA, USA) prior to imaging in the IVIS Lumina using the Living Image Software 4.3.1 (Perkin Elmer, MA, USA).

Transgenic GTML/*Trp53*$^{KI/KI}$ animals with bioluminescence signals higher than $1.5e^9$ photons/seconds (20-30 days of life) were randomised to treatment groups of 4-6 mice, and treated with 30mg kg^{-1} MLN8237 (kindly provided by Millennium, MA, USA), 50mg/kg GDC-0449 (Vismodegib, LC Laboratories, MA, USA), 1mg kg^{-1} Tamoxifen (Harlan Laboratories, IN, USA), 200mg/kg^{-1} doxycycline (Harlan Laboratories, IN, USA) and vehicle. MLN8237, GDC-0449 and the respective vehicles were dosed orally on a daily basis. Tamoxifen and doxycycline were given via chow at 1mg kg^{-1} and 200mg kg^{-1} respectively. Animals were monitored twice a week for bioluminescence signal and were sacrificed upon detection of a signal higher than $9e^9$ photons/second or overt signs of intracranial expansion associated with tumour growth.

4.2.5 MRI imaging

Multi-slice 1H MRI was performed on a 7T Bruker horizontal bore microimaging system (Bruker, Ettlingen, Germany) using a 3cm birdcage coil and a 2.5cm x 2.5cm field of view. Anaesthesia was induced with a 10 ml kg^{-1} intraperitoneal injection of fentanyl citrate (0.315 mg ml^{-1}) plus fluanisone (10 mg ml^{-1} (Hypnorm; Janssen Pharmaceutical Ltd. High Wycombe, UK), midazolam (5mg/ml (Hypnovel; Roche, CT, USA)), and sterile water (1:1:2). Core body temperature was maintained by warm air blown through the magnet bore. Magnetic field homogeneity was optimized by shimming over the entire brain using an automated shimming routine (FASTmap). T_2-weighted images acquired using a rapid acquisition with refocused echoes (RARE) sequence (12 contiguous 1mm sagittal slices or 20 contiguous 1mm axial slices, 256 x 256 matrix, 4 averages, echo times (TE) = 36 and 132 ms, repetition time (TR) = 4.5 s, RARE factor = 8) were used for localization of the tumour and measurement of tumour volume.

4.2.6 Neurosphere isolation and culture

Tissue was isolated from GTML/Trp53$^{KI/KI}$ tumours and transferred into cold HBSS (Life Sciences, CT, USA). The tissues were then cut into 2-3mm^2 pieces and dissociated before the cells were titrated in medium and filtered through a 70µm mesh. Subsequently the cells were cultured under self-renewal conditions in DMEM/F12

medium (Life Technologies, CA, USA) supplemented with 2% B27 supplement (Life Technologies, CA, USA), 20ng ml^{-1} epidermal growth factor (EGF, Sigma-Aldrich, MO, USA), 20ng ml^{-1} fibroblast growth factor (bFGF-basic, Life Technologies, CA, USA) and 100units ml^{-1} penicillin/streptomycin. To examine cell division rates, cells were treated with the following concentrations of drugs: DMSO or ethanol, 100nM 4-OHT (Sigma-Aldrich, MO, USA), 1µg ml^{-1} doxycycline (Sigma-Aldrich, MO, USA), 100 nM MLN8237, 500 nM GDC-0449 up to 7 days. At each time-point cells were counted as follows: neurospheres were dissociated, trypan blue (Sigma-Aldrich, MO, USA) was added and cells were counted using a haemocytometer. To assess neurosphere formation, cells were plated in limiting dilutions from 1000 to 60 cells in 96-well plates. Drugs were added as before and neurospheres were counted after 3 days in culture using the Celigo S Imaging Cell Cytometer (Brooks Life Science Systems, MA, USA).

4.2.7 Western blot analysis

Tumour or spleen tissues were homogenized using T-PER buffer as previously described (Brockmann *et al.*, 2013). Neurospheres were cultured in the presence or absence of MLN8237 or GDC-0449 for 24hrs before cells were suspended in RIPA lysis buffer (Santa Cruz Biotechnology, TX, USA) as per manufacturer's protocol. Western blot analysis was performed as previously described (Chesler *et al.*, 2006). Antibodies used included MYCN (OP-13, Merck-Millipore, Darmstadt, Germany), Phospo-S10-Histone H3 (9706, Cell Signalling Technology, MA, USA), phospho-AurkABC (2914, Cell Signalling Technology, MA, USA), AurkA (4718, Cell Signalling Technology, MA, USA), Sonic Hedgehog (Ab73958, Abcam, Cambridge, UK), Gli-1 (2534, Cell Signalling Technology, MA, USA) and GAPDH (2118, Cell Signalling Technology, MA, USA).

4.2.8 Gene expression analysis

RNA was isolated from cells or tumour tissue using the miRNAeasy minikit (Qiagen, Venlo, Netherlands) according to the manufacturer's protocol. Total RNA was reverse transcribed into complementary DNA (cDNA) using Superscript II Reverse Transcriptase (Life Technologies, CA, USA) according to manufacturer's protocol. Quantitative PCR (QT-PCR) was performed in triplicates using Taqman Gene Expression mix (Life Technologies, CA, USA). Primers used were mouse *Cdkn1a* (Mm04205640), mouse *Mdm2* (Mm01233136), human *MYCN* (Hs00232074) and mouse β-actin (Mm00607939; Life Technologies, CA, USA). Relative expression was calculated

according to the $\Delta\Delta C_T$ relative quantification method using the average expression of control cells treated with ethanol or vehicle treated tumours as calibrator.

4.2.9 Trp53 mutational analysis

Genomic DNA was extracted from cell lines, tumours and where available, normal brain tissue using a Qiagen QIAamp DNA Mini kit (Qiagen, Venlo, Netherlands). PCR amplification of exons 5-9 was performed using primers detailed in Figure 4.1 . Products were sequenced with the original PCR primers using the BigDye Terminator Cycle Sequencing Kit (Life Technologies, Paisley, UK) and an ABI 3730 Genetic Analyser (Applied Biosystems, Foster City, CA, USA). Sequences were analysed using Mutation Surveyor software v3.97 (DNA Variant Analysis, SoftGenetics, PA, USA).

Location	Forward sequence 5'-3'	Reverse sequence 5'-3'
Exon 5/6	GATCGTTACTCGGCTTGTCC	AAGACGCACAAACCAAAACA
Exon 7	CTATAGCCAGCCATTCCCG	AGGCAGAAGCTGGGGAAG
Exon 8/9	TACACACAGTCAGGATGGGG	ATGCGAGAGACAGAGGCAAT

Figure 4.1 Primers for *Trp53* PCR reaction.

4.2.10 Expression analysis

Affymetrix (Affymetrix, CA, USA) HGU133plus2 expression profiles of primary tumours from 110 individuals with a diagnosis of medulloblastoma were taken from previously published studies (Kool *et al.*, 2008; Fattet *et al.*, 2009). Raw data were normalised and processed using gcRMA in R (R Development Core Team, 2014). Processed data was converted to four metagenes representing the four subgroups using NMF, and these metagenes projected onto the mouse tumour/cell line expression profiles using an adaption of the procedure described by Tamayo *et al* (Tamayo et al., 2007). Mouse expression profiles were generated using Illumina Mouse v8 arrays (Illumina Inc., CA, USA) according to manufacturer's instructions. Raw data was processed using the beadarray package in R (R Development Core Team, 2014). Expression profiles from primary murine medulloblastoma samples and cell lines included a total of 47 from our GTML mouse models as well as 6 from a *Myc/Trp53*-deficient mouse model (Kawauchi *et al.*, 2012) (a kind gift from Dr Martine Roussel, St. Jude Children's Research Hospital, TN, USA) and 36 from *Ptch*$^{+/-}$ mice (Lastowska *et al.*, 2013). We also included published

Ptch$^{+/-}$ and *Myc/Trp53*-deficient mouse model expression profiles (Kawauchi *et al.*, 2012), which were downloaded from Gene Expression Omnibus (Elsevier, London, UK) and processed using gcRMA. Subgroup calls for the mouse tumours were made using a Support Vector Machine algorithm trained on the four human subgroup metagenes and tested on the projected mouse metagenes.

4.2.11 Pharmacokinetic analysis

4.2.11.1 Calibration standards

Calibration and quality control solutions were prepared in dimethyl sulfoxide (DMSO) from individual 1mM MLN8237 and GDC-0449 stocks. Calibration standards used for spiking were prepared over the dynamic range 20-100000nM by serial dilution of the calibration stock solution with DMSO to give final matrix concentrations of 2-10000nM. QC standards were also prepared at 250, 2500, 7500 and 25000nM by serial dilution of the quality control stock solution with DMSO to give a final concentration of 25, 250, 750 and 2500nM. A stock solution of Olomoucine (Sigma-Aldrich, MO, USA) internal standard (IS) was prepared in DMSO at a concentration of 1mM and further diluted in methanol to give a working IS solution of 250nM for quenching.

4.2.11.2 Plasma and tissue sample preparation

Plasma and tissue samples were thawed on ice. All tissues were homogenised in either 3 or 5ml g^{-1} PBS and kept on ice. 100µl aliquots of untreated mouse plasma or tissue homogenates were spiked with 10µl of the appropriate calibration or QC standard solutions. 100µl aliquots of the unknown samples were spiked with 10µl DMSO. Where necessary, plasma and tissue samples were diluted with untreated (blank) matrix.

4.2.11.3 LC-MS/MS method

Extracted plasma and tissue samples were analysed by LC-MS/MS for the quantification of MLN8237, GDC-0449 and Olomoucine (Sigma-Aldrich, MO, USA) using a Waters Xevo TQ-S mass spectrometer (Waters, MA, USA) coupled with an Acquity ultra-performance liquid chromatography UPLC H-class system (Waters, MA, USA). Chromatography was carried out using a Phenomenex (Macclesfield, UK) C18 X-B column (2.6µm, 50mm x 2.1mm ID) with a gradient mobile phase consisting of 0.1 % formic acid and methanol. 2ml of sample was injected on to the column using a flow rate of 0.6ml min^{-1} with a 5 minute run time. Both analytes and IS were ionized using

electrospray interface in positive ion mode. Detection was via tandem mass spectrometry (MS/MS) in the multiple reaction monitoring (MRM) mode. The transitions m/z 519.12 – 139.04, 421.11 – 110.87 and m/z 299.19 – 177.29 were monitored for MLN8237, GDC-0449 and IS respectively. Data acquisition was performed using Targetlynx, version 4.1 (Waters, MA, USA). The assay was linear over the range 2-10,000nM.

4.3 Results

4.3.1 Trp53 and MYCN interact directly in medulloblastoma development and generate locally aggressive tumours

The observations reported in Chapter 3 (section 3.4), alongside other medulloblastoma mouse models reported by Kawauchi *et al*., (2012) and Pei *et al*., (2012, section 1.8.8.3.3), suggested that upregulation of *MYC/MYCN* interacts with inactivation of p53 to form aggressive types of medulloblastoma. To investigate this hypothesis further we elected to examine the *Trp53* status of medulloblastomas arising in the *MYCN*-driven GTML (*Glt1–tTA/TRE–MYCN–Luc*) mouse model. This model is an established doxycycline (dox) regulatable transgenic *MYCN*-driven model (Swartling *et al.*, 2010). Medulloblastoma tumours in this immunocompetent model are spontaneously arising, retain their appropriate anatomical and developmental context, and have an intact blood brain barrier.

Acquired somatic *Trp53* mutations within the DNA binding domain of the gene, which were comparable to the location of mutations in human medulloblastomas, were found in 10/12 of GTML mice examined (83%, Table 3.7 and Table 4.1). Tumours in these mice were also non-metastatic, but locally aggressive, with LCA histology (Figure 4.2), reflective of the clinicopathological features noted in the human medulloblastomas with combined p53-MYC defects (Table 3.11).

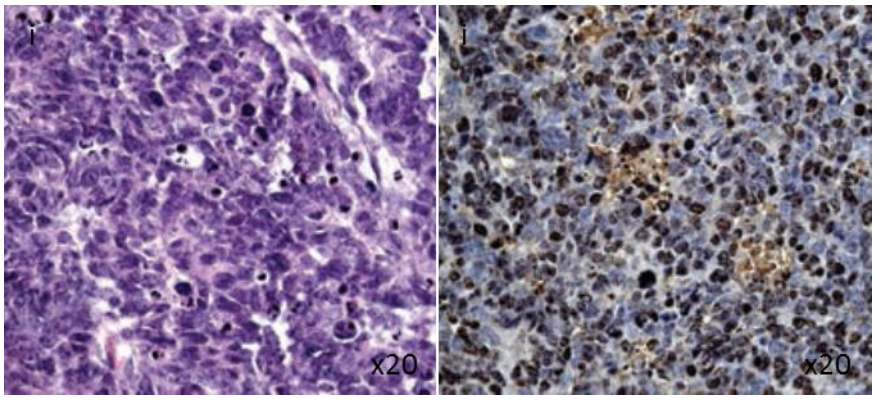

Figure 4.2 GTML mice demonstrate aggressive histopathological features. (i) H&E stain of tumours arising from GTML mice with a spontaneous *Trp53* mutation showing LCA histology and a high proliferation rate on Ki-67 staining (ii).

Mouse ID	Tissue	Sequence variant		Somatic *TP53* mutation count in human cancer*
		cDNA	Protein	
10519	Tumor	734G>GA	Arg245Arg/His	1544 (Arg248)[#]
10519	Brain	None detected	Wild type	na
10087	Tumor	404C>CT	Ala135Ala/Val	110 (Ala138)
10087	Brain	None detected	Wild type	na
26826	Tumor	464G>GC	Arg155Arg/Pro	264 (Arg158)
26826	Brain	None detected	Wild type	na
10933	Tumor	464G>GC	Arg155Arg/Pro	264 (Arg158)
10933	Brain	None detected	Wild type	na
14658	Tumor	701T>C	Met234Thr	214 (Met237)
14658	Brain	None detected	Wild type	na
11185	Tumor	839G>T, 841A>C	Arg280Leu, Thr281Pro	103 (Arg283), 30 (Thr284)
14634	Tumor	382_405 het_delAATAAGCTATTCTGCCAGCTGGCG	Wild type	na
10545	Tumor	577C>CG	Arg193Arg/Gly	230 (Arg196)
19780	Tumor	734G>A	Arg245His	1544 (Arg248)
2737	Tumor	526C>T	His176Tyr	341 (His179)
9303	Tumor	None detected	Wild type	na
9303	Tail	None detected	Wild type	na
11153	Tumor	None detected	Wild type	na

*Soussi *et al.* , 2006

[#]Equivalent human p53 amino acids are shown in parenthesis.

Ala, Alanine; Arg, Arginine; Cys, Cysteine; Gly, Glycine; His, Histidine; Leu, Leucine; Met, Methionine; Pro, Proline; Thr, Threonine; Tyr, Tyrosine; Val, Valine; na, not applicable.

Table 4.1 Spontaneously developing *Trp53* mutations in GTML mice. Table demonstrating the nature of somatic *Trp53* mutations acquired in GTML mouse including nucleotide change, amino acid change and equivalency of mutation to those observed in human cancers.

To examine the interaction between *MYCN* and *Trp53*, and test whether tumour growth was dependent on the dysregulation of both these genes, GTML mice, deficient for p53 from the outset were developed. This novel model was generated by replacing the endogenous *Trp53* gene with a knock-in allele encoding a 4-hydroxytamoxifen (4-OHT) regulatable p53-ER^{TAM} fusion protein (Christophorou *et al.*, 2005). The function of this fusion protein was completely dependent on the administration of ectopic tamoxifen (tam) which is metabolised to 4-OHT, allowing p53 to be readily activated or inactivated. Consequently, this GTML mouse model had both a *MYCN* regulatable (dox) and *Trp53* (4-OHT) regulatable allele, enabling the interaction of these two genes to be studied directly.

The three GTML genotypes developed, (GTML, GTML/*Trp53*$^{KI/WT}$ and GTML/*Trp53*$^{KI/KI}$), were next investigated for tumour penetrance and survival. Both GTML/*Trp53*$^{KI/WT}$ and GTML/*Trp53*$^{KI/KI}$ mice, when compared to GTML mice alone, demonstrated significantly increased penetrance and reduced OS ($p=0.0022$ and $p < 0.0001$, respectively, Log-rank test, Figure 4.3), with GTML/*Trp53*$^{KI/KI}$ displaying 100% tumour penetrance (43/43).

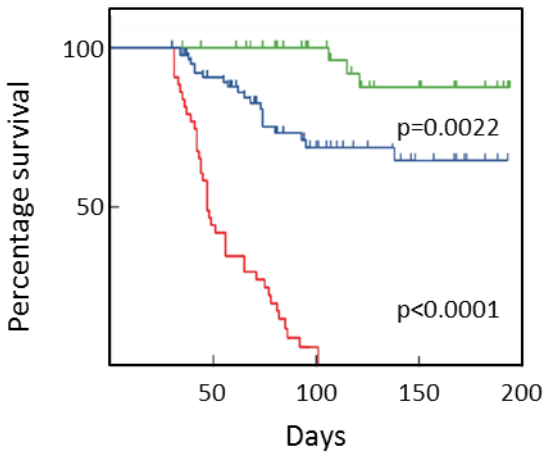

Figure 4.3 Kaplan-Meier survival curves for GTML, GTML/*Trp53*$^{KI/WT}$ and GTML/*Trp53*$^{KI/KI}$ mice. Green line, GTML (n=50); blue line, GTML/*Trp53*$^{KI/WT}$ (n=83); red line, GTML/*Trp53*$^{KI/KI}$ (n=43). p, Log rank test.

Similar to the clinicopathological features noted in the human medulloblastomas with combined p53-MYC defects, and GTML mice with spontaneously arising *Trp53* mutations (Table 3.11 and Figure 4.2), tumours from GTML/*Trp53*$^{KI/WT}$ and GTML/*Trp53*$^{KI/KI}$ displayed locally aggressive pathological features with LCA and a high proliferation rate (Figure 4.4).

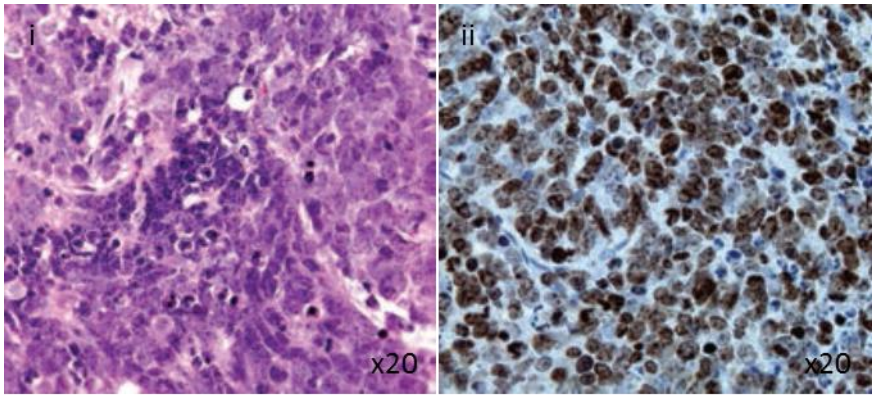

Figure 4.4 GTML/*Trp53*$^{KI/KI}$ mice demonstrate aggressive histopathological features. (i) H&E stain of tumours arising from GTML/*Trp53*$^{KI/KI}$ showing LCA histology and a high proliferation rate on Ki-67 staining (ii).

These tumours, as already described for GTML mice in section 1.8.8.3.3, displayed expression profiles which clustered with human MB_{Group3} expression profiles (Figure 4.5).

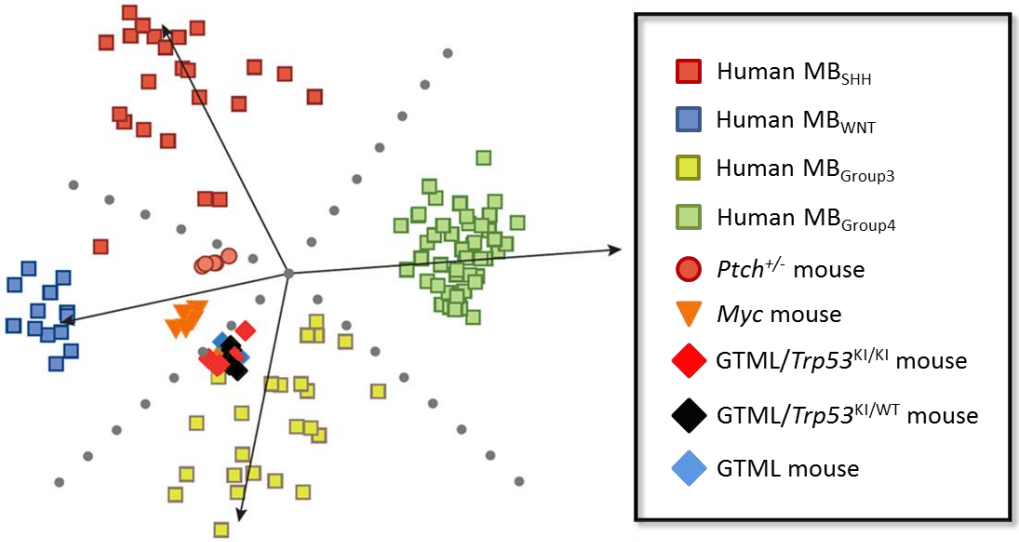

Figure 4.5 Subgroup classification using a support vector machine (SVM) trained on expression profiles of human medulloblastomas. Principal component analysis of murine and human medulloblastomas demonstrated that all 3 GTML genotypes (GTML, GTML/*Trp53*$^{KI/WT}$ and GTML/*Trp53*$^{KI/KI}$) clustered with human MB_{Group3}. (For descriptions of the other mouse models and expression analysis see sections 1.8.8 and 4.2.10 respectively.)

4.3.2 Tumour maintenance is dependent on Trp53 and MYCN status in GTML/Trp53$^{KI/KI}$ mice

We next wanted to investigate in this regulatable model, whether tumour maintenance was reliant on both *MYCN* upregulation and *Trp53* downregulation. Firstly, in GTML/*Trp53*$^{KI/KI}$ neurospheres, suppression of *MYCN* expression with dox, and reactivation of p53 with tam separately lead to a significant reduction in the number of spheres formed, and decreased overall growth ($p<0.0001$, unpaired t test, Figure 4.6). Reduced expression of *MYCN*, and induction of p53 target genes (*e.g. Cdkn1a*, Figure 1.6) was also demonstrated following treatment with dox or tam respectively by real-time quantitative PCR (Figure 4.7).

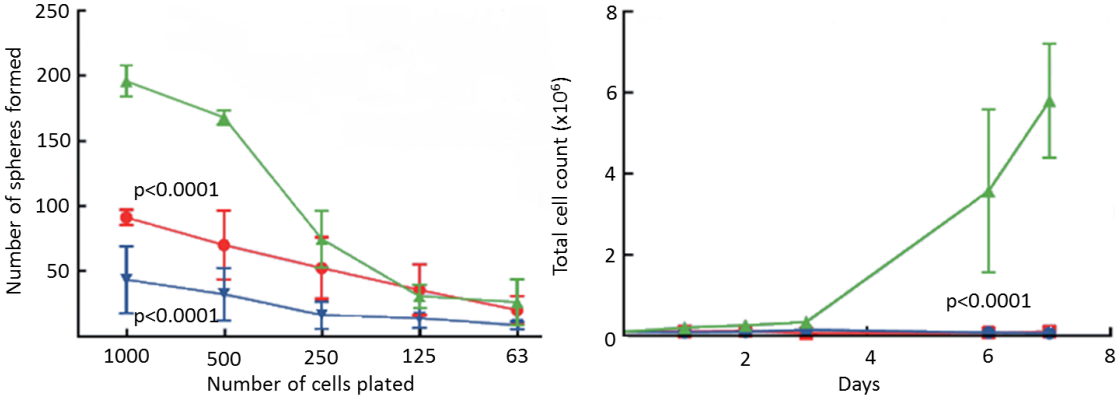

Figure 4.6 GTML/*Trp53*$^{KI/KI}$ derived primary cells depend on both loss of p53 function and expression of *MYCN* for survival. Neurosphere formation (left) and growth (right) following dox (red) or tam (blue) administration compared to untreated control (green). p, unpaired t test.

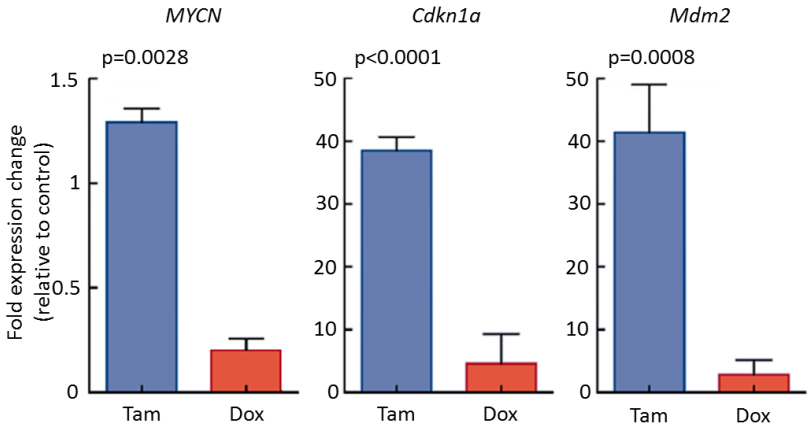

Figure 4.7 Expression levels of human *MYCN* after doxycycline (Dox) treatment and *Cdkn1a* and *Mdm2* after tamoxifen (Tam) treatment. p, unpaired t test.

Secondly, in GTML/*Trp53*$^{KI/KI}$ mice, administration of dox led to tumour regression, and tam inhibited tumour growth revealing a significant survival benefit with both agents (p=0.0101, Log rank test, Figure 4.8 and Figure 4.9).

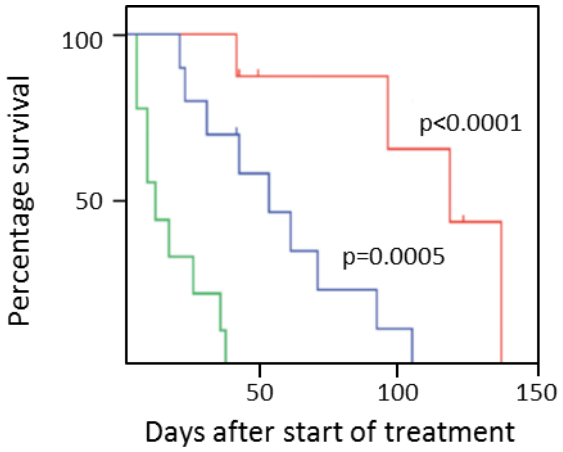

Figure 4.8 Kaplan-Meier curve illustrating the difference in survival of GTML/*Trp53*$^{KI/KI}$ mice treated with doxycycline or tamoxifen. Red line, dox; blue line, tam; green line, vehicle. p, Log rank test.

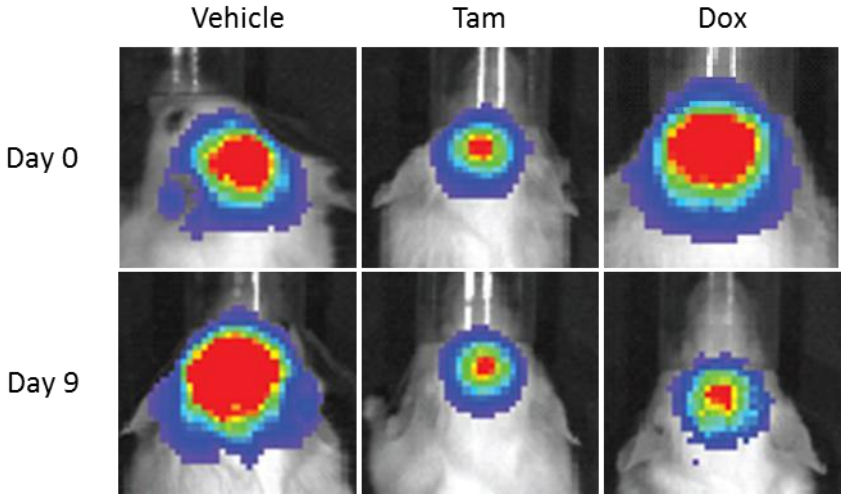

Figure 4.9 GTML/*Trp53*$^{KI/KI}$ mice demonstrate tumour growth inhibition and regression following tamoxifen and doxycycline. Bioluminescence images demonstrating tumour progression is observed between day 0-9 in vehicle control, tumour inhibition is observed between day 0-9 following the administration of tam whereas tumour regression is observed between day 0-9 following the administration of dox.

Similarly MYCN protein expression was reduced in dox treated mice and *Cdkn1a* RNA expression (p53 target gene) increased following the administration of tam (Figure 4.10 and Figure 4.11).

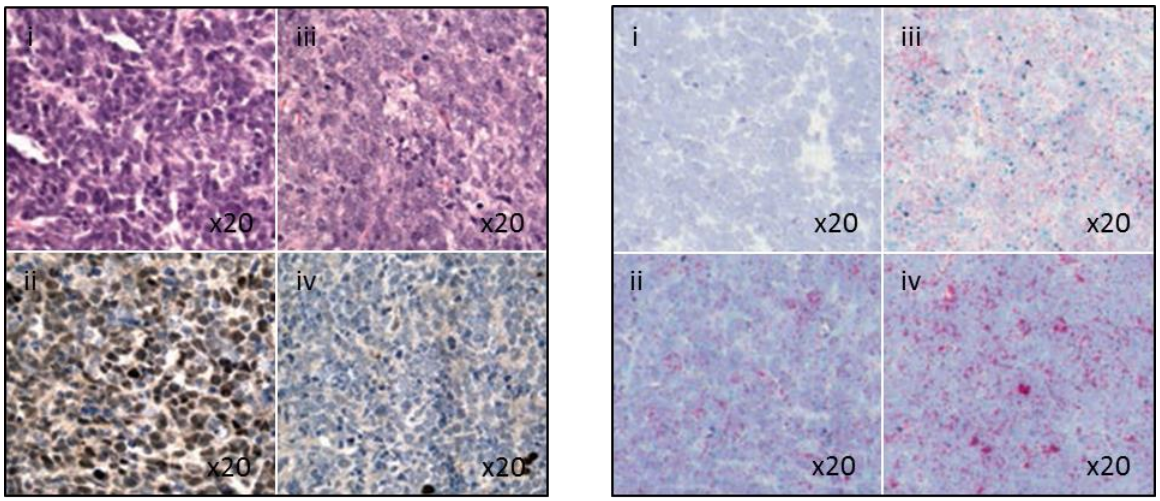

Figure 4.10 GTML/*Trp53*$^{KI/KI}$ mice treated with doxycycline or tamoxifen. Left, H&E of vehicle (i) and doxycycline treated (iii) GTML/*Trp53*$^{KI/KI}$ mice with reduction of MYCN expression in doxycycline (iv) treated GTML/*Trp53*$^{KI/KI}$ versus vehicle (ii). Right, RNA scope demonstrating RNA expression of *Cdkn1a* in negative (i) and positive control (iii) followed by increased expression in tam treated GTML/*Trp53*$^{KI/KI}$ mice (iv) compared to vehicle (ii).

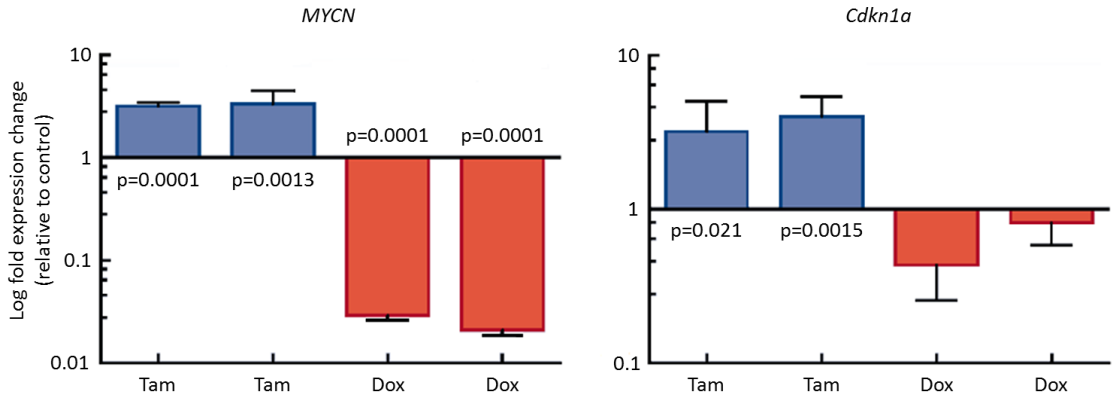

Figure 4.11 Fold difference in human *MYCN* and *Cdkn1a* RNA levels in GTML/*Trp53*$^{KI/KI}$ mice following treatment with either tamoxifen (tam) or doxycycline (dox). p, unpaired t test.

These combined findings validated the dependency of *MYCN*-driven tumour growth in the GTML mouse models on both *MYCN* and *Trp53* defects. As such, the demonstrated dependency of tumour growth and maintenance on this critical interaction provided a potential opportunity for therapeutic intervention in this aggressive tumour model.

4.3.3 Therapeutic targeting and inhibition of Aurora A kinase in GTML/*Trp53*$^{KI/KI}$ mice with MLN8237 reduces tumour growth and prolongs survival

Following this discovery of the reliance of tumour growth and maintenance on the *Trp53-MYCN* interaction in GTML/*Trp53*$^{KI/KI}$ mice, the second generation Aurora A kinase inhibitor MLN8237 was used to treat both GTML/*Trp53*$^{KI/KI}$ neurospheres and mice. MLN8237, described in section 1.5.2.2.1, is a small-molecule that targets the kinase domain of Aurora A, which disrupts the complex formed between Aurora A and MYCN and leads to the degradation of MYCN. This agent has previously demonstrated *in vitro* efficacy in MYCN-driven neuroblastoma cell lines (Brockmann *et al.*, 2013). In our GTML/*Trp53*$^{KI/KI}$ neurospheres, MLN8237 significantly inhibited growth and clonogenic capacity ($p<0.001$, unpaired t test, Figure 4.12).

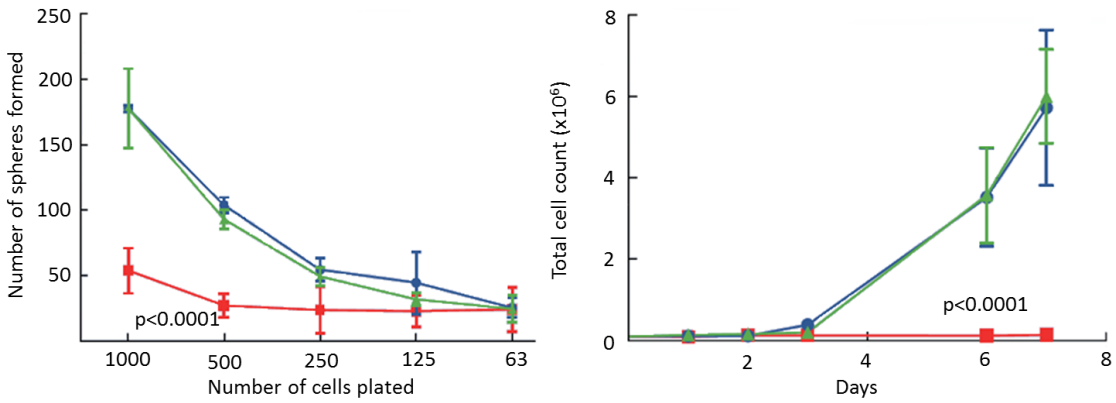

Figure 4.12 Limiting dilution assays following treatment with MLN8237.
Neurosphere formation (left) and growth (right) following MLN8237 (red) or GDC-0449 (blue) administration compared to untreated control (green). p, unpaired t test.

In vivo administration of the agent also significantly prolonged survival of GTML/*Trp53*$^{KI/KI}$ mice ($p<0.0001$, Log rank test, Figure 4.13) and, consistent with their expression profiles (MB_{Group3}, Figure 4.5), neither *in vitro*, nor *in vivo* treatment with the SHH inhibitor GDC-0449, which was selected as a second control agent (section 1.8.8.2), demonstrated an effect on growth or survival. Tumour growth was also visibly inhibited following the administration of MLN8237 in GTML/*Trp53*$^{KI/KI}$ mice as measured by MRI and bioluminescence (Figure 4.14).

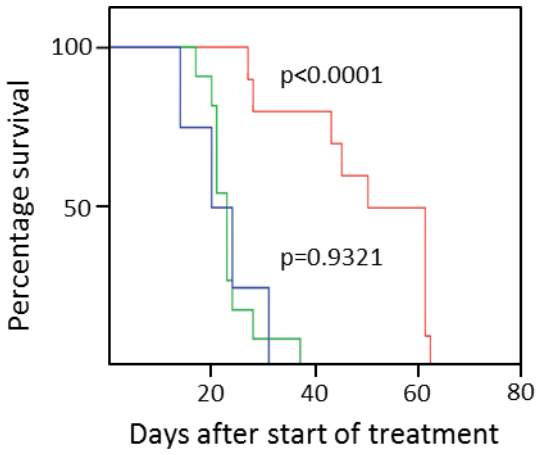

Figure 4.13 Kaplan-Meier plot illustrating prolonged survival in GTML/*Trp53*$^{KI/KI}$ mice treated with MLN8237. Red line, MLN8237; blue line, GDC-0449 (SHH inhibitor) and green line, vehicle. p, Log rank test.

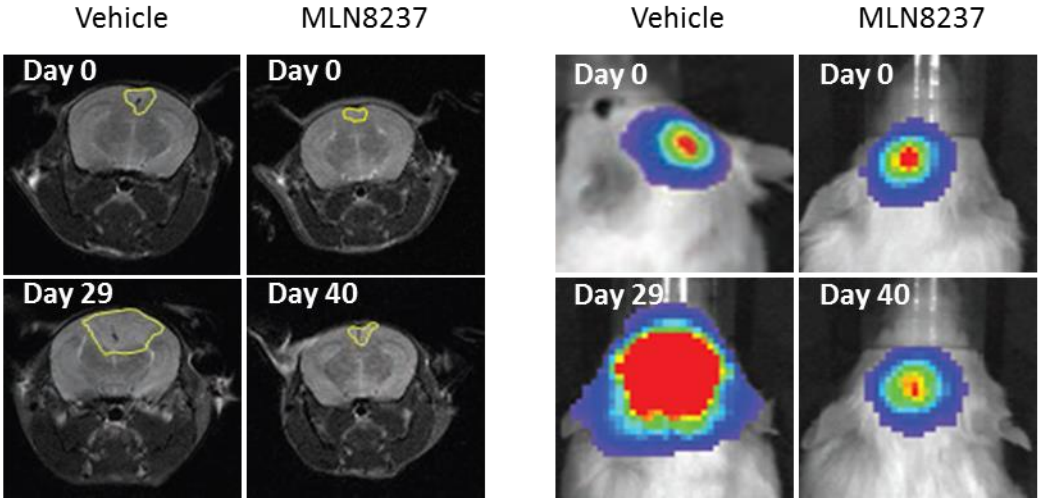

Figure 4.14 Inhibition of tumour growth in GTML/*Trp53*$^{KI/KI}$ mice following treatment with MLN8237. Left, MRI images demonstrate no tumour growth on day 40 following administration of MLN8237. Right, bioluminescence confirms no tumour growth following MLN8237 compared to vehicle control.

Importantly MLN8237 penetrated the blood brain barrier and demonstrated target-dependent activity, as its administration in GTML/*Trp53*$^{KI/KI}$ mice led to reductions in MYCN and Ki-67 expression and accumulation of phosphorylated histone H3 in G2 and mitosis because of Aurora A inhibition (Figure 4.15).

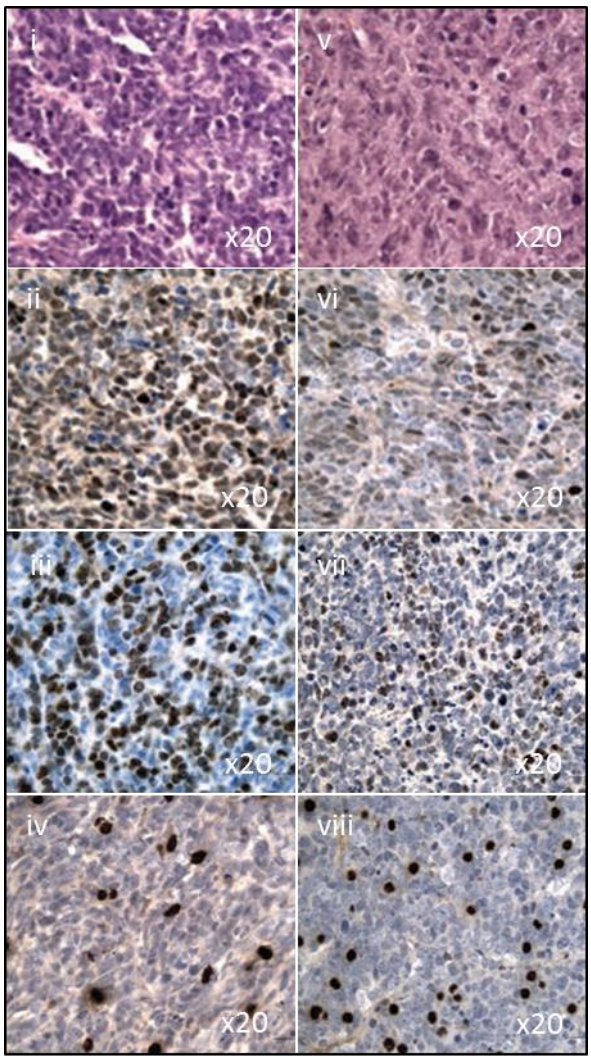

Figure 4.15 Target dependent activity of MLN8237 in GTML/*Trp53*$^{KI/KI}$ mice. H&E of vehicle (i) and MLN8237 treated (v) GTML/*Trp53*$^{KI/KI}$ mice with reduction of MYCN expression in MLN8237 (vi) treated GTML/*Trp53*$^{KI/KI}$ mice versus vehicle (ii). Reduction of Ki-67 following MLN8237 administration (vii) compared to vehicle (iii) and increased levels of phosphorylated histone H3 (viii) due to Aurora A kinase inhibition compared to vehicle alone (iv).

4.4 Discussion

4.4.1 GTML/Trp53 $^{KI/KI}$ mice model locally aggressive medulloblastoma disease

GTML mice provide an important model for understanding the biology of p53-MYC interactions in medulloblastoma. The initial discovery of spontaneous *Trp53* mutations in GTML mice, followed by the direct modelling of this interaction in the novel GTML/*Trp53*$^{KI/WT}$ and GTML/*Trp53*$^{KI/KI}$ mice validated the observations in chapter 3; *MYCN* and *Trp53* defects interact directly to generate tumours (section 4.3.1). Importantly, tumours sampled from GTML/*Trp53*$^{KI/KI}$ faithfully modelled the clinicopathological features of the locally aggressive disease witnessed in the human relapsed tumours with combined p53-MYC defects. The murine tumours were non-metastatic, and displayed LCA histology with high proliferation rates (Figure 4.4). Furthermore, the regulatable nature of both the *MYCN* and *Trp53* alleles enabled us to demonstrate the reliance of tumour growth and maintenance on disruption of both *MYCN* and *Trp53* dysregulation (section 4.3.2).

4.4.2 Aurora A kinase inhibition is a promising strategy for indirect targeting of MYCN in medulloblastoma

The indirect targeting of MYCN with the Aurora A kinase inhibitor, MLN8237, significantly prolonged survival in GTML/*Trp53*$^{KI/KI}$ derived neurospheres and mice (Figure 4.12 and Figure 4.13). MLN8237 demonstrated target-dependent activity leading to a reduction in MYCN expression, alongside a reduction in cell proliferation and accumulation of phosphorylation of histone H3 (Figure 4.15). Importantly, MLN8237 penetrated the blood brain barrier, which is intact in this mouse model. These pre-clinical trials provided proof-of-concept for the potential therapeutic use of Aurora A kinase inhibition in MYCN-driven human medulloblastomas.

4.4.3 Therapeutic reactivation of p53 as a potential strategy in medulloblastoma

The dependency of tumour growth and maintenance on loss of function of p53 demonstrated in this study (section 4.3.2) suggests an additional opportunity for therapies that reactivate wild type p53 by inhibiting the p53-MDM2 interaction (Figure 1.6). One group of agents which target the p53-MDM2 interaction are nutlins

(discussed in section 1.5.1.1). Nutlins have already been shown to have anti-tumorigenic activity *in vitro* and *in vivo* in a variety of paediatric tumour types including medulloblastoma cells lines (Kunkele *et al.*, 2012; Carol *et al.*, 2013; Van Maerken *et al.*, 2013). However, this therapeutic trial was not possible in the GTML/*Trp53*$^{KI/KI}$ model as nutlin therapy requires wild type p53 to be effective. Use of this agent in medulloblastoma, including relapsed medulloblastoma, where the majority of tumours in this study had functioning wild type p53 at relapse (15/22, 68%, Table 3.5) holds promise as an alternative targeted intervention.

4.5 Summary

Here we describe a novel mouse model which faithfully mimics key clinicopathological and molecular features identified in an extremely poor prognosis subgroup of patients with relapsed medulloblastoma. Utilising the GTML/*Trp53*$^{KI/KI}$ mouse model we have validated the dependency of tumour growth and maintenance on both *MYCN* and *Trp53* disruption, and successfully targeted MYCN indirectly with MLN8237, a second generation Aurora A kinase inhibitor. MLN8237 crosses the blood brain barrier, and is now an attractive targeted therapy for MYCN driven relapsed medulloblastoma. Moreover, establishment of it wider relevance in all MYCN driven tumours, including medulloblastoma at diagnosis, is essential. This study further emphasises that modelling and targeting the evolving biology of medulloblastoma at relapse is vital to improve outcomes in this devastating and almost always fatal disease.

Chapter 5. Identification of the T-box and Homeobox families as candidate epigenetically regulated genes which play a role in MB_{Group4} at relapse

5.1 Introduction

Epigenetic aberrations are increasingly implicated in the development and maintenance of cancer. The four best defined epigenetic mechanisms which can regulate the level of gene expression are; DNA methylation, histone modifications, chromatin remodelling and miRNAs and their role in promoter methylation (section 1.4.5). While DNA methylation is the most studied epigenetic feature in medulloblastoma, recent advances through WGS and WES techniques have also discovered subgroup-specific mutations in genes associated with chromatin remodelling and histone modifications which are discussed in detail in section 1.8.8 (Parsons *et al.*, 2011; Jones *et al.*, 2012; Northcott *et al.*, 2012a; Pugh *et al.*, 2012; Robinson *et al.*, 2012).

DNA methylation patterns in medulloblastoma reproducibly and reliably identify the four consensus molecular subgroups observed in the disease, and have been proposed to reflect the developmental origins for each of the four subgroups (Gibson *et al.*, 2010; Grammel *et al.*, 2012). Importantly, specific methylation events have been reported to be prognostically and biologically relevant in the disease. Recent examples of methylation markers which improve prognostication are *MXI1* and *IL8*; hypomethylation of both these genes in non-MB_{WNT} tumours is associated with a poor prognosis (Schwalbe *et al.*, 2013b). In addition, individual methylation events have been reported to show negative and positive correlations with gene expression in medulloblastoma, implying a biologically important role in the epigenetic regulation of gene expression in the disease. The most recent example is aberrant DNA methylation upstream of the TSS of *TERT* (detailed in section 1.4.7) which positively correlates with gene expression in MB_{SHH} (Lindsey *et al.*, 2014).

DNA methylation patterns have not previously been examined at relapse in medulloblastoma. Consequently the utility of DNA methylation patterns as either prognostic biomarkers, or biologically important drivers of tumour development at relapse has not been explored. This chapter focuses on characterising, for the first time, DNA methylation patterns and events in recurrent disease. Here, DNA methylation in paired samples taken from tumours at both diagnosis and relapse are profiled on the Infinium methylation 450K array (Illumina Inc. San Diego, CA, USA), and analysed to identify DNA methylation features that are either acquired at disease

recurrence or may be predictive of relapse. Events identified are subsequently correlated with expression in an independent medulloblastoma cohort for which DNA methylation and expression profiles are available (unpublished data, PBTG), to distinguish epigenetic events with a potential regulatory role in gene expression at relapse. Any new discoveries will provide the platform for future functional work to define the biological mechanisms underlying these findings, and their utility as either prognostic biomarkers or therapeutic targets at relapse.

5.2 Aims

The aims of this chapter are to;

- Assemble a cohort of tumour samples taken at medulloblastoma relapse alongside their paired diagnostic counterpart.

- Interrogate the DNA methylation patterns of this cohort utilising the Infinium methylation 450K array (Illumina Inc. San Diego, CA, USA).

- Analyse this dataset both cohort-wide, and by molecular subgroup, to identify single CpG residue events and regional DNA methylation patterns that are either acquired or maintained at relapse.

- Interpret these discoveries utilising an independent methylation-expression dataset to investigate the correlation of DNA methylation events identified at relapse with gene expression.

- Provide a platform for future functional work aimed at defining the biological mechanisms underlying these epigenetic events and exploring their utility as either prognostic biomarkers or therapeutic targets.

5.3 Materials and methods

5.3.1 DNA extraction and quality control

DNA from tumour and normal cerebellar tissue was extracted as described in section 2.1.1. Where DNA was of sufficient quantity and quality, as determined by the Qubit fluorometer (section 2.1.2.2), samples were analysed on the Infinium methylation 450K array at the Wellcome Trust Clinical Research Facility, University of Edinburgh, UK, according to the manufacturer's protocols (section 5.3.6, Illumina Inc. San Diego, CA, USA). Sample requirements for this array were a DNA concentration of ≥50ng/µl and total amount of 2µg extracted from FFPE material or 750ng extracted from frozen tissue. FFPE sample requirements were greater to allow for degraded FFPA DNA to be restored using the Infinium HD FFPE restore protocol (Illumina Inc. San Diego, CA, USA).

5.3.2 Assembly of a paired relapse cohort of medulloblastoma tumours sampled at diagnosis and relapse

The assembly of the cohort of paired tumours sampled at both diagnosis and relapse has been described in detail in section 3.3.1. In total, twenty-nine tumours sampled at relapse and twenty-six counterpart tumours sampled at diagnosis were available for profiling on the Infinium methylation 450K array (Illumina Inc. San Diego, CA, USA). Twenty-seven tumour samples taken at relapse and twenty-two tumour samples taken at diagnosis met the DNA requirements for this array (total number of paired samples = 20). To expand this cohort, seven further pairs of tumours sampled at diagnosis and relapse, kindly provided by Dr Michael Taylor and Prof Stefan Pfister, (Arthur and Sonia Labatt Brain Tumour Research Centre, Hospital for Sick Children, University of Toronto, Toronto, Canada and Department of Paediatric Haematology and Oncology, Heidelberg University Hospital, Heidelberg, Germany, respectively), were profiled.

5.3.3 Assembly of a control cohort of medulloblastoma tumours sampled at diagnosis for the assessment and comparison of DNA methylation events between diagnosis and relapse

A control cohort of medulloblastoma samples taken at diagnosis (n=139) was assembled and utilised for a comparative analysis to identify DNA methylation events enriched or novel in relapse disease. These samples were collated from the Newcastle

Medulloblastoma (NMB) cohort. Entry criteria for the cases were; successful analysis on the Infinium methylation 450K array, availability of complete clinical data and molecular subgrouping data, and DNA available for further validation work. To assess the suitability of this cohort, clinical and demographic features were assessed and a survival analysis performed (section 2.8) to ensure the cohort was reflective and representative of medulloblastomas sampled at diagnosis. The results of this analysis are reported below (Table 5.1, Figure 5.1-Figure 5.5).

Clinicopathological features and molecular subgroup		Historic studies [#] Diagnosis	Present study Control cohort
Gender	Male	585/952 (61%)	85/139 (61%)
	Female	367/952 (39%)	54/139 (39%)
	Male:female ratio	1.6:1	1.6:1
Age	Age range in years	0.3-52	0.2-43
	Infants (<4 years)	167/943 (17%)	35/139 (25%)
	Children (4-16 years)	599/943 (64%)	97/139 (70%)
	Adults (>16 years)	177/943 (19%)	7/139 (5%)
Pathology	CLA	938/1277 (74%)	96/134 (71%)
	DN	183/1277 (14%)	17/134 (13%)
	LCA	156/1277 (12%)	21/134 (16%)
Metastatic stage	M-	608/834 (73%)	67/118 (57%)
	M+	226/834 (27%)	51/118 (43%)
Resection	GTR	267/317 (84%)	95/122 (78%)
	STR	50/317 (16%)	27/122 (22%)
Molecular subgroup	MB_{SHH}	153/550 (28%)	45/139 (32%)
	MB_{WNT}	60/550 (11%)	14/139 (10%)
	MB_{Group3}	149/550 (27%)	29/139 (21%)
	MB_{Group4}	188/550 (34%)	51/139 (37%)

Table 5.1 Clinicopathological features and molecular subgroup demographics of the Infinium methylation 450K array control cohort. All clinicopathological and demographic features are shown alongside their expected distribution as reported in historic studies. [#] Historic studies (McManamy *et al.*, 2007; Kool *et al.*, 2012; Lannering *et al.*, 2012). CLA, classic histology; DN, desmoplastic/nodular histology; LCA, large cell/anaplastic histology; M-, M0 disease; M+, M1+ disease; GTR, gross total resection; STR, subtotal resection.

As demonstrated in Table 5.1, the demographic features of patients included in the control cohort reflected the age and gender distribution observed in larger historic independent cohorts. There was an equivalent male predominance (1.6:1, male:female) in the present cohort and the majority of patients were diagnosed between the ages of 4-16 years (64% (historic studies) versus 70% (present study)).

Similarly, pathological variant, resection status and molecular subgroup frequencies within the present control cohort were in line with the large independent cohorts reported here. However, in the present control cohort there was a greater number of metastatic cases observed (27% (historic studies) versus 43% (present study)) which was most likely due to many of the cases (n=21) not having their CSF sampled and therefore unable to be categorised as M0 or M1 disease (Table 1.6) and excluded from this comparison.

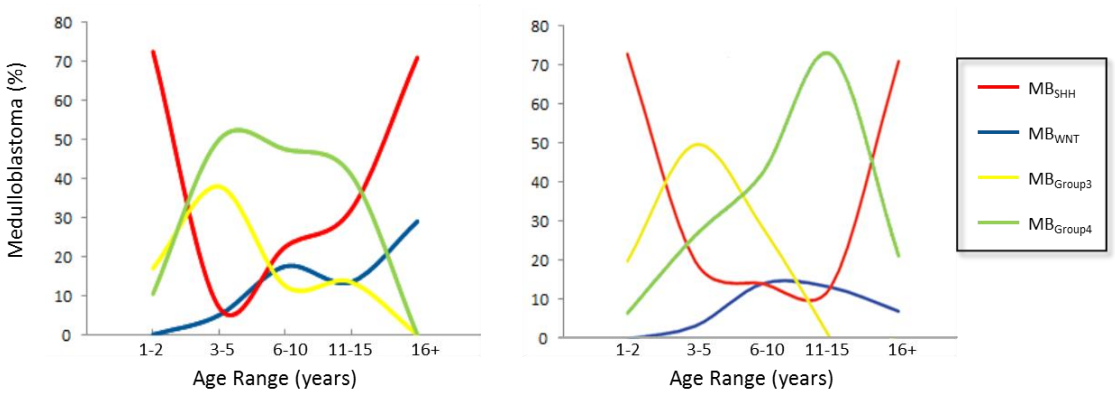

Figure 5.1 Illustrative example of age distribution within the four molecular subgroups within the Infinium methylation 450K array control cohort (left) and an independent historic study (right). Historic study (Northcott *et al.*, 2011b).

As illustrated in Figure 5.1, MB_{SHH} showed a peak in infancy and teenagers in the control cohort (left panel) similar to that of the independent historic study (right panel). In both cohorts MB_{WNT} was most commonly seen between 6-10 years, MB_{Group3} was observed in infants whereas MB_{Group4}, the largest subgroup, was witnessed throughout childhood (Northcott *et al.*, 2011b). These comparisons demonstrated that the subgroup-specific age distribution within the independent Infinium methylation 450K array control cohort was reflective of medulloblastoma tumours sampled at diagnosis.

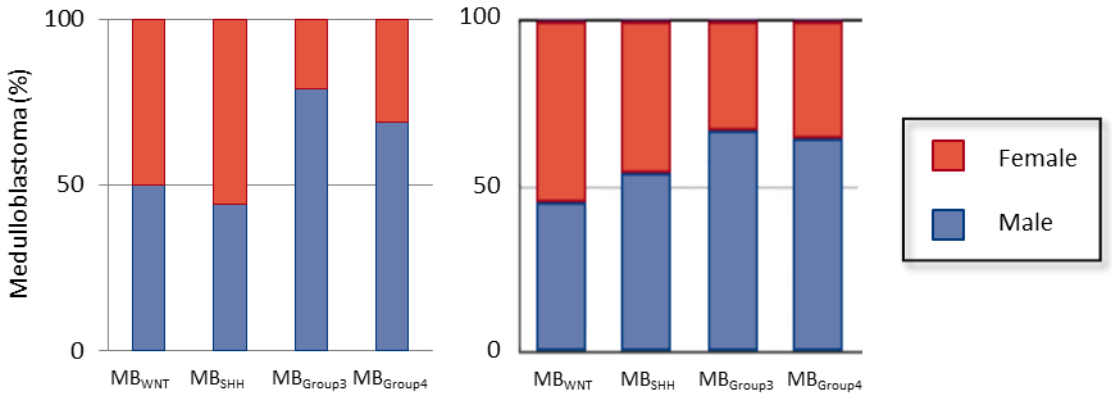

Figure 5.2 Gender distribution by molecular subgroup in the Infinium methylation 450K array control cohort (left) and an independent historic study (right). Historic study (Kool *et al.*, 2012).

As illustrated in Figure 5.2, the bar graphs demonstrated equal male: female ratio in MB_{WNT} and MB_{SHH} and male predominance in MB_{Group3} and MB_{Group4} in both the Infinium methylation 450K array control cohort and the historic study (Kool *et al.*, 2012).

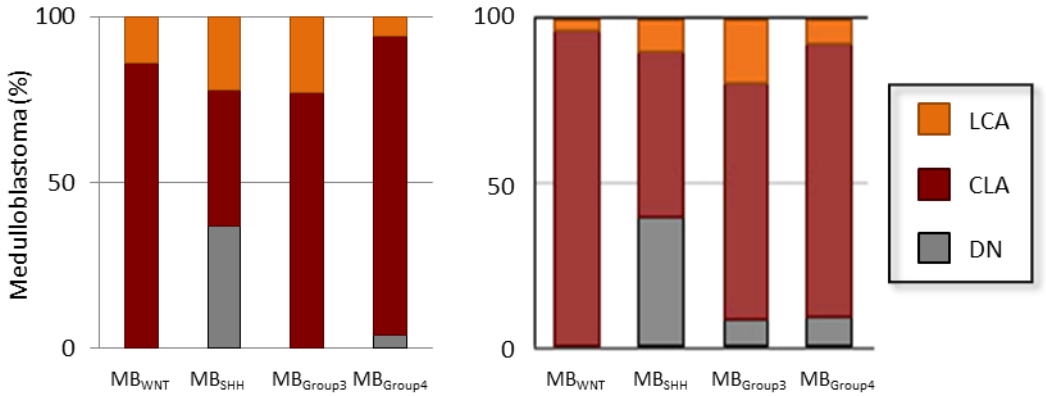

Figure 5.3 Histology distribution by molecular subgroup in the Infinium methylation 450K array control cohort (left) and an independent historic study (right). Historic study (Kool *et al.*, 2012). CLA, classic histology; DN, desmoplastic/nodular histology; LCA, large cell/anaplastic histology.

In Figure 5.3 the bar graphs demonstrated the expected pathological variants by molecular subgroup in the Infinium methylation 450K array control cohort when compared to the historic study (Kool *et al.*, 2012). There was an enrichment of DN in MB_{SHH}, predominantly CLA in MB_{WNT}, MB_{Group3} and MB_{Group4} and a significant presence of LCA in MB_{Group3}.

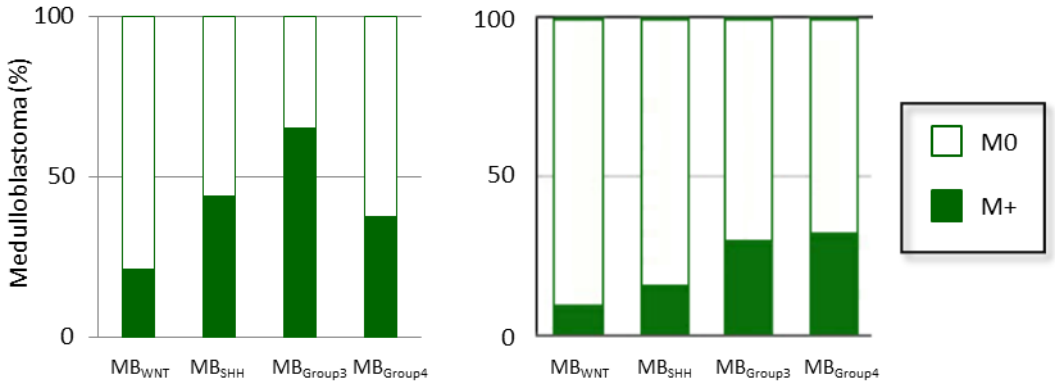

Figure 5.4 Metastatic disease by molecular subgroup in the Infinium methylation 450K array control cohort (left) and an independent historic study (right). Historic study (Kool *et al.*, 2012). M-, M0 disease; M+, M1+ disease.

Figure 5.4 demonstrates less metastatic disease in MB_{WNT} but enrichment of metastatic disease in MB_{Group3} and MB_{Group4} for both cohorts. Overall there was an increased number of patients presenting with metastatic disease in the Infinium methylation 450K array control cohort, which was most likely reflective of the incomplete staging of 21 patients who were excluded from this comparison as they could not be classified as either M0 or M1 disease (Table 5.1).

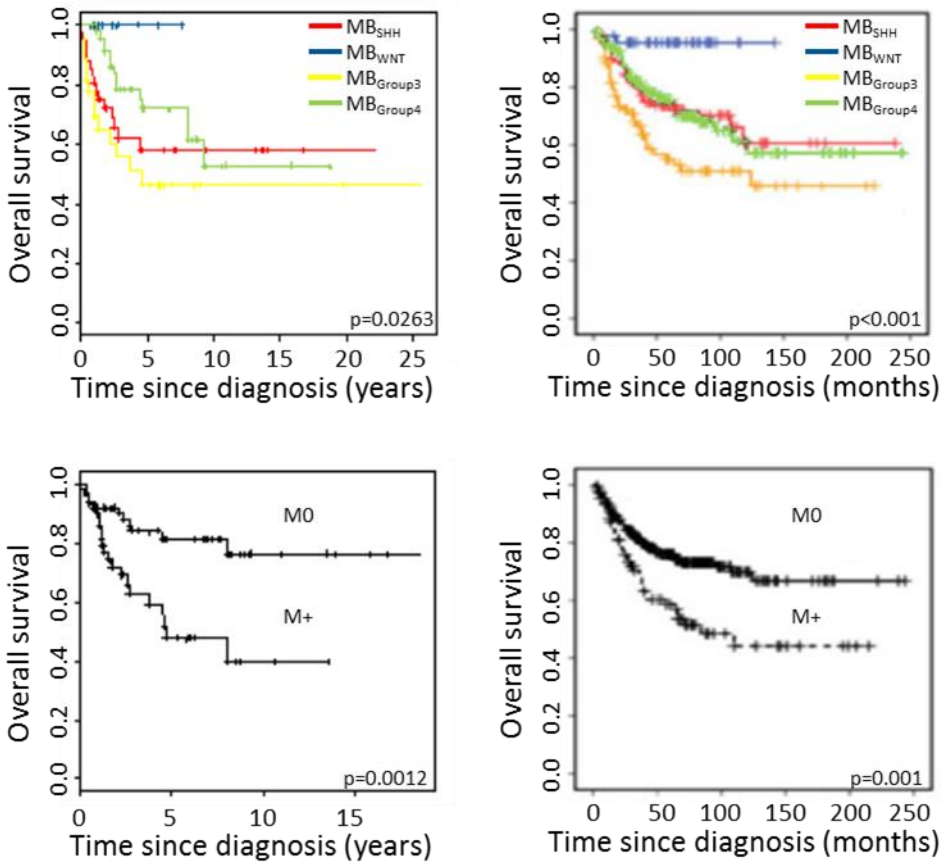

Figure 5.5 Kaplan-Meier curve illustrating the overall survival difference between molecular subgroups (top) and metastatic disease (bottom) in the Infinium methylation 450K array control cohort (left) and an independent historic study (right). Historic study (Kool *et al.*, 2012). M-, M0 disease; M+, M1+ disease.

As demonstrated in Figure 5.5, MB_{WNT} had a good overall survival rate in both the Infinium methylation 450K array control cohort (top left) and in the independent historic cohort (top right). Similarly metastatic disease conveyed a poorer prognosis in both cohorts (bottom panels).

Overall, the control cohort was reflective and representative of medulloblastoma at diagnosis when compared to large historic studies (McManamy *et al.*, 2007; Northcott *et al.*, 2011b; Kool *et al.*, 2012; Lannering *et al.*, 2012), and demonstrated the appropriate subgroup-specific clinicopathological features (Table 5.1, Figure 5.1 - Figure 5.5). Age distribution amongst the subgroups revealed a bimodal trend in MB_{SHH}, enrichment of MB_{Group3} in infants and the prevalence of both MB_{WNT} and

MB_{Group4} in childhood (Figure 5.1). There was an enrichment of males in both MB_{Group3} and MB_{Group4} consistent with other datasets in medulloblastoma (Figure 5.2). Similarly, pathology variants were represented appropriately within the four subgroups, with DN witnessed most frequently in MB_{SHH}, CLA histology predominating in MB_{WNT}, and MB_{Group3} showing the highest number of LCA cases (Figure 5.3). Metastatic disease was observed most frequently in MB_{Group3} (Figure 5.4), consistent with the current understanding of the disease (Taylor *et al.*, 2012). Finally, survival relationships with molecular subgroup and metastatic disease were as expected, with MB_{WNT} having the best prognosis, and metastatic disease demonstrating a poor overall survival (Figure 5.5).

5.3.4 Selection and assembly of a cohort for the assessment of DNA methylation patterns and their correlation with gene expression levels

Subgroup-specific analysis of DNA methylation patterns, as profiled on the Infinium methylation 450K array, focused on MB_{Group4} as this was the largest, uniformly treated (upfront CSI), molecular subgroup within the paired relapse cohort. In addition, proceeding with the analysis in MB_{Group4} alone, controlled for the DNA methylation heterogeneity observed between the four molecular subgroups (Hovestadt *et al.*, 2013; Schwalbe *et al.*, 2013b). To analyse DNA methylation patterns and relate them to gene expression, an independent NMB cohort of medulloblastomas with matched expression and DNA methylation data (HiSeq 2000 RNA-seq and Infinium methylation 450K array respectively, Illumina Inc., CA, USA) was used to assess the correlation between methylation and expression. This aspect of the analysis was performed by Dr Sirintra Nakjang (PBTG). In brief, Pearson's product-moment correlation coefficient (*r*) was calculated to assess the strength of relationships between DNA methylation at specific CpG residues of interest and their associated gene expression levels. These analyses were performed across all four molecular subgroups and in MB_{Group4} alone. A strong positive relationship was defined by a correlation coefficient r value > 0.75 and a p value < 0.05; a strong inverse relationship was defined by an r value < -0.75 and a p value < 0.05. The clinicopathological, demographic features and molecular subgroup distribution of this cohort are detailed in Table 5.2, and represent the expected disease features and distribution of all these parameters at diagnosis.

Clinicopathological features and molecular subgroup		Historic studies [#] Diagnosis	Present study Control cohort
Gender	Male	585/952 (61%)	109/168 (65%)
	Female	367/952 (39%)	59/168 (35%)
	Male:female ratio	1.6:1	1.8:1
Age	Age range in years	0.3-52	0.2-43
	Infants (<4 years)	167/943 (17%)	37/168 (22%)
	Children (4-16 years)	599/943 (64%)	118/168 (70%)
	Adults (>16 years)	177/943 (19%)	13/168 (8%)
Pathology	CLA	938/1277 (74%)	115/157 (74%)
	DN	183/1277 (14%)	21/157 (13%)
	LCA	156/1277 (12%)	21/157 (13%)
Metastatic stage	M-	608/834 (73%)	97/151 (64%)
	M+	226/834 (27%)	54/151 (36%)
Resection	GTR	267/317 (84%)	120/148 (81%)
	STR	50/317 (16%)	28/148 (19%)
Molecular subgroup	MB_{SHH}	153/550 (28%)	41/168 (25%)
	MB_{WNT}	60/550 (11%)	19/168 (11%)
	MB_{Group3}	149/550 (27%)	39/168 (23%)
	MB_{Group4}	188/550 (34%)	69/168 (41%)

Table 5.2 Clinicopathological features and molecular subgroup overview of the control cohort for the assessment of DNA methylation patterns and their correlation with gene expression. All clinicopathological and demographic features are shown alongside their expected distribution as reported in historic studies. [#] Historic studies (McManamy *et al.*, 2007; Kool *et al.*, 2012; Lannering *et al.*, 2012). CLA, classic histology; DN, desmoplastic/nodular histology; LCA, large cell/anaplastic histology; M-, M0 disease; M+, M1+ disease; GTR, gross total resection; STR, subtotal resection.

As demonstrated in Table 5.2, the demographic features of patients included in the control cohort reflected the age and gender distribution observed in larger historic independent cohorts. There was a male predominance observed in both cohorts (1.6:1, male:female (historic studies) versus 1.8:1, male:female (present study)). The majority of patients in both cohorts were diagnosed between the ages of 4-16 years (64% (historic studies) versus 70% (present study)). Similarly, the frequency and distribution of pathological variants, metastatic disease, resection status and molecular subgroup within the present control cohort were representative of medulloblastoma tumours sampled at diagnosis, when compared alongside the large independent historic cohorts reported here.

5.3.5 Selection and assembly of a control cohort of normal cerebella

DNA methylation of normal brain tissue is known to vary according to the developmental stage of the CNS (section 1.4.6.1.1). To identify tumour-specific DNA methylation events in medulloblastoma, a cohort of DNA samples (n=17) from normal cerebella at different stages of development, extracted as described in section 2.1.1, was collated and analysed on the Infinium methylation 450K array.

Sample number	Developmental stage	Tissue type
CB1	Foetal	Frozen
CB2	Foetal	Frozen
CB3	Foetal	Frozen
CB5	Infant	Frozen
CB6	Infant	Frozen
CB7	Adult	Frozen
CB9	Adult	Frozen
CB11	Infant	Frozen
CB13	Infant	Frozen
CB15	Unknown	Frozen
CB17	Infant	Frozen
CB18	Adult	Frozen
CB21	Infant	Frozen
CB22	Child	Frozen
CB23	Child	Frozen
CB24	Child	Frozen
CB25	Infant	Frozen

Table 5.3 Cohort of normal cerebella tissue samples. Infant, <3 years old; child 3-16 years old; adult >16 years old. CB, cerebellum.

5.3.6 The Infinium methylation 450K array

As discussed in section 1.4.6.1, DNA methylation patterns vary widely in cancer. While bisulfite genomic sequencing provides the highest resolution for investigating the DNA methylome (Bibikova *et al.*, 2011; Dedeurwaerder *et al.*, 2011), the Infinium methylation 450K array enables the assessment of >480 000 CpG residues which are distributed across the entire human genome. This recent technology provides, at present, the best compromise for high throughput, cost effective biomarker and target discovery. Importantly, this array interrogates >95% of CpG islands (section 1.4.6.1.1) as well as island shores and distant sites (Figure 5.6), and coverage includes 99% of all Reference Sequence (RefSeq) genes (Dedeurwaerder *et al.*, 2011).

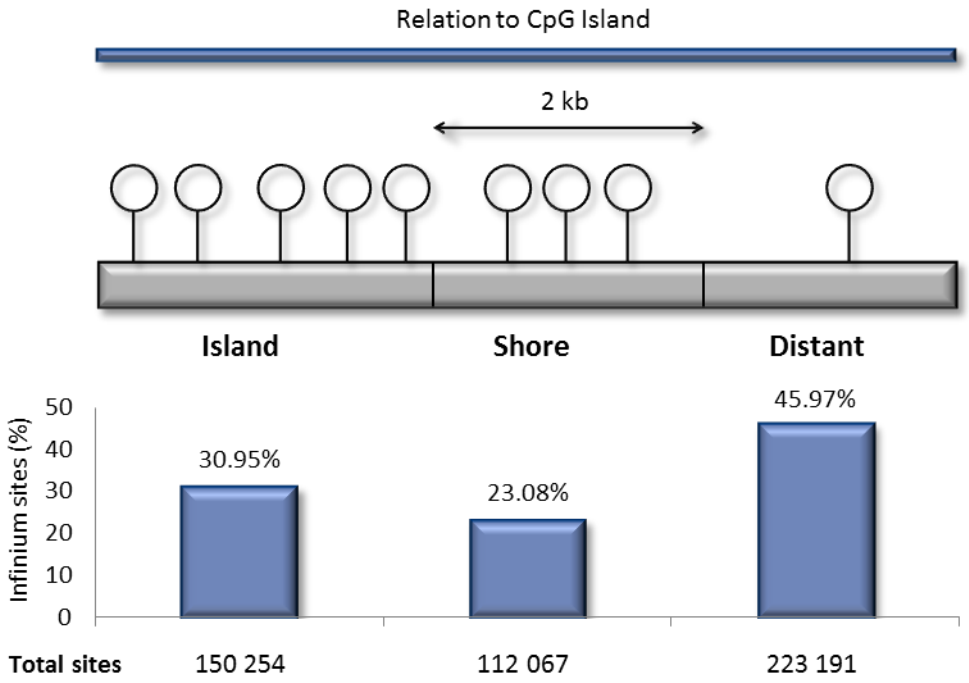

Figure 5.6 Distribution of probes across the genome on the Infinium methylation 450K array. Island shores are defined as those regions within a 2 kilobase (2kb) distance of a CpG island (Irizarry *et al.*, 2009). Figure adapted from Dedeurwaerder *et al*., (2011).

5.3.6.1 The Infinium methylation assay

The Infinium DNA methylation assay combines DNA bisulfite conversion and whole genome amplification (WGA) as sample preparation, before directly capturing and scoring each individual CpG locus on the array. Bisulfite treatment introduces single nucleotide changes within the DNA that are dependent on the methylation status of cytosine residues, as demonstrated in Figure 5.7, which enables the analysis of DNA methylation patterns (Krueger *et al.*, 2012).

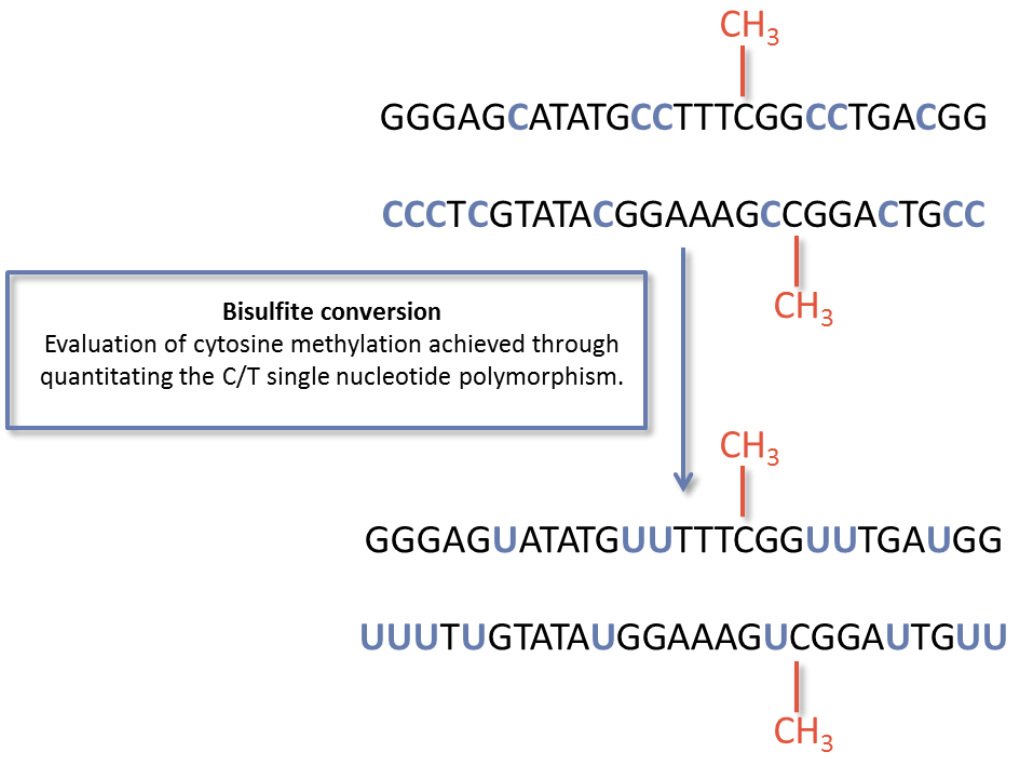

Figure 5.7 DNA bisulfite conversion. Schematic demonstrating the cytosine (C) to thymine (T/U) polymorphism that is introduced at unmethylated cytosine nucleotides alone, allowing for quantitative genotyping of this polymorphism. CH_3, methylated residue.

Following bisulfite conversion, DNA is denatured with sodium hydroxide (NaOH), neutralised and isothermally amplified over 20-24 hours to produce several thousand copies of the converted DNA. The amplified DNA sample is enzymatically fragmented, precipitated in 100% isopropanol and centrifuged at 3000 rpm for 20 minutes at 4°C to facilitate DNA collection. Precipitated DNA is then resuspended in hybridisation buffer, dispensed onto BeadChips and incubated overnight. Any non-specifically hybridised or unhybridised DNA is washed off and the oligonucleotides on the BeadChip undergo single bp extension, incorporating labels which can then determine the methylation levels of the CpG loci of interest (Illumina, 2010; Bibikova *et al.*, 2011; Dedeurwaerder *et al.*, 2011).

5.3.6.2 Infinium I and II assay probes

There are two different types of probes on the Infinium methylation 450K platform; type I assay probes and type II assay probes, which are illustrated and described in Figure 5.8. The Infinium II probe is preferentially used on the array (72%), however in high density CpG regions such as islands, type I probes (28%) are used. This is due to the fact that type II probes can have up to three CpG sites corresponding to one probe. Consequently in regions of the genome which are densely populated with CpG residues, specificity and hybridisation kinetics would be deleteriously affected if type II probes were used and data quality would suffer (Maksimovic *et al.*, 2012).

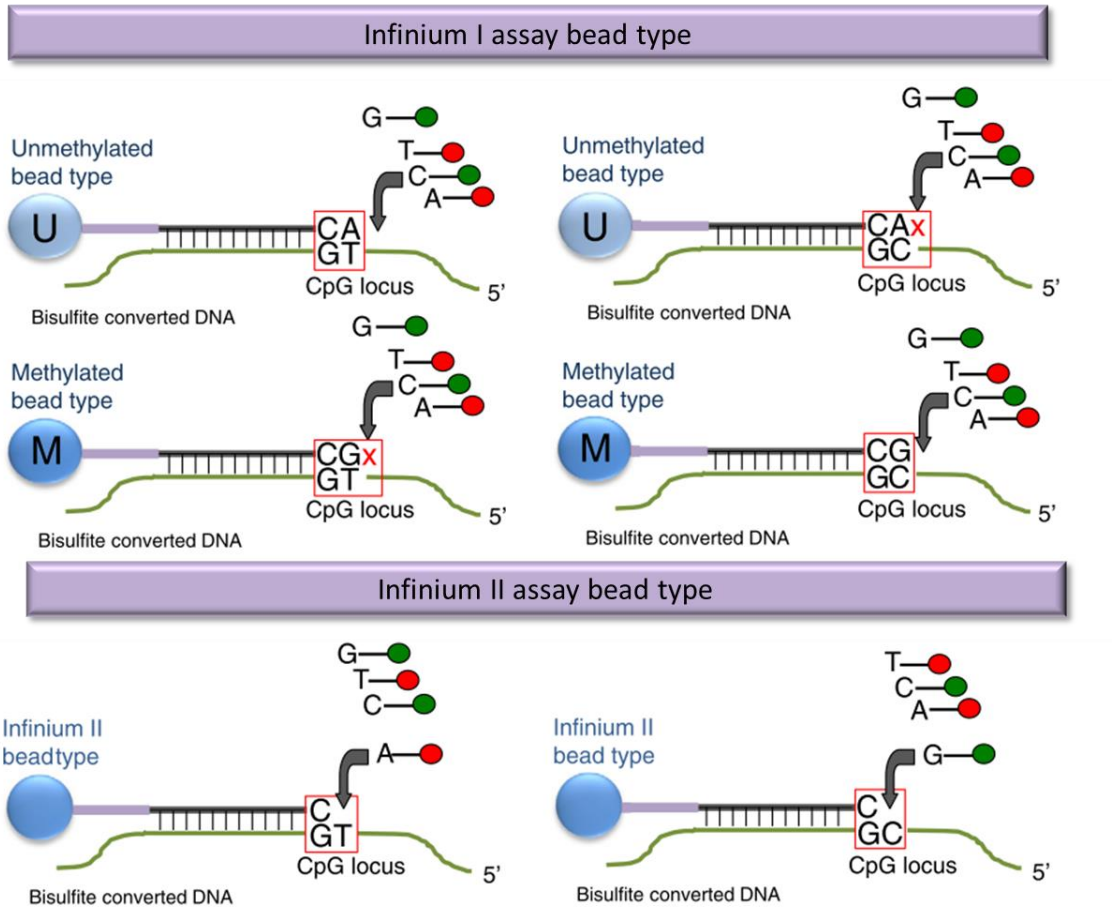

Figure 5.8 The Infinium methylation 450K array assay scheme. Infinium I assay bead type; two bead types correspond to each locus, one for methylated cytosine (C) residues, one for unmethylated (T) bisulfite converted residues. Both bead types are detected in the same colour channel. This 50bp probe design assumes that the methylation state of the interrogated site corresponds to that of any other underlying adjacent sites. Infinium II assay bead type; one bead type corresponds to each locus which is detected in two colours. 'A' is incorporated at an unmethylated site (left) and 'G' at a methylated site (right). The Infinium II probe design can contain up to three CpG loci. Figure adapted from Bibikova *et al.,* 2011.

Technical differences in performance and a divergence of β-values between the Infinium I and Infinium II assays have been reported (Bibikova *et al.*, 2011; Dedeurwaerder *et al.*, 2011; Maksimovic *et al.*, 2012; Teschendorff *et al.*, 2013). The dynamic range of β-values reported by the Infinium II probes is reduced, with less accuracy and reproducibility of β-values particularly at the extremes of methylation (hypo or hyper methylation, Figure 5.9). To overcome this variablity and enable analysis of both assays simultaneously, various normalisation techniques have been descibed and are discussed below.

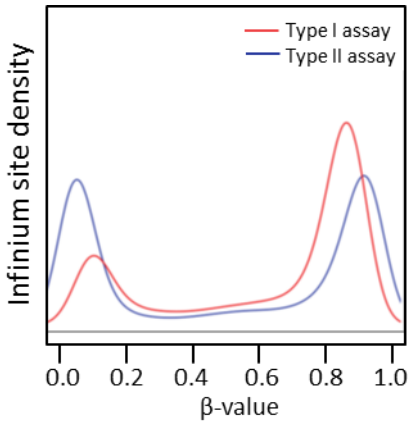

Figure 5.9 Density plots demonstrating the divergence in β-values between the type I and type II assays on the Infinium methylation 450K array. Figure adapted from Dedeurwaerder *et al.*, 2011.

5.3.6.3 Peak-based correction

Peak-based correction (PBC) utilises the peak summits of the β-values to align and match the reported β-values from type I and type II probes. β-values are transformed to M-values (Figure 5.10), peak summits for both probe types are independently determined and raw M-values are corrected using the reference peak summits. The corrected M-values are rescaled to the Infinium I assay probe range (greater than the Infinium II assay probe) and M-values are converted back to β-values. As illustrated in Figure 5.11, this correction provides a better distribution of type II assay probe β-values, which align more closely to the distribution of type I assay probes (Dedeurwaerder *et al.*, 2011).

β-value: $\beta = \frac{M}{M+U+100}$

M-value: $Mval = \log\left(\frac{M}{U}\right)$

Figure 5.10 Conversion of β-values to M-values. *M*, methylated signal*; U*, unmethylated signal.

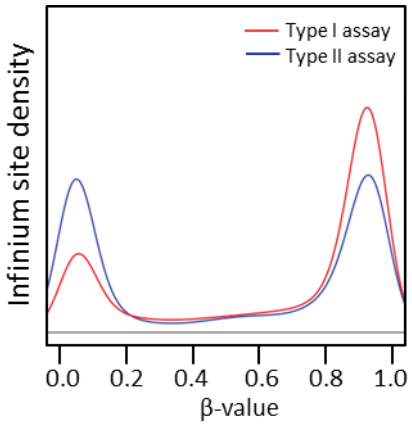

Figure 5.11 Density plots demonstrating the improved alignment between type I and type II assays reported β-values following peak-based correction. Figure adapted from Dedeurwaerder *et al*., 2011.

5.3.6.4 Subset-quantile within array normalisation

Subset-quantile within array normalization (SWAN) is a technique available within the *minfi* package written for R (R Development Core Team, 2014) and downloadable from Bioconductor.org. It is a technique which has evolved from normalisation methods used for microarray expression platforms and applies a within-array quantile normalisation to match the type I and type II probes β-value distribution. This method is designed to remove technical variation whilst preserving any true biological differences observed between the two probe types. Biological differences between the two probes will occur because of their differences in distribution (section 5.3.6.2). Type I Infinium probes are more readily found in CpG dense regions such as islands, which will often have differing methylation states when compared to low density CpG regions more readily corresponding to type II Infinium probes. As a result of this unequal distribution across the genome, standard normalisation techniques cannot be applied.

To overcome this difficulty the SWAN algorithm randomly selects a subset of Infinium type I and II probes deemed to be biologically similar based on their underlying CpG content *i.e.* it selects from a pool of type I and II probes (3n pairs) which have one, two or three underlying CpG sites (n=number of probes for each underlying CpG variant). The methylated and unmethylated channel from each subset of probe types is organised in increasing intensity for each of the 3n pairs. The mean value of each of the 3n pairs becomes the mean intensity for that 'quantile' and all remaining probes are separately normalised to the subset of probes using linear interpolation (Maksimovic *et al.*, 2012). This algorithm again provides a better distribution of type II assay probe β-values, illustrated in Figure 5.12, and supersedes PBC, which struggles to normalise probes which are hemi-methylated.

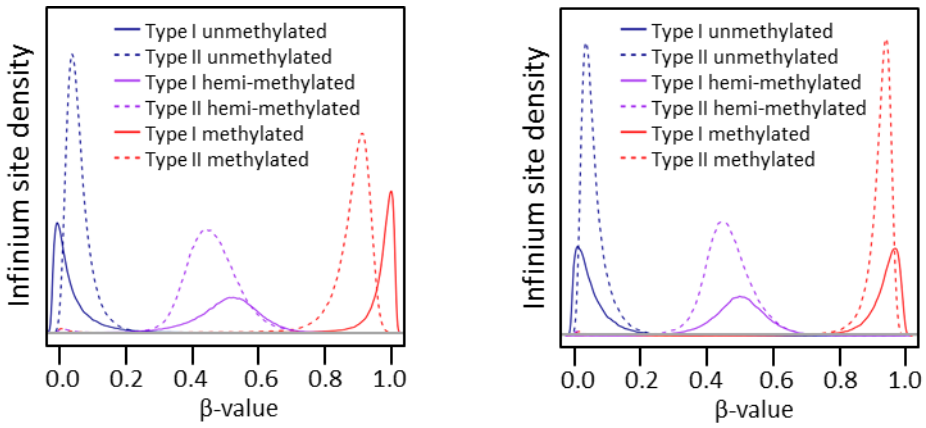

Figure 5.12 Differences in β-values before and after subset-quantile within array normalisation. Left panel, varying β-value distribution at unmethylated, hemi-methylated and methylated CpG sites for type I and type II Infinium assay probes. Right panel, improved β-value distribution at unmethylated, hemi-methylated and methylated CpG sites for type I and type II Infinium assay probes following SWAN procedure. Figure adapted from Maksimovic *et al.*, 2012.

5.3.6.5 Beta-mixture quantile normalisation

Beta-mixture quantile (BMIQ) normalisation is another technique which uses quantiles to match the density distributions of type II probes to that of type I probes. It is an assumption free algorithm, which fits fully methylated, unmethylated and hemi-methylated type II probes to the distribution of type I probes but does not rely on normalisation of a subset of probes with biologically similar characteristics. In

comparison to the two other methods described, (PBC and SWAN), BMIQ performs better, generating a smoother density distribution. In particular PBC struggles when a probe does not have a bimodal distribution of β-values as demonstrated in Figure 5.13.

BMIQ also outperforms in eliminating the type I enrichment bias, which is observed due to the greater dynamic range of type I probes providing more statistical power in analyses which leads to their over-representation as top ranked probes. The reduction in technical variation following BMIQ is superior to PBC and SWAN and crucially does not affect biological findings (Teschendorff *et al.*, 2013). Overall, BMIQ normalisation outperforms all other current techniques for correcting the type I and II probe differences and was selected as the algorithm to utilise in this study. BMIQ was downloaded from http://bmiq.googlecode.com/files/BMIQ_1.2.R and is a series of functions written for use in R (R Development Core Team, 2014).

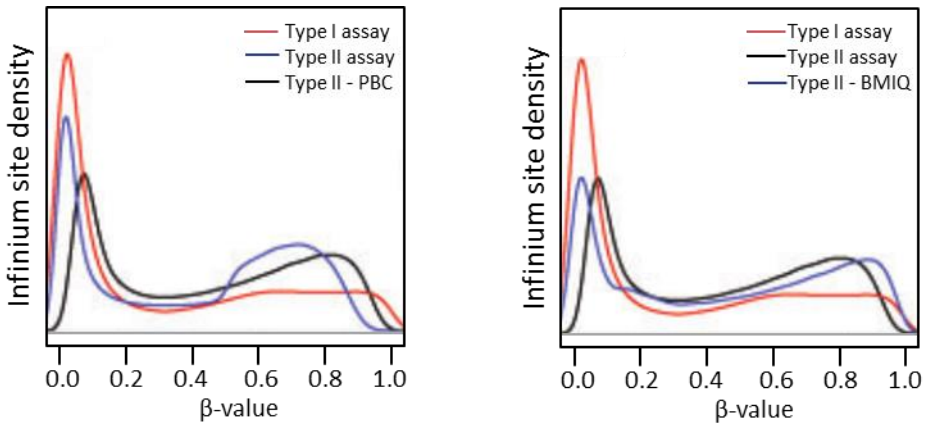

Figure 5.13 Comparison of peak-based correction versus beta-mixture quantile normalisation. Illustrative examples of both correction techniques showing a superior fit following BMIQ (left) when compared to PBC (right). Figure adapted from Teschendorff *et al*., 2013.

5.3.6.6 Quality control measures

IDAT data files of the raw β-values were read into R (R Foundation for Statistical Computing, 2014) and the BMIQ normalisation was applied (section 5.3.6.5). Quality control reports were generated to assess the data and array performance, and batch controls were analysed to look for inter-array batch variation. As demonstrated in Figure 5.14, inter array batch controls did not vary in their β-value distribution but data quality was variable with a proportion (8/65, 12%) of samples not demonstrating a

clear bimodal distribution typically observed for β-values (*e.g.* Patient 11 at diagnosis, Figure 5.14). This related most closely to sample type, with frozen samples outperforming the more degraded DNA obtained from FFPE samples. This was not uncommon for FFPE samples at this time, with previous experience from within the PBTG, observing approximately a 10% failure rate for FFPE samples on historic DNA methylation arrays such as the GoldenGate array (Illumina Inc., CA, USA).

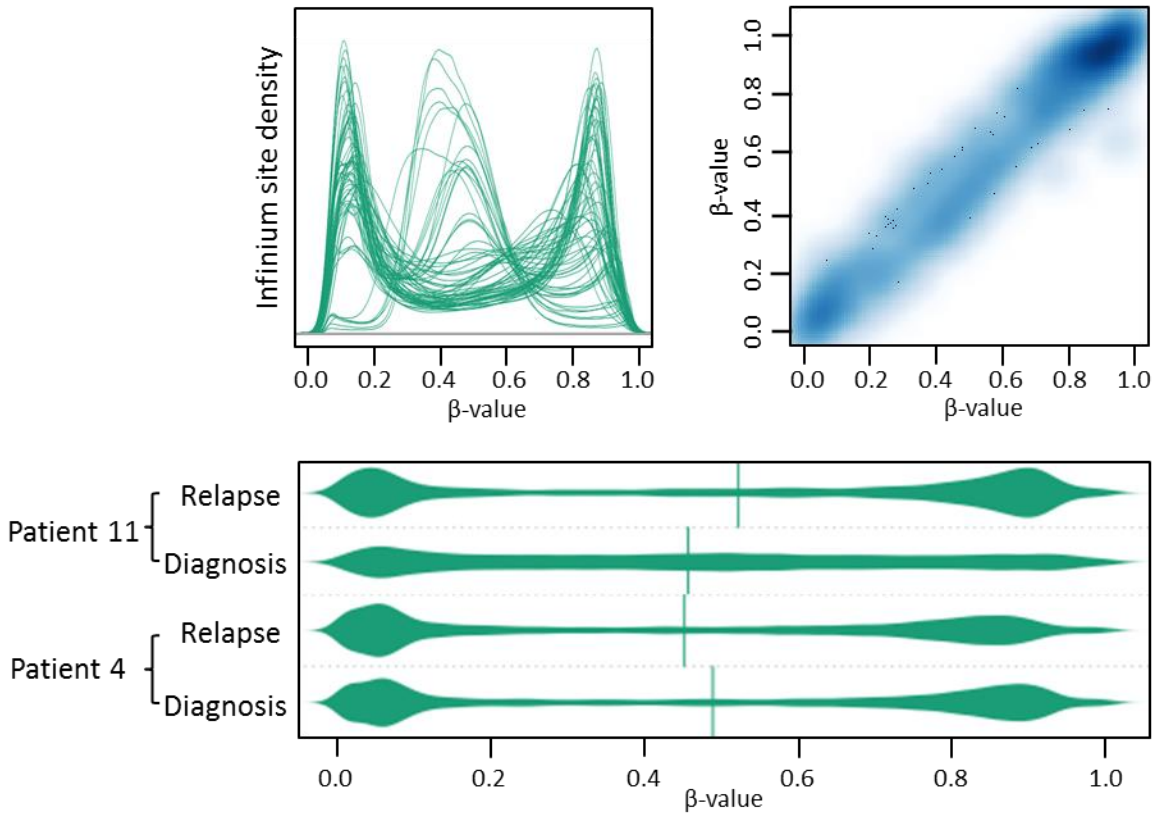

Figure 5.14 Quality control report of β-values in the paired relapsed cohort. Variable data quality demonstrated in density plot (top left) and beanplot (bottom). Batch control (top right) demonstrating minimal batch variation and good correlation between β-values of the same DNA sample on different batches at different times.

5.3.7 Study design

In order to maximise the opportunities for discovery work from the paired relapse cohort methylation dataset, several analytical approaches were conceived and undertaken. The workflow pipeline is summarised in Figure 5.15. In brief, analyses were undertaken using either a regional approach, looking for widespread changes in methylation states across multiple CpG loci, or by identifying single CpG sites which show alterations in methylation states between diagnosis and relapse. Individual

analyses required control cohorts to compare and correlate against, which were introduced in section 5.3.3 - 5.3.5. Each analysis arm will be discussed separately in section 5.3.7.1 - 5.3.7.3.

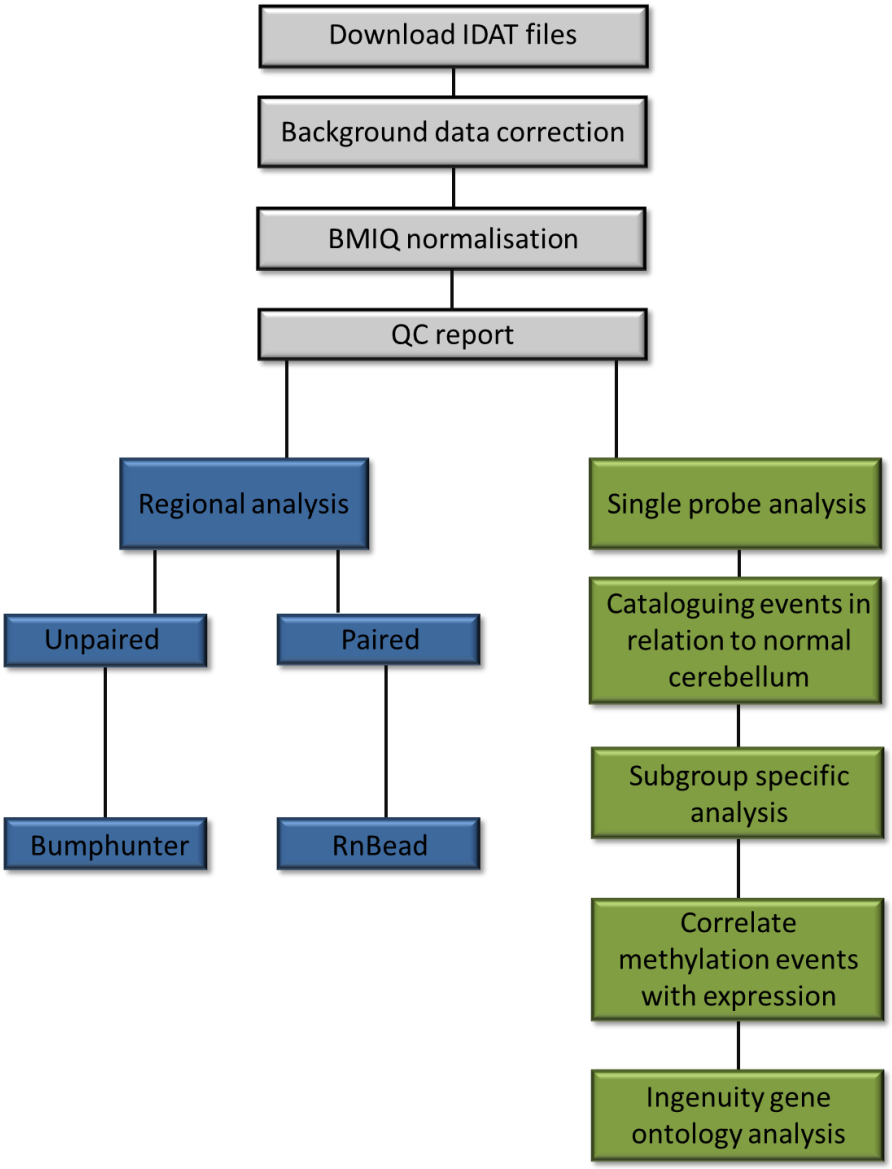

Figure 5.15 Pipeline for analysis of the Infinium methylation 450K array dataset in the paired relapse cohort.

5.3.7.1 Bumphunter analyses

DNA methylation events demonstrating relationships with gene expression, have been described for both genomic CpG regions such as islands and island shores as well as single site events (Irizarry *et al.*, 2009; Jaffe *et al.*, 2012; Lindsey *et al.*, 2014). 'Bumphunting' was first described to look for transcription factor binding sites utilising chromatin immunoprecipitation (ChIP). While not directly applicable in this context, due to the nature and greater variability of epigenetic 'bumps', this technique has been adapted for use in DNA methylation analyses (Jaffe *et al.*, 2012).

In brief, for each genomic location there is a β-value for several individuals. Regression analysis for each individual is performed giving one estimate value. Candidate regions between the two populations are identified and permutation analyses performed to assess uncertainty. The output of this analysis is a table of candidate regions with permutation-based family-wise error rates and an assigned p value. The p value should be interpreted with caution, and represents the percentage of candidate regions obtained from the permutations that are as extreme as the original observation, identifying this region as a candidate. Bumphunter is a function within the *minfi* package written for R (R Development Core Team, 2014) and was applied to detect differentially methylated genomic regions of interest between two different populations. The analysis workflow is depicted in Figure 5.16.

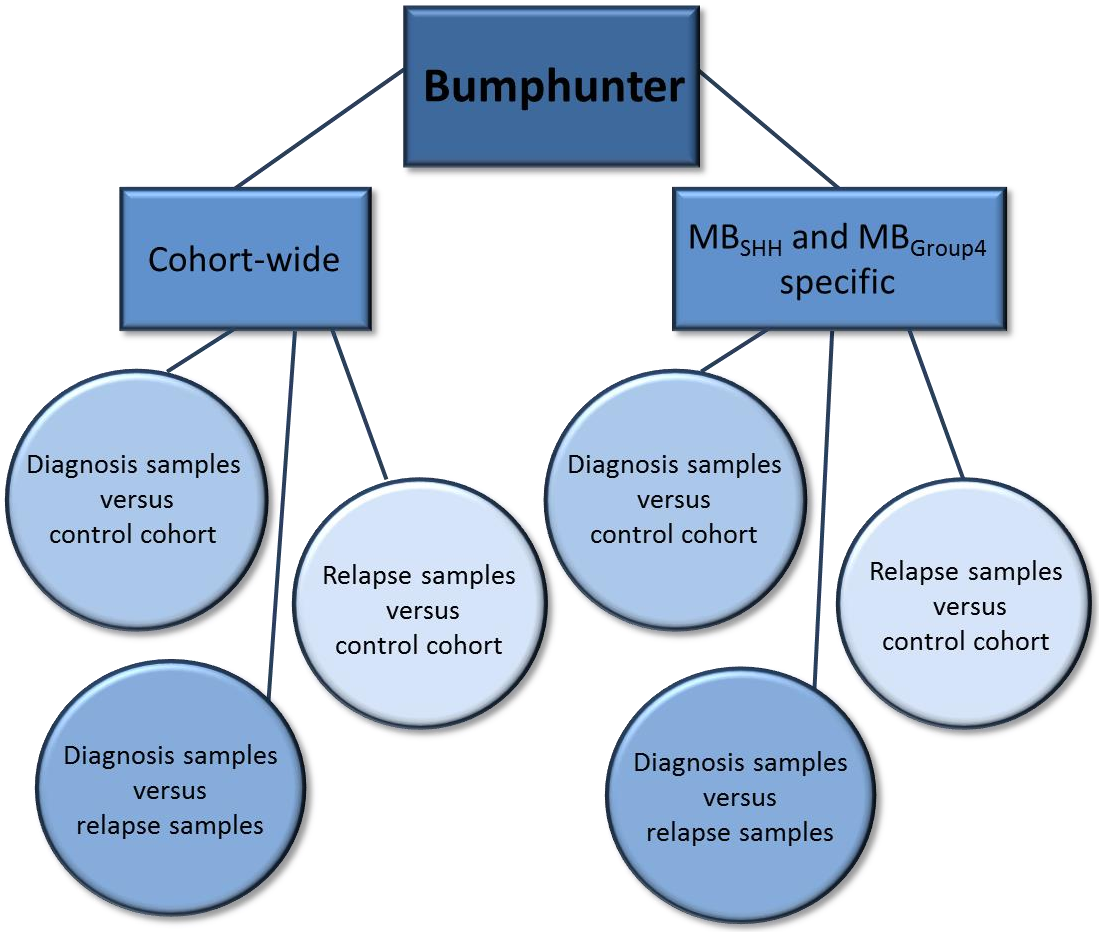

Figure 5.16 Analysis pipeline utilising Bumphunter. Diagnosis and relapse samples represent the paired relapse cohort (section 5.3.2). The control cohort is a collection of independent tumours sampled at diagnosis and described in section 5.3.3.

Bumphunter can only interrogate two populations; consequently three different comparisons were conceived to identify prognostic events (samples taken at diagnosis from the paired relapse cohort (n=29) versus control cohort (n=139)), relapse specific events (samples taken at relapse from the paired relapse cohort (n=34) versus control cohort) and acquired events (samples taken at diagnosis from the paired relapse cohort versus samples taken at relapse). This was performed cohort wide as well as in a subgroup-specific manner for the two well represented subgroups in these analyses (MB_{SHH}, 16/29 (55%) sampled at diagnosis, 17/34 (50%) sampled at relapse, and MB_{Group4} 9/29 (31%) sampled at diagnosis, 11/34 (32%) sampled at relapse). MB_{WNT} and MB_{Group3} subgroups were limited in numbers and unsuitable for this analysis in isolation (both 1/29 (3%) sampled at diagnosis, 2/34 (6%) sampled at relapse).

5.3.7.2 RnBeads analyses

RnBeads is an open source R package (R Development Core Team, 2014) for analysis of multiple types of methylation data, including the Infinium methylation 450K array. It is capable of analysing genomic regions as well as single CpG sites. Genomic regions, inferred from the annotation data are separated into promoter, CpG island and gene body locations. RnBeads has the advantage of being able to perform paired analyses, for example, compare methylation states of a sample taken at diagnosis with its counterpart sample taken at relapse. In this type of analysis the paired Student's *t*-test is applied and reported alongside a false discovery rate (FDR) adjusted p value. For this reason an analysis workflow was developed (Figure 5.17) using RnBeads, to directly interrogate in a pairwise manner whether genomic regions acquired changes in methylation between diagnosis and relapse.

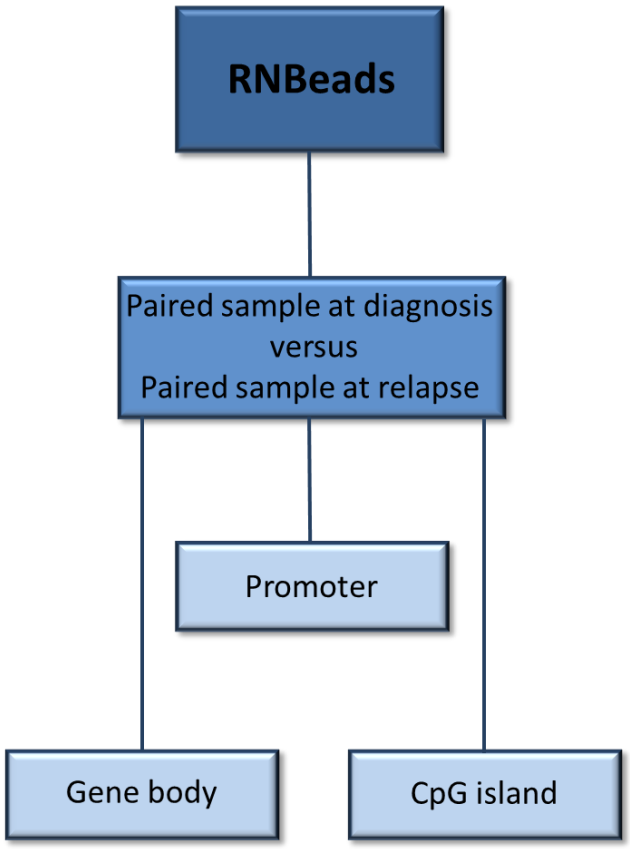

Figure 5.17 Workflow for RnBeads analyses. Paired samples at diagnosis and relapse samples refer to the paired relapse cohort (section 5.3.2).

5.3.7.3 Single probe analysis

This proof-of-concept analysis was designed to detect methylation events that were either acquired at relapse or maintained at relapse. It was hypothesis driven following the observations in Chapter 3, where maintained and acquired defects such as *TP53* mutation were significant events observed at relapse. To capture methylation events that behaved in an equivalent manner, the following pipeline was conceived and implemented.

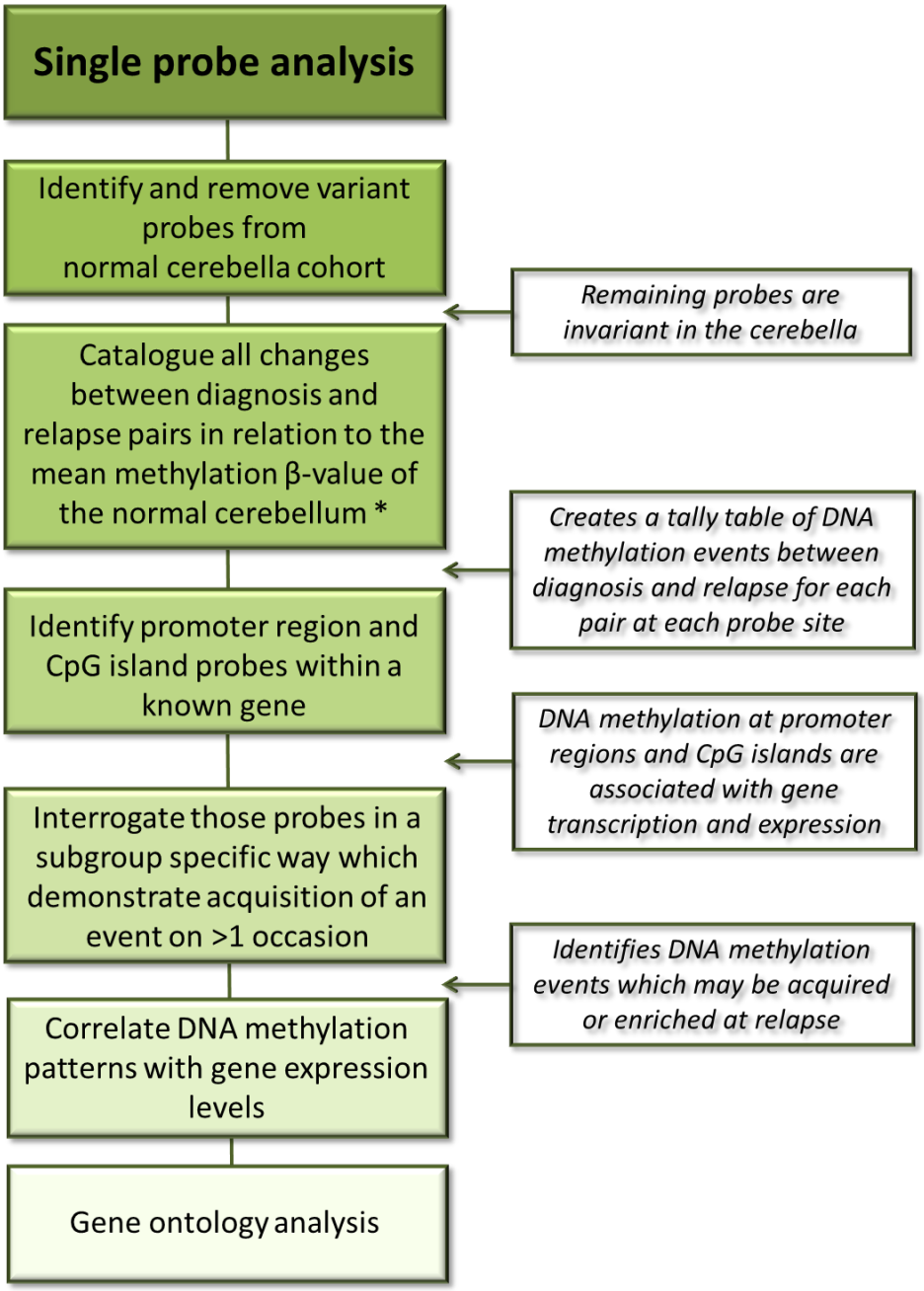

Figure 5.18 Analysis pipeline to detect single CpG site alterations between diagnosis and relapse. *Description of cataloguing events is discussed in section 5.3.7.3.1.

5.3.7.3.1 Cataloguing events with relation to the normal cerebella

The cerebella cohort (n=17, section 5.3.5) methylation dataset was normalised using the BMIQ method (section 5.3.6.5). Probes which contained potentially confounding single nucleotide polymorphisms (SNPs) were removed from both the normal cerebella and paired relapsed cohort methylation datasets. Invariant probes in the normal cerebellum were identified as those probes with a standard deviation from the mean of β-value <0.02. This identified a total of 410 350 probes with a consistent methylation status in normal tissue which could be used to interrogate tumour-specific methylation states in the paired relapsed cohort. Every invariant probe was next categorised according to their methylation status at diagnosis and relapse in every individual patient matched sample, to determine whether DNA methylation status was altered from the normal cerebellum at diagnosis and relapse.

This created 5 criteria; changed methylation state from abnormal (tumour-specific) to normal (same as normal cerebellum) between diagnosis and relapse, changed methylation state from normal to abnormal between diagnosis and relapse, unchanged normal methylation state between diagnosis and relapse, unchanged abnormal methylation state between diagnosis and relapse and NA due to missing data. Examples of two of these criteria, acquired events and maintained events (changed methylation state from normal to abnormal between diagnosis and relapse and unchanged abnormal DNA methylation state between diagnosis and relapse respectively) are illustrated in Figure 5.19. The threshold for a change in DNA methylation state was set at an absolute β-value difference of 0.4. This was to capture true differences in β-values which has previous been defined as a β-value change of 0.25-0.33 (Maksimovic *et al.*, 2012; Schwalbe *et al.*, 2013b). The R script for this analysis is reported in section 9.1: Appendix I.

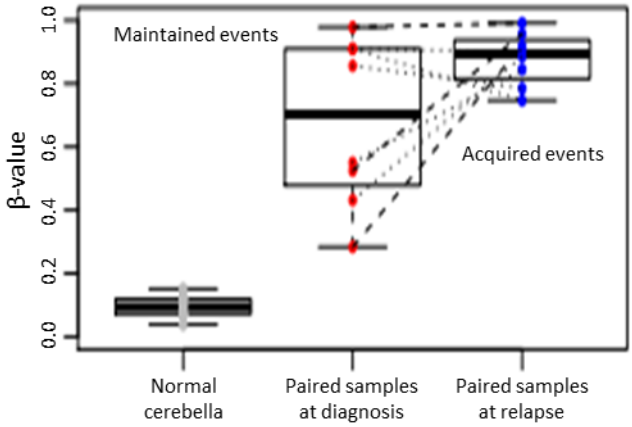

Figure 5.19 Illustrative example in MB_{Group4} of a single CpG residue (probe cg05431842) showing acquired and maintained tumour-specific methylation states between diagnosis and relapse in relation to the normal cerebella. Dashed and dotted lines connect paired tumours sampled from the same patient at diagnosis and relapse.

5.3.7.3.2 Analysis of MB_{Group4} methylation events

Subsequent analyses of the paired relapse cohort methylation dataset focused on the MB_{Group4} pairs sampled at diagnosis and relapse. The MB_{Group4} pairs were the largest, uniformly treated (upfront CSI), molecular subgroup, and proceeding with the analysis in MB_{Group4} alone controlled for the DNA methylation heterogeneity observed between the four molecular subgroups (Hovestadt *et al.*, 2013; Schwalbe *et al.*, 2013b). This analysis focused on identifying single CpG residues located in either a CpG island or promoter region, which demonstrated acquisition or maintenance of a tumour-specific DNA methylation state, with regards to the normal cerebella, whilst excluding those CpG sites which showed loss of an event and a return to normal methylation state at relapse. See section 9.2: Appendix II for the fully annotated R script of this analysis and section 5.4.2 and Figure 5.22 for the output tally table of results.

5.3.7.3.3 Correlation of methylation events with expression

An independent cohort with matched DNA methylation and gene expression data was utilised to identify DNA methylation events in MB_{Group4} that demonstrated a relationship with gene expression. This analysis is detailed in section 5.3.4.

5.3.7.3.4 Gene ontology analysis

Candidate genes showing acquired and maintained tumour-specific DNA methylation events in MB_{Group4} at relapse, which also demonstrated a strong relationship to expression (correlation coefficient *r* value >0.75 or <-0.75, section 5.3.4) were taken forward for gene ontology analyses. Ingenuity Pathway Analysis (IPA, Qiagen, Venlo, Netherlands) is an interactive software package which performs multiple types of analyses, such as pathway analysis, predictive causal analytics, as well as the integration and analyses of complex datasets. This software was utilised to identify relationships between candidate genes, pathway interactions and predict downstream effects of the upregulation or downregulation of a gene of interest.

5.4 Results

5.4.1 Relapse specific differentially methylated regions in medulloblastoma are an uncommon event

Two approaches, Bumphunting and RnBeads, were undertaken to interrogate the epigenome for the presence of differentially methylated regions that were associated with relapsed disease. These analyses are described in sections 5.3.7.1 and 5.3.7.2. The following table summarises the result from the Bumphunting analyses, including the number of candidate regions identified for each type of comparative analyses (Table 5.4).

Comparison		Results	
Paired relapse cohort	**Independent control cohort**	**Number of candidate regions**	**p value range**
Cohort wide			
Diagnosis	Diagnosis	20	**<0.0001-0.05**
Relapse	Diagnosis	56	**<0.0001-0.05**
MB_{SHH}			
Diagnosis	Diagnosis	27	**0.0008-0.05**
Relapse	Diagnosis	193	**<0.0001-0.04**
MB_{Group4}			
Diagnosis	Diagnosis	274	**<0.0001-0.05**
Relapse	Diagnosis	255	**<0.0001-0.05**
Comparison		**Results**	
Paired relapse cohort	**Paired relapse cohort**	**Number of candidate regions**	**p value range**
Cohort wide			
Diagnosis	Relapse	8	**0.006-0.02**
MB_{SHH}			
Diagnosis	Relapse	0	na
MB_{Group4}			
Diagnosis	Relapse	196	**<0.0001-0.05**

Table 5.4 Summary of Bumphunter analysis results in the paired relapse cohort compared to an independent control cohort of tumours sampled at diagnosis. p value, see section 5.3.7.1.

As already discussed in section 5.3.7.1, the p value reported should be interpreted with caution. Therefore, all candidate regions were visualised to examine the absolute difference in average β-values between the 2 populations of interest. Illustrative examples, reflective of the candidate regions identified are shown in Figure 5.20.

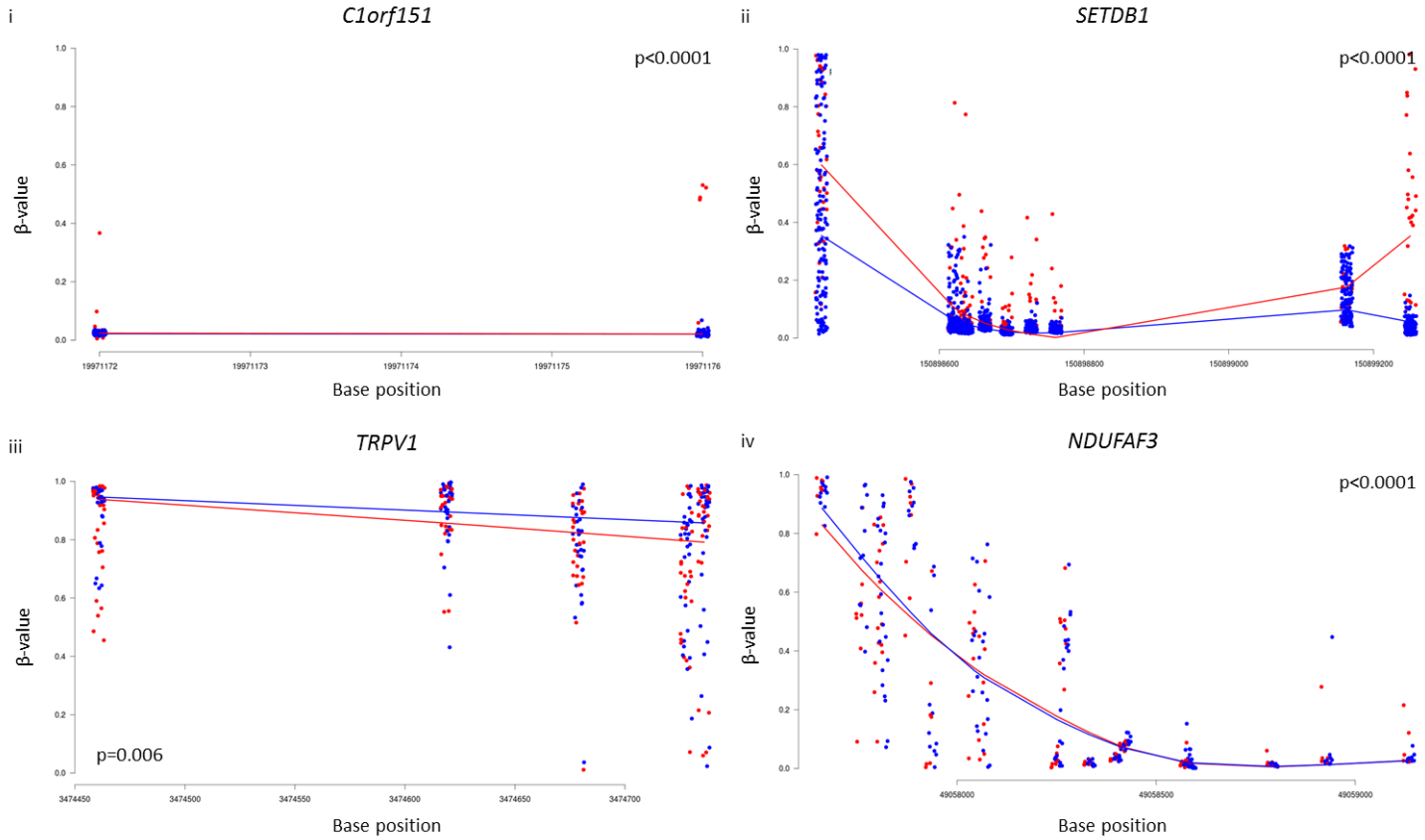

Figure 5.20 Illustrative examples of candidate regions identified by Bumphunter analysis. i) Tumours sampled at diagnosis (red) from paired relapse cohort versus tumours sampled at diagnosis (blue) from control cohort, ii) tumours sampled at relapse (red) from paired relapse cohort versus tumours sampled at diagnosis (blue) from control cohort, iii) tumours sampled at diagnosis (red) from paired relapse cohort versus tumours sampled at relapse (blue) from paired relapse cohort, iv) MB_{Group4} tumours sampled at diagnosis (red) from paired relapse cohort versus MB_{Group4} tumours sampled at relapse (blue) from paired relapse cohort. p value, see section 5.3.7.1.

Candidate regions identified by the Bumphunter analyses did demonstrate significant differences in β-values between the two comparative populations. However an absolute β-value difference >0.33 is typically reported as a significant change in DNA methylation which could lead to an epigenetically regulated change in gene transcription, and therefore may be of biological importance (Maksimovic *et al.*, 2012; Schwalbe *et al.*, 2013b). An example of this is shown in Figure 5.20i, where outlying cases sampled at diagnosis from the paired relapsed cohort (red) demonstrated a β-value difference of >0.33 when compared to the independent control cohort (blue). However, other regions were more difficult to interpret. For example, the region in NADH dehydrogenase assembly factor 3 (*NDUFAF3,* Figure 5.20iv) identified in the MB_{Group4} analysis between tumours sampled at diagnosis and relapse in the paired relapse cohort. This candidate region demonstrated a wide range of β-values in both populations interrogated, with little separation in the two mean β-values across the region and despite being significant was unlikely to be of biological relevance.

One of the limitations of the Bumphunter algorithm is that it only assesses and compares two populations of tumour samples. To overcome this, and undertake an analysis based on the individual patient matched tumour samples taken at diagnosis and relapse, a paired regional analysis was performed using RnBeads. This analysis, described in section 5.3.7.2, compared all tumours sampled at diagnosis that had a matched sample taken at relapse (n=27) and was undertaken to specifically identify acquired regional changes in DNA methylation between diagnosis and relapse within each individual patient. The results of this analysis are summarised in Table 5.5 and examples of differentially methylated regions are illustrated in Figure 5.21.

Comparison		Results	
Paired relapse cohort	**Paired relapse cohort**	**Number of candidate regions**	**p value range**
CpG Island			
Diagnosis	Relapse	429	**<0.01-0.05**
Promoter			
Diagnosis	Relapse	194	**<0.01-0.05**
Gene body			
Diagnosis	Relapse	136	**<0.01-0.05**

Table 5.5 Summary of RnBeads analysis in the paired relapse cohort reported by genomic region. p, paired Student's *t*-test.

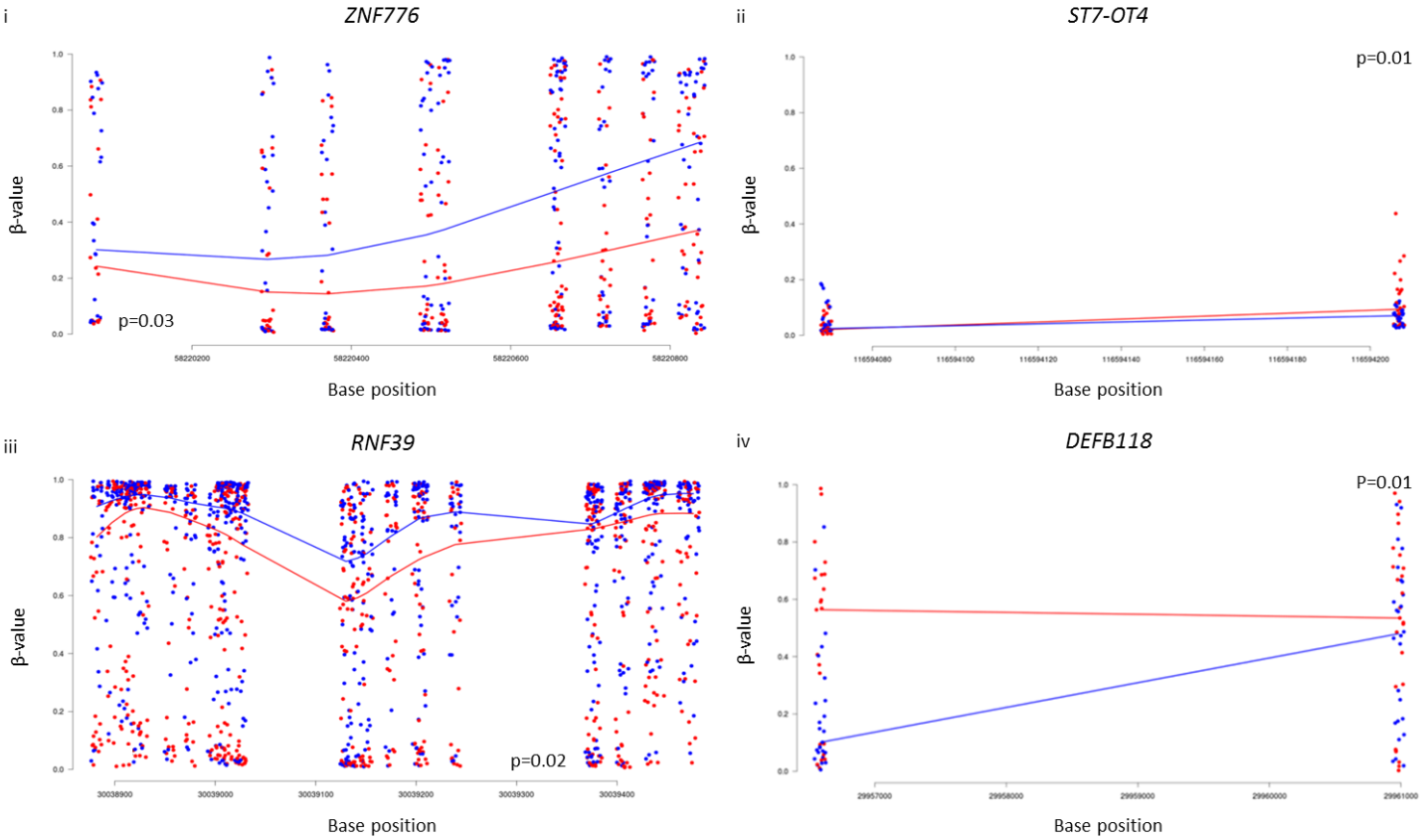

Figure 5.21 Illustrative examples of candidate regions identified by paired RnBeads analysis. i) Promoter region, ii) CpG island, iii) CpG island and iv) gene body. Red, tumours sampled at diagnosis from the paired relapse cohort; blue, tumours sampled at relapse from the paired relapse cohort. p, paired Student's *t*-test.

The results following the RnBeads analyses also required careful interpretation. While significant results were obtained following the paired Student's *t*-test, after controlling for the FDR, no results remained significant. Furthermore, on examining the differentially methylated genomic regions identified in this analysis (Figure 5.21), the absolute differences in β-values were <0.33 and therefore unlikely to be of biological importance (Maksimovic *et al.*, 2012; Schwalbe *et al.*, 2013b).

5.4.1.1 Challenges of analysing global DNA methylation patterns in the paired relapsed cohort

Following review of both approaches to examine any regional DNA methylation changes between diagnosis and relapse in medulloblastoma, it was evident that DNA methylation events of potential biological relevance were occurring, as illustrated in Figure 5.20i; isolated cases sampled at diagnosis from the paired relapsed cohort (red) demonstrated a β-value difference of >0.33 when compared to the independent control cohort (blue). However, given the heterogeneous DNA methylation patterns displayed by the four molecular subgroups (Hovestadt *et al.*, 2013; Schwalbe *et al.*, 2013b) which were all included in these analyses, it was likely that DNA methylation events were masked between diagnosis and relapse. Moreover, to identify DNA methylation events that behaved in an equivalent manner to the events reported in Chapter 3, *i.e.* acquired and maintained events between diagnosis and relapse, required a more focused and hypothesis driven approach as these types of events were unlikely to reach significance in regional analyses where β-values were averaged.

To address these challenges, a novel analysis was developed to identify single CpG residues located in biologically important regions of the genome (CpG islands or promoter regions), that either acquired or maintained tumour-specific DNA methylation states at relapse. These genomic regions were interrogated initially as it is well established that promoter DNA methylation can regulate gene transcription and expression (Bird, 2002; Issa, 2004; Baylin and Jones, 2011). This analysis was next expanded to incorporate a regional overview looking at CpG residues across an entire gene in a subgroup-specific manner. As described in section 5.3.7.3, this approach addressed both the limited numbers and epigenetic heterogeneity within the paired relapse cohort by cataloguing every methylation event for each pair according to their molecular subgroup.

MB_{SHH}, while overall was the largest subgroup in the paired relapse cohort (n=16 pairs), contained both infants and older children who received variable upfront treatment strategies *i.e.* infants did not receive upfront CSI. Given the findings reported in Chapter 3, and the impact upfront treatment appears to have on relapse medulloblastoma biology, further analyses focused on MB_{Group4}, the largest uniformly treated molecular subgroup represented in the paired relapse cohort. It is also the most poorly understood of the four subgroups ((Kool *et al.*, 2012; Northcott *et al.*, 2012a; Taylor *et al.*, 2012)). Therefore, to further our understanding in this subgroup, the methylation events cataloged in MB_{Group4} paired tumour samples were investigated in more detail and correlated with expression.

5.4.2 T-box gene family and Homeobox gene family acquire methylation events at relapse which correlate with gene expression in MB_{Group4}

As described in section 5.3.7.3.1, every probe that was invariant in the cerebella, with a β-value standard deviation of <0.02 (n=410 350), on the Infinium methylation 450K array, was categorised according to its DNA methylation state at diagnosis versus relapse for each individual MB_{Group4} paired sample. Only probes located in promoter regions or CpG islands of known genes were included in this analysis. This approach was taken because of the current understanding in cancer of epigenetic regulation of gene expression by aberrant promoter region DNA methylation, which is discussed in section 1.4.6.1.2 (Costello and Plass, 2001; Sidransky, 2002; Baylin and Jones, 2011; Dedeurwaerder *et al.*, 2011).

Probes that showed loss of an event, *i.e.* a tumour-specific DNA methylation state at diagnosis returning to a normal state at relapse were excluded (section 9.2: Appendix II). Finally, an output tally table was created which focused on scoring probes according to how many acquired (normal DNA methylation state at diagnosis, tumour-specific state at relapse) or maintained events (tumour-specific state at both diagnosis and relapse) they demonstrated (Figure 5.22). Those probes which demonstrated acquisition of an event between diagnosis and relapse on >1 occasion (n=2170 probes) were taken forward into the expression analysis.

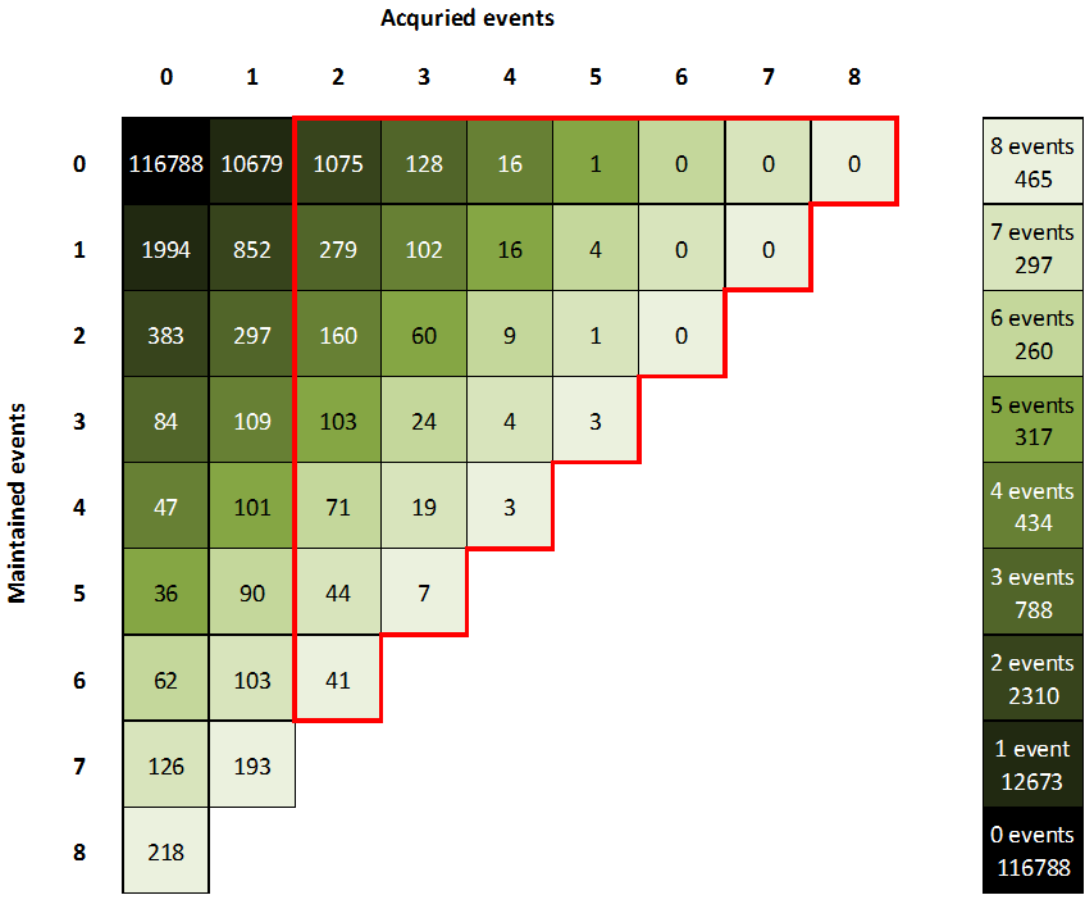

Figure 5.22 Tally table of acquired and maintained methylation events in gene CpG islands and promoter regions between MB_{Group4} paired samples at diagnosis and relapse. Number in each box represents the number of probes in this dataset fulfilling the criteria of the acquired (horizontal axis) and maintained (vertical axis) events. Squares outlined in red; number of selected probes taken forward for correlative expression analysis.

Correlation of DNA methylation and expression events was performed as described in section 5.3.4. This identified 23 CpG residues with DNA methylation events in MB_{Group4} relapse tumours which demonstrated a strong positive or negative relationship with expression (correlation coefficient *r* value >0.75 or <-0.75 respectively). Several of these probes were located within the same CpG island or gene promoter region. In total, 15 candidate genes showed a significant association between DNA methylation and gene expression levels, strongly suggestive of epigenetic mechanisms which regulate transcription of these candidate genes in MB_{Group4} tumours (Table 5.6). Most notably, genes from the T-box and Homeobox gene families represented 8/15 (53%) of the candidates identified.

Infinium methylation 450K array		Expression analysis		
Probe	**Location**	***r* value in MB_{Group4}**	***r* value across all subgroups**	**Gene name**
		Positive correlation		
cg00347620	Island	0.77	0.68	*TBX3*
cg22635491	CpG island	0.8	0.71	*TBX3*
cg09413529	CpG island	0.8	0.71	*TBX3*
cg11246938	CpG island	0.79	0.71	*TBX3*
cg18161956	CpG island	0.82	0.74	*TBX3*
cg18173058	CpG island	0.92	0.7	*TBX5*
cg05769349	CpG island	0.79	0.75	*TBX5*
cg16732616	CpG island	0.94	0.82	*DMRTA2*
cg12756396	CpG island	0.93	0.79	*DMRTA2*
cg16406967	CpG island	0.81	0.75	*HOXA3*
cg19999161	CpG island	0.83	0.78	*HOXA3*
cg14230397	Promoter	0.81	0.66	*PRAC*
cg20945566	Promoter	0.84	0.68	*PRAC*
cg22149137	CpG island	0.85	0.57	*HOXB13*
cg20403938	Promoter	0.79	0.69	*HOXC10*
cg11664987	CpG island	0.78	0.75	*EPHA10*
cg00204782	CpG island	0.85	0.88	*TBX1*
cg18843682	CpG island	0.75	0.77	*HOXC5*
		Negative correlation		
cg26459500	CpG island	-0.8	-0.82	*NUDT16*
cg15270892	CpG island	-0.91	-0.79	*EOMES*
cg26614816	CpG island	-0.84	-0.85	*EID3*
cg07064066	Promoter	-0.87	-0.87	*DSCR4*
cg08460435	CpG island	-0.88	-0.86	*HENMT1*

Table 5.6 MB_{Group4} candidate gene list with DNA methylation events at medulloblastoma relapse which are significantly associated with gene expression levels. Infinium methylation 450K array probes with acquisition of tumour-specific DNA methylation events between diagnosis and relapse are shown according to their relationship with expression in an independent methylation-expression dataset of medulloblastomas (section 5.3.4). *r* values are reported across all four molecular subgroups in this independent cohort and in MB_{Group4} alone.

5.4.2.1 TBX3 exhibits regional DNA methylation changes between diagnosis and relapse which positively correlate with expression

As illustrated in Table 5.6, the most notable findings in this analysis were the enrichment of T-box transcription factors (*TBX1, TBX3*, *TBX5* and *EOMES*) and the Homeobox gene family (*HOXA3, HOXB13, HOXC10* and *HOXC5*). In particular the relationship between DNA methylation and gene expression for *TBX3*, the T-box transcription factor located on chromosome 12, which exhibited multiple CpG sites with either maintained tumour-specific DNA methylation or acquired DNA methylation of these sites at relapse (Figure 5.23). For example DNA methylation was acquired at

several CpG residues in patient 21 and 31 and also maintained in patient 17 and 18 (Figure 5.23, highlighted in grey). Importantly, on examining the CpG sites across the entire gene, acquired DNA methylation changes were also observed outside of the CpG residues identified in this analysis, for example in patient 21 probe cg16277169 (Figure 5.23). This suggests that while DNA methylation of individual CpG residues identified in this analysis may correlate with gene expression, they may also be reflective of the wider DNA methylation status observed in that gene region. The DNA methylation at 5 CpG residues which all positively correlated with expression in the independent expression control cohort are illustrated in Figure 5.24, and were significantly associated with levels of gene expression in both MB_{Group4} and all medulloblastoma tumours in the independent expression control cohort.

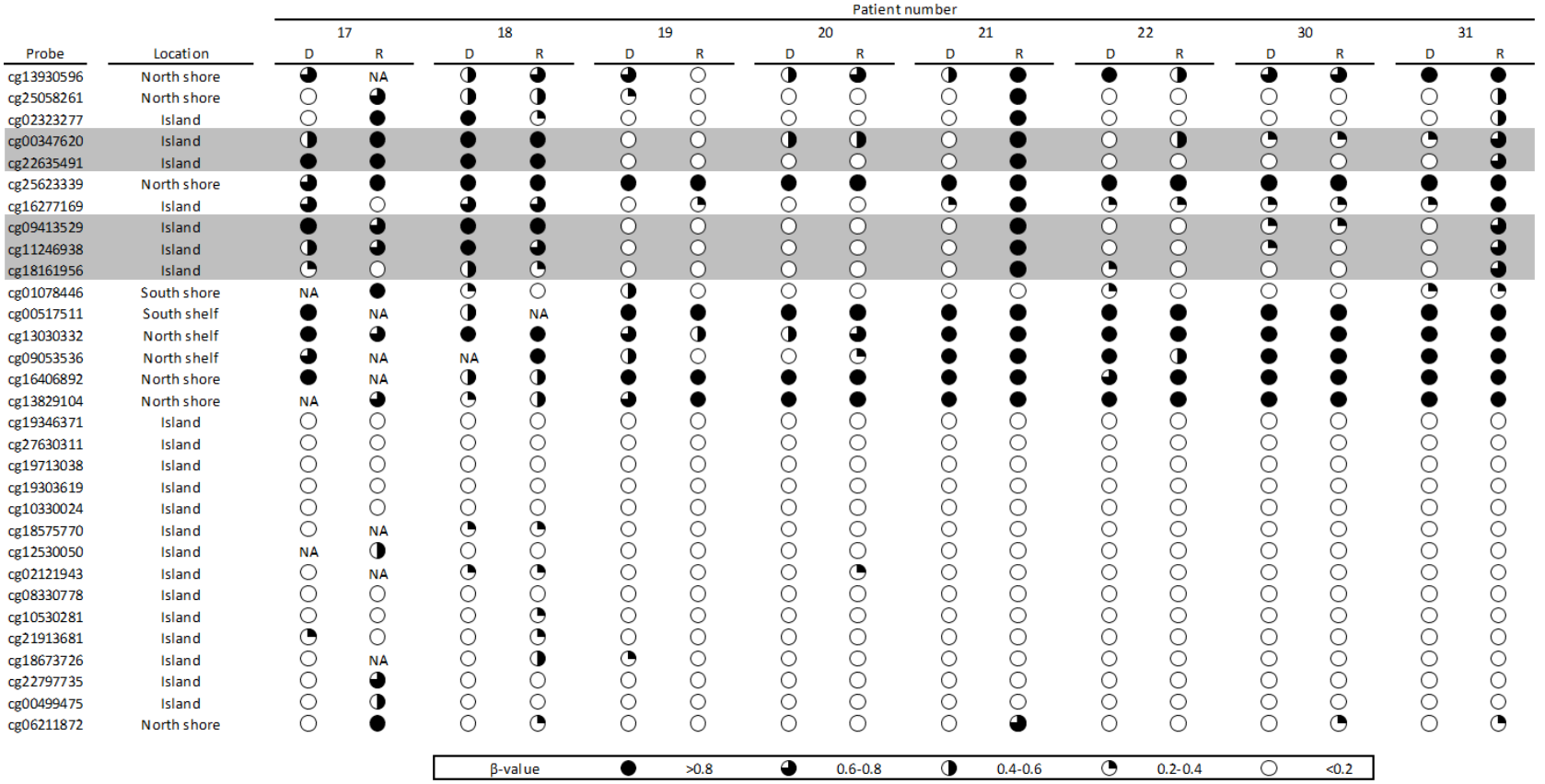

Figure 5.23 Illustration demonstrating the DNA methylation changes for *TBX3* between diagnosis and relapse in the MB_{Group4} paired samples. Circles represent the β-value for each sample as detected by the CpG probes on the Infinium methylation 450K array. CpG probes are arranged in order along the gene (5'-3'). Grey rows, probes of interest; D, diagnosis; R, relapse.

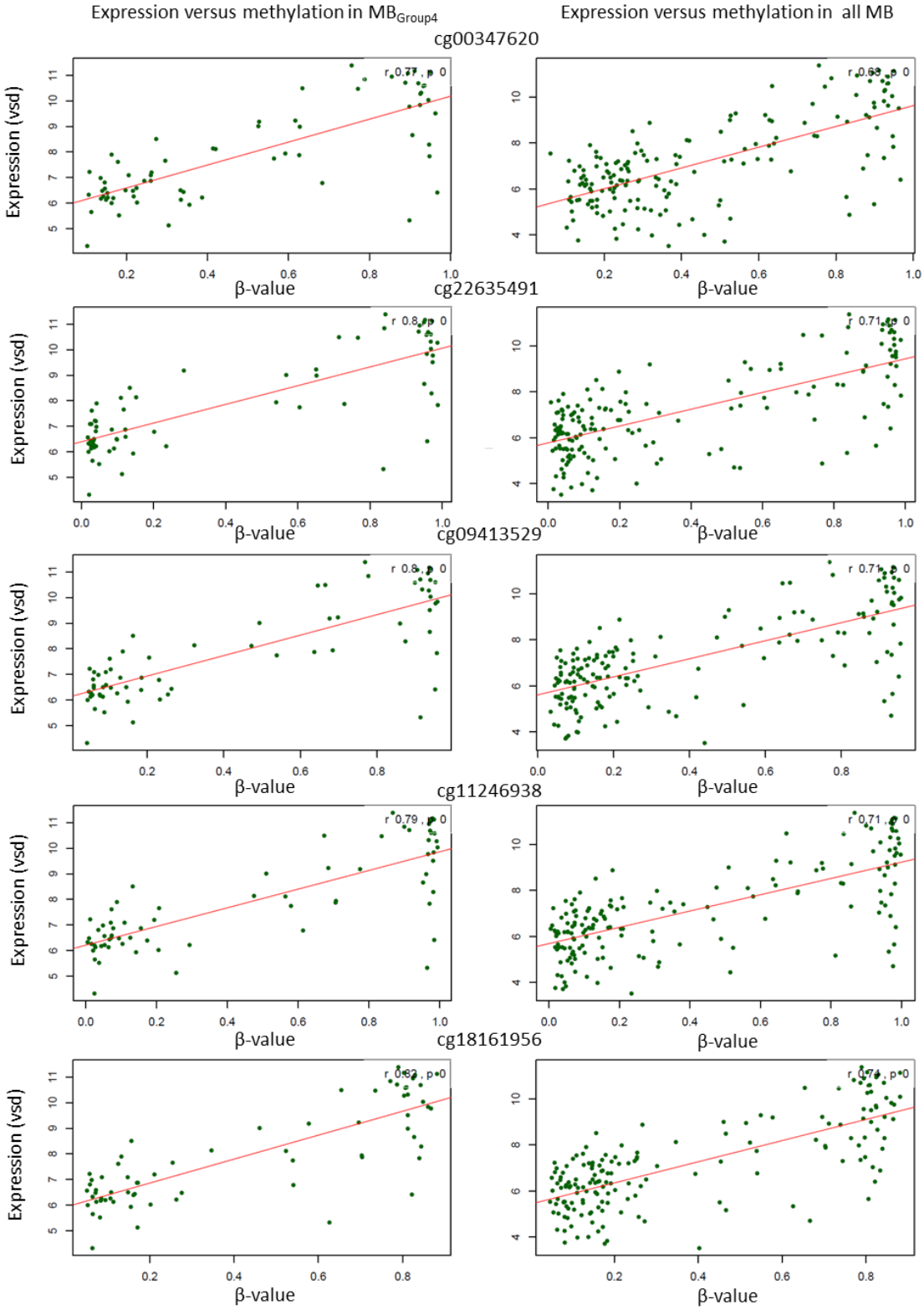

Figure 5.24 Linear regression plot demonstrating the positive correlation between gene expression and DNA methylation for 5 CpG residues located in the gene *TBX3*. VSD, variance-stabilising data.

While a positive correlation between DNA methylation and gene expression is contrary to the typical epigenetic mechanism proposed for the regulation of gene expression (*i.e.* promoter hypermethylation normally leads to gene silencing (section 1.4.6.1.2)), this type of observation is not unique. Recent work within medulloblastoma and other brain tumours has reported similar findings, with for example, hypermethylation upstream of the TSS of *TERT* linked to increased expression of the gene (Castelo-Branco *et al.*, 2013; Lindsey *et al.*, 2014). Given this strong correlation between DNA methylation and gene expression across multiple sites in the *TBX3* gene, pathway analysis was undertaken to investigate the role of *TBX3* methylation and expression in tumourigenesis.

5.4.2.2 TBX3 gene expression inhibits $p14^{ARF}$ and TP53 in pathway analysis

Pathway analysis using the IPA software as described in section 5.3.7.3.4 was undertaken to identify gene networks associated with *TBX3.* The predictive causal analysis was also explored to assess the downstream effects of increased expression in *TBX3*, which corresponded with the positively correlated increase in DNA methylation observed at relapse in MB_{Group4} tumours (Figure 5.23). The result of this analysis is shown in Figure 5.25. Most notably, increased expression of *TBX3* was predicted to inhibit both *TP53*, and *CDKN2A*, which has an alternatively spliced transcript encoding $p14^{ARF}$, a stabiliser of the p53 protein (Figure 1.6). This is suggestive of another aberrant mechanism leading to p53 pathway disruption at medulloblastoma relapse, in keeping with the discoveries reported in Chapter 3.

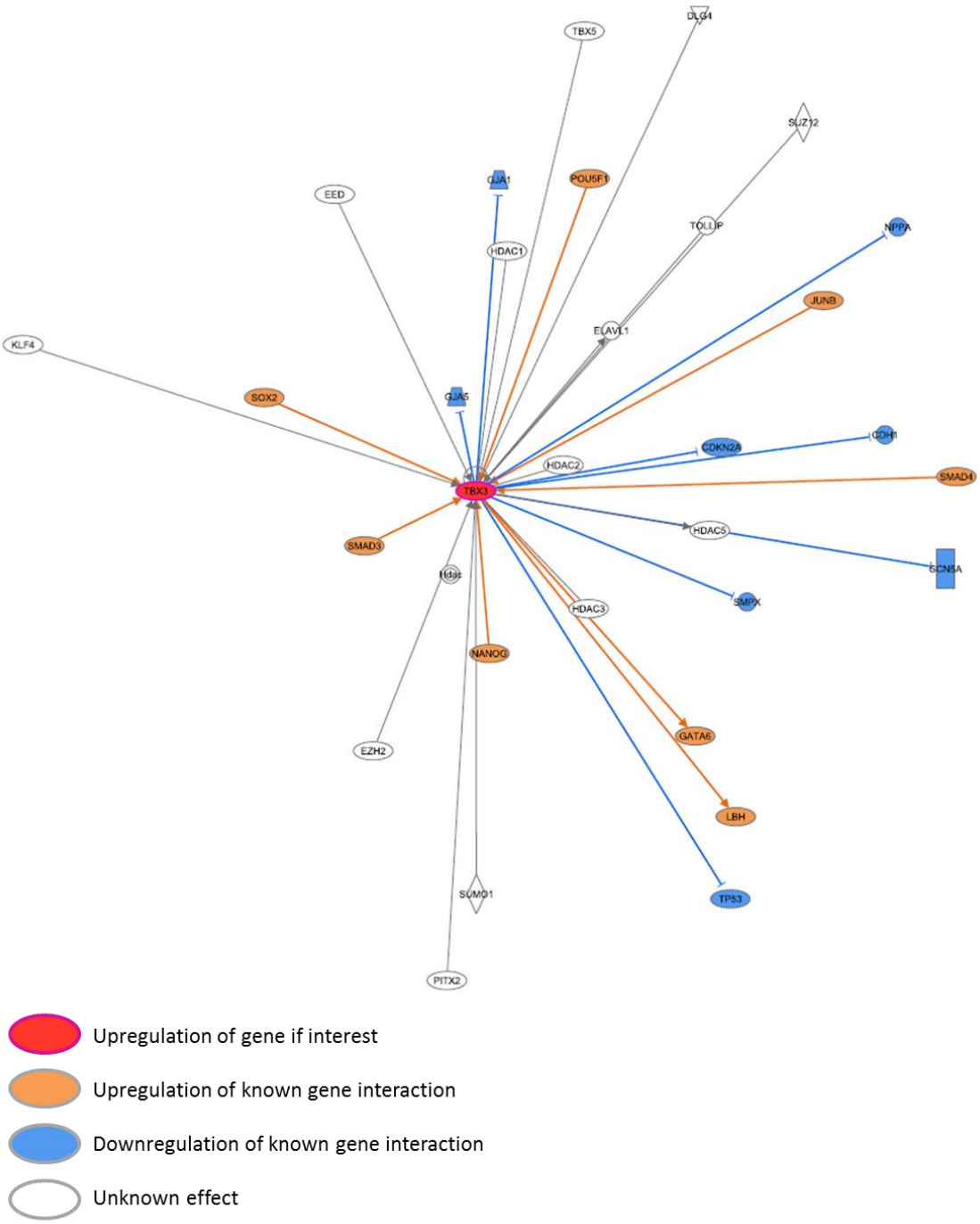

Figure 5.25 Downstream effects of *TBX3* upregulation as predicted by Ingenuity Pathway Analysis. Illustration shows only the networks with strong relationships to the gene of interest, *TBX3*.

5.4.2.3 TBX5 and TBX1 exhibit DNA methylation changes between diagnosis and relapse which positively correlate with gene expression

In addition*, TBX5* and *TBX1* of the T-box gene family also demonstrated acquisition and maintenance of DNA methylation of individual CpG residues at relapse in MB_{Group4} (Figure 5.26, Figure 5.27 and Figure 5.29). For example, in *TBX5* acquisition of DNA methylation was observed in patient 17 and 20, and maintenance of DNA methylation at relapse for patient 18, 22, 30 and 31 (Figure 5.26, grey row). Further downstream in *TBX5*, acquisition of DNA methylation was also observed in patient 17, 18 and 22 (Figure 5.27, grey row). As illustrated in both these figures, the CpG residues of interest at relapse appeared to be more widely reflective of the DNA methylation patterns of that region of the gene. This was particularly noticeable for patient 18, 22, 30 and 31 in the CpG island associated with the probe of interest, cg18173058 (Figure 5.26).

TBX1 demonstrated a similar pattern of DNA methylation at relapse, with acquisition observed in two patients (patient 17 and 21) and maintenance of DNA methylation witnessed in several patients which was reflective of the regional DNA methylation status (19, 20, 22, 30 and 31, Figure 5.29). For both *TBX5* and *TBX1*, gene expression levels correlated positively with DNA methylation in the independent expression control cohort (Figure 5.28 and Figure 5.30). These findings further reinforced the potential role of the T-box gene family in MB_{Group4} medulloblastoma at relapse, alongside highlighting the complex relationship between the epigenetic regulation of gene expression (discussed in section 5.5.2).

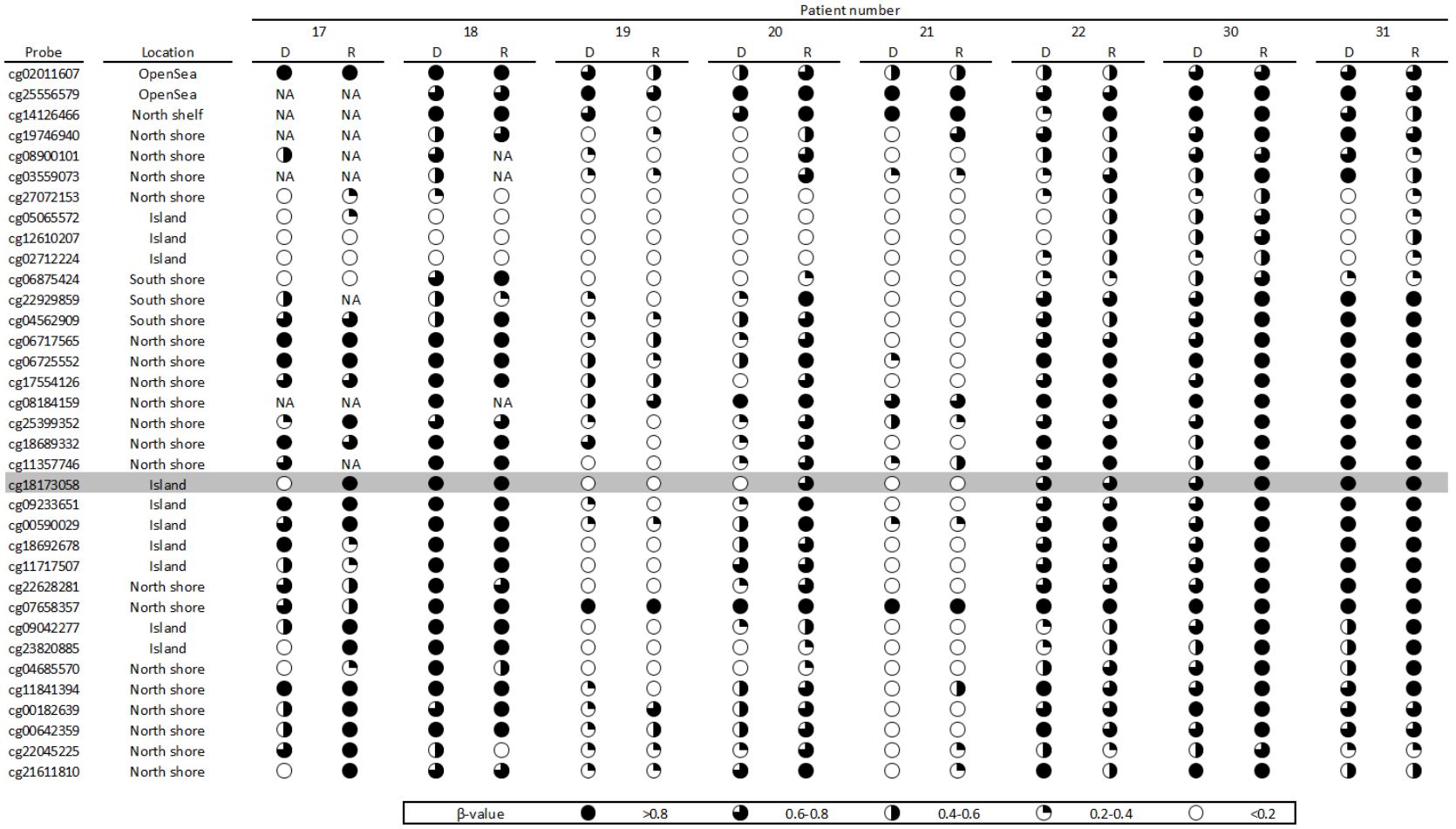

Figure 5.26 Illustration demonstrating the DNA methylation changes for *TBX5* between diagnosis and relapse in the MB_{Group4} paired samples. Circles represent the β-value for each sample as detected by the CpG probes on the Infinium methylation 450K array. CpG probes are arranged in order along the gene (5'-3'). Grey row, probe of interest; D, diagnosis; R, relapse.

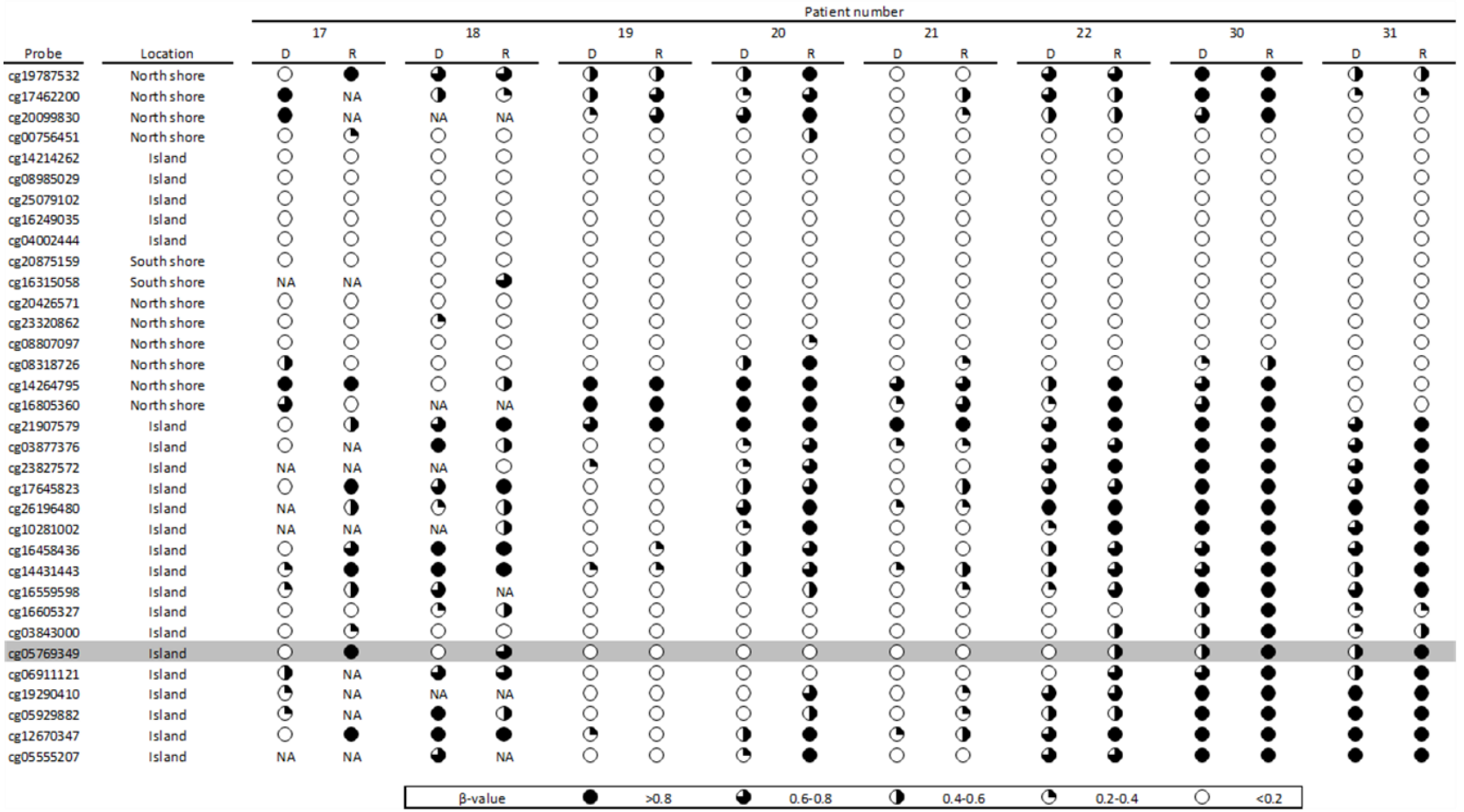

Figure 5.27 Illustration continued demonstrating the DNA methylation changes for *TBX5* between diagnosis and relapse in the MB_{Group4} paired samples. Circles represent the β-value for each sample as detected by the CpG probes on the Infinium methylation 450K array. CpG probes are arranged in order along the gene (5'-3'). Grey row, probe of interest; D, diagnosis; R, relapse.

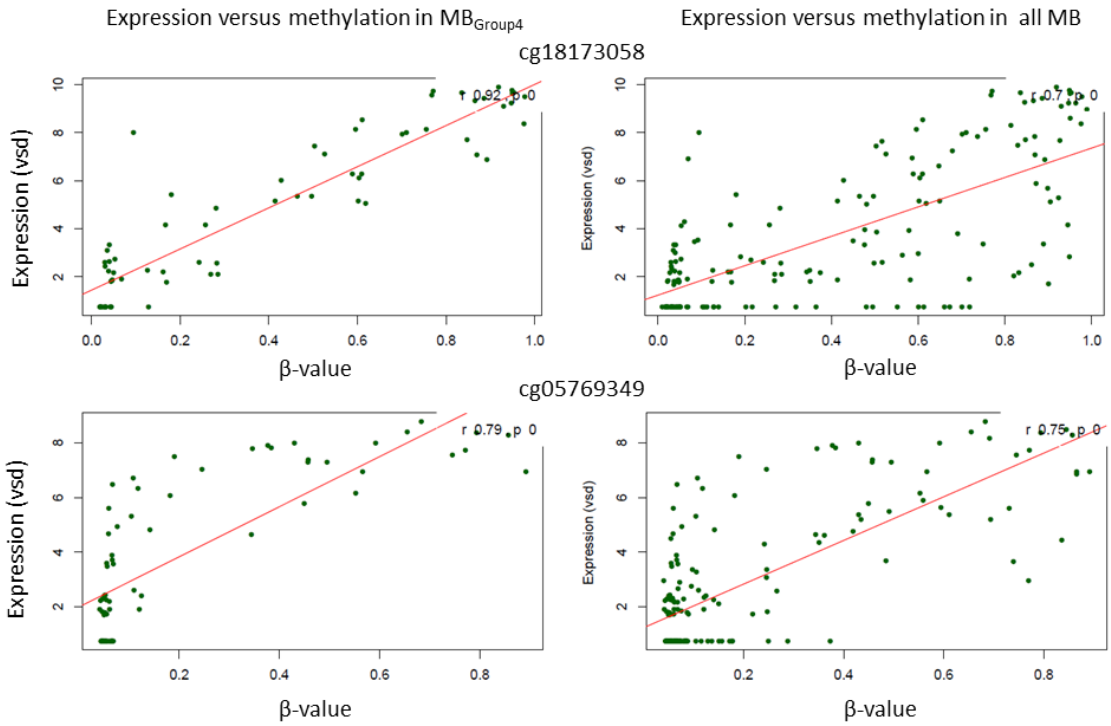

Figure 5.28 Linear regression plot demonstrating the positive correlation between gene expression and DNA methylation for 2 CpG residues located in the gene *TBX5.* VSD, variance-stabilising data.

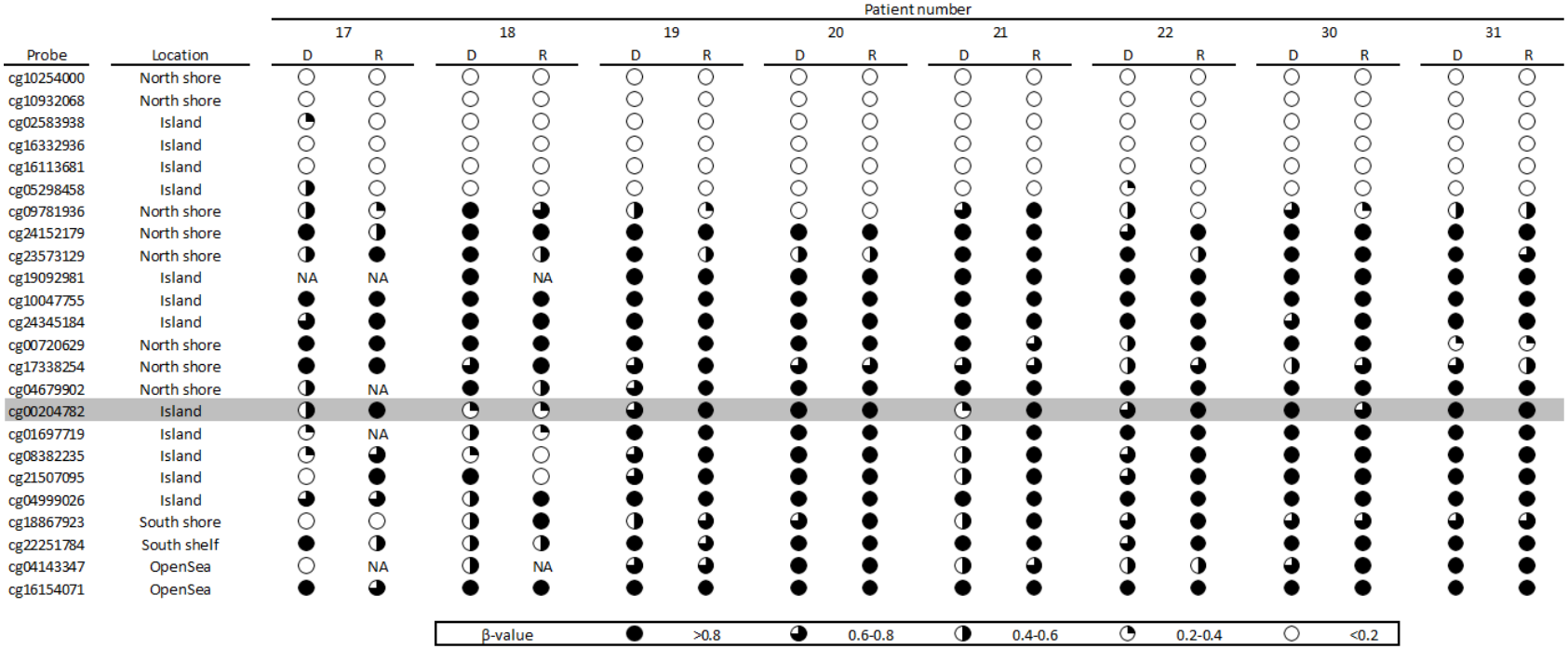

Figure 5.29 Illustration demonstrating the DNA methylation changes for *TBX1* between diagnosis and relapse in the MB_{Group4} paired samples. Circles represent the β-value for each sample as detected by the CpG probes on the Infinium methylation 450K array. CpG probes are arranged in order along the gene (5'-3'). Grey row, probe of interest; D, diagnosis; R, relapse.

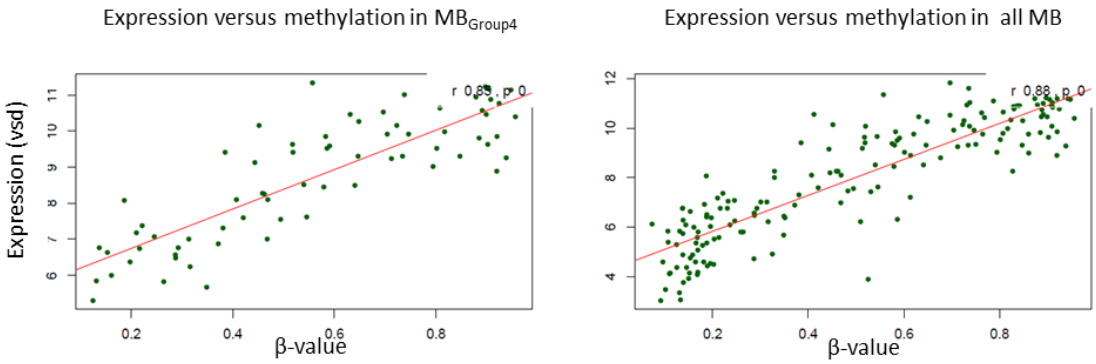

Figure 5.30 Linear regression plot demonstrating the positive correlation between gene expression and DNA methylation for 1 CpG residue located in the gene *TBX1.* VSD, variance-stabilising data.

5.4.2.4 EOMES DNA methylation inversely correlates with gene expression in MB$_{Group4}$ tumours at relapse

Five genes demonstrated a significantly inverse relationship between DNA methylation and gene expression (Table 5.6, section 9.3: Appendix III and section 9.4: Appendix IV). One of these genes, *EOMES* located on chromosome 3, is another member of the T-box gene family. One CpG residue located within a CpG island demonstrated acquisition of DNA methylation in two patients (19 and 22) and maintenance of DNA methylation in three patients (20, 30 and 31, Figure 5.32). DNA methylation at this CpG residue (cg15270892) appeared reflective of the DNA methylation upstream, for example, in the north shore in patient 19 and 22 (acquisition of DNA methylation) and patient 20, 30 and 31 (maintenance of DNA methylation). DNA methylation at this CpG residue strongly correlated inversely with gene expression (Figure 5.31) suggesting a possible role for epigenetic silencing of *EOMES* in MB$_{Group4}$ at relapse.

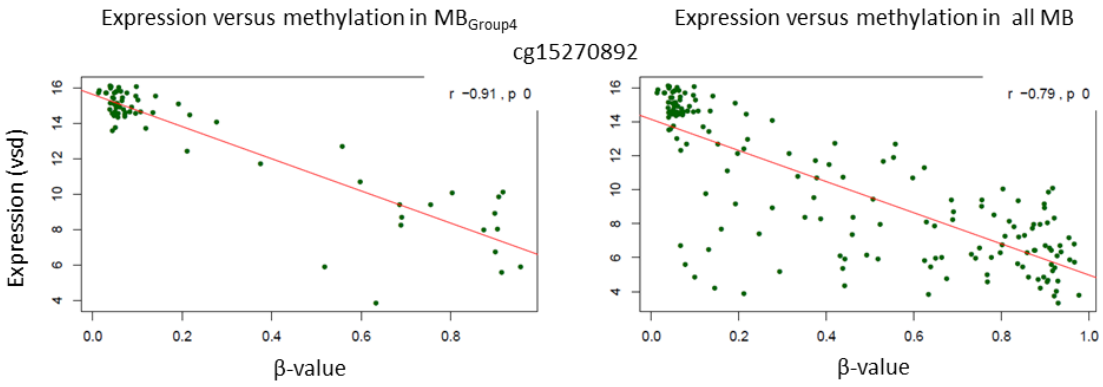

Figure 5.31 Linear regression plot demonstrating the inverse correlation between gene expression and DNA methylation for CpG residue cg15270892 located in the CpG island of *EOMES*. VSD, variance-stabilising data.

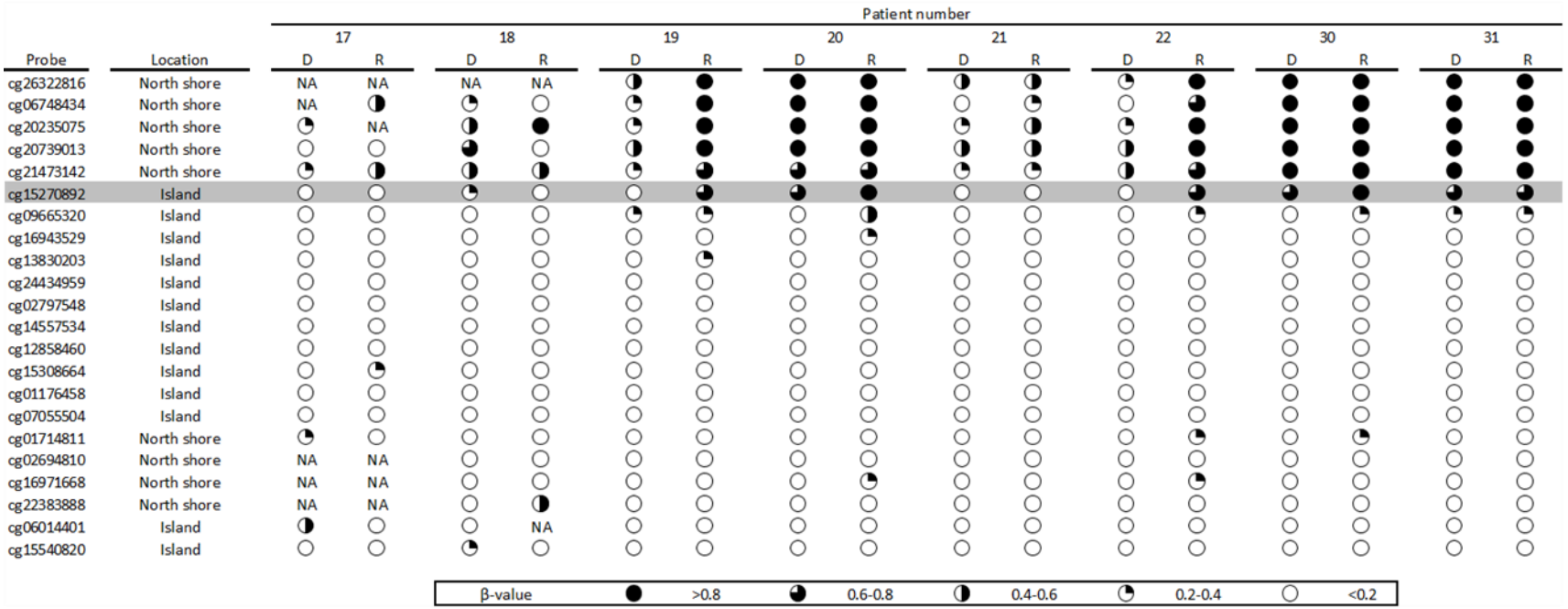

Figure 5.32 Illustration demonstrating the DNA methylation changes for *EOMES* between diagnosis and relapse in the MB_{Group4} paired samples. Circles represent the β-value for each sample as detected by the CpG probes on the Infinium methylation 450K array. CpG probes are arranged in order along the gene (5'-3'). Grey row, probe of interest; D, diagnosis; R, relapse.

5.4.2.5 All MB_{Group4} tumours at relapse demonstrate acquisition or maintenance of DNA methylation in a T-box gene CpG residue which correlates with gene expression

To understand the overall involvement of the T-box gene family in MB_{Group4} at relapse a summary of the DNA methylation status at the CpG residues associated with gene expression is shown in Figure 5.33. On examining the DNA methylation patterns for each gene it was clear, for example in *TBX3*, that in patient 17, 18, 21 and 31 the DNA methylation status at diagnosis and relapse was equivalent at each CpG site associated with gene expression (n=5). This was either acquisition of DNA methylation (*e.g.* patient 21) or maintenance of DNA methylation (*e.g.* patient 18). A similar pattern was observed in *TBX5*, for example in patient 17, where acquisition of DNA methylation was witnessed at both CpG sites associated with gene expression.

Importantly, on examining the patterns of DNA methylation for all four T-box genes identified in these analyses, every MB_{Group4} tumour demonstrated either acquisition or maintenance of a tumour-specific DNA methylation event at relapse. In particular, *TBX1* displayed a DNA methylation event in 7/8 (88%) of MB_{Group4} between diagnosis and relapse. Together, these findings suggest the epigenetic regulation and involvement of the T-box gene family in MB_{Group4} at relapse.

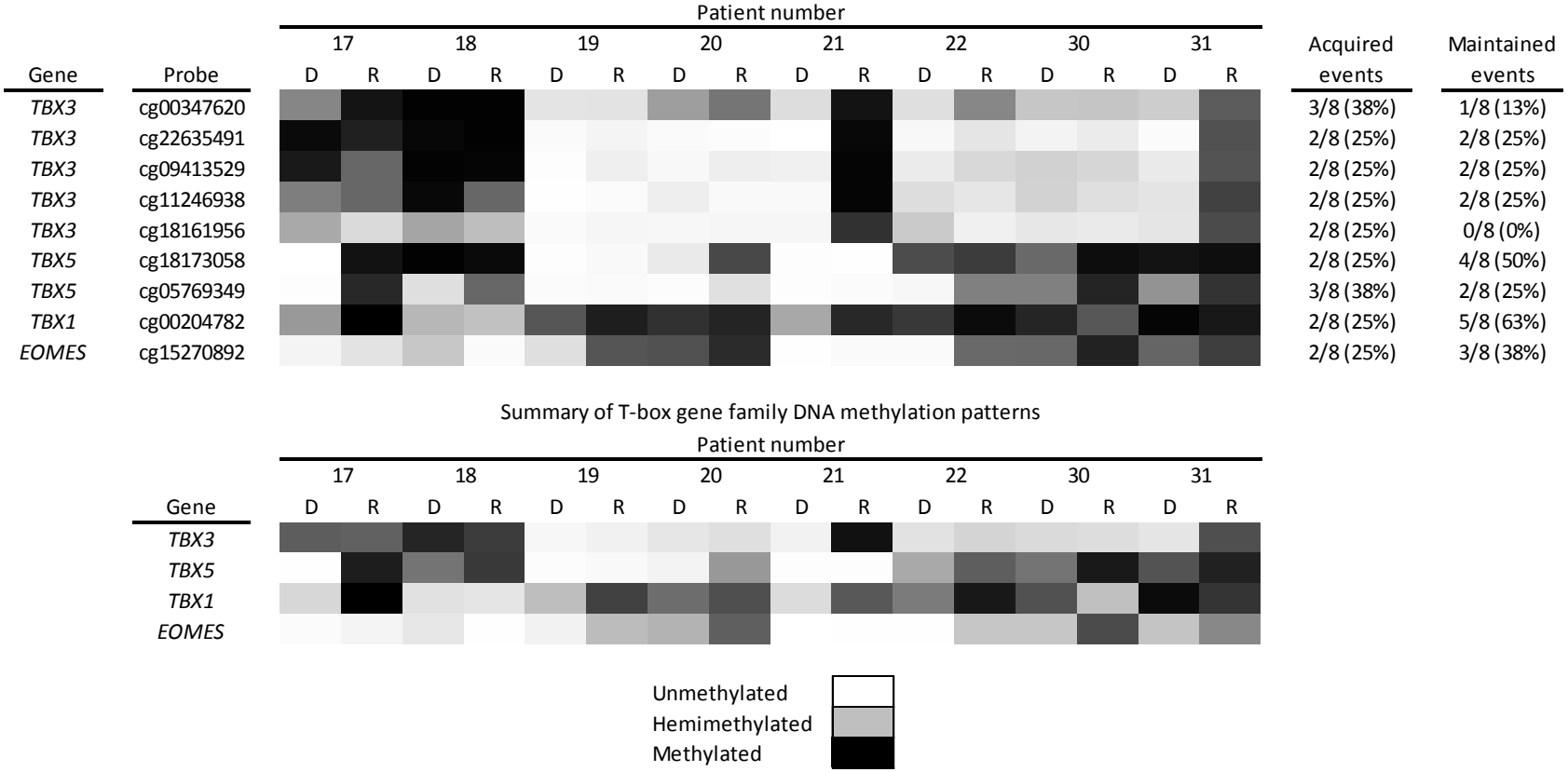

Figure 5.33 Heat-map demonstrating the DNA methylation status for each CpG residue associated with gene expression in the T-box gene family. Top panel displays DNA methylation at individual CpG residues with a summary of the number of acquired and maintained tumour-specific events observed at each site. Bottom panel summarises the four T-box genes with an average β-value for the two genes, *TBX3* and *TBX5,* which have multiple CpG residues of interest. D, diagnosis; R, relapse.

5.4.2.6 Homeobox gene family demonstrates acquisition of DNA methylation events in MB_{Group4} at relapse which positively correlate with gene expression

As already reported in Table 5.6, four members of the Homeobox gene family (*HOXA3, HOXB13, HOXC10* and *HOXC5*) at MB_{Group4} relapse also acquired DNA methylation at individual CpG residues which were associated with gene expression. These findings are illustrated in Figure 5.34 - Figure 5.38. *HOXA3* displayed two CpG sites with acquired or maintained tumour-specific DNA methylation at relapse which, similar to the DNA methylation patterns observed in the T-box gene family, was reflective of the DNA methylation of the CpG island associated with these two residues (*e.g.* patient 20 and 30, Figure 5.34). Similar patterns at adjacent probes were also witnessed for *HOXC10* and *HOXC5* (*e.g.* patient 20 and 30, Figure 5.36 and Figure 5.37). However, the regional DNA methylation pattern was less clear for *HOXB13* and only an isolated CpG residue demonstrated acquired tumour-specific DNA methylation (*e.g.* patient 17, 18 and 21, Figure 5.35). In the Homeobox gene family, DNA methylation patterns at the five CpG residues identified through this analysis (Table 5.6), were significantly and positively associated with gene expression in the independent expression cohort (Figure 5.38).

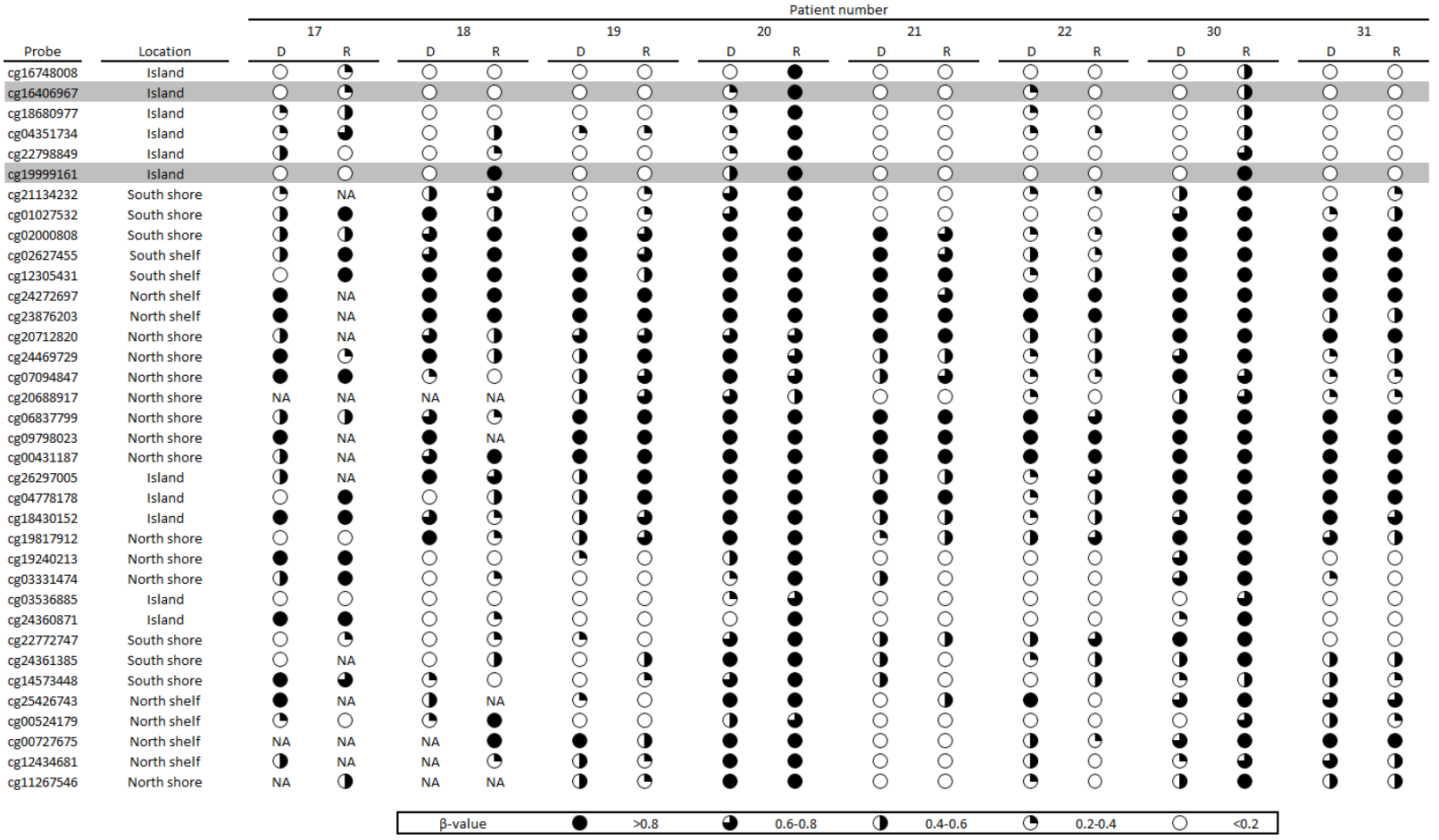

Figure 5.34 Illustration demonstrating the DNA methylation changes for *HOXA3* between diagnosis and relapse in the MB_{Group4} paired samples. Circles represent the β-value for each sample as detected by the CpG probes on the Infinium methylation 450K array. CpG probes are arranged in order along the gene (5'-3'). Grey row, probe of interest; D, diagnosis; R, relapse.

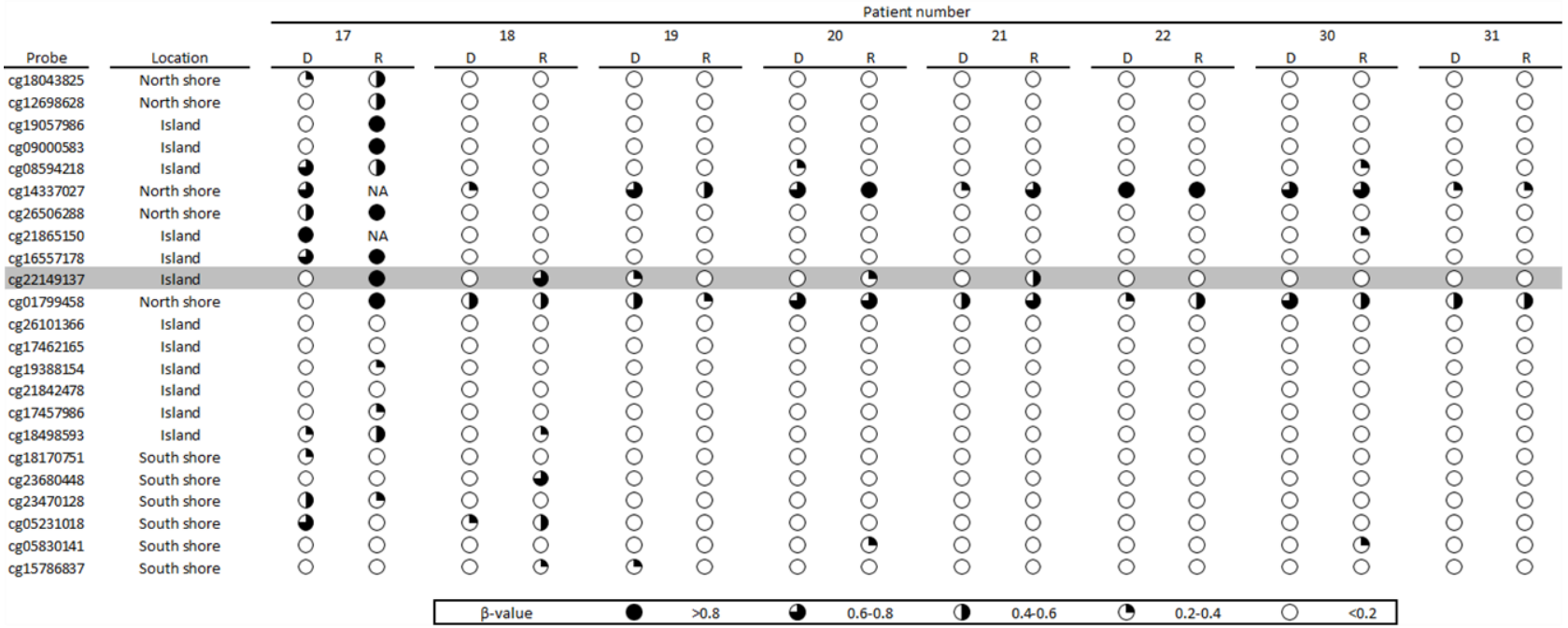

Figure 5.35 Illustration demonstrating the DNA methylation changes for *HOXB13* between diagnosis and relapse in the MB_{Group4} paired samples. Circles represent the β-value for each sample as detected by the CpG probes on the Infinium methylation 450K array. CpG probes are arranged in order along the gene (5'-3'). Grey row, probe of interest; D, diagnosis; R, relapse.

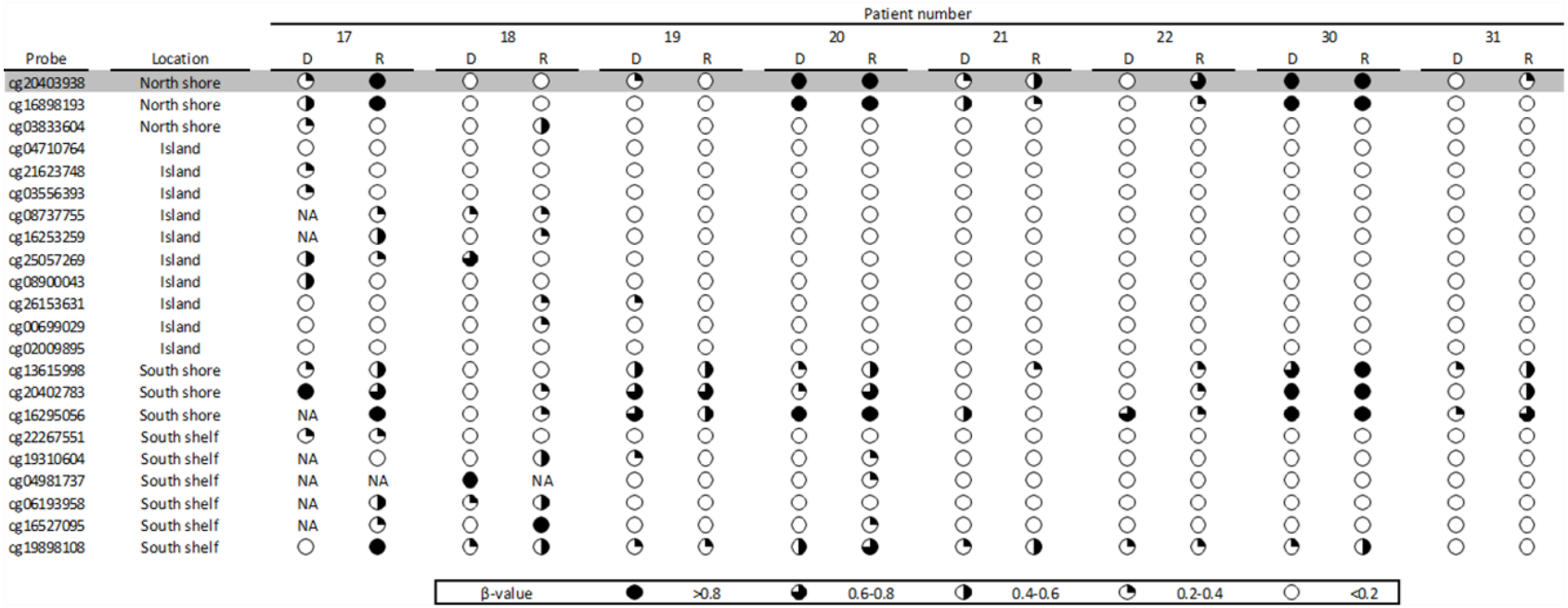

Figure 5.36 Illustration demonstrating the DNA methylation changes for *HOXC10* between diagnosis and relapse in the MB_{Group4} paired samples. Circles represent the β-value for each sample as detected by the CpG probes on the Infinium methylation 450K array. CpG probes are arranged in order along the gene (5'-3'). Grey row, probe of interest; D, diagnosis; R, relapse.

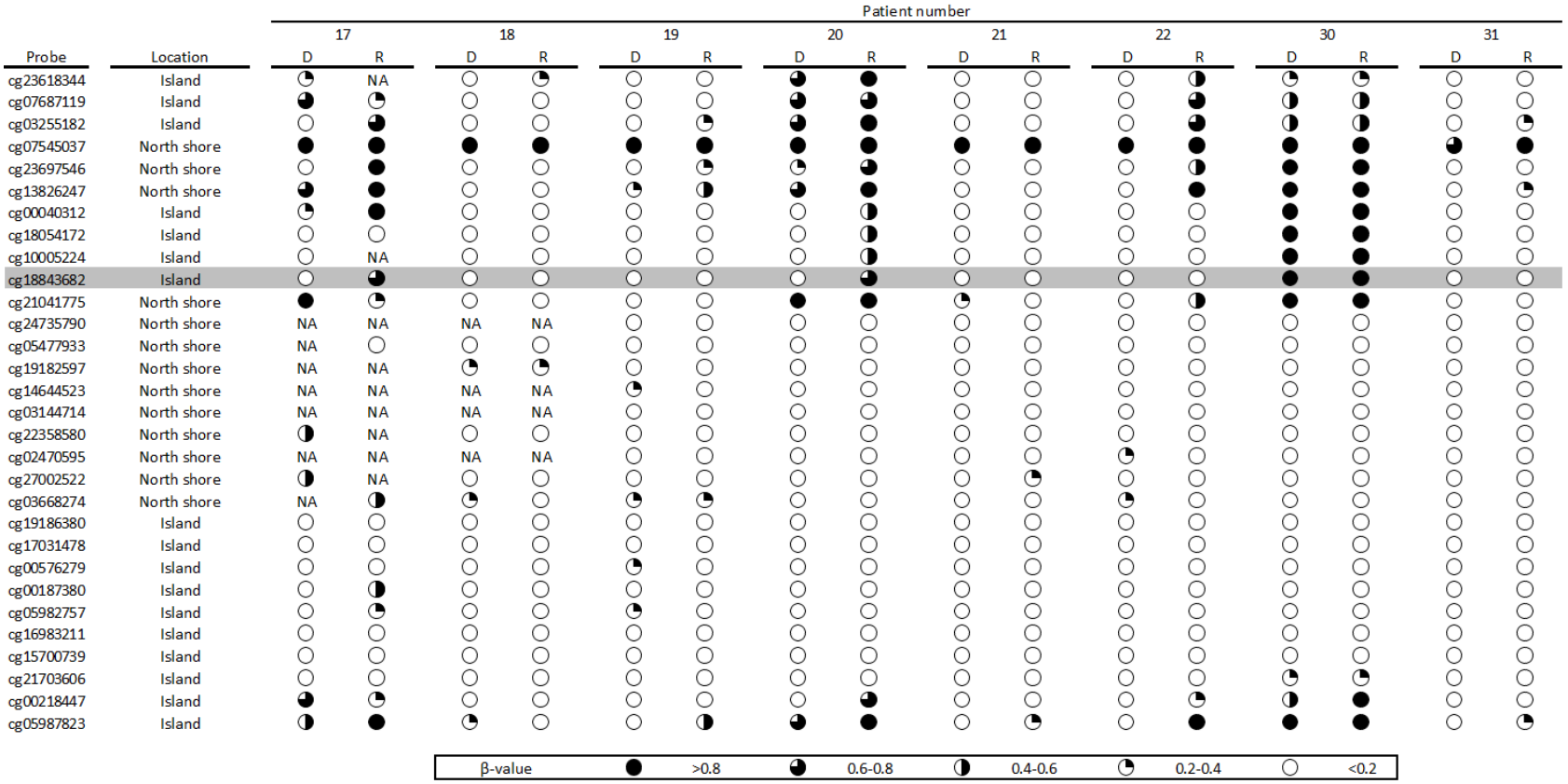

Figure 5.37 Illustration demonstrating the DNA methylation changes for *HOXC5* between diagnosis and relapse in the MB_{Group4} paired samples. Circles represent the β-value for each sample as detected by the CpG probes on the Infinium methylation 450K array. CpG probes are arranged in order along the gene (5'-3'). Grey row, probe of interest; D, diagnosis; R, relapse.

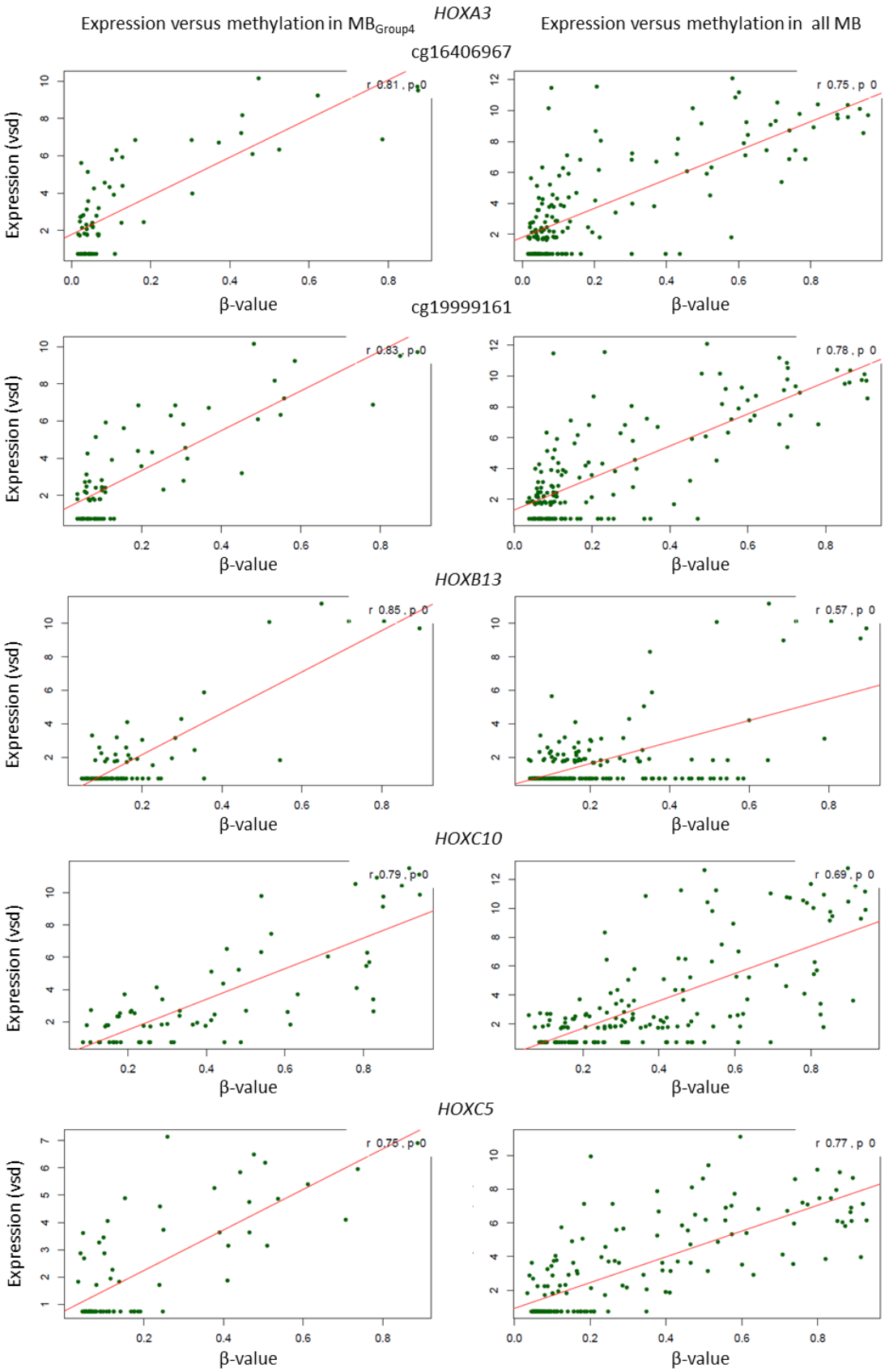

Figure 5.38 Linear regression plots demonstrating the positive correlation between gene expression and DNA methylation for the Homeobox gene family. VSD, variance-stabilising data.

5.4.2.7 Tumour-specific DNA methylation in the Homeobox gene family is frequently observed in MB_{Group4} at relapse

Tumour-specific DNA methylation at the CpG sites of interest identified in these analyses were observed in the majority of MB_{Group4} tumours at relapse (5/8, 63%). These DNA methylation patterns are illustrated in Figure 5.39 and highlight that a DNA methylation event occurred in one or more of the Homeobox genes for patient 17, 18, 20, 22 and 30. In particular, patient 17, 20 and 30 demonstrated either maintenance or acquisition of a DNA methylation event at relapse across multiple Homeobox genes (Figure 5.39). Combined these findings suggest a role for the Homeobox gene family in MB_{Group4} at relapse.

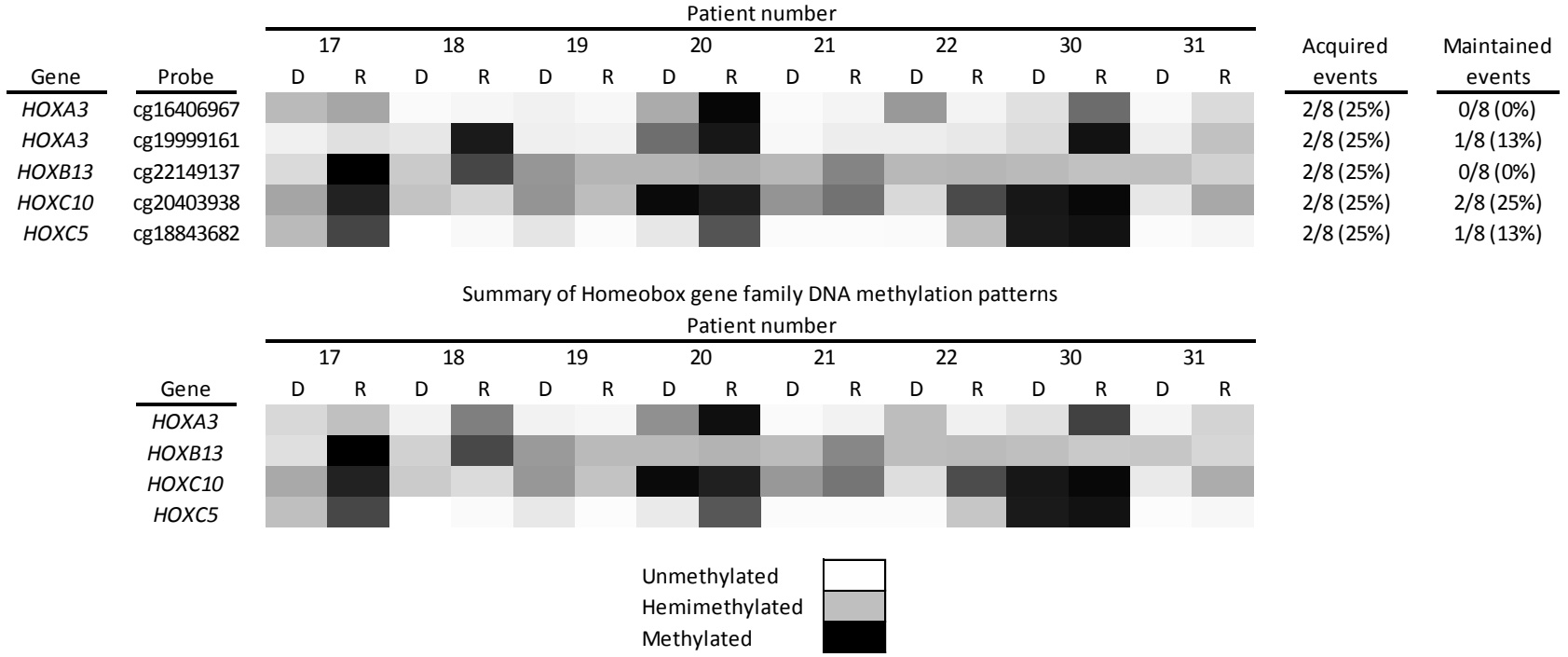

Figure 5.39 Heat-map demonstrating the DNA methylation status for each CpG residue associated with gene expression in the Homeobox gene family. Top panel displays DNA methylation at individual CpG residues with a summary of the number of acquired and maintained tumour-specific events observed at each site. Bottom panel summarises the four Homeobox genes with an average β-value for *HOXA3,* which has two CpG residues of interest. D, diagnosis; R, relapse.

5.5 Discussion

5.5.1 DNA methylation patterns differ between diagnosis and relapse in medulloblastoma

This study was the first to examine and identify differences in medulloblastoma DNA methylation patterns between diagnosis and relapse. These findings were in contrast to earlier discoveries reported in Chapter 3, where the subgroup-specific DNA methylation patterns remain stable between both time-points (Table 3.5). Three approaches were adopted to determine whether CpG residues either acquired or lost DNA methylation at relapse and if, in turn, this correlated with expression. Regional analysis of the medulloblastoma methylome in an unpaired (Bumphunter, section 5.4.1) and paired (RnBeads, section 5.4.1) analysis revealed initial insights into the temporal changes of DNA methylation but did not identify regions that displayed significantly different DNA methylation between diagnosis and relapse.

Following these provisional findings, subsequent analyses focused on the MB_{Group4} matched pairs. This was the largest molecular subgroup represented in the paired cohort of medulloblastoma tumours sampled at both diagnosis and relapse that received similar initial treatment, including upfront CSI (section 5.4.1.1). This novel approach addressed the heterogeneity of the methylome between subgroups in medulloblastoma and also compensated for the modest numbers in the cohort by interrogating for tumour-specific DNA methylation changes. Through this analysis, 2170 probes residing in CpG islands or promoter regions were identified to show tumour-specific DNA methylation states that emerged at relapse on multiple occasions. These findings demonstrated that changes in DNA methylation between diagnosis and relapse were present and, given that the changes were observed on more than one occasion, suggested a potential biological role in tumour development and progression.

5.5.2 T-box gene family and Homeobox gene family methylation patterns positively correlate with expression and suggest a novel epigenetic mechanism for gene regulation

Further analysis revealed that DNA methylation of 23/2170 (1%) CpG probes, which corresponded to 15 genes in total, showed a significant correlation with gene

expression and, on several occasions, DNA methylation of multiple CpG sites within the same gene demonstrated a positive relationship with gene expression (*e.g.TBX3,* Figure 5.24). This relationship does not correspond with the typical epigenetic model proposed of promoter DNA hypermethylation and gene silencing for the regulation of gene transcription (Costello and Plass, 2001; Sidransky, 2002; Baylin and Jones, 2011; Dedeurwaerder *et al.*, 2011).

However, the repeated discovery of positive correlations between DNA methylation and gene expression levels within the same gene, and within two particular gene families (T-box and Homeobox), further supported that these were significant findings that may be of biologically relevance. These two gene families are discussed below with particular emphasis on; *TBX3* (section 5.5.2.1 and 5.5.2.2), in view of the frequent association of gene expression and DNA methylation at multiple CpG sites within the gene; *EOMES* (section 5.5.2.3), which has previously been reported in medulloblastoma; and the Homeobox gene family in general which has been reported to have complex epigenetic mechanisms which regulate gene expression and may also play a role in medulloblastoma tumour development (section 5.5.2.4 and 5.5.2.5).

5.5.2.1 TBX3 expression has important roles in other cancers

TBX3 belongs to the T-box family of transcription factors and is closely related to *TBX2*, which shares the same ancestral gene. *TBX3* is important in embryological development and has been implicated in cell cycle regulation in cancer development. Mutations in *TBX3* lead to the rare condition known as ulnar mammary syndrome whereby there is abnormal development of the limbs, heart and genitalia, as well as mammary gland hypoplasia. There are also multiple reports of its overexpression in a variety of cancer types including head and neck carcinomas, melanoma, breast, bladder, liver, pancreatic and ovarian tumours (Rodriguez *et al.*, 2008; Cavard *et al.*, 2009; Peres *et al.*, 2010; Burgucu *et al.*, 2012; Douglas and Papaioannou, 2013; Peres and Prince, 2013; Peters *et al.*, 2013).

TBX3 has been shown to interact with a variety of pathways implicated in tumour development and its function as a transcriptional repressor is increasingly found to play a major role in disrupting key pathways in tumourigenesis. For example, *in vivo* and *in vitro* work in melanoma has demonstrated that *TBX3* can repress the adhesion

molecule E-cadherin by directly binding near the TSS, potentially enhancing the invasive capabilities of the tumour (Hoogaars *et al.*, 2008; Rodriguez *et al.*, 2008). Similarly, it also directly represses *CDKN1A*$^{p21/CIP1/WAF1}$, a downstream target of p53, (Figure 1.6) and *PTEN in vitro*, another tumour suppressor gene frequently downregulated in cancer (Hoogaars *et al.*, 2008; Lu *et al.*, 2010; Burgucu *et al.*, 2012).

Recent work in transgenic mice has also shown that *TBX3* directly binds to, and represses *NFκBIB* an inhibitor of NF-κB. Dysregulation of the NF-κB pathway leads to elevated levels of NF-κB, promotes cell proliferation and mammary hyperplasia and plays a role in breast cancer development (Liu *et al.*, 2011). In addition, *TBX3* is a downstream target of β-catenin in liver cancer (heptocellular carcinoma and hepatoblastoma), and activating mutations of the *CTNNB1* gene which encodes for β-catenin protein is associated with overexpression of *TBX3* (Hoogaars *et al.*, 2008; Rodriguez *et al.*, 2008; Yarosh *et al.*, 2008; Lu *et al.*, 2010; Liu *et al.*, 2011; Burgucu *et al.*, 2012; Douglas and Papaioannou, 2013).

One of the most reported functions of *TBX3* is its repression and downregulation of *p14*^{ARF} (*p19*^{ARF} in mice) which was also predicted in this study following IPA analysis (section 5.4.2.2). The mechanisms of interaction between *p14*^{ARF} and *TBX3* are diverse and complex. Some studies have shown *in vitro* that *TBX3* interacts with HDACs to regulate the expression of *p14*^{ARF} (Yarosh et al., 2008), whereas others demonstrate that expression of *TBX3* can regulate the p53 pathway to suppress apoptosis or bypass cell senescence via repression of *p14*^{ARF} through a variant T-box binding element located near the TSS of *p14*^{ARF} (Brummelkamp *et al.*, 2002; Lingbeek *et al.*, 2002; Rowley *et al.*, 2004; Lu *et al.*, 2010; Liu *et al.*, 2011; Douglas and Papaioannou, 2013).

In contrast, knockdown of *TBX3* in melanoma cell lines has been shown to increase rather than decrease cell proliferation. However, in these experiments *TBX3* did contribute to tumour formation and migration both in melanoma cell lines and upon orthotopic implantation *in vivo* (Peres *et al.*, 2010; Peres and Prince, 2013). This in turn led to a more aggressive phenotype, most likely through the inhibition of E-cadherin described above (Hoek *et al.*, 2004; Hoogaars *et al.*, 2008; Rodriguez *et al.*, 2008). More recently, *TBX3* expression has been proposed as marker for cancer stem cells that could have potential in diagnosing or predicting tumour progression (Amini *et al.*,

2014). A summary of the key pathways that interact with *TBX3* and are believed to play a role in tumour formation are shown in Figure 5.40.

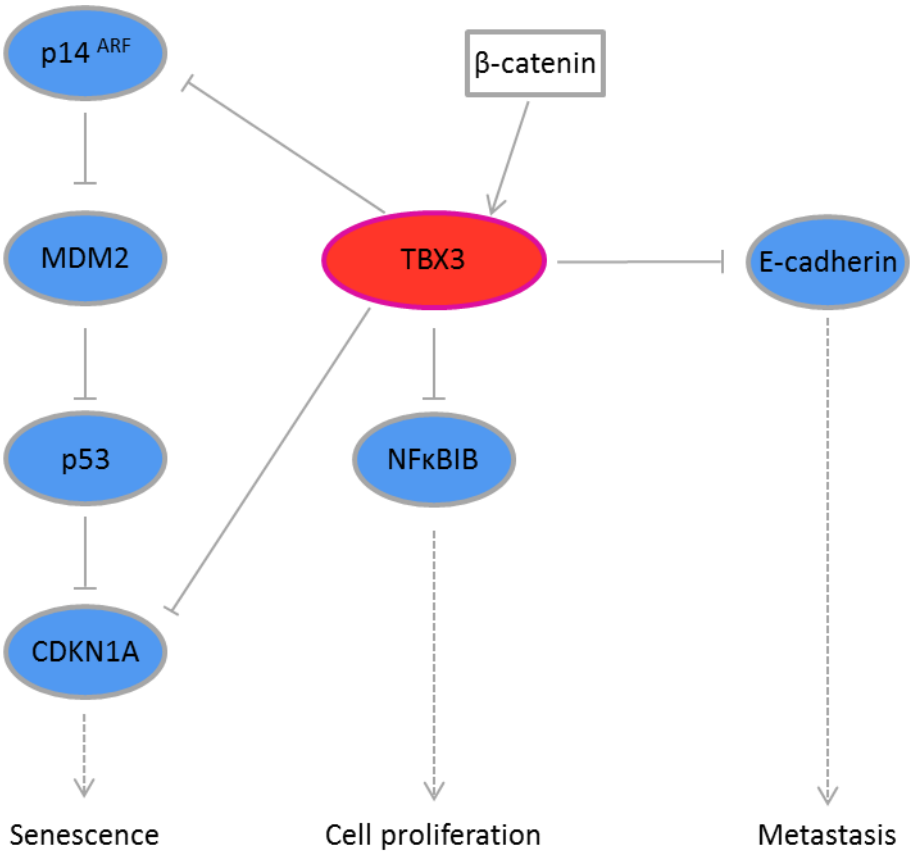

Figure 5.40 Summary of the proposed mechanisms for the role of *TBX3* in tumourigenesis. *TBX3* represses *CDKN1A* and *p14*^{ARF} leading to the bypassing of cellular senescence, increases cellular proliferation by the inhibition of *NFκBIB*, and promotes metastases by repressing E-cadherin. It is also a downstream target of β-catenin, of the WNT signaling pathway. Figure adapted from Lu *et al*., (2010).

5.5.2.2 TBX3 hypermethylation conveys a poor prognosis and is associated with disease progression in glioblastoma and bladder cancer

Genome-wide integrative analyses of both gene expression profiles and DNA methylation in GBM on 40 patients have reported tumour-specific DNA methylation changes which are inversely correlated with gene expression, such as the hypermethylation of *CDKN2A* leading to gene silencing (Etcheverry *et al.*, 2010). In total, the study undertaken by Etcheverry *et al*., (2010) reported 421 CpG sites

corresponding to 321 genes which displayed an inverse correlation with expression (*r* value < -0.5). While they utilised the Infinium HumanMethylation 27 beadchip array (Illumina Inc. San Diego, CA, USA) a predecessor to the Infinium methylation 450K array, CpG probes corresponding to the promoter region of the *TBX3* gene were interrogated and no inverse relationship was reported.

Importantly however, in the same study, a multivariate survival analysis, performed on 50 patients, demonstrated that hypermethylation in the promoter region of *TBX3* identified patients who did not respond to treatment and had an extremely poor survival. In summary, while this analysis was limited, it reports that DNA methylation of *TBX3* may also play a role in tumour progression and response. Moreover, similar to the present study, Etcheverry *et al*., (2010) does not find an inverse correlation between methylation and expression of the *TBX3* gene. While they do not support a positive correlation between gene expression and DNA methylation it is clear they interrogated their datasets for inverse relationships alone. Finally, in a study of bladder cancer, hypermethylation of the *TBX3* CpG island was associated with disease progression in multivariate analysis. Direct comparison with gene expression was not performed as part of this study, but again these findings highlight the potential role of *TBX3* methylation in tumour progression (Kandimalla *et al.*, 2012).

5.5.2.3 Epigenetic gene silencing of the T-box transcription factor, EOMES in medulloblastoma

Methylation of *EOMES,* another T-box transcription factor also known as *TBR*-2, has been demonstrated in other cancers. In medulloblastoma, hypermethylation of *EOMES* has been shown to have an inverse correlation with gene expression with subgroup-specific differential expression observed in MB_{Group4}, (Jones *et al.*, 2012), supporting the findings in this study and suggesting a potential role in MB_{Group4} tumourigenesis (Figure 5.31 and Figure 5.32). *EOMES* is implicated in the process of differentiation and maturation of natural killer (NK) cells and, alongside *TBX21* (T-bet), is a key transcription factor required for the expression of the IL-15Rβ-chain by NK cells. One role of NK cells is to prevent tumour development. *EOMES* is potentially important in dictating the normal NK cell response to tumours and down regulation of *EOMES* has been shown to lead to loss of the NK anti-tumour effect. While the nature of this relationship is not fully understood, the discovery of hypermethylation of *EOMES* in

MB_{Group4} at relapse suggests a mechanism for silencing a gene that normally has a protective role against tumour development (Atreya *et al.*, 2007; Ivascu *et al.*, 2007; Reinert *et al.*, 2011; Gordon *et al.*, 2012; Jones *et al.*, 2012; Malaise *et al.*, 2014).

5.5.2.4 The diverse relationship between DNA methylation and gene expression in the Homeobox gene family

The example of *TBX3* discovered in this study, coupled with the multiple recurrent hits of other genes demonstrating a positive correlation between DNA methylation and gene expression (Table 5.6, section 9.3: Appendix III and section 9.4: Appendix IV) suggests that the current mechanisms for the epigenetic regulation of gene expression are not fully understood. Homeobox genes, similar to the T-box gene family, are important in normal development and are a family of transcription factors involved in many cellular processes such as growth, proliferation, and differentiation (Shah and Sukumar, 2010; Bhatlekar *et al.*, 2014). Again they can act as transcriptional activators and repressors in cancer and *HOXB13,* (identified in this study, Table 5.6), in adult solid malignancies, is one of the most commonly disrupted genes from this family (Shah and Sukumar, 2010; Bhatlekar *et al.*, 2014). Their behaviour in tumour development is again varied and reported to be tissue and cancer specific. They can act as tumour suppressors as well as drivers of aggressive disease (Shah and Sukumar, 2010; Bhatlekar *et al.*, 2014).

Interestingly, the regulation of Homeobox gene expression, via epigenetic mechanism such as the methylation of miRNAs (section 1.4.6.1.4) to regulate Homeobox gene expression, has been proposed. DNA promoter hypermethylation leading to gene silencing has also been noted (Shah and Sukumar, 2010). Conversely, in other studies, Homeobox gene family expression in some instances was shown to be depressed upon DNA demethylation. Moreover, *HOXB* and *HOXC* gene clusters, three genes of which were highlighted in the present study, (*HOXB13*, *HOXC10* and *HOXC5*, Table 5.6), have been reported to display DNA hypermethylation in certain regions which was associated with moderate or strong gene expression in specific tissue types (Flagiello *et al.*, 1996; Tsumagari *et al.*, 2013). Proposed explanations for these findings included the necessity for more than one epigenetic mechanism to silence gene expression, such as repressive histone modifications and DNA methylation, or that DNA methylation is present to control the differential splicing observed in this family of

genes (Tsumagari *et al.*, 2013). These discoveries suggest that DNA methylation plays a diverse role in controlling the expression of Homeobox genes in specific cell types, and further supports the relationships observed in the present study.

5.5.2.5 The role of the Homeobox gene family in medulloblastoma

While the role of the Homeobox gene family in medulloblastoma has not yet been fully elucidated, early reports have described strong protein expression, detected immunohistochemically, of *HOXB3* and *HOXB4* in medulloblastoma suggestive of a role in tumour development (Bodey *et al.*, 2000). Amplification of *OTX2*, another member of the Homeobox gene family has been recently reported in medulloblastoma at diagnosis (Parsons *et al.*, 2011; Northcott *et al.*, 2012a; Robinson *et al.*, 2012). Moreover, Homeobox gene expression can be regulated by the MLL family of histone modifiers. Mutations within the MLL gene family have been reported in medulloblastoma at diagnosis (discussed in section 1.8.8), suggestive of common pathways inclusive of the MLL and Homeobox gene families that could be involved in tumour development (Parsons *et al.*, 2011; Jones *et al.*, 2012; Northcott *et al.*, 2012a; Pugh *et al.*, 2012; Robinson *et al.*, 2012). Together these findings alongside the reports of epigenetic regulation of the Homeobox genes in other cancer types (section 5.5.2.4) support the discoveries in the present study and the role of the Homeobox gene family in MB_{Group4} at relapse.

5.6 Summary

MB_{Group4} is the largest and yet poorest understood of the molecular subgroups in medulloblastoma. As such, it represents a large proportion of recurrent tumours, and all patients who relapsed with MB_{Group4} in the paired relapse cohort (Chapter 3) died of their disease. Novel routes of investigation are required to understand the mechanisms of tumourigenesis and disease recurrence in this subgroup and to identify new treatment strategies and targets. This study reports DNA methylation events that emerge at relapse and show significant relationships with gene expression. Importantly, two gene families (T-box and Homeobox gene families) consistently showed DNA methylation events at relapse which, in an independent cohort, correlated with gene expression.

Both the T-box gene family and the Homeobox gene family are important in development and their dysregulation has been demonstrated in several cancers. The role of these two gene families has not been detailed in medulloblastoma, with the exception of the potential epigenetic regulation of the T-box gene *EOMES*, which is differentially expressed in MB_{Group4}. This observation is consistent with the findings in this study (section 5.4.2.4) and the traditional epigenetic paradigm of DNA promoter hypermethylation leading to gene silencing. However, the majority of reported correlations in the present study were contrary to the paradigm, with DNA hypermethylation corresponding to an increase in gene expression. The epigenetic control of gene expression is increasingly studied and many observations have noted a relationship between hypermethylation and increased gene expression. In medulloblastoma, this has been observed for *TERT*, and the expression of Homeobox genes in other cell types has been reported to display diverse and complex relationships with DNA methylation and other epigenetic mechanisms (section 5.5.2.4).

Further work is now required to validate and expand on these findings in the T-box and Homeobox gene families alongside all the other MB_{Group4} candidates identified in this analysis (Table 5.6, section 9.3: Appendix III and section 9.4: Appendix IV). A separate paired relapse cohort with frozen tissue samples taken at diagnosis and recurrence would enable the interrogation of DNA methylation events between these two time-points and their direct assessment with gene expression. Cohort expansion in this way

would potentially allow for similar analyses to be undertaken on the other three subgroups which were not interrogated in this aspect of the study. Cross validation in all subgroups of any significant findings would also be important to elicit whether observations were subgroup specific, relapse specific, or both. This cross validation is important as while interrogating medulloblastoma in the context of subgroup is essential, common aberrations in all molecular subgroups, such as p53-MYC defects described in Chapter 3, may be observed across all the subgroups in the disease at relapse.

Moreover, *in vitro* and *in vivo* work is required to discern the epigenetic mechanisms of gene regulation. Experiments such as the treatment of medulloblastoma cell lines with 5-azacitidine to decrease DNA methylation and assess the effect (upregulation or downregulation) on gene expression should be undertaken, alongside functional work to explore the role of candidate genes in cellular processes such as apoptosis, senescence, proliferation and migration. In addition, developing suitable medulloblastoma mouse models to evaluate the downstream effects of these candidate genes on tumour penetrance, maintenance and aggression, similar in nature to the work described in Chapter 4, could also be undertaken.

Chapter 6. Patterns and timings of medulloblastoma relapse are associated with radiotherapy and molecular subgroup

6.1 Introduction

Biopsies of medulloblastoma recurrences are rarely performed in current clinical practice and as a consequence, investigating the biology of disease at relapse is a challenge. At present, only two studies (section 1.9.2), alongside this study, have collated and interrogated a cohort of tumours sampled at disease recurrence (Korshunov *et al.*, 2008; Ramaswamy *et al.*, 2013). Understanding the biology of medulloblastoma at relapse is essential to identify novel treatment strategies. This was highlighted by the findings of combined p53-MYC defects (Chapter 3) as a biomarker of aggressive disease behaviour post-recurrence, alongside the pre-clinical results reported in Chapter 4 of the successful targeting of this interaction with the Aurora A kinase inhibitor MLN8237. However, until biopsies are routinely performed in the clinical setting and larger cohorts are compiled of tumours sampled at disease relapse, additional informative approaches are required to supplement and expand on the initial findings by this study and others (Korshunov *et al.*, 2008; Ramaswamy *et al.*, 2013).

Medulloblastoma is a heterogeneous disease comprising of four molecular subgroups with varying clinicopathological, demographic and molecular features, and current hypotheses suggest that these four subgroups develop from four distinct tumour cells of origin (Gibson *et al.*, 2010; Grammel *et al.*, 2012; Taylor *et al.*, 2012). This study, alongside Ramaswamy *et al*., (2013), supports this theory by demonstrating that molecular subgroup does not alter over time between diagnosis and relapse. Moreover, these findings provide an opportunity to study medulloblastoma at diagnosis, in a subgroup-specific way and interrogate the disease features of those patients who subsequently relapse with their disease.

This chapter describes the identification, assembly, clinicopathological and molecular characterisation of a cohort comprised of medulloblastoma tumours, sampled at diagnosis, from a population of patients who are known to subsequently suffer from disease recurrence. Detailed clinical and pathological features, including patterns of disease relapse, are compiled alongside the investigation of molecular features understood to play a role in relapse disease. These include molecular subgroup, *MYC* gene family amplification and *TP53* mutation. This large relapsing cohort provides a valuable opportunity to evaluate the patterns of recurrence in a subgroup-specific way

and identify features which may be enriched at diagnosis, and predictive of relapse. In addition, this cohort provides the foundation for future studies to validate the utility of potential biomarkers identified in this study, such as promoter hypermethylation of the T-box gene, *EOMES*, in MB_{Group4}, which is both maintained between diagnosis and relapse, and acquired at disease relapse (section 5.4.2.4). Moreover, it will enable the unbiased assessment of molecular features from profiling data, (genomic and DNA methylation events), and the relationship of these features with the patterns and timings of relapse disease.

6.2 Aims

The aims of this chapter are to;

- Compile an extensive database for the cohort of medulloblastoma samples taken at diagnosis and assembled in Newcastle for investigation (Newcastle Medulloblastoma Cohort, NMB cohort). Centrally review, and encode all clinical data affiliated with each tumour sample.

- Coordinate and align all centrally reviewed pathology data and molecular data related to each tumour sample within the NMB cohort.

- Identify from the NMB cohort, all patients who have relapsed and have tumour material taken at diagnosis available (relapsing cohort).

- Characterise this relapsing cohort with respect to patterns and timings of disease recurrence, clinical demographics, pathological variant and molecular features.

- Utilise this cohort to analyse the patterns of disease relapse and perform an exploratory survival analysis to identify features at diagnosis that are associated with time to relapse, time to death and overall survival.

- Provide the foundation for further multivariate survival analyses and future work to identify and validate potential relapse-specific biomarkers.

6.3 Materials and methods

6.3.1 Assembly of a cohort of medulloblastoma samples taken at diagnosis

Tumour tissue was collected from UK CCLG institutions and collaborating centres as part of the wider remit of work undertaken by the PBTG. To date, 718 tumours sampled at diagnosis have been collected and entered into the NMB database for further annotation, characterisation and review. All investigations carried out on human tissue in this study were part of a CCLG-approved biological study (BS-2007-04) with ethics approval from the Newcastle/North Tyneside Research Ethics Committee (reference 07/Q0905/71). All biological material was recorded and logged in accordance with the Human Tissue Act, 2004.

6.3.2 Collation and review of cohort clinical data

Detailed clinical data was collated by Prof Simon Bailey (PBTG) from all treatment centres, centrally reviewed and coded to create a database of NMB tumour samples with annotated clinical data (n=718). The clinical features and categories of information obtained are illustrated in Table 6.1. Strict inclusion criteria were applied to tumour samples and their corresponding clinical data and cases which did not meet the minimum essential criteria (Table 6.1) were excluded from detailed survival analyses. A total of 597/718 (83%) diagnostic tumour samples were suitable for future survival and correlative analyses (sections 2.8 and 2.9).

	Clinical feature	Category
Details at disease diagnosis		
Patient demographics	**Gender**	Male/female
	Age at diagnosis	Years
	Diagnosis	Medulloblastoma/ATRT/CNS-PNET/other
Staging	Site of tumour	
	Metastatic stage	M0/M1/M2/M3/M4/M0/1
	Extent of tumour resection	GTR/STR/biopsy
Treatment	Radiotherapy	Yes/no
	Radiotherapy type	Focal/CSI
	CSI dose	Low (24-27Gy)/high (35-39Gy)/hyperfractionated/other (40-54Gy)
	Chemotherapy	Yes/no
	Chemotherapy regimen	
Survival	**Status**	Alive/dead
	Overall survival	ADF/AWD/DOD/DOOC
	Disease specific PFS	Yes/no
	Second malignancy	Yes, no
	PFS	Years
	Follow up	Years
Other	Family history cancer predisposition	Gorlin syndrome/LFS
Details at disease recurrence		
Patient demographics	**Age at relapse**	Years
	Progression vs relapse	Progression/relapse
Treatment	Treatment at recurrence	
	Curative intent	Yes/no
	Surgery	Yes/no
	Extent of surgery	GTR, STR, biopsy
	Radiotherapy	Yes/no
	Chemotherapy	Yes/no
Overall survival	**Time to 1st recurrence**	Years
	Time to 2nd recurrence	Years
	Time to 3rd recurrence	Years
	Time from relapse to death	Years
Patterns of relapse	Site of relapse	Local/distant/both
	Character of relapse	Nodular/diffuse/both
	Metastatic stage	M0/M1/M2/M3/M4/M0/1

Table 6.1 Overview of the clinical and demographic patient information obtained for tumour samples in the NMB cohort. Essential criteria for inclusion into studies at diagnosis and relapse are highlighted in bold. ATRT, Atypical teratoid/rhabdoid tumours; CNS-PNET, CNS primitive neuroectodermal tumours; GTR, gross total resection; STR, subtotal resection; CSI, craniospinal irradiation; Gy, Gray; ADF, alive disease free; AWD, alive with disease; DOD, died of disease; DOOC, died of other complications; PFS, progression free survival; LFS, Li-Fraumeni syndrome; empty category line, free text entered.

6.3.3 Central pathology review

All tumour samples within the NMB cohort with FFPE tissue available were centrally reviewed by a panel of four neuropathologists (Prof David Ellison, St Jude Children's Research Hospital, Memphis, TN, Dr Thomas Jacques, Prof Stephen Wharton and Dr Keith Robson from the UK CCLG), as described in section 2.2. Coordination of this review was undertaken by Ms Sarah Leigh-Nicholson (former member of the PBTG), myself and more recently Dr Stephen Crosier (PBTG). Tumour samples were excluded if, on review, the diagnosis of a medulloblastoma was in question or changed, for example to an ATRT. Pathological variant was categorised according to the current WHO guidelines as CLA, DN, MBEN, LCA or MB_{NOS} and entered alongside the clinical data for each tumour sample (Louis *et al.*, 2007). Separate entries for reticulin, p53 and β-catenin immunohistochemical results were completed to support individual projects within the PBTG. In total 527/597 (88%) underwent central pathology review.

6.3.4 Molecular data

The NMB cohort has been extensively characterised according to the current understanding of the key molecular features in the disease which are outlined in section 1.8.8. Molecular data was available on large subsets of the cohort including; molecular subgroup (GoldenGate Methylation array and Infinium methylation 450K array, Illumina Inc., CA, USA), copy number variation (SNP6, Affymetrix Inc., CA, USA; Infinium methylation 450K array and Illumina omniexpress array, Illumina Inc., CA, USA), RNA seq (HiSeq2000, Illumina Inc., CA, USA), *TP53* mutation status (section 2.3.1), *CTNNB1* mutation status (section 2.3.2), *MYC* and *MYCN* amplification status as determined by FISH (section 2.6) or MLPA (section 2.7) and more recently *TERT* methylation and mutation status (section 1.4.7). Data points to represent the molecular analyses undertaken, and data results for *MYC* gene family amplification, *TERT* status, *CTNNB1* and *TP53* mutations were compiled alongside clinical and pathological data to create an Excel spreadsheet (Microsoft Office 2010, Microsoft Corporation, WA, USA), containing all pertinent data in relation to each tumour sample.

6.3.5 Assembly of the relapsing cohort

Clinical data was extensively reviewed and all patients documented to have relapsed with a medulloblastoma and have biological material available from their tumour sampled at diagnosis (DNA, FFPE block, paraffin curl or frozen tissue), were identified and included in the relapsing cohort. Relapse was differentiated from progression, and defined as having no evidence of disease at one time-point (disease remission) either during initial treatment or after completion of initial therapy prior to the disease returning. Progression was defined as patients who displayed evidence of medulloblastoma (local or metastatic) throughout their disease course.

In total 204/718 (28%) cases were identified in the NMB cohort, which had tissue available from their tumour sampled at diagnosis, alongside confirmatory clinical evidence of relapsed disease. This number was inclusive of the twenty-six samples taken at diagnosis that were analysed in the paired relapse cohort (Chapter 3). To supplement the relapsing NMB cohort, a well annotated trials based medulloblastoma cohort from the SIOP-UK Children's Cancer Study Group PNET3 study was utilised (Schwalbe *et al.*, 2013b). Relapsed cases were identified from this cohort as defined above, and cases with available tumour material, (n=31, DNA, FFPE block or paraffin curl), were included in the relapsing cohort to make a total of 235 cases available for further investigation and analyses.

6.3.6 Molecular characterisation of the relapsing cohort

Many of the molecular features associated with medulloblastoma (section 1.8.8) had already been interrogated for a selected number of cases in the relapsing cohort as part of the wider remit of work within the PBTG. Cases with missing data were identified and investigated for molecular subgroup, *TP53* mutations and *MYC* gene family amplification.

6.3.6.1 Molecular subgrouping of the relapsing cohort on the Infinium methylation 450K array

Molecular subgroup was assigned as previously described in section 2.11. Where DNA was of sufficient quantity and quality, as determined by the Qubit fluorometer (section 2.1.2.2), samples were analysed on the Infinium methylation 450K array at the Wellcome Trust Clinical Research Facility, University of Edinburgh, UK, as discussed in

section 3.3.2.1. More recently samples were analysed on the Infinium methylation 450K array by Aros (Department of Clinical Biochemistry, Aarhus, Denmark) according to the manufacturer's protocols which are described in section 5.3.6 (Illumina Inc. San Diego, CA, USA). Revised sample requirements for the analysis by Aros were a total tumour DNA amount of 1µg extracted using standard techniques, (section 2.1.1), from either FFPE or frozen material at a concentration of ≥23ng/µl. Samples that did not meet these revised criteria were analysed using a novel DNA minimal methylation signature assay developed in the PBTG (section 6.3.6.2).

6.3.6.2 Assigning molecular subgroup in the relapsing cohort using a minimal methylation signature

This novel technique employs the use of a minimal methylation signature to determine the molecular subgroup of the medulloblastoma tumour and was developed by Dr Ed Schwalbe of the PBTG (unpublished data). The experimental procedures were performed by Dr Debbie Hicks (PBTG). In brief, a panel of CpG loci were identified through ranking the most informative subgrouping probes on the Infinium methylation 450K array and sequentially removing each of the top ranking probes to enable the assessment of their contribution to the subgrouping confidence call. In total, a panel of 19 CpG residues were identified to be the most robust loci whose methylation signature confidently determined molecular subgroup.

6.3.6.3 TP53 mutation analysis

TP53 mutation analysis using PCR based direct sequence analysis of exons 5-8 was undertaken as previously described in section 2.3.1. Exons 5-8 were interrogated as a result of the findings by this study (Chapter 3) and others whereby these exons were the most frequently observed region within the DNA binding zone of the *TP53* gene, to harbour a mutation in medulloblastoma (Zhukova *et al.*, 2013). Sanger sequencing was outsourced to Eurofins Genomics (Ebersberg, Germany) and sequence analysis was performed on SeqMan 5.05, MegAlign 5.05 (©1993-2002 DNASTAR) and Mutation Surveyor (Dna Variant Analysis, SoftGenetics, PA, USA).

6.3.6.4 MYC gene family amplification

Analyses of the *MYC* gene family in the relapsing cohort for evidence of amplification were undertaken firstly by MLPA as described in section 2.7. Fragment analysis was

outsourced to DBS GENOMICS (Durham University, Durham, UK). Any sample demonstrating evidence of copy number aberration by MLPA of either *MYC* or *MYCN*, as defined in section 2.7.4, proceeded to be analysed by FISH (section 2.6).

6.3.7 Data analysis

Comparative, correlative and univariate survival analyses were undertaken as previously described in section 2.8-2.10 and performed in GraphPad Prism version 6.05 (GraphPad Software, Inc., San Diego, CA, USA) and R (R Development Core Team, 2014) respectively.

6.4 Results

6.4.1 Relapsing cohort demographics and outcomes

Overall, 235 medulloblastoma tumours sampled at diagnosis, with clinical data confirming disease recurrence, were assembled to form the relapsing cohort. There was a significant male preponderance within the cohort (male: female ratio 2.18: 1 versus 1.6:1, p=0.0499, Fisher's exact test, Table 6.2) suggesting that males were more likely to relapse then females. The median age at diagnosis was 6.8 years (range 0.01-33.7 year). The median age at recurrence was 8.9 years (range 1.3-36.3 years) with a median time to recurrence of 1.5 years (range 0.1-8.9 years). Overall 16/235 (7%) patients were alive and disease free at the point of clinical data collection, 17/235 patients (7%) were alive with evidence of disease, 195/235 patients (83%) died of their disease with the remaining 7/235 patients (3%) dying of other causes. The factors influencing long term survival within the relapsing cohort are discussed further in section 6.4.9.

6.4.2 Established high-risk clinicopathological features are enriched

In Chapter 3 (section 3.4.1), a comparative analysis was performed between the paired relapse cohort and independent published studies of medulloblastoma tumours sampled at diagnosis. This revealed that high-risk clinical features, such as metastatic disease, were enriched at diagnosis in the paired relapse cohort, whereas high-risk molecular features such as *MYC* gene family amplification and *TP53* mutation were not significantly more frequent at diagnosis in the paired relapse cohort (section 3.4.1.2). Similar comparisons were performed between the larger relapsing cohort (n=235) and the same independent, published historic studies of medulloblastomas sampled at diagnosis (McManamy *et al.*, 2007; Pfaff *et al.*, 2010; Kool *et al.*, 2012; Lannering *et al.*, 2012; Ryan *et al.*, 2012). The results of these comparisons are reported in Table 6.2, and demonstrate that all current established clinical and pathological high-risk features (Pizer *et al.*, 2011b), are enriched at diagnosis in the relapsing cohort. These features were; infant age group (p=0.0003, Fisher's exact test), metastatic disease (p<0.001, Fisher's exact test), subtotal resection (p<0.001, Fisher's exact test) and LCA histology (p=0.0493, Fisher's exact test).

Examining the molecular features characterised thus far in the relapsing cohort, revealed a significantly lower incidence of MB_{WNT} in the relapsing cohort when compared to the independent historic studies, (5/206 (2%) versus 60/550 (11%), p<0.0001, Fisher's exact test, Table 6.2). This low relapse rate is unsurprising given the overall good EFS and OS associated with MB_{WNT} (Clifford *et al.*, 2006; Kool *et al.*, 2012; Northcott *et al.*, 2012a; Taylor *et al.*, 2012; Shih *et al.*, 2014). Interestingly, and in contrast to the findings reported in the paired relapse cohort, (section 3.4.1.2 and Table 3.4), there was not an enrichment of MB_{SHH} (60/206 (29%) versus 153/550 (28%), p=0.7174, Fisher's exact test, Table 6.2) or paucity of MB_{Group3} (57/206 (28%) versus 149/550 (27%), p=0.9269, Fisher's exact test, Table 6.2) observed in the relapsing cohort. This suggests that current clinical practice does not sample medulloblastoma tumours at relapse in a subgroup reflective way. This observation is explored and discussed further in section 6.4.3.

There was a moderate enrichment of *MYC* gene family amplification in the relapsing cohort (p=0.0313, Fisher's exact test, Table 6.2) which was not significant when *MYC* and *MYCN* were compared in isolation. This supports the role of *MYC* gene family amplification as a biomarker of high-risk disease at diagnosis and its use for treatment stratification in upcoming clinical trials (Pizer and Clifford, 2009). *TP53* mutations in exons 5-8, which encode the DNA binding domain of the gene, were not enriched at diagnosis in the relapsing cohort. A schematic illustration demonstrating the nature and subgroup distribution of the *TP53* mutations is shown in Figure 6.1. As expected there was a preponderance for mutations in MB_{SHH} and MB_{WNT} (15/19, 79% and 2/19, 11% respectively, section 1.8.8) and on correlative analysis (reported in Figure 6.2) *TP53* mutations and MB_{SHH} were significantly associated (p<0.0001, Fisher's exact test, Bonferroni corrected). No mutations were found in MB_{Group3} and only an isolated example was observed in MB_{Group4} (Figure 6.1).

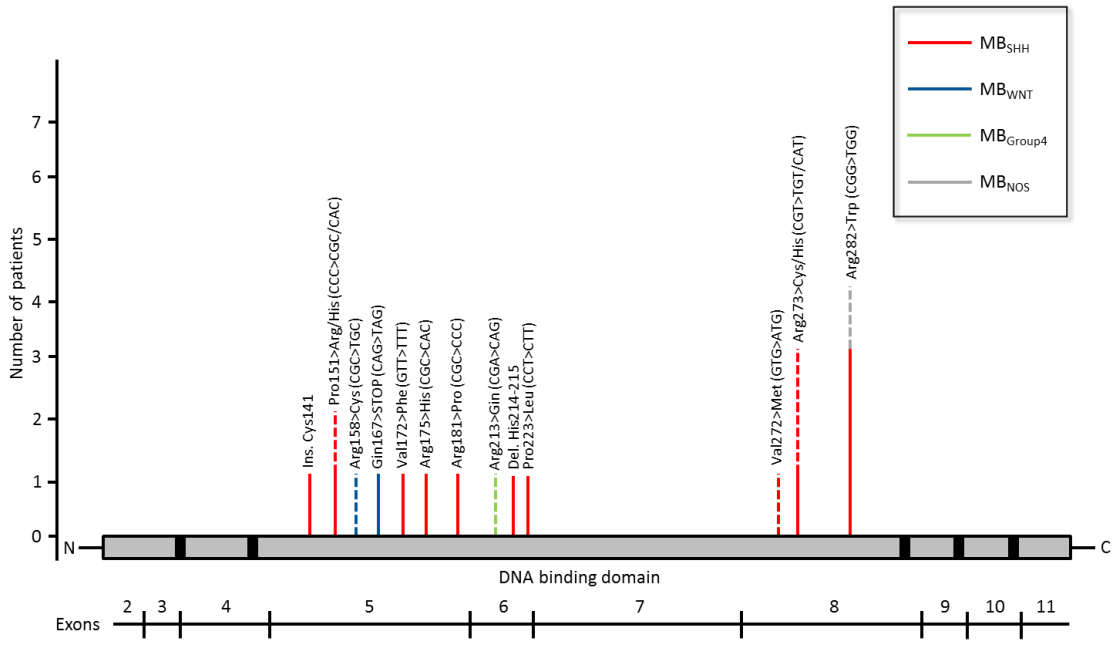

Figure 6.1 Schematic demonstrating the nature and subgroup distribution of *TP53* mutations in the relapsing cohort. Solid line, homozygous mutation; dashed line, heterozygous mutation; Ins, insertion; Cys, Cysteine; Pro, Proline; Arg, Arginine; Gin, glutamine; Val, Valine; Phe, Phenylalanine; His, Histidine; Del, deletion; Leu, Leucine; Met, Methionine; Trp, Tryptophan.

Importantly, there was not an enrichment of combined p53-MYC defects in the relapsing cohort (9/230, 4%, versus 8/310, 3%, p=0.4574, Fisher's exact test, Table 6.2) and all p53-MYC combined defects were observed in MB_{SHH}, consistent with reports by others (Zhukova *et al.*, 2013). This observation supports the significant findings reported in Chapter 3 where combined p53-MYC defects frequently emerged at medulloblastoma relapse and were observed in all four molecular subgroups (Table 3.11).

Clinicopathological and molecular features		Independent published studies	Present study	
		Historic studies [#]	Relapsing cohort	
		Diagnosis	Diagnosis	p value
Gender	Male	585/952 (61%)	161/235 (69%)	**0.0499**
	Female	367/952 (39%)	74/235 (31%)	
	Male:female ratio	1.6:1	2.18:1	
Age	Age range in years	0.3-52	0.01-33.73	
	Infants (<4 years)	167/943 (17%)	67/235 (29%)	**0.0003***
	Children (4-16 years)	599/943 (64%)	160/235 (68%)	
	Adults (>16 years)	177/943 (19%)	8/235 (3%)	
Pathology	CLA	938/1277 (74%)	154/219 (71%)	
	DN	183/1277 (14%)	27/219 (12%)	
	LCA	156/1277 (12%)	38/219 (17%)	**0.0493***
Metastatic stage	M-	608/834 (73%)	93/183 (51%)	**<0.0001**
	M+	226/834 (27%)	90/183 (49%)	
Resection	GTR	267/317 (84%)	154/227 (68%)	**<0.0001**
	STR	50/317 (16%)	73/227 (32%)	
Molecular subgroup	MB_{SHH}	153/550 (28%)	60/206 (29%)	0.7174
	MB_{WNT}	60/550 (11%)	5/206 (2%)	**<0.0001**
	MB_{Group3}	149/550 (27%)	57/206 (28%)	0.9269
	MB_{Group4}	188/550 (34%)	84/206 (41%)	0.1058
Molecular defects	*MYC/MYCN* amplification	50/552 (9%)	29/198 (15%)	**0.0313**
	MYC amplification	17/552 (3%)	9/212 (4%)	0.5034
	MYCN amplification	33/552 (6%)	20/199 (10%)	0.0742
	TP53 mutations	21/310 (7%)	19/215 (9%)	0.4058
Combined molecular defects	*TP53* mutation and *MYC/MYCN* amplification	8/310 (3%)	9/230 (4%)	0.4574
	TP53 mutation and *MYC* amplification	1/310 (<1%)	0/232 (0%)	1
	TP53 mutation and *MYCN* amplification	7/310 (2%)	9/230 (4%)	0.309

Table 6.2 Comparison of clinicopathological and molecular features in the relapsing cohort with historic studies of tumours sampled at diagnosis. [#] Historic studies (McManamy *et al.*, 2007; Pfaff *et al.*, 2010; Kool *et al.*, 2012; Lannering *et al.*, 2012; Ryan *et al.*, 2012). * Cases with the specific feature were compared against all others without that feature. CLA, classic histology; DN, desmoplastic/nodular histology; LCA, large cell/anaplastic histology; M-, M0 disease; M+, M1+ disease; GTR, gross total resection; STR, subtotal resection; bold results, significant p value. p, Fisher's exact test.

6.4.3 MB_{Group3} tumours are not frequently biopsied at relapse

Comparisons between the molecular subgroup distribution of the relapsing cohort (n=206 with subgroup available) and historic studies of medulloblastoma tumours sampled at diagnosis revealed that subgroup distribution of MB_{SHH}, MB_{Group3} and MB_{Group4} was not significantly different (Table 6.2). However, tumours sampled at relapse in the paired relapse cohort (Chapter 3), when compared to the same historic studies (Table 3.4), demonstrated an enrichment at relapse for MB_{SHH} (12/25,48%, versus 153/550, 28%, p=0.0402, Fisher's exact test) and a paucity for MB_{Group3} tumours (2/25, 8%, versus 149/550, 27%, p=0.0355, Fisher's exact test). This raises the question of sampling bias which potentially may be due to a difference in clinical practice influenced by the subgroup-specific disease presentation at relapse. To explore this further, direct comparisons of subgroup distribution were performed between the paired relapse cohort (Chapter 3), the present relapsing cohort and the only other independent cohort of subgrouped medulloblastomas sampled at relapse (Ramaswamy *et al.*, 2013).

These comparisons, reported in Table 6.3, revealed that the subgroup distribution of the paired relapse cohort (Chapter 3) does differ significantly in its number of MB_{Group3} when compared to the number of MB_{Group3} in the present relapsing cohort (57/206, 28%, versus 2/25,8%, p=0.0489, Fisher's exact test). However, on comparing the subgroup distribution of the paired relapse cohort with the tumours sampled at relapse reported by Ramaswamy *et al*., (2013) the number of MB_{Group3} relapse tumours does not differ significantly (p=0.3215, Fisher's exact test). This suggests that while MB_{Group3} tumours do recur frequently, as would be expected given their poor overall prognosis (section 1.8.8.3), they are not routinely sampled at relapse. Clinical practice of tumour sampling at recurrence is most likely influenced by the nature and presentation of the disease at this time-point. The subgroup-specific patterns of disease relapse, alongside an exploratory survival analysis, are discussed in sections 6.4.4.2-6.4.8.3 where the presentation of MB_{Group3} disease at recurrence is explored further.

	Present study				
	Paired relapse cohort	Relapsing cohort		Independent published study *	
Molecular subgroup	Relapse	Diagnosis	p value	Relapse	p value
MB_{SHH}	12/25 (48%)	60/206 (29%)	0.0676	21/51 (41%)	0.6275
MB_{WNT}	2/25 (8%)	5/206 (2%)	0.1684	1/51 (2%)	0.2504
MB_{Group3}	2/25 (8%)	57/206 (28%)	**0.0489**	9/51 (18%)	0.3215
MB_{Group4}	9/25 (36%)	84/206 (41%)	0.8295	20/51 (39%)	1

Table 6.3 Comparison between the subgroup distribution of the paired relapse cohort, relapsing cohort and independent cohort of medulloblastoma tumours sampled at relapse. *Independent published study (Ramaswamy *et al.*, 2013). p, Fisher's exact test.

6.4.4 Assessing the clinicopathological and molecular features at diagnosis and their association with patterns of relapse in medulloblastoma

Medulloblastoma comprises of four molecularly distinct subgroups which are associated with specific clinicopathological and additional molecular features (Thompson *et al.*, 2006; Kool *et al.*, 2008; Cho *et al.*, 2011; Northcott *et al.*, 2011b; Taylor *et al.*, 2012). Consequently, all subsequent analyses were undertaken on the cases within the relapsing cohort which had molecular subgroup successfully assigned (n=206, section 6.3.6.1 and 6.3.6.2). To interrogate the relapsing cohort for associations between patterns of disease relapse and all other features (clinical, pathological and molecular), a correlative analyses (section 2.9) of the 206 relapsing tumours with known molecular subgroup was performed and is summarised in Figure 6.2.

6.4.4.1 Local relapses are associated with nodular disease, whereas distant relapse is associated with diffuse disease

Several expected associations were observed in this analysis, whereas no unexpected associations were observed (Figure 6.2). This provided confidence in the assembly and assessment of the relapsing cohort. Established associations observed included the significant positive correlations between MB_{SHH} and; infant age group (p=0.0247, Fisher's exact test, Bonferroni corrected), *MYCN* amplification (p=0.0134, Fisher's exact

test, Bonferroni corrected), *TP53* mutation (p<0.0001, Fisher's exact test, Bonferroni corrected) and DN histology (p<0.0001, Fisher's exact test, Bonferroni corrected, section 1.8.8.2). Other established associations observed were the relationships between *TP53* mutation and *MYCN* amplification (p<0.0001, Fisher's exact test Bonferroni corrected), MB_{Group4} and CLA histology (p=0.0006, Fisher's exact test Bonferroni corrected) and the absence of MB_{Group4} in the infant age group (p=0.0005, Fisher's exact test, Bonferroni corrected). All of these established associations in medulloblastoma at diagnosis are discussed in section 1.8.8.

Most notably the nature of disease relapse (diffuse or nodular) was significantly associated with disease location *i.e.* local or distant relapse (p<0.0001, Fisher's exact test, Bonferroni corrected). This can be attributed to the typical clinical presentation of medulloblastoma recurrence, whereby nodular disease is more likely to occur locally and diffuse leptomeningeal disease is more widespread and distant (Perreault *et al.*, 2013). Following correction for multiple testing, no other feature demonstrated a significant association with the nature, or location of disease relapse. However, both MB_{SHH} and DN histology were associated with disease location before correction for multiple testing (p=0.0199 and 0.0462 respectively, Fisher's exact test). In view of the demonstrated association between DN histology and MB_{SHH} (p<0.0001, Fisher's exact test, Bonferroni corrected) and the stronger association between MB_{SHH} and location of relapse, the subgroup-specific patterns of relapse were explored further (section 6.4.4.2).

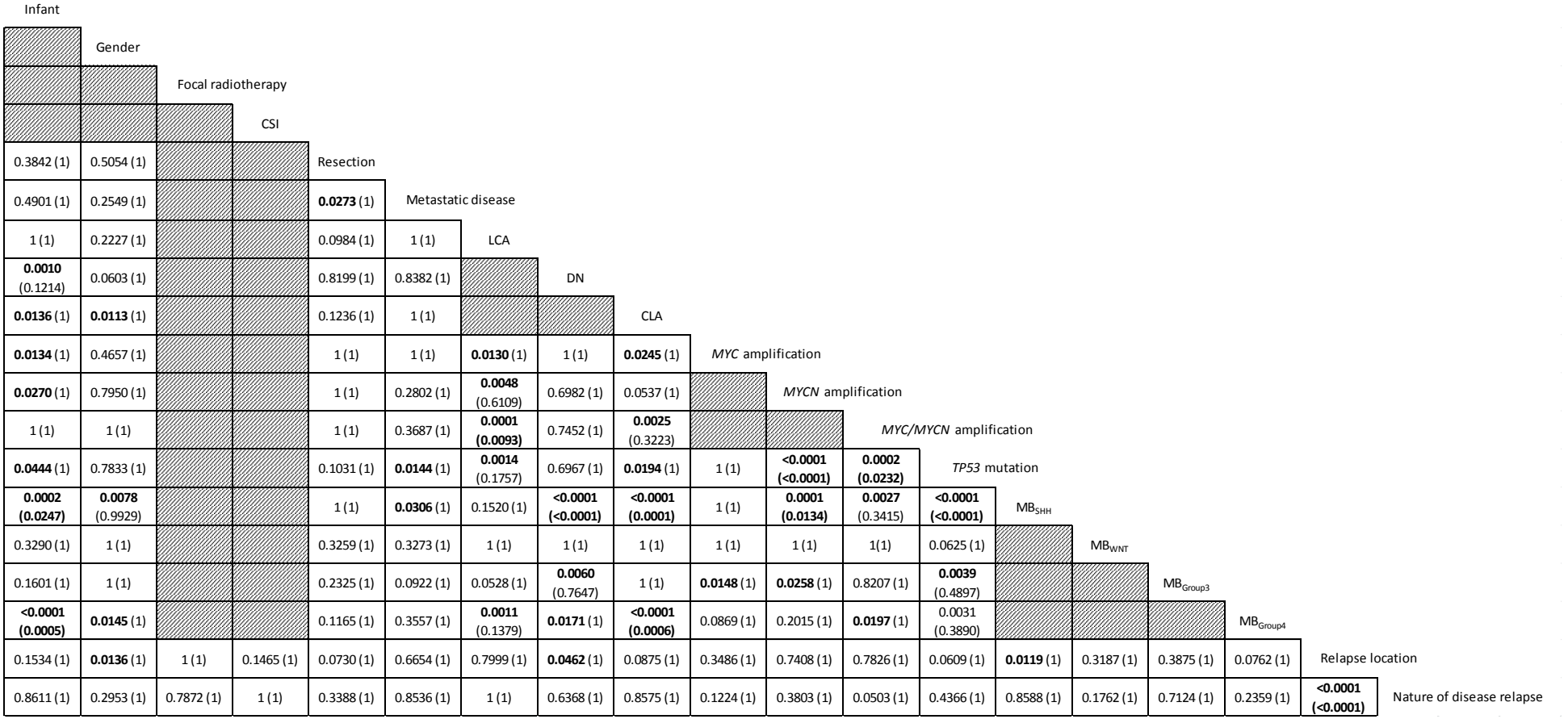

Figure 6.2 Correlative analysis of the association between clinicopathological, molecular features and patterns of relapse in the relapsing cohort. Raw p values (Fisher's exact test) reported in individual boxes, Bonferroni corrected p values in parentheses. CSI, craniospinal irradiation; LCA, large cell/anaplastic histology; DN, Desmoplastic/nodular histology; CLA, classic histology; Relapse location, distant; Nature of disease relapse, diffuse; diagonally hatched boxes, comparison not appropriate/available; bold, significant p value.

6.4.4.2 MB_{Group3} and MB_{Group4} are commonly metastatic at disease relapse

To assess the subgroup-specific patterns of relapse, three comparative analyses were performed on; the whole relapsing cohort, those patients who received upfront CSI and those patients that did not receive upfront CSI. These were undertaken to account for the differing age distribution of the molecular subgroups and the variable upfront treatment that each age group received (*i.e.* infants do not have CSI upfront, section 1.8.5, and are enriched for MB_{SHH} and MB_{Group3}, section 1.8.8). In addition, recent observations by Ramaswamy *et al*., (2013) noted a difference in the subgroup-specific patterns of relapse depending on the delivery of upfront CSI to MB_{Group4} patients. The structure of the analysis of the present study would thus allow similar comparisons to be made. Overall, MB_{SHH} recurred more frequently in the posterior fossa (31/47, 66%, p=0.0052, Fisher's exact test, Table 6.4) than MB_{Group3} and MB_{Group4}, both of which typically relapsed at distant sites (34/41, 83% and 52/61, 85%, p=0.0119, Fisher's exact test, Table 6.4). This is consistent with recent reports by Ramaswamy *et al*., (2013, section 1.9.2.2), although they report a lower rate of distant disease in MB_{SHH} (18/58, 31%) than described in this study where distant relapse in MB_{SHH} is still a common event (30/47, 64%).

Whole cohort				
	Relapse pattern frequency by molecular subgroup			
Molecular subgroup	Local	p value	Distant	p value
MB_{SHH}	31/47 (66%)	**0.0052**	30/47 (64%)	**0.0119**
MB_{WNT}	2/5 (40%)	1	3/5 (60%)	0.3187
MB_{Group3}	16/41 (39%)	0.2015	34/41 (83%)	0.3875
MB_{Group4}	26/61 (43%)	0.2507	52/61 (85%)	0.0762
Upfront CSI cohort				
	Relapse pattern frequency by molecular subgroup			
Molecular subgroup	Local	p value	Distant	p value
MB_{SHH}	13/20 (65%)	**0.0245**	11/20 (55%)	**0.0034**
MB_{WNT}	2/5 (40%)	1	3/5 (60%)	0.2492
MB_{Group3}	8/27 (30%)	0.1788	22/27 (81%)	1
MB_{Group4}	22/56 (41%)	0.6969	51/56 (91%)	**0.0066**
No upfront CSI cohort				
	Relapse pattern frequency by molecular subgroup			
Molecular subgroup	Local	p value	Distant	p value
MB_{SHH}	18/27 (67%)	1	19/27 (70%)	1
MB_{Group3}	8/14 (57%)	0.5115	12/14 (86%)	0.1692
MB_{Group4}	4/5 (80%)	0.6446	1/5 (20%)	**0.0248**

Table 6.4 Subgroup-specific patterns of disease relapse. CSI, craniospinal irradiation; bold, significant p value; local disease, M0/1; distant disease, M2+; p, Fisher's exact test, compares the rate of local or distant relapse for each subgroup versus all other subgroups.

The subgroup-specific patterns of disease relapse and association of MB_{SHH} with local disease relapse (Figure 6.2) also reflects the predominance of distant relapse in MB_{Group3} and MB_{Group4} (34/41, 83% and 52/61, 85% in the whole cohort, Table 6.4). This is particularly true for those patients who received upfront CSI, whereby in MB_{Group4}, distant relapse occurs in 91% of patients (51/56, p=0.0066, Table 6.4). However, in MB_{Group4} patients not receiving upfront CSI, distant relapse occurred infrequently (1/5, 20%, p=0.0248, Fisher's exact test). While this finding is drawn from a small population of patients, it is consistent with other reports (Ramaswamy *et al.*, 2013).

Further analysis revealed that the patterns of MB_{Group4} relapse in patients who did not receive upfront CSI, differs significantly from the pattern of relapse observed in MB_{Group4} patients who did receive upfront CSI, with patients typically relapsing at distant sites following upfront CSI (51/56,91%, versus 1/5, 20%, p=0.0011, Fisher's exact test, Table 6.5).

MB_{Group4}				
	Relapse pattern			
Cohort	Local	p value	Distant	p value
Upfront CSI	22/56 (41%)	0.1536	51/56 (91%)	**0.0011**
No upfront CSI	4/5 (80%)		1/5 (20%)	

Table 6.5 Differing patterns of relapse in MB_{Group4} patients with and without upfront CSI. Local disease, M0/1; distant disease, M2+; p, Fisher's exact test.

6.4.4.3 Distant disease is frequently acquired in all molecular subgroups at medulloblastoma relapse

In view of the high rate of distant disease at relapse, particularly in MB_{Group3} and MB_{Group4}, the frequency of distant disease (M2+) at diagnosis was reviewed cohort-wide and compared to the frequency of distant disease at relapse. This revealed that distant disease at relapse (119/154, 77%) was significantly more common than distant disease at diagnosis (63/202, 31%, p<0.0001, Fisher's exact test). In view of these findings, and the enrichment of distant disease in MB_{Group3} and MB_{Group4} (Table 6.4), further analysis was undertaken to determine whether there was a subgroup-specific difference in disease location at diagnosis in those patients who went on to relapse at a distant site. The following results (Table 6.6) demonstrate that across all four subgroups, the majority of patients who suffer a distant relapse, regardless of whether they received upfront CSI, have only local disease at diagnosis.

Overall, distant disease (M2+) at diagnosis in patients who go on to develop distant relapse is observed more frequently in MB_{Group3} and MB_{Group4} patients at diagnosis (12/34, 35% and 16/50, 32%, respectively) when compared to MB_{SHH} and MB_{WNT} (5/30, 17% and 0/3, 0%, respectively). This is consistent with the increased overall rate of metastatic disease associated with these two subgroups (Thompson *et al.*, 2006; Kool *et al.*, 2008; Cho *et al.*, 2011; Northcott *et al.*, 2011b; Taylor *et al.*, 2012). However,

there was not a statistical difference in the frequency of M2+ disease at diagnosis in MB_{Group3} and MB_{Group4} when individually compared to the rest of the cohort (p=0.3654 and p=0.5339 respectively, Fisher's exact test). These findings indicate that disease location at diagnosis is not predictive of disease location at relapse in all four subgroups, and distant disease sites are commonly acquired at relapse. This is again consistent with the findings in Chapter 3 (section 3.4.2.2), where high-risk disease features, including distant relapse, were commonly acquired at recurrence. Fully annotated data on the subgroup-specific patterns of disease relapse alongside all other currently characterised molecular, clinicopathological and demographic features are provided in section 9.5: Appendix V.

Whole cohort				
	Acquisition and maintenance of distant disease			
Molecular subgroup	Distant disease at relapse	Location of disease at diagnosis		p value
MB_{SHH}	30/47 (64%)	Local disease Distant disease	25/30 (83%) 5/30 (17%)	0.157
MB_{WNT}	3/5 (60%)	Local disease Distant disease	3/3 (100%) 0/3 (0%)	0.5578
MB_{Group3}	34/41 (83%)	Local disease Distant disease	22/34 (65%) 12/34 (35%)	0.3654
MB_{Group4}	52/61 (85%)	Local disease Distant disease	34/50 (68%)* 16/50 (32%)*	0.5339
Upfront CSI cohort				
	Acquisition and maintenance of distant disease			
Molecular subgroup	Distant disease at relapse	Location of disease at diagnosis		p value
MB_{SHH}	11/20 (55%)	Local disease Distant disease	9/11 (82%) 2/11 (18%)	0.4952
MB_{WNT}	3/5 (60%)	Local disease Distant disease	3/3 (100%) 0/3 (0%)	0.552
MB_{Group3}	22/27 (81%)	Local disease Distant disease	15/22 (68%) 7/22 (32%)	0.7904
MB_{Group4}	51/56 (91%)	Local disease Distant disease	33/49 (63%)* 16/49 (33%)*	0.4800
No upfront CSI cohort				
	Acquisition and maintenance of distant disease			
Molecular subgroup	Distant disease at relapse	Location of disease at diagnosis		p value
MB_{SHH}	19/27 (70%)	Local disease Distant disease	16/19 (84%) 3/19 (16%)	0.0652
MB_{Group3}	12/14 (86%)	Local disease Distant disease	7/12 (58%) 5/12 (42%	0.1161
MB_{Group4}	1/5 (20%)	Local disease Distant disease	1/1 (100%) 0/1 (0%)	1

Table 6.6 Acquisition of distant disease at medulloblastoma relapse across all four molecular subgroups. Data reported at diagnosis are the proportion of patients who go on to have distant relapses (also shown at relapse). CSI, craniospinal irradiation. * Data not available for two MB_{Group4} patients at diagnosis. p, Fisher's exact test comparing the frequency of distant disease at diagnosis in an individual subgroup with the frequency of distant disease in all other subgroups.

6.4.4.4 Tumours with combined TP53 mutations and MYCN amplification display locally aggressive disease at diagnosis

The patterns of disease relapse in patients with combined p53-MYC defects, (Chapter 3), were also interrogated in the cohort of patients who relapsed following upfront CSI. In total, 7/152 cases (5%, two cases not characterised) displayed combined *TP53* mutations and *MYCN* amplification at diagnosis, and were all MB_{SHH}. This is consistent

with the current understanding of the disease at diagnosis (section 1.8.8.2) where these features are infrequent at diagnosis and not observed outside of MB_{SHH} (Pfaff *et al.*, 2010; Jones *et al.*, 2012; Zhukova *et al.*, 2013; Kool *et al.*, 2014). All of the seven patients (100%) demonstrated local disease alone, and 5/6 (83%, one case MB_{NOS}) displayed LCA histology at diagnosis, consistent with the locally aggressive disease features reported at relapse in patients who acquired combined p53-MYC defects (Table 3.11). Interestingly, 5/6 p53-*MYCN* cases (83%, one case had no data) developed metastatic disease, typically leptomeningeal, at relapse. While this was in contrast to the findings reported in Chapter 3 these events are not directly comparable.

Firstly, these observations are based on the assumption in the relapsing cohort that the combined p53-*MYCN* defects at diagnosis are maintained at relapse, which cannot be confirmed in the absence of a biopsy sample taken at relapse. Secondly, these comparisons do not account for the temporal evolution of the tumour. If we consider the time-point where both molecular aberrations are known to be present, whether it be at diagnosis (present study) or at relapse (Chapter 3), then both cohorts of patients display locally aggressive disease (M0/M1 disease and LCA histology). The observations in this study suggest that if the combined p53-MYC defects are demonstrated early (*i.e.* at diagnosis) then over time the tumour can recur and metastasise to distant sites.

6.4.5 Features associated with time to relapse in the relapsing cohort

An exploratory, univariate survival analyses undertaken on all cases with molecular subgroup available in the relapsing cohort (n=206), revealed several molecular features that were associated with a more rapid time to relapse.

6.4.5.1 Upfront CSI, molecular subgroup membership and MYC amplification are associated with time to relapse

Patients not receiving upfront CSI relapsed more quickly than those who did receive this treatment modality at diagnosis (Table 6.7 and Figure 6.3, p=0.0045, Log rank test, Bonferroni corrected). These patients were predominately infants (38/47, 81%, section 9.5: Appendix V), consistent with current clinical practice whereby CSI is typically avoided in this age group due to the long term side effects on the developing brain (Ashford *et al.*, 2014; Bull *et al.*, 2014; Knight *et al.*, 2014). MB_{Group4} was also predictive

of a slower time to relapse in the whole cohort (Table 6.7 and Figure 6.3, p=0.0008, Log rank test, Bonferroni corrected).

In contrast to the findings in the paired relapse cohort (section 3.4.4.3, Table 3.9), *TP53* mutation did not predict a shortened time to relapse in this larger, relapsing cohort (Table 6.7). However, other high-risk disease features (Pizer and Clifford, 2009; Northcott *et al.*, 2012a) which were associated with a more rapid time to relapse included MB_{Group3} (Table 6.7 and Figure 6.3, p=0.0022, Log rank test, Bonferroni corrected) and *MYC* amplification (Table 6.7 and Figure 6.3, p<0.0001, Log rank test, Bonferroni corrected). On comparing in isolation the time to relapse across all four subgroups there remained a significant difference between the rate of relapse (p<0.0001, Log rank test, Figure 6.3) which was most likely born out of the more rapid time to relapse of MB_{Group3} and the slower time to relapse of MB_{Group4} (Table 6.7 and Figure 6.3, p=0.0022 and p=0.0008 respectively, Log rank test, Bonferroni corrected).

Whole cohort				
Variable		**Number of patients**	**Univariate**	
			raw p value	corrected p value
Age	Infant	54/206 (26%)	**0.0048**	0.076
	Non infant	152/206 (74%)		
Gender	Male	142/206 (69%)	0.39046	1
	Female	64/206 (31%)		
CSI at diagnosis	Yes	154/201 (77%)	**0.0003**	**0.0045**
	No	47/201 (23%)		
Resection	STR	61/199 (31%)	0.9624	1
	GTR	138/199 (69%)		
Pathology	CLA	134/194 (69%)	0.0919	1
	LCA	35/194 (18%)	**0.0128**	0.2050
	DN	25/194 (13%)	0.8053	1
Metastatic stage	M+	63/202 (31%)	0.3486	1
	M-	139/202 (69%)		
Subgroup	MB_{SHH}	60/206 (29%)	0.0965	1
	MB_{WNT}	5/206 (2%)	0.3947	1
	MB_{Group3}	57/206 (28%)	**0.0001**	**0.0022**
	MB_{Group4}	84/206 (41%)	**0.0001**	**0.0008**
Molecular defects	*MYC/MYCN* amplification	27/181 (15%)	**0.0001**	**0.0014**
	MYC amplification	9/191 (5%)	**<0.0001**	**<0.0001**
	MYCN amplification	18/182 (10%)	0.0557	1
	TP53 mutations	17/193 (9%)	0.5160	1

Table 6.7 Univariate time to relapse analysis on the whole relapsing cohort. Demographic frequencies are shown as a proportion and percentage of the data available for each variable. Infant, <4 years; STR, subtotal resection; GTR, gross total resection; CLA, classic; LCA, large-cell/anaplastic; DN, desmoplastic/nodular; M-, M0/M1; M+, M2+. p, Log rank test, significant results are highlighted in bold.

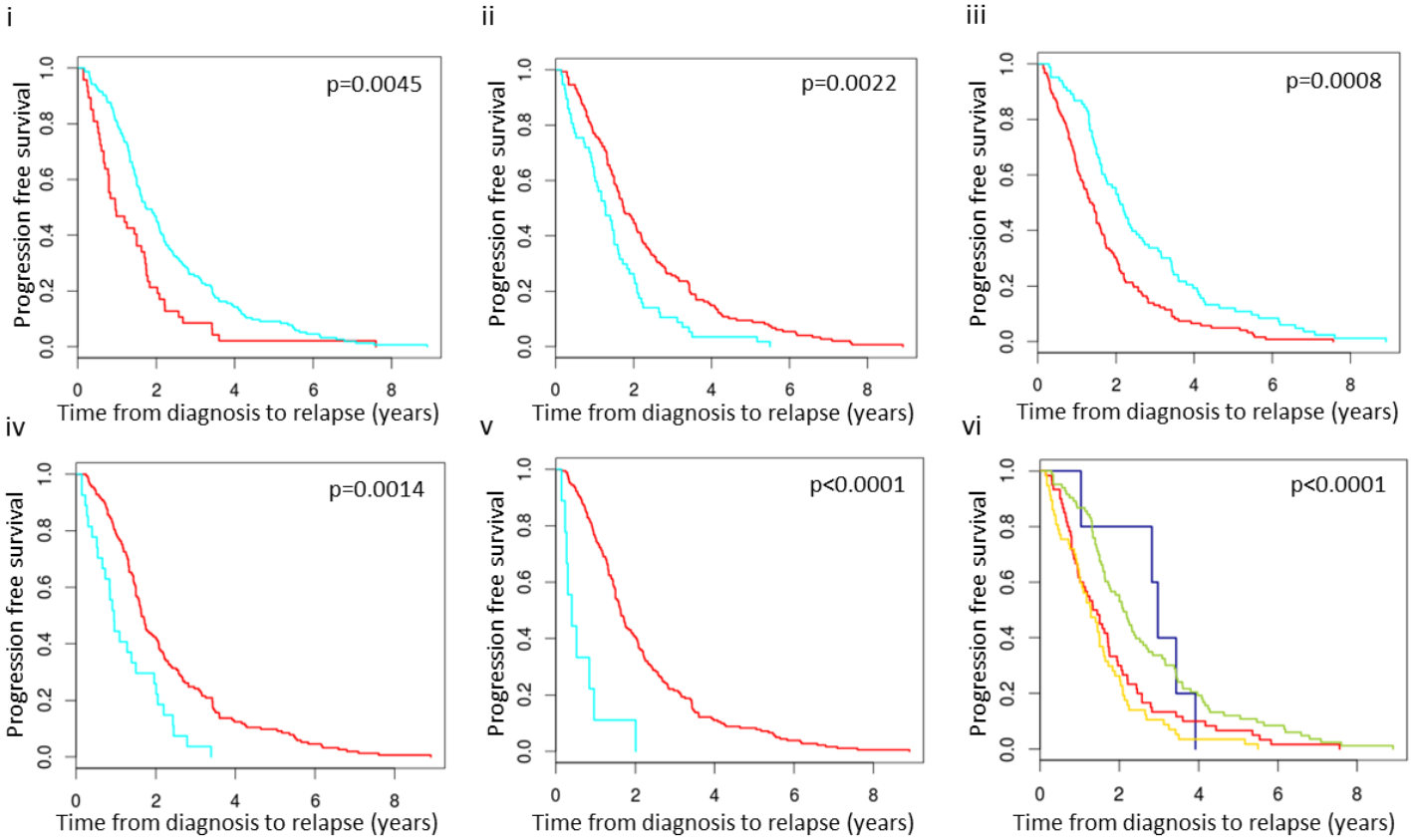

Figure 6.3 Kaplan-Meier plots demonstrating the difference in time to relapse between different treatment groups, molecular subgroups and molecular features in the whole relapsing cohort. (i) Patients receiving upfront CSI (blue) versus no upfront CSI (red). (ii) MB_{Group3} tumours (blue) versus non-MB_{Group3} tumours (red). (iii) MB_{Group4} tumours (blue) versus non-MB_{Group4} tumours (red). (iv) *MYC/MYCN* amplified tumours (blue) versus non-amplified tumours (red). (v) *MYC* amplified tumours (blue) versus non-*MYC* amplified tumours (red). p, Log rank test, Bonferroni corrected. (vi) Comparison of all four molecular subgroups; blue, MB_{WNT}; red, MB_{SHH}; yellow, MB_{Group3}; green, MB_{Group4}. p, Log rank test.

6.4.5.2 MB_{Group3} tumours relapse more quickly in patients receiving upfront CSI

In view of the demonstrated association between upfront CSI and time to relapse (Table 6.7), further survival analyses were undertaken on the two previously defined treatment groups within the relapsing cohort; those patients who received upfront CSI and those patients who did not receive upfront CSI. This highlighted that in patients who received upfront CSI only MB_{Group3} membership was significantly associated with a rapid time to relapse with a median time to recurrence of 1.28 years (range 0.17-5.5 years), compared to an overall median time to recurrence of 2.75 years in the remaining three molecular subgroups (range 0.29-8.91, p=0.0022, Log rank test, Bonferroni corrected, Table 6.8 and Figure 6.4). The difference in time to relapse remained significant when all four subgroups were compared in isolation (p=0.0013, Log rank test, Figure 6.4). These findings were consistent with the current understanding of medulloblastoma where MB_{Group3} has the poorest OS (section 1.8.8.3), and most aggressive disease course of all four subgroups (Kool *et al.*, 2012; Northcott *et al.*, 2012a; Taylor *et al.*, 2012; Shih *et al.*, 2014).

Upfront CSI cohort				
Variable		**Number of patients**	**Univariate**	
			raw p value	corrected p value
Age	Infant	14/154 (9%)	**0.0326**	0.5210
	Non infant	140/154 (91%)		
Gender	Male	111/154 (72%)	0.3998	1
	Female	43/154 (28%)		
Resection	STR	51/152 (34%)	0.9524	1
	GTR	101/152 (66%)		
Pathology	CLA	106/144 (74%)	0.7830	1
	LCA	25/144 (17%)	0.1462	1
	DN	13/144 (9%)	0.2370	1
Metastatic stage	M+	49/152 (32%)	0.3276	1
	M-	103/152 (68%)		
Subgroup	MB_{SHH}	33/154 (22%)	0.7957	1
	MB_{WNT}	5/154 (3%)	0.5662	1
	MB_{Group3}	42/154 (27%)	**0.0001**	**0.0022**
	MB_{Group4}	74/154 (48%)	**0.0050**	0.0795
Molecular defects	*MYC/MYCN* amplification	18/132 (14%)	**0.0139**	0.2221
	MYC amplification	3/140 (2%)	**0.0353**	0.5646
	MYCN amplification	15/133 (11%)	0.0661	1
	TP53 mutations	15/141 (11%)	0.4081	1
	TP53 mutation and *MYC /MYCN* amplification	7/152 (5%)	0.3277	1

Table 6.8 Univariate time to relapse analysis on patients receiving upfront CSI in the relapsing cohort. Demographic frequencies are shown as a proportion and percentage of the data available for each variable. Infant, <4 years; STR, subtotal resection; GTR, gross total resection; CLA, classic; LCA, large-cell/anaplastic; DN, desmoplastic/nodular; M-, M0/M1; M+, M2+. p, Log rank test, significant results are highlighted in bold.

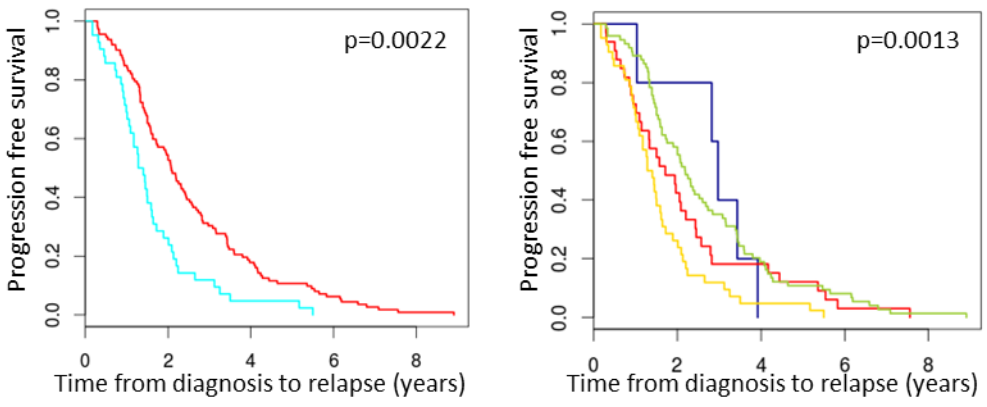

Figure 6.4 Kaplan-Meier plots demonstrating the difference in time to relapse between molecular subgroups in patients who received upfront CSI. (i) MB_{Group3} tumours (blue) versus non-MB_{Group3} tumours (red). p, Log rank test, Bonferroni corrected. (ii) Comparison of all four molecular subgroups; blue, MB_{WNT}; red, MB_{SHH}; yellow, MB_{Group3}; green, MB_{Group4}. p, Log rank test.

6.4.5.3 Combined TP53 mutations and MYCN do not predict a rapid time to relapse following upfront CSI

As already described in section 6.4.4.4, 7/152 cases (5%) demonstrated combined *TP53* mutation and *MYCN* amplification at diagnosis. These tumours were locally aggressive at diagnosis, similar in nature to the clinicopathological features of the p53-MYC tumours discovered at relapse and described in Chapter 3 (Table 3.11). Similar to the observations in Chapter 3, patients with combined p53-*MYCN* defects did not relapse more quickly than patients without combined defects (p=1, Log rank test, Bonferroni corrected, Table 6.8 and Figure 6.5).

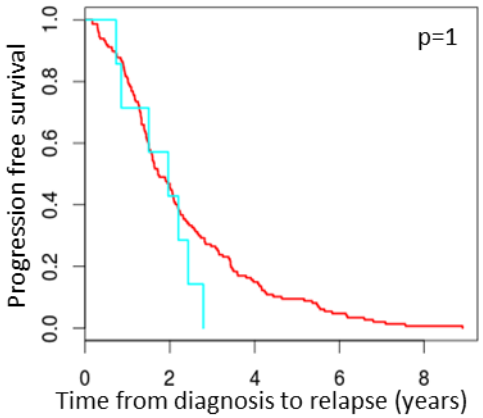

Figure 6.5 Kaplan-Meier plot demonstrating, in patients who received upfront CSI, the difference in time to relapse between cases with and without p53-*MYCN* defects at diagnosis. Combined p53-*MYCN* defects (blue) versus all cases without combined p53-*MYCN* defects (red). p, Log rank test, Bonferroni corrected.

6.4.5.4 Pathological and molecular features predict a rapid time to relapse in patients not receiving upfront CSI

As already demonstrated on the whole cohort, *MYC* amplification was significantly associated with a rapid time to relapse (section 6.4.5.1, Table 6.7 and Figure 6.3). This finding was not maintained in the cohort patients who received upfront CSI (p=0.5646, Log rank test, Bonferroni corrected, Table 6.8). However, on assessing patients who did not receive upfront CSI, *MYC* amplification was significantly associated with a rapid time to relapse (p=0.0003, Log rank test, Bonferroni corrected, Table 6.9 and Figure 6.6). In addition to this finding, LCA histology, another established high-risk disease feature (Pizer and Clifford, 2009; Ellison, 2010; Pizer *et al.*, 2011b) was also associated

with a shortened time to relapse (p=0.0004, Log rank test, Bonferroni corrected, Table 6.9 and Figure 6.6). *MYCN* amplification appeared predictive of a shortened time to relapse (p=0.0357, Log rank test, Table 6.9 and Figure 6.6), but did not retain significance after correction for multiple testing. Overall, *MYC* gene family amplification (*MYC/MYCN* amplification) in the cohort of patients not receiving upfront CSI was significantly associated with a more rapid recurrence when compared to tumours without *MYC* gene family amplification (p<0.0001, Log rank test, Bonferroni corrected, Table 6.9 and Figure 6.6).

Interestingly, of the six patients who displayed *MYC* amplification at diagnosis, 4/6 (67%) also displayed LCA histology at diagnosis with an additional five cases displaying LCA who did not have *MYC* amplification at diagnosis. These findings suggest that *MYC* gene amplification and LCA histology are significant in predicting rapid recurrence in patients not receiving upfront CSI, but there is also a cross-over of these high-risk features which may compound the rapid time to relapse witnessed in this group of patients. Finally, molecular subgroup was not predictive of a differing time to relapse (p=0.5404, Log rank test, Table 6.9 and Figure 6.6), unlike the findings reported for patients who received upfront CSI, where MB_{Group3} was predictive of a shortened time to relapse (section 6.4.5.2).

No upfront CSI cohort				
Variable		**Number of patients**	**Univariate**	
			raw p value	corrected p value
Age	Infant	38/47 (81%)	0.1029	1
	Non infant	9/47 (19%)		
Gender	Male	27/47 (57%)	0.90889	1
	Female	20/47 (43%)		
Resection	STR	10/47 (21%)	0.2898	1
	GTR	37/47 (79%)		
Pathology	CLA	24/45 (53%)	0.0314	0.4389
	LCA	9/45 (20%)	**<0.0001**	**0.0004**
	DN	12/45 (27%)	0.9774	1
Metastatic stage	M+	13/47 (28%)	0.9963	1
	M-	34/47 (72%)		
Subgroup	MB_{SHH}	27/47 (57%)	0.7330	1
	MB_{WNT}	0/47 (0%)	na	na
	MB_{Group3}	14/47 (30%)	0.5975	1
	MB_{Group4}	6/47 (13%)	0.2788	1
Molecular defects	*MYC/MYCN* amplification	9/44 (20%)	**<0.0001**	**<0.0001**
	MYC amplification	6/46 (13%)	**<0.0001**	**0.0003**
	MYCN amplification	3/44 (7%)	**0.0357**	0.4991
	TP53 mutations	2/47 (4%)	0.1105	1

Table 6.9 Univariate time to relapse analysis on patients not receiving upfront CSI in the relapsing cohort. Demographic frequencies are shown as a proportion and percentage of the data available for each variable. Infant, <4 years; STR, subtotal resection; GTR, gross total resection; CLA, classic; LCA, large-cell/anaplastic; DN, desmoplastic/nodular; M-, M0/M1; M+, M2+; na, not applicable. p, Log rank test, significant results are highlighted in bold.

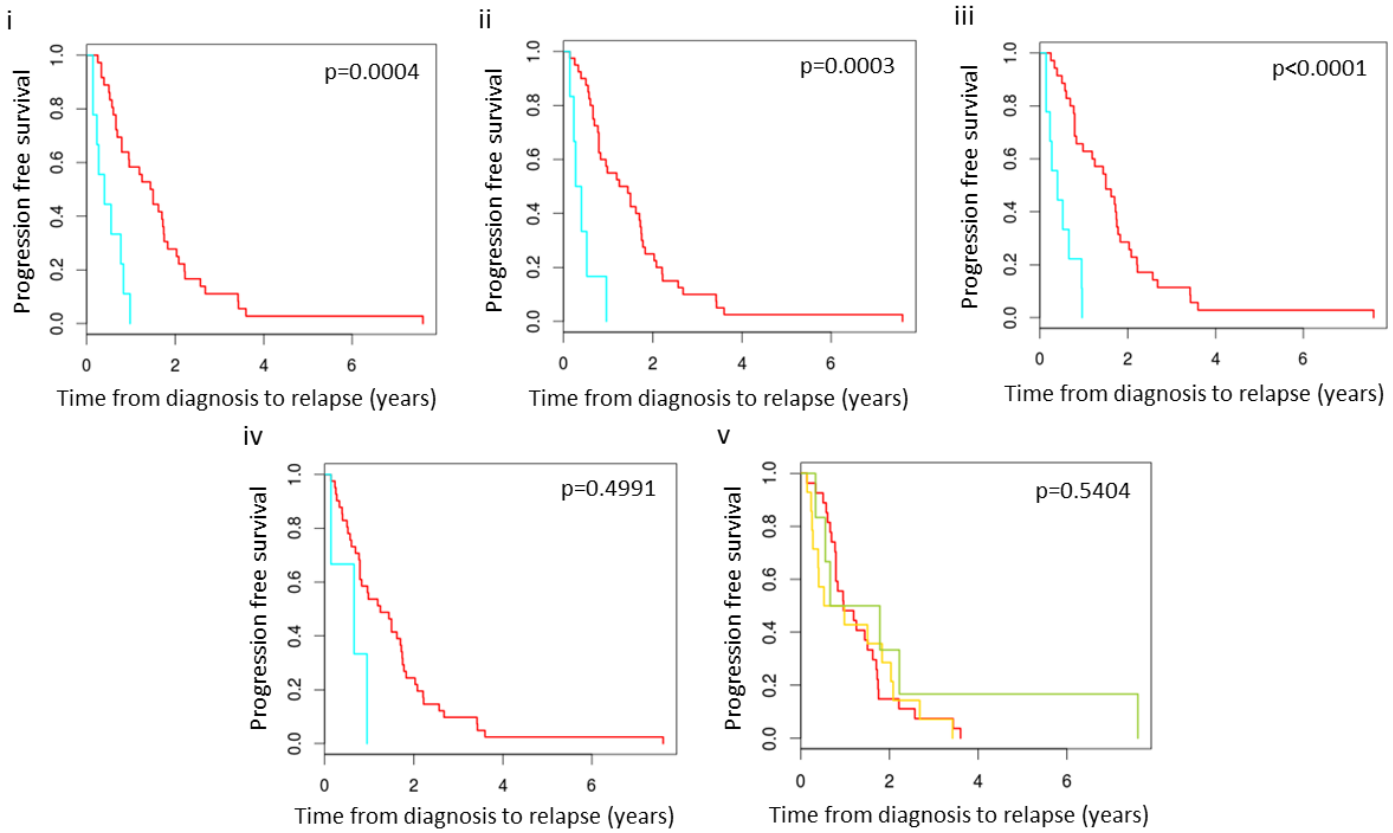

Figure 6.6 Kaplan-Meier plots demonstrating the difference in time to relapse in patients not receiving upfront CSI according to histological variant, *MYC* gene family amplification and molecular subgroup (i) LCA histology (blue) versus non-LCA histology (red). (ii) *MYC* amplified tumours (blue) versus non-*MYC* amplified tumours (red). (iii) *MYC* gene family amplified tumours (blue) versus non-*MYC* gene family amplified tumours (red). (iv) *MYCN* amplified tumours (blue) versus non-*MYCN* amplified tumours (red). p, Log rank test, Bonferroni corrected. (v) Comparison of all molecular subgroups; red, MB_{SHH}; yellow, MB_{Group3}; green, MB_{Group4}. p, Log rank test.

6.4.6 Assessing the clinicopathological and molecular features associated with time to death following relapse

All clinical, pathological and molecular features at diagnosis and relapse that could influence disease behaviour from the point of relapse onwards; *i.e.* age, gender, molecular subgroup, molecular defects at diagnosis, pathology at diagnosis, radiotherapy at relapse, relapse location and pattern of relapse, were included in a univariate TTD analysis.

6.4.6.1 No molecular features are associated with time to death following relapse in patients who received upfront CSI

In the cohort of patients receiving upfront CSI, *MYCN* amplification and LCA histology at diagnosis and diffuse disease at relapse were associated with a shortened TTD prior to performing the Bonferroni procedure for multiple testing (section 2.10, Table 6.10). Similarly, prior to correction for multiple testing, MB_{Group4} and radiotherapy at relapse were associated with a prolonged TTD (section 2.10, Table 6.10). Importantly, no feature, upon correcting for multiple testing, demonstrated a significant relationship with TTD. These findings were supportive of the results in Chapter 3, whereby it was the emerging molecular features of the tumour at relapse, (*e.g.* p53-MYC combined defects), and not diagnosis that identified patients with rapidly progressive disease post-recurrence (section 3.4.4.4).

Upfront CSI cohort				
Variable		**Number of patients**	**Univariate**	
			raw p value	corrected p value
Age	Infant	14/154 (9%)	0.5988	1
	Non infant	140/154 (91%)		
Gender	Male	111/154 (72%)	0.6828	1
	Female	43/154 (28%)		
Subgroup at diagnosis	MB_{SHH}	33/154 (22%)	0.0952	1
	MB_{WNT}	5/154 (3%)	0.2537	1
	MB_{Group3}	42/154 (27%)	0.0883	1
	MB_{Group4}	74/154 (48%)	**0.0253**	0.4298
Molecular defects at diagnosis	*MYC/MYCN* amplification	18/132 (14%)	**0.0152**	0.2576
	MYC amplification	3/140 (2%)	0.2261	1
	MYCN amplification	15/133 (11%)	**0.0375**	0.6382
	TP53 mutations	15/141 (11%)	0.8971	1
	TP53 mutation and *MYC/MYCN* amplification	7/152 (5%)	0.8146	1
Pathology at diagnosis	CLA	106/144 (74%)	0.0653	1
	LCA	25/144 (17%)	**0.0418**	0.7106
	DN	13/144 (9%)	0.7225	1
RT at relapse	Yes	13/102 (13%)	**0.0188**	0.3189
	No	89/102 (87%)		
Relapse location	Distant	87/108 (81%)	0.2231	1
	Local	21/108 (19%)		
Pattern of relapse	Diffuse	57/104 (55%)	**0.0058**	0.0981
	Nodular	47/104 (45%)		

Table 6.10 Univariate time to death analysis on patients receiving upfront CSI in the relapsing cohort. Demographic frequencies are shown as a proportion and percentage of the data available for each variable. Infant, <4 years; CLA, classic; LCA, large-cell/anaplastic; DN, desmoplastic/nodular; Distant, M2+; Local, M0/M1. p, Log rank test, significant results are highlighted in bold.

6.4.6.2 Patients treated with upfront CSI, who display combined TP53 mutations and MYCN amplification at diagnosis, progress rapidly following disease recurrence

Despite the non-significant findings of this aspect of the analysis, closer inspection of the patients who displayed combined p53-*MYCN* defects at diagnosis (n=7) revealed that, with the exception of one patient who survived for 3.34 years, all other patients (n=5) died rapidly following recurrence (Figure 6.7) with a median TTD of 0.58 years (range 0.12-0.87 years). This compared to a median TTD of 0.79 (range 0- 4.31 years) in the remainder of the cohort. In addition, one patient who displayed combined p53-*MYCN* defects at diagnosis had recently been diagnosed with a recurrent

medulloblastoma and was still alive with evidence of disease at the point of clinical data collection (follow-up post-recurrence of 0.04 years).

This comparison does not consider other p53 pathway defects which are yet to be assessed in this cohort (*e.g.* $p14^{ARF}$ deletion). Moreover, as it is a cohort of tumours sampled at diagnosis, there is no accounting for any cases that may have acquired p53-MYC defects at relapse, as reported in Chapter3, which may influence disease behavior post-recurrence. However, if the p53-*MYCN* defects discovered at diagnosis in the relapsing cohort were maintained at relapse, these findings compliment the findings reported in Chapter 3, as the majority of patients with p53-*MYCN* defects at diagnosis (5/7, 71%) rapidly progress and succumb to their disease within a year post-relapse (Figure 6.7).

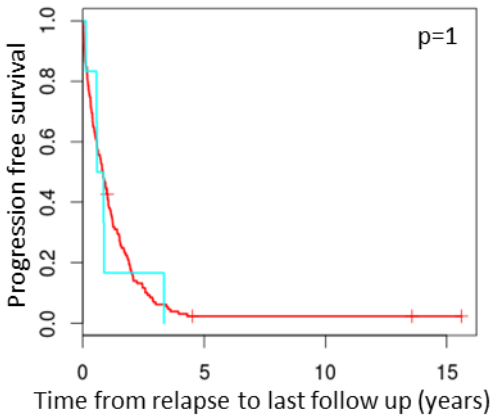

Figure 6.7 Kaplan-Meier plot demonstrating, in patients who received upfront CSI, the difference in time to death following relapse between cases with and without p53-*MYCN* defects at diagnosis. Combined p53-*MYCN* defects (blue) versus all cases without combined p53-MYC defects (red). p, Log rank test, Bonferroni corrected.

6.4.6.3 MYC amplification predicts a rapid time to death in patients who do not receive upfront CSI

In patients who did not receive upfront CSI, *MYC* amplification was predictive of rapid time to death following relapse (p=0.0003, Log rank test, Bonferroni corrected, Table 6.11 and Figure 6.8). All patients with *MYC* amplified tumours at diagnosis rapidly progressed after recurrence and died of disease, with a median TTD of 0.02 years (range 0.01-0.22 years, Figure 6.8). Other features also associated with a rapid demise post recurrence, prior to correction for multiple testing, were MB_{Group3} and LCA (Table

6.11 and Figure 6.8). As already discussed in section 6.4.5.4, there was overlap between these variables and 5/6 (83%) *MYC* amplified tumours belonged to MB_{Group3}, and 4/5 (80%) of these tumours also displayed LCA histology (Table 9.3).

No upfront CSI cohort				
Variable		**Number of patients**	**Univariate**	
			raw p value	corrected p value
Age	Infant	38/47 (81%)	0.5689	1
	Non infant	9/47 (19%)		
Gender	Male	27/47 (57%)	0.5167	1
	Female	20/47 (43%)		
Subgroup at diagnosis	MB_{SHH}	27/47 (57%)	0.0905	1
	MB_{WNT}	0/47 (0%)	na	na
	MB_{Group3}	14/47 (30%)	**0.0254**	0.3816
	MB_{Group4}	6/47 (13%)	0.7081	1
Molecular defects at diagnosis	*MYC/MYCN* amplification	9/44 (20%)	**0.0004**	**0.0053**
	MYC amplification	6/46 (13%)	**<0.0001**	**0.0003**
	MYCN amplification	3/44 (7%)	0.4866	1
	TP53 mutations	2/47 (4%)	0.7380	1
Pathology at diagnosis	CLA	24/45 (53%)	0.0341	0.5116
	LCA	9/45 (20%)	**0.0065**	0.0972
	DN	12/45 (27%)	**0.0038**	0.0564
RT at relapse	Yes	19/43 (44%)	**<0.0001**	**0.0003**
	No	24/43 (56%)		
Relapse location	Distant	32/46 (70%)	0.6182	1
	Local	14/46 (30%)		
Pattern of relapse	Diffuse	24/44 (55%)	0.5182	1
	Nodular	20/44 (45%)		

Table 6.11 Univariate time to death analysis on patients not receiving upfront CSI in the relapsing cohort. Demographic frequencies are shown as a proportion and percentage of the data available for each variable. Infant, <4 years; CLA, classic; LCA, large-cell/anaplastic; DN, desmoplastic/nodular; Distant, M2+; Local, M0/M1; na, not applicable. p, Log rank test, significant results are highlighted in bold.

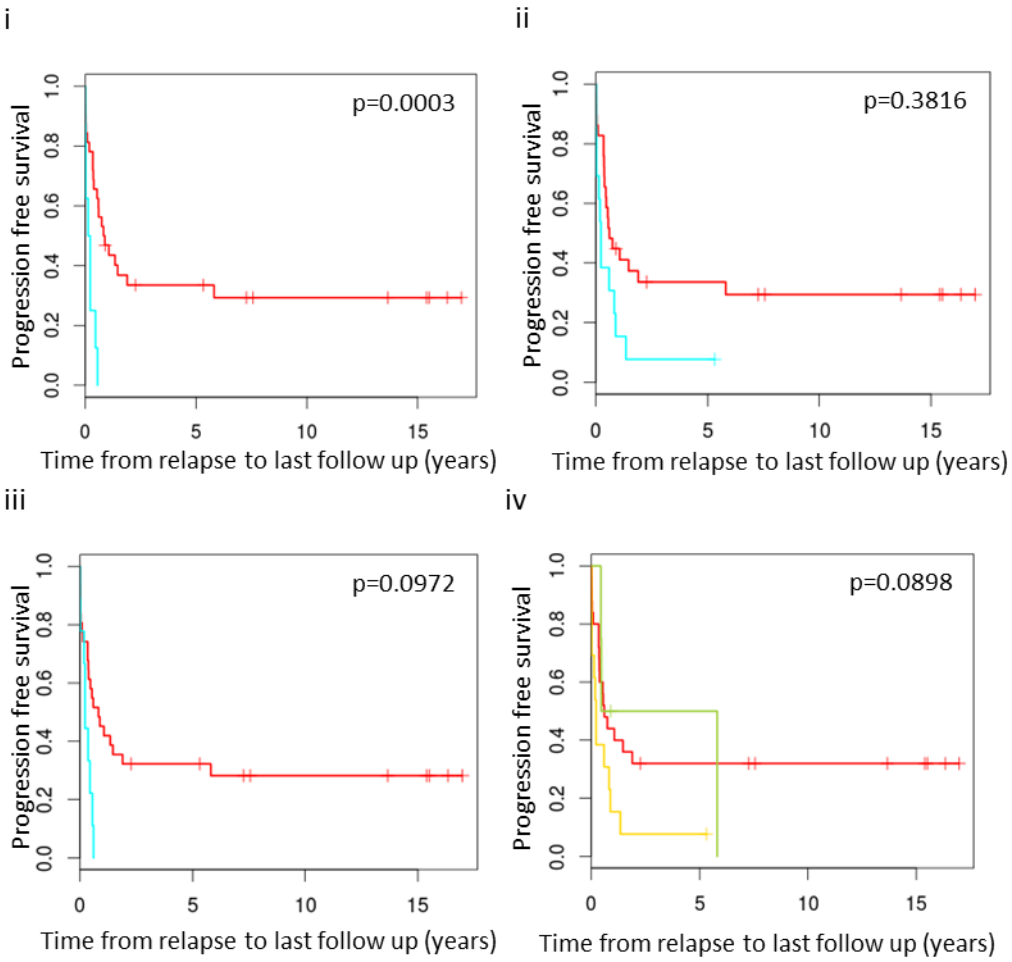

Figure 6.8 Kaplan-Meier plots demonstrating the features associated with time to death post-recurrence in CSI naïve patients. (i) *MYC* amplified tumours (blue) versus non-*MYC* amplified tumours (red). (ii) MB_{Group3} tumours (blue) versus non-MB_{Group3} tumours (red). (iii) LCA (blue) versus non-LCA tumours. p, Log rank test, Bonferroni corrected. (iv) Comparison of all molecular subgroups; red, $MB_{SHH;}$ yellow, MB_{Group3}; green, MB_{Group4}. p, Log rank test.

6.4.7 Radiotherapy at relapse is associated with time to death in those patients who are CSI naïve at disease recurrence

Radiotherapy at relapse (both CSI and focal radiotherapy) was the only factor following correction for multiple testing which was significantly associated with an increased TTD and survival in patients who did not receive upfront CSI (p=0.0003, Log rank test, Bonferroni corrected, Figure 6.9 and Table 6.11). This supports work by others (Muller *et al.*, 2014), who report that radiotherapy is a potentially curative option at medulloblastoma relapse in this group of patients who are CSI naïve and is explored further in section 6.4.9. DN histology also conveyed a survival benefit in the cohort of

patients not receiving upfront CSI although this was not significant following correction for multiple testing (p=0.0564, Log rank test, Bonferroni corrected, Table 6.11). This finding compliments the current understanding of disease behavior in infants where DN histology conveys a better prognosis at diagnosis (McManamy *et al.*, 2007; Rutkowski *et al.*, 2009; Ellison, 2010; Leary *et al.*, 2011).

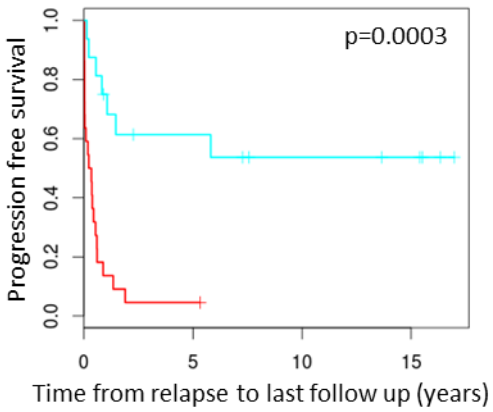

Figure 6.9 Kaplan-Meier plot demonstrating the difference in survival between CSI naïve patients at relapse who received radiotherapy at recurrence. Blue line, radiotherapy at recurrence; red line, no radiotherapy at recurrence. p, Log rank test, Bonferroni corrected.

6.4.8 Features that are associated with overall survival in the relapsing cohort

Overall survival analyses was undertaken to investigate associations with the clinicopathological and molecular features interrogated at both diagnosis and relapse in the relapsing cohort.

6.4.8.1 Only MYC gene family amplification is associated with a reduced overall survival in patients receiving upfront CSI

In the cohort of patients receiving CSI at diagnosis, OS analysis clearly demonstrated that apart from *MYC* gene family amplification, no other feature was associated with OS (p=0.0481, Log rank test, Bonferroni corrected, Table 6.12). There was a subgroup-specific difference between OS in MB_{Group3} and MB_{Group4} tumours prior to correction for multiple testing (p=0.0082 and p=0.0078 respectively, Log rank test, Table 6.12 and Figure 6.10) and comparison of the four molecular subgroups in isolation demonstrated a significant difference in OS (p=0.0208, Log rank test, Figure 6.10).

These findings most likely relate to the differing times to relapse in the molecular subgroups, with MB_{Group3} relapsing quickly and MB_{Group4} relapsing more slowly (section 6.4.5.2 and Table 6.8).

Upfront CSI cohort				
Variable		**Number of patients**	**Univariate**	
			raw p value	corrected p value
Age	Infant	14/154 (9%)	0.7843	1
	Non infant	140/154 (91%)		
Gender	Male	111/154 (72%)	0.7352	1
	Female	43/154 (28%)		
Subgroup at diagnosis	MB_{SHH}	33/154 (22%)	0.3224	1
	MB_{WNT}	5/154 (3%)	0.4468	1
	MB_{Group3}	42/154 (27%)	**0.0082**	0.1554
	MB_{Group4}	74/154 (48%)	**0.0078**	0.1476
Pathology at diagnosis	CLA	106/144 (74%)	0.2703	1
	LCA	25/144 (17%)	0.0630	1
	DN	13/144 (9%)	0.6988	1
Metastatic stage at diagnosis	M+	49/152 (32%)	0.1033	1
	M-	103/152 (68%)		
Resection at diagnosis	STR	51/152 (34%)	0.1855	1
	GTR	101/152 (66%)		
Molecular defects at diagnosis	*MYC/MYCN* amplification	18/132 (14%)	**0.0025**	**0.0481**
	MYC amplification	3/140 (2%)	**0.0238**	0.4513
	MYCN amplification	15/133 (11%)	**0.0216**	0.4096
	TP53 mutations	15/141 (11%)	0.5871	1
	TP53 mutation and *MYC*/*MYCN* amplification	7/152 (5%)	0.6556	1
RT at relapse	Yes	13/102 (13%)	**0.0425**	0.8071
	No	89/102 (87%)		
Relapse location	Distant	87/108 (81%)	0.9376	1
	Local	21/108 (19%)		
Pattern of relapse	Diffuse	57/104 (55%)	0.0551	1
	Nodular	47/104 (45%)		

Table 6.12 Univariate overall survival analysis performed on patients receiving upfront CSI in the relapsing cohort. Demographic frequencies are shown as a proportion and percentage of the data available for each variable. Infant, <4 years; CLA, classic; LCA, large-cell/anaplastic; DN, desmoplastic/nodular; M+, M2+; M-, M0/1; STR, subtotal resection; GTR, gross total resection; RT, radiotherapy; distant, M2+; local, M0/M1. p, Log rank test, significant results are highlighted in bold.

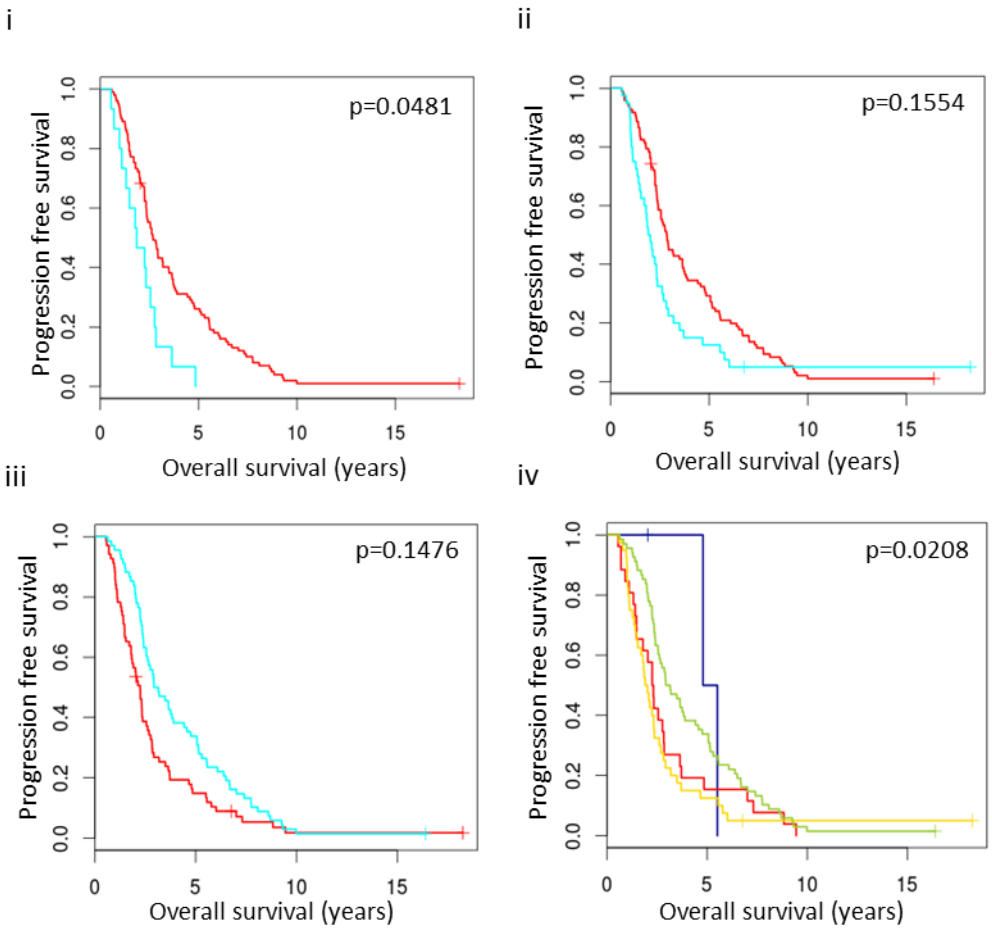

Figure 6.10 Kaplan-Meier plots illustrating the features that are associated with overall survival in those patients who received upfront CSI in the relapsing cohort (i) *MYC* gene family amplified tumours (blue) versus non amplified tumours (red). (ii) MB_{Group3} tumours (blue) versus non-MB_{Group3} tumours (red). (iii) MB_{Group4} tumours (blue) versus non-MB_{Group4} tumours (red). p, Log rank test, Bonferroni corrected. (iv) Comparison of all four molecular subgroups; blue, MB_{WNT}; red, MB_{SHH}; yellow, MB_{Group3}; green, MB_{Group4}. p, Log rank test.

6.4.8.2 Radiotherapy at relapse conveys a significant survival benefit to those patients who did not receive CSI at initial diagnosis

Similar to the TTD analysis (Table 6.11), radiotherapy at relapse was significantly associated with OS in patients who did not receive upfront CSI at diagnosis (p=0.0058, Log rank test, Bonferroni corrected, Table 6.13 and Figure 6.11). Overall, 9/10 (90%) long term survivors in this cohort received radiotherapy at disease recurrence. This finding was consistent with the findings reported in Chapter 3, where radiotherapy at medulloblastoma relapse conveyed an OS benefit to those patients who were CSI naïve and is discussed further in section 6.4.9 (Figure 3.8 and Figure 6.11).

6.4.8.3 MYC gene family amplification is significantly associated with a reduced OS in patients not receiving upfront CSI

Similar to the time to relapse and TTD analyses, *MYC* gene family amplification was significantly associated with a reduced OS (p<0.0001, Fisher's exact test, Bonferroni corrected, Table 6.13 and Figure 6.11). Patients who had a *MYC* gene family amplified tumour and did not receive CSI at diagnosis both relapsed more quickly (Table 6.9 and Figure 6.6) and died rapidly (Table 6.11 and Figure 6.8). *MYC* amplification was more frequently observed in this cohort (6/46, 13%, data not available for one case) compared to *MYCN* (3/44, 7%, data not available for three cases) which mainly comprised of infants (38/47, 81%). Of those tumours that exhibited *MYC* amplification at diagnosis, 5/6 (83%) were MB_{Group3} (1/6, 17%, MB_{SHH}).

LCA histology, another feature associated with MB_{Group3} (Kool *et al.*, 2012; Northcott *et al.*, 2012a; Taylor *et al.*, 2012), was also associated with a reduced OS (p=0.0003, Fisher's exact test, Bonferroni corrected, Table 6.13 and Figure 6.11). Similarly, those cases with LCA histology were assigned MB_{Group3} membership in 5/9 cases (56%; MB_{SHH}, 3/9 (33%) and MB_{Group4}, 1/9 (11%)). MB_{Group3} did not retain an association with OS following correction for multiple testing (p=0.4976, Fisher's exact test, Bonferroni corrected, Table 6.13 and Figure 6.11) suggesting that it was the aggressive phenotypes of LCA and *MYC* amplification which drove tumourgenesis and not MB_{Group3} in isolation.

No upfront CSI cohort				
Variable		**Number of patients**	**Univariate**	
			raw p value	corrected p value
Age	Infant	38/47 (81%)	0.1694	1
	Non infant	9/47 (19%)		
Gender	Male	27/47 (57%)	0.4460	1
	Female	20/47 (43%)		
Subgroup at diagnosis	MB_{SHH}	27/47 (57%)	0.0649	1
	MB_{WNT}	0/47 (0%)	na	na
	MB_{Group3}	14/47 (30%)	**0.0293**	0.4976
	MB_{Group4}	6/47 (13%)	0.9003	1
Pathology at diagnosis	CLA	24/45 (53%)	0.6676	1
	LCA	9/45 (20%)	**<0.0001**	**0.0003**
	DN	12/45 (27%)	**0.0039**	0.0660
Metastatic stage at diagnosis	M+	13/47 (28%)	0.5886	1
	M-	34/47 (72%)		
Resection at diagnosis	STR	10/47 (21%)	0.3025	1
	GTR	37/47 (79%)		
Molecular defects at diagnosis	*MYC/MYCN* amplification	9/44 (20%)	**<0.0001**	**<0.0001**
	MYC amplification	6/46 (13%)	**<0.0001**	**<0.0001**
	MYCN amplification	3/44 (7%)	**0.0421**	0.7159
	TP53 mutations	2/47 (4%)	0.0502	0.8531
RT at relapse	Yes	19/43 (44%)	**0.0003**	**0.0058**
	No	24/43 (56%)		
Relapse location	Distant	32/46 (70%)	0.7922	1
	Local	14/46 (30%)		
Pattern of relapse	Diffuse	24/44 (55%)	0.4894	1
	Nodular	20/44 (45%)		

Table 6.13 Univariate overall survival analysis performed on patients who did not receive upfront CSI. Demographic frequencies are shown as a proportion and percentage of the data available for each variable. Infant, <4 years; CLA, classic; LCA, large-cell/anaplastic; DN, desmoplastic/nodular; M+, M2+; M-, M0/1; STR, subtotal resection; GTR, gross total resection; RT, radiotherapy; distant, M2+; local, M0/M1; na, not applicable. p, Log rank test, significant results are highlighted in bold.

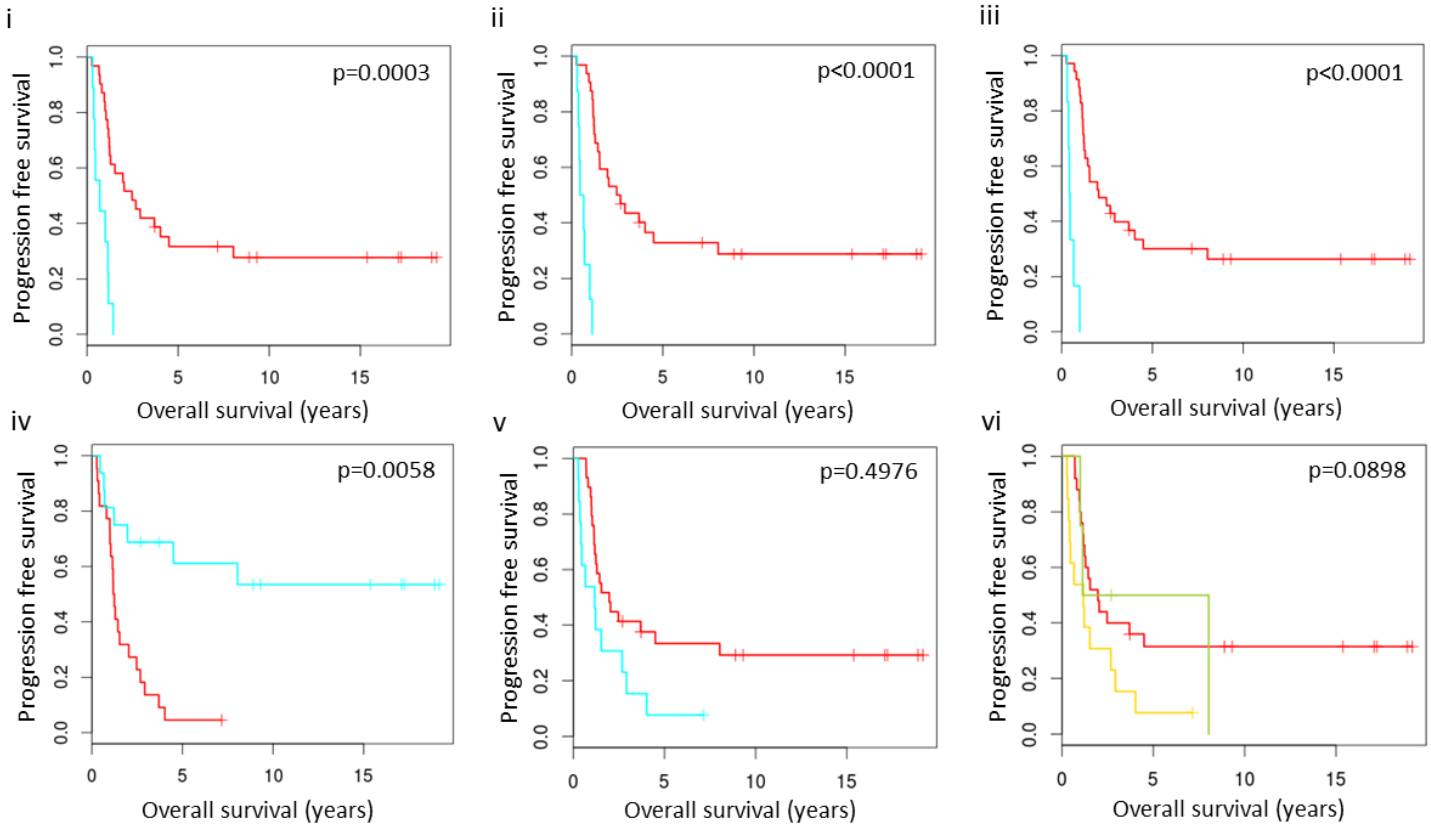

Figure 6.11 Kaplan-Meier plots illustrating the clinicopathological and molecular features that are associated with overall survival in those patients who did not receive upfront CSI in the relapsing cohort. (i) LCA histology (blue) versus non-LCA histology (red). (ii) *MYC* gene family amplified tumours (blue) versus non amplified tumours (red). (iii) *MYC* amplified tumours (blue) versus non-*MYC* amplified tumours (red). (iv) Radiotherapy at relapse (blue) versus no radiotherapy at relapse (red). (v) MB_{Group3} tumours (blue) versus non-MB_{Group3} tumours (red). p, Log rank test, Bonferroni corrected. (vi) Comparison of all molecular subgroups; red, MB_{SHH}; yellow, MB_{Group3}; green, MB_{Group4}. p, Log rank test.

6.4.9 Long term survival after medulloblastoma relapse

As already discussed, radiotherapy at relapse conveyed a significant survival benefit to those patients who did not receive upfront CSI (section 6.4.7 and 6.4.8.2). In the entire relapsing cohort (n=206) there were fourteen patients alive and disease free after disease recurrence (Table 6.14). Of these fourteen patients, twelve (86%) received radiotherapy at relapse (CSI; 8/12, 67% and focal radiotherapy; 4/12, 33%). Eight patients (67%) relapsed at distant sites (2/8, 25%, relapsed at both distant and local site) and 7/8 patients (88%) with a distant recurrence received CSI at relapse (Table 6.14). The twelve patients receiving radiotherapy at relapse had a median follow-up after recurrence of 10.6 years (range 0.9-17 years) and comprised of all four molecular subgroups (MB_{SHH} 8/12, (67%); MB_{WNT} 1/12, (8%); MB_{Group3} 2/12, (17%) and MB_{Group4} 1/12 (8%)). MB_{SHH} was the most frequently observed molecular subgroup in this population of survivors. This may reflect the better prognosis of DN histology in infancy which is associated with MB_{SHH} (McManamy *et al.*, 2007; Rutkowski *et al.*, 2009; Ellison, 2010; Leary *et al.*, 2011) and observed at diagnosis in 7/8 (88%) of MB_{SHH} survivors (Table 6.14).

Two patients, (Table 6.14), both with follow-up after relapse beyond 5 years (5.3 and 13.6 years) survived their disease recurrence without radiotherapy or neurosurgical resection. One patient had MB_{Group3} and developed a nodular, frontal lobe relapse but responded to high dose chemotherapy with stem cell rescue (discussed in section 1.9.1). The other case, MB_{Group4}, relapsed distantly and diffusely and similarly responded to high dose chemotherapy and stem cell rescue. These findings reinforce the results of Chapter 3 and others (Pizer *et al.*, 2011a; Ramaswamy *et al.*, 2013) whereby recurrent medulloblastoma is almost universally fatal. Radiotherapy is the critical treatment modality which offers a chance of survival at relapse (Muller *et al.*, 2014) . In the two isolated cases which did not receive radiotherapy, high dose chemotherapy was the treatment modality which achieved disease control and long term survival after recurrence. However, radiotherapy and high dose chemotherapy, are often not successful at controlling disease after relapse. A greater number of patients who received radiotherapy at recurrence died of their disease (n=14). Similarly, high dose chemotherapy did not achieve disease control or long term survival in at least twenty-one cases where data was available.

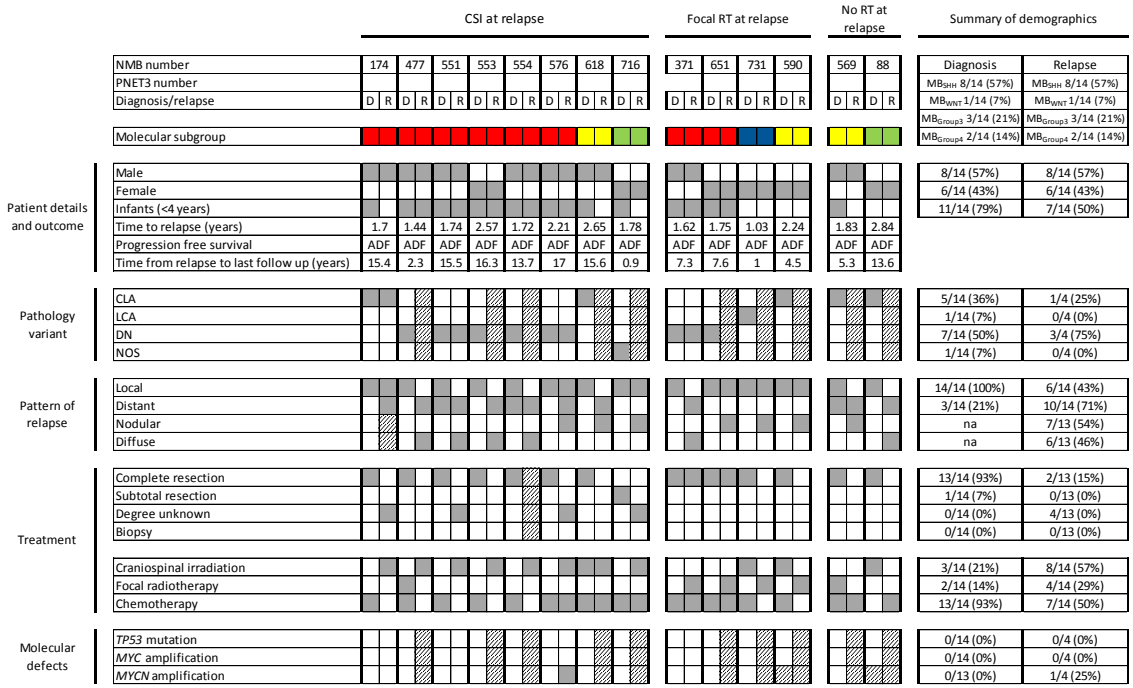

Table 6.14 Detailed clinical, pathological, patterns of relapse and molecular characteristics at diagnosis (D) and relapse (R) of the long term survivors in the relapsing cohort. Demographic frequencies are shown as a proportion and percentage of the data available for each variable. CSI, craniospinal irradiation; RT, radiotherapy; NMB, Newcastle medulloblastoma. Molecular subgroup (red, MB_{SHH}; blue, MB_{WNT}; yellow, MB_{Group3}; green, MB_{Group4}). Progression free survival (ADF, alive disease-free). Pathology variant (CLA, classic; LCA, large-cell/anaplastic; DN, desmoplastic/nodular; NOS, medulloblastoma not otherwise specified). Disease location (local, M0/M1; distant, M2+). Feature present, grey square; feature absent, white square; data not available, diagonal hatching.

6.5 Discussion

6.5.1 High-risk features are enriched at diagnosis in patients who subsequently relapse with medulloblastoma

As already discussed in Chapter 3, high-risk features are commonly observed at diagnosis in patients who go on to relapse. All established high-risk clinicopathological features in the disease; infant age group, metastatic disease, LCA histology and STR, (Pizer *et al.*, 2011b) were significantly enriched at diagnosis in the relapsing cohort. This finding further validates their role in identifying patients at diagnosis who require more intensive treatment. However, the fact that these patients went on to relapse, despite many of them having increased upfront therapy, suggests that current therapeutic options for patients with high-risk disease is not sufficient. *MYC* gene family amplification was also enriched at diagnosis in the relapsing cohort, supporting its role in aggressive tumourigenesis and its inclusion in new and upcoming clinical trials as an additional biomarker of high-risk disease (Pizer and Clifford, 2009; Morfouace *et al.*, 2014).

6.5.2 Tumours with TP53 mutations and MYCN amplification at diagnosis are locally aggressive and typically progress quickly post-recurrence

The combination of p53-MYC defects, a novel biomarker of aggressive disease at relapse (Chapter 3), was not enriched in the relapsing cohort at diagnosis (Table 6.2). This supports the findings discussed in Chapter 3 of combined p53-MYC defects as a biomarker which emerges at relapse in a group of patients who receive upfront CSI. Within the relapsing cohort those patients who received upfront CSI and displayed p53-*MYCN* defects typically had local tumours (7/7 100%), and displayed LCA histology (5/6, (83%), at diagnosis (section 6.4.4.4), again supportive of the findings reported in Chapter 3 (Table 3.11). In contrast to the reports in Chapters 3, p53-*MYCN* tumours in the relapsing cohort, had distant relapses which may reflect the temporal evolution of tumour biology (section 6.4.4.4). Tumours which demonstrated p53-*MYCN* defects at diagnosis did not recur more quickly. However, whilst the result was not significant, 5/7 patients (71%), with p53-*MYCN* defects at diagnosis had a rapid time to death post-recurrence (section 6.4.6.2).

6.5.3 MB_{Group3} tumours relapse quickly, with aggressive disease and are not frequently biopsied

As discussed in section 6.4.3, while MB_{Group3} accounted for 28% of medulloblastoma tumours in the relapsing cohort, this was not reflected in the tumour samples obtained at relapse in this study (Chapter 3). MB_{Group3} were commonly metastatic at relapse (section 6.4.4.2) and also recurred quickly (section 6.4.5 and 6.4.5.2). These two factors are likely to influence clinical practice and biopsy is firstly, less likely to be performed to confirm diagnosis as, given the short time to relapse, the recurrent tumour is unlikely to be anything other than a medulloblastoma. Secondly, in view of the frequent metastatic disease of MB_{Group3} at relapse, neurosurgical intervention is less likely to be performed as part of a curative strategy.

Neither MB_{SHH} nor MB_{Group4}, the other two well represented subgroups in the relapsing cohort (29% and 41% respectively, Table 6.2) exhibited both a rapid recurrence and distant disease at relapse. For example, MB_{SHH} was not as frequently metastatic at relapse as MB_{Group3} and MB_{Group4} and was not associated with a rapid time to relapse (section 6.4.4.2 and section 6.4.5.1-6.4.5.4). MB_{Group4} were commonly metastatic at relapse, particularly in those patients who received upfront CSI (section 6.4.4.2), but had a significantly slower overall time to relapse than any of the other three subgroups (Table 6.7 and Figure 6.3). Typically the majority of children (approximately 75%) with a medulloblastoma will relapse within 2 years of initial diagnosis (Crawford *et al.*, 2007). In this cohort, MB_{Group4} had a median time to relapse of 2.1 years (range 0.29-8.91 years). The prolonged time to relapse observed in MB_{Group4}, may bring about some doubt in the diagnosis of a recurrent medulloblastoma and raise the question of a possible secondary malignancy and therefore necessitate a biopsy to confirm the diagnosis. These findings are the most likely explanation for the under-representation of MB_{Group3} tumours in comparison to the MB_{SHH} and MB_{Group4} tumours in the paired relapse cohort (Chapter 3). Moreover, the subgroup distribution of the relapsing cohort (Table 6.2) highlights the necessity for routine biopsy at relapse, if we are to understand the biology at recurrence of all the molecular subgroups in medulloblastoma.

6.5.4 Distant disease is frequently acquired and enriched at relapse

While MB_{SHH} tumours had local disease at relapse more frequently than MB_{Group3} and MB_{Group4}, all four molecular subgroups frequently acquired distant disease at relapse (section 6.4.4.3). This was observed in patients who received upfront CSI as well as those who did not. However, in MB_{SHH} distant disease at relapse was more frequently observed in patients who did not receive upfront CSI (Table 6.6) supporting the role of CSI in preventing distant recurrence and in contrast to reports by others (Ramaswamy *et al.*, 2013). Interestingly, MB_{Group4} tumours tended to relapse locally in patients who did not receive upfront CSI (Table 6.6) a pattern which is also supported by the study from Ramaswamy *et al.,* (2013). This finding is counter-intuitive and highlights the lack of understanding in MB_{Group4} tumour biology. It also potentially suggests that MB_{Group4} tumours behave differently in infants compared to young children. Further studies in MB_{Group4}, such as the novel investigations undertaken in Chapter 5, are now essential to advance our knowledge and treatment options for this, the most frequently relapsing tumour subgroup.

6.5.5 Survival analyses in patients receiving upfront CSI demonstrates that very few clinicopathological and molecular features are associated with outcome

Univariate survival analyses, assessing time to relapse, TTD and OS demonstrated that few disease features, following correction for multiple testing, were associated with survival in patients receiving upfront CSI. As already discussed (section 6.5.3), MB_{Group3} tumours typically recurred more rapidly in this treatment group (p=0.0022, Log rank test, Bonferroni corrected, section 6.4.5.2). No other factor influenced time to relapse or TTD after correction for multiple testing. *MYC* gene family amplification was associated with a poorer OS in this treatment group (section 6.4.8) supporting its role in aggressive disease at both diagnosis (Pizer and Clifford, 2009; Ryan *et al.*, 2012) and, potentially at relapse if the amplification was maintained.

6.5.6 Tumour biology at diagnosis is associated with time to death and OS in patients who did not receive upfront CSI

Patients who did not receive upfront CSI and demonstrated LCA histology or *MYC* amplification at diagnosis relapsed quickly (section 6.4.5.4), reinforcing both these features as markers of aggressive disease (Pizer and Clifford, 2009; Ellison, 2010; Ryan *et al.*, 2012). Moreover, *MYC* amplification retained its significance in the TTD analysis in this treatment cohort (p=0.0003, Log rank test, Bonferroni corrected), potentially suggesting that this defect persisted in the tumour at relapse and continued to influence disease behaviour. Both LCA and *MYC* amplification were also significantly associated with a poorer overall survival (section 6.4.8.3). As already discussed (section 6.4.5.4, 6.4.6.3 and 6.4.8.3) there was overlap between *MYC* amplification, LCA histology and MB_{Group3} with 5/6 (83%) *MYC* amplified tumours belonging to MB_{Group3}, and 4/5 (80%) of these tumours also displaying LCA histology (Table 9.3). This overlap suggests that multiple high-risk features at diagnosis may combine and influence disease course at all three time-points (time to relapse, TTD and OS).

Moreover, the consistent finding of *MYC* amplification at diagnosis and its association with a poor outcome in all three analyses in this treatment group, (time to relapse, TTD and OS), suggests that in the absence of upfront CSI, tumour molecular biology at diagnosis continues to influence disease behaviour at relapse. This supports the theory, as discussed in section 3.5.4, that selective pressure following treatment, such as upfront CSI, occurs and alters the molecular biology of a tumour at relapse. This may also explain why, in the relapsing cohort, no molecular feature characterised at diagnosis, was associated with TTD in those patients who received CSI (section 6.4.6).

In the absence of CSI, one could hypothesise that in the relapsing cohort, *MYC* amplification is unchanged in the recurrent tumour, and hence is still associated with a rapid TTD. This is further supported by the observations in the paired relapse cohort (Chapter 3), where expansion or acquisition of molecular defects are less frequent between diagnosis and relapse in those patients who did not receive upfront CSI (Table 3.5). Acquired molecular defects such as *MYC* gene family amplification, p53 pathway defects, Ch17 defects, polyploidy and microsatellite instability, were only observed on three occasions in the seven paired tumour samples which did not receive CSI at diagnosis (Table 3.5). Importantly, acquired molecular defects were observed on

fifteen occasions in the nineteen paired tumour samples that did receive upfront CSI, (Table 3.5), giving an average number of acquired defects per patient of 0.43 (no upfront CSI) versus 0.79 (upfront CSI). Therefore, the findings in this study reported here and in Chapter 3 both support the temporal evolution and clonal expansion of treatment resistant cells in medulloblastoma, which is more evident in patients who receive upfront CSI.

6.5.7 Long term survival following medulloblastoma relapse is rare and significantly associated with the administration of radiotherapy at disease recurrence

Radiotherapy at relapse is the treatment modality most likely to achieve long term disease control. It was significantly associated with OS in those patients who did not receive upfront CSI (p=0.0058, Log rank test, Bonferroni corrected, Table 6.13) and did provide long term benefit when administered focally to two patients who received upfront CSI (Table 6.14). Two patients also survived their disease recurrence after re-treatment with high dose chemotherapy (section 6.4.9). However, both these treatment strategies (radiotherapy and high dose chemotherapy) failed to achieve long term survival after relapse more frequently than they succeeded (section 6.4.9).

These findings highlight that successful upfront treatment of medulloblastoma provides our best chance of cure and that relapse is exceptionally challenging to retreat and current therapeutic options are inadequate. Nonetheless, in CSI naïve patients, radiotherapy at relapse currently provides the best option for long term cure. However, the majority of survivors who received radiotherapy at relapse, were less than 4 years old at the time of radiotherapy delivery (7/12, 58%, Table 6.14). The consequences of this treatment modality on such a young and developing brain will likely be severe (section 1.8.6) and survival will have come with significant co-morbidities and long term neurological sequelae (Ashford *et al.*, 2014; Bull *et al.*, 2014; Knight *et al.*, 2014; Muller *et al.*, 2014). As reported by others, (Pizer *et al.*, 2011a) high dose chemotherapy is rarely successful in controlling disease at relapse and novel treatment strategies are now essential if we are offer a chance of cure to children who suffer from recurrent medulloblastoma.

6.5.8 Comparison of the patterns and timings of medulloblastoma relapse with other published studies

As already discussed in section 1.9.2.2, there has been one other recent study which interrogated the subgroup-specific patterns of medulloblastoma relapse (Ramaswamy *et al.*, 2013). The present study alongside the report by Ramaswamy *et al*., (2013) confirmed that molecular subgroup did not change between diagnosis and relapse. In addition, they also investigate the patterns and timings of medulloblastoma relapse according to molecular subgroup, which are discussed further below.

Overall, they reported that distant relapses were more commonly observed in MB_{Group3} and MB_{Group4} (62/68, 91% and 60/67 respectively) with local recurrences occurring more frequently in MB_{SHH} (18/58, 31%). These are consistent with the findings reported in this study where distant relapses were most frequently observed in MB_{Group3} and MB_{Group4} (34/41, 83% and 52/61, 85%, Table 6.4). However, while distant MB_{SHH} relapses were significantly less frequent in this study when compared to the other molecular subgroups (30/47, 64%, p=0.0199, Fisher's exact test, Table 6.4) there was still a significantly higher rate of distant relapses observed in MB_{SHH} when compared to the study by Ramaswamy *et al*., (30/47, 64% versus 18/58, 31%, p=0.0009). Moreover, the frequency of distant relapses in patients with MB_{SHH} who did not receive upfront CSI, in this study is higher still (19/27, 70%, Table 6.4). The findings of the present study would therefore not support the suggestions by Ramaswamy *et al*., (2013) to intensify local therapy and reduce CSI in MB_{SHH}. Failure to prevent distant relapse in MB_{SHH} was still a common event and was observed more frequently in those patients who did not receive upfront CSI (19/27, 70%, versus 11/20, 55%, Table 6.4), suggesting that CSI does have a role in preventing distant relapse in MB_{SHH}.

In addition to this finding, Ramaswamy *et al*., (2013) also demonstrated that local recurrences tended to be higher in MB_{Group4} patients who did not receive CSI upfront than in MB_{Group4} tumours that did receive upfront CSI (p=0.031, Fisher's exact test). This supports the findings of this study where distant recurrences were rare in MB_{Group4} patients who did not receive upfront CSI compared those children who did receive upfront CSI (1/5, 20%, versus 51/56, 91%, respectively, p=0.0011, Fisher's exact test, Table 6.5). As already discussed (section 6.5.4), this is an unusual finding that may

reflect the differing biology of MB_{Group4} either in particular age groups or following different treatments.

MB_{Group4} tumours also had a significantly prolonged time to relapse across the whole cohort in the present study (p=0.0008, Log Rank test, Bonferroni corrected, Table 6.7). This was also observed in two out of the three cohorts examined by Ramaswamy *et al*., (2013, cohort 1 and 2). Here they also reported that MB_{Group4} had a prolonged survival following relapse, a significant finding in the patients who received upfront CSI in the present study prior to correction for multiple testing (p=0.0253, Log rank test, Table 6.10). These findings, in two independent studies, now warrant further investigation, with cohort expansion to validate these discoveries along with more frequent biopsy at relapse to interrogate the molecular features of MB_{Group4} tumours at both time-points.

6.5.9 Future work

These analyses highlight that the timings and patterns of medulloblastoma relapse are strongly associated with radiotherapy (upfront or at relapse) and molecular subgroup. Further analyses are now required to understand the initial findings reported here. Cohort expansion and molecular subgrouping is ongoing and likely to exceed 250 cases with clinicopathological and molecular subgrouping data available. This would assemble the largest reported cohort of medulloblastoma tumours, sampled from patients at diagnosis who have subsequently relapsed with their disease. In addition to the molecular characterisation already described in section 6.3.6, further molecular investigations are also required to characterise all the established molecular features associated with disease outcome. These would include for example; chromosome 17 status, polyploidy and *TERT* mutation status (Pfister *et al.*, 2009; Ellison *et al.*, 2011; Jones *et al.*, 2012; Northcott *et al.*, 2012a; Taylor *et al.*, 2012; Remke *et al.*, 2013; Shih *et al.*, 2014). In addition, further characterisation of the p53 pathway defects is required, given the finding of an acquired $p14^{ARF}$ deletion reported at relapse in Chapter 3 (section 3.4.2.3.2), and similar reports of methylation or deletion of $p14^{ARF}$ by others in medulloblastoma at diagnosis (Frank *et al.*, 2004).

Following expansion and characterisation of the relapsing cohort, univariate analyses should first be repeated as described in this chapter, to confirm the findings reported and analyse the significance of additional molecular variables interrogated in the

cohort. Subsequent multivariate analyses will be undertaken cohort-wide and in the two defined treatment groups (patients who received upfront CSI and patients who did not received upfront CSI). Multivariate survival analyses would be particularly useful in understanding the findings reported in the cohort of patients who did not receive upfront CSI where *MYC* amplification, LCA and MB_{Group3} frequently coincided at diagnosis and were associated with time to relapse, TTD and OS (section 6.4.5.4, 6.4.6.3 and 6.4.8.3). In addition, correlative, univariate and multivariate analyses should be undertaken in the cohort in a subgroup-specific manner, to interrogate the differing behaviours and disease biology of the four distinct tumour entities in medulloblastoma.

The relapsing cohort also provides an important resource to interrogate the already identified candidates in MB_{Group4} described in Chapter 5 (*e.g.* T-box and Homeobox gene families), and assess their prognostic utility in the disease at diagnosis. In addition, profiling of the relapsing cohort (genomic and DNA methylation events) provides a valuable opportunity to identify new candidates that may be predicative of relapse in medulloblastoma either across all four subgroups or in a subgroup-specific manner.

6.6 Summary

Relapsed medulloblastoma is almost universally fatal and in this study 83% of patients died of their disease. High-risk disease features were enriched at diagnosis in patients who go on to relapse. In CSI naïve patients the high-risk molecular feature, *MYC* amplification, was associated with a more rapid time to relapse and TTD. Certain factors were also associated with TTD following upfront CSI, such as *MYCN* amplification and LCA histology (shortened TTD), and MB_{Group4} and RT at relapse (prolonged TTD). However, following correction for multiple testing, no clinicopathological or molecular features examined at diagnosis were associated with TTD in patients who received upfront CSI. Together, these findings support the discoveries in Chapter 3, where in those patients who received upfront CSI, it was the emergent biology of the tumour at relapse which was most strongly associated with disease course following relapse.

The frequency, rate and patterns of disease relapse do vary according to molecular subgroup. Unsurprisingly, given their overall good prognosis, MB_{WNT} tumours were rare in the relapsing cohort when compared to the other three molecular subgroups. However, MB_{WNT} tumours did recur following standard upfront therapy (n=5) and therefore MB_{WNT} is not 100% curable with 2/5 (40%) of these patients dying of disease and 2/5 (40%) alive but with disease. MB_{SHH} at relapse was associated with both local and distant disease and was the subgroup most frequently represented in patients who survived their relapse (8/14, 57%). All the long term survivors with MB_{SHH} tumours received delayed radiotherapy at relapse and the majority displayed the favourable DN histology variant at diagnosis (7/8, 88%, Table 6.14). However, despite these findings, no patients with MB_{SHH} who received upfront CSI survived their disease relapse. Overall, MB_{Group3} tumours relapsed more quickly and at distant sites, and both these features are likely to contribute to treatment decisions at this time-point and their infrequent biopsy. MB_{Group4} also relapsed at distant sites but at a slower rate, and in the absence of upfront CSI disease tended to recur locally. These observations could inform treatment decisions at relapse with aggressive strategies for prolonging life potentially being of less benefit in MB_{Group3} tumours compared to MB_{Group4} tumours.

This chapter has described the subgroup-specific patterns of relapse and provided an exploratory overview of the clinicopathological and molecular factors which influence

time to relapse, TTD and OS. A more detailed analysis is now required to assess all the features with established relationships to prognosis at diagnosis such as chromosome 17 status and polyploidy (section 6.5.9) as well as molecular features such as *TERT* mutations recently associated with MB_{SHH} and MB_{Group4} survival (Remke *et al.*, 2013). Following the completion of this characterisation a multivariate survival analysis will aid in identifying any clinicopathological or molecular features at diagnosis which are predictive of relapse. Moreover, the assembly of a large and well annotated relapsing cohort provides a valuable resource to examine new events (genomic and DNA methylation) and candidates, such as the methylation events in T-box and Homeobox gene families discovered in MB_{Group4} described Chapter 5.

Chapter 7. Summary and Discussion

7.1 Introduction

Medulloblastoma is the most common malignant brain tumour in childhood. Approximately 90 new cases are diagnosed annually in the UK, which equates to around 650 cases per annum in the European Union (Pizer and Clifford, 2008; Pizer and Clifford, 2009). There is a male predominance with an annual incidence of 0.48 per 100 000 in girls and 0.75 per 100 000 in boys (Crawford *et al.*, 2007). Current OS rates for standard-risk disease following multimodal therapy are approximately 80%. However, for patients with high-risk disease (section 1.8.5), long term survival is significantly worse despite frequent escalation of upfront treatment, and survival rates between 25-65% are reported (Crawford *et al.*, 2007; Pizer and Clifford, 2009; Ellison, 2010; Gajjar *et al.*, 2012).

Typically the disease course is such that remission is achieved following upfront treatment but, over time, approximately 30% of all patients will develop a recurrent tumour, with most relapses occurring during the first 2 years following initial diagnosis (Crawford *et al.*, 2007; Jones *et al.*, 2012). Relapse disease is almost universally fatal, particularly if the patient has already received CSI (Pizer *et al.*, 2011a; Ramaswamy *et al.*, 2013). Consequently, disease recurrence is the single greatest cause of death in children diagnosed with a medulloblastoma (Pizer and Clifford, 2008; Jones *et al.*, 2012; Muller *et al.*, 2014).

It is now understood that, at diagnosis, medulloblastoma comprises of four subgroups which are molecularly defined and believed to originate from different cell types. The four molecular subgroups; MB_{WNT}, MB_{SHH}, MB_{Group3} and MB_{Group4}, have characteristic demographic, clinicopathological, genetic and epigenetic features alongside established differences in outcome (Gibson *et al.*, 2010; Grammel *et al.*, 2012; Northcott *et al.*, 2012a; Taylor *et al.*, 2012). These discoveries have guided both the clinical trials and research studies now undertaken in medulloblastoma at diagnosis. Clinical trials with subgroup-specific treatment stratification, founded on this new knowledge, are underway in the USA (SJMB12) and imminently due to open in Europe (PNET5, section 1.8.8).

To date, however, very little is understood about disease biology at medulloblastoma recurrence. This is due in part to the rarity of recurrent samples to investigate, as biopsy at relapse is performed infrequently in current clinical practice. There are only two published studies which have investigated the features of disease biology at medulloblastoma recurrence (Korshunov *et al.*, 2008; Ramaswamy *et al.*, 2013). The study by Korshunov *et al*., (2008) was the first published dataset to provide initial insights into the biology of recurrent disease, and demonstrated temporal progression of both histopathological and molecular events. This study was undertaken in the pre-subgrouping era of medulloblastoma research (section 1.9.2.1).

Ramaswamy *et al*., (2013) investigated the subgroup-specific patterns of relapse medulloblastoma in three independent cohorts. Here they demonstrated subgroup stability over time, alongside highlighting subgroup-specific differences in the timings and patterns of relapse (section 1.9.2.2). However, until now, medulloblastoma disease features at diagnosis with established importance and relationships with disease outcome, such as *MYC* gene family amplification, chromosome 17 status and p53 pathway defects, have yet to be comprehensively interrogated in the disease at relapse. Moreover, discovery work in recurrent disease to interrogate events that are either enriched or novel at this time-point, such as the analyses of DNA methylation patterns and their potential role in the regulation of gene expression, has not been performed. These events could in the future, be explored for their utility as either prognostic biomarkers or therapeutic targets at relapse.

The current study was conceived and undertaken to provide critical new understanding of the biological mechanisms of medulloblastoma relapse. Through comprehensive investigation of the clinicopathological and molecular characteristics of recurrent disease, this study aimed to identify features that were either enriched or novel in the disease at relapse. Any events identified could firstly be assessed as potential biomarkers predictive of relapse, or relapse disease behaviour, which could be incorporated into therapeutic stratification of the disease at diagnosis, or used to inform treatment decisions at recurrence respectively. Secondly, relapse disease features could be investigated for their therapeutic utility, and provide the foundation for functional and pre-clinical work, with the ultimate aim of developing future

targeted therapeutic strategies for the disease at relapse and potentially the disease at diagnosis if the target is present (section 1.10).

The approaches taken in this study were firstly to assemble a cohort of medulloblastoma tumours sampled at relapse, characterise the clinicopathological and molecular disease features of the tumours sampled at relapse, and contrast them with their diagnostic counterparts (Chapter 3). As a result of these investigations, with the exception of molecular subgroup, it was demonstrated that all clinicopathological and molecular features examined, showed evidence of alteration and predominantly acquisition of poor prognosis features. Most notably, the emergence of combined p53-MYC defects were identified as a biomarker of locally aggressive relapsed disease which occurred across all four molecular subgroups. As a result of this discovery, collaborative work was undertaken by Dr Louis Chesler and his group, (Pediatric Solid Tumour Biology and Therapeutics Team, ICR, Sutton, UK). Here, they developed a novel mouse model of the p53-MYCN interaction in medulloblastoma (GTML/*Trp53*$^{KI/KI}$) which faithfully mimicked the key features of the human p53-MYC relapsed tumours. As detailed in Chapter 4, the dependency of tumour growth and maintenance on the p53-MYCN genetic interaction was demonstrated. The Aurora A kinase inhibitor, MLN8237, an agent which disrupts the complex formed between Aurora A and MYCN and promotes MYCN degradation, reduced tumour formation and prolonged survival in this mouse model, and therefore may have therapeutic utility in medulloblastoma at relapse (Chapter 4).

The second approach, reported in Chapter 5, describes the analysis of DNA methylation patterns in medulloblastoma at relapse, and compares these patterns with the disease at diagnosis in both an unpaired and paired manner. In this chapter, a novel analysis was developed and undertaken, focussed on MB_{Group4}, to interrogate the DNA methylation status of CpG sites located in gene promoter regions and CpG islands. This analysis identified 15 candidate genes (Table 5.6) that displayed tumour-specific DNA methylation states which were acquired at disease relapse, and correlated with gene expression in an independent cohort. Importantly, 8/15 (53%) of the candidate genes belonged to two gene families (T-box and Homeobox gene families) which are both reported in other cancers to be potentially epigenetically regulated (section 5.4). These candidates now provide the foundation for functional

work and their utility for therapeutic targeting or disease stratification should be further explored (section 7.5).

In the final approach, the assembly and characterisation of a large relapsing cohort (n=206), described in Chapter 6, has enabled the subgroup-specific patterns and timings of disease relapse to be studied more widely. The findings reported here, validate the current use of high-risk disease features (section 1.8.5) to identify patients more likely to have a poor outcome, as all high-risk features investigated were enriched in this relapsing cohort. Moreover, high-risk molecular features at diagnosis, such as *MYC* amplification in patients who were CSI naïve, demonstrated an association with a rapid time to death and reduced OS (section 6.4.6.3 and 6.4.8.3). The findings in this chapter highlighted that the timings and patterns of disease recurrence are also strongly associated with radiotherapy and molecular subgroup. Moreover, while the molecular features identified at diagnosis in tumours that did not receive upfront CSI are still associated with disease course at relapse (*e.g. MYC* amplification), for patients that did receive upfront CSI, the features of the tumour at diagnosis were not significantly associated with disease course post-recurrence. These findings compliment the discoveries reported in Chapter 3 where it was the biology of the tumour at relapse which was most strongly associated with disease behaviour at this time-point.

In addition to these findings, characterisation of the relapsing cohort has enabled the features associated with survival following relapse to be assessed, and highlighted a significant benefit following the administration of radiotherapy at relapse (section 6.4.9 and 6.5.7). Radiotherapy, both focal and CSI, should be considered at present the critical treatment modality as part of a curative strategy for recurrent disease. While this treatment may not be a suitable option for all patients, particularly for those who have already received upfront CSI, radiotherapy does have utility at relapse. However radiotherapy can lead to significant morbidity in infants who, as demonstrated in this cohort (Table 6.14), are the group of patients commonly administered radiotherapy as part of their salvage strategy at relapse (Muller *et al.*, 2014).

In summary, this study provides the most comprehensive investigation of relapsed medulloblastoma to date which could influence both current and future clinical practice. Emergent, combined p53-MYC defects at relapse have potential utility as a biomarker of aggressive disease and could inform treatment decisions at disease recurrence. Through collaborative work, the modelling and targeting of p53-MYCN combined defects, has identified the agent MLN8237, which should be consider for use in medulloblastoma at recurrence. Moreover, the investigation of the DNA methylation patterns of relapsed disease has identified candidate genes (*e.g.* T-box and Homeobox gene families) which should be explored as either potential biomarkers or therapeutic targets in relapsed disease. Combined with the reported patterns and timing of disease relapse (described in Chapter 6), these discoveries also underscore the urgent need for further investigation of medulloblastoma recurrence and how these discoveries could be translated into patient benefit. The key themes (section 7.2-7.4) and ideas (section 7.5) to advance all the findings from this study are discussed below.

7.2 The temporal evolution of the molecular biology in medulloblastoma is dependent on upfront treatment

The temporal evolution of tumour molecular biology has been reported for many types of paediatric cancers including, for example, neuroblastoma, LGG and HGG (Phillips *et al.*, 2006; Carr-Wilkinson *et al.*, 2010; Castelo-Branco *et al.*, 2013; Sottoriva *et al.*, 2013). A single report in medulloblastoma, prior to this study, identified acquisition at relapse of histological features such as anaplasia, as well as the development of cytogenetic aberrations such as 17q gain and *MYCN* amplification (Korshunov *et al.*, 2008). In contrast, a more recent study reported that molecular subgroup remained stable between diagnosis and relapse (Ramaswamy *et al.*, 2013).

This study has advanced the discoveries of the two earlier reports in the disease at relapse and describes findings which support the conclusions of both studies (Korshunov *et al.*, 2008; Ramaswamy *et al.*, 2013). In the paired relapse cohort assembled in this study (Chapter 3), molecular disease features with established roles in disease prognosis at diagnosis were interrogated. Here, it was demonstrated that molecular subgroup, as assessed on the Infinium methylation 450K array, remained stable between 15/15 (100%) paired medulloblastoma tumours sampled at both diagnosis and relapse (section 3.4.2.1). Moreover, the DNA methylation patterns of tumour pairs correlated most closely with each other before any other tumour sampled from within the same molecular subgroup (Figure 2.8 and Figure 3.3). Therefore, the cancer cells that populate the tumour at recurrence, demonstrate the same DNA methylation signature as the cancer cells in the tumour at diagnosis. This finding further supports the hypothesis that the four molecular subgroups identified in medulloblastoma arise from distinct cells of origin and the cell of origin, with its distinct DNA methylation pattern, is unchanged over time (Gibson *et al.*, 2010; Grammel *et al.*, 2012). In addition, this discovery suggests that subgroup directed therapy such as SHH inhibitors (Low and de Sauvage, 2010), may have utility in the disease at recurrence which can be determined from the molecular subgroup identified at diagnosis (section 1.8.8.2.2).

In contrast, all other molecular features interrogated at medulloblastoma relapse demonstrated evidence of alteration; predominantly acquisition, of high-risk features (Table 3.5). This was particularly noticeable for patients who received upfront CSI

where the acquisition of fifteen molecular events was observed in the nineteen paired tumours, (acquisition rate 0.79 per patient), compared to only three events in the seven paired tumours sampled from patients who did not receive upfront CSI (acquisition rate of 0.43 per patient, Table 3.5). Importantly, in those patients who received upfront CSI it was the emergent molecular biology of the tumour at relapse which was associated with disease behavior from this time-point. Combined p53-MYC defects were frequently observed at medulloblastoma relapse in this treatment group (7/22, 32%), across all four molecular subgroups (Table 3.11) and was significantly associated with rapid progression after relapse, independent of the time taken to relapse (p=0.0165 and p=1 respectively, Log rank test, Bonferroni corrected, Figure 3.11).

These findings suggest that the molecular biology of recurrent disease in patients treated with upfront CSI is more frequently altered than the biology of recurrent tumours in patients not receiving upfront CSI. Ionizing radiotherapy works on the principle of causing extensive cellular damage. This is achieved by the creation of free radicals, which leads to either single stranded or double stranded DNA breaks. Damaged cells are then either repaired or, as is the aim with cancer cells, directed into apoptosis and cell death (Pelengaris and Khan, 2006). However, intratumoural heterogeneity at a cellular level exists and is observed in the present study, for example *MYC* and *MYCN* amplification, where the defect was not present in all nuclei assessed by FISH (Figure 3.7 and Figure 3.10). Intratumoural heterogeneity in medulloblastoma may therefore account for variable response rates, at a cellular level, to treatment modalities such as CSI. Clones of cells, which contain the original driving defect, *e.g.* SHH pathway aberrations, may also contain additional aberrations such as *MYCN* amplification which convey a survival advantage and resistance to CSI (Wang *et al.*, 2013).

The administration of treatment such as CSI, potentially applies selective pressure, and inadvertently isolates treatment resistant clones which return to populate the tumour at recurrence. The evolutionary theory of tumour development, known as clonal expansion, is discussed in section 1.4 and section 3.5.4 and was first proposed by Nowell (1976). However, theories have evolved and now include the possibility of CSCs accounting for a treatment resistant population of cells (section 1.4.4) and the

existence of a medulloblastoma stem cell or brain tumour-initiating cell (BTIC) that is radiotherapy resistant has been postulated (Manoranjan *et al.*, 2012). It is likely that these models are not mutually exclusive, moreover neither model accounts for the *de novo* acquisition of molecular aberrations also reported in this study (Figure 3.10).

Two hypotheses exist to explain the *de novo* acquisition of defects observed, for example, the discovery of an emergent *TP53* mutation at relapse in patient 22 in the paired relapse cohort. This mutation was not evident at diagnosis following assessment by next generation sequencing (Figure 3.10). Firstly, the mutation may have been present at low-levels in the tumour at diagnosis but was simply not detected. This could be due tumour sampling failing to obtain a population of cells with the mutation present or because the sample was not sequenced to enough depth to detect the low-level mutation.

The alternative explanation is that the molecular defect was not present at diagnosis and occurred in a population of cancer cells later on in tumour development, after tumour sampling was performed at initial diagnosis. This clone of cells would not be a CSC but a cancer cell with a survival advantage, which over time was favourably selected and populated the tumour at recurrence (Figure 1.9 and Figure 3.10). *De novo* acquisition could therefore also be attributed to treatment induced DNA damage following therapies such as CSI which could introduce the aberration after the tumour had been sampled at initial diagnosis (Boss *et al.*, 2014). Experiments such as next-generation sequencing have the ability to explore both these theories, by either identifying the low-level clones of cells at diagnosis which are treatment resistant and populate the tumour at relapse or, as reported in this study (Figure 3.10), demonstrate the absence of the molecular defect at diagnosis, supporting the theory of *de novo* acquisition at medulloblastoma relapse.

While the effect of treatment has not been explored directly in this study, the findings in Chapter 3 alongside the discoveries in Chapter 6 support a different course of tumour evolution depending on upfront treatment. For example, patients who received upfront CSI in the relapsing study, relapsed more slowly and had no molecular features identified at diagnosis which influenced disease behaviour at relapse (Table 6.7 and Table 6.10). Patients, who did not receive upfront CSI, relapsed quickly but had

molecular features detectable at diagnosis which continued to be associated with tumour behavior at relapse (Table 6.11 and Figure 6.8). Ionizing radiation, may therefore alter the course of the molecular evolution within a tumour. This could either be due to treatment induced selective pressure or the introduction of defects as a direct result of the DNA damaging effects of ionizing radiotherapy.

If it is the upfront treatment that is the most important factor directing the molecular evolution of a tumour, it follows that to understand these treatment effects further, tumours at relapse, following all different types of upfront treatment must be sampled. Moreover, to test these theories pre-clinically, we must model treatment effects directly (section 7.5.5) as well as the downstream aberrations that emerge at relapse, such as combined p53-MYC defects (Chapter 4). Given that the majority of patients receive upfront CSI, it is likely to be the emergent molecular biology of the tumour at relapse which informs disease behavior and these are the events that must be characterised and targeted if we are to improve and potentially cure patients of their relapsed disease.

7.3 Pre-clinical models of relapsed medulloblastoma are needed to further our understanding of its underlying biology and trial promising novel therapies

Through collaborative work, a mouse model, which faithfully recapitulated the key clinicopathological and molecular features identified in an aggressive form of human relapsed medulloblastoma, was developed. As reported in the human data (Chapter 3), the common emergence of p53-MYC defects at relapse suggested that these two combined aberrations provided a particular survival advantage to the cancer cell, whether they were considered as CSCs or treatment resistant clones. Given the frequency of this occurrence it was likely that these two aberrations co-existed, as was demonstrated in one tumour (patient 22, Figure 3.10), at a cellular level to drive tumour development and progression at relapse. The development of the novel GTML/*Trp53*$^{KI/KI}$ mouse model facilitated the exploration of this hypothesis and demonstrated that the interaction between these two aberrations was critical to tumour development, and was similarly associated with aggressive disease.

This proof-of-concept study highlighted the importance of appropriately modelling the molecular biology of the disease at relapse to firstly validate the findings of the human data and secondly provide an appropriate pre-clinical model to study further. When we consider the disease course of medulloblastoma, the majority of patients will die of their relapsed disease and not their primary disease. Therefore it follows that to improve survival in the disease as a whole, it is the biology of the disease at relapse that we need to understand further and faithfully model.

By modelling combined p53-MYC defects disease in a GTML/ *Trp53*$^{KI/KI}$ mouse we have firstly validated the dependency of MYCN-driven tumour growth on both MYCN and *Trp53* defects. Secondly, we have demonstrated that we can therapeutically target p53-MYCN driven medulloblastoma with an appropriate agent such as MLN8237. MLN8237, is an Aurora A kinase inhibitor which works by disrupting the complex which forms between MYCN and Aurora A, which as a consequence, leads to the degradation of MYCN. The use of MLN8237 in the GTML/*Trp53*$^{KI/KI}$ mouse model highlights the importance of agent selection for the desired target, as well as utilising a drug which is already approved for use in phase II trials, which will facilitate the more rapid translation of these findings into clinical practice (Table 1.5). MLN8237, has potential utility for treatment of recurrent disease and should be considered for use in patients with p53-MYCN driven relapsed medulloblastoma.

Currently we do undertake phase I and II studies of new agents on patients with relapsed medulloblastoma, such as the SHH inhibitor GDC-0449 (section 1.8.8.2.2). However, while SHH pathway inhibition may still have utility in the disease at relapse, given the findings in this study of subgroup stability over time; other potential new agents identified through pre-clinical work may not have efficacy in the disease at relapse, or if they do, may only have effect in a subgroup of the population at relapse who still display the target. Most reported mouse models focus on mimicking the disease features identified in medulloblastoma at diagnosis (section 1.8.8). Therefore agents developed through this route will be typically trialled on pre-clinical models of the disease at diagnosis, and targeted at the disease features at this time-point. However, at present, agents developed through this route are given to patients at disease relapse, where the driving events of tumour biology, as demonstrated in Chapter 3, are likely to have evolved.

It therefore follows that to improve outcomes in patients with relapsed medulloblastoma we should alter our approach. As demonstrated in this study, molecular target identification should be driven out of the interrogation of relapsed tumour biology. These events should next be modelled and targeted pre-clinically. To facilitate more rapid translation of potential agents into the clinic we should look first towards agents that are either in development or use in other cancers and expedite any therapeutic agent with demonstrated pre-clinical utility into the clinic. Importantly these agents should be administered to patients who display the target at relapse to allow appropriate understanding of the tumour responses (section 7.5).

7.4 Novel and focused analyses of the features of relapse medulloblastoma provides important new insights into the epigenetics of tumour development

The findings in Chapter 5 describe changes in DNA methylation patterns between diagnosis and relapse in both the T-box and Homeobox gene families in MB_{Group4}. Both these families display either maintenance or acquisition of tumour-specific DNA methylation within CpG islands or promoter regions of the gene between these two time-points which, in turn, correlates with expression. These findings suggest that DNA methylation may play a role in regulating gene transcription in these gene families and that these candidate genes may be important in MB_{Group4} tumour development at relapse. Several important points are highlighted by these discoveries to consider when investigating medulloblastoma.

Firstly, the consideration of medulloblastoma molecular subgroup at all time-points in the disease is crucial to interpret findings. Had the analysis described in section 5.3.7.3 only considered all relapsed tumour samples together, and not in a subgroup-specific way, it is possible that these important findings would not have been discovered due to the heterogeneity of the DNA methylation patterns between the subgroups (Hovestadt *et al.*, 2013; Schwalbe *et al.*, 2013b), and the dilution of any important discoveries. This may be counter-intuitive as the numbers in the study group were consequently small. However, the analysis has generated candidate genes from the same gene families which are known to play a role in other cancers (section 5.4). Moreover, one candidate gene, *EOMES*, has been identified by others to potentially be epigenetically regulated and have a role in tumourigenesis MB_{Group4} tumours (Jones *et*

al., 2012). Secondly, when characterising the DNA methylation events between diagnosis and relapse it is important to consider the current understanding of these mechanisms. For example, the threshold for a change in DNA methylation state was set at an absolute β-value difference of 0.4 to capture true differences in β-values, previously defined as a β-value change of 0.25-0.33, that may reflect the epigenetic regulation of gene transcription (Maksimovic *et al.*, 2012; Schwalbe *et al.*, 2013b).

This novel approach has yielded important findings which should be interrogated further and taken forward into functional work (section 7.5). The identification in this study, of several potentially epigenetically regulated genes highlights the importance of considering both genetics and epigenetics in cancer development as a whole, and in medulloblastoma specifically. In addition, the positive correlation between DNA methylation and gene expression demonstrated consistently across multiple CpG sites in several genes (Table 5.6) suggests that the current understanding of the epigenetic mechanisms which control gene expression is not complete, as these findings do not conform to the current paradigm of DNA methylation and its typically inverse relationship with gene expression (Baylin and Jones, 2011).

Characterisation of the epigenetic mechanisms associated with cancer development has until recently focused on the linear, inverse correlation between DNA methylation and gene expression (Baylin and Jones, 2011) and in particular the epigenetic silencing of tumour suppressor genes (Table 1.3). However, it is now evident that this understanding is limited. This is supported by the present study, other reports in medulloblastoma (*e.g. TERT* expression regulation) and studies in the Homeobox gene families (Flagiello *et al.*, 1996; Castelo-Branco *et al.*, 2013; Tsumagari *et al.*, 2013; Lindsey *et al.*, 2014). The complex relationships between all epigenetic mechanisms that regulate gene expression needs to be further investigated.

DNA methylation patterns do not only exhibit negative linear relationships with gene expression levels, and both non-linear relationships and negative associations, should also be explored. For example, analyses separate to the ones described in Chapter 5 (section 5.3.4) identifying the associations between DNA methylation and gene expression whereby, for example, DNA methylation has to reach a threshold before gene expression levels are affected (non-linear relationship) may also uncover

important epigenetically regulated genes. Moreover, patterns of DNA methylation may also be responsible for determining alternate gene transcripts rather than simply levels of gene expression, and hence may explain the positive correlations observed. Similarly, DNA methylation in isolation may not be the only epigenetic mechanism required to control gene expression (Tsumagari *et al.*, 2013). Histone and chromatin modifications are also critical in controlling gene transcription and the recent discovery in medulloblastoma of mutations in several genes responsible for modifying histones and chromatin supports this (Parsons *et al.*, 2011; Jones *et al.*, 2012; Northcott *et al.*, 2012a; Pugh *et al.*, 2012; Robinson *et al.*, 2012). Further investigation into these less well understood aspects of the epigenetic machinery is now warranted in the disease and ideas for future work are discussed in section 7.5.

7.5 Future work

The present study has demonstrated that the molecular biology of relapsed disease is different to that of the disease at diagnosis (Chapter 3 and Chapter 5), emergent events at relapse are associated with disease behaviour (Chapter 3), and the patterns and timings of relapse vary according to molecular subgroup and radiotherapy (Chapter 6). These findings underscore the importance of sampling and interrogating medulloblastoma disease at relapse further if we are to advance treatments and improve outcome in this almost always fatal diagnosis (Pizer *et al.*, 2011a; Ramaswamy *et al.*, 2013). The discoveries reported in the current study could lead to several potential lines of investigations which are discussed in detail below. These novel findings in medulloblastoma at relapse, have also provided the platform for wider translational research in the field and ideas for future studies are explored in section 7.5.5.

7.5.1 Validation of combined p53-MYC defects and translation into clinical practice

The discovery of emergent and combined p53-MYC defects at medulloblastoma relapse requires validating in a separate cohort of paired tumour samples taken at both diagnosis and relapse. The techniques employed in this study such as a focused PCR-based direct sequence analysis of the hotspot regions for *TP53* mutations (exon 5-8) alongside MLPA and FISH for the assessment of *MYC* and *MYCN* amplification could be readily undertaken in relapse biopsies, as they require limited amounts of DNA extracted from FFPE material (Chapter 3). While in this study the Infinium methylation 450K array was utilised to determine subgroup for the majority of tumour samples, where DNA may be limited, the additional use of a minimal signature DNA methylation assay (section 6.3.6.2) to determine molecular subgroup would also be important to assign subgroup on all samples obtained.

Confirmation of the frequent acquisition of combined p53-MYC defects at relapse in a separate cohort and its association with aggressive disease, would reinforce the clinical use of these combined aberrations as a biomarker of rapidly progressing disease at recurrence. Moreover, therapeutic targeting of this interaction should next be expedited for patient use. In this study the compound MLN8237 had demonstrated efficacy in the tumours spontaneously arising in GTML/*Trp53*$^{KI/KI}$ mice. Other agents

may also have utility, for example the BET inhibitor JQ1, which is described in section 1.5.2.3.1, and has demonstrated efficacy against both *MYC* and *MYCN* oncogenes (Puissant *et al.*, 2013; Di Costanzo *et al.*, 2014). Given the findings of both combined p53-*MYC* and p53-*MYCN* defects emerging at relapse in the human tumours (Chapter 3), JQ1 may also be more widely appropriate for trial in the disease at relapse.

7.5.2 Expansion of the paired relapsed cohort is essential to identify more genetic and epigenetic events important in disease recurrence

Expansion of the paired relapse cohort is now essential to elicit further key biological mechanisms in medulloblastoma relapse. While much has been achieved from DNA extracted from FFPE samples, to maximise the opportunity to characterise recurrent disease, tissue sampled at relapse should be freshly frozen, to enable the analysis of both DNA and RNA. The correlation of DNA methylation patterns and gene expression profiles at relapse would provide further evidence, for example, of the epigenetic regulation of T-box and Homeobox gene families at relapse (Chapter 5). Moreover, high molecular weight DNA samples and good quality RNA samples would facilitate techniques such as WES, WGS, whole genome bisulfite sequencing, RNA seq analysis and ChIP which could further explore the role of epigenetic mechanisms in the regulation of gene expression in relapsed medulloblastoma (Laird, 2010; Bibikova *et al.*, 2011; Dedeurwaerder *et al.*, 2011). These techniques could also be utilised to expand on the findings in Chapter 5 and aid in explaining the positive correlations between DNA methylation and gene expression levels (section 5.4).

Expansion of the paired relapse cohort, with improvement of the of quality material, would also allow for more detailed interrogation genome-wide. Targeted deep sequencing at a greater resolution could be used to further explore whether acquired defects such as *TP53* mutation are truly acquired or simply not detected at the depth investigated in this study (Figure 3.10). Moreover, WGS or WES of tumours at relapse could be utilised to identify new candidate genes important in disease evolution at relapse. In addition, the general expansion of the paired relapse cohort would expand the data available for all four molecular subgroups at relapse. This would firstly facilitate a greater understanding of the underrepresented MB_{Group3} tumours. Moreover, subgroup-specific analyses of paired tumour samples taken at both

diagnosis and relapse, would maximise the opportunity for finding further major mechanisms important in the disease at relapse.

7.5.3 Interrogation of the DNA methylation patterns of MB_{WNT}, MB_{SHH} and MB_{Group3} at relapse

As described above (section 7.5.3) the expansion of the paired relapse cohort is crucial to understanding the mechanisms of disease relapse in medulloblastoma. In the future, this would facilitate similar types of assessment of the DNA methylation patterns in the three subgroups that were not interrogated in this study (MB_{WNT}, MB_{SHH} and MB_{Group3}, Chapter 5). Initial approaches would be to replicate the analyses described in section 5.3.7.3 across all subgroups. Candidates identified through these analyses, such as the T-box and Homeobox gene families in MB_{Group4}, should be cross investigated in each subgroup to understand whether these events are subgroup-specific or relapse specific.

Potential epigenetically regulated candidate genes, discovered through these investigations, would provide the platform for *in vitro* and *in vivo* work. Experiments such as the treatment of medulloblastoma cell lines with 5-azacitidine to decrease DNA methylation and assess the downstream effect (upregulation or downregulation) on gene expression levels should be undertaken. Other assays utilising, for example, siRNAs in medulloblastoma cells lines to interrupt the expression of candidate genes could be developed to assess the role of the candidate genes in cellular processes such as apoptosis, senescence, proliferation and migration. Together these approaches would validate genes as epigenetically regulated and confirm their role in cellular processes that are important in tumourigenesis.

7.5.4 Characterisation of the relapsing cohort and validation of DNA methylation markers predictive of disease relapse

The assembly and analysis of the relapsing cohort reported in Chapter 6 needs to be completed and a comprehensive multivariate analyses undertaken. Clinical data on patterns of relapse are awaited on 31 cases and will aid in interpreting the initial findings described in section 6.4. Moreover, the molecular characterisation of other established disease features which are associated with prognosis is important. Aberrations such as chromosome 17 status, ploidy and *TERT* mutation status should be

assessed, before incorporating all clinicopathological features into a large multivariate survival analysis. The results of this analysis will expand the findings reported in Chapter 6 and provide further information on the impact of tumour molecular biology at diagnosis on disease behavior at relapse.

In addition to analysing established features of medulloblastoma in the relapsing cohort, additional work should be undertaken in this cohort to assess any current or future candidate genes that are discovered through analyses such as those reported in Chapter 5. The analysis described in section 5.3.7.3 is designed to identify methylation events that are either maintained or acquired at relapse. It therefore follows that through this analysis, potential candidates might also have prognostic utility in the disease at diagnosis. The relapsing cohort (section 6.3.5) alongside the larger NMB cohort (section 6.3.1-6.3.4) provides a valuable resource to enable the validation of prognostic biomarkers at diagnosis. Approximately 250 of the tumour samples in the NMB cohort and 160 tumours in the relapsing cohort have been characterised on the Infinium methylation 450K array. Consequently any candidate gene identified at relapse could be investigated in these independent cohorts to assess their prognostic utility.

In addition, DNA methylation at CpG residues could be investigated seperately, in these large cohorts of tumours sampled at diagnosis, to assess their utility as biomarkers predictive of relapse. A multivariate analysis which incorporates all features with an established association to disease prognosis, similar to previous studies (Schwalbe *et al.*, 2013b), could be performed to assess the prognostic utility of any selected probe of interest. Unbiased entry of bi-modally methylated probes into a Cox proportional hazard model could be performed as previously described (Schwalbe *et al.*, 2013b), or a correlative analysis of DNA methylation events which are associated with, or enriched in tumours sampled from patients at diagnosis who subsequently relapse, could be undertaken to identify CpG residues of interest. This analysis should be performed cohort-wide and in a subgroup-specific manner.

Looking further ahead, the identification of a small number of CpG residues whose DNA methylation status is predictive of relapse, could be interrogated using a minimal signature methylation assay similar to the one described in section 6.3.6.2. This assay

is practical, successful on small amounts on DNA and, as a medulloblastoma molecular subgrouping technique, is being considered for development as a clinically suitable method to subgroup patients (PBTG, unpublished work). Our best treatment strategy at present is to cure our patients with upfront therapy, and a sensitive and specific clinical test, predictive of relapse, could direct initial treatment stratification.

7.5.5 The future landscape of translational research in relapsed medulloblastoma

To improve the clinical outcome of patients with relapsed medulloblastoma, combined research and clinical efforts must focus on understanding the disease at relapse. This study has raised the possibility that upfront treatment directs the temporal evolution of the molecular biology of tumours (section 7.2). Pre-clinical work could firstly utilise some of the tools already available, such as the established medulloblastoma cell lines (Xu *et al.*, 2014). The molecular biology of these established medulloblastoma cells lines (*e.g.* DNA methylation patterns, gene expression levels and copy number aberrations) could be investigated, both before and after applying selective treatment pressure with radiotherapy. This would enable the extensive characterisation of molecular aberrations that expand or emerge as a result of radiotherapy. These findings would provide further understanding of the potential mechanisms of treatment resistance and facilitate the comparison between the aberrations discovered through these experiments and the aberrations discovered in tumours at relapse (Chapter 3).

Exploring this idea further, these experiments could be designed and undertaken in the medulloblastoma mouse models. A recent elegant study, undertaken in *Ptch1*$^{+/-}$ MB_{SHH} mouse models, reports the identification of a potentially treatment resistant population of cells (Vanner *et al.*, 2014). Here, Vanner *et al*., (2014) describes the discovery of a low frequency, quiescent population of $Sox2^{+}$ cells which expanded following treatment with chemotherapy, implying treatment resistance, but upon targeting these cells with the antineoplastic agent, mithramycin, tumour growth reduction was observed. While this report does not explore the effect of radiotherapy on tumour biology it does support the hypothesis of clonal evolution over time in medulloblastoma (section 3.5.4), and provides rationale for the future experiments outlined here.

At present there are mouse models that represent three out of the four molecular subgroups in the disease (Northcott *et al.*, 2012a; Poschl *et al.*, 2014). Future experiments in mouse models, representative of all possible molecular subgroups, could be designed to recapitulate the treatment of human disease. For example, following the development of a primary medulloblastoma tumour, exposing these various mouse models to the equivalent treatment administered to patients, such as chemotherapy and radiotherapy, and allowing tumours to return would provide access to valuable relapse tumour material that again should be interrogated at the epigenetic and genetic level. These investigations could identify aberrations that have emerged at relapse and are important in relapsed biology. In addition, next generation sequencing of tumours at both diagnosis and relapse could identify treatment resistant clonal populations of cells which may be present at low levels in tumours sampled at diagnosis but expand to populate tumours at relapse.

In order to appropriately model the disease at relapse, large numbers of combination experiments, with mice representative of all possible molecular subgroups, would be required. Each subgroup would need a cohort of mice to receive upfront CSI with adjuvant chemotherapy as well as just chemotherapy alone, to recapitulate the treatment received by patients at diagnosis. This approach would also be able to accommodate any changes that occur in the upfront treatment of patients which may affect the nature, patterns, frequency and tumour biology of medulloblastoma relapses. Employing an adaptive strategy like this would enable the pre-clinical study of relapse disease to be relevant to the present day and reflective of our current upfront treatment strategies.

Following the development of appropriate cell lines and mouse models, whether after exposure to treatment in mouse models of the primary disease (described above) or modelling the molecular biology of relapsed disease as described in Chapter 4, therapeutic options should next be explored. Two approaches could be undertaken. With an identified target, such as MYCN, appropriate and available targeted therapy could be trialled on mouse models which model and display that target (Brockmann *et al.*, 2013). Similar to the experiment described in Chapter 4, conformation of successful targeting by the agent by interrogating for a reduction in the target at both the protein level (Western blotting and IHC) or the gene level (RNA extraction a QT-PCR) should

also be undertaken. Alternatively, in mouse models where tumours have recurred following treatment, and do not have an identifiable target, high throughput drug screening could be performed.

High throughput drug screening has already been undertaken for other paediatric brain tumours such as ependymoma (section 1.6.1.3), and have successfully identified potential cytotoxic agents with efficacy in the disease, for example 5-fluoruracil (Atkinson *et al.*, 2011). Similarly, a recent report of *in vitro* and *in vivo* drug screening in MB_{Group3} mouse models and neurospheres, identified gemcitabine and pemetrexed as agents with utility in this subgroup (Morfouace *et al.*, 2014). Both these findings are now being translated into clinical practice. Approaches similar to these reports could therefore be undertaken in the *in vitro* and *in vivo* relapsed medulloblastoma models described. In addition, after the identification of an appropriate drug through both these avenues, agents should be used in the relapse setting on the appropriate patients. Otherwise if a targeted therapy is trialled on patients who do not exhibit the target, the likelihood of observing an effect on tumour growth is small (Kool *et al.*, 2014). The incorrect use of a targeted agent in early phase trials could lead to the rejection of a potentially useful drug in the relapsed setting.

Efforts to improve our understanding of the biology of relapsed disease should also be driven out of current clinical practice. The importance of sampling medulloblastoma tumours at relapse has already been highlighted (section 7.2). The molecular biology of tumours has been shown to evolve over time; therefore further information could also be attained from sampling tumours at post mortem. While this is not common practice in medulloblastoma, it has been undertaken for other childhood brain tumours such as diffuse intrinsic pontine gliomas (DIPGs), a HGG which is not normally biopsied, and therefore understanding of the molecular biology of the disease has, until recently, remained elusive. Nucleic acids extracted from DIPGs sampled at post mortem, have successfully been extracted and utilised in experiments to characterise the molecular biology of this tumour, and the discoveries from these samples have furthered the understanding in this fatal disease (Jones and Baker, 2014).

Medulloblastoma tumours sampled at three time-points would aid in determining whether the molecular evolution of the tumour is as a result of treatment, the natural

biology of the tumour, or both. Moreover sampling at post mortem of tumours that have progressed through all treatments, and never achieved remission may also reveal mechanisms and pathways that are associated with progressive disease (section 6.3.5). While rapidly progressive disease is rare, it is difficult to investigate, as the clinical need to sample a tumour at disease progression rarely occurs. Post mortem sampling, and comparison between the molecular features of relapsed disease and progressive disease, could provide the first insights into this aspect of disease behaviour, and help to determine whether rapidly progressive disease is an accelerated version of recurrence or a separate entity with differing tumour biology.

Finally exploring the biology of relapsed disease more widely in other childhood tumours should also be considered. As already discussed in section 1.7, relapse in paediatric brain tumours and other tumours such as neuroblastoma also occurs, and in certain tumour types, for example ependymoma, recurrent disease is frequently witnessed on multiple occasions. In this study we have already demonstrated that p53 pathway defects emerge at medulloblastoma relapse, similar to the findings reported in neuroblastoma (Carr *et al.*, 2006; Carr-Wilkinson *et al.*, 2010). Other common mechanisms may be involved in tumour evolution and treatment resistance, and therefore an integrated understanding of many tumour types is more likely to identify targetable mechanisms, as well as safe and effective therapies for use in the relapse setting.

7.5.6 Summary

This study has identified emergent and combined p53-MYC pathway defects which are associated with locally aggressive relapsed disease, DNA methylation events in MB_{Group4} which are acquired or maintained at relapse and associated with gene expression in the T-box and Homeobox gene families, and patterns or timings of relapse disease which are related to features at diagnosis, such as, molecular subgroup or radiotherapy. Together, these findings have provided the foundation for future research into relapsed medulloblastoma. These initial discoveries demonstrate that both genetic and epigenetic events contribute to the molecular evolution of medulloblastoma at relapse. In addition, upfront treatment such as CSI appears to play a critical role in the frequency and nature of molecular aberrations discovered at

recurrence. Combined efforts both pre-clinically and clinically are now required to further the understanding of this almost universally fatal disease.

Efforts should now focus on developing appropriate models of relapse to trial therapeutic agents which, if successful, should be expedited into the clinic. In the clinic, biopsy of tumours at relapse should be incorporated into routine clinical practice. Ideally tumour samples should be freshly frozen, which would improve the nuclei acid quality and yield, and enable more extensive analysis of the genome and epigenome to be undertaken. Post mortem biopsies should also now be considered, not just for relapse medulloblastoma, but for all patients dying of disease. Finally, collaborative efforts into relapse disease across all paediatric tumours should enable the identification of any common mechanisms and agents that may have cross-tumour utility. This will maximise potential patient groups for trial of new treatment strategies and therapeutic agents. Together, these approaches should expand our understanding of the disease, provide potential agents with efficacy at recurrence, and ultimately improve the outcome for patients with relapse medulloblastoma.

Chapter 8. References

Aguilera, D., Mazewski, C., Fangusaro, J., MacDonald, T.J., McNall-Knapp, R.Y., Hayes, L.L., Kim, S. and Castellino, R.C. (2013) 'Response to bevacizumab, irinotecan, and temozolomide in children with relapsed medulloblastoma: a multi-institutional experience', *Childs Nerv Syst*, 29(4), pp. 589-96.

Aguilera, D.G., Goldman, S. and Fangusaro, J. (2011) 'Bevacizumab and irinotecan in the treatment of children with recurrent/refractory medulloblastoma', *Pediatr Blood Cancer*, 56(3), pp. 491-4.

Aktipis, C.A., Kwan, V.S., Johnson, K.A., Neuberg, S.L. and Maley, C.C. (2011) 'Overlooking evolution: a systematic analysis of cancer relapse and therapeutic resistance research', *PLoS One*, 6(11), p. e26100.

Ali, M.J., Parsam, V.L., Honavar, S.G., Kannabiran, C., Vemuganti, G.K. and Reddy, V.A. (2010) 'RB1 gene mutations in retinoblastoma and its clinical correlation', *Saudi J Ophthalmol*, 24(4), pp. 119-23.

Amini, S., Fathi, F., Mobalegi, J., Sofimajidpour, H. and Ghadimi, T. (2014) 'The expressions of stem cell markers: Oct4, Nanog, Sox2, nucleostemin, Bmi, Zfx, Tcl1, Tbx3, Dppa4, and Esrrb in bladder, colon, and prostate cancer, and certain cancer cell lines', *Anat Cell Biol*, 47(1), pp. 1-11.

Andor, N., Harness, J.V., Muller, S., Mewes, H.W. and Petritsch, C. (2014) 'EXPANDS: expanding ploidy and allele frequency on nested subpopulations', *Bioinformatics*, 30(1), pp. 50-60.

Archer, T.C. and Pomeroy, S.L. (2011) 'Posterior fossa ependymomas: a tale of two subtypes', *Cancer Cell*, 20(2), pp. 133-4.

Ashford, J.M., Netson, K.L., Clark, K.N., Merchant, T.E., Santana, V.M., Wu, S. and Conklin, H.M. (2014) 'Adaptive functioning of childhood brain tumor survivors following conformal radiation therapy', *J Neurooncol*, 118(1), pp. 193-9.

Atkinson, J.M., Shelat, A.A., Carcaboso, A.M., Kranenburg, T.A., Arnold, L.A., Boulos, N., Wright, K., Johnson, R.A., Poppleton, H., Mohankumar, K.M., Feau, C., Phoenix, T., Gibson, P., Zhu, L., Tong, Y., Eden, C., Ellison, D.W., Priebe, W., Koul, D., Yung, W.K., Gajjar, A., Stewart, C.F., Guy, R.K. and Gilbertson, R.J. (2011) 'An integrated in vitro and in vivo high-throughput screen identifies treatment leads for ependymoma', *Cancer Cell*, 20(3), pp. 384-99.

Atreya, I., Schimanski, C.C., Becker, C., Wirtz, S., Dornhoff, H., Schnurer, E., Berger, M.R., Galle, P.R., Herr, W. and Neurath, M.F. (2007) 'The T-box transcription factor eomesodermin controls CD8 T cell activity and lymph node metastasis in human colorectal cancer', *Gut*, 56(11), pp. 1572-8.

Baeriswyl, V. and Christofori, G. (2009) 'The angiogenic switch in carcinogenesis', *Semin Cancer Biol*, 19(5), pp. 329-37.

Banine, F., Bartlett, C., Gunawardena, R., Muchardt, C., Yaniv, M., Knudsen, E.S., Weissman, B.E. and Sherman, L.S. (2005) 'SWI/SNF chromatin-remodeling factors induce changes in DNA methylation to promote transcriptional activation', *Cancer Res*, 65(9), pp. 3542-7.

Baylin, S.B. and Jones, P.A. (2011) 'A decade of exploring the cancer epigenome - biological and translational implications', *Nat Rev Cancer*, 11(10), pp. 726-34.

Bender, S., Tang, Y., Lindroth, A.M., Hovestadt, V., Jones, D.T., Kool, M., Zapatka, M., Northcott, P.A., Sturm, D., Wang, W., Radlwimmer, B., Hojfeldt, J.W., Truffaux, N., Castel, D., Schubert, S., Ryzhova, M., Seker-Cin, H., Gronych, J., Johann, P.D., Stark, S., Meyer, J., Milde, T., Schuhmann, M., Ebinger, M., Monoranu, C.M., Ponnuswami, A., Chen, S., Jones, C., Witt, O., Collins, V.P., von Deimling, A., Jabado, N., Puget, S., Grill, J., Helin, K., Korshunov, A., Lichter, P., Monje, M., Plass, C., Cho, Y.J. and Pfister, S.M. (2013) 'Reduced H3K27me3 and DNA hypomethylation are major drivers of gene expression in K27M mutant pediatric high-grade gliomas', *Cancer Cell*, 24(5), pp. 660-72.

Bhatlekar, S., Fields, J.Z. and Boman, B.M. (2014) 'HOX genes and their role in the development of human cancers', *J Mol Med (Berl)*, 92(8), pp. 811-23.

Bibikova, M., Barnes, B., Tsan, C., Ho, V., Klotzle, B., Le, J.M., Delano, D., Zhang, L., Schroth, G.P., Gunderson, K.L., Fan, J.B. and Shen, R. (2011) 'High density DNA methylation array with single CpG site resolution', *Genomics*, 98(4), pp. 288-95.

Bird, A. (2002) 'DNA methylation patterns and epigenetic memory', *Genes Dev*, 16(1), pp. 6-21.

Bland, J.M. and Altman, D.G. (1995) 'Multiple significance tests: the Bonferroni method', *BMJ*, 310(6973), p. 170.

Bland, J.M. and Altman, D.G. (1998) 'Survival probabilities (the Kaplan-Meier method)', *BMJ*, 317(7172), p. 1572.

Bland, J.M. and Altman, D.G. (2004) 'The logrank test', *BMJ*, 328(7447), p. 1073.

Bode, U., Zimmermann, M., Moser, O., Rutkowski, S., Warmuth-Metz, M., Pietsch, T., Kortmann, R.D., Faldum, A. and Fleischhack, G. (2014) 'Treatment of recurrent primitive neuroectodermal tumors (PNET) in children and adolescents with high-dose chemotherapy (HDC) and stem cell support: results of the HITREZ 97 multicentre trial', *J Neurooncol*.

Bodey, B., Bodey, B., Jr., Siegel, S.E. and Kaiser, H.E. (2000) 'Immunocytochemical detection of the homeobox B3, B4, and C6 gene products in childhood medulloblastomas/primitive neuroectodermal tumors', *Anticancer Res*, 20(3A), pp. 1769-80.

Boss, M.K., Bristow, R. and Dewhirst, M.W. (2014) 'Linking the history of radiation biology to the hallmarks of cancer', *Radiat Res*, 181(6), pp. 561-77.

Bouffet, E., Hawkins, C.E., Ballourah, W., Taylor, M.D., Bartels, U.K., Schoenhoff, N., Tsangaris, E., Huang, A., Kulkarni, A., Mabbot, D.J., Laperriere, N. and Tabori, U. (2012)

'Survival benefit for pediatric patients with recurrent ependymoma treated with reirradiation', *Int J Radiat Oncol Biol Phys*, 83(5), pp. 1541-8.

Bradburn, M.J., Clark, T.G., Love, S.B. and Altman, D.G. (2003) 'Survival analysis part II: multivariate data analysis--an introduction to concepts and methods', *Br J Cancer*, 89(3), pp. 431-6.

Bretones, G., Delgado, M.D. and Leon, J. (2014) 'Myc and cell cycle control', *Biochim Biophys Acta*.

Brockmann, M., Poon, E., Berry, T., Carstensen, A., Deubzer, H.E., Rycak, L., Jamin, Y., Thway, K., Robinson, S.P., Roels, F., Witt, O., Fischer, M., Chesler, L. and Eilers, M. (2013) 'Small molecule inhibitors of aurora-a induce proteasomal degradation of N-myc in childhood neuroblastoma', *Cancer Cell*, 24(1), pp. 75-89.

Brummelkamp, T.R., Kortlever, R.M., Lingbeek, M., Trettel, F., MacDonald, M.E., van Lohuizen, M. and Bernards, R. (2002) 'TBX-3, the gene mutated in Ulnar-Mammary Syndrome, is a negative regulator of p19ARF and inhibits senescence', *J Biol Chem*, 277(8), pp. 6567-72.

Bull, K.S., Kennedy, C.R., Bailey, S., Ellison, D.W. and Clifford, S.C. (2014) 'Improved health-related quality of life outcomes associated with SHH subgroup medulloblastoma in SIOP-UKCCSG PNET3 trial survivors', *Acta Neuropathol*.

Burgucu, D., Guney, K., Sahinturk, D., Ozbudak, I.H., Ozel, D., Ozbilim, G. and Yavuzer, U. (2012) 'Tbx3 represses PTEN and is over-expressed in head and neck squamous cell carcinoma', *BMC Cancer*, 12, p. 481.

Cakir, B., Tarhan, N.C., Coskun, M., Ozdemir, B.H., Bozkurt, A. and Ozyilkan, O. (2004) 'Metastatic cerebellar medulloblastoma in the liver mimicking a complicated cyst: sonographic and MDCT findings', *AJR Am J Roentgenol*, 183(6), pp. 1608-10.

Carol, H., Reynolds, C.P., Kang, M.H., Keir, S.T., Maris, J.M., Gorlick, R., Kolb, E.A., Billups, C.A., Geier, B., Kurmasheva, R.T., Houghton, P.J., Smith, M.A. and Lock, R.B.

(2013) 'Initial testing of the MDM2 inhibitor RG7112 by the Pediatric Preclinical Testing Program', *Pediatr Blood Cancer*, 60(4), pp. 633-41.

Carr-Wilkinson, J., O'Toole, K., Wood, K.M., Challen, C.C., Baker, A.G., Board, J.R., Evans, L., Cole, M., Cheung, N.K., Boos, J., Kohler, G., Leuschner, I., Pearson, A.D., Lunec, J. and Tweddle, D.A. (2010) 'High Frequency of p53/MDM2/p14ARF Pathway Abnormalities in Relapsed Neuroblastoma', *Clin Cancer Res*, 16(4), pp. 1108-18.

Carr, J., Bell, E., Pearson, A.D., Kees, U.R., Beris, H., Lunec, J. and Tweddle, D.A. (2006) 'Increased frequency of aberrations in the p53/MDM2/p14(ARF) pathway in neuroblastoma cell lines established at relapse', *Cancer Res*, 66(4), pp. 2138-45.

Castelo-Branco, P., Choufani, S., Mack, S., Gallagher, D., Zhang, C., Lipman, T., Zhukova, N., Walker, E.J., Martin, D., Merino, D., Wasserman, J.D., Elizabeth, C., Alon, N., Zhang, L., Hovestadt, V., Kool, M., Jones, D.T., Zadeh, G., Croul, S., Hawkins, C., Hitzler, J., Wang, J.C., Baruchel, S., Dirks, P.B., Malkin, D., Pfister, S., Taylor, M.D., Weksberg, R. and Tabori, U. (2013) 'Methylation of the TERT promoter and risk stratification of childhood brain tumours: an integrative genomic and molecular study', *Lancet Oncol*, 14(6), pp. 534-42.

Cavard, C., Audebourg, A., Letourneur, F., Audard, V., Beuvon, F., Cagnard, N., Radenen, B., Varlet, P., Vacher-Lavenu, M.C., Perret, C. and Terris, B. (2009) 'Gene expression profiling provides insights into the pathways involved in solid pseudopapillary neoplasm of the pancreas', *J Pathol*, 218(2), pp. 201-9.

Cavenee, W.K., Dryja, T.P., Phillips, R.A., Benedict, W.F., Godbout, R., Gallie, B.L., Murphree, A.L., Strong, L.C. and White, R.L. (1983) 'Expression of recessive alleles by chromosomal mechanisms in retinoblastoma', *Nature*, 305(5937), pp. 779-84.

Chang, C.H., Housepian, E.M. and Herbert, C., Jr. (1969) 'An operative staging system and a megavoltage radiotherapeutic technic for cerebellar medulloblastomas', *Radiology*, 93(6), pp. 1351-9.

Chen, C., Zhao, M., Yin, N., He, B., Wang, B., Yuan, Y., Yu, F., Hu, J., Yin, B. and Lu, Q. (2011) 'Abnormal histone acetylation and methylation levels in esophageal squamous cell carcinomas', *Cancer Invest*, 29(8), pp. 548-56.

Chene, P. (2003) 'Inhibiting the p53-MDM2 interaction: an important target for cancer therapy', *Nat Rev Cancer*, 3(2), pp. 102-9.

Chesler, L., Schlieve, C., Goldenberg, D.D., Kenney, A., Kim, G., McMillan, A., Matthay, K.K., Rowitch, D. and Weiss, W.A. (2006) 'Inhibition of phosphatidylinositol 3-kinase destabilizes Mycn protein and blocks malignant progression in neuroblastoma', *Cancer Res*, 66(16), pp. 8139-46.

Cheung, N.K. and Dyer, M.A. (2013) 'Neuroblastoma: developmental biology, cancer genomics and immunotherapy', *Nat Rev Cancer*, 13(6), pp. 397-411.

Cho, Y.J., Tsherniak, A., Tamayo, P., Santagata, S., Ligon, A., Greulich, H., Berhoukim, R., Amani, V., Goumnerova, L., Eberhart, C.G., Lau, C.C., Olson, J.M., Gilbertson, R.J., Gajjar, A., Delattre, O., Kool, M., Ligon, K., Meyerson, M., Mesirov, J.P. and Pomeroy, S.L. (2011) 'Integrative genomic analysis of medulloblastoma identifies a molecular subgroup that drives poor clinical outcome', *J Clin Oncol*, 29(11), pp. 1424-30.

Chompret, A., Brugieres, L., Ronsin, M., Gardes, M., Dessarps-Freichey, F., Abel, A., Hua, D., Ligot, L., Dondon, M.G., Bressac-de Paillerets, B., Frebourg, T., Lemerle, J., Bonaiti-Pellie, C. and Feunteun, J. (2000) 'P53 germline mutations in childhood cancers and cancer risk for carrier individuals', *Br J Cancer*, 82(12), pp. 1932-7.

Christophorou, M.A., Martin-Zanca, D., Soucek, L., Lawlor, E.R., Brown-Swigart, L., Verschuren, E.W. and Evan, G.I. (2005) 'Temporal dissection of p53 function in vitro and in vivo', *Nat Genet*, 37(7), pp. 718-26.

Clark, T.G., Bradburn, M.J., Love, S.B. and Altman, D.G. (2003) 'Survival analysis part I: basic concepts and first analyses', *Br J Cancer*, 89(2), pp. 232-8.

Clifford, S.C., Lusher, M.E., Lindsey, J.C., Langdon, J.A., Gilbertson, R.J., Straughton, D. and Ellison, D.W. (2006) 'Wnt/Wingless pathway activation and chromosome 6 loss characterize a distinct molecular sub-group of medulloblastomas associated with a favorable prognosis', *Cell Cycle*, 5(22), pp. 2666-70.

Computing, R.F.f.S. (2014) *R: A Language and Environment for Statistical Computing* [Computer program]. Available at: http://www.R-project.org.

Costello, J.F. and Plass, C. (2001) 'Methylation matters', *J Med Genet*, 38(5), pp. 285-303.

Crawford, J.R., MacDonald, T.J. and Packer, R.J. (2007) 'Medulloblastoma in childhood: new biological advances', *Lancet Neurol*, 6(12), pp. 1073-85.

CRUK (2010) *Childhood Cancer - Great Britain & UK*.

CRUK (2011) *Cancer Worldwide and in the UK*.

CRUK (2014a) *Brain, other CNS and intracranial tumours incidence statistics*.

CRUK (2014b) *Cancer incidence and mortality in the UK*.

CRUK (2014c) *Childhood cancer key facts*.

Dasgupta, T. and Haas-Kogan, D.A. (2013) 'The combination of novel targeted molecular agents and radiation in the treatment of pediatric gliomas', *Front Oncol*, 3, p. 110.

de Bont, J.M., Packer, R.J., Michiels, E.M., den Boer, M.L. and Pieters, R. (2008) 'Biological background of pediatric medulloblastoma and ependymoma: a review from a translational research perspective', *Neuro Oncol*, 10(6), pp. 1040-60.

de Vries, A., Flores, E.R., Miranda, B., Hsieh, H.M., van Oostrom, C.T., Sage, J. and Jacks, T. (2002) 'Targeted point mutations of p53 lead to dominant-negative inhibition of wild-type p53 function', *Proc Natl Acad Sci U S A*, 99(5), pp. 2948-53.

Dedeurwaerder, S., Defrance, M., Calonne, E., Denis, H., Sotiriou, C. and Fuks, F. (2011) 'Evaluation of the Infinium Methylation 450K technology', *Epigenomics*, 3(6), pp. 771-84.

Di Costanzo, A., Del Gaudio, N., Migliaccio, A. and Altucci, L. (2014) 'Epigenetic drugs against cancer: an evolving landscape', *Arch Toxicol*, 88(9), pp. 1651-68.

Dieffenbach, C.W., Lowe, T.M. and Dveksler, G.S. (1993) 'General concepts for PCR primer design', *PCR Methods Appl*, 3(3), pp. S30-7.

Dietlein, F., Thelen, L. and Reinhardt, H.C. (2014) 'Cancer-specific defects in DNA repair pathways as targets for personalized therapeutic approaches', *Trends Genet*, 30(8), pp. 326-39.

Douglas, N.C. and Papaioannou, V.E. (2013) 'The T-box transcription factors TBX2 and TBX3 in mammary gland development and breast cancer', *J Mammary Gland Biol Neoplasia*, 18(2), pp. 143-7.

Druker, B.J., Talpaz, M., Resta, D.J., Peng, B., Buchdunger, E., Ford, J.M., Lydon, N.B., Kantarjian, H., Capdeville, R., Ohno-Jones, S. and Sawyers, C.L. (2001) 'Efficacy and safety of a specific inhibitor of the BCR-ABL tyrosine kinase in chronic myeloid leukemia', *N Engl J Med*, 344(14), pp. 1031-7.

Druker, B.J., Tamura, S., Buchdunger, E., Ohno, S., Segal, G.M., Fanning, S., Zimmermann, J. and Lydon, N.B. (1996) 'Effects of a selective inhibitor of the Abl tyrosine kinase on the growth of Bcr-Abl positive cells', *Nat Med*, 2(5), pp. 561-6.

Dufour, C., Beaugrand, A., Le Deley, M.C., Bourdeaut, F., Andre, N., Leblond, P., Bertozzi, A.I., Frappaz, D., Rialland, X., Fouyssac, F., Edan, C., Grill, J., Quidot, M. and Varlet, P. (2012a) 'Clinicopathologic prognostic factors in childhood atypical teratoid and rhabdoid tumor of the central nervous system: a multicenter study', *Cancer*, 118(15), pp. 3812-21.

Dufour, C., Beaugrand, A., Pizer, B., Micheli, J., Aubelle, M.S., Fourcade, A., Couanet, D., Laplanche, A., Kalifa, C. and Grill, J. (2012b) 'Metastatic Medulloblastoma in Childhood: Chang's Classification Revisited', *Int J Surg Oncol*, 2012, p. 245385.

Dunkel, I.J., Gardner, S.L., Garvin, J.H., Jr., Goldman, S., Shi, W. and Finlay, J.L. (2010) 'High-dose carboplatin, thiotepa, and etoposide with autologous stem cell rescue for patients with previously irradiated recurrent medulloblastoma', *Neuro Oncol*, 12(3), pp. 297-303.

Ellison, D.W. (2010) 'Childhood medulloblastoma: novel approaches to the classification of a heterogeneous disease', *Acta Neuropathol*, 120(3), pp. 305-16.

Ellison, D.W., Kocak, M., Dalton, J., Megahed, H., Lusher, M.E., Ryan, S.L., Zhao, W., Nicholson, S.L., Taylor, R.E., Bailey, S. and Clifford, S.C. (2011) 'Definition of disease-risk stratification groups in childhood medulloblastoma using combined clinical, pathologic, and molecular variables', *J Clin Oncol*, 29(11), pp. 1400-7.

Ellison, D.W., Onilude, O.E., Lindsey, J.C., Lusher, M.E., Weston, C.L., Taylor, R.E., Pearson, A.D. and Clifford, S.C. (2005) 'beta-Catenin status predicts a favorable outcome in childhood medulloblastoma: the United Kingdom Children's Cancer Study Group Brain Tumour Committee', *J Clin Oncol*, 23(31), pp. 7951-7.

Esposito, M.T. and So, C.W. (2014) 'DNA damage accumulation and repair defects in acute myeloid leukemia: implications for pathogenesis, disease progression, and chemotherapy resistance', *Chromosoma*.

Etcheverry, A., Aubry, M., de Tayrac, M., Vauleon, E., Boniface, R., Guenot, F., Saikali, S., Hamlat, A., Riffaud, L., Menei, P., Quillien, V. and Mosser, J. (2010) 'DNA methylation in glioblastoma: impact on gene expression and clinical outcome', *BMC Genomics*, 11, p. 701.

Fabbri, M., Garzon, R., Cimmino, A., Liu, Z., Zanesi, N., Callegari, E., Liu, S., Alder, H., Costinean, S., Fernandez-Cymering, C., Volinia, S., Guler, G., Morrison, C.D., Chan, K.K., Marcucci, G., Calin, G.A., Huebner, K. and Croce, C.M. (2007) 'MicroRNA-29 family

reverts aberrant methylation in lung cancer by targeting DNA methyltransferases 3A and 3B', *Proc Natl Acad Sci U S A*, 104(40), pp. 15805-10.

Fangusaro, J. (2012) 'Pediatric high grade glioma: a review and update on tumor clinical characteristics and biology', *Front Oncol*, 2, p. 105.

Fattet, S., Haberler, C., Legoix, P., Varlet, P., Lellouch-Tubiana, A., Lair, S., Manie, E., Raquin, M.A., Bours, D., Carpentier, S., Barillot, E., Grill, J., Doz, F., Puget, S., Janoueix-Lerosey, I. and Delattre, O. (2009) 'Beta-catenin status in paediatric medulloblastomas: correlation of immunohistochemical expression with mutational status, genetic profiles, and clinical characteristics', *J Pathol*, 218(1), pp. 86-94.

Fearon, E.R. and Vogelstein, B. (1990) 'A genetic model for colorectal tumorigenesis', *Cell*, 61(5), pp. 759-67.

Feinberg, A.P. and Tycko, B. (2004) 'The history of cancer epigenetics', *Nat Rev Cancer*, 4(2), pp. 143-53.

Flagiello, D., Poupon, M.F., Cillo, C., Dutrillaux, B. and Malfoy, B. (1996) 'Relationship between DNA methylation and gene expression of the HOXB gene cluster in small cell lung cancers', *FEBS Lett*, 380(1-2), pp. 103-7.

Frank, A.J., Hernan, R., Hollander, A., Lindsey, J.C., Lusher, M.E., Fuller, C.E., Clifford, S.C. and Gilbertson, R.J. (2004) 'The TP53-ARF tumor suppressor pathway is frequently disrupted in large/cell anaplastic medulloblastoma', *Brain Res Mol Brain Res*, 121(1-2), pp. 137-40.

Gajjar, A., Chintagumpala, M., Ashley, D., Kellie, S., Kun, L.E., Merchant, T.E., Woo, S., Wheeler, G., Ahern, V., Krasin, M.J., Fouladi, M., Broniscer, A., Krance, R., Hale, G.A., Stewart, C.F., Dauser, R., Sanford, R.A., Fuller, C., Lau, C., Boyett, J.M., Wallace, D. and Gilbertson, R.J. (2006) 'Risk-adapted craniospinal radiotherapy followed by high-dose chemotherapy and stem-cell rescue in children with newly diagnosed medulloblastoma (St Jude Medulloblastoma-96): long-term results from a prospective, multicentre trial', *Lancet Oncol*, 7(10), pp. 813-20.

Gajjar, A., Mulhern, R.K., Heideman, R.L., Sanford, R.A., Douglass, E.C., Kovnar, E.H., Langston, J.A., Jenkins, J.J. and Kun, L.E. (1994) 'Medulloblastoma in very young children: outcome of definitive craniospinal irradiation following incomplete response to chemotherapy', *J Clin Oncol*, 12(6), pp. 1212-6.

Gajjar, A., Packer, R.J., Foreman, N.K., Cohen, K., Haas-Kogan, D. and Merchant, T.E. (2012) 'Children's Oncology Group's 2013 blueprint for research: Central nervous system tumors', *Pediatr Blood Cancer*.

Gajjar, A. and Pizer, B. (2010) 'Role of high-dose chemotherapy for recurrent medulloblastoma and other CNS primitive neuroectodermal tumors', *Pediatr Blood Cancer*, 54(4), pp. 649-51.

Gajjar, A., Stewart, C.F., Ellison, D.W., Kaste, S., Kun, L.E., Packer, R.J., Goldman, S., Chintagumpala, M., Wallace, D., Takebe, N., Boyett, J.M., Gilbertson, R.J. and Curran, T. (2013) 'Phase I study of vismodegib in children with recurrent or refractory medulloblastoma: a pediatric brain tumor consortium study', *Clin Cancer Res*, 19(22), pp. 6305-12.

Gandola, L., Massimino, M., Cefalo, G., Solero, C., Spreafico, F., Pecori, E., Riva, D., Collini, P., Pignoli, E., Giangaspero, F., Luksch, R., Berretta, S., Poggi, G., Biassoni, V., Ferrari, A., Pollo, B., Favre, C., Sardi, I., Terenziani, M. and Fossati-Bellani, F. (2009) 'Hyperfractionated accelerated radiotherapy in the Milan strategy for metastatic medulloblastoma', *J Clin Oncol*, 27(4), pp. 566-71.

Garzon, R., Liu, S., Fabbri, M., Liu, Z., Heaphy, C.E., Callegari, E., Schwind, S., Pang, J., Yu, J., Muthusamy, N., Havelange, V., Volinia, S., Blum, W., Rush, L.J., Perrotti, D., Andreeff, M., Bloomfield, C.D., Byrd, J.C., Chan, K., Wu, L.C., Croce, C.M. and Marcucci, G. (2009) 'MicroRNA-29b induces global DNA hypomethylation and tumor suppressor gene reexpression in acute myeloid leukemia by targeting directly DNMT3A and 3B and indirectly DNMT1', *Blood*, 113(25), pp. 6411-8.

Gibson, P., Tong, Y., Robinson, G., Thompson, M.C., Currle, D.S., Eden, C., Kranenburg, T.A., Hogg, T., Poppleton, H., Martin, J., Finkelstein, D., Pounds, S., Weiss, A., Patay, Z.,

Scoggins, M., Ogg, R., Pei, Y., Yang, Z.J., Brun, S., Lee, Y., Zindy, F., Lindsey, J.C., Taketo, M.M., Boop, F.A., Sanford, R.A., Gajjar, A., Clifford, S.C., Roussel, M.F., McKinnon, P.J., Gutmann, D.H., Ellison, D.W., Wechsler-Reya, R. and Gilbertson, R.J. (2010) 'Subtypes of medulloblastoma have distinct developmental origins', *Nature*, 468(7327), pp. 1095-9.

Gilbertson, R.J. and Rich, J.N. (2007) 'Making a tumour's bed: glioblastoma stem cells and the vascular niche', *Nat Rev Cancer*, 7(10), pp. 733-6.

Gonzalez, K.D., Noltner, K.A., Buzin, C.H., Gu, D., Wen-Fong, C.Y., Nguyen, V.Q., Han, J.H., Lowstuter, K., Longmate, J., Sommer, S.S. and Weitzel, J.N. (2009) 'Beyond Li Fraumeni Syndrome: clinical characteristics of families with p53 germline mutations', *J Clin Oncol*, 27(8), pp. 1250-6.

Goodrich, L.V., Milenkovic, L., Higgins, K.M. and Scott, M.P. (1997) 'Altered neural cell fates and medulloblastoma in mouse patched mutants', *Science*, 277(5329), pp. 1109-13.

Gordon, S.M., Chaix, J., Rupp, L.J., Wu, J., Madera, S., Sun, J.C., Lindsten, T. and Reiner, S.L. (2012) 'The transcription factors T-bet and Eomes control key checkpoints of natural killer cell maturation', *Immunity*, 36(1), pp. 55-67.

Gorovoy, I.R. and de Alba Campomanes, A. (2014) 'A potential life-saving diagnosis--recognizing Turcot syndrome', *J AAPOS*, 18(2), pp. 186-8.

Grammel, D., Warmuth-Metz, M., von Bueren, A.O., Kool, M., Pietsch, T., Kretzschmar, H.A., Rowitch, D.H., Rutkowski, S., Pfister, S.M. and Schuller, U. (2012) 'Sonic hedgehog-associated medulloblastoma arising from the cochlear nuclei of the brainstem', *Acta Neuropathol*, 123(4), pp. 601-14.

Greer, E.L. and Shi, Y. (2012) 'Histone methylation: a dynamic mark in health, disease and inheritance', *Nat Rev Genet*, 13(5), pp. 343-57.

Grill, J., Geoerger, B., Gesner, L., Perek, D., Leblond, P., Canete, A., Aerts, I., Madero, L., de Toledo Codina, J.S., Verlooy, J., Estlin, E., Cisar, L., Breazna, A., Dorman, A., Bailey, S., Nicolin, G., Grundy, R.G., Hargrave, D., European Consortium Innovative Therapies for Children with, C. and the European Society for Paediatric Oncology brain tumor, g. (2013) 'Phase II study of irinotecan in combination with temozolomide (TEMIRI) in children with recurrent or refractory medulloblastoma: a joint ITCC and SIOPE brain tumor study', *Neuro Oncol*, 15(9), pp. 1236-43.

Grodman, H., Wolfe, L. and Kretschmar, C. (2009) 'Outcome of patients with recurrent medulloblastoma or central nervous system germinoma treated with low dose continuous intravenous etoposide along with dose-intensive chemotherapy followed by autologous hematopoietic stem cell rescue', *Pediatr Blood Cancer*, 53(1), pp. 33-6.

Gros, C., Fahy, J., Halby, L., Dufau, I., Erdmann, A., Gregoire, J.M., Ausseil, F., Vispe, S. and Arimondo, P.B. (2012) 'DNA methylation inhibitors in cancer: recent and future approaches', *Biochimie*, 94(11), pp. 2280-96.

Grossmann, V., Kohlmann, A., Zenger, M., Schindela, S., Eder, C., Weissmann, S., Schnittger, S., Kern, W., Muller, M.C., Hochhaus, A., Haferlach, T. and Haferlach, C. (2011) 'A deep-sequencing study of chronic myeloid leukemia patients in blast crisis (BC-CML) detects mutations in 76.9% of cases', *Leukemia*, 25(3), pp. 557-60.

Hadnagy, A., Beaulieu, R. and Balicki, D. (2008) 'Histone tail modifications and noncanonical functions of histones: perspectives in cancer epigenetics', *Mol Cancer Ther*, 7(4), pp. 740-8.

Hallahan, A.R., Pritchard, J.I., Hansen, S., Benson, M., Stoeck, J., Hatton, B.A., Russell, T.L., Ellenbogen, R.G., Bernstein, I.D., Beachy, P.A. and Olson, J.M. (2004) 'The SmoA1 mouse model reveals that notch signaling is critical for the growth and survival of sonic hedgehog-induced medulloblastomas', *Cancer Res*, 64(21), pp. 7794-800.

Hanahan, D. and Weinberg, R.A. (2000) 'The hallmarks of cancer', *Cell*, 100(1), pp. 57-70.

Hanahan, D. and Weinberg, R.A. (2011) 'Hallmarks of cancer: the next generation', *Cell*, 144(5), pp. 646-74.

Hargrave, D. (2009) 'Paediatric high and low grade glioma: the impact of tumour biology on current and future therapy', *Br J Neurosurg*, 23(4), pp. 351-63.

Hasselblatt, M., Gesk, S., Oyen, F., Rossi, S., Viscardi, E., Giangaspero, F., Giannini, C., Judkins, A.R., Fruhwald, M.C., Obser, T., Schneppenheim, R., Siebert, R. and Paulus, W. (2011) 'Nonsense mutation and inactivation of SMARCA4 (BRG1) in an atypical teratoid/rhabdoid tumor showing retained SMARCB1 (INI1) expression', *Am J Surg Pathol*, 35(6), pp. 933-5.

Hatton, B.A., Villavicencio, E.H., Tsuchiya, K.D., Pritchard, J.I., Ditzler, S., Pullar, B., Hansen, S., Knoblaugh, S.E., Lee, D., Eberhart, C.G., Hallahan, A.R. and Olson, J.M. (2008) 'The Smo/Smo model: hedgehog-induced medulloblastoma with 90% incidence and leptomeningeal spread', *Cancer Res*, 68(6), pp. 1768-76.

Helms, A.W., Abney, A.L., Ben-Arie, N., Zoghbi, H.Y. and Johnson, J.E. (2000) 'Autoregulation and multiple enhancers control Math1 expression in the developing nervous system', *Development*, 127(6), pp. 1185-96.

Hoek, K., Rimm, D.L., Williams, K.R., Zhao, H., Ariyan, S., Lin, A., Kluger, H.M., Berger, A.J., Cheng, E., Trombetta, E.S., Wu, T., Niinobe, M., Yoshikawa, K., Hannigan, G.E. and Halaban, R. (2004) 'Expression profiling reveals novel pathways in the transformation of melanocytes to melanomas', *Cancer Res*, 64(15), pp. 5270-82.

Hoffman, L.M., Plimpton, S.R., Foreman, N.K., Stence, N.V., Hankinson, T.C., Handler, M.H., Hemenway, M.S., Vibhakar, R. and Liu, A.K. (2014) 'Fractionated stereotactic radiosurgery for recurrent ependymoma in children', *J Neurooncol*, 116(1), pp. 107-11.

Hoogaars, W.M., Barnett, P., Rodriguez, M., Clout, D.E., Moorman, A.F., Goding, C.R. and Christoffels, V.M. (2008) 'TBX3 and its splice variant TBX3 + exon 2a are functionally similar', *Pigment Cell Melanoma Res*, 21(3), pp. 379-87.

Hovestadt, V., Remke, M., Kool, M., Pietsch, T., Northcott, P.A., Fischer, R., Cavalli, F.M., Ramaswamy, V., Zapatka, M., Reifenberger, G., Rutkowski, S., Schick, M., Bewerunge-Hudler, M., Korshunov, A., Lichter, P., Taylor, M.D., Pfister, S.M. and Jones, D.T. (2013) 'Robust molecular subgrouping and copy-number profiling of medulloblastoma from small amounts of archival tumour material using high-density DNA methylation arrays', *Acta Neuropathol*, 125(6), pp. 913-6.

Huang, Y., Nayak, S., Jankowitz, R., Davidson, N.E. and Oesterreich, S. (2011) 'Epigenetics in breast cancer: what's new?', *Breast Cancer Res*, 13(6), p. 225.

Illumina (2010) *Infinium HD Assay Methylation Protocol Guide*.

Irizarry, R.A., Ladd-Acosta, C., Wen, B., Wu, Z., Montano, C., Onyango, P., Cui, H., Gabo, K., Rongione, M., Webster, M., Ji, H., Potash, J.B., Sabunciyan, S. and Feinberg, A.P. (2009) 'The human colon cancer methylome shows similar hypo- and hypermethylation at conserved tissue-specific CpG island shores', *Nat Genet*, 41(2), pp. 178-86.

Issa, J.P. (2004) 'CpG island methylator phenotype in cancer', *Nat Rev Cancer*, 4(12), pp. 988-93.

Ivascu, C., Wasserkort, R., Lesche, R., Dong, J., Stein, H., Thiel, A. and Eckhardt, F. (2007) 'DNA methylation profiling of transcription factor genes in normal lymphocyte development and lymphomas', *Int J Biochem Cell Biol*, 39(7-8), pp. 1523-38.

Jaffe, A.E., Murakami, P., Lee, H., Leek, J.T., Fallin, M.D., Feinberg, A.P. and Irizarry, R.A. (2012) 'Bump hunting to identify differentially methylated regions in epigenetic epidemiology studies', *Int J Epidemiol*, 41(1), pp. 200-9.

Jones, C. and Baker, S.J. (2014) 'Unique genetic and epigenetic mechanisms driving paediatric diffuse high-grade glioma', *Nat Rev Cancer*.

Jones, D.T., Jager, N., Kool, M., Zichner, T., Hutter, B., Sultan, M., Cho, Y.J., Pugh, T.J., Hovestadt, V., Stutz, A.M., Rausch, T., Warnatz, H.J., Ryzhova, M., Bender, S., Sturm, D.,

Pleier, S., Cin, H., Pfaff, E., Sieber, L., Wittmann, A., Remke, M., Witt, H., Hutter, S., Tzaridis, T., Weischenfeldt, J., Raeder, B., Avci, M., Amstislavskiy, V., Zapatka, M., Weber, U.D., Wang, Q., Lasitschka, B., Bartholomae, C.C., Schmidt, M., von Kalle, C., Ast, V., Lawerenz, C., Eils, J., Kabbe, R., Benes, V., van Sluis, P., Koster, J., Volckmann, R., Shih, D., Betts, M.J., Russell, R.B., Coco, S., Tonini, G.P., Schuller, U., Hans, V., Graf, N., Kim, Y.J., Monoranu, C., Roggendorf, W., Unterberg, A., Herold-Mende, C., Milde, T., Kulozik, A.E., von Deimling, A., Witt, O., Maass, E., Rossler, J., Ebinger, M., Schuhmann, M.U., Fruhwald, M.C., Hasselblatt, M., Jabado, N., Rutkowski, S., von Bueren, A.O., Williamson, D., Clifford, S.C., McCabe, M.G., Collins, V.P., Wolf, S., Wiemann, S., Lehrach, H., Brors, B., Scheurlen, W., Felsberg, J., Reifenberger, G., Northcott, P.A., Taylor, M.D., Meyerson, M., Pomeroy, S.L., Yaspo, M.L., Korbel, J.O., Korshunov, A., Eils, R., Pfister, S.M. and Lichter, P. (2012) 'Dissecting the genomic complexity underlying medulloblastoma', *Nature*, 488(7409), pp. 100-5.

Jones, P.A. and Baylin, S.B. (2007) 'The epigenomics of cancer', *Cell*, 128(4), pp. 683-92.

Jung, H.L., Wang, K.C., Kim, S.K., Sung, K.W., Koo, H.H., Shin, H.Y., Ahn, H.S., Shin, H.J. and Cho, B.K. (2004) 'Loss of heterozygosity analysis of chromosome 17p13.1-13.3 and its correlation with clinical outcome in medulloblastomas', *J Neurooncol*, 67(1-2), pp. 41-6.

Kandimalla, R., van Tilborg, A.A., Kompier, L.C., Stumpel, D.J., Stam, R.W., Bangma, C.H. and Zwarthoff, E.C. (2012) 'Genome-wide analysis of CpG island methylation in bladder cancer identified TBX2, TBX3, GATA2, and ZIC4 as pTa-specific prognostic markers', *Eur Urol*, 61(6), pp. 1245-56.

Kawauchi, D., Robinson, G., Uziel, T., Gibson, P., Rehg, J., Gao, C., Finkelstein, D., Qu, C., Pounds, S., Ellison, D.W., Gilbertson, R.J. and Roussel, M.F. (2012) 'A mouse model of the most aggressive subgroup of human medulloblastoma', *Cancer Cell*, 21(2), pp. 168-80.

Khoury, H.J., Cortes, J.E., Kantarjian, H.M., Gambacorti-Passerini, C., Baccarani, M., Kim, D.W., Zaritskey, A., Countouriotis, A., Besson, N., Leip, E., Kelly, V. and Brummendorf, T.H. (2012) 'Bosutinib is active in chronic phase chronic myeloid

leukemia after imatinib and dasatinib and/or nilotinib therapy failure', *Blood*, 119(15), pp. 3403-12.

Killela, P.J., Reitman, Z.J., Jiao, Y., Bettegowda, C., Agrawal, N., Diaz, L.A., Jr., Friedman, A.H., Friedman, H., Gallia, G.L., Giovanella, B.C., Grollman, A.P., He, T.C., He, Y., Hruban, R.H., Jallo, G.I., Mandahl, N., Meeker, A.K., Mertens, F., Netto, G.J., Rasheed, B.A., Riggins, G.J., Rosenquist, T.A., Schiffman, M., Shih Ie, M., Theodorescu, D., Torbenson, M.S., Velculescu, V.E., Wang, T.L., Wentzensen, N., Wood, L.D., Zhang, M., McLendon, R.E., Bigner, D.D., Kinzler, K.W., Vogelstein, B., Papadopoulos, N. and Yan, H. (2013) 'TERT promoter mutations occur frequently in gliomas and a subset of tumors derived from cells with low rates of self-renewal', *Proc Natl Acad Sci U S A*, 110(15), pp. 6021-6.

Kim, H., Kang, H.J., Lee, J.W., Park, J.D., Park, K.D., Shin, H.Y. and Ahn, H.S. (2013) 'Irinotecan, vincristine, cisplatin, cyclophosphamide, and etoposide for refractory or relapsed medulloblastoma/PNET in pediatric patients', *Childs Nerv Syst*, 29(10), pp. 1851-8.

Kirschbaum, M., Gojo, I., Goldberg, S.L., Bredeson, C., Kujawski, L.A., Yang, A., Marks, P., Frankel, P., Sun, X., Tosolini, A., Eid, J.E., Lubiniecki, G.M. and Issa, J.P. (2014) 'A phase 1 clinical trial of vorinostat in combination with decitabine in patients with acute myeloid leukaemia or myelodysplastic syndrome', *Br J Haematol*.

Kleinman, C.L., Gerges, N., Papillon-Cavanagh, S., Sin-Chan, P., Pramatarova, A., Quang, D.A., Adoue, V., Busche, S., Caron, M., Djambazian, H., Bemmo, A., Fontebasso, A.M., Spence, T., Schwartzentruber, J., Albrecht, S., Hauser, P., Garami, M., Klekner, A., Bognar, L., Montes, J.L., Staffa, A., Montpetit, A., Berube, P., Zakrzewska, M., Zakrzewski, K., Liberski, P.P., Dong, Z., Siegel, P.M., Duchaine, T., Perotti, C., Fleming, A., Faury, D., Remke, M., Gallo, M., Dirks, P., Taylor, M.D., Sladek, R., Pastinen, T., Chan, J.A., Huang, A., Majewski, J. and Jabado, N. (2014) 'Fusion of TTYH1 with the C19MC microRNA cluster drives expression of a brain-specific DNMT3B isoform in the embryonal brain tumor ETMR', *Nat Genet*, 46(1), pp. 39-44.

Kleinsmith, L.J. and Pierce, G.B., Jr. (1964) 'Multipotentiality of Single Embryonal Carcinoma Cells', *Cancer Res*, 24, pp. 1544-51.

Knight, S.J., Conklin, H.M., Palmer, S.L., Schreiber, J.E., Armstrong, C.L., Wallace, D., Bonner, M., Swain, M.A., Evankovich, K.D., Mabbott, D.J., Boyle, R., Huang, Q., Zhang, H., Anderson, V.A. and Gajjar, A. (2014) 'Working memory abilities among children treated for medulloblastoma: parent report and child performance', *J Pediatr Psychol*, 39(5), pp. 501-11.

Knudson, A.G., Jr. (1971) 'Mutation and cancer: statistical study of retinoblastoma', *Proc Natl Acad Sci U S A*, 68(4), pp. 820-3.

Koelsche, C., Sahm, F., Capper, D., Reuss, D., Sturm, D., Jones, D.T., Kool, M., Northcott, P.A., Wiestler, B., Bohmer, K., Meyer, J., Mawrin, C., Hartmann, C., Mittelbronn, M., Platten, M., Brokinkel, B., Seiz, M., Herold-Mende, C., Unterberg, A., Schittenhelm, J., Weller, M., Pfister, S., Wick, W., Korshunov, A. and von Deimling, A. (2013) 'Distribution of TERT promoter mutations in pediatric and adult tumors of the nervous system', *Acta Neuropathol*.

Kollareddy, M., Zheleva, D., Dzubak, P., Brahmkshatriya, P.S., Lepsik, M. and Hajduch, M. (2012) 'Aurora kinase inhibitors: progress towards the clinic', *Invest New Drugs*, 30(6), pp. 2411-32.

Kool, M., Jones, D.T., Jager, N., Northcott, P.A., Pugh, T.J., Hovestadt, V., Piro, R.M., Esparza, L.A., Markant, S.L., Remke, M., Milde, T., Bourdeaut, F., Ryzhova, M., Sturm, D., Pfaff, E., Stark, S., Hutter, S., Seker-Cin, H., Johann, P., Bender, S., Schmidt, C., Rausch, T., Shih, D., Reimand, J., Sieber, L., Wittmann, A., Linke, L., Witt, H., Weber, U.D., Zapatka, M., Konig, R., Beroukhim, R., Bergthold, G., van Sluis, P., Volckmann, R., Koster, J., Versteeg, R., Schmidt, S., Wolf, S., Lawerenz, C., Bartholomae, C.C., von Kalle, C., Unterberg, A., Herold-Mende, C., Hofer, S., Kulozik, A.E., von Deimling, A., Scheurlen, W., Felsberg, J., Reifenberger, G., Hasselblatt, M., Crawford, J.R., Grant, G.A., Jabado, N., Perry, A., Cowdrey, C., Croul, S., Zadeh, G., Korbel, J.O., Doz, F., Delattre, O., Bader, G.D., McCabe, M.G., Collins, V.P., Kieran, M.W., Cho, Y.J., Pomeroy, S.L., Witt, O., Brors, B., Taylor, M.D., Schuller, U., Korshunov, A., Eils, R., Wechsler-

Reya, R.J., Lichter, P., Pfister, S.M. and Project, I.P.T. (2014) 'Genome Sequencing of SHH Medulloblastoma Predicts Genotype-Related Response to Smoothened Inhibition', *Cancer Cell*, 25(3), pp. 393-405.

Kool, M., Korshunov, A., Remke, M., Jones, D.T., Schlanstein, M., Northcott, P.A., Cho, Y.J., Koster, J., Schouten-van Meeteren, A., van Vuurden, D., Clifford, S.C., Pietsch, T., von Bueren, A.O., Rutkowski, S., McCabe, M., Collins, V.P., Backlund, M.L., Haberler, C., Bourdeaut, F., Delattre, O., Doz, F., Ellison, D.W., Gilbertson, R.J., Pomeroy, S.L., Taylor, M.D., Lichter, P. and Pfister, S.M. (2012) 'Molecular subgroups of medulloblastoma: an international meta-analysis of transcriptome, genetic aberrations, and clinical data of WNT, SHH, Group 3, and Group 4 medulloblastomas', *Acta Neuropathol*, 123(4), pp. 473-84.

Kool, M., Koster, J., Bunt, J., Hasselt, N.E., Lakeman, A., van Sluis, P., Troost, D., Meeteren, N.S., Caron, H.N., Cloos, J., Mrsic, A., Ylstra, B., Grajkowska, W., Hartmann, W., Pietsch, T., Ellison, D., Clifford, S.C. and Versteeg, R. (2008) 'Integrated genomics identifies five medulloblastoma subtypes with distinct genetic profiles, pathway signatures and clinicopathological features', *PLoS One*, 3(8), p. e3088.

Korshunov, A., Benner, A., Remke, M., Lichter, P., von Deimling, A. and Pfister, S. (2008) 'Accumulation of genomic aberrations during clinical progression of medulloblastoma', *Acta Neuropathol*, 116(4), pp. 383-90.

Korshunov, A., Remke, M., Kool, M., Hielscher, T., Northcott, P.A., Williamson, D., Pfaff, E., Witt, H., Jones, D.T., Ryzhova, M., Cho, Y.J., Wittmann, A., Benner, A., Weiss, W.A., von Deimling, A., Scheurlen, W., Kulozik, A.E., Clifford, S.C., Peter Collins, V., Westermann, F., Taylor, M.D., Lichter, P. and Pfister, S.M. (2011) 'Biological and clinical heterogeneity of MYCN-amplified medulloblastoma', *Acta Neuropathol*.

Korshunov, A., Sturm, D., Ryzhova, M., Hovestadt, V., Gessi, M., Jones, D.T., Remke, M., Northcott, P., Perry, A., Picard, D., Rosenblum, M., Antonelli, M., Aronica, E., Schuller, U., Hasselblatt, M., Woehrer, A., Zheludkova, O., Kumirova, E., Puget, S., Taylor, M.D., Giangaspero, F., Peter Collins, V., von Deimling, A., Lichter, P., Huang, A., Pietsch, T., Pfister, S.M. and Kool, M. (2014) 'Embryonal tumor with abundant neuropil and true

rosettes (ETANTR), ependymoblastoma, and medulloepithelioma share molecular similarity and comprise a single clinicopathological entity', *Acta Neuropathol*, 128(2), pp. 279-89.

Krueger, F., Kreck, B., Franke, A. and Andrews, S.R. (2012) 'DNA methylome analysis using short bisulfite sequencing data', *Nat Methods*, 9(2), pp. 145-51.

Kujawski, L. and Talpaz, M. (2007) 'Strategies for overcoming imatinib resistance in chronic myeloid leukemia', *Leuk Lymphoma*, 48(12), pp. 2310-22.

Kulis, M., Heath, S., Bibikova, M., Queiros, A.C., Navarro, A., Clot, G., Martinez-Trillos, A., Castellano, G., Brun-Heath, I., Pinyol, M., Barberan-Soler, S., Papasaikas, P., Jares, P., Bea, S., Rico, D., Ecker, S., Rubio, M., Royo, R., Ho, V., Klotzle, B., Hernandez, L., Conde, L., Lopez-Guerra, M., Colomer, D., Villamor, N., Aymerich, M., Rozman, M., Bayes, M., Gut, M., Gelpi, J.L., Orozco, M., Fan, J.B., Quesada, V., Puente, X.S., Pisano, D.G., Valencia, A., Lopez-Guillermo, A., Gut, I., Lopez-Otin, C., Campo, E. and Martin-Subero, J.I. (2012) 'Epigenomic analysis detects widespread gene-body DNA hypomethylation in chronic lymphocytic leukemia', *Nat Genet*, 44(11), pp. 1236-42.

Kunkele, A., De Preter, K., Heukamp, L., Thor, T., Pajtler, K.W., Hartmann, W., Mittelbronn, M., Grotzer, M.A., Deubzer, H.E., Speleman, F., Schramm, A., Eggert, A. and Schulte, J.H. (2012) 'Pharmacological activation of the p53 pathway by nutlin-3 exerts anti-tumoral effects in medulloblastomas', *Neuro Oncol*, 14(7), pp. 859-69.

Laird, P.W. (2010) 'Principles and challenges of genomewide DNA methylation analysis', *Nat Rev Genet*, 11(3), pp. 191-203.

Lamont, J.M., McManamy, C.S., Pearson, A.D., Clifford, S.C. and Ellison, D.W. (2004) 'Combined histopathological and molecular cytogenetic stratification of medulloblastoma patients', *Clin Cancer Res*, 10(16), pp. 5482-93.

Langdon, J.A., Lamont, J.M., Scott, D.K., Dyer, S., Prebble, E., Bown, N., Grundy, R.G., Ellison, D.W. and Clifford, S.C. (2006) 'Combined genome-wide allelotyping and copy

number analysis identify frequent genetic losses without copy number reduction in medulloblastoma', *Genes Chromosomes Cancer*, 45(1), pp. 47-60.

Lannering, B., Rutkowski, S., Doz, F., Pizer, B., Gustafsson, G., Navajas, A., Massimino, M., Reddingius, R., Benesch, M., Carrie, C., Taylor, R., Gandola, L., Bjork-Eriksson, T., Giralt, J., Oldenburger, F., Pietsch, T., Figarella-Branger, D., Robson, K., Forni, M., Clifford, S.C., Warmuth-Metz, M., von Hoff, K., Faldum, A., Mosseri, V. and Kortmann, R. (2012) 'Hyperfractionated versus conventional radiotherapy followed by chemotherapy in standard-risk medulloblastoma: results from the randomized multicenter HIT-SIOP PNET 4 trial', *J Clin Oncol*, 30(26), pp. 3187-93.

Lastowska, M., Al-Afghani, H., Al-Balool, H.H., Sheth, H., Mercer, E., Coxhead, J.M., Redfern, C.P., Peters, H., Burt, A.D., Santibanez-Koref, M., Bacon, C.M., Chesler, L., Rust, A.G., Adams, D.J., Williamson, D., Clifford, S.C. and Jackson, M.S. (2013) 'Identification of a neuronal transcription factor network involved in medulloblastoma development', *Acta Neuropathol Commun*, 1(1), p. 35.

Leary, S.E., Zhou, T., Holmes, E., Geyer, J.R. and Miller, D.C. (2011) 'Histology predicts a favorable outcome in young children with desmoplastic medulloblastoma: a report from the children's oncology group', *Cancer*, 117(14), pp. 3262-7.

Levan, A., Nichols, W. and Norden, A. (1963) 'A case of chronic myeloid leukemia with two leukemic stemlines in the blood', *Hereditas*, 49(3), pp. 433-441.

Levesley, J., Lusher, M.E., Lindsey, J.C., Clifford, S.C., Grundy, R. and Coyle, B. (2011) 'RASSF1A and the BH3-only mimetic ABT-737 promote apoptosis in pediatric medulloblastoma cell lines', *Neuro Oncol*, 13(12), pp. 1265-76.

Lindsey, J.C., Anderton, J.A., Lusher, M.E. and Clifford, S.C. (2005) 'Epigenetic events in medulloblastoma development', *Neurosurg Focus*, 19(5), p. E10.

Lindsey, J.C., Hill, R.M., Megahed, H., Lusher, M.E., Schwalbe, E.C., Cole, M., Hogg, T.L., Gilbertson, R.J., Ellison, D.W., Bailey, S. and Clifford, S.C. (2011) 'TP53 mutations in

favorable-risk Wnt/Wingless-subtype medulloblastomas', *J Clin Oncol*, 29(12), pp. e344-6; author reply e347-8.

Lindsey, J.C., Schwalbe, E.C., Potluri, S., Bailey, S., Williamson, D. and Clifford, S.C. (2014) 'TERT promoter mutation and aberrant hypermethylation are associated with elevated expression in medulloblastoma and characterise the majority of non-infant SHH subgroup tumours', *Acta Neuropathol*, 127(2), pp. 307-9.

Lingbeek, M.E., Jacobs, J.J. and van Lohuizen, M. (2002) 'The T-box repressors TBX2 and TBX3 specifically regulate the tumor suppressor gene p14ARF via a variant T-site in the initiator', *J Biol Chem*, 277(29), pp. 26120-7.

Liu, J., Esmailpour, T., Shang, X., Gulsen, G., Liu, A. and Huang, T. (2011) 'TBX3 over-expression causes mammary gland hyperplasia and increases mammary stem-like cells in an inducible transgenic mouse model', *BMC Dev Biol*, 11, p. 65.

Louis, D.N., Ohgaki, H., Wiestler, O.D., Cavenee, W.K., Burger, P.C., Jouvet, A., Scheithauer, B.W. and Kleihues, P. (2007) 'The 2007 WHO classification of tumours of the central nervous system', *Acta Neuropathol*, 114(2), pp. 97-109.

Low, J.A. and de Sauvage, F.J. (2010) 'Clinical experience with Hedgehog pathway inhibitors', *J Clin Oncol*, 28(36), pp. 5321-6.

Lowe, S.W., Bodis, S., McClatchey, A., Remington, L., Ruley, H.E., Fisher, D.E., Housman, D.E. and Jacks, T. (1994) 'p53 status and the efficacy of cancer therapy in vivo', *Science*, 266(5186), pp. 807-10.

Lu, J., Li, X.P., Dong, Q., Kung, H.F. and He, M.L. (2010) 'TBX2 and TBX3: the special value for anticancer drug targets', *Biochim Biophys Acta*, 1806(2), pp. 268-74.

Mack, S.C., Witt, H., Piro, R.M., Gu, L., Zuyderduyn, S., Stutz, A.M., Wang, X., Gallo, M., Garzia, L., Zayne, K., Zhang, X., Ramaswamy, V., Jager, N., Jones, D.T., Sill, M., Pugh, T.J., Ryzhova, M., Wani, K.M., Shih, D.J., Head, R., Remke, M., Bailey, S.D., Zichner, T., Faria, C.C., Barszczyk, M., Stark, S., Seker-Cin, H., Hutter, S., Johann, P., Bender, S.,

Hovestadt, V., Tzaridis, T., Dubuc, A.M., Northcott, P.A., Peacock, J., Bertrand, K.C., Agnihotri, S., Cavalli, F.M., Clarke, I., Nethery-Brokx, K., Creasy, C.L., Verma, S.K., Koster, J., Wu, X., Yao, Y., Milde, T., Sin-Chan, P., Zuccaro, J., Lau, L., Pereira, S., Castelo-Branco, P., Hirst, M., Marra, M.A., Roberts, S.S., Fults, D., Massimi, L., Cho, Y.J., Van Meter, T., Grajkowska, W., Lach, B., Kulozik, A.E., von Deimling, A., Witt, O., Scherer, S.W., Fan, X., Muraszko, K.M., Kool, M., Pomeroy, S.L., Gupta, N., Phillips, J., Huang, A., Tabori, U., Hawkins, C., Malkin, D., Kongkham, P.N., Weiss, W.A., Jabado, N., Rutka, J.T., Bouffet, E., Korbel, J.O., Lupien, M., Aldape, K.D., Bader, G.D., Eils, R., Lichter, P., Dirks, P.B., Pfister, S.M., Korshunov, A. and Taylor, M.D. (2014) 'Epigenomic alterations define lethal CIMP-positive ependymomas of infancy', *Nature*, 506(7489), pp. 445-50.

Maksimovic, J., Gordon, L. and Oshlack, A. (2012) 'SWAN: Subset-quantile within array normalization for illumina infinium HumanMethylation450 BeadChips', *Genome Biol*, 13(6), p. R44.

Malaise, M., Rovira, J., Renner, P., Eggenhofer, E., Sabet-Baktach, M., Lantow, M., Lang, S.A., Koehl, G.E., Farkas, S.A., Loss, M., Agha, A., Campistol, J.M., Schlitt, H.J., Geissler, E.K. and Kroemer, A. (2014) 'KLRG1+ NK cells protect T-bet-deficient mice from pulmonary metastatic colorectal carcinoma', *J Immunol*, 192(4), pp. 1954-61.

Malkin, D. (2011) 'Li-fraumeni syndrome', *Genes Cancer*, 2(4), pp. 475-84.

Manoranjan, B., Venugopal, C., McFarlane, N., Doble, B.W., Dunn, S.E., Scheinemann, K. and Singh, S.K. (2012) 'Medulloblastoma stem cells: where development and cancer cross pathways', *Pediatr Res*, 71(4 Pt 2), pp. 516-22.

Martinez-Garcia, E. and Licht, J.D. (2010) 'Deregulation of H3K27 methylation in cancer', *Nat Genet*, 42(2), pp. 100-1.

Massimino, M., Gandola, L., Spreafico, F., Biassoni, V., Luksch, R., Collini, P., Solero, C.N., Simonetti, F., Pignoli, E., Cefalo, G., Poggi, G., Modena, P., Mariani, L., Potepan, P., Podda, M., Casanova, M., Pecori, E., Acerno, S., Ferrari, A., Terenziani, M., Meazza, C., Polastri, D., Ravagnani, F. and Fossati-Bellani, F. (2009) 'No salvage using high-dose

chemotherapy plus/minus reirradiation for relapsing previously irradiated medulloblastoma', *Int J Radiat Oncol Biol Phys*, 73(5), pp. 1358-63.

McManamy, C.S., Pears, J., Weston, C.L., Hanzely, Z., Ironside, J.W., Taylor, R.E., Grundy, R.G., Clifford, S.C. and Ellison, D.W. (2007) 'Nodule formation and desmoplasia in medulloblastomas-defining the nodular/desmoplastic variant and its biological behavior', *Brain Pathol*, 17(2), pp. 151-64.

Merchant, T.E., Boop, F.A., Kun, L.E. and Sanford, R.A. (2008) 'A retrospective study of surgery and reirradiation for recurrent ependymoma', *Int J Radiat Oncol Biol Phys*, 71(1), pp. 87-97.

Messahel, B., Ashley, S., Saran, F., Ellison, D., Ironside, J., Phipps, K., Cox, T., Chong, W.K., Robinson, K., Picton, S., Pinkerton, C.R., Mallucci, C., Macarthur, D., Jaspan, T., Michalski, A., Grundy, R.G. and Children's Cancer Leukaemia Group Brain Tumour, C. (2009) 'Relapsed intracranial ependymoma in children in the UK: patterns of relapse, survival and therapeutic outcome', *Eur J Cancer*, 45(10), pp. 1815-23.

Milde, T., Pfister, S., Korshunov, A., Deubzer, H.E., Oehme, I., Ernst, A., Starzinski-Powitz, A., Seitz, A., Lichter, P., von Deimling, A. and Witt, O. (2009) 'Stepwise accumulation of distinct genomic aberrations in a patient with progressively metastasizing ependymoma', *Genes Chromosomes Cancer*, 48(3), pp. 229-38.

Morfouace, M., Shelat, A., Jacus, M., Freeman, B.B., 3rd, Turner, D., Robinson, S., Zindy, F., Wang, Y.D., Finkelstein, D., Ayrault, O., Bihannic, L., Puget, S., Li, X.N., Olson, J.M., Robinson, G.W., Guy, R.K., Stewart, C.F., Gajjar, A. and Roussel, M.F. (2014) 'Pemetrexed and gemcitabine as combination therapy for the treatment of group3 medulloblastoma', *Cancer Cell*, 25(4), pp. 516-29.

Muller, K., Mynarek, M., Zwiener, I., Siegler, N., Zimmermann, M., Christiansen, H., Budach, W., Henke, G., Warmuth-Metz, M., Pietsch, T., von Hoff, K., von Bueren, A., Bode, U., Rutkowski, S., Kortmann, R.D., Fleischhack, G. and Tippelt, S. (2014) 'Postponed is not canceled: role of craniospinal radiation therapy in the management

of recurrent infant medulloblastoma--an experience from the HIT-REZ 1997 & 2005 studies', *Int J Radiat Oncol Biol Phys*, 88(5), pp. 1019-24.

Mullis, K., Faloona, F., Scharf, S., Saiki, R., Horn, G. and Erlich, H. (1986) 'Specific enzymatic amplification of DNA in vitro: the polymerase chain reaction', *Cold Spring Harb Symp Quant Biol*, 51 Pt 1, pp. 263-73.

Ng, J.M. and Curran, T. (2011) 'The Hedgehog's tale: developing strategies for targeting cancer', *Nat Rev Cancer*, 11(7), pp. 493-501.

Nguyen, L.V., Vanner, R., Dirks, P. and Eaves, C.J. (2012) 'Cancer stem cells: an evolving concept', *Nat Rev Cancer*, 12(2), pp. 133-43.

Nicholson, J., Wickramasinghe, C., Ross, F., Crolla, J. and Ellison, D. (2000) 'Imbalances of chromosome 17 in medulloblastomas determined by comparative genomic hybridisation and fluorescence in situ hybridisation', *Mol Pathol*, 53(6), pp. 313-9.

Northcott, P.A., Hielscher, T., Dubuc, A., Mack, S., Shih, D., Remke, M., Al-Halabi, H., Albrecht, S., Jabado, N., Eberhart, C.G., Grajkowska, W., Weiss, W.A., Clifford, S.C., Bouffet, E., Rutka, J.T., Korshunov, A., Pfister, S. and Taylor, M.D. (2011a) 'Pediatric and adult sonic hedgehog medulloblastomas are clinically and molecularly distinct', *Acta Neuropathol*, 122(2), pp. 231-40.

Northcott, P.A., Jones, D.T., Kool, M., Robinson, G.W., Gilbertson, R.J., Cho, Y.J., Pomeroy, S.L., Korshunov, A., Lichter, P., Taylor, M.D. and Pfister, S.M. (2012a) 'Medulloblastomics: the end of the beginning', *Nat Rev Cancer*, 12(12), pp. 818-34.

Northcott, P.A., Korshunov, A., Witt, H., Hielscher, T., Eberhart, C.G., Mack, S., Bouffet, E., Clifford, S.C., Hawkins, C.E., French, P., Rutka, J.T., Pfister, S. and Taylor, M.D. (2011b) 'Medulloblastoma comprises four distinct molecular variants', *J Clin Oncol*, 29(11), pp. 1408-14.

Northcott, P.A., Shih, D.J., Peacock, J., Garzia, L., Morrissy, A.S., Zichner, T., Stutz, A.M., Korshunov, A., Reimand, J., Schumacher, S.E., Beroukhim, R., Ellison, D.W., Marshall,

C.R., Lionel, A.C., Mack, S., Dubuc, A., Yao, Y., Ramaswamy, V., Luu, B., Rolider, A., Cavalli, F.M., Wang, X., Remke, M., Wu, X., Chiu, R.Y., Chu, A., Chuah, E., Corbett, R.D., Hoad, G.R., Jackman, S.D., Li, Y., Lo, A., Mungall, K.L., Nip, K.M., Qian, J.Q., Raymond, A.G., Thiessen, N.T., Varhol, R.J., Birol, I., Moore, R.A., Mungall, A.J., Holt, R., Kawauchi, D., Roussel, M.F., Kool, M., Jones, D.T., Witt, H., Fernandez, L.A., Kenney, A.M., Wechsler-Reya, R.J., Dirks, P., Aviv, T., Grajkowska, W.A., Perek-Polnik, M., Haberler, C.C., Delattre, O., Reynaud, S.S., Doz, F.F., Pernet-Fattet, S.S., Cho, B.K., Kim, S.K., Wang, K.C., Scheurlen, W., Eberhart, C.G., Fevre-Montange, M., Jouvet, A., Pollack, I.F., Fan, X., Muraszko, K.M., Gillespie, G.Y., Di Rocco, C., Massimi, L., Michiels, E.M., Kloosterhof, N.K., French, P.J., Kros, J.M., Olson, J.M., Ellenbogen, R.G., Zitterbart, K., Kren, L., Thompson, R.C., Cooper, M.K., Lach, B., McLendon, R.E., Bigner, D.D., Fontebasso, A., Albrecht, S., Jabado, N., Lindsey, J.C., Bailey, S., Gupta, N., Weiss, W.A., Bognar, L., Klekner, A., Van Meter, T.E., Kumabe, T., Tominaga, T., Elbabaa, S.K., Leonard, J.R., Rubin, J.B., et al. (2012b) 'Subgroup-specific structural variation across 1,000 medulloblastoma genomes', *Nature*, 488(7409), pp. 49-56.

Northcott, P.A., Shih, D.J., Remke, M., Cho, Y.J., Kool, M., Hawkins, C., Eberhart, C.G., Dubuc, A., Guettouche, T., Cardentey, Y., Bouffet, E., Pomeroy, S.L., Marra, M., Malkin, D., Rutka, J.T., Korshunov, A., Pfister, S. and Taylor, M.D. (2011c) 'Rapid, reliable, and reproducible molecular sub-grouping of clinical medulloblastoma samples', *Acta Neuropathol*.

Nowell, P. and Hungerford, D. (1960) 'A minute chromosome in human chronic granulocytic leukemia', *Science*, 132, p. 1497.

Nowell, P.C. (1976) 'The clonal evolution of tumor cell populations', *Science*, 194(4260), pp. 23-8.

Otto, T., Horn, S., Brockmann, M., Eilers, U., Schuttrumpf, L., Popov, N., Kenney, A.M., Schulte, J.H., Beijersbergen, R., Christiansen, H., Berwanger, B. and Eilers, M. (2009) 'Stabilization of N-Myc is a critical function of Aurora A in human neuroblastoma', *Cancer Cell*, 15(1), pp. 67-78.

Packer, R.J., Gajjar, A., Vezina, G., Rorke-Adams, L., Burger, P.C., Robertson, P.L., Bayer, L., LaFond, D., Donahue, B.R., Marymont, M.H., Muraszko, K., Langston, J. and Sposto, R. (2006) 'Phase III study of craniospinal radiation therapy followed by adjuvant chemotherapy for newly diagnosed average-risk medulloblastoma', *J Clin Oncol*, 24(25), pp. 4202-8.

Padovani, L., Andre, N., Gentet, J.C., Figarella Branger, D., Scavarda, D., Verschuur, A., Chinot, O., Cowen, D. and Muracciole, X. (2011) 'Reirradiation and concomitant metronomic temozolomide: an efficient combination for local control in medulloblastoma disease?', *J Pediatr Hematol Oncol*, 33(8), pp. 600-4.

Panigrahy, A., Krieger, M.D., Gonzalez-Gomez, I., Liu, X., McComb, J.G., Finlay, J.L., Nelson, M.D., Jr., Gilles, F.H. and Bluml, S. (2006) 'Quantitative short echo time 1H-MR spectroscopy of untreated pediatric brain tumors: preoperative diagnosis and characterization', *AJNR Am J Neuroradiol*, 27(3), pp. 560-72.

Parker, M., Mohankumar, K.M., Punchihewa, C., Weinlich, R., Dalton, J.D., Li, Y., Lee, R., Tatevossian, R.G., Phoenix, T.N., Thiruvenkatam, R., White, E., Tang, B., Orisme, W., Gupta, K., Rusch, M., Chen, X., Li, Y., Nagahawhatte, P., Hedlund, E., Finkelstein, D., Wu, G., Shurtleff, S., Easton, J., Boggs, K., Yergeau, D., Vadodaria, B., Mulder, H.L., Becksford, J., Gupta, P., Huether, R., Ma, J., Song, G., Gajjar, A., Merchant, T., Boop, F., Smith, A.A., Ding, L., Lu, C., Ochoa, K., Zhao, D., Fulton, R.S., Fulton, L.L., Mardis, E.R., Wilson, R.K., Downing, J.R., Green, D.R., Zhang, J., Ellison, D.W. and Gilbertson, R.J. (2014) 'C11orf95-RELA fusions drive oncogenic NF-kappaB signalling in ependymoma', *Nature*, 506(7489), pp. 451-5.

Parsons, D.W., Li, M., Zhang, X., Jones, S., Leary, R.J., Lin, J.C., Boca, S.M., Carter, H., Samayoa, J., Bettegowda, C., Gallia, G.L., Jallo, G.I., Binder, Z.A., Nikolsky, Y., Hartigan, J., Smith, D.R., Gerhard, D.S., Fults, D.W., VandenBerg, S., Berger, M.S., Marie, S.K., Shinjo, S.M., Clara, C., Phillips, P.C., Minturn, J.E., Biegel, J.A., Judkins, A.R., Resnick, A.C., Storm, P.B., Curran, T., He, Y., Rasheed, B.A., Friedman, H.S., Keir, S.T., McLendon, R., Northcott, P.A., Taylor, M.D., Burger, P.C., Riggins, G.J., Karchin, R., Parmigiani, G., Bigner, D.D., Yan, H., Papadopoulos, N., Vogelstein, B., Kinzler, K.W. and Velculescu,

V.E. (2011) 'The genetic landscape of the childhood cancer medulloblastoma', *Science*, 331(6016), pp. 435-9.

Pei, Y., Moore, C.E., Wang, J., Tewari, A.K., Eroshkin, A., Cho, Y.J., Witt, H., Korshunov, A., Read, T.A., Sun, J.L., Schmitt, E.M., Miller, C.R., Buckley, A.F., McLendon, R.E., Westbrook, T.F., Northcott, P.A., Taylor, M.D., Pfister, S.M., Febbo, P.G. and Wechsler-Reya, R.J. (2012) 'An animal model of MYC-driven medulloblastoma', *Cancer Cell*, 21(2), pp. 155-67.

Pelengaris, S. and Khan, M. (2006) *The Molecular Biology of Cancer*. Wiley-Blackwell.

Peres, J., Davis, E., Mowla, S., Bennett, D.C., Li, J.A., Wansleben, S. and Prince, S. (2010) 'The Highly Homologous T-Box Transcription Factors, TBX2 and TBX3, Have Distinct Roles in the Oncogenic Process', *Genes Cancer*, 1(3), pp. 272-82.

Peres, J. and Prince, S. (2013) 'The T-box transcription factor, TBX3, is sufficient to promote melanoma formation and invasion', *Mol Cancer*, 12(1), p. 117.

Perreault, S., Lober, R.M., Carret, A.S., Zhang, G., Hershon, L., Decarie, J.C., Yeom, K., Vogel, H., Fisher, P.G. and Partap, S. (2013) 'Relapse patterns in pediatric embryonal central nervous system tumors', *J Neurooncol*, 115(2), pp. 209-15.

Peters, U., Jiao, S., Schumacher, F.R., Hutter, C.M., Aragaki, A.K., Baron, J.A., Berndt, S.I., Bezieau, S., Brenner, H., Butterbach, K., Caan, B.J., Campbell, P.T., Carlson, C.S., Casey, G., Chan, A.T., Chang-Claude, J., Chanock, S.J., Chen, L.S., Coetzee, G.A., Coetzee, S.G., Conti, D.V., Curtis, K.R., Duggan, D., Edwards, T., Fuchs, C.S., Gallinger, S., Giovannucci, E.L., Gogarten, S.M., Gruber, S.B., Haile, R.W., Harrison, T.A., Hayes, R.B., Henderson, B.E., Hoffmeister, M., Hopper, J.L., Hudson, T.J., Hunter, D.J., Jackson, R.D., Jee, S.H., Jenkins, M.A., Jia, W.H., Kolonel, L.N., Kooperberg, C., Kury, S., Lacroix, A.Z., Laurie, C.C., Laurie, C.A., Le Marchand, L., Lemire, M., Levine, D., Lindor, N.M., Liu, Y., Ma, J., Makar, K.W., Matsuo, K., Newcomb, P.A., Potter, J.D., Prentice, R.L., Qu, C., Rohan, T., Rosse, S.A., Schoen, R.E., Seminara, D., Shrubsole, M., Shu, X.O., Slattery, M.L., Taverna, D., Thibodeau, S.N., Ulrich, C.M., White, E., Xiang, Y., Zanke, B.W., Zeng, Y.X., Zhang, B., Zheng, W., Hsu, L., Colon Cancer Family, R., the, G. and Epidemiology of

Colorectal Cancer, C. (2013) 'Identification of Genetic Susceptibility Loci for Colorectal Tumors in a Genome-Wide Meta-analysis', *Gastroenterology*, 144(4), pp. 799-807 e24.

Petroni, M., Veschi, V., Gulino, A. and Giannini, G. (2012) 'Molecular mechanisms of MYCN-dependent apoptosis and the MDM2-p53 pathway: an Achille's heel to be exploited for the therapy of MYCN-amplified neuroblastoma', *Front Oncol*, 2, p. 141.

Pezzolo, A., Coco, S., Raso, A., Parodi, F., Pistorio, A., Valdora, F., Capra, V., Zollo, M., Aschero, S., Basso, E., Cama, A., Nozza, P., Gambini, C., Cinalli, G., Garre, M.L., Iolascon, A., Pistoia, V. and Tonini, G.P. (2011) 'Loss of 10q26.1-q26.3 in association with 7q34-q36.3 gain or 17q24.3-q25.3 gain predict poor outcome in pediatric medulloblastoma', *Cancer Lett*, 308(2), pp. 215-24.

Pfaff, E., Remke, M., Sturm, D., Benner, A., Witt, H., Milde, T., von Bueren, A.O., Wittmann, A., Schottler, A., Jorch, N., Graf, N., Kulozik, A.E., Witt, O., Scheurlen, W., von Deimling, A., Rutkowski, S., Taylor, M.D., Tabori, U., Lichter, P., Korshunov, A. and Pfister, S.M. (2010) 'TP53 mutation is frequently associated with CTNNB1 mutation or MYCN amplification and is compatible with long-term survival in medulloblastoma', *J Clin Oncol*, 28(35), pp. 5188-96.

Pfister, S., Remke, M., Benner, A., Mendrzyk, F., Toedt, G., Felsberg, J., Wittmann, A., Devens, F., Gerber, N.U., Joos, S., Kulozik, A., Reifenberger, G., Rutkowski, S., Wiestler, O.D., Radlwimmer, B., Scheurlen, W., Lichter, P. and Korshunov, A. (2009) 'Outcome prediction in pediatric medulloblastoma based on DNA copy-number aberrations of chromosomes 6q and 17q and the MYC and MYCN loci', *J Clin Oncol*, 27(10), pp. 1627-36.

Phillips, H.S., Kharbanda, S., Chen, R., Forrest, W.F., Soriano, R.H., Wu, T.D., Misra, A., Nigro, J.M., Colman, H., Soroceanu, L., Williams, P.M., Modrusan, Z., Feuerstein, B.G. and Aldape, K. (2006) 'Molecular subclasses of high-grade glioma predict prognosis, delineate a pattern of disease progression, and resemble stages in neurogenesis', *Cancer Cell*, 9(3), pp. 157-73.

Picard, D., Miller, S., Hawkins, C.E., Bouffet, E., Rogers, H.A., Chan, T.S., Kim, S.K., Ra, Y.S., Fangusaro, J., Korshunov, A., Toledano, H., Nakamura, H., Hayden, J.T., Chan, J., Lafay-Cousin, L., Hu, P., Fan, X., Muraszko, K.M., Pomeroy, S.L., Lau, C.C., Ng, H.K., Jones, C., Van Meter, T., Clifford, S.C., Eberhart, C., Gajjar, A., Pfister, S.M., Grundy, R.G. and Huang, A. (2012) 'Markers of survival and metastatic potential in childhood CNS primitive neuro-ectodermal brain tumours: an integrative genomic analysis', *Lancet Oncol*, 13(8), pp. 838-48.

Piekarz, R.L., Robey, R.W., Zhan, Z., Kayastha, G., Sayah, A., Abdeldaim, A.H., Torrico, S. and Bates, S.E. (2004) 'T-cell lymphoma as a model for the use of histone deacetylase inhibitors in cancer therapy: impact of depsipeptide on molecular markers, therapeutic targets, and mechanisms of resistance', *Blood*, 103(12), pp. 4636-43.

Pinkerton, R., Shankar, A. and Matthay, K. (2007) *Evidence-based Pediatric Oncology*. Second edn. Blackwell Publishing.

Pizer, B. and Clifford, S. (2008) 'Medulloblastoma: new insights into biology and treatment', *Arch Dis Child Educ Pract Ed*, 93(5), pp. 137-44.

Pizer, B., Donachie, P.H., Robinson, K., Taylor, R.E., Michalski, A., Punt, J., Ellison, D.W. and Picton, S. (2011a) 'Treatment of recurrent central nervous system primitive neuroectodermal tumours in children and adolescents: results of a Children's Cancer and Leukaemia Group study', *Eur J Cancer*, 47(9), pp. 1389-97.

Pizer, B., Traunecker, H. and Saran, F. (2011b) *CCLG guidelines for standard risk medulloblastoma (for children 3 years of age and older)*. Group, C.P.

Pizer, B.L. and Clifford, S.C. (2009) 'The potential impact of tumour biology on improved clinical practice for medulloblastoma: progress towards biologically driven clinical trials', *Br J Neurosurg*, 23(4), pp. 364-75.

Plass, C., Pfister, S.M., Lindroth, A.M., Bogatyrova, O., Claus, R. and Lichter, P. (2013) 'Mutations in regulators of the epigenome and their connections to global chromatin patterns in cancer', *Nat Rev Genet*, 14(11), pp. 765-80.

Poschl, J., Stark, S., Neumann, P., Grobner, S., Kawauchi, D., Jones, D.T., Northcott, P.A., Lichter, P., Pfister, S.M., Kool, M. and Schuller, U. (2014) 'Genomic and transcriptomic analyses match medulloblastoma mouse models to their human counterparts', *Acta Neuropathol*, 128(1), pp. 123-36.

Pugh, T.J., Weeraratne, S.D., Archer, T.C., Pomeranz Krummel, D.A., Auclair, D., Bochicchio, J., Carneiro, M.O., Carter, S.L., Cibulskis, K., Erlich, R.L., Greulich, H., Lawrence, M.S., Lennon, N.J., McKenna, A., Meldrim, J., Ramos, A.H., Ross, M.G., Russ, C., Shefler, E., Sivachenko, A., Sogoloff, B., Stojanov, P., Tamayo, P., Mesirov, J.P., Amani, V., Teider, N., Sengupta, S., Francois, J.P., Northcott, P.A., Taylor, M.D., Yu, F., Crabtree, G.R., Kautzman, A.G., Gabriel, S.B., Getz, G., Jager, N., Jones, D.T., Lichter, P., Pfister, S.M., Roberts, T.M., Meyerson, M., Pomeroy, S.L. and Cho, Y.J. (2012) 'Medulloblastoma exome sequencing uncovers subtype-specific somatic mutations', *Nature*, 488(7409), pp. 106-10.

Puissant, A., Frumm, S.M., Alexe, G., Bassil, C.F., Qi, J., Chanthery, Y.H., Nekritz, E.A., Zeid, R., Gustafson, W.C., Greninger, P., Garnett, M.J., McDermott, U., Benes, C.H., Kung, A.L., Weiss, W.A., Bradner, J.E. and Stegmaier, K. (2013) 'Targeting MYCN in neuroblastoma by BET bromodomain inhibition', *Cancer Discov*, 3(3), pp. 308-23.

R Development Core Team (2014) *R: A language and environment for statistical computing* [Computer program]. R Foundation for Statistical Computing.

Ramaswamy, V., Remke, M., Bouffet, E., Faria, C.C., Perreault, S., Cho, Y.J., Shih, D.J., Luu, B., Dubuc, A.M., Northcott, P.A., Schuller, U., Gururangan, S., McLendon, R., Bigner, D., Fouladi, M., Ligon, K.L., Pomeroy, S.L., Dunn, S., Triscott, J., Jabado, N., Fontebasso, A., Jones, D.T., Kool, M., Karajannis, M.A., Gardner, S.L., Zagzag, D., Nunes, S., Pimentel, J., Mora, J., Lipp, E., Walter, A.W., Ryzhova, M., Zheludkova, O., Kumirova, E., Alshami, J., Croul, S.E., Rutka, J.T., Hawkins, C., Tabori, U., Codispoti, K.E., Packer, R.J., Pfister, S.M., Korshunov, A. and Taylor, M.D. (2013) 'Recurrence patterns across medulloblastoma subgroups: an integrated clinical and molecular analysis', *Lancet Oncol*.

Randerson-Moor, J.A., Harland, M., Williams, S., Cuthbert-Heavens, D., Sheridan, E., Aveyard, J., Sibley, K., Whitaker, L., Knowles, M., Bishop, J.N. and Bishop, D.T. (2001) 'A germline deletion of p14(ARF) but not CDKN2A in a melanoma-neural system tumour syndrome family', *Hum Mol Genet*, 10(1), pp. 55-62.

Rausch, T., Jones, D.T., Zapatka, M., Stutz, A.M., Zichner, T., Weischenfeldt, J., Jager, N., Remke, M., Shih, D., Northcott, P.A., Pfaff, E., Tica, J., Wang, Q., Massimi, L., Witt, H., Bender, S., Pleier, S., Cin, H., Hawkins, C., Beck, C., von Deimling, A., Hans, V., Brors, B., Eils, R., Scheurlen, W., Blake, J., Benes, V., Kulozik, A.E., Witt, O., Martin, D., Zhang, C., Porat, R., Merino, D.M., Wasserman, J., Jabado, N., Fontebasso, A., Bullinger, L., Rucker, F.G., Dohner, K., Dohner, H., Koster, J., Molenaar, J.J., Versteeg, R., Kool, M., Tabori, U., Malkin, D., Korshunov, A., Taylor, M.D., Lichter, P., Pfister, S.M. and Korbel, J.O. (2012) 'Genome sequencing of pediatric medulloblastoma links catastrophic DNA rearrangements with TP53 mutations', *Cell*, 148(1-2), pp. 59-71.

Ray-Coquard, I., Blay, J.Y., Italiano, A., Le Cesne, A., Penel, N., Zhi, J., Heil, F., Rueger, R., Graves, B., Ding, M., Geho, D., Middleton, S.A., Vassilev, L.T., Nichols, G.L. and Bui, B.N. (2012) 'Effect of the MDM2 antagonist RG7112 on the P53 pathway in patients with MDM2-amplified, well-differentiated or dedifferentiated liposarcoma: an exploratory proof-of-mechanism study', *Lancet Oncol*, 13(11), pp. 1133-40.

Reinert, T., Modin, C., Castano, F.M., Lamy, P., Wojdacz, T.K., Hansen, L.L., Wiuf, C., Borre, M., Dyrskjot, L. and Orntoft, T.F. (2011) 'Comprehensive genome methylation analysis in bladder cancer: identification and validation of novel methylated genes and application of these as urinary tumor markers', *Clin Cancer Res*, 17(17), pp. 5582-92.

Remke, M., Ramaswamy, V., Peacock, J., Shih, D.J., Koelsche, C., Northcott, P.A., Hill, N., Cavalli, F.M., Kool, M., Wang, X., Mack, S.C., Barszczyk, M., Morrissy, A.S., Wu, X., Agnihotri, S., Luu, B., Jones, D.T., Garzia, L., Dubuc, A.M., Zhukova, N., Vanner, R., Kros, J.M., French, P.J., Van Meir, E.G., Vibhakar, R., Zitterbart, K., Chan, J.A., Bognar, L., Klekner, A., Lach, B., Jung, S., Saad, A.G., Liau, L.M., Albrecht, S., Zollo, M., Cooper, M.K., Thompson, R.C., Delattre, O.O., Bourdeaut, F., Doz, F.F., Garami, M., Hauser, P., Carlotti, C.G., Van Meter, T.E., Massimi, L., Fults, D., Pomeroy, S.L., Kumabe, T., Ra, Y.S.,

Leonard, J.R., Elbabaa, S.K., Mora, J., Rubin, J.B., Cho, Y.J., McLendon, R.E., Bigner, D.D., Eberhart, C.G., Fouladi, M., Wechsler-Reya, R.J., Faria, C.C., Croul, S.E., Huang, A., Bouffet, E., Hawkins, C.E., Dirks, P.B., Weiss, W.A., Schuller, U., Pollack, I.F., Rutkowski, S., Meyronet, D., Jouvet, A., Fevre-Montange, M., Jabado, N., Perek-Polnik, M., Grajkowska, W.A., Kim, S.K., Rutka, J.T., Malkin, D., Tabori, U., Pfister, S.M., Korshunov, A., von Deimling, A. and Taylor, M.D. (2013) 'TERT promoter mutations are highly recurrent in SHH subgroup medulloblastoma', *Acta Neuropathol*.

Robinson, G., Parker, M., Kranenburg, T.A., Lu, C., Chen, X., Ding, L., Phoenix, T.N., Hedlund, E., Wei, L., Zhu, X., Chalhoub, N., Baker, S.J., Huether, R., Kriwacki, R., Curley, N., Thiruvenkatam, R., Wang, J., Wu, G., Rusch, M., Hong, X., Becksfort, J., Gupta, P., Ma, J., Easton, J., Vadodaria, B., Onar-Thomas, A., Lin, T., Li, S., Pounds, S., Paugh, S., Zhao, D., Kawauchi, D., Roussel, M.F., Finkelstein, D., Ellison, D.W., Lau, C.C., Bouffet, E., Hassall, T., Gururangan, S., Cohn, R., Fulton, R.S., Fulton, L.L., Dooling, D.J., Ochoa, K., Gajjar, A., Mardis, E.R., Wilson, R.K., Downing, J.R., Zhang, J. and Gilbertson, R.J. (2012) 'Novel mutations target distinct subgroups of medulloblastoma', *Nature*, 488(7409), pp. 43-8.

Rodriguez, M., Aladowicz, E., Lanfrancone, L. and Goding, C.R. (2008) 'Tbx3 represses E-cadherin expression and enhances melanoma invasiveness', *Cancer Res*, 68(19), pp. 7872-81.

Rowley, M., Grothey, E. and Couch, F.J. (2004) 'The role of Tbx2 and Tbx3 in mammary development and tumorigenesis', *J Mammary Gland Biol Neoplasia*, 9(2), pp. 109-18.

Rudin, C.M., Hann, C.L., Laterra, J., Yauch, R.L., Callahan, C.A., Fu, L., Holcomb, T., Stinson, J., Gould, S.E., Coleman, B., LoRusso, P.M., Von Hoff, D.D., de Sauvage, F.J. and Low, J.A. (2009) 'Treatment of medulloblastoma with hedgehog pathway inhibitor GDC-0449', *N Engl J Med*, 361(12), pp. 1173-8.

Ruggiero, A., Rizzo, D., Attina, G., Lazzareschi, I., Mastrangelo, S., Maurizi, P., Migliorati, R., Bertolini, P., Pastore, M., Colosimo, C. and Riccardi, R. (2010) 'Phase I study of temozolomide combined with oral etoposide in children with recurrent or progressive medulloblastoma', *Eur J Cancer*, 46(16), pp. 2943-9.

Rumboldt, Z., Camacho, D.L., Lake, D., Welsh, C.T. and Castillo, M. (2006) 'Apparent diffusion coefficients for differentiation of cerebellar tumors in children', *AJNR Am J Neuroradiol*, 27(6), pp. 1362-9.

Rutkowski, S., Gerber, N.U., von Hoff, K., Gnekow, A., Bode, U., Graf, N., Berthold, F., Henze, G., Wolff, J.E., Warmuth-Metz, M., Soerensen, N., Emser, A., Ottensmeier, H., Deinlein, F., Schlegel, P.G., Kortmann, R.D., Pietsch, T. and Kuehl, J. (2009) 'Treatment of early childhood medulloblastoma by postoperative chemotherapy and deferred radiotherapy', *Neuro Oncol*, 11(2), pp. 201-10.

Ryan, S.L., Schwalbe, E.C., Cole, M., Lu, Y., Lusher, M.E., Megahed, H., O'Toole, K., Nicholson, S.L., Bognar, L., Garami, M., Hauser, P., Korshunov, A., Pfister, S.M., Williamson, D., Taylor, R.E., Ellison, D.W., Bailey, S. and Clifford, S.C. (2012) 'MYC family amplification and clinical risk-factors interact to predict an extremely poor prognosis in childhood medulloblastoma', *Acta Neuropathol*, 123(4), pp. 501-13.

Saglio, G., Hochhaus, A., Goh, Y.T., Masszi, T., Pasquini, R., Maloisel, F., Erben, P., Cortes, J., Paquette, R., Bradley-Garelik, M.B., Zhu, C. and Dombret, H. (2010) 'Dasatinib in imatinib-resistant or imatinib-intolerant chronic myeloid leukemia in blast phase after 2 years of follow-up in a phase 3 study: efficacy and tolerability of 140 milligrams once daily and 70 milligrams twice daily', *Cancer*, 116(16), pp. 3852-61.

Sanger, F., Nicklen, S. and Coulson, A.R. (1977) 'DNA sequencing with chain-terminating inhibitors', *Proc Natl Acad Sci U S A*, 74(12), pp. 5463-7.

Schiffman, J.D., Hodgson, J.G., VandenBerg, S.R., Flaherty, P., Polley, M.Y., Yu, M., Fisher, P.G., Rowitch, D.H., Ford, J.M., Berger, M.S., Ji, H., Gutmann, D.H. and James, C.D. (2010) 'Oncogenic BRAF mutation with CDKN2A inactivation is characteristic of a subset of pediatric malignant astrocytomas', *Cancer Res*, 70(2), pp. 512-9.

Schouten, J.P., McElgunn, C.J., Waaijer, R., Zwijnenburg, D., Diepvens, F. and Pals, G. (2002) 'Relative quantification of 40 nucleic acid sequences by multiplex ligation-dependent probe amplification', *Nucleic Acids Res*, 30(12), p. e57.

Schuller, U., Zhao, Q., Godinho, S.A., Heine, V.M., Medema, R.H., Pellman, D. and Rowitch, D.H. (2007) 'Forkhead transcription factor FoxM1 regulates mitotic entry and prevents spindle defects in cerebellar granule neuron precursors', *Mol Cell Biol*, 27(23), pp. 8259-70.

Schwalbe, E.C., Hayden, J.T., Rogers, H.A., Miller, S., Lindsey, J.C., Hill, R.M., Nicholson, S.L., Kilday, J.P., Adamowicz-Brice, M., Storer, L., Jacques, T.S., Robson, K., Lowe, J., Williamson, D., Grundy, R.G., Bailey, S. and Clifford, S.C. (2013a) 'Histologically defined central nervous system primitive neuro-ectodermal tumours (CNS-PNETs) display heterogeneous DNA methylation profiles and show relationships to other paediatric brain tumour types', *Acta Neuropathol*, 126(6), pp. 943-6.

Schwalbe, E.C., Lindsey, J.C., Straughton, D., Hogg, T.L., Cole, M., Megahed, H., Ryan, S.L., Lusher, M.E., Taylor, M.D., Gilbertson, R.J., Ellison, D.W., Bailey, S. and Clifford, S.C. (2011) 'Rapid diagnosis of medulloblastoma molecular subgroups', *Clin Cancer Res*, 17(7), pp. 1883-94.

Schwalbe, E.C., Williamson, D., Lindsey, J.C., Hamilton, D., Ryan, S.L., Megahed, H., Garami, M., Hauser, P., Dembowska-Baginska, B., Perek, D., Northcott, P.A., Taylor, M.D., Taylor, R.E., Ellison, D.W., Bailey, S. and Clifford, S.C. (2013b) 'DNA methylation profiling of medulloblastoma allows robust subclassification and improved outcome prediction using formalin-fixed biopsies', *Acta Neuropathol*.

Sedlackova, T., Repiska, G., Celec, P., Szemes, T. and Minarik, G. (2013) 'Fragmentation of DNA affects the accuracy of the DNA quantitation by the commonly used methods', *Biol Proced Online*, 15(1), p. 5.

Shackney, S.E., Pollice, A.A., Smith, C.A., Alston, L., Singh, S.G., Janocko, L.E., Brown, K.A., Petruolo, S., Groft, D.W., Yakulis, R. and Hartsock, R.J. (1996) 'The accumulation of multiple genetic abnormalities in individual tumor cells in human breast cancers: clinical prognostic implications', *Cancer J Sci Am*, 2(2), pp. 106-13.

Shah, N. and Sukumar, S. (2010) 'The Hox genes and their roles in oncogenesis', *Nat Rev Cancer*, 10(5), pp. 361-71.

Shay, J.W. and Wright, W.E. (2011) 'Role of telomeres and telomerase in cancer', *Semin Cancer Biol*, 21(6), pp. 349-53.

Shih, D.J., Northcott, P.A., Remke, M., Korshunov, A., Ramaswamy, V., Kool, M., Luu, B., Yao, Y., Wang, X., Dubuc, A.M., Garzia, L., Peacock, J., Mack, S.C., Wu, X., Rolider, A., Morrissy, A.S., Cavalli, F.M., Jones, D.T., Zitterbart, K., Faria, C.C., Schuller, U., Kren, L., Kumabe, T., Tominaga, T., Shin Ra, Y., Garami, M., Hauser, P., Chan, J.A., Robinson, S., Bognar, L., Klekner, A., Saad, A.G., Liau, L.M., Albrecht, S., Fontebasso, A., Cinalli, G., De Antonellis, P., Zollo, M., Cooper, M.K., Thompson, R.C., Bailey, S., Lindsey, J.C., Di Rocco, C., Massimi, L., Michiels, E.M., Scherer, S.W., Phillips, J.J., Gupta, N., Fan, X., Muraszko, K.M., Vibhakar, R., Eberhart, C.G., Fouladi, M., Lach, B., Jung, S., Wechsler-Reya, R.J., Fevre-Montange, M., Jouvet, A., Jabado, N., Pollack, I.F., Weiss, W.A., Lee, J.Y., Cho, B.K., Kim, S.K., Wang, K.C., Leonard, J.R., Rubin, J.B., de Torres, C., Lavarino, C., Mora, J., Cho, Y.J., Tabori, U., Olson, J.M., Gajjar, A., Packer, R.J., Rutkowski, S., Pomeroy, S.L., French, P.J., Kloosterhof, N.K., Kros, J.M., Van Meir, E.G., Clifford, S.C., Bourdeaut, F., Delattre, O., Doz, F.F., Hawkins, C.E., Malkin, D., Grajkowska, W.A., Perek-Polnik, M., Bouffet, E., Rutka, J.T., Pfister, S.M. and Taylor, M.D. (2014) 'Cytogenetic prognostication within medulloblastoma subgroups', *J Clin Oncol*, 32(9), pp. 886-96.

Sidransky, D. (2002) 'Emerging molecular markers of cancer', *Nat Rev Cancer*, 2(3), pp. 210-9.

Slany, R.K. (2009) 'The molecular biology of mixed lineage leukemia', *Haematologica*, 94(7), pp. 984-93.

Sondhi, V., Arun Kurkure, P., Jalali, R., Rangarajan, V., Sridhar, E., Medhi, S. and Arora, B. (2012) 'Complete remission and long-term survival in a child with relapsed medulloblastoma with extensive osteosclerotic bony metastasis with a novel metronomic chemobiological approach', *J Pediatr Hematol Oncol*, 34(5), pp. e195-8.

Sottoriva, A., Spiteri, I., Piccirillo, S.G., Touloumis, A., Collins, V.P., Marioni, J.C., Curtis, C., Watts, C. and Tavare, S. (2013) 'Intratumor heterogeneity in human glioblastoma reflects cancer evolutionary dynamics', *Proc Natl Acad Sci U S A*, 110(10), pp. 4009-14.

Soussi, T., Asselain, B., Hamroun, D., Kato, S., Ishioka, C., Claustres, M. and Beroud, C. (2006) 'Meta-analysis of the p53 mutation database for mutant p53 biological activity reveals a methodologic bias in mutation detection', *Clin Cancer Res*, 12(1), pp. 62-9.

Sterba, J., Pavelka, Z., Andre, N., Ventruba, J., Skotakova, J., Bajciova, V., Bronisova, D., Dubska, L. and Valik, D. (2010) 'Second complete remission of relapsed medulloblastoma induced by metronomic chemotherapy', *Pediatr Blood Cancer*, 54(4), pp. 616-7.

Stiller, C.A. (2004) 'Epidemiology and genetics of childhood cancer', *Oncogene*, 23(38), pp. 6429-44.

Sturm, D., Witt, H., Hovestadt, V., Khuong-Quang, D.A., Jones, D.T., Konermann, C., Pfaff, E., Tonjes, M., Sill, M., Bender, S., Kool, M., Zapatka, M., Becker, N., Zucknick, M., Hielscher, T., Liu, X.Y., Fontebasso, A.M., Ryzhova, M., Albrecht, S., Jacob, K., Wolter, M., Ebinger, M., Schuhmann, M.U., van Meter, T., Fruhwald, M.C., Hauch, H., Pekrun, A., Radlwimmer, B., Niehues, T., von Komorowski, G., Durken, M., Kulozik, A.E., Madden, J., Donson, A., Foreman, N.K., Drissi, R., Fouladi, M., Scheurlen, W., von Deimling, A., Monoranu, C., Roggendorf, W., Herold-Mende, C., Unterberg, A., Kramm, C.M., Felsberg, J., Hartmann, C., Wiestler, B., Wick, W., Milde, T., Witt, O., Lindroth, A.M., Schwartzentruber, J., Faury, D., Fleming, A., Zakrzewska, M., Liberski, P.P., Zakrzewski, K., Hauser, P., Garami, M., Klekner, A., Bognar, L., Morrissy, S., Cavalli, F., Taylor, M.D., van Sluis, P., Koster, J., Versteeg, R., Volckmann, R., Mikkelsen, T., Aldape, K., Reifenberger, G., Collins, V.P., Majewski, J., Korshunov, A., Lichter, P., Plass, C., Jabado, N. and Pfister, S.M. (2012) 'Hotspot Mutations in H3F3A and IDH1 Define Distinct Epigenetic and Biological Subgroups of Glioblastoma', *Cancer Cell*, 22(4), pp. 425-37.

Swartling, F.J., Grimmer, M.R., Hackett, C.S., Northcott, P.A., Fan, Q.W., Goldenberg, D.D., Lau, J., Masic, S., Nguyen, K., Yakovenko, S., Zhe, X.N., Gilmer, H.C., Collins, R., Nagaoka, M., Phillips, J.J., Jenkins, R.B., Tihan, T., Vandenberg, S.R., James, C.D., Tanaka, K., Taylor, M.D., Weiss, W.A. and Chesler, L. (2010) 'Pleiotropic role for MYCN in medulloblastoma', *Genes Dev*, 24(10), pp. 1059-72.

Tabori, U., Baskin, B., Shago, M., Alon, N., Taylor, M.D., Ray, P.N., Bouffet, E., Malkin, D. and Hawkins, C. (2010) 'Universal poor survival in children with medulloblastoma harboring somatic TP53 mutations', *J Clin Oncol*, 28(8), pp. 1345-50.

Taketo, M., Schroeder, A.C., Mobraaten, L.E., Gunning, K.B., Hanten, G., Fox, R.R., Roderick, T.H., Stewart, C.L., Lilly, F., Hansen, C.T. and et al. (1991) 'FVB/N: an inbred mouse strain preferable for transgenic analyses', *Proc Natl Acad Sci U S A*, 88(6), pp. 2065-9.

Talmadge, J.E. and Fidler, I.J. (2010) 'AACR centennial series: the biology of cancer metastasis: historical perspective', *Cancer Res*, 70(14), pp. 5649-69.

Tamayo, P., Scanfeld, D., Ebert, B.L., Gillette, M.A., Roberts, C.W. and Mesirov, J.P. (2007) 'Metagene projection for cross-platform, cross-species characterization of global transcriptional states', *Proc Natl Acad Sci U S A*, 104(14), pp. 5959-64.

Taylor, M.D., Northcott, P.A., Korshunov, A., Remke, M., Cho, Y.J., Clifford, S.C., Eberhart, C.G., Parsons, D.W., Rutkowski, S., Gajjar, A., Ellison, D.W., Lichter, P., Gilbertson, R.J., Pomeroy, S.L., Kool, M. and Pfister, S.M. (2012) 'Molecular subgroups of medulloblastoma: the current consensus', *Acta Neuropathol*, 123(4), pp. 465-72.

Tekautz, T.M., Fuller, C.E., Blaney, S., Fouladi, M., Broniscer, A., Merchant, T.E., Krasin, M., Dalton, J., Hale, G., Kun, L.E., Wallace, D., Gilbertson, R.J. and Gajjar, A. (2005) 'Atypical teratoid/rhabdoid tumors (ATRT): improved survival in children 3 years of age and older with radiation therapy and high-dose alkylator-based chemotherapy', *J Clin Oncol*, 23(7), pp. 1491-9.

Teschendorff, A.E., Marabita, F., Lechner, M., Bartlett, T., Tegner, J., Gomez-Cabrero, D. and Beck, S. (2013) 'A beta-mixture quantile normalization method for correcting probe design bias in Illumina Infinium 450 k DNA methylation data', *Bioinformatics*, 29(2), pp. 189-96.

Thompson, M.C., Fuller, C., Hogg, T.L., Dalton, J., Finkelstein, D., Lau, C.C., Chintagumpala, M., Adesina, A., Ashley, D.M., Kellie, S.J., Taylor, M.D., Curran, T.,

Gajjar, A. and Gilbertson, R.J. (2006) 'Genomics identifies medulloblastoma subgroups that are enriched for specific genetic alterations', *J Clin Oncol*, 24(12), pp. 1924-31.

Tolstorukov, M.Y., Sansam, C.G., Lu, P., Koellhoffer, E.C., Helming, K.C., Alver, B.H., Tillman, E.J., Evans, J.A., Wilson, B.G., Park, P.J. and Roberts, C.W. (2013) 'Swi/Snf chromatin remodeling/tumor suppressor complex establishes nucleosome occupancy at target promoters', *Proc Natl Acad Sci U S A*, 110(25), pp. 10165-70.

Torrelo, A., Vicente, A., Navarro, L., Planaguma, M., Bueno, E., Gonzalez-Sarmiento, R., Hernandez-Martin, A., Noguera-Morel, L., Requena, L., Colmenero, I., Parareda, A., Gonzalez-Ensenat, M.A. and Haple, R. (2014) 'Early-onset acral basal cell carcinomas in Gorlin syndrome', *Br J Dermatol*.

Tsumagari, K., Baribault, C., Terragni, J., Chandra, S., Renshaw, C., Sun, Z., Song, L., Crawford, G.E., Pradhan, S., Lacey, M. and Ehrlich, M. (2013) 'DNA methylation and differentiation: HOX genes in muscle cells', *Epigenetics Chromatin*, 6(1), p. 25.

Van Maerken, T., Rihani, A., Van Goethem, A., De Paepe, A., Speleman, F. and Vandesompele, J. (2013) 'Pharmacologic activation of wild-type p53 by nutlin therapy in childhood cancer', *Cancer Lett*.

Vanner, R.J., Remke, M., Gallo, M., Selvadurai, H.J., Coutinho, F., Lee, L., Kushida, M., Head, R., Morrissy, S., Zhu, X., Aviv, T., Voisin, V., Clarke, I.D., Li, Y., Mungall, A.J., Moore, R.A., Ma, Y., Jones, S.J., Marra, M.A., Malkin, D., Northcott, P.A., Kool, M., Pfister, S.M., Bader, G., Hochedlinger, K., Korshunov, A., Taylor, M.D. and Dirks, P.B. (2014) 'Quiescent sox2(+) cells drive hierarchical growth and relapse in sonic hedgehog subgroup medulloblastoma', *Cancer Cell*, 26(1), pp. 33-47.

Visvader, J.E. and Lindeman, G.J. (2012) 'Cancer stem cells: current status and evolving complexities', *Cell Stem Cell*, 10(6), pp. 717-28.

Vita, M. and Henriksson, M. (2006) 'The Myc oncoprotein as a therapeutic target for human cancer', *Semin Cancer Biol*, 16(4), pp. 318-30.

Wang, F., Flanagan, J., Su, N., Wang, L.C., Bui, S., Nielson, A., Wu, X., Vo, H.T., Ma, X.J. and Luo, Y. (2012) 'RNAscope: a novel in situ RNA analysis platform for formalin-fixed, paraffin-embedded tissues', *J Mol Diagn*, 14(1), pp. 22-9.

Wang, X., Ramaswamy, V., Remke, M., Mack, S.C., Dubuc, A.M., Northcott, P.A. and Taylor, M.D. (2013) 'Intertumoral and intratumoral heterogeneity as a barrier for effective treatment of medulloblastoma', *Neurosurgery*, 60 Suppl 1, pp. 57-63.

Wani, K., Armstrong, T.S., Vera-Bolanos, E., Raghunathan, A., Ellison, D., Gilbertson, R., Vaillant, B., Goldman, S., Packer, R.J., Fouladi, M., Pollack, I., Mikkelsen, T., Prados, M., Omuro, A., Soffietti, R., Ledoux, A., Wilson, C., Long, L., Gilbert, M.R., Aldape, K. and Collaborative Ependymoma Research, N. (2012) 'A prognostic gene expression signature in infratentorial ependymoma', *Acta Neuropathol*, 123(5), pp. 727-38.

Wetmore, C., Eberhart, D.E. and Curran, T. (2000) 'The normal patched allele is expressed in medulloblastomas from mice with heterozygous germ-line mutation of patched', *Cancer Res*, 60(8), pp. 2239-46.

Wijnhoven, S.W., Speksnijder, E.N., Liu, X., Zwart, E., vanOostrom, C.T., Beems, R.B., Hoogervorst, E.M., Schaap, M.M., Attardi, L.D., Jacks, T., van Steeg, H., Jonkers, J. and de Vries, A. (2007) 'Dominant-negative but not gain-of-function effects of a p53.R270H mutation in mouse epithelium tissue after DNA damage', *Cancer Res*, 67(10), pp. 4648-56.

Witt, H., Mack, S.C., Ryzhova, M., Bender, S., Sill, M., Isserlin, R., Benner, A., Hielscher, T., Milde, T., Remke, M., Jones, D.T., Northcott, P.A., Garzia, L., Bertrand, K.C., Wittmann, A., Yao, Y., Roberts, S.S., Massimi, L., Van Meter, T., Weiss, W.A., Gupta, N., Grajkowska, W., Lach, B., Cho, Y.J., von Deimling, A., Kulozik, A.E., Witt, O., Bader, G.D., Hawkins, C.E., Tabori, U., Guha, A., Rutka, J.T., Lichter, P., Korshunov, A., Taylor, M.D. and Pfister, S.M. (2011) 'Delineation of two clinically and molecularly distinct subgroups of posterior fossa ependymoma', *Cancer Cell*, 20(2), pp. 143-57.

Witt, O., Milde, T., Deubzer, H.E., Oehme, I., Witt, R., Kulozik, A., Eisenmenger, A., Abel, U. and Karapanagiotou-Schenkel, I. (2012) 'Phase I/II intra-patient dose escalation

study of vorinostat in children with relapsed solid tumor, lymphoma or leukemia', *Klin Padiatr*, 224(6), pp. 398-403.

Workman, P., Aboagye, E.O., Balkwill, F., Balmain, A., Bruder, G., Chaplin, D.J., Double, J.A., Everitt, J., Farningham, D.A.H., Glennie, M.J., Kelland, L.R., Robinson, V., Stratford, I.J., Tozer, G.M., Watson, S., Wedge, S.R. and Eccles, S.A. (2010) 'Guidelines for the welfare and use of animals in cancer research', *Br J Cancer*, 102(11), pp. 1555-1577.

Wu, X., Northcott, P.A., Dubuc, A., Dupuy, A.J., Shih, D.J., Witt, H., Croul, S., Bouffet, E., Fults, D.W., Eberhart, C.G., Garzia, L., Van Meter, T., Zagzag, D., Jabado, N., Schwartzentruber, J., Majewski, J., Scheetz, T.E., Pfister, S.M., Korshunov, A., Li, X.N., Scherer, S.W., Cho, Y.J., Akagi, K., MacDonald, T.J., Koster, J., McCabe, M.G., Sarver, A.L., Collins, V.P., Weiss, W.A., Largaespada, D.A., Collier, L.S. and Taylor, M.D. (2012) 'Clonal selection drives genetic divergence of metastatic medulloblastoma', *Nature*, 482(7386), pp. 529-33.

Xu, J., Margol, A., Asgharzadeh, S. and Erdreich-Epstein, A. (2014) 'Pediatric Brain Tumor Cell Lines', *J Cell Biochem*.

Yang, Z.J., Ellis, T., Markant, S.L., Read, T.A., Kessler, J.D., Bourboulas, M., Schuller, U., Machold, R., Fishell, G., Rowitch, D.H., Wainwright, B.J. and Wechsler-Reya, R.J. (2008) 'Medulloblastoma can be initiated by deletion of Patched in lineage-restricted progenitors or stem cells', *Cancer Cell*, 14(2), pp. 135-45.

Yarosh, W., Barrientos, T., Esmailpour, T., Lin, L., Carpenter, P.M., Osann, K., Anton-Culver, H. and Huang, T. (2008) 'TBX3 is overexpressed in breast cancer and represses p14 ARF by interacting with histone deacetylases', *Cancer Res*, 68(3), pp. 693-9.

Zacharoulis, S., Ashley, S., Moreno, L., Gentet, J.C., Massimino, M. and Frappaz, D. (2010) 'Treatment and outcome of children with relapsed ependymoma: a multi-institutional retrospective analysis', *Childs Nerv Syst*, 26(7), pp. 905-11.

Zhukova, N., Ramaswamy, V., Remke, M., Pfaff, E., Shih, D.J., Martin, D.C., Castelo-Branco, P., Baskin, B., Ray, P.N., Bouffet, E., von Bueren, A.O., Jones, D.T., Northcott,

P.A., Kool, M., Sturm, D., Pugh, T.J., Pomeroy, S.L., Cho, Y.J., Pietsch, T., Gessi, M., Rutkowski, S., Bognar, L., Klekner, A., Cho, B.K., Kim, S.K., Wang, K.C., Eberhart, C.G., Fevre-Montange, M., Fouladi, M., French, P.J., Kros, M., Grajkowska, W.A., Gupta, N., Weiss, W.A., Hauser, P., Jabado, N., Jouvet, A., Jung, S., Kumabe, T., Lach, B., Leonard, J.R., Rubin, J.B., Liau, L.M., Massimi, L., Pollack, I.F., Shin Ra, Y., Van Meir, E.G., Zitterbart, K., Schuller, U., Hill, R.M., Lindsey, J.C., Schwalbe, E.C., Bailey, S., Ellison, D.W., Hawkins, C., Malkin, D., Clifford, S.C., Korshunov, A., Pfister, S., Taylor, M.D. and Tabori, U. (2013) 'Subgroup-Specific Prognostic Implications of TP53 Mutation in Medulloblastoma', *J Clin Oncol*, 31(23), pp. 2927-35.

Chapter 9. Appendices

9.1 Appendix I: R script characterising methylation events between diagnosis and relapse

```
##Normal cerebella cohort dataset object; betas.BMIQ.NC

##Paired relapsed cohort dataset object (number of pairs=27);
##betas.BMIQ.D.R

##Convert to M values

library(minfi)

library(multicore)

M.CB <- ilogit2(betas.BMIQ.NC)

##Calculate standard deviation

CB.sd <- mclapply(mc.cores=16, 1:nrow(M.CB), function(i)
sd(na.rm=TRUE, M.CB[i,]))

CB.sd <- unlist(CB.sd)

plot(CB.sd[order(decreasing=TRUE, CB.sd)], pch=".")

selectedProbes <- rownames(M.CB)[which(CB.sd < 0.02)]

##interrogate invariant probes only for both datasets and check they
##match

betas.BMIQ.D.R.trim <- betas.BMIQ.D.R[rownames(betas.BMIQ.D.R) %in%
selectedProbes,]

betas.BMIQ.NC.trim <- betas.BMIQ.NC[rownames(betas.BMIQ.NC) %in%
selectedProbes,]

all(rownames(betas.BMIQ.NC.trim) == rownames(betas.BMIQ.D.R.trim))

##create a matrix of values of the difference in beta values between
##diagnosis and relapse

betas.BMIQ.D.R.diffs <- betas.BMIQ.D.R.trim [,1:27] -
betas.BMIQ.D.R.trim[,28:54]

##calculate the mean of the cerebella beta values

CB.mean <- apply(betas.BMIQ.NC.trim,1,function(x) mean(x, na.rm=TRUE))

##set the change in methylation value which is biologically important

threshold <- 0.4

diagChange <- lapply(1:nrow(betas.BMIQ.D.R.trim), function(i)

            which(abs(betas.BMIQ.D.R.trim[i,1:27] - CB.mean[i]) >
      threshold))

relapChange <- lapply(1:nrow(betas.BMIQ.D.R.trim), function(i)

            which(abs(betas.BMIQ.D.R.trim[i,28:54] - CB.mean[i]) >
threshold))

diagUnchange <- lapply(1:nrow(betas.BMIQ.D.R.trim), function(i)
```

```
            which(abs(betas.BMIQ.D.R.trim[i,1:27] - CB.mean[i]) <
threshold))

relapUnchange <- lapply(1:nrow(betas.BMIQ.D.R.trim), function(i)

            which(abs(betas.BMIQ.D.R.trim[i,28:54] - CB.mean[i]) <
threshold))

NAcount <- lapply(1:nrow(betas.BMIQ.D.R.diffs), function(i)

            which(is.na(betas.BMIQ.D.R.trim[i,1:27]) |
            is.na(betas.BMIQ.D.R.trim[i,28:54])))

##Count 1. Change D -> R, back to cerebellar-like state

func1 <- function(i) {  tmpD <- diagChange[[i]]

                  tmpD <- tmpD[!tmpD %in% NAcount[[i]]]

                  tmpR <- relapChange[[i]]

                  tmpR <- tmpR[!tmpR %in% NAcount[[i]]]

                  out <- tmpD[!tmpD %in% tmpR]

                  if(length(out)==0) {x <- length(out)} else {x <-
out}

 }

outcome1          <- lapply(1:nrow(betas.BMIQ.D.R.diffs), function(i)
func1(i))

##Count 2. Change D -> R, away from cerebellar-like state

func2 <- function(i) {  tmpD <- diagChange[[i]]

                  tmpD <- tmpD[!tmpD %in% NAcount[[i]]]

                  tmpR <- relapChange[[i]]

                  tmpR <- tmpR[!tmpR %in% NAcount[[i]]]

                  out <- tmpR[!tmpR %in% tmpD]

                  if(length(out)==0) {x <- length(out)} else {x <-
            out} x}

outcome2          <- lapply(1:nrow(betas.BMIQ.D.R.diffs), function(i)
func2(i))

##Count 3. Unchanging D -> R, in cerebellar-like state

func3 <- function(i) {  tmpD <- diagUnchange[[i]]

                  tmpD <- tmpD[!tmpD %in% NAcount[[i]]]

                  tmpR <- relapUnchange[[i]]

                  tmpR <- tmpR[!tmpR %in% NAcount[[i]]]

                  out <- tmpD[tmpD %in% tmpR]

                  if(length(out)==0) {x <- length(out)} else {x <-
            out} x}
```

```
outcome3          <- lapply(1:nrow(betas.BMIQ.D.R.diffs), function(i)
func3(i))

##Count 4. Unchanging D -> R, maintained in abnormal state

func4 <- function(i) {  tmpD <- diagChange[[i]]

                  tmpD <- tmpD[!tmpD %in% NAcount[[i]]]

                  tmpR <- relapChange[[i]]

                  tmpR <- tmpR[!tmpR %in% NAcount[[i]]]

                  out <- tmpD[tmpD %in% tmpR]

                  if(length(out)==0) {x <- length(out)} else {x<- out}
x}

outcome4           <- lapply(1:nrow(betas.BMIQ.D.R.diffs), function(i)
func4(i))

##Count 5. Magnitude of change between diagnosis and relapse

func5 <- function(i) {  diffs <- abs(betas.BMIQ.D.R.trim [i,1:27] -

                  betas.BMIQ.D.R.trim i,28:54])

                  x <- length(diffs[diffs > threshold]) x}

outcome5          <- lapply(1:nrow(betas.BMIQ.D.R.diffs), function(i)
func5(i))

##populate a results matrix

results <- matrix(nrow=nrow(betas.BMIQ.D.R.diffs), ncol=6)

colnames(results) <-    c("Change_D_R_to_CB_state",
                  "Change_D_R_away_CB_state", "Unchange_maintain_CB",
                  "Unchange_maintain_abnormal", "NA"
                  "D_R_difference>threshold")

rownames(results)       <- rownames(betas.BMIQ.D.R.diffs)

for(i in 1:nrow(results))

{

      tmp <- outcome1[[i]]

      if(tmp[1]!=0) { results[i,1] <- length(tmp) } else {results[i,1]
<- 0}

      tmp <- outcome2[[i]]

      if(tmp[1]!=0) {results[i,2] <- length(tmp) } else {results[i,2]
<- 0}

      tmp <- outcome3[[i]]

      if(tmp[1]!=0) {results[i,3] <- length(tmp) } else {results[i,3]
<- 0}

      tmp <- outcome4[[i]]

      if(tmp[1]!=0) {results[i,4] <- length(tmp) } else {results[i,4]
<- 0}
```

```
       tmp <- NAcount[[i]]

      if(length(tmp)!=0) {results[i,5] <- length(tmp) } else
{results[i,5] <- 0}

      tmp <- outcome5[[i]]

      if(tmp[1]!=0) {results[i,6] <- tmp } else {results[i,6] <- 0}

}

## Check all should add up to 27 pairs

all(rowSums(results [, 1:5]) == 27)
```

9.2 Appendix II: R script tallying methylation events between diagnosis and relapse

```
##Table of categorises events in MB_Group4;
##Grp4_Threshold_0.4_Comparison_CB

##Headings for table Grp4_Threshold_0.4_Comparison_CB

      ##Count 1. "Change_D_R_to_CB_state"

      ##Count 2. "Change_D_R_away_CB_state"

      ##Count 3. "Unchange_maintain_CB",

      ##Count 4. "Unchange_maintain_abnormal"

      ##Count 5. "NA"

      ##Count 6. "D_R_difference>threshold"

##Load annotation data

library(IlluminaHumanMethylation450kanno.ilmn12.hg19)

library(minfiData)

data(RGsetEx)

A     <- getAnnotation(RGsetEx)

##match annotation data to Grp4_Threshold_0.4_Comparison_CB

A     <- A[match(rownames(Grp4_Threshold_0.4_Comparison_CB),
rownames(A)),]
```

```
##Include probes that are in an Island in a known gene

Island                  <-A[A$Relation_to_Island =="Island",]

Island_Body             <-Island[Island$UCSC_RefGene_Name !="",]

##Include probes that are in promoter regions defined as 1500 bp
##upstream of the TSS and 500 bp downstream of TSS

library(Homo.sapiens)

txsByGene         <- transcriptsBy(TxDb.Hsapiens.UCSC.hg19.knownGene,
'gene')

names(txsByGene)  <- mget(names(txsByGene), org.Hs.egSYMBOL,
ifnotfound=NA)

promotersByGene   <- promoters(txsByGene, upstream=1500,
downstream=500)

library(minfiData)

data(MsetEx)

tmp                     <- mapToGenome(MsetEx)

promoterProbes          <- subsetByOverlaps(tmp, promotersByGene)

promoterProbeNames      <- rownames(promoterProbes)

##Combine with CpG Island probes; Island_Body

probesOfInterest <- unique(c(promoterProbeNames,
rownames(Island_Body)))

##Filter table Grp4_Threshold_0.4_Comparison_CB to match our
##probesOfInterest

Grp4_Threshold_0.4_Comparison_CB_trim <-
Grp4_Threshold_0.4_Comparison_CB[rownames(Grp4_Threshold_0.4_Compariso
n_CB) %in% probesOfInterest, ]
```

```
##Create an event table to tally acquired
##(Count 2. "Change_D_R_away_CB_state") and maintained
##(Count 4. "Unchange_maintain_abnormal") events whilst excluding
##probes which demonstrate lost methylation events
##(Count 1. "Change_D_R_to_CB_state")

noOfProbes<-c()

for(xIn in 0:8)

{

  for(yIn in 0:8)

  {

tmp         <-    Grp4_Threshold_0.4_Comparison_CB_trim

                  [Grp4_Threshold_0.4_Comparison_CB_trim[,2] == xIn

                                          &
Grp4_Threshold_0.4_Comparison_CB_trim[,6] == xIn

                                                  &
Grp4_Threshold_0.4_Comparison_CB_trim[,4] == yIn

                                                  &
Grp4_Threshold_0.4_Comparison_CB_trim[,1] == 0, , drop=F]

                  noOfProbes<-c(noOfProbes, nrow(tmp))

  }

}

Tally_table       <-    matrix(noOfProbes, 9, 9, byrow=F)

Tally_table
```

9.3 Appendix III: Candidate gene illustrations of DNA methylation at diagnosis and relapse in MB_{Group4} paired samples.

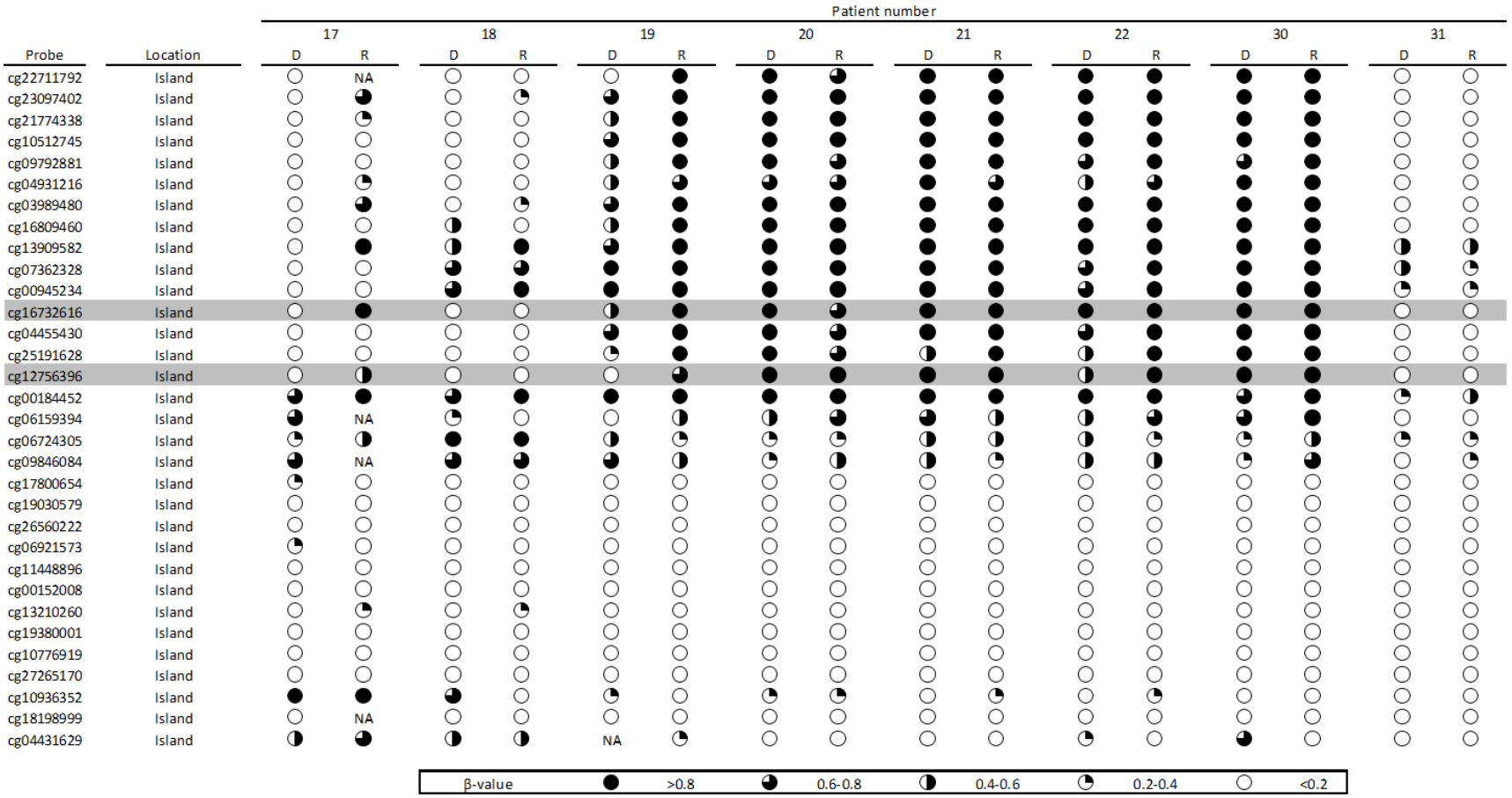

Figure 9.1 Illustration demonstrating the DNA methylation changes for *DMRTA2* between diagnosis and relapse in the MB_{Group4} paired samples. Circles represent the β-value for each sample as detected by the CpG probes on the Infinium methylation 450K array. CpG probes are arranged in order along the gene (5'-3'). Grey rows, probes of interest; D, diagnosis; R, relapse.

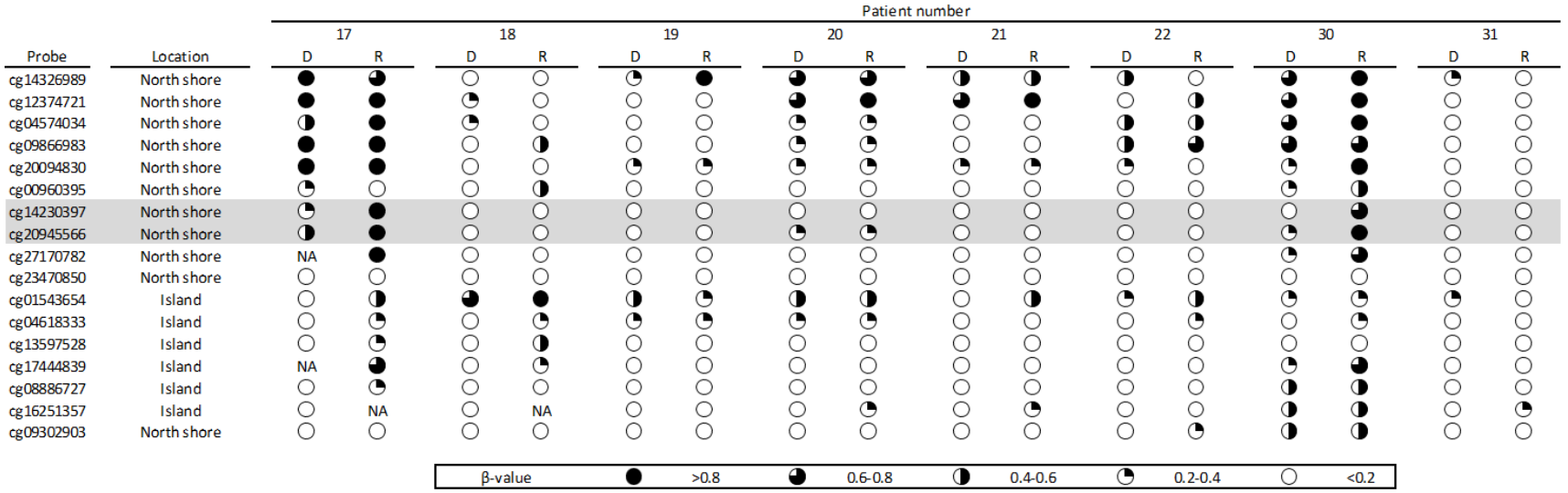

Figure 9.2 Illustration demonstrating the DNA methylation changes for *PRAC* between diagnosis and relapse in the MB_{Group4} paired samples. Circles represent the β-value for each sample as detected by the CpG probes on the Infinium methylation 450K array. CpG probes are arranged in order along the gene (5'-3'). Grey rows, probes of interest; D, diagnosis; R, relapse.

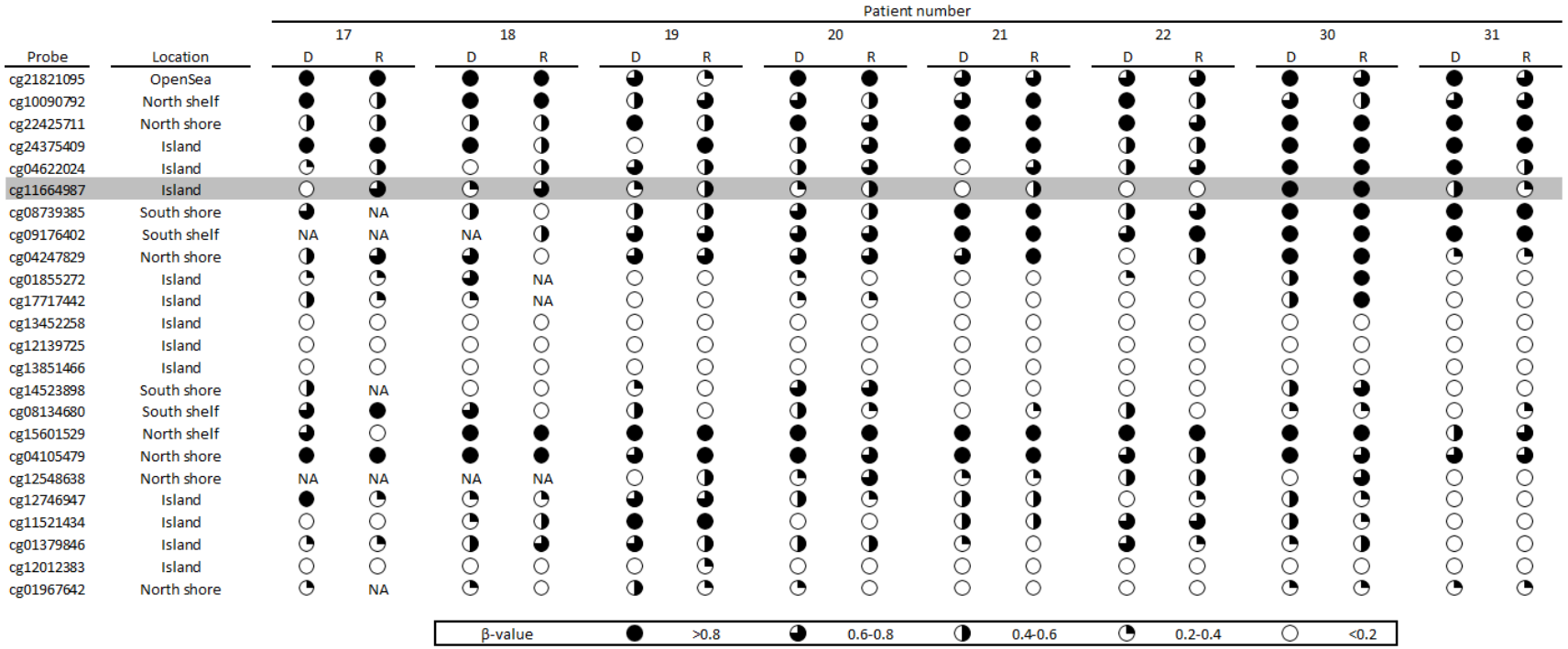

Figure 9.3 Illustration demonstrating the DNA methylation changes for *EPHA10* between diagnosis and relapse in the MB_{Group4} paired samples. Circles represent the β-value for each sample as detected by the CpG probes on the Infinium methylation 450K array. CpG probes are arranged in order along the gene (5'-3'). Grey row, probe of interest; D, diagnosis; R, relapse.

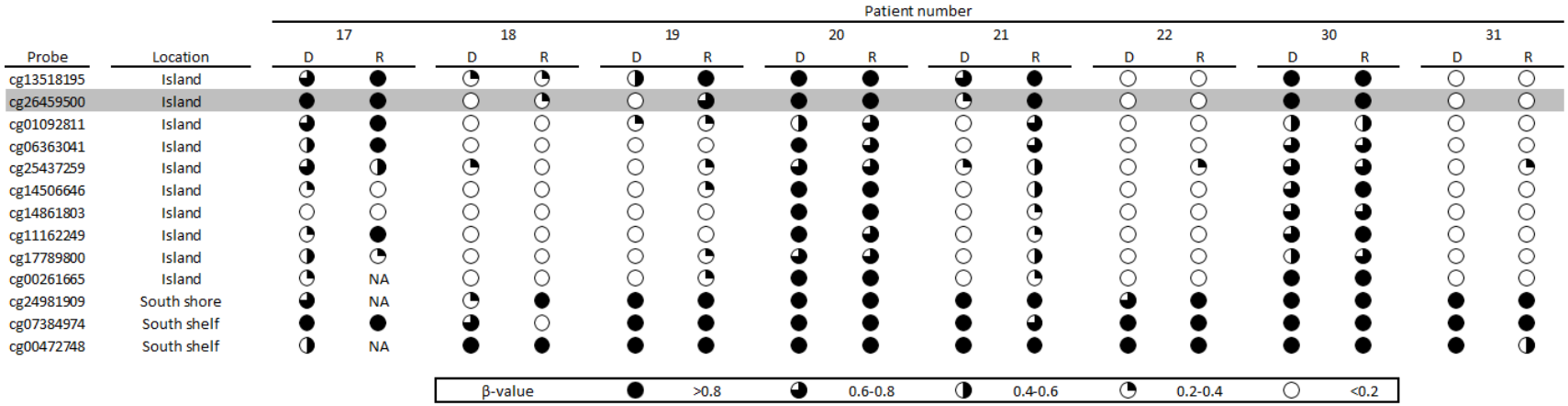

Figure 9.4 Illustration demonstrating the DNA methylation changes for *NUDT16* between diagnosis and relapse in the MB_{Group4} paired samples. Circles represent the β-value for each sample as detected by the CpG probes on the Infinium methylation 450K array. CpG probes are arranged in order along the gene (5'-3'). Grey row, probe of interest; D, diagnosis; R, relapse.

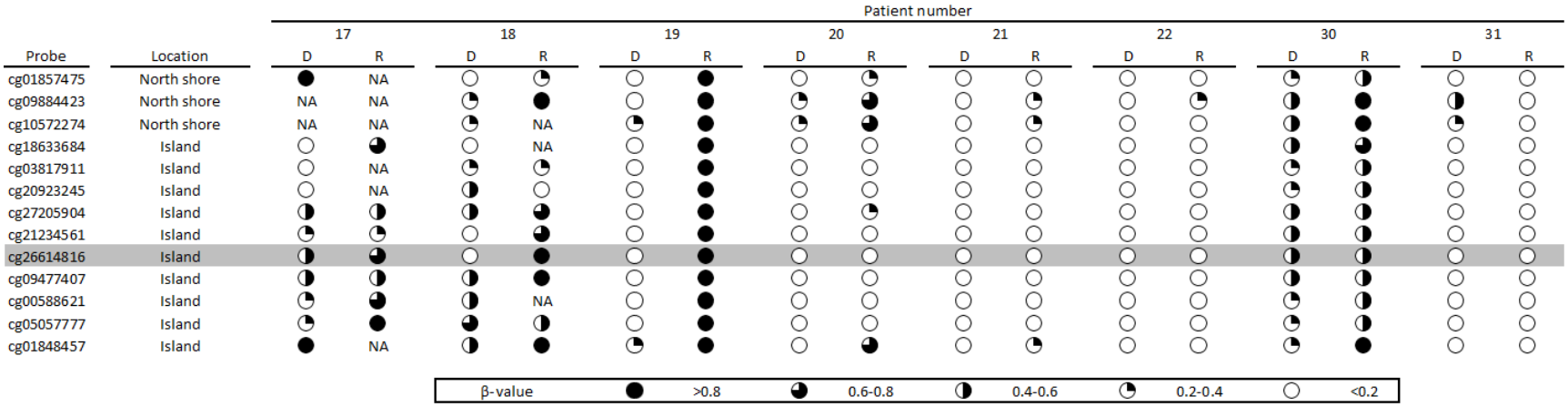

Figure 9.5 Illustration demonstrating the DNA methylation changes for *EID3* between diagnosis and relapse in the MB_{Group4} paired samples. Circles represent the β-value for each sample as detected by the CpG probes on the Infinium methylation 450K array. CpG probes are arranged in order along the gene (5'-3'). Grey row, probe of interest; D, diagnosis; R, relapse.

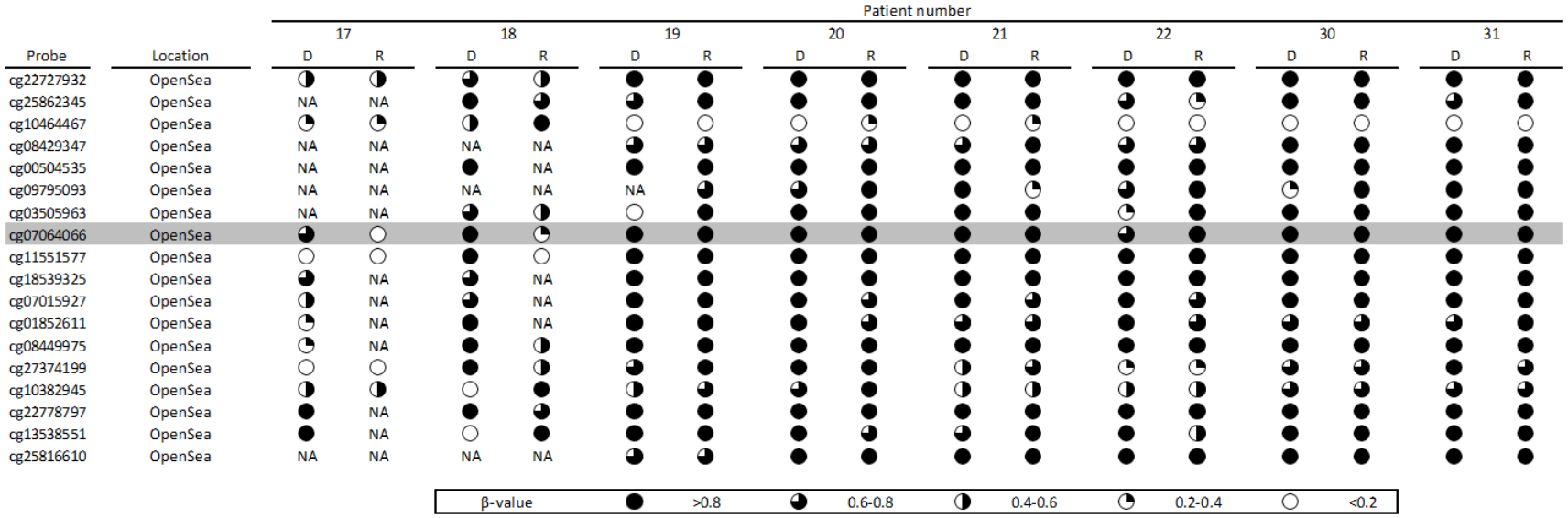

Figure 9.6 Illustration demonstrating the DNA methylation changes for *DSCR4* between diagnosis and relapse in the MB_{Group4} paired samples. Circles represent the β-value for each sample as detected by the CpG probes on the Infinium methylation 450K array. CpG probes are arranged in order along the gene (5'-3'). Grey row, probe of interest; D, diagnosis; R, relapse.

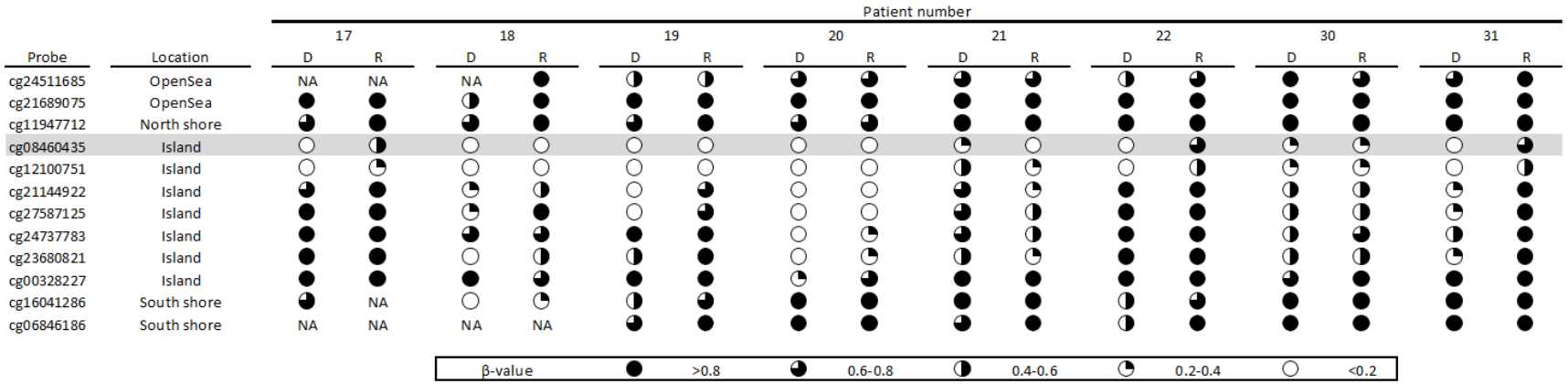

Figure 9.7 Illustration demonstrating the DNA methylation changes for *HENTM1* between diagnosis and relapse in the MB_{Group4} paired samples. Circles represent the β-value for each sample as detected by the CpG probes on the Infinium methylation 450K array. CpG probes are arranged in order along the gene (5'-3'). Grey row, probe of interest; D, diagnosis; R, relapse.

9.4 Appendix IV: Linear regression plots demonstrating the correlation between gene expression and DNA methylation for the candidate genes in MB_{Group4} tumours

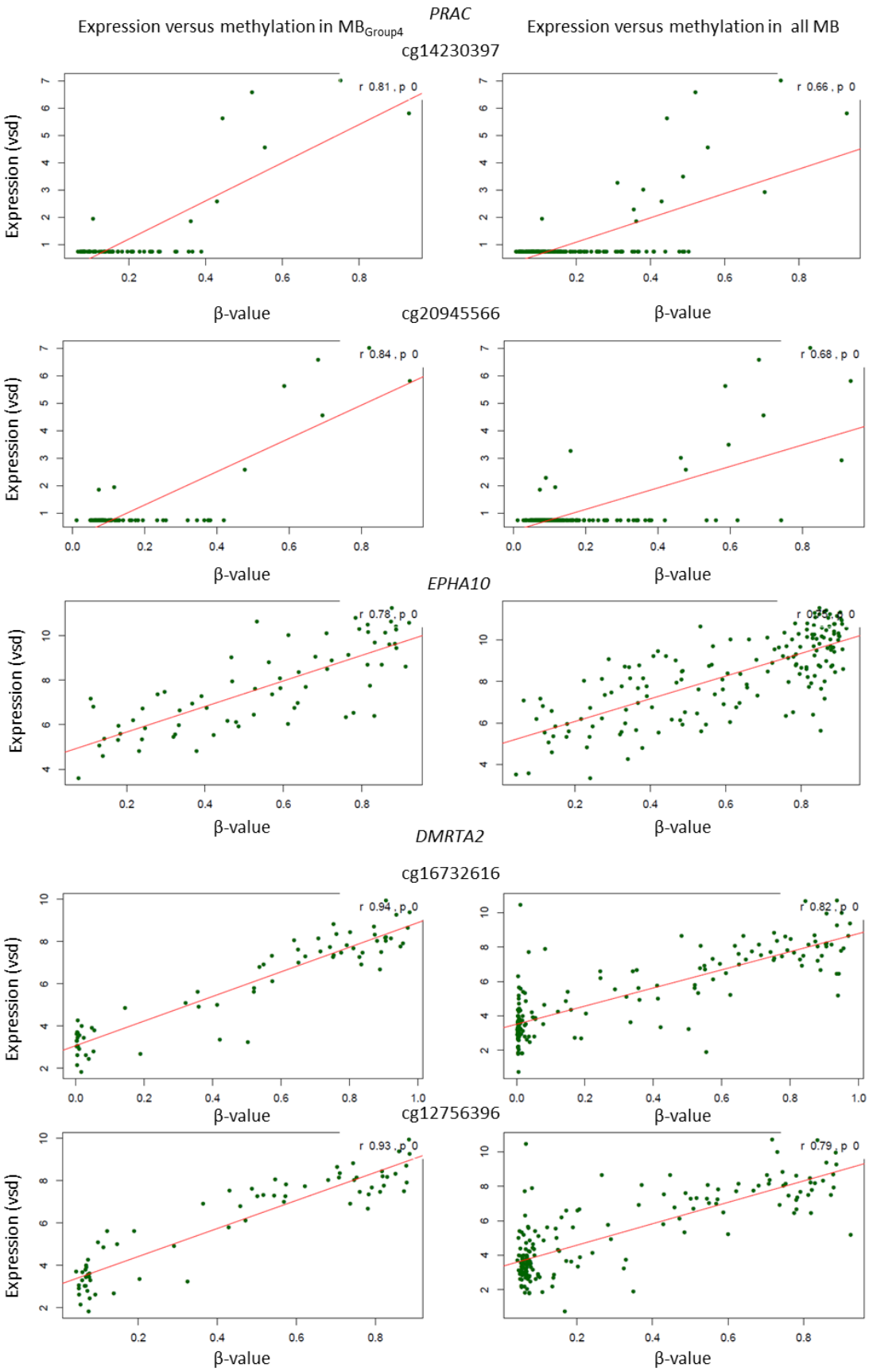

Figure 9.8 Linear regression plot illustrating the positive correlation between methylation and expression in *PRAC*, *EPHA10* and *DMRTA2*. VSD, variance-stabilising data.

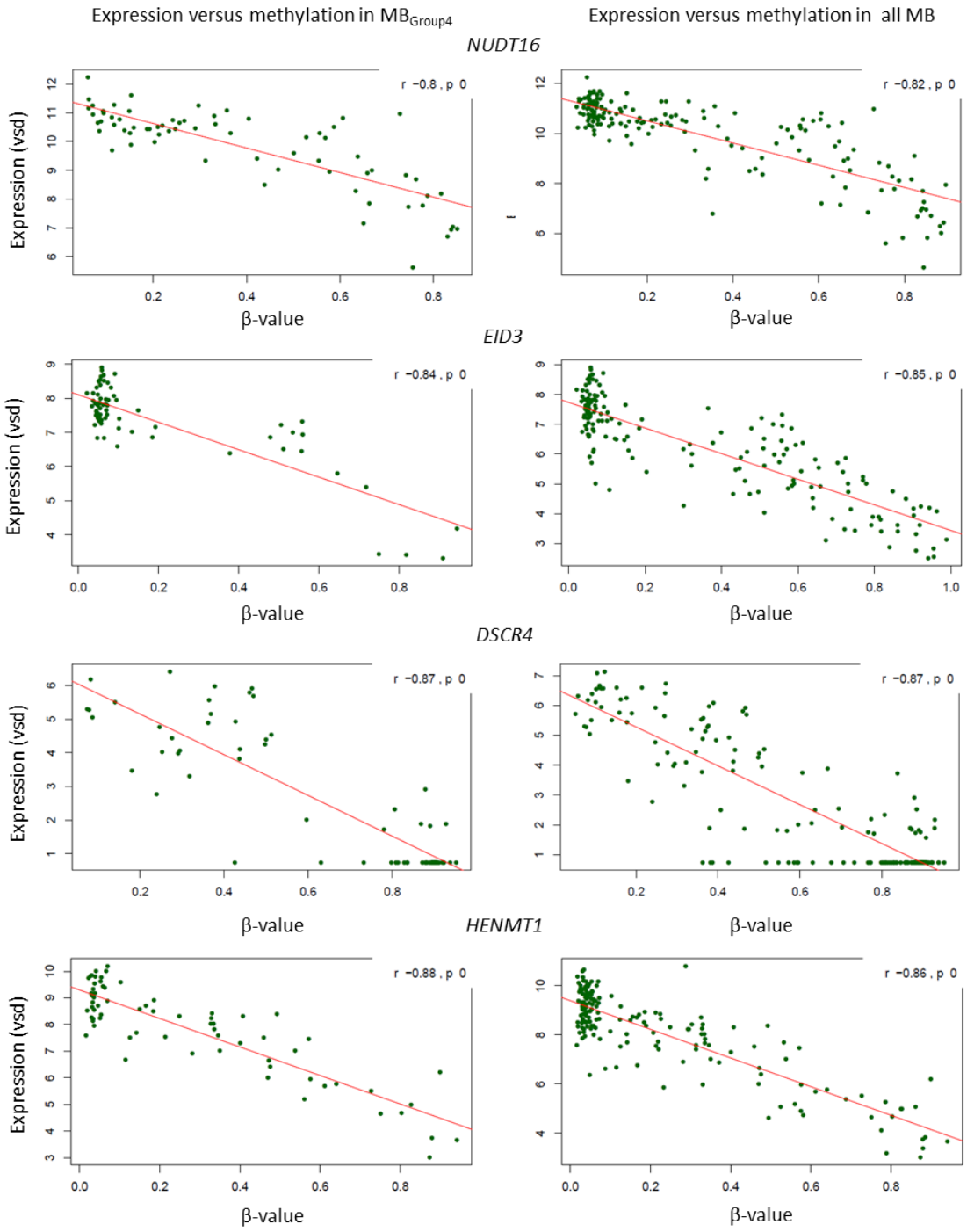

Figure 9.9 Linear regression plot illustrating the inverse correlation between methylation and expression at single CpG residues for *NUD16*, *EID3*, *DSCR4* and *HENMT1*. VSD, variance-stabilising data.

9.5 Appendix V: Relapsing cohort data tables illustrating the patterns of medulloblastoma relapse according to molecular subgroup and upfront therapy.

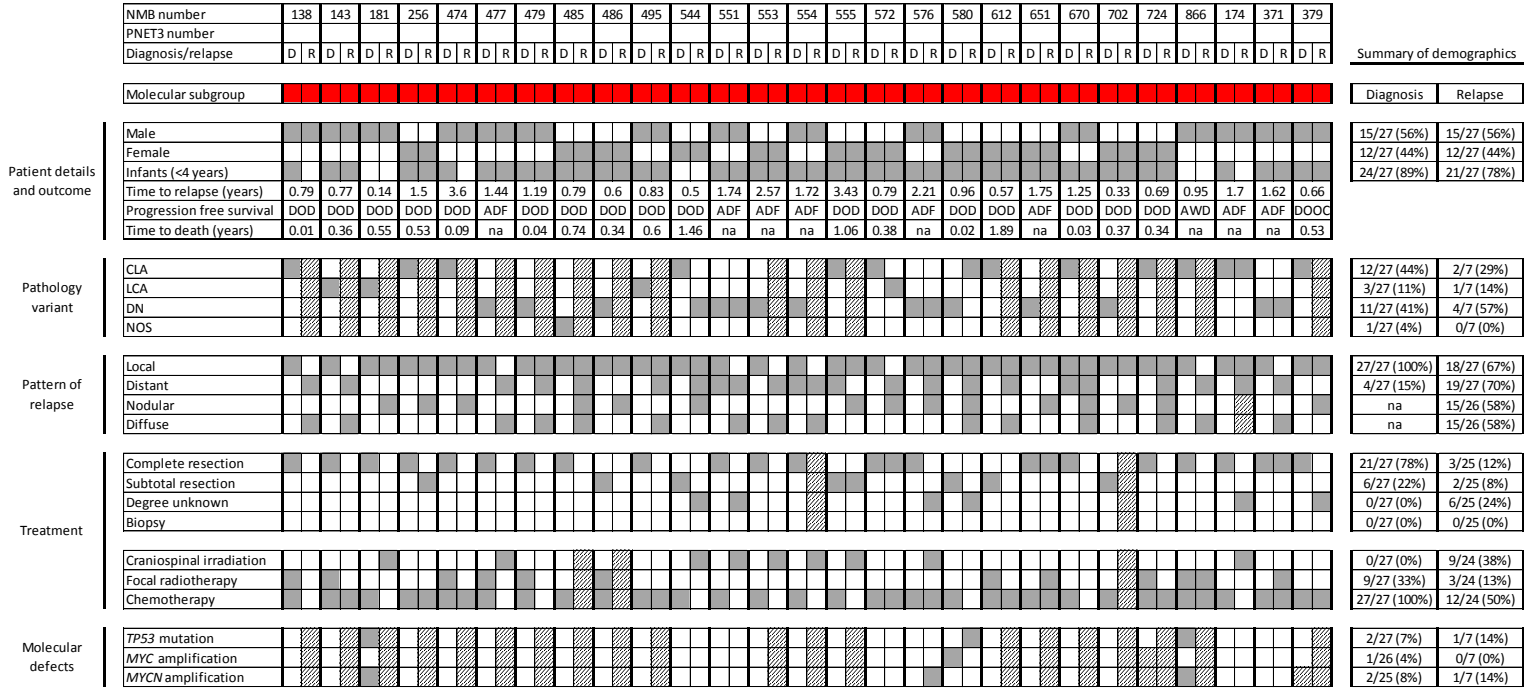

Table 9.1 Detailed clinical, pathological, patterns of relapse and molecular characteristics at diagnosis (D) and relapse (R) of the MB_{SHH} (red) relapsing cohort who did not receive upfront craniospinal radiotherapy. Demographic frequencies are shown as a proportion and percentage of the data available for each variable. NMB, Newcastle medulloblastoma. Progression free survival (ADF, alive disease-free; AWD, alive with disease; DOD, died of disease; DOOC, died of other complications). Pathology variant (CLA, classic; LCA, large-cell/anaplastic; DN, desmoplastic/nodular; NOS, medulloblastoma not otherwise specified). Disease location (local, M0/M1; distant, M2+). Feature present, grey square; feature absent, white square; data not available, diagonal hatching.

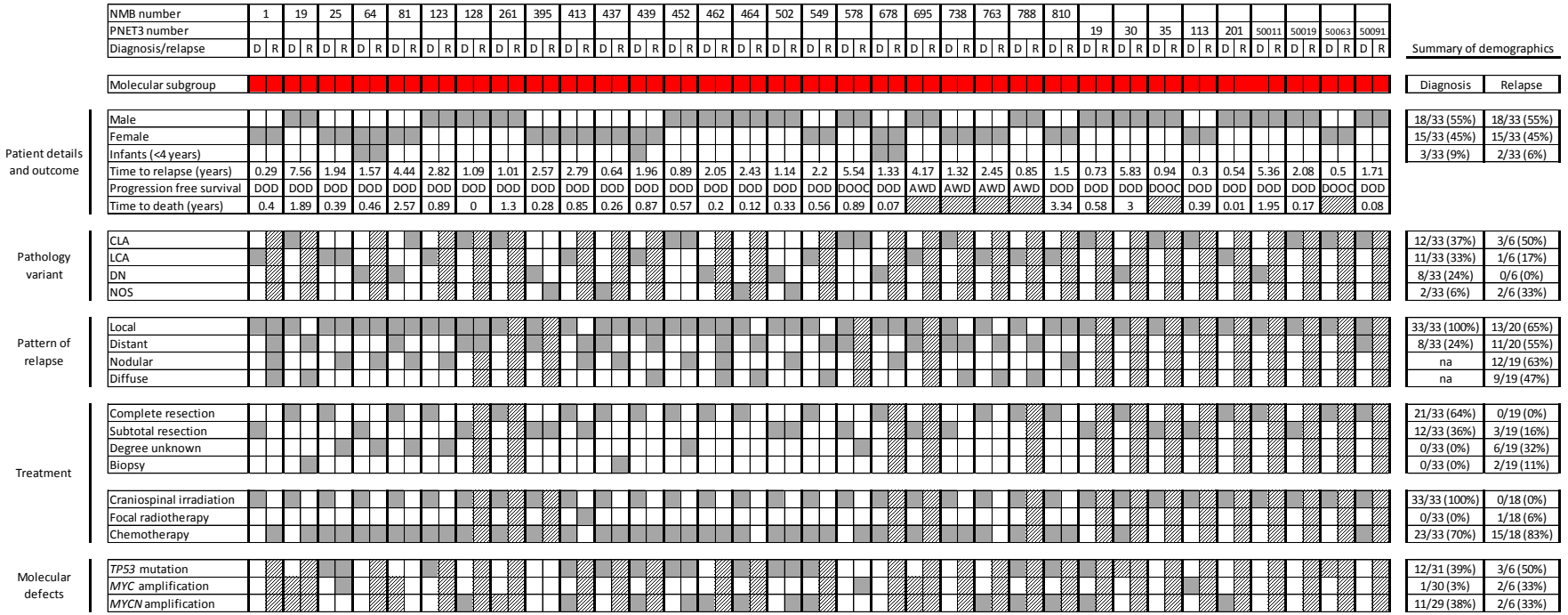

Table 9.2 Detailed clinical, pathological, patterns of relapse and molecular characteristics at diagnosis (D) and relapse (R) of the MB_{SHH} (red) relapsing cohort who did receive upfront craniospinal radiotherapy. Demographic frequencies are shown as a proportion and percentage of the data available for each variable. NMB, Newcastle medulloblastoma. Progression free survival (ADF, alive disease-free; AWD, alive with disease; DOD, died of disease; DOOC, died of other complications). Pathology variant (CLA, classic; LCA, large-cell/anaplastic; DN, desmoplastic/nodular; NOS, medulloblastoma not otherwise specified). Disease location (local, M0/M1; distant, M2+). Feature present, grey square; feature absent, white square; data not available, diagonal hatching.

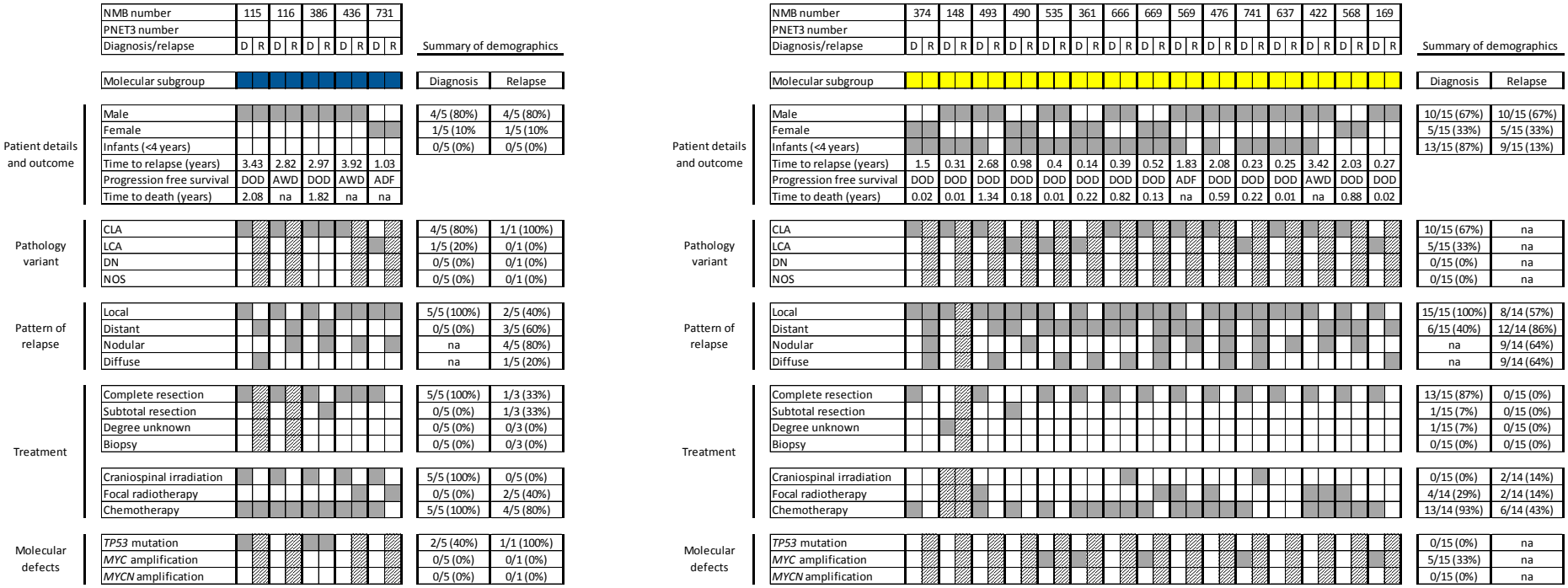

Table 9.3 Detailed clinical, pathological, patterns of relapse and molecular characteristics at diagnosis (D) and relapse (R) of the MB_{WNT} (blue) relapsing cohort who did receive upfront craniospinal radiotherapy and MB_{Group3} (yellow) relapsing cohort who did not receive upfront craniospinal radiotherapy. Demographic frequencies are shown as a proportion and percentage of the data available for each variable. NMB, Newcastle medulloblastoma. Progression free survival (ADF, alive disease-free; AWD, alive with disease; DOD, died of disease). Pathology variant (CLA, classic; LCA, large-cell/anaplastic; DN, desmoplastic/nodular; NOS, medulloblastoma not otherwise specified). Disease location (local, M0/M1; distant, M2+). Feature present, grey square; feature absent, white square; data not available, diagonal hatching.

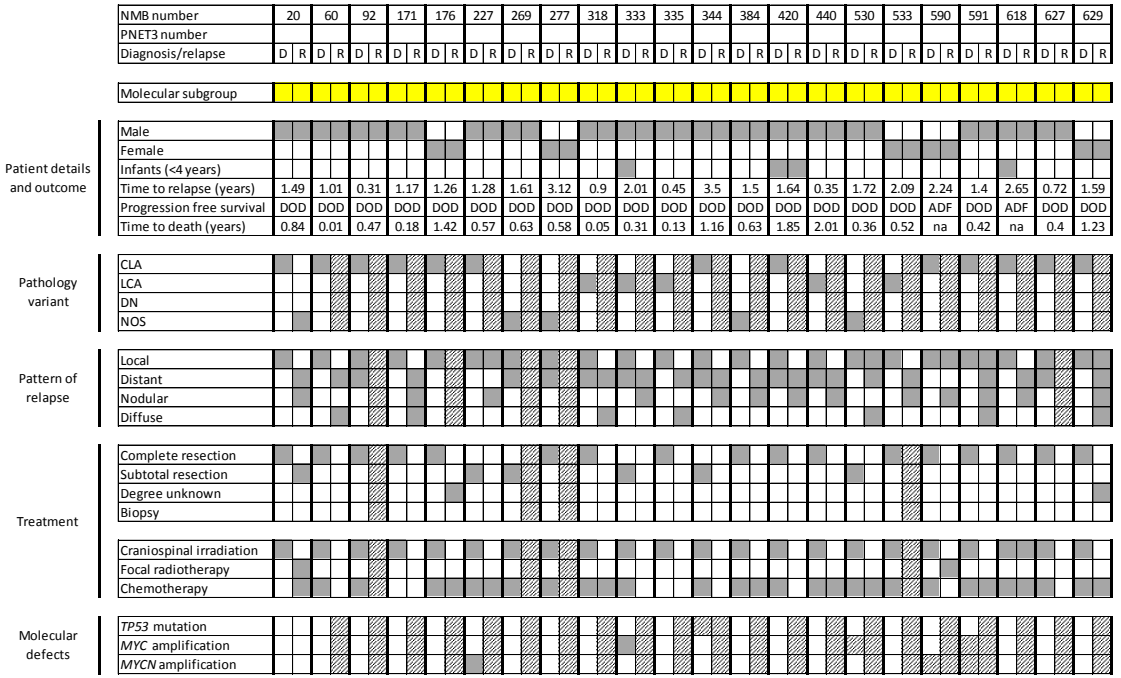

Table 9.4 Detailed clinical, pathological, patterns of relapse and molecular characteristics at diagnosis (D) and relapse (R) of the MB_{Group3} (yellow) relapsing cohort who did receive upfront craniospinal radiotherapy. Demographic frequencies are shown in Table 9.5. NMB, Newcastle medulloblastoma. Progression free survival (ADF, alive disease-free; DOD, died of disease). Pathology variant (CLA, classic; LCA, large-cell/anaplastic; DN, desmoplastic/nodular; NOS, medulloblastoma not otherwise specified). Disease location (local, M0/M1; distant, M2+). Feature present, grey square; feature absent, white square; data not available, diagonal hatching.

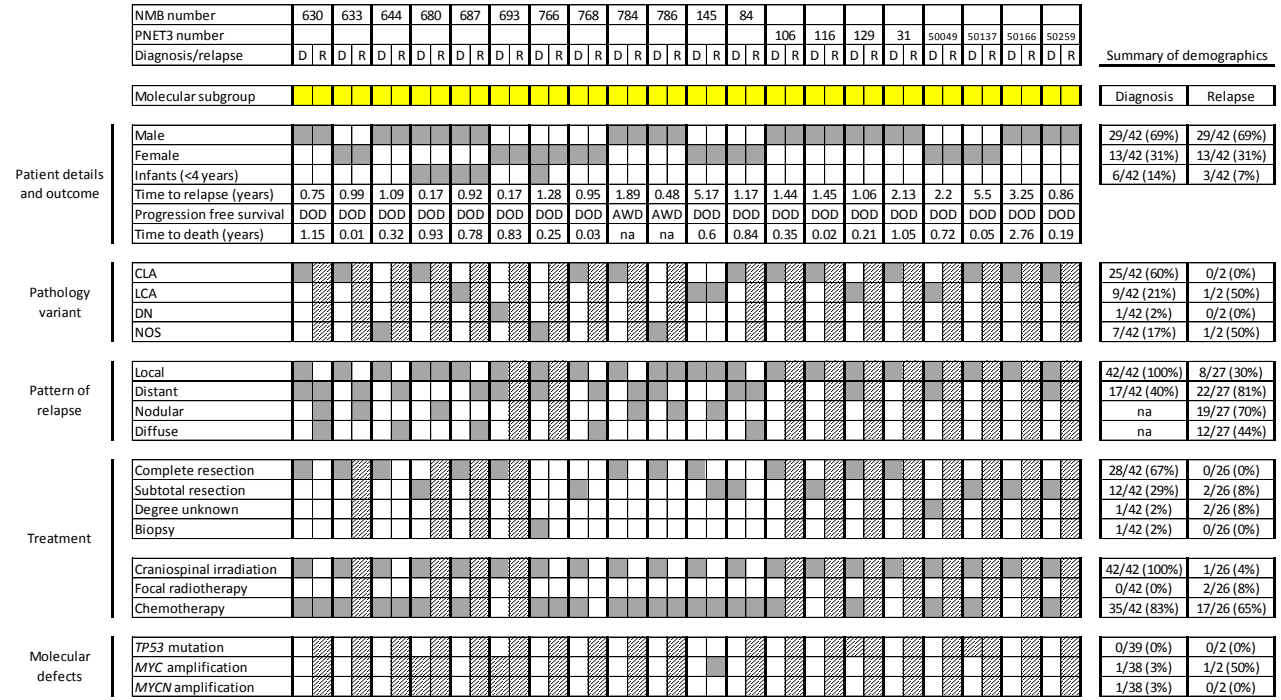

Table 9.5 Detailed clinical, pathological, patterns of relapse and molecular characteristics at diagnosis (D) and relapse (R) of the MB_{Group3} (yellow) relapsing cohort who did receive upfront craniospinal radiotherapy. Demographic frequencies are shown as a proportion and percentage of the data available for each variable. NMB, Newcastle medulloblastoma. Progression free survival (AWD, alive with disease; DOD, died of disease). Pathology variant (CLA, classic; LCA, large-cell/anaplastic; DN, desmoplastic/nodular; NOS, medulloblastoma not otherwise specified). Disease location (local, M0/M1; distant, M2+). Feature present, grey square; feature absent, white square; data not available, diagonal hatching.

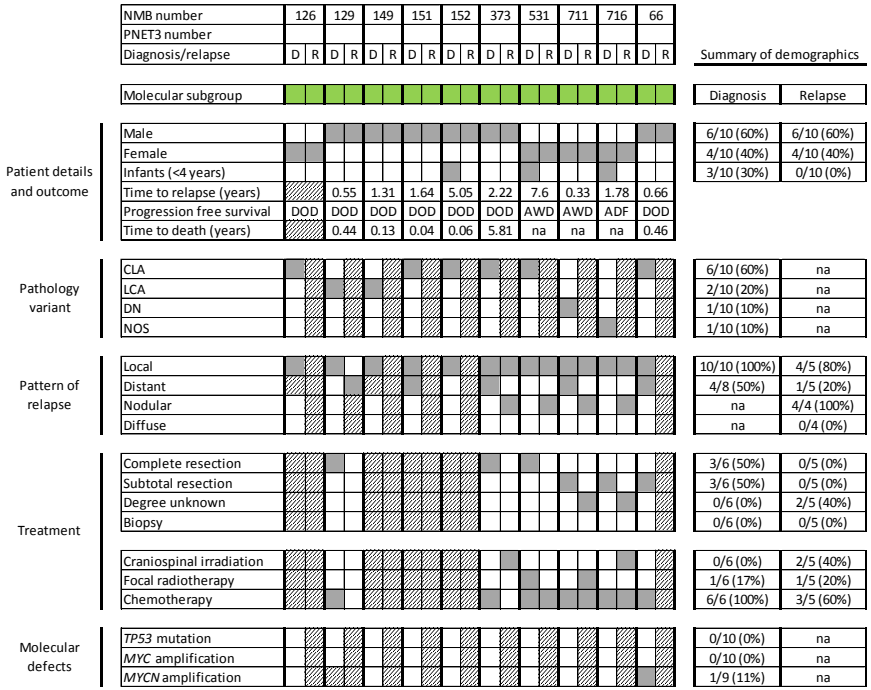

Table 9.6 Detailed clinical, pathological, patterns of relapse and molecular characteristics at diagnosis (D) and relapse (R) of the MB_{Group4} (green) relapsing cohort who did not receive upfront craniospinal radiotherapy. Demographic frequencies are shown as a proportion and percentage of the data available for each variable. NMB, Newcastle medulloblastoma. Progression free survival (ADF, alive disease-free; AWD, alive with disease: DOD, died of disease). Pathology variant (CLA, classic; LCA, large-cell/anaplastic; DN, desmoplastic/nodular; NOS, medulloblastoma not otherwise specified). Disease location (local, M0/M1; distant, M2+). Feature present, grey square; feature absent, white square; data not available, diagonal hatching.

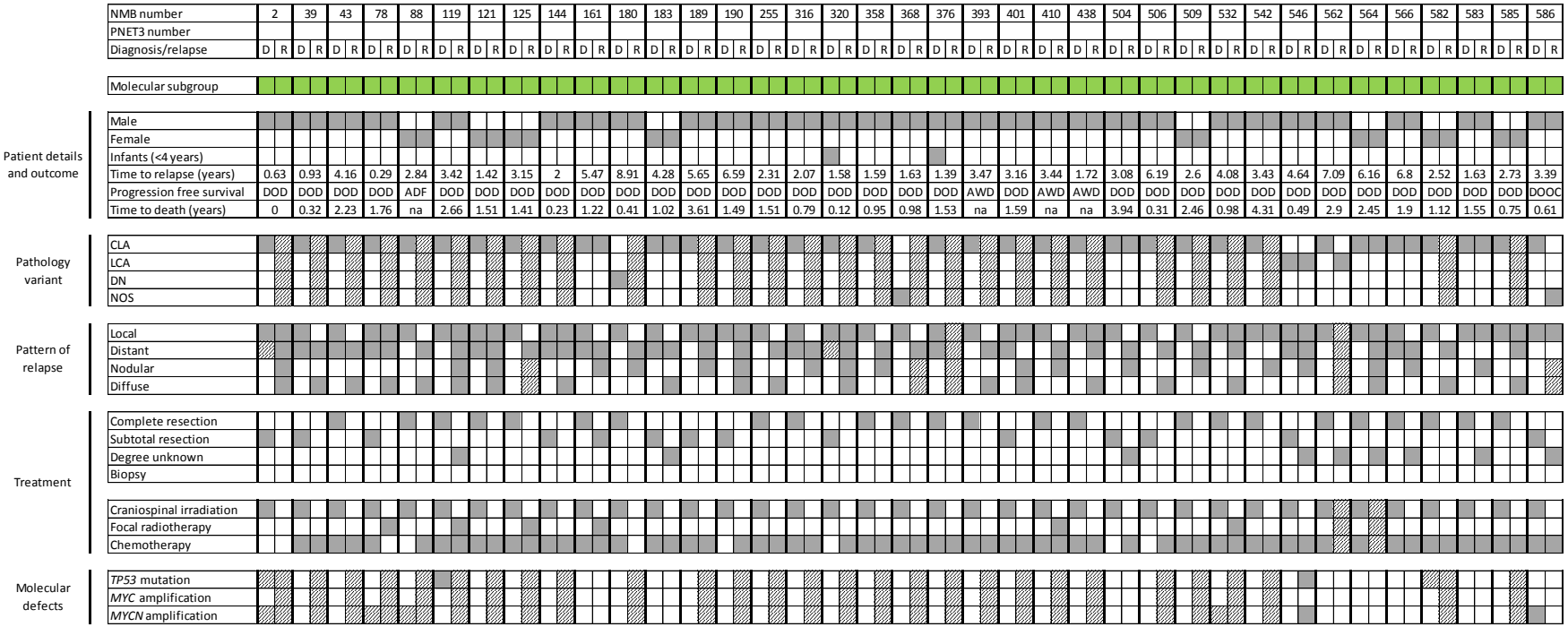

NMB number	2	39	43	78	88	119	121	125	144	161	180	183	189	190	255	316	320	358	368	376	393	401	410	438	504	506	509	532	542	546	562	564	566	582	583	585	586
PNET3 number																																					
Diagnosis/relapse	D R	D R	D R	D R	D R	D R	D R	D R	D R	D R	D R	D R	D R	D R	D R	D R	D R	D R	D R	D R	D R	D R	D R	D R	D R	D R	D R	D R	D R	D R	D R	D R	D R	D R	D R	D R	D R
Molecular subgroup																																					
Male																																					
Female																																					
Infants (<4 years)																																					
Time to relapse (years)	0.63	0.93	4.16	0.29	2.84	3.42	1.42	3.15	2	5.47	8.91	4.28	5.65	6.59	2.31	2.07	1.58	1.59	1.63	1.39	3.47	3.16	3.44	1.72	3.08	6.19	2.6	4.08	3.43	4.64	7.09	6.16	6.8	2.52	1.63	2.73	3.39
Progression free survival	DOD	DOD	DOD	DOD	ADF	DOD	DOD	DOD	DOD	DOD	DOD	DOD	DOD	DOD	DOD	DOD	DOD	DOD	DOD	DOD	AWD	DOD	AWD	AWD	DOD	DOD	DOD	DOD	DOD	DOD	DOD	DOD	DOD	DOD	DOD	DOD	DOOC
Time to death (years)	0	0.32	2.23	1.76	na	2.66	1.51	1.41	0.23	1.22	0.41	1.02	3.61	1.49	1.51	0.79	0.12	0.95	0.98	1.53	na	1.59	na	na	3.94	0.31	2.46	0.98	4.31	0.49	2.9	2.45	1.9	1.12	1.55	0.75	0.61
CLA																																					
LCA																																					
DN																																					
NOS																																					
Local																																					
Distant																																					
Nodular																																					
Diffuse																																					
Complete resection																																					
Subtotal resection																																					
Degree unknown																																					
Biopsy																																					
Craniospinal irradiation																																					
Focal radiotherapy																																					
Chemotherapy																																					
TP53 mutation																																					
MYC amplification																																					
MYCN amplification																																					

Table 9.7 Detailed clinical, pathological, patterns of relapse and molecular characteristics at diagnosis (D) and relapse (R) of the MB_{Group4} (green) relapsing cohort who did receive upfront craniospinal radiotherapy. Demographic frequencies are shown in Table 9.8. NMB, Newcastle medulloblastoma. Progression free survival (ADF, alive disease-free; AWD, alive with disease; DOD, died of disease; DOOC, died of other complications). Pathology variant (CLA, classic; LCA, large-cell/anaplastic; DN, desmoplastic/nodular; NOS, medulloblastoma not otherwise specified). Disease location (local, M0/M1; distant, M2+). Feature present, grey square; feature absent, white square; data not available, diagonal hatching.

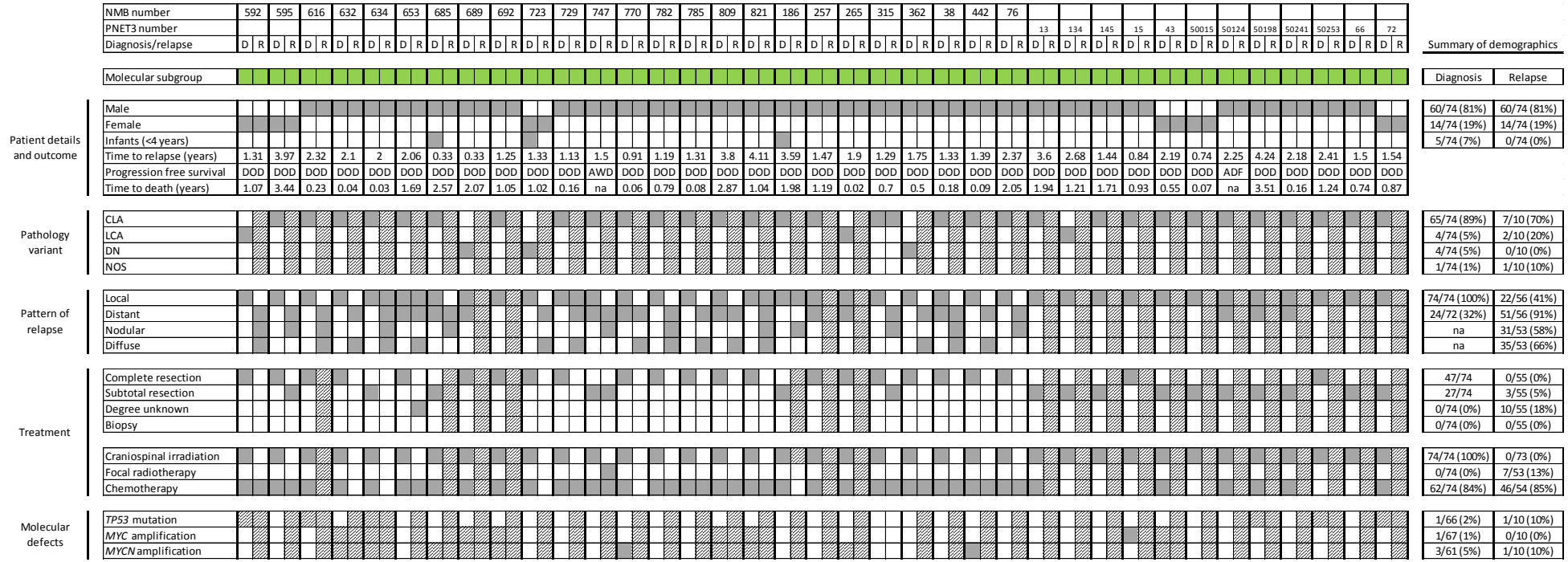

Table 9.8 Detailed clinical, pathological, patterns of relapse and molecular characteristics at diagnosis (D) and relapse (R) of the MB_{Group4} (green) relapsing cohort who did receive upfront craniospinal radiotherapy. Demographic frequencies are shown as a proportion and percentage of the data available for each variable. NMB, Newcastle medulloblastoma. Progression free survival (ADF, alive disease-free; AWD, alive with disease; DOD, died of disease). Pathology variant (CLA, classic; LCA, large-cell/anaplastic; DN, desmoplastic/nodular; NOS, medulloblastoma not otherwise specified). Disease location (local, M0/M1; distant, M2+). Feature present, grey square; feature absent, white square; data not available, diagonal hatching.

Chapter 10. Publications